Remote Sensing Data Handbook

New Technology, Incorporated Huntsville, Alabama July 1978

U.S. DEPARTMENT OF COMMERCE National Technical Information Service





# NASA CONTRACTOR REPORT

NASA CR-150837

(NASA-CR-150837) REMOTE SENSING DATA HANDBOOK (New Technology, Inc.) 469 p HC A20/MF A01 CSCL 14B N79-14499

Unclas G3/43 35417

REMOTE SENSING DATA HANDBOOK

Prepared by

New Technology, Inc. 3313 Memorial Parkway, S. W. Huntsville, Alabama 35801

Contract NAS8-31423

July 31, 1978

REPRODUCED BY
NATIONAL TECHNICAL
INFORMATION SERVICE
U.S. DEPARTMENT OF COMMERCE
SPRINGFIELD, VA 22161

Prepared for

NASA - George C. Marshall Space Flight Center Marshall Space Flight Center, Alabama 35812

#### NOTICE

THIS DOCUMENT HAS BEEN REPRODUCED FROM THE BEST COPY FURNISHED US BY THE SPONSORING AGENCY. ALTHOUGH IT IS RECOGNIZED THAT CERTAIN PORTIONS ARE ILLEGIBLE, IT IS BEING RELEASED IN THE INTEREST OF MAKING AVAILABLE AS MUCH INFORMATION AS POSSIBLE.

REPORT NO. 2. GOVERNMENT ACCESSION NO.	
NASA CR-150837	3. RECIPIENT'S CATALOG NO.
TITLE AND SUBTITLE	5. REPORT DATE
Dometo Concina Data Handbook	July 31, 1978
Remote Sensing Data Handbook	6. PERFORMING ORGANIZATION CODE
AUTHOR(S)	8. PERFORMING ORGANIZATION REPORT
PERFORMING ORGANIZATION NAME AND ADDRESS	10. WORK UNIT NO.
New Technology, Inc.	
3313 Memorial Parkway, S. W.	11. CONTRACT OR GRANT NO.
Huntsville, Alabama 35801	NAS8-31423
<u> </u>	13. TYPE OF REPORT & PERIOD COVERED
SPONSORING AGENCY NAME AND ADDRESS	Contro et au Bau aut
National Aeronautics and Space Administration	Contractor Report
Washington, D. C. 20546	14. SPONSORING AGENCY CODE
SUPPLEMENTARY NOTES	
This work was done under the technical supervision of Marshall Space Flight Center.	f Mr. David Schaefer, George C.
, ABSTRACT	
characteristics of space-borne sensors and the supportive sy therewith. It also includes end-to-end systems information t	<b>▼</b>
appraising total data system impact produced by a sensor. To for anticipating the complexity of systems and potential data needs are generated. Materials in this handbook span sensor those planned for use in the 1990's. Sensor systems on all pin digest form, condensed from data as available at the time are made of anticipated systems.	The objective is to provide a tool system problems as new user r systems from the present to lanned missions are presented
for anticipating the complexity of systems and potential data needs are generated. Materials in this handbook span sensor those planned for use in the 1990's. Sensor systems on all p in digest form, condensed from data as available at the time	The objective is to provide a tool system problems as new user r systems from the present to lanned missions are presented
for anticipating the complexity of systems and potential data needs are generated. Materials in this handbook span sensor those planned for use in the 1990's. Sensor systems on all p in digest form, condensed from data as available at the time	The objective is to provide a tool system problems as new user r systems from the present to lanned missions are presented
for anticipating the complexity of systems and potential data needs are generated. Materials in this handbook span sensor those planned for use in the 1990's. Sensor systems on all p in digest form, condensed from data as available at the time	The objective is to provide a tool system problems as new user r systems from the present to lanned missions are presented
for anticipating the complexity of systems and potential data needs are generated. Materials in this handbook span sensor those planned for use in the 1990's. Sensor systems on all p in digest form, condensed from data as available at the time	The objective is to provide a tool system problems as new user r systems from the present to lanned missions are presented
for anticipating the complexity of systems and potential data needs are generated. Materials in this handbook span sensor those planned for use in the 1990's. Sensor systems on all p in digest form, condensed from data as available at the time	The objective is to provide a tool system problems as new user r systems from the present to lanned missions are presented
for anticipating the complexity of systems and potential data needs are generated. Materials in this handbook span sensor those planned for use in the 1990's. Sensor systems on all p in digest form, condensed from data as available at the time	The objective is to provide a tool system problems as new user r systems from the present to lanned missions are presented
for anticipating the complexity of systems and potential data needs are generated. Materials in this handbook span sensor those planned for use in the 1990's. Sensor systems on all pin digest form, condensed from data as available at the time are made of anticipated systems.	The objective is to provide a tool system problems as new user r systems from the present to lanned missions are presented of compilation. Projections
for anticipating the complexity of systems and potential data needs are generated. Materials in this handbook span sensor those planned for use in the 1990's. Sensor systems on all p in digest form, condensed from data as available at the time	The objective is to provide a tool system problems as new user r systems from the present to lanned missions are presented of compilation. Projections
for anticipating the complexity of systems and potential data needs are generated. Materials in this handbook span sensor those planned for use in the 1990's. Sensor systems on all pin digest form, condensed from data as available at the time are made of anticipated systems.	The objective is to provide a tool system problems as new user r systems from the present to lanned missions are presented of compilation. Projections
for anticipating the complexity of systems and potential data needs are generated. Materials in this handbook span sensor those planned for use in the 1990's. Sensor systems on all pin digest form, condensed from data as available at the time are made of anticipated systems.	The objective is to provide a tool system problems as new user r systems from the present to lanned missions are presented of compilation. Projections
for anticipating the complexity of systems and potential data needs are generated. Materials in this handbook span sensor those planned for use in the 1990's. Sensor systems on all pin digest form, condensed from data as available at the time are made of anticipated systems.	The objective is to provide a tool system problems as new user r systems from the present to lanned missions are presented of compilation. Projections
for anticipating the complexity of systems and potential data needs are generated. Materials in this handbook span sensor those planned for use in the 1990's. Sensor systems on all pin digest form, condensed from data as available at the time are made of anticipated systems.	The objective is to provide a tool system problems as new user r systems from the present to lanned missions are presented of compilation. Projections
for anticipating the complexity of systems and potential data needs are generated. Materials in this handbook span sensor those planned for use in the 1990's. Sensor systems on all pin digest form, condensed from data as available at the time are made of anticipated systems.	The objective is to provide a tool system problems as new user r systems from the present to lanned missions are presented of compilation. Projections
for anticipating the complexity of systems and potential data needs are generated. Materials in this handbook span sensor those planned for use in the 1990's. Sensor systems on all pin digest form, condensed from data as available at the time are made of anticipated systems.	The objective is to provide a tool system problems as new user r systems from the present to lanned missions are presented of compilation. Projections
for anticipating the complexity of systems and potential data needs are generated. Materials in this handbook span sensor those planned for use in the 1990's. Sensor systems on all pin digest form, condensed from data as available at the time are made of anticipated systems.	The objective is to provide a tool system problems as new user r systems from the present to lanned missions are presented of compilation. Projections
for anticipating the complexity of systems and potential data needs are generated. Materials in this handbook span sensor those planned for use in the 1990's. Sensor systems on all pin digest form, condensed from data as available at the time are made of anticipated systems.	The objective is to provide a tool system problems as new user r systems from the present to lanned missions are presented of compilation. Projections

#### **FOREWORD**

This handbook was prepared by New Technology, Inc., under Contract NAS8-31423, entitled, "User Technology Study." The Remote Sensing Data Handbook (RSDH) presently contains summary information on remote sensors of earth resources and related data system elements. Technical monitors for this handbook are Messrs. Harvey Golden (EF-21) and Dave Schaefer (EF-23) of the Data Systems Laboratory of the Marshall Space Flight Center, Alabama. Principal investigators for the handbook are James L. Ellison and R. R. DeWitt of New Technology, Inc., Huntsville, Alabama.

Questions, comments and suggestions concerning the contents and format of this handbook are invited. Communications may be made via the RSDH Change Request Forms (located at the end of Section 2) or by telephone to the following individual:

Mr. Dave Schaefer (205) 453-4064

Revisions of this document and/or quarterly updates are available through the National Technical Information Service and/or the Marshall Space Flight Center Documentation Repository.

#### TABLE OF CONTENTS

Section		Contents		Page
•	FOREWOR	ap · · ·	•	i
	TABLE O	OF CONTENTS	ORIGINAL PA	GF is ii
•	REVISIO	N CONTROL SHEET	OF POOR QUA	ALITY iv
1	INTRODU	CTION		1-1
	1.1 Re	evision Control		1-2
	1.2 Cr	oss Indexing		1-2
	1.3 Se	ensor Data Sheets	•	1-2
2	RSDH RE	VISION CONTROL		2-1
	2.1 Re	vision Control Struc	cture	2-1
	2.2 Re	vision Control Proce	edure	2-2
3	RSDH CR	ROSS INDEXES		3-1
	3.1 A1	phabetical and Senso	or Category I <b>nd</b>	ex 3-3
	3.2 Pr	ogram and Developmer	nt Index	3-5
	3.3 Di	scipline and Major I	unction Index	3-7
	3.4 Sp	ectrum and Coverage	Index	3-10
4	DEFINIT	TONS AND ACRONYMS		4-1
	4.1 De	finition of Terms	•	4-1
	4.2 Ac	cronyms		4-2
5	SENSOR	CATEGORIES		5-1
	5.1 Sy	nthetic Aperture Rac	lars	5.1-1
	5.2 A1	timeters		5.2-1
	5.3 Sc	atterometers		5.3-1
	5.4 La	iser Radars		5.4-1

REV. NO.:

2

#### RSDH

5.5	Multispectral and Mapping Cameras	5.5-1
5.6	Other Active Radiance Measuring Sensors	TBD
5.7	Imaging Spectroradiometers	5.7-1
5.8	Atmospheric Sounders	5.8-1
5.9	Other Passive Radiance Measuring Sensors	TBD
5.10	Field Measuring Sensors	5.10-1
APPEN	NDIK AInfrared Detectors	A-1

### RSDH REVISION CONTROL SHEET

SECTION NUMBER PAGE		EFFECTIV	VE .	
NUMBÉR	OF PAGES	NUMBER	REV. DATE	REV. N
FOREWORD	1	i	31 JUL 78	3
TABLE OF CONTENTS	2	ii iii .	31 JAN 78 31 JAN 78	. 2
RSDH REVISION CONTROL	2	iv v	31 JUL 78 31 JUL 78	3 3
1	5	1-1 1-2 1-3 1-4 1-5	31 JAN 78 31 JAN 78 31 JUL 78 31 JUL 78 30 JUN 77	2 2 3 3 0
2	5	2-1 2-2 2-3 2-4 2-5	31 JAN 78 31 JAN 78 31 JAN 78 31 JAN 78 30 JUN 78	2 2 2 2 0
3	16	3-1 3-2 3-3 3-4 3-5 3-6 3-7 3-8 3-9 3-10 3-11 3-12 3-13 3-14 3-15 3-16	31 JAN 78 31 JAN 78 31 JUL 78	2 2 3 3 2 3 3 3 3 3 3 3 3 3 3 3 3 3 3 3
4	8	4-1 4-2 4-3 4-4 4-5 4-6 4-7 4-8	31 JAN 78 31 JUL 78	2 3 3 3 3 3 3 3 3

RSDH REVISION CONTROL SHEET

SECTION	NUMBER	PAGE	EFFECTIV	/E
NUMBER	OF PAGES	NUMBER	REV. DATE	REV. NO.
5		5-1	31 JAN 78	2
	*(See individual Ta Sheets at the fron	ble of Contents and t of each sensor ca	Revision Control tegory in Section 5	<b>.</b> )
APPENDIX A				
AFFERDIA A	*(See Revision Cont	rol Sheet and Table	of Contents	
	at the front of A	ppendix A.)		
and the state of t	Carlos Agreements and Carlos Agreement and Carlos A			
			• . • .	
			•	
i vita	to the second		, , ,	

### HORR CONTRACTOR

erive erice	3443		en montale acom	ETHERINA PRESIDENCE E A L'ARRENT LA CONTRA DE L'ARRENT E LA CONTRA DE L'ARRENT E L'ARREN
REV. NO.	REV. DATE	1. 18 1 1 1 1 1 1 1 1 1 1 1 1 1 1 1 1 1	NUMBER OF PAGES	SECTION
S	31 JAN 78	THE RESERVENCE OF THE PROPERTY	Committee Commit	And the second s
on 3.)	Revision Contr tegory in Secti	ole of Control and t of each sensor ca	*(See individual la Shaets at the fron	·
MENGRAP ENTER SERVICE			क्त	APPENDIY A
if pyraside constraints of the district of the	of Contents	rol Sheet and Table ppendix A.)	*(See Revision Cont at the front of A	
AND THE PROPERTY OF THE PROPER				
escape en l'orizonne de l'oriz	<i>i</i>			
C pose (C2) conservation of the Cartesian of the Cartesia	· .			
Paris Landau de la companya de la co	•			
SHEET ALL AND				
To prove Piller in the a Committee Committee	, ,	·		

Revised 31 July 1978 (Revision 3)

## Section 1 INTRODUCTION

This handbook is a digest of information on remote sensor data systems. It includes characteristics of space-borne sensors and the supportive systems immediately associated therewith. It also includes end-to-end systems information that will assist the user in appraising total data system impact produced by a sensor. The objective is to provide a tool for anticipating the complexity of systems and potential data system problems as new user needs are generated. Materials in this handbook span sensor systems from the present to those planned for use in the 1990's. Sensor systems on all planned missions are presented in digest form, condensed from data as available at the time of compilation. Projections are made of anticipated systems.

Remote sensing systems encompass many disciplines. To provide the handbook user with a perspective between the discipline and the specific sensor information, an introduction to each sensor group (e.g., Scatterometers) is included in each sensor category. This introductory section will assist the user in understanding the principles of the operation of the instrument and the meaning of terms associated with specific sensors. Sources of additional information and trends in the field are also discussed. The information in each introductory section addresses a particular category of sensors and is outlined as follows:

- Historical Information
- Principles of Operation
- Performance Limiting Factors
- Data System and Output Products
- Trends in R & D

- Prominent Contributors
- References

Information on specific sensor systems is presented in a data sheet format which is discussed in Paragraph 1.3.

#### 1.1 Revision Control

A revision control structure and procedure is provided in Section 2, such that this handbook may be maintained by periodic revision and/or republications. All sensor related information and data sheets in this handbook are dated, numbered and controlled via this procedure.

#### 1.2 RSDH Cross Indexing

To further assist the handbook user, four cross indexes are provided to facilitate entry into the sensor systems information from any of four different perspectives:

- Alphabetical Listing of Sensors vs. Sensor Category
- Program Alignment and Development Schedule Information
- Discipline Alignment and Major Function Information
- Sensor Spectrum and Coverage Characteristics

These indexes are described and contained in Section 3.

#### 1.3 Sensor Data Sheets

Information on specific sensor systems is presented in a data sheet format which organizes the information without restricting it. The same data sheet format is used throughout the handbook and is illustrated in Figure 1-1. As shown in Figure 1-1, the data sheet is structured into thirteen information cells plus a continuation sheet. To familiarize the user with the sensor data sheets, Figure 1.1 gives a short description of the information content for each information cell.

**REV. NO.:** 2

nd garrand, if applicable) r to primary application (3) SusDISCIPLINE: secondary discipline(s)	(b) SENSON DATA MENSUNCMENT AND INFORMATION STOLEM - BLUCK CINDRAM.
discripting of application	
APPLICATION - Describes has sensor to used	
OBJECTIVE - Describes the intended purpose of the sensor	
(6) HERITAGE/KEY PERSONNEL:  Identifies the lineage of the primary sensor components  and sensor representatives or sponsors	Includes information sufficient to describe the trouts
(6) SENSOR DEPLOYMENT:	nits on board i
Description of the platform(s) upon which the sensor is mounted (type of satellite, altitude, eccentricity, inclination, period, etc.)	bandriths and data retesall pertinent units bothsen the detector and the downlink anterna are included.
SENSOR CHARACTERISTICS	
(7A) CAPABILITIES AND CONSTRAINTS OF THE SENSOR TO ACQUIRE THE MEASURED PARAMETER:	
Identifies exath, scan rate, scan pattern, spatial resolution, accuracy characteristics. This information relates to the means by which radiant energy is collected.	
(18) ACTIVE SOURCE CHARACTERISTICS (FOR ACTIVE SENSORS):	(9) MEASUREMENT AND TRANSMISSION SYSTEM – NARRATIVE:
identifies operating frequency, power level, modulation antenna pattern, etc., of the artificial source for the illumination of the target (if used).	CE PO
(7C) DETECTOR MEASUREMENTS CHARACTERISTICS:	of housekeeping and correlative data, description of O S storage and pre-processing equipment, etc.
Describes detector size and resolution, rise time, noise, amplifier bandridth, dynamic range, linearity, repeatability, sto. This section characterizes the device used for converting the reastved radiant energy into electrical energy.	PAGE IS QUALITY
SECTION NO: SENSOR CATEGORY:	NO:
REV. DATE:	REV. NO.: REV. DATE:

, a partie de la constante de	SHEET OF	20 - T33-K2
		<u> </u>   •
<del>•••••</del>		
<del></del>		
·		
	Includes information and functional diagram to describe the ground processing related to the sensor generated data. This diagram shall include all data system impacting elements between the ground receiving antenna disk and the output data product. Transmission and/or shipment times of ant products shall be even.	This block diagram shows the distribution routes and times to various users and identifies distribution centers.
**************************************		
REV. N		
<b>O</b> .: 3	(11) RECEIVING AND PROCESSING – NARRATIVE:	(13) DATA DISTRIBUTION – NARRATIVE:
'RE'	This section provides a narrative description of the sensor data receiving and proceesing function that extends and provides further definition of the functional diagram above.	This section provides a narrative description of the data distribution related to this sensor. This information provides additional definition to the block diagram presented in (12) above.
V. DATE		
: 31	SECTION NO.: SENSOR CATEGORY: REV. NO.: REV. DATE:	SECTION NO.: SENSOR CATEGORY: REV. NO.: REV. DATE:
July 19	FIGURE 1-1	Data Sheet Format and Content (Page 2 of 3)
78		

CE EOOR QUALITY

This continuation sheet is used to accommodate overflow from information cells on the standard sensor data sheets and to present tables, figures and other tillustrations required to sufficiently describe sensors and related systems. Continuation sheets will irredictely follow the standard data sheets being continued.

Follow the standard data sheets being continued.

SHEET

CONTINUATION SHEET:

FIGURE 1-1 Data Sheet Format and Content (Page 3 of 3)

REV. NO.:

0

REV. DATE: 30 June 1977

This page intentionally left blank. REV. DATE: 30 June 1977 REV. NO.:

## Section 2 RSDH REVISION CONTROL

In order for the RSDH to be current and useful, a communication mechanism is required between the Data Systems Laboratory (DSL) personnel, who are responsible for the publication and maintenance of the RSDH, and the RSDH users. This communication link is provided by a revision control structure and associated updating procedures outlined and described in this section. It is anticipated that, in many cases, RSDH users will be major contributors to the handbook's technical content. This mechanism provides a means for these users to contribute new, additional or corrective information to the RSDH.

#### 2.1 Revision Control Structure

The revision control structure for the RSDH is separated into three activities as follows:

- Overall RSDH Revision and Distribution Control
- Sensor Category Revision Control
- RSDH Change Requests

Overall RSDH Revision and Distribution Control - The users of the RSDH will include Data Systems Laboratory and associated contractor personnel, other NASA personnel, contractors, and other government agencies. Each user will be issued a RSDH bound in a looseleaf folder so that he may make page additions and deletions. The RSDH Table of Contents will be followed by a "RSDH Revision Control Sheet" which will reflect the current content status of Sections 1 through 4 and the structure (titles only) of the sensor categories in Section 5. The internal content of each sensor category is controlled by a different form as explained later.

In order to provide revisions and other RSDH changes to users, a "RSDH Distribution List" is maintained. This list identifies all RSDH recipients by name,

REV. NO.:

organization/company, address and number of copies provided.

Sensor Category Revision Control - A separate table of contents and revision control form entitled, "Sensor Category Table of Contents and Revision Control Sheet," is maintained for each sensor category in Section 5. These control forms are located at the front of each sensor category and provide content and revision status on an individual sensor group basis.

RSDH Change Requests - The RSDH will be updated periodically as new information is available. It is recognized that RSDH users may be a major source of up-to-date sensor information as it is released. Users may originate a request for change to the RSDH via the Change Request (CR) forms provided at the end of this section. The CR forms permit users to note outdated information and input new information and other suggested improvements to the RSDH.

The responsibilities and procedures for accomplishing revision, distribution and change request activities are discussed in the next paragraph.

#### 2.2 Revision Control Procedure

Revisions are made on a periodic basis to improve and expand the information content of the RSDH. The initial copy of this handbook (Baseline Issue, dated 30 June 1977) represents a concentrated effort by Data Systems Laboratory to accumulate, condense, categorize and format sensor information into a useful reference document. RSDH users utilizing this manual to perform requirements analyses, sensor system studies or other sensor related evaluations will be able to contribute significantly to keeping this handbook as current and up-to-date as practical. The CR form discussed in Section 2.1 and contained at the end of Section 2 is provided for this purpose. In order that new and corrective information from CR's, as well as

ORIGINAL PAGE IS

OPICINAL QUALITY

those generated by Data Systems Laboratory, can be inserted into the RSDH on a timely and effective basis, the following revision control procedures are established

- Revision Frequency New material developed or received by Data Systems Laboratory for inclusion into the RSDH will be reviewed for approval on an as-received basis. Updated material will be formulated into revision packages and released to RSDH users on a frequency of at least semi-annually, but not more than quarterly.
- Revision Control Authority The authority for approving new and/or revised content for the RSDH is vested with the Requirements Analysis Branch (EF-23) of the Data Systems Laboratory. Revision control is accomplished by one or more designees of the Requirements Analysis Branch in the form of a RSDH Revision Control Unit (RCU). The functions of the RSDH RCU are as follows:
  - (1) control the list of recipients of the RSDH,
  - (2) approve material that is to be added to or deleted from the RSDH,
  - (3) insure that all CR's are reviewed, answered and/or implemented,
  - (4) insure that the RSDH is maintained as current as practical.
- <u>Preparation of Revised Material</u> <u>Preparation of revision packages is</u> the responsibility of the RSDH Investigative Unit (IU). The RSDH IU is composed of Data Systems Laboratory personnel from the Requirements Analysis Branch and/or contractor personnel. The functions of this unit are to:
  - (1) perform research on sensors or related systems for inclusion into the RSDH as directed by the RCU,
  - (2) review, research and implement CR's as approved by the RCU,
  - (3) control and maintain the originals (master copies) of the RSDII and revision packages, and
  - (4) print and release RSDH revision packages as approved by the RCU.

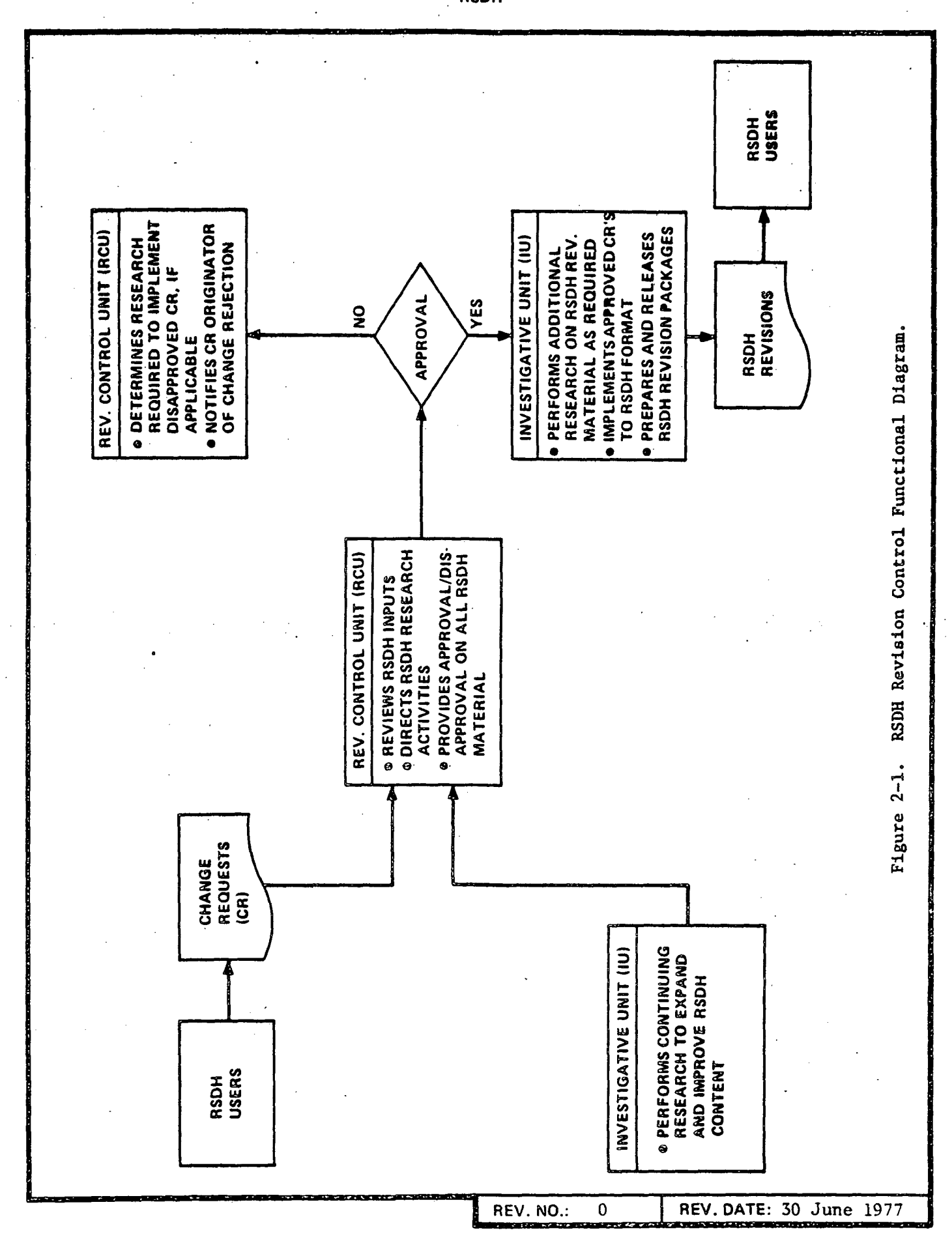
**REV. DATE:** 31 Jan 1978

2

· <u>Contents of Revision Packages</u> - Change material approved by the RCU will be issued on a periodic basis in the form of RSDH revision packages. These packages will contain the following:

- (1) Revision Instruction Sheet This sheet will provide the revision number, revision date, pages to be deleted, pages to be added and special instructions as appropriate,
- (2) New RSDH pages, as required, annotated with revision date and number,
- (3) Changed RSDH pages as required, annotated with revision date, revision number and revision section indicator,
- (4) Updated Revision Control Sheets for those sections and/or sensor categories which have been modified.

The functional diagram in Figure 2-1 illustrates revision control activities for the RSDH.



This page intentionally left blank.

REV. NO.: 0 REV. DATE: 30 June 1977

## Section 3 RSDH CROSS INDEXES

The sensor information maintained in this document is structured into ten (10) categories which are representative of the major remote sensing devices presently used or planned for use in space programs and related discipline activities. These ten categories are identified in the Table of Contents by category title, section number and page. An additional "Sensor Category Table of Contents and Revision Control Sheet" is located in front of each sensor category section to provide content information and revision control for that sensor group.

To utilize the RSDH by the "Table of Contents" structure, one may select the sensor category of interest and scan the "Sensor Category Table of Contents and Revision Control Sheet" to locate the specific sensor(s) desired. Four (4) cross indexes are provided in this section which allows entry into the RSDH in other ways. A brief description is provided for each cross index, followed by the specific cross indexed information.

Alphabetical and Sensor Category Index - This index provides a complete alphabetical listing of all sensors contained in the RSDH. This list is cross-indexed to sensor categories and page numbers which allows entry into the handbook by sensor name, title or acronym.

Program and Development Index - This index provides a list of current and planned space programs relative to the sensors contained in the RSDH. Sensor titles, sensor development schedule data and RSDH page numbers for sensor location are indexed to the sponsoring program. This index allows one to locate specific sensors in the RSDH, relative to a given program. Programs are listed in alphabetical order.

<u>Discipline and Major Function Index</u> - The Discipline and Major Function Index provides the user with a means of locating sensors which align to a particular

REV. NO.: 2 REV. DATE: 31 Jan 1978

discipline or application. The major function associated with the sensor and RSDH page information are also provided.

Spectrum and Coverage Index - Sensors are grouped by category and listed alphabetically within each group. Spectral characteristics, IFOV, FOV and page numbers are provided for each sensor.

REV. NO.:

2

#### RSDH ALPHABETICAL AND SENSOR CATEGORY INDEX

DEV NO. 3 DEV DATE: 31 July 1978					<del></del>			
Imaging Radar [AASIR]  Advanced Very High Resolution Radiometer [AVHRR]  Altimeter, Radar [ALT]  Coastal Zone Color Scanner [CZCS]  Earth Terrain Camera (S190B)  Fluxgate Magnetometer [FMAG]  Gradiometer, Rotating [GRAD]  Heat Capacity Mapping Radiometer [HGMR]  Large Earth Survey Telescope [LEST]  Laser Altimeter/Profilometer Experiment (OP-06-S)  LIDAR (APE-01)  Miltispectral and Mapping Cameras (Section 5.4)  Laser Radars (Section 5.7)  Multispectradiometers (Section 5.7)  Laser Radars (Section 5.7)  Multispectradiometers (Section 5.7)  Laser Radars (Section 5.7)  Multispectral and Mapping Cameras (Section 5.7)  Laser Radars (Section 5.7)  Laser Radars (Section 5.7)  Miltispectral and Mapping Cameras (Section 5.7)  Laser Radars (Section 5.4)  Multispectral and Mapping Cameras (Section 5.5)  Microwave Atmospheric Sounding Radiometer [MASR]  Microwave Sounding Unit [MSU]  Multispectral and Mapping Camera (Section 5.8)  Multispectral and Mapping Camera (Section 5.5)	ALPHABETICAL LISTING	3	SENSOR CATEGO	RY				
Radiometer [AVHRR]  Altimeter, Radar [ALT]  Coastal Zone Color Scanner [CZCS]  Earth Terrain Camera (S190B)  Fluxgate Magnetometer [FMAG]  Gradiometer, Rotating [GRAD]  Heat Capacity Mapping Radiometer [HCMR]  High Resolution Infrared Radiation Sounder [HIRS]  Large Earth Survey Telescope [LEST]  Laser Altimeter/Profilometer Experiment (OP-06-S)  LIDAR (APE-01)  Metric Camera (E0E-1)  Microwave Atmospheric Sounding Radiometer [MASR]  Microwave Sounding Unit [MSU]  Microwave Sounding Unit [MSU]  Optical Bar Panoramic Camera (S163)  Multispectral and Mapping Cameras (Section 5.5)  Micrownous State (Section 5.7)  Altimeters (Section 5.7)  Imaging Septororadiometers (Section 5.7)  Atmospheric Sounders (Section 5.7)  Laser Radars (Section 5.4)  Laser Radars (Section 5.4)  Multispectral and Mapping Cameras (Section 5.5)  Microwave Sounding Unit [MSU]  Atmospheric Sounders (Section 5.8)  Multispectral and Mapping Camera (Section 5.5)  SECTION NO. 3.1  Altimeters (Section 5.7)  Altimeters (Section 5.	• •	nding and						
Coastal Zone Color Scanner [CZCS]  Earth Terrain Camera (S190B)  Fluxgate Magnetometer [FMAG]  Fluxgate Magnetometer [FMAG]  Gradiometer, Rotating [GRAD]  Heat Capacity Mapping Radiometer [HCMR]  High Resolution Infrared Radiation Sounder [HIRS]  Large Earth Survey Telescope [LEST]  Laser Altimeter/Profilometer Experiment (OP-06-S)  LIDAR (APE-01)  Multispectral and Mapping Cameras (Section 5.10)  Field Measuring Sensors (Section 5.7)  Atomspheric Sounders (Section 5.7)  Atomspheric Sounders (Section 5.7)  Laser Radiars (Section 5.7)  Laser Radiars (Section 5.4)  Lidar (APE-01)  Multispectral and Mapping Cameras (Section 5.4)  Multispectral and Mapping Cameras (Section 5.5)  Microwave Atmospheric Sounding Radiometer [MASR]  Microwave Sounding Unit [MSU]  Microwave Sounding Unit [MSU]  Optical Bar Panoramic Camera (S163)  Multispectral and Mapping Camera (Section 5.5)  SECTION NO. 3.1  SECTION NO. 3.1  SECTION TITLE: RSDH Cross-Indexing	• •	ution		ters	5.8-83			
Earth Terrain Camera (S190B)  Multispectral and Mapping Cameras (Section 5.5)  Fluxgate Magnetometer [FMAG]  Field Measuring Sensors (Section 5.10)  Field Measuring Sensors (Section 5.10)  Heat Capacity Mapping Radiometer (Section 5.10)  Heat Capacity Mapping Radiometer (Section 5.10)  High Resolution Infrared Radiation Sounder (HIRS)  Large Earth Survey Telescope (LEST)  Laser Altimeter/Profilometer Experiment (OP-06-S)  LIDAR (APE-01)  Metric Camera (EOE-1)  Microwave Atmospheric Sounding Radiometer (Section 5.4)  Microwave Atmospheric Sounding Radiometer (MASR)  Microwave Sounding Unit [MSU]  Microwave Sounding Unit [MSU]  Multispectral and Mapping Camera (Section 5.8)  Multispectral Photographic (Section 5.5)  Multispectral and Mapping Camera (Section 5.8)  Multispectral and Mapping Camera (Section 5.5)	Altimeter, Radar [ALT]				5.2-19			
Fluxgate Magnetometer [FMAG]  Field Measuring Sensors (Section 5.10)  Field Measuring Sensors (Section 5.7)  Field Measuring Pensor  Field Measuring Pensor  Field Measuring Pensor  Field Measuri	Coastal Zone Color Scanne	er [CZCS]		ters	5.7-77			
Gradiometer, Rotating [GRAD]  Heat Capacity Mapping Radiometer [HCMR]  High Resolution Infrared Radiation Sounder [HIRS]  Large Earth Survey Telescope [LEST]  Laser Altimeter/Profilometer Experiment (OP-06-S)  LIDAR (APE-01)  Metric Camera (E0E-1)  Microwave Atmospheric Sounding Radiometer [MASR]  Microwave Sounding Unit [MSU]  Multispectral and Mapping Camera (Section 5.8)  Microwave Sounding Unit [MSU]  Atmospheric Sounders (Section 5.8)  Multispectral and Mapping Camera (Section 5.8)  Optical Bar Panoramic Camera (S163)  Multispectral and Mapping Camera (Section 5.5)  SECTION NO.: 3.1  SECTION TITLE: RSDH Cross-Indexing	Earth Terrain Camera (S1	90B)		ing Cameras	5.5-21			
Heat Capacity Mapping Radiometer [HCMR]  High Resolution Infrared Radiation Sounder [HIRS]  Large Earth Survey Telescope [LEST]  Laser Altimeter/Profilometer Experiment (OP-06-S)  LIDAR (APE-01)  Metric Camera (EOE-1)  Microwave Atmospheric Sounding Radiometer [MASR]  Microwave Sounding Unit [MSU]  Multispectral and Mapping Camera (Section 5.8)  Multispectral Photographic Facility (S190A)  Optical Bar Panoramic Camera (S163)  Multispectral and Mapping Cameras (Section 5.5)  Multispectral and Mapping Camera (Section 5.8)  Multispectral and Mapping Camera (Section 5.5)  SECTION NO:  3.1  SECTION TITLE:  RSDH Cross-Indexing	Fluxgate Magnetometer [Fl	MAG]		<b>s</b>	5.10-31			
High Resolution Infrared Radiation Sounder [HIRS]  Large Earth Survey Telescope [LEST]  Laser Altimeter/Profilometer Experiment (OP-06-S)  LIDAR (APE-01)  Metric Camera (EOE-1)  Microwave Atmospheric Sounding Radiometer [MASR]  Microwave Sounding Unit [MSU]  Microwave Sounding Unit [MSU]  Multispectral and Mapping Camera (Section 5.8)  Multispectral Photographic Facility (S190A)  Optical Bar Panoramic Camera (S163)  Multispectral and Mapping Cameras (Section 5.5)  Multispectral and Mapping Camera (Section 5.8)  Multispectral and Mapping Camera (Section 5.8)  Multispectral and Mapping Camera (Section 5.8)  Multispectral and Mapping Camera (Section 5.5)  Multispectral and Mapping Camera (Section 5.5)  SECTION NO.: 3.1  SECTION TITLE: RSDH Cross-Indexing	Gradiometer, Rotating [G	RAD]		S	5.10-35			
Sounder [HIRS]  Large Earth Survey Telescope [LEST]  Laser Altimeter/Profilometer Experiment (OP-06-S)  LIDAR (APE-01)  Metric Camera (E0E-1)  Microwave Atmospheric Sounding Radiometer [MASR]  Microwave Sounding Unit [MSU]  Multispectral and Mapping Cameras (Section 5.8)  Atmospheric Sounders (Section 5.8)  Multispectral Photographic Facility (S190A)  Optical Bar Panoramic Camera (S163)  Multispectral and Mapping Cameras (Section 5.5)  Multispectral and Mapping Camera (Section 5.8)  Multispectral and Mapping Camera (Section 5.5)  Multispectral and Mapping Camera (Section 5.5)  Multispectral and Mapping Camera (Section 5.5)  SECTION NO.: 3.1  SECTION TITLE: RSDH Cross-Indexing				5.7-69				
Laser Altimeter/Profilometer Experiment (OP-06-S)  Lidaser Radars (Section 5.4)  Lidaser Radars (Section 5.4)  Lidaser Radars (Section 5.4)  Laser Radars (Section 5.4)  Multispectral and Mapping Cameras (Section 5.5)  Microwave Atmospheric Sounding Radiometer [MASR]  Microwave Sounding Unit [MSU]  Microwave Sounding Unit [MSU]  Atmospheric Sounders (Section 5.8)  Multispectral Photographic Facility (S190A)  Optical Bar Panoramic Camera (S163)  Multispectral and Mapping Camera (Section 5.5)  Multispectral and Mapping Camera (Section 5.5)  Multispectral and Mapping Camera (Section 5.5)  SECTION NO: 3.1  SECTION TITLE: RSDH Cross-Indexing				5.8-75				
Experiment (OP-06-S)  LIDAR (APE-01)  Laser Radars (Section 5.4)  Metric Camera (E0E-1)  Multispectral and Mapping Cameras (Section 5.5)  Microwave Atmospheric Sounding Radiometer [MASR]  Microwave Sounding Unit [MSU]  Atmospheric Sounders (Section 5.8)  Multispectral Photographic (Section 5.8)  Multispectral Photographic (Section 5.8)  Multispectral and Mapping Camera (Section 5.5)  Optical Bar Panoramic Camera (S163)  Multispectral and Mapping Camera (Section 5.5)  SECTION NO.: 3.1  SECTION TITLE: RSDH Cross-Indexing				5.7-87				
Metric Camera (EOE-1)  Multispectral and Mapping Cameras (Section 5.5)  Microwave Atmospheric Sounding Radiometer [MASR]  Microwave Sounding Unit [MSU]  Atmospheric Sounders (Section 5.8)  Microwave Sounding Unit [MSU]  Atmospheric Sounders (Section 5.8)  Multispectral Photographic (Section 5.8)  Multispectral and Mapping Camera (Section 5.5)  Optical Bar Panoramic Camera (S163)  Multispectral and Mapping Cameras (Section 5.5)  SECTION NO.: 3.1  SECTION TITLE: RSDH Cross-Indexing		eter		5.4-21				
Microwave Atmospheric Sounding Radiometer [MASR]  Microwave Sounding Unit [MSU]  Microwave Sounding Unit [MSU]  Multispectral Photographic Facility (S190A)  Optical Bar Panoramic Camera (S163)  Multispectral and Mapping Camera (Section 5.5)  Multispectral and Mapping Camera (Section 5.5)  Multispectral and Mapping Camera (Section 5.5)  SECTION NO.: 3.1  SECTION TITLE: RSDH Cross-Indexing	LIDAR (APE-01)				5.4-15			
Microwave Sounding Unit [MSU]  Microwave Sounding Unit [MSU]  Multispectral Photographic (Section 5.8)  Multispectral and Mapping Camera (Section 5.5)  Optical Bar Panoramic Camera (S163)  Multispectral and Mapping Cameras (Section 5.5)  SECTION NO.: 3.1  SECTION TITLE: RSDH Cross-Indexing	Metric Camera (E0E-1)			ing Cameras	5.5-15			
Multispectral Photographic Facility (S190A)  Optical Bar Panoramic Camera (S163)  SECTION NO.: 3.1  SECTION TITLE: RSDH Cross-Indexing  (Section 5.8)  Multispectral and Mapping Camera (S.5-27 (Section 5.5)  SECTION NO.: 3.1  SECTION TITLE: RSDH Cross-Indexing				5.8-69				
Facility (S190A)  Optical Bar Panoramic Camera (S163) Multispectral and Mapping Cameras (Section 5.5)  SECTION NO.: 3.1 SECTION TITLE: RSDH Cross-Indexing	Microwave Sounding Unit [MSU]			5.8-79				
(Section 5.5)  SECTION NO.: 3.1 SECTION TITLE: RSDH Cross-Indexing				5.5-27				
DEV NO. 3 DEV DATE: 31 July 1978	Optical Bar Panoramic Car	mera (S163)	obj mestered and military					
DEV NO. 3 DEV DATE: 31 July 1978	SECTION NO.: 3 1 SE	3 1 SECTION TITLE: RSDH Cross-Indexing						
		૩.૩		REV. DATE: 3	l July 1978			

### ALPHABETICAL AND SENSOR CATEGORY INDEX

			and the second s		
ALPHABETICAL LISTII	NG		SENSOR CATEGO	PRY	PAGE NUMBER
Scanning Multichannel M Radiometer [SMMR]	icrowave	Atmos (Sect	pheric Sounders ion 5.8)		5.8-89
Scatterometer, Microwav	e [SCAT]		erometers ion 5.3)	ŗ.	5.3-17
Shuttle Imaging Radar [	SIR-B]		etic Aperture Rad	lar	5.1-45
Spaceborne Laser Rangin (OP-16-S)	g System		Radars ion 5.4)		5.4-21
Stratospheric and Mesos Sounder [SAMS]	pheric		pheric Sounders		5.8-57
Stratospheric Sounding	Unit [SSU]		pheric Sounders ion 5.8)		5.8-85
Synthetic Aperture Rada	r [SAR]	Synth	etic Aperture Rad	lar	5.1-41
Temperature/Humidity In Radiometer [THIR]	frared		pheric Sounders ion 5.8)		5.8-33
Thematic Mapper [TM]			ng Spectroradiome	eters	5.7-45
Vertical Temperature Pr Radiometer [VTPR]	ofile		pheric Sounders ion 5.8)		5.8-51
Very High Resolution Ra [VHRR]	diometer		ng Spectroradiome	eters	5.7-63
Visible Infrared Spin-S meter Atmospheric Sound			spheric Sounders sion 5.8)		5.8-63
Visible Infrared Spin-S Radiometer [VISSR]	can		ng Spectroradiome	eters	5.7-49
	·				
			•		
					,
3.4	•				
SECTION NO.: 3.1	SECTION TITLE:	RSDI	l Cross-Indexing		
			REV. NO.: 3	REV. DATE:	31 July 1978

#### RSDH PROGRAM AND DEVELOPMENT INDEX

222244	DEVELOPMENT SCHEDULE								SCHEDULE			PAGE		
PROGRAM	SENSOR	76	77	78	79	80	81	82	8	3 8	34	85	POST 1985	NUMBER
AEM/HCMM	Heat Capacity Mapping Radiometer [HCMR] (Section 5.7)			<b>-</b>										5.7+69
GOES/NOAA	Visible-Infrared Spin-Scan Radio- meter [VISSR] (Section 5.7)	Oi	PEF	ΓA	10	NA:	L							5.7-49
GOES/NOAA	Visible-Infrared Spin-Scan Radio- meter Atmospheric Sounder [VAS] (Section 5.8)					*								5.8-63
Gravity Gradiometer Satellite (Shuttle OP-Ø2-A)	Gravity Gradiometer, Rotating [GRAD] (Section 5.10)					<b> </b>								5.10-35
ITOS/NOAA	Vertical Temperature Profile Radiometer [VTPR] (Section 5.8)	0	PEF	A1	10	NA.								5.8-51
ITOS/NOAA	Very High Resolution Radiometer [VHRR] (Section 5.7)	. 0	EF	A7	10	NA				£.		j.;	6 Tes	5.7±63
LANDSAT-D	Thematic Mapper [TM] (Section 5.7)					*				-				5.7-45
NIMBUS	Coastal Zone Color Scanner [CZCS] (Section 5.7)		<u> </u>	<b> </b> *										5.7-77
NIMBUS	Stratospheric and Mesospheric Sounder [SAMS] (Section 5.8)			<b> </b> -			ŀ							5.8-57
NIMBUS	Temperature/Humidity Infrared Radiometer [THIR] (Section 5.8)	0	PEI	RA7	10	NA					-			5.8-33
SEASAT-A	Altimeter, Radar [ALT] (Section 5.2)		·	]*										5.2-19
SEASAT-A	Scanning Multichannel Microwave Radiometer [SMMR] (Section 5.8)			<u> </u>										5.8-89
SEASAT-A	Scatterometer, Microwave [SCAT] (Section 5.3)			1										5.3-17
SECTION NO.: 3.	SECTION TITLE: RSDH Cross-1	nde	xi	ng										

### RSDH PROGRAM AND DEVELOPMENT INDEX

SEASAT-A  Synthetic Aperture Radar [SAR] (Section 5.1)  SEOS  Large Earth Survey Telescope [LEST] (Section 5.7)  Shuttle Mission #4  Shuttle Sortie)  Shuttle Sortie)  Shuttle Sortie)  Shuttle Sortie)  Shuttle Sortie  Shuttle Sortie Shuttle Sortie Shuttle Sortie Shuttle Sortie Shuttle Shutt			DEVELOPMENT SCHEDULE PAGE
SEOS  Large Earth Survey Telescope [LEST] (Section 5.7)  Shuttle Mission #4  Multispectral Photographic Facility (Section 5.5)  Shuttle Mission #4  Optical Bar Panoramic Camera (Section 5.5)  Shuttle Mission #4  Shuttle Imaging Radar [SIR-B] (Shuttle Section 5.1)  Sortie)  SMS-2  Visible-Infrared Spin-Scan Radiometer [VISSR] (Section 5.7)  Spacelab  Metric Camera (Section 5.5)  Spacelab  Laser Altimeter/Profilometer Experiment (Section 5.4)  Spacelab  LIDAR (Section 5.4)  Spacelab  Spaceborne Laser Ranging (Section 5.4)  Spaceborne Laser Ranging (Section 5.8)  STORMSAT  Microwave Atmospheric Sounding and Imaging Radiometer [AASIR] (Section 5.8)  TIROS-N  Advanced Very High Resolution Radiometer [AVIRR] (Section 5.7)	PROGRAM	SENSOR	76 77 78 79 80 81 82 83 84 85 POST NUMBE
Shuttle Mission #4 (Section 5.5)  Shuttle Multispectral Photographic Facility (Section 5.5)  Shuttle Mission #4 (Section 5.5)  Shuttle Imaging Radar [SIR-B] (Section 5.1)  SIR-B (Shuttle Imaging Radar [SIR-B] (Section 5.1)  SMS-2 Visible-Infrared Spin-Scan Radiometer [VISSR] (Section 5.7)  Spacelab Metric Camera (Section 5.5)  Spacelab Laser Altimeter/Profilometer Experiment (Section 5.4)  Spacelab LIDAR (Section 5.4)  Spacelab Spaceborne Laser Ranging (Section 5.4)  Spacelab Spaceborne Laser Ranging (Section 5.4)  STORMSAT Advanced Atmospheric Sounding and Imaging Radiometer [AASIR] (Section 5.8)  STORMSAT Microwave Atmospheric Sounding Radiometer [MASR] (Section 5.8)  TIROS-N Advanced Very High Resolution Radiometer [AVHRR] (Section 5.7)	SEASAT-A		AR] 5.1-4
Mission #4 (Section 5.5)  Shuttle Mission #4 (Section 5.5)  Shuttle Optical Bar Panoramic Camera (Section 5.5)  Shuttle (Section 5.5)  SIR-B (Shuttle Imaging Radar [SIR-B] (Section 5.1)  Sortie)  SMS-2 Visible-Infrared Spin-Scan Radiometer (VISSR) (Section 5.7)  Spacelab Metric Camera (Section 5.5)  Spacelab Laser Altimeter/Profilometer Experiment (Section 5.4)  Spacelab LIDAR (Section 5.4)  Spacelab Spaceborne Laser Ranging (Section 5.4)  Stormsat Advanced Atmospheric Sounding and Imaging Radiometer [AASIR] (Section 5.8)  STORMSAT Microwave Atmospheric Sounding Radiometer [MASR] (Section 5.8)  TIROS-N Advanced Very High Resolution Radiometer [AVHRR] (Section 5.7)	SEOS		E [LEST] * 5.7-8
Mission #4  Facility (Section 5.5)  Shuttle (Section 5.5)  SIR-B (Shuttle (Section 5.1)  SMS-2 Visible-Infrared Spin-Scan Radiometer [VISSR] (Section 5.7)  Spacelab Metric Camera (Section 5.5)  Spacelab Laser Altimeter/Profilometer Experiment (Section 5.4)  Spacelab LIDAR (Section 5.4)  Spacelab Spaceborne Laser Ranging (Section 5.4)  STORMSAT Advanced Atmospheric Sounding and Imaging Radiometer [AASIR] (Section 5.8)  STORMSAT Microwave Atmospheric Sounding Radiometer [MASR] (Section 5.8)  TIROS-N Advanced Very High Resolution Radiometer [AVHRR] (Section 5.7)			5.5-2
Mission #4  (Section 5.5)  SIR-B (Shuttle   Shuttle   Imaging Radar   SIR-B   (Section 5.1)  SMS-2   Visible-Infrared Spin-Scan   Radiometer   VISSR   (Section 5.7)  Spacelab   Metric Camera   Section 5.5)  Spacelab   Laser Altimeter/Profilometer   Experiment   Section 5.4)  Spacelab   LIDAR   Spacelab   Spaceborne   Laser Ranging   Section 5.4)  Spacelab   Spaceborne   Laser Ranging   Section 5.4)  STORMSAT   Advanced Atmospheric Sounding   Advanced Atmospheric Sounding   Radiometer   MASR   Section 5.8  STORMSAT   Microwave Atmospheric Sounding   Radiometer   MASR   Section 5.8)  TIROS-N   Advanced Very High Resolution   Radiometer   AVHRR   Section 5.7)		Facility	5.5-2
(Shuttle Sortie)  SMS-2 Visible-Infrared Spin-Scan Radiometer [VISSR] (Section 5.7)  Spacelab Metric Camera (Section 5.5)  Spacelab Laser Altimeter/Profilometer Experiment (Section 5.4)  Spacelab LIDAR (Section 5.4)  Spacelab Spaceborne Laser Ranging (Section 5.4)  STORMSAT Advanced Atmospheric Sounding and Imaging Radiometer [AASIR] (Section 5.8)  STORMSAT Microwave Atmospheric Sounding Radiometer [MASR] (Section 5.8)  TIROS-N Advanced Very High Resolution Radiometer [AVHRR] (Section 5.7)	· · · · · · · · · · · · · · · · · · ·		5.5-3
SMS-2 Visible-Infrared Spin-Scan Radiometer [VISSR] (Section 5.7)  Spacelab Metric Camera (Section 5.5)  Spacelab Laser Altimeter/Profilometer Experiment (Section 5.4)  Spacelab LIDAR (Section 5.4)  Spacelab Spaceborne Laser Ranging (Section 5.4)  STORMSAT Advanced Atmospheric Sounding and Imaging Radiometer [AASIR] (Section 5.8)  STORMSAT Microwave Atmospheric Sounding Radiometer [MASR] (Section 5.8)  TIROS-N Advanced Very High Resolution Radiometer [AVHRR] (Section 5.7)	(Shuttle		5.1-4
Spacelab Laser Altimeter/Profilometer Experiment (Section 5.4)  Spacelab LIDAR (Section 5.4)  Spacelab Spaceborne Laser Ranging (Section 5.4)  STORMSAT Advanced Atmospheric Sounding and Imaging Radiometer [AASIR] (Section 5.8)  STORMSAT Microwave Atmospheric Sounding Radiometer [MASR] (Section 5.8)  TIROS-N Advanced Very High Resolution Radiometer [AVHRR] (Section 5.7)	Marie Control of the	Radiometer [VISSR]	OPERATIONAL 5.7-4
Experiment (Section 5.4)  Spacelab  LIDAR (Section 5.4)  Spacelab  Spaceborne Laser Ranging (Section 5.4)  STORMSAT  Advanced Atmospheric Sounding and Imaging Radiometer [AASIR] (Section 5.8  STORMSAT  Microwave Atmospheric Sounding Radiometer [MASR] (Section 5.8)  TIROS-N  Advanced Very High Resolution Radiometer [AVHRR] (Section 5.7)	Späcelab .		5.5-1
Spacelab (Section 5.4)  Spacelab Spaceborne Laser Ranging (Section 5.4)  STORMSAT Advanced Atmospheric Sounding and Imaging Radiometer [AASIR] (Section 5.8  STORMSAT Microwave Atmospheric Sounding Radiometer [MASR] (Section 5.8)  TIROS-N Advanced Very High Resolution Radiometer [AVHRR] (Section 5.7)	Spacelab	Experiment	r 5.4-2
STORMSAT  Advanced Atmospheric Sounding and Imaging Radiometer [AASIR] (Section 5.8  STORMSAT  Microwave Atmospheric Sounding Radiometer [MASR] (Section 5.8)  TIROS-N  Advanced Very High Resolution Radiometer [AVHRR] (Section 5.7)	Spacelab	·	5.4-1
Imaging Radiometer [AASIR] (Section 5.8  STORMSAT Microwave Atmospheric Sounding Radiometer [MASR] (Section 5.8)  TIROS-N Advanced Very High Resolution Radiometer [AVHRR] (Section 5.7)	Spacelab		*
Radiometer [MASR] (Section 5.8)  Advanced Very High Resolution Radiometer [AVHRR] (Section 5.7)	STORMSAT	Imaging Radiometer [AASIR]	ng and 5.8-3
Radiometer [AVHRR] (Section 5.7)	STORMSAT	Radiometer [MASR]	ing 5.8-6
	TIROS-N	Radiometer [AVHRR]	on 5.7-8
SECTION NO.: 3.2 SECTION TITLE: RSDH Cross-Indexing  REV. NO.: 3 REV. DATE: 31 July 1978	SECTION NO.: 3.	and the second s	and the contract of the contra

### RSDH PROGRAM AND DEVELOPMENT INDEX

					C			DUI		VT			PAGE
PROGRAM	SENSOR	76	77	78	79	80	81	82	83	84	85	POST 1985	NUMBER
TIROS-N	High Resolution Infrared Radiation Sounder [HIRS] (Section 5.8)			*									5.8-75
TIROS-N	Microwave Sounding Unit [MSU] (Section 5.8)			*							ļ.		5.8-79
TIROS-N	Stratospheric Sounding Unit [SSU] (Section 5.8)			*									5.8-85
Vector Satellite System (Shuttle OP-Ø5-A)	Fluxgate Magnetometer [FMAG] (Section 5.10)					<b>D</b> *							5.10-3
						•							
SECTION NO.: 3.2	SECTION TITLE: RSDH Cross-In  3.7 REV. NO.			g		T_	EV.					July	

DISCIPLINE(S)	SENSOR AND MAJOR FUNCTION(S)	PAGE NUMBER
EARTH AND OCEAN PHYSICS		•
Global Surveying & Mapping	Fluxgate Magnetometer [FMAG] (Section 5.10) Global Magnetic Field Mapping	5.10-31
Land Monitoring	Thematic Mapper [TM] (Section 5.7) Earth Resource Imagery (Reflective & Emissive)	5.7-45
Ocean Dynamics	Altimeter, Radar [ALT] (Section 5.2) Altimetry, Sea State	5.2-19
Ocean Dynamicș	Laser Altimeter/Profilometer Experiment (Section 5.4) Altimetry, Sea State Ocean and Coastal Bottom Topography, Sub-	5.4-21
	surface Ocean Temperature Pro- filing, Fish School Detection and Track, Marine Plankton Productivity, Oil and Hazardous Material Detection, Ocean Cur- rents Mapping	
Ocean Dynamics	Scanning Multichannel Microwave Radiometer [SMMR] (Section 5.8) Ocean Surface Wind Speed and Temperature Data, Polar Ice Canopy Characteristics and Ocean Mapping	5.8-89
Ocean Dynamics	Scatterometer, Microwave [SCAT] (Section 5.3) Wind Vector Measurements	5.3-17
Ocean Dynamics	Synthetic Aperture Radar [SAR] (Section 5.1) Sea Ice, Coastal Features, Ocean Wavelength & Direction	5.1-41
Solid Earth Dynamics	Gradiometer, Rotating Gravity [GRAD] (Section 5.10) Global Gravity Mapping	5.10-35
SECTION NO.: 3.3 SECTION TITLE:	RSDH Cross-Indexing	
8.8		July 1978

Solid Earth Dynamics  Spaceborne Laser Ranging System (Section 5.4) Earthquake Events  Advanced Atmospheric Sounding and Imaging Radiometer [ASSIR] (Section 5.8) Visible and Infrared Imagery and Temperature and Humidity Soundings  Atmospheric Monitoring  Advanced Very High Resolution Radiometer [AVHRR] (Section 5.7) Sea Surface Temperature Ice, Snow and Cloud Information  High Resolution Infrared Radiation Sounder [HIRS] (Section 5.7) Soundings  Atmospheric Monitoring  LIDAR (Section 5.4) Atmospheric Winds, Temperature Profiles, Constituent Abundances, Cloud Top Altitudes, Cirrus Cloud Reflectivities and Thickness  Atmospheric Monitoring  Microwave Atmospheric Sounding Radiometer [MASR] (Section 5.8) Temperature and Humidity Profiles  Atmospheric Monitoring  Microwave Atmospheric Sounding Radiometer [MASR] (Section 5.8) Temperature and Humidity Profiles  Atmospheric Temperature Profile Sounding Unit [MSU] (Section 5.8) Atmospheric Temperature Profile Soundings from Surface to 40 Km	DISCIPLINE(S)	SENSOR AND MAJOR FUNCTION(S)	PAGE NUMBER
Atmospheric Monitoring  Advanced Atmospheric Sounding and Imaging Radiometer [AASIR] (Section 5.8)  Visible and Infrared Imagery and Temperature and Humidity Soundings  Atmospheric Monitoring  Advanced Very High Resolution Radiometer [AVHRR] (Section 5.7) Sea Surface Temperature Ice, Snow and Cloud Information  Atmospheric Monitoring  High Resolution Infrared Radiation Sounder [HIRS] (Section 5.8) Temperature and Humidity Soundings  Atmospheric Monitoring  LIDAR (Section 5.4) Atmospheric Winds, Temperature Profiles, Constituent Abundances, Cloud Top Attitudes, Cirrus Cloud Reflectivities and Thickness  Atmospheric Monitoring  Microwave Atmospheric Sounding Radiometer [MASR] (Section 5.8) Temperature and Humidity Profiles  Atmospheric Monitoring  Microwave Sounding Unit [MSU] (Section 5.8) Atmospheric Temperature Profile Soundings from	Solid Earth Dynamics	(Section 5.4)	5.4-21
Imaging Radiometer [AASIR] (Section S.8) Visible and Infrared Imagery and Temperature and Humidity Soundings  Advanced Very High Resolution Radiometer [AVHRR] (Section S.7) Sea Surface Temperature Ice, Snow and Cloud Information  High Resolution Infrared Radiation Sounder [HRR] (Section S.8) Temperature and Humidity Soundings  Atmoshperic Monitoring  LIDAR (Section S.4) Atmospheric Winds, Temperature Profiles, Constituent Abundances, Cloud Top Altitudes, Cirrus Cloud Reflectivities and Thickness  Atmospheric Monitoring  Microwave Atmospheric Sounding Radiometer [MASR] (Section S.8) Temperature and Humidity Profiles  Atmospheric Monitoring  Microwave Sounding Unit [MSU] (Section S.8) Atmospheric Temperature Profile Soundings from	EARTH OBSERVATIONS		
Radiometer [AVHRR] (Section 5.7) Sea Surface Temperature Ice, Snow and Cloud Information  High Resolution Infrared Radiation Sounder [HIRS] (Section 5.8) Temperature and Humidity Soundings  Atmoshperic Monitoring  LIDAR (Section 5.4) Atmospheric Winds, Temperature Profiles, Constituent Abundances, Cloud Top Altitudes, Cirrus Cloud Reflectivities and Thickness  Atmospheric Monitoring  Microwave Atmospheric Sounding Radiometer [MASR] (Section 5.8) Temperature and Humidity Profiles  Atmospheric Monitoring  Microwave Sounding Unit [MSU] (Section 5.8) Atmospheric Temperature Profile Soundings from	Atmospheric Monitoring	Imaging Radiometer [AASIR] (Section 5.8) Visible and Infrared Imagery and Temperature and Humidity	5.8-39
Sounder [HIRS] (Section 5.8) Temperature and Humidity Soundings  Atmoshperic Monitoring  LIDAR (Section 5.4) Atmospheric Winds, Temperature Profiles, Constituent Abundances, Cloud Top Altitudes, Cirrus Cloud Reflectivities and Thickness  Atmospheric Monitoring  Microwave Atmospheric Sounding Radiometer [MASR] (Section 5.8) Temperature and Humidity Profiles  Atmospheric Monitoring  Microwave Sounding Unit [MSU] (Section 5.8) Atmospheric Temperature Profile Soundings from	Atmospheric Monitoring	Radiometer [AVHRR] (Section 5.7) Sea Surface Temperature	5.7-83
(Section 5.4) Atmospheric Winds, Temperature Profiles, Constituent Abundances, Cloud Top Altitudes, Cirrus Cloud Reflectivities and Thickness  Atmospheric Monitoring  Microwave Atmospheric Sounding Radiometer [MASR] (Section 5.8) Temperature and Humidity Profiles  Atmospheric Monitoring  Microwave Sounding Unit [MSU] (Section 5.8) Atmospheric Temperature Profile Soundings from	Atmospheric Monitoring	Sounder [HIRS] (Section 5.8) Temperature and Humidity	5.8-75
Radiometer [MASR] (Section 5.8) Temperature and Humidity Profiles  Atmospheric Monitoring  Microwave Sounding Unit [MSU] (Section 5.8) Atmospheric Temperature Profile Soundings from	Atmoshperic Monitoring	(Section 5.4) Atmospheric Winds, Temperature Profiles, Constituent Abundances, Cloud Top Altitudes, Cirrus Cloud Reflectivities and	5.4-15
(Section 5.8) Atmospheric Temperature Profile Soundings from	Atmospheric Monitoring	Radiometer [MASR] (Section 5.8) Temperature and Humidity	5.8-69
	Atmospheric Monitoring	(Section 5.8) Atmospheric Temperature Profile Soundings from	5.8-79
3.9			<b>3</b> .9

REV. NO.: 3

REV. DATE: 31 July 1978

DISCIPLINE(S)	SENSOR AND MAJOR FUNCTION(S)	PAGE NUMBER
EARTH OBSERVATIONS (continued)	·	
Atmospheric Monitoring	Stratospheric and Mesospheric Sounder [SAMS] (Section 5.8)	5.8-57
	Temperature Profile and Element Concentration Soundings from 10 Km to 120 Km	
Atmospheric Monitoring	Stratospheric Sounding Unit [SSU] (Section 5.8) Temperature Soundings from	5.8-85
	25 Km to 50 Km	
Atmospheric Monitoring	Temperature/Humidity Infrared Radiometer [THIR]	5.8-33
	(Section 5.8) Temperature Humidity Soundings and Cloud Cover Imagery	
Atmospheric Monitoring	Vertical Temperature Profile Radiometer [VTPR]	5.8-51
	(Section 5.8) Temperature and Water Vapor Soundings up to 30 Km	
Atmospheric Monitoring	Very High Resolution Radiometer [VHRR] (Section 5.7)	5.7-63
	Cloud Imaging (Day and Night)	
Atmospheric Monitoring	Visible Infrared Spin-Scan Radiometer [VISSR] (Section 5.7) Visible and Infrared Imaging	5.7-49
Atmospheric Monitoring	Visible Infrared Spin-Scan Radio- meter Atmospheric Sounder [VAS] (Section 5.8) Sea Surface and Cloud Top Temperatures (Soundings and Imaging)	5.8-63
Land Monitoring	Earth Terrain Camera (Section 5.5) High Resolution Imagery	5.5-21
3.10		
SECTION NO.: 3.3 SECTION TITLE	RSDH Cross-Indexing	
	REV. NO.: 3 REV. DATE: 31	July 1978

DISCIPLINE(S)	SENSOR AND MAJOR FUNCTION(S)	PAGE NUMBER
EARTH OBSERVATIONS (continued)		,
Land Monitoring	Heat Capacity Mapping Radiometer [HCMR] (Section 5.7) Thermal Mapping Data High Spatial Resolution	5.7-69
Land Monitoring	Metric Camera (Section 5.5) High Resolution Imagery	5.5-15
Land Monitoring	Multispectral Photographic Facility (Section 5.5) High Resolution Multispectral Imagery	5.5-27
Land Monitoring	Optical Bar Panoramic Camera (Section 5.5) High Resolution Imagery	5.5-33
Land Monitoring	Shuttle Imaging Radar [SIR-B] (Section 5.1) Microwave Image Data	5.1-45 .
Land/Atmospheric Monitoring	Large Earth Survey Telescope [LEST] (Section 5.7) Visible and Infrared Imagery and Atmospheric Temperature Soundings	5.7-87
Ocean Monitoring	Coastal Zone Color Scanner [CZCS] (Section 5.7) Visible and Infrared Imagery of Coastal Waters and Open Ocean Parameters	5.7-77
	·	
• •		•
·	3-11	
SECTION NO.: 3.3 SECTION TITLE:	RSDH Cross-Indexing	

<u> </u>	SENSOR	 SPECT	RAL C	HARAC 10	TERIS	TICS M	100 100	SPECTRAL CHARACTERISTICS MILLIMETERS(mm) 10 10	mm)	(mr.)	F 2	FOV (deg.)	PAGE NUMBER
	Shuttle Imaging Radar [SIR-B] (Section 5.1)									925	· · · · · · · · · · · · · · · · · · ·	53	5.1-45
	Synthetic Aperture Radar [SAR] (Section 5.1)							/		.03	-	<b>Z</b>	5.1-41
	Radar Altimeter [ALT] (Section 5.2)		-#.:							.026	1.5	رى د	5.2-19
_	Microwave Scatterometer [SCAT] (Section 5.3)									8.7		30	5.3-17
	Microwave Atmospheric Sounding Radiometer [MASR] (Section 5.8)	•••								.7 (nadir		36	5.8-69
	Microwave Sounding Unit [MSU] (Section 5.8)		Giras ·							.13	94	<u> </u>	5.8-79
	Scanning Multichannel Microwave Radiometer [SMMR] (SEction 5.8)					4340				12-67.	v	20	5.8-89
		 									· ·		
		 						· · · · · · · · · · · · · · · · · · ·					

RSDH SPECTRUM AND COVERAGE INDEX

_		territoria (n. 1. de la company) e propiedad de la companya de la companya de la companya de la companya de la	,				14 301 E	ANOME	(ma) SO JERNOMETERS (ma)	1 40	7021	202	2000	-
	SEC	SENSOR	., 8	SPECTMAL	L CHARAL	AC 1 E N 1	3	10000			(mr.)	(deg.)	NUMBER	-
	TIOI													
<del></del>	N NO	Laser Altimeter/Profilometer				· · · · ·					A/X	10_3	5.4-21	-
	.: 3	Experiment (Section 5.4)					<del> </del>					·		
-	. 4	Spaceborne Laser Ranging System (Section 5.4)									N/A	10-3	5.4-21	سبأت بالثاث
	T	TAD									Α/ N	10.3	5.4-15	-
	SECT	(Section 5.4)	•									10.	•	<del></del>
	ION													
	TITL	Metric Lamera (Section 5.5)	• ,								99.	<del>-</del>	•	
	E:	Bouth Townsin Comers									.025	15x15	5.5-21	
	RSI				E						to		)	
	H C:										Depends	···		-
	ros										on spectral			-
	s-Inc										band)	· · · · · · · · · · · · · · · · · · ·		
3	dexing	Multispectral Photographic Facility (Section 5.5)			- (a)						.050	21.2x21.2	5.5-27	
	3	Optical Bar Panoramic Camera									.015	10.7 × 108	5.5-33	<del></del>
RE		1 5.5)										·		-
EV. C									-, -, -, -, -, -, -, -, -, -, -, -, -, -			·		
ATE:	• • • • • • • • • • • • • • • • • • • •					• :							· .	-
31														
Jul												· · · · · · · · · · · · · · · · · · ·	· · · · · · ·	
y 19					74. 4.								•	
78												, ·		
-					1111									: 1

S	GCNED	SPECTRAL CH		Fov	PAGE
EC		100 10000	(mr.)	(deg.)	NUMBER
TION NO					
3.4	Advanced Very High Resolution Radiometer [AVHRR] (Section 5.7)			360	5.7-83
SE	Coastal Zone Color Scanner [CZCS] (Section 5.7)		.865	08	5.7-77
CTION TIT	Heat Capacity Mapping Radiometer [HCMR] (Section 5.7)		∞.	Horizon	5.7-69
LE: RSDH	<pre>Large Earth Survey Telescope [LEST] (Section 5.7)</pre>		.03 to 0.33	9.0	5.7-87
Cross-Indexi	Thematic Mapper [TM] (Section 5.7)		.04 (visible) .16 (infra- red)	e) 15	5.7-45
ng	Very High Resolution Radiometer · [VHRR] (Section 5.7)		.00018 to .00028	360	5.7-63
REV. DATE:	Visible Infrared Spin-Scan Radio- meter [VISSR] (Section 5.7)		.021 x .025 (visible)	36	5.7-49
31 July			(infra-	· · ·	es and a second
1978					

ZDEX	
=	
ΡĀG	
COVERAGE	
S	
Q N N	
<u>S</u>	
PECTRU	-
SPE	
RSDH	
Œ	

Advanced Atmospheric Sounding and finaging Resolution Infrared Radiation Sounder [HIRS]  Stratospheric Sounding Unit [SSU]  Stratospheric Sounding Unit [SSU]  Stratospheric Sounding Unit [SSU]  Stratospheric Sounding Unit [SSU]  SpecTRAL CHARACTERISTICS NANOMETERS (nm)
Atmospheric Sounding and tadiometer [AASIR] 5.8) Sounder [HIRS] 5.8) eric and Mesospheric SAMS] 5.8) eric Sounding Unit [SSU] 5.8)
SENSOR  Atmospheric Sounding and tadiometer [AASIR] 5.8)  lution Infrared Sounder [HIRS] 5.8)  heric and Mesospheric SAMS] 5.8)  heric Sounding Unit [SSU] 5.8)
Atmospheric Sounding and tadiometer [AASIR] 5.8) Sounder [HIRS] 5.8) Fric and Mesospheric (SAMS) 5.8) Fric SAMS] 5.8) Fric Sounding Unit [SSU] 5.8)
SENSOR Atmospheric Sounding tadiometer [AASIR] 5.8) Sounder [HIRS] 5.8) eric and Mesospheric SAMS] 5.8) heric Sounding Unit [Seric Sounding Unit [Seric Same]
<u> </u>

This page intentionally left blank.

**REV. NO.:** 3

REV. DATE: 31 July 1978

## Section 4 DEFINITIONS AND ACRONYMS

Definitions and acronyms presented in this section are basic to the RSDH in its entirety and are provided to establish a common framework between a varying category of users and the information contained in this handbook.

Definitions which pertain to only one sensor category will be covered in the Introduction Section for that particular sensor group.

#### 4.1 Definition of Terms

- Detector That element in a sensor which is illuminated by the output of the radiation gathering means and which has an (electrical) output that is relatable to the intensity of the input radiation over a frequency range which characterizes the radiation.
- Sensor A combination of facilities including an antenna, lens, focusing mirror or other radiation gathering means, and a detector with auxiliary devices which can be used to collect radiation of a desired nature, produce an output proportional to that radiation and organize the output into a recognizable format.
- Instrument A class of apparatus including sensors which, in the broadest sense can be said to be intended to be responsive to physical phenomena in some consistent way as opposed to a tool which can be said to be intended to bring about an alteration of physical properties.
- Experiment An experiment is an organized thrust into an unexplored sphere of knowledge or the utilization of unproven methods with the purpose in mind to illustrate the plausibility of a concept. In the area of interest here, an experiment may involve one or more sensors and other instruments and one or more satellites.
- Payload A space vehicle system payload, in the context of this handbook, consists of the sensors plus the supportive space-borne hardware required to maintain them in the desired orbit and convey their information back to earth (including life support system where applicable).

Geoid - An imaginary surface that coincides with the mean sea level in the ocean and its extension through the continents. (The geometric figure formed by this surface is an ellipsoid flattened at the poles.)

Backscatter Coefficient - The backscattered power per unit area normalized for antenna gain, range loss, and transmitted power.

#### 4.2 Acronyms

A/D - Analog to Digital

AAFE - Advanced Application Flight Experiments

AASIR - Advanced Atmospheric Sounding and Imaging Radar

ADC - Analog-to-Digital Converter

ADP - Automatic Data Processing

AEM - Applications Explorer Missions

AFOS - Automation of Field Operations and Services

ALT - Altimeter

APE - Atmospheric Physics Experiment

ARS - Agriculture Research Service

ASCU - Archive Station Communication Units

ATS - Advanced Technology Satellite

AUS - Agriculture Utilization Subsystem

AVHRR - Advanced Very High Resolution Radiometer

BIL - Band-Interleaved-by-Line

BLIP - Background-Limited Infrared Photoconductor

CCD - Charge-Coupled-Device

CCT - Computer Compatible Tape

CDAS - Command Data Acquisition Station

CDDF - Central Data Distribution Facility

CDPF - Central Data Processing Facility

CIT - California Institute of Technology

CMG - Control Moment Gyro

CNRS - Centre National de Recherches Spatiales

CONUS - Continental United States

CPU - Central Processor Unit

CR - Change Request

CW - Continuous Wave

CZCS - Coastal Zone Color Scanner

D\* - Detectivity

DACS - Data Acquisition and Control Subsystem

DAPS - Data Processing Subsystem

dBm - Ration referenced to a particular impedance

DDHS - Digital Data Handling System

DEC - Digital Equipment Corporation

DIP - Digital Information Processor

DIS - Data Input Subsystem

DMD - Digital Muirhead Display

DOD - Department of Defense

DSL - Data Systems Laboratory

EFL - Equivalent Focal Length

EOE - Earth Observation Experiment

EOS - Earth Observation Satellite

ESA - European Space Agency

ETA - Earth Terrain Camera

EU - Etövös Units (1 EU =  $10^{-9}$  gal/cm; 1 gal - 1 cm/sec<sup>2</sup>)

FFT - Fast Fourier Transform

FOV - Field of View

FMAG - Fluxgate Magnetometer

FMC - Forward Motion Compensation

FNWC - Fleet Numeric Weather Central

GARP - Global Atmospheric Research Program

Ge - Germanium

GISS - Goddard Institute for Space Studies

GOES - Geostationary Operational Environmental Satellite

GRAD - Gravity Gradiometer

GRE - Ground Resolution Element

GSFC - Goddard Space Flight Center

HCMM - Heat Capacity Mapping Missions

HCMR - Heat Capacity Mapping Radiometer

HDDR - High Density Digital Tape Recorder

HDDT - High Density Digital Tape

**HDT** - High Density Tape

HDTR - High Density Tape Recorder

HgCdTe - Mercury-Cadmium Telluride

HIRS - High Resolution Infrared Radiation Sounder

HRE - High Resolution Etalon

HRPT - High Resolution Picture Transmission

IFOV - Instantaneous Field of View

InAs - Indium Arsenide

InS - Indium Sulfide

InSb - Indium Antimonide

IPD - Information Processing Divison

IR - Infrared

ITOS - Improved TIROS Operational Satellite

IU - Investigative Unit

JPL - Jet Propulsion Laboratory

J-T - Joule-Thompson

Kbps - Kilo bits per second

LaRC - Langley Research Center

LEST - Large Earth Survey Telescope

LIDAR - Light Detection and Ranging

LSI - Large Scale Integration

MA - Multiple Acess (TDRSS Mode)

MASR - Microwave Atmospheric Sounding Radiometer

Mbps - Mega bits per second

MDHS - Meteorological Data Handling System

MHz - Mega Hertz

MLE - Maximum Likelihood Estimator

MMIPS - Man-Machine-Interactive Processing System

MPF - Multispectral Photographic Facility

MRE - Medium Resolution Etalon

MRIR - Medium Resolution Infrared Radiometer

MSS - Multispectral Scanner

MSSCC - Multicolor Spin-Scan Cloud Camera

MSIJ - Microwave Sounding Unit

NADUC - NIMBUS/ATS Data Utilization Center

NASCOM - NASA Communications Link

NEDT - Noise Equivalent Differential Temperature

NEP - Noise Equivalent Power

NESS - National Environmental Satellite Service

NIR - Near Infrared

**REV. NO.:** 

NOAA - National Oceanographic and Atmospheric Agency

NMRT - NIMBUS Meteorological Radiation Tape

NRL - Naval Research Laboratory

NRZ - Non-Return to Zero

NSSDC - National Space Science Data Center

NWS - National Weather Service

OP - Ocean Physics

OPBR - Optical Bar Panoramic Camera

P/B - Playback

PbS - Lead Sulfide

PbSe - Lead Selenide

PbSnTe - Lead Tin Telluride

PCM - Pulse Code Modulation

PDPF - Project Data Processing Facility

PDPS - Project Data Processing System

PGDF - Product Generation and Dissemination Facility

PI - Principle Investigator

PIXEL - Picture Element

PM - Pulse Moduleation

PMT - Photomultiplier Tube

PMC - Pressure Modulated Cell

PN - Pseudorandom Biphase Modulation

POCC - Project Operations Control Center

PPU - Patch Panel Unit

PSK - Phase Shift Keyed

QE - Quantum Efficiency

RAU - Remote Acquisition Unit

RCU - Revision Control Unit

RMS - Root Mean Square

RSDH - Remote Sensing Data Handbook

R&D - Research and Development

SAMS - Stratospheric and Mesospheric Sounder

SAR - Synthetic Aperture Radar

SASS - SEASAT-A Satellite Scatterometer

SATCOM - Satellite Communications

SCAT - Scatterometer

S/DB - Synchronizer - Data Buffer

SDPF - Satellite Data Processing Facility

SDR - Supplementry Data Record

SEOS - Synchronous Earth Observation Satellite

SESS - Satellite Field Service Site

Si - Silicon

SIPS - Satellite Input Processing System

SIR - Shuttle Imaging Radar

SIRS - Satellite Infrared Sounding

SIU - Serial Interface Unit

SMMR - Scanning Multichannel Microwave Radiometer

SMS - Synchronous Meteorological Satellite

S/N - Signal to Noise

SOCC - Satellite Operations Control Center

SOPS - Satellite Output Processing System

SRI - Standford Research Institute

SSU - Stratospheric Sounding Unit

STDN - Spaceflight Tracking and Data Network

TBD - to be determined

REV. NO.:

3

REV. DATE: 31 July 1978

TELOPS - Telemetry On-Line Processing System

TDRS - Tracking and Data Relay Satellite

TDRSS - Tracking and Data Relay Satellite System

TGS - Triglycine Sulfate

THIR - Temperature/Humidity Infrared Radiometer

TIR - Thermal Infrared

TLM - Telemetry

TM - Thematic Mapper

TTY - Teletype

TWT - Traveling Wave Tube (Amplifier)

ULE - Ultra Low Expansion

USB - Unified S-Band

USDA - United States Department of Agriculture

UT - Universal Time

UV - Ultra Violet

VAS - Visible Infrared Spin-Scan Radiometer Atmospheric Sounder

VDM - VISSR Digital Multiplexer

VHRR - Very High Resolution Radiometer

VIC - VISSR Ingest Computer

VIP - Versatile Information Processor

VIS - Visible

VISSR - Visible Infrared Spin-Scan Radiometer

VTPR - Vertical Temperature Profile Radiometer

VTU - Video Terminal Unit

WFC - Wallops Flight Center

WWB - World Weather Building

ZIP - CZCS Information Processor

ZnSe - Zinc Selenide

REV. NO.: 3 REV. DATE: 31 July 1978

### SENSOR CATEGORY TABLE OF CONTENTS AND REVISION CONTROL SHEET

SENSOR NAME NUMBER EFFECTIVE				
OR	OF	PAGE	EFFECTIVE	
OTHER ENTRY	PAGES	NUMBER	REV. DATE	REV. NO.
Section 5.1 Table of Contents	2	5.1-i	31 JAN 78	2 2
Introduction to Synthetic Aperture		5.1-ii	31 JAN 78	2
Radars	40	. 5.1-1	31 JAN 78	2
		5.1-2	31 JAN 78	2
		5.1-3	30 SEPT 77 31 JAN 78	1 2
		5.1-4 5.1-5	31 JAN 78 30 SEPT 77	1
		5.1-6	30 SEPT 77	1
	,	5.1-7	30 SEPT 77	1
	1	5.1-8	30 SEPT 77	1
	•	5.1-9 5.1-10	30 JUN 77 30 SEPT 77	0 1
	ı	5.1-10	30 SEPT 77	1
		5.1-12	30 JUN 77	0
•		5.1-13	30 SEPT 77	1 .
·		5.1-14	30 JUN 77	0
		5.1-15 5.1-16	31 JAN 78 30 SEPT 77	2
		5.1-17	30 SEPT 77	i
		5.1-18	30 SEPT 77	1
	•	5.1-19	30 SEPT 77	<u>1</u>
		5.1-20 5.1-21	31 JAN 78 31 JAN 78	2 2
		5.1-22	30 SEPT 77	1
		5.1-23	31 JAN 78	2
		5.1-24	30 SEPT 77	1
	1	5.1-25	31 JAN 78 30 SEPT 77	2
		5.1-26 5.1-27	30 SEPT 77	1 .
		5.1-28	31 JAN 78	2
		5.1-29	31 JAN 78	2
		5.1-30	31 JAN 78	2
,		5.1-31 5.1-32	31 JAN 78 30 SEPT 77	2 1
·	İ	5.1-33	31 JAN 78	2
		5.1-34	31 JAN 78	2
		5.1-35	30 SEPT 77	1
·		5.1-36	30 SEPT 77	1
		5.1-37 5.1-38	31 JAN 78 30 SEPT 77	2 1
	Į	5.1-39	30 SEPT 77	1
		5.1-40	31 JAN 78	2
SEASAT-A Synthetic Aperture Radar	4	5.1-41	31 JAN 78	2
	1	5.1-42	31 JAN 78	2
	1	5.1-43	31 JAN 78	2
	1	5.1-44	31 JAN 78	2
SECTION NO.: 5.1 SENSOR CATEGORY	: Synthetic	Aperture Rad	ars	
5-1-1	REV. NO.:		EV.DATE: 31 J	an 1078

5-1-1 REV. NO.: 2 REV. DAT

### SENSOR CATEGORY TABLE OF CONTENTS AND REVISION CONTROL SHEET

Sensor Name Or Other Entry	E	NUMBER OF	PAGE	EFFECTIVE	
	Υ	PAGES	NUMBER	REV. DATE	REV. NO.
Shuttle Imaging Radar		4	5.4-45 5.4-46 5.4-47 5.4-48	31 JAN 78 31 JAN 78 31 JAN 78 31 JAN 78	2 2 2 2
	·				
		• , •		7	
					·
. · •					
			-		
	•				
•	5.1-ii				
SECTION NO.: 5.1	SENSOR CATEGORY	: Syntheti REV.NO.	c Aperture R	adars EV.DATE: 31 J	1000

# Section 5

Section 5 consists of ten sensor categories as listed in the Table of Contents. Each category is identified by an index tab and contains three basic parts; an introduction, a listing of research material and RSDH Data Sheets.

The introduction provides the user with a general overview, operating principles and other background information for a particular category of sensors. The listing of research material, which follows the introduction is made up of the following:

- Active Contributors A partial list of workers in the discipline who have distinguished themselves by their leadership.
- References These lists identify those publications of which specific mention is made in the introduction and/or data sheets. Numbers in brackets (e.g., [13]) in the text refer to this list.
- <u>Bibliographies</u> These lists are documents and papers relevant to the sensor category. In some cases, Bibliographies are broken down to show applicability to particular sensors.
- · Illustration Credits This list provides acknowledgement of the sources for illustrations used in the RSDH. The listings consist of four columns. The first two give the figure number and page with respect to the RSDH. The second two columns identify the research material (reference number and page) from which the illustration was drawn.

All pages in Section 5 are numbered consecutively with the section number preceding the page number (e.g., 5.2-1, 5.2-2, etc.).

Specific information on infrared detectors is presented in Appendix A.

This page intentionally left blank.

REV. NO.:

REV. DATE: 30 June 1977

# Section 5.1 INTRODUCTION TO SYNTHETIC APERTURE RADAR (SAR)

The wavelengths in the microwave region of the spectrum are long compared with the size of scattering centers associated with most weather phenomena. As a result, remote sensors built to operate in this spectral region have the potential to provide an all-weather capability because the relatively long waves are not effectively reflected or scattered by the small centers. Most weather phenomena are, therefore, transparent to microwaves. Microwave remote sensors can provide operation on the dark side of the earth as well as the lighted side. Various radiometers measure passive microwave radiation to determine atmospheric temperature and these devices are addressed in another section. This section deals with an active microwave sensor known variously as the Synthetic Aperture Radar (SAR), coherent radar or sidelooking radar. As with conventional radars, the area of with the conventional radars, the conventional radars are the conventional radars. interest is flooded with microwave radiation of controllable characteristics and the return reflections are operated upon. As will be shown later, it is primarily the processing at the receiver which gives the SAR its uniqueness. Advantages other than all-weather operation are gained using microwave energy rather than visible or One such advantage is the capability of the longer wavelengths infrared radiation. to penetrate solids and liquids, and return radiation from beneath the surface. This characteristic can be utilized to map subsurface terrain features as on the Apollo Lunar Sounder where a SAR was operated at other than microwave frequencies (5 MHz, 15 MHz, and 150 MHz) in an environment of low attenuation surfaces to realize deep penetrations of the order of several meters. The reflection and absorption of terrestrial soils have been found to vary with water content, salinity, chemical composition and other factors. Researchers have recognized the potential

REV. NO.: 2 | REV. DATE: 31 Jan 1978

of microwave sensors for mapping soil moisture for agricultural purposes, for locating soil salt problems caused by irrigation water, for determining the type of rock in certain outcroppings and for penetrating vegetative cover.

The SAR is a microwave imager and has much in common with the Multispectral Scanner and Thematic Mapper in that the output product is a photograph of a subsatellite swath. The image has its own set of unique characteristics owing to the properties of the interaction of the radiation with the ground targets. Images can also be developed using passive microwave devices where a highly directional antenna is scanned and the output of the detector is plotted against scan angle. Conventional radar may also be used to produce images. The problem with both of these alternatives is resolution. The beam width in a "straightforward" radar or a microwave receiver is proportional to the size of the antenna and the wavelength of the radiation. For a given antenna size (diameter), as the wavelength is reduced the beam width is reduced but the influence of small scattering centers is increased If wavelength reduction is used as a method of improving resolution, weather penetration capability suffers. Likewise, we are limited by structural considerations in increasing antenna size to improve resolution. The constraints of nature, then, limit even the potential for improving microwave imaging unless a more subtle approach is utilized. In the following paragraphs, we will attempt to aid the reader in visualizing the principles upon which the SAR is founded. A rigorious or even thorough treatment of these principles is beyond the scope of this manual and the reader whose requirements are not satisfied by this coverage is referred to more detailed material [1]. Goodyear Aircraft Corp., The University of Michigan and the University of Illinois figure heavily into the first work with synthetic apertures in the early fifties. The hardware was first approached with airborne equipment using an x-band coherent radar, a conventional oscilloscope and film

REV. NO.: 2 RI

REV. DATE: 30 Jan 1978

camera for display with a tape recorder used as a memory in processing the data.

The object of the early experiments was to demonstrate the concept of Doppler beam sharpening. The geometry of a typical airborne SAR operation is shown in Figure 5.1-1.

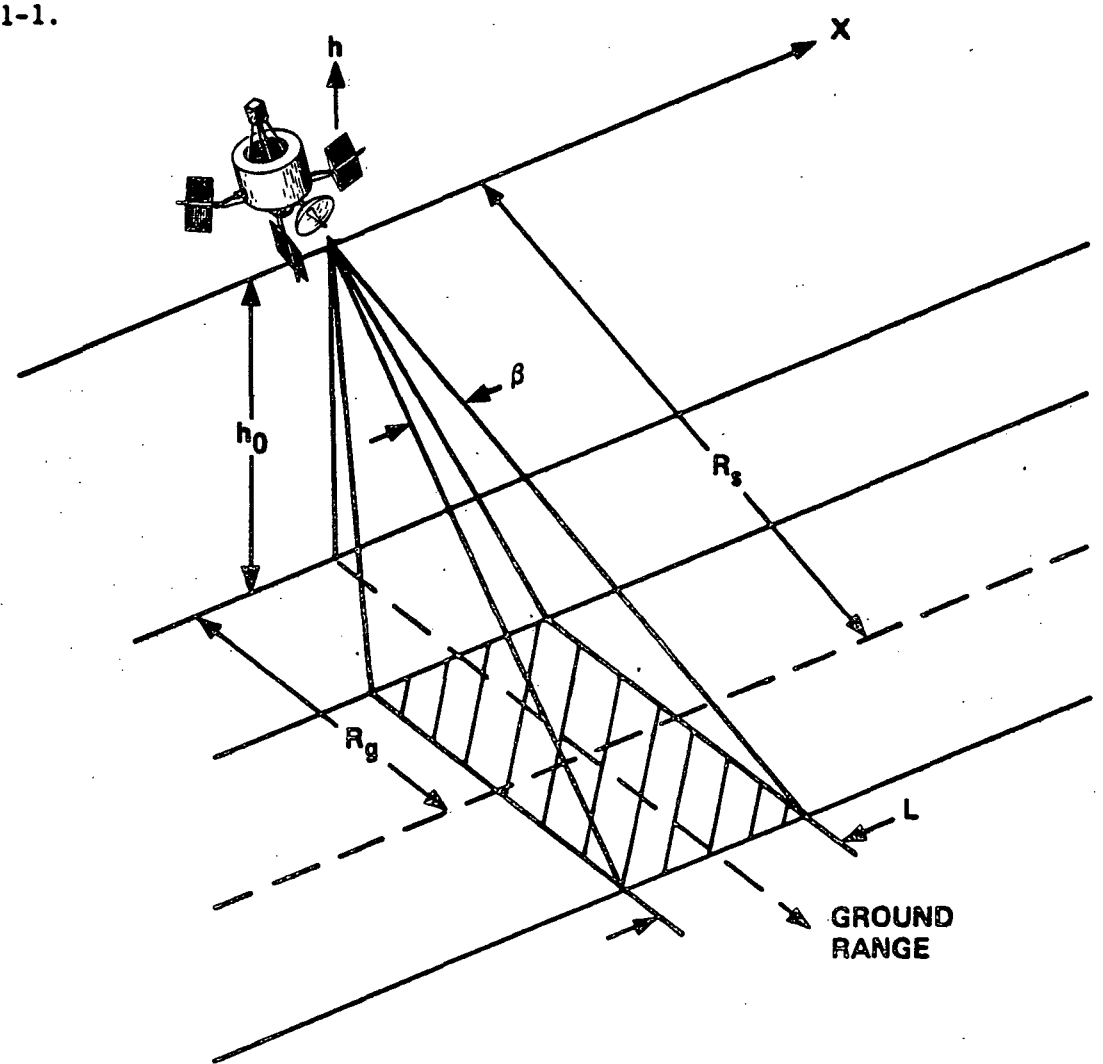


FIGURE 5.1-1 SAR Operation Perspective View

The antenna is placed and pattern chosen so that radiation leaving it illuminates a strip parallel to the flight path (shaded area Figure 5.1-1). Scan of the strip is achieved by the forward motion of the spacecraft. The antenna is not scanned nor is it rolled or yawed to compensate for spacecraft motion. These errors, together

with spacecraft velocity variations, will be dealt with later. For now, let us assume ideal circumstances.

As shown in Figure 5.1-2, the wavefront leaving the antenna propagates onto the illuminated area along slant range  $R_{\rm S}$ . If the reflections from the ground were specular, angle of incidence and reflection would equal and no return would be received, but for the majority of targets in the strip, the reflection is diffused. The wavefront is disturbed and individual reflections from points within the strip are returned to the antenna at times proportionate to slant range  $R_{\rm S}$ . The round trip propagation time between the antenna and the target is

$$\Delta T = \frac{2R_S}{C} \tag{1}$$

where C is essentially the speed of light (propagation speed for the medium) and can be visualized at about one foot per nanosecond.

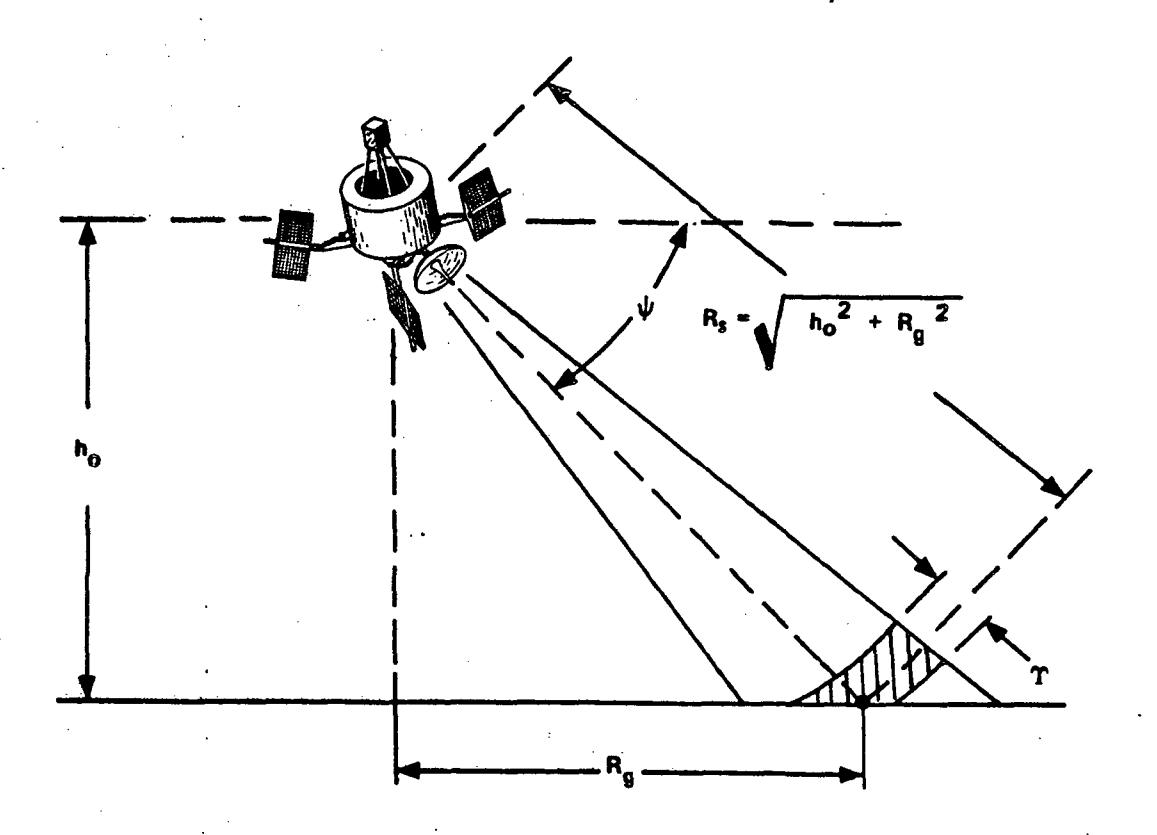


FIGURE 5.1-2 SAR Operation Rear View

REV. NO.. 2 | REV. DATE: 31 Jan 1978

Were the transmitted pulse a single wavefront, all the returns from various targets at different slant ranges would be distinct and separable. However, since the transmitted pulse is a sequence of wavefronts, it has a finite length or thickness and two or more targets at different values of R<sub>S</sub> will be illuminated simultaneously and, therefore, will not be separable. In theory, reflections from targets are separable if they are staggered in tandem by a distance greater than the transmitted pulse length. Since the echos have traveled the round trip to the targets, they will be sufficiently staggered if they originate from targets whose slant ranges are different by an amount equal to one half the physical length of the pulse

$$\Delta R_{\rm g} \ge \frac{\rm CT}{2} \tag{2}$$

We can call this separation slant range resolution or

$$\rho_r = \frac{CT}{2} \tag{3}$$

and the corresponding ground range resolution is

$$\rho g = \frac{CT}{2} \cos \Psi \tag{4}$$

where  $\Psi$  is the antenna depression angle as shown in Figure 5.1-2. The pulse width or wavefront thickness is reduced by using wide bandwidth radars and <u>pulse compression</u> techniques [2].

The along-track dimension or azimuthal cross section (horizontal plane dimension of the pulse) is determined by the antenna pattern. As shown in Figure 5.1-3, the width of a pulse produced by an antenna, with half-power beamwidth of  $\beta$  radians, at range  $R_s$  is  $L = \beta R_s$ .

If L is a measure of the along-track resolution ( $\rho x$ ), then the only recourse open for use in "straightforward" radars is to make  $\beta$  small. Beamwidth is related to antenna aperture in a diffraction limited system: one where the errors in the

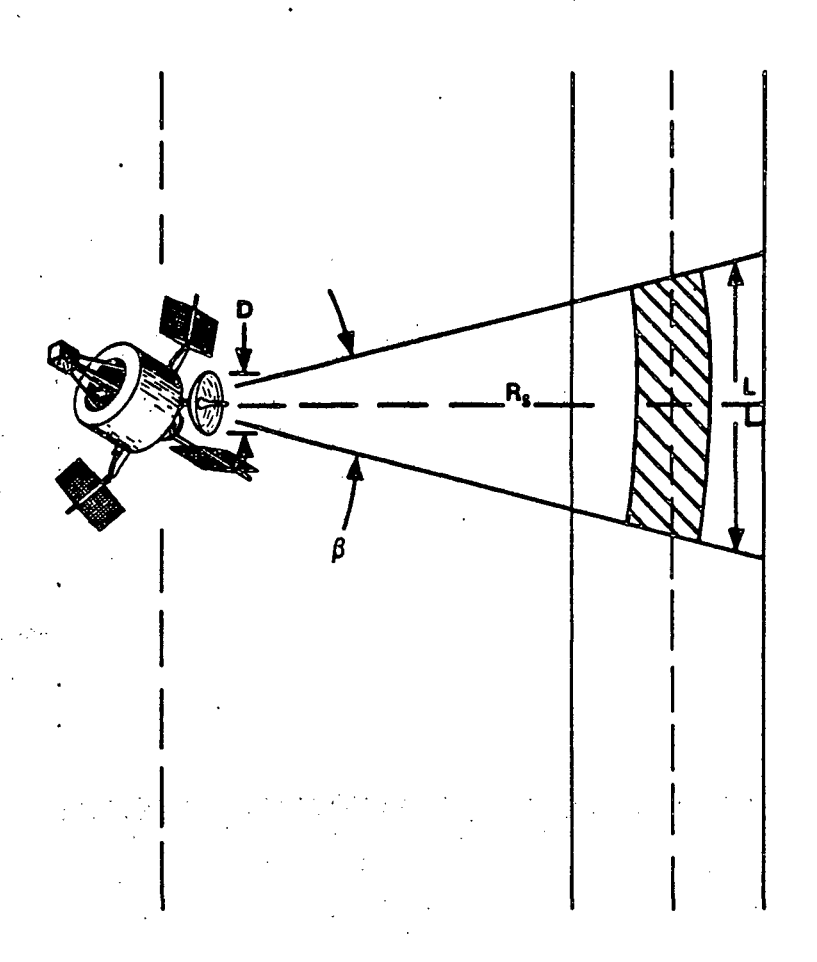


FIGURE 5.1-3 SAR Operation Plan View

reflecting surfaces are essentially non-existant. The relationship, which is known as the Rayleigh Criterion, was first applied in optics and simplifies to:

$$\beta = \frac{\lambda}{D}$$
 radians,

where  $\lambda$  is the wavelength of the radiation and D is the dimension (aperture) of the antenna in the plane being considered (horizontal).

Therefore, we can rewrite the expression for along-track resolution as:

$$\rho x = R_g \beta 
\beta = \frac{\lambda}{D}$$
(5)

$$\frac{\lambda R}{Dx} = \frac{D}{D}$$
 (6)

As was pointed out earlier, to keep  $\beta$  small,  $\lambda$  may be reduced or D increased but both of these alternatives become unattractive if carried beyond certain limits. Therefore, to improve  $\beta$  beyond the limits of the Rayleigh Criterion, we employ a synthetic aperture technique.

If the radar emits a sinusoid at a frequency  $f_0$ , then since the spacecraft is in motion with some velocity v, the reflected signal will have undergone a shift in frequency.

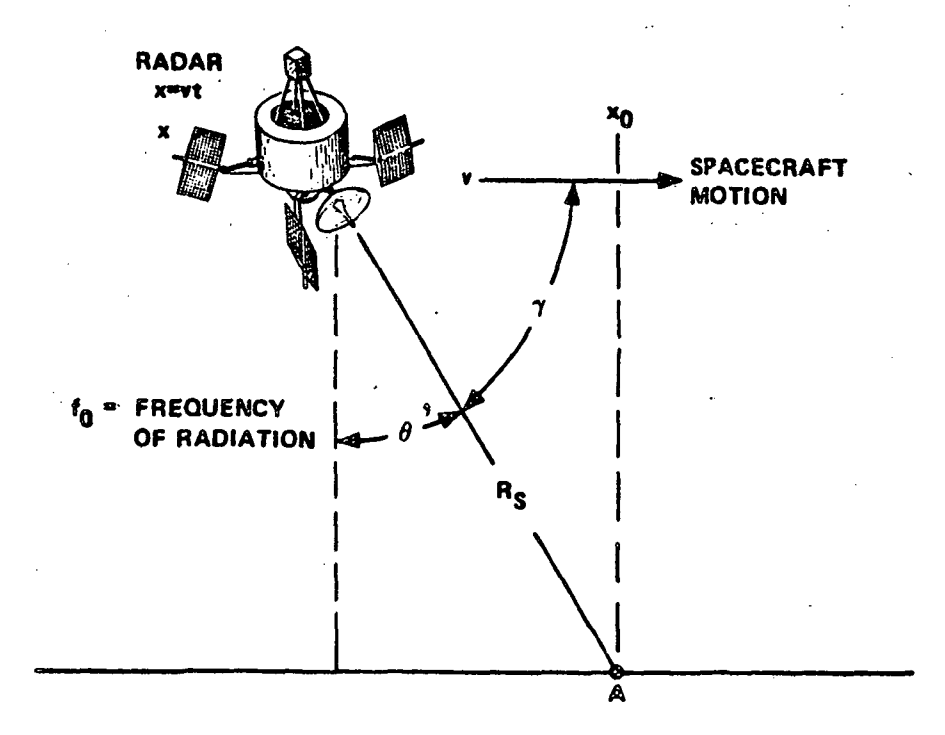


FIGURE 5.1-4 SAR Operation Side View

The amount of Doppler shift is proportional to the propagation speed C and the relative velocity between the source and the point of observation. If the point of observation were on the ground at point A, the Doppler shift would be proportional to the rate of change of  $R_{\rm c}$ .

$$F_{D} = \frac{D_{t}R_{s}}{C} \quad f_{o} \tag{7}$$

Since the "observation" point is on-board the spacecraft, not on the ground, the radiation travels twice  $R_s$  and the shift is doubled. The change in  $R_s$  can be equated to spacecraft velocity v as follows:

$$D_{\uparrow}R_{s} = v \cos \gamma \tag{8}$$

and the expression for the Doppler shift from a specific target can be rewritten:

$$f_{D} = \frac{2vCos\gamma f_{O}}{C}$$
 (9)

$$\frac{\mathbf{f_o}}{C} = \frac{1}{\lambda} \tag{10}$$

$$\cos \gamma = \frac{x - x_0}{R_s} \tag{11}$$

and 
$$f_o = \frac{2v}{\lambda R_s} (x - x_o)$$
 (12)

Clearly then, if a projection is made abeam the spacecraft, echos from targets not lying on the projection are undergoing a Doppler frequency displacement from the original radiation and echos from targets lying on the projection are not shifted. We can, therefore, exclude some returns by a narrow bandpass filter centered at f<sub>0</sub>. The passband of the filter determines the frequency limits of "acceptable" signals. The received signals then are discriminated against linearily as a function of x-x<sub>0</sub> for any value of range. The radar beam then can be said to be collimated.

The synthetic aperture technique, although first conceived from the Doppler viewpoint, can also be approached from an entirely different but mathematically equivalent viewpoint. Following from Figure 5.1-1, observe that a reflection at range  $R_s$  is illuminated by the radar while the latter moves through a distance of  $L = \beta R_s$ .

If the physical antenna is regarded as one element of a linear array which is elongated only in the direction of flight, occupying in time sequence all the

**REV. NO.: 1** 

**REV. DATE:** 30 Sept 1977

elemental positions germane to the array, then intuitively, it should be possible to "synthesize" an aperture of length L by suitably storing the received signal before processing the data. The processed data then has nearly all the qualities of data that would have been generated by an antenna of length L. Actually, the data is better in several ways.

In a physical array, n equally spaced dipoles transmit signals in phase (thus the beam is normal) to the array, all n dipoles receive signals from a target and all these signals are added in the antenna itself. In the synthetic antenna, n signals are transmitted in sequence (one for each radar pulse), received in sequence and stored in such a manner that their phases and amplitudes are preserved. Finally, during the signal-processing operation the stored signals are added together, thus reconstructing the effective aperture.

By manipulating phase upon readout, the synthetic aperture radar can be made to focus on any range to further improve the resolution at that range. These focused SAR's have the requirement that small pertubations in the flight path of the spacecraft must be taken into account in image reconstruction. An accelerometer compensates for positional shifts along the flight path by altering the phase of the transmitted or received pulses.

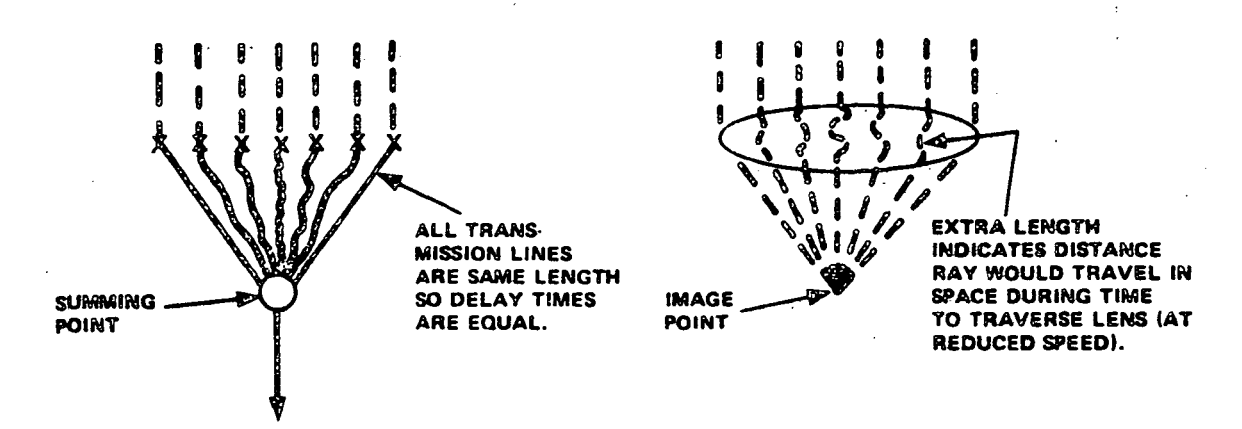


FIGURE 5.1-5 Comparison of Broadside Antenna Array with Lens Focused at Infinity

REV. NO.: 0 | REV. DATE: 30 June 1977

Most real aperture radar antennas are focused at infinity, as illustrated in Figure 5.1-5, but synthetic aperture antennas (see discussion below) often are focused at a nearer point, as shown in Figure 5.1-6. For the lens seen in the figure, the paths from object 0 to image point I through a, b, c, d and e all experience the same delay, the extra delay for the shorter path through c being due to an extra distance traveled in the low-velocity path within the lens. For the antenna the same effect can be achieved by adjusting the lengths of the transmission lines from the various elements to the summing point. Thus the delays along paths (OaS, ObS, OcS, OdS, and OeS are all the same. Hence, the antenna is focused at point 0.

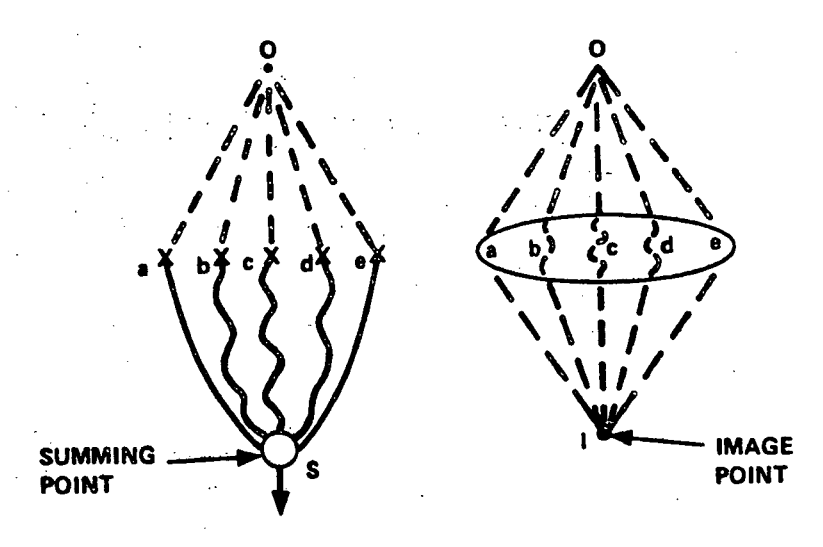


FIGURE 5.1-6 Comparison of Focused Antenna Array with Lens Focused at Point O

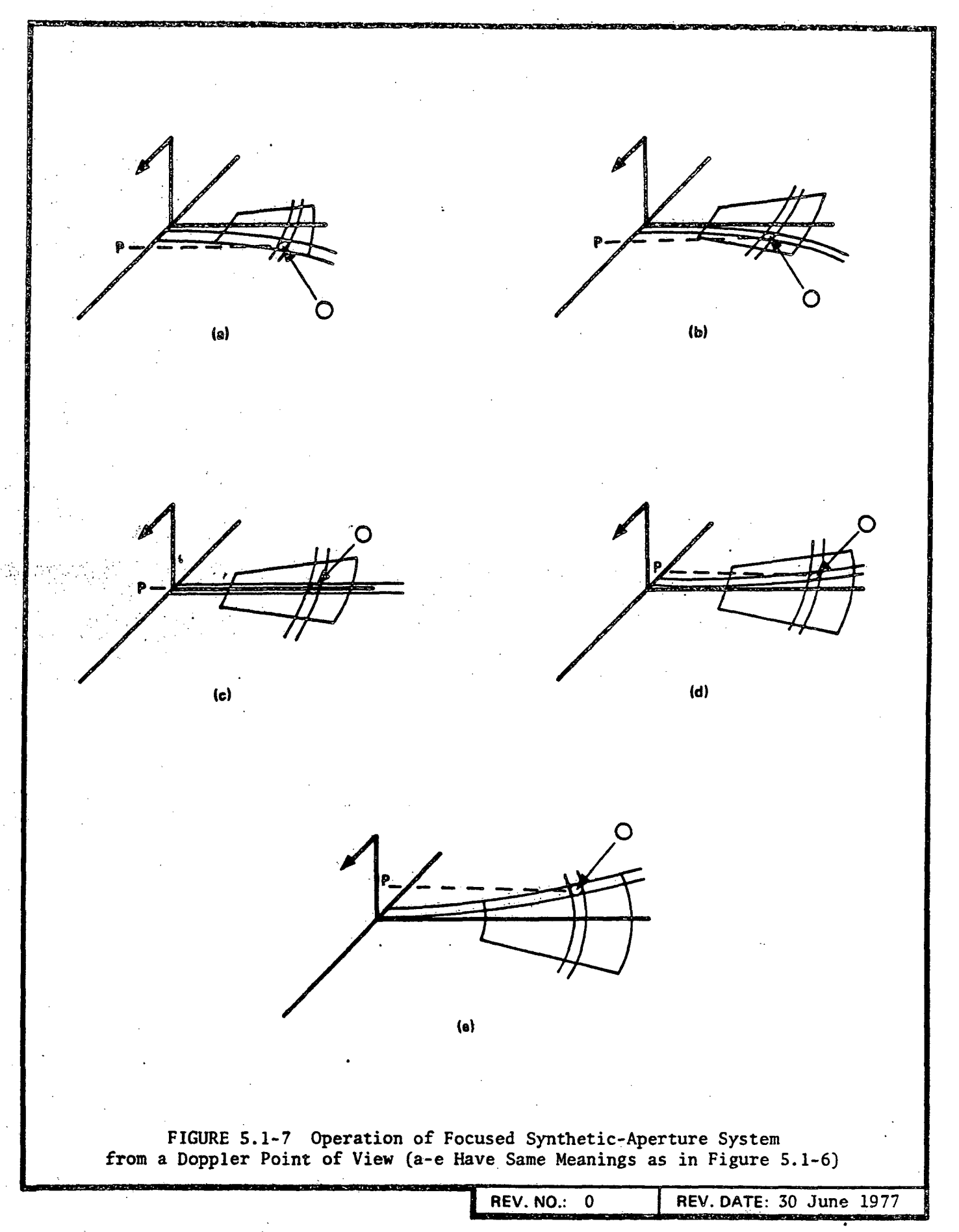
The synthetic aperture can be built either in the form of an array focused at infinity, as in Figure 5.1-5 (called an unfocused synthetic aperture), or in the form of an array focused at some closer point, as in Figure 5.1-6. The element positions of the array (a-e in the figures) are not simultaneously occupied by physical antennas. Rather, the radar travels first to a, then b, then c, then d, then e, etc. The signal received at each point is compared in phase with the signal

**REV. NO.: 1** 

REV. DATE: 30 Sept 1977

transmitted at that point, and the result stored in a memory. Either in the space-craft or on the ground, the signals stored in the memory are processed to achieve the equivalent of the transmission line lengths shown in Figures 5.1-5 and 5.1-6. A common way to store this information is on signal film.

To focus at a closer point like the antenna of Figure 5.1-6, a method must be devised to use all the information available from the time the target first enters the beam of the real antenna until it leaves this beam. Not only will this give a better resolution, but also it does not waste power as does the system diagrammed in Figure 5.1-3. Figure 5.1-7 is a simplified illustration of the way in which the focused synthetic aperture system operates, as viewed from a Doppler frequency point of view. Here we assume that each of the sketches represents what happens in the general vicinity of one of the points (a through e) of Figure 5.1-6. Actually, this means that each of the points shown in Figure 5.1-6 represents tens or hundreds of elements for this situation; otherwise there would be insufficient samples to achieve the Doppler filtering of Figure 5.1-7. Figure 5.1-7(a) shows the situation when the target 0 has just been illuminated by the real aperture. At this time the set of Doppler frequencies (relative velocities) corresponding to the forward edge of the real aperture is filtered and used for target 0. Range lines are also shown The point P on the ground track of the spacecraft is the foot of a perpendicular from point 0. The spacecraft has not yet reached this point. In Figure 5.1-7(b). corresponding to point b of Figure 5.1-6, the Doppler frequencies used are those midway through the forward part of the beam, and the spacecraft is closer to point In Figure 5.1-7(c), the spacecraft is directly over point P and abreast of point 0. The Doppler filter here is the same as that of Figure 5.1-3. In Figures 5.1-7(d) and 5.1-7(e), the mirror-image situation prevails as the spacecraft moves on past P. The results of each of these five filtering operations are stored and combined in the processing system to produce the equivalent focused synthetic



aperture. In a real system the filter moves continuously rather than incrementally as indicated here. Furthermore, additional filters are at work for each of the elements within the real aperture. Obviously, the mechanization is quite complicated.

The type of storage used depends on whether the synthetic aperture processing is to be performed immediately or on return of the data to a ground station. With immediate processing the information may be stored in a recirculating delay line, which may also serve as part of the processor. Storage can also be achieved by separately gating returns from each range element into a capacitor with a long decay time constant. A technique for temporary storage that appears more suitable for a fully focused processor involves the use of one or more storage tubes.

Storage for later processing can be achieved by recording the signal on magnetic tape if the tape recorder has sufficient bandwidth. This is reasonable with the present state-of-the-art as long as the range resolution is not too fine.

Recording the received signal on film with the same type of recorder employed for the real aperture system permits use of a wider band width than does magnetic tape. At present this is the most commonly used method for focused synthetic aperture systems. Systems presently planned for spacecraft application (SEASAT-A) are designed to transmit SAR output video directly to Earth on a separate wide-band data link with no storage whatever. The film record is produced on the ground upon receipt of the video signal.

The returning radar signals will have a bandwidth determined by the rangeresolution capability built into the radar system. A photographic process permits
recording of wide-band signals with greater ease than is possible with certain
other recording systems; consequently, it is well suited for use with synthetic
aperture radars, provided one can tolerate some of the film-processing inconven-

iences. Photographic recording also permits high-density storage, another quality which is desirable in fine-resolution imaging systems.

The radar receiver output is a sequence of reflected range pulses; these are used to intensity-modulate a cathode-ray tube, the electron beam of which is swept synchronously with the returning pulses. Successive range traces are recorded side-by-side, producing a two-dimensional format in which the dimension across the film represents range and the dimension along the film represents the along-track dimension. This format is shown in Figure 5.1-8.

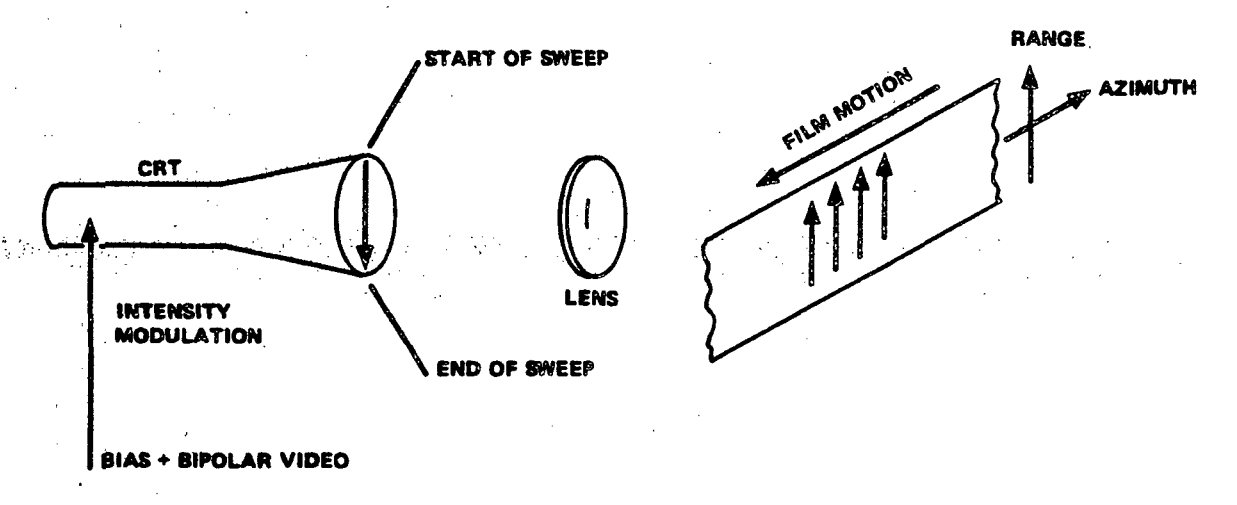


FIGURE 5.1-8 Radar Signals are Sent Through a Biased CRT, and then Recorded on Film for Subsequent Optical Processing

The film recording of the output of the coherent detector is like a hologram in that the phase information is contained in interference fringes on the film [3]. This point is illustrated by Figure 5.1-9 which shows how a hologram is constructed. With the hologram a sample of the illuminating beam is mirrored onto the photographic plate, where it interferes with the scattered light from the object viewed to produce the well-known holographic interference fringes. In the radar the same effect is achieved by the homodyne receiver, in which the interference is between the sample of the transmitter signal and the scattered signal received on the antenna.

REV. NO.: 0 REV. DATE: 30 June 1977

Just as an image is reproduced from the hologram by illuminating it with monochromatic light, so an image can be produced from the radar film by similar illumination.

The film recorded at the output of the synthetic-aperture receiver, which is in effect a microwave hologram, is called signal film. Like an optical hologram, it is an interference pattern which is difficult to interpret when viewed by itself. Thus, it must be processed to produce an image film for use by the interpreter. Each scattering object on the ground produces a one-dimensional Fresnel zone plate corresponding to the range of the object, and with a focal length proportional to this range. Reflectors, at the same range but with different along-track coordinates appear as zone plates with displaced centers; their radar cross sections are manifested in the modulation intensity of the zone plate.

When this collection of one-dimensional holograms is illuminated by a coherent, collimated beam of light, a one-dimensional wavefront reconstruction takes place. The spatial pattern associated with each reflector generates a real and virtual image, each having a focal length proportional to range.

The conventional optical processor configuration using conical, cylindrical, and spherical lenses is described elsewhere, [4], [7], (2). The description given below represents the current state-of-the-art in optical processing and will be utilized for Seasat-A SAR data by the Jet Propulsion Laboratory in Pasadena, California.

Although the applicability of optical processing for future missions (because of the increasing resolution and accuracy requirements) is questionable, the technique has significant heritage and its requirements are well understood.

REV. DATE: 31 Jan 1978

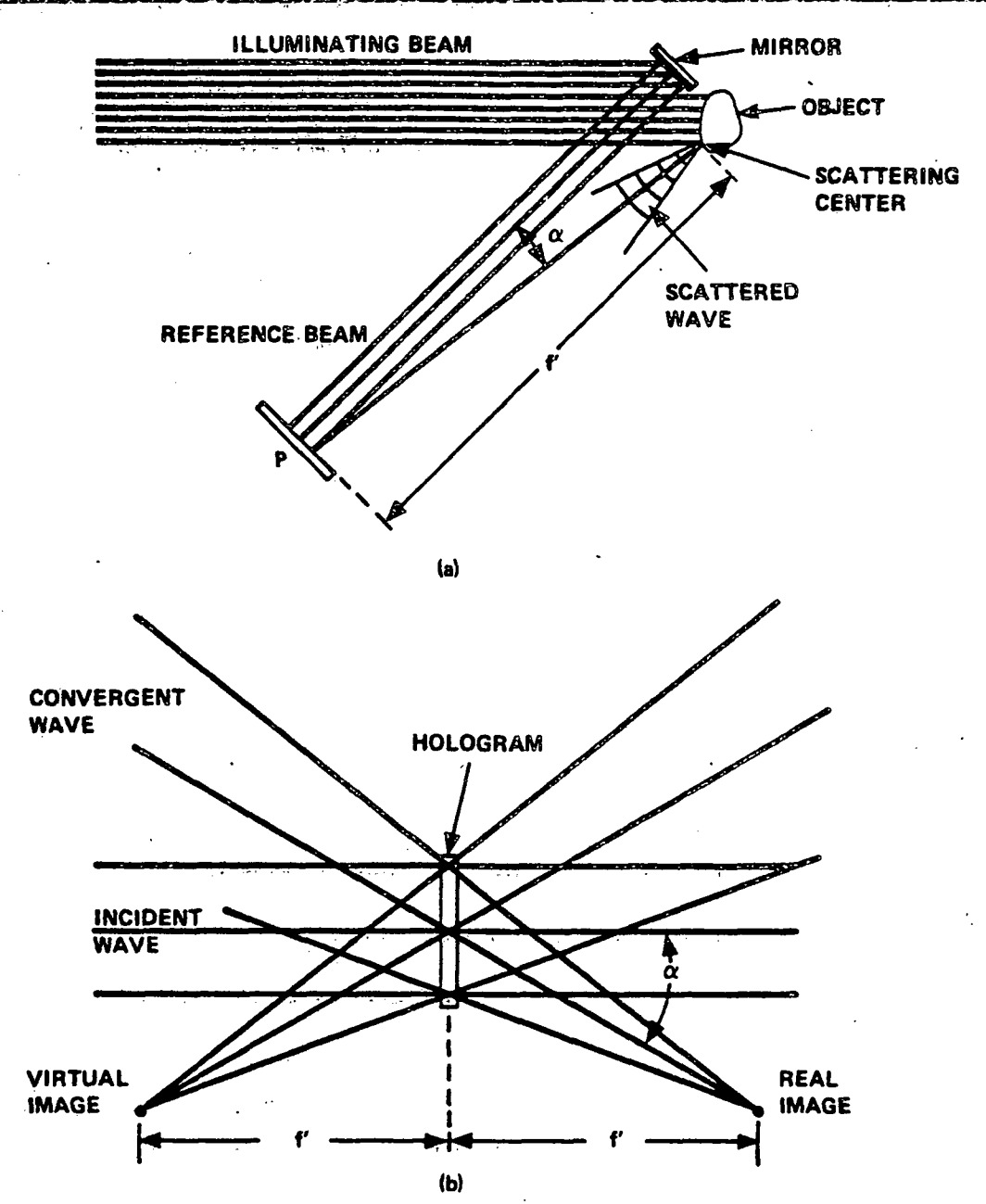


FIGURE 5.1-9 Top diagram (a) depicts conventional optical setup for producing a hologram. Hologram (b) can, in turn, reproduce both a virtual and a real three-dimensional image.

Figure 5.1-10 shows a block diagram of optical processing data flow. The processing is simplified by maintaining a constant film speed to spacecraft speed

ratio. In this way, the azimuth focus in the correlator remains constant throughout the pass. If this were not done, it would be necessary to compensate dynamically in the correlator for the azimuth focus. The signal film, then, is processed through the optical correlator, and the image can be digitized or exposed on photographic film to obtain a transparency.

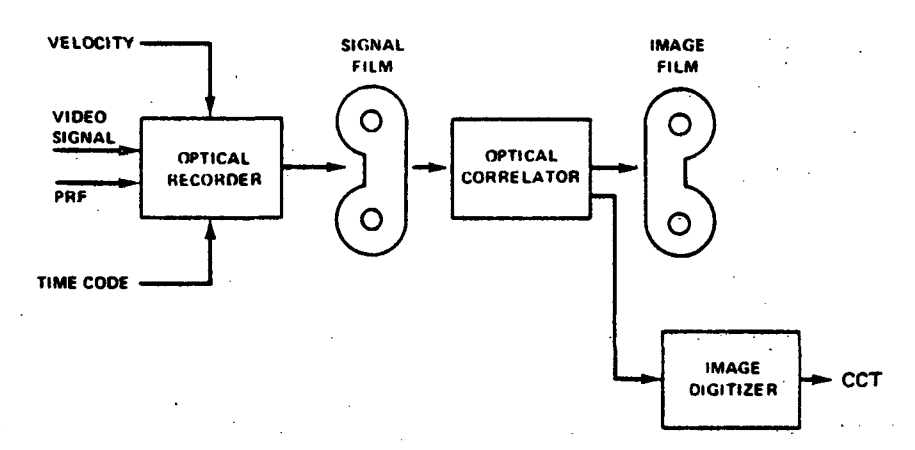


FIGURE 5.1-10 Optical Processing

Figure 5.1-11 is a simplified diagram of an optical processor. A collimated laser beam illuminates the signal film. The film is tilted to take into account the linear increase in the azimuth focus with increasing slant range. The first lens transforms the data, and the phase correction is made for range migration in the transform plane. Both azimuth and range-frequency filtering is performed. The

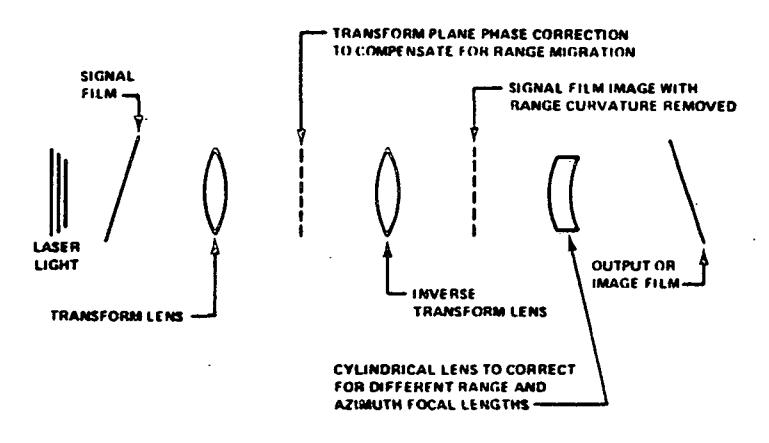


FIGURE 5.1-11 Simplified Diagram of Optical Processing

transform of a point target with the range curvature corrected is a uniform amplitude light wave with quadratic phase variation in the range and azimuth dimension. The second lens then transforms the data after it has been partially processed. A cylindrical lens telescope then images the data in azimuth to bring the range and azimuth focal lengths into coincidence. The input and output film planes are tilted with respect to each other to compensate for change in the azimuth focal length with range.

Figure 5.1-12 shows the generation of multiple looks by optical means. The phase history of a point target is spread out over the distance indicated by the double-headed arrow. If the aperture is stopped down to look at only one quarter of that distance with the laser beam, the light would focus through the correlator to a point at one quarter of the full resolution. Illumination of any one of these four segments would produce a different pixel intensity at the output focus. Thus, four looks could be obtained at the output focus by moving the beam across the signal. Instead of doing that, however, the film is moved past the beam, the focus point moves at the output in the same direction as the output film so that the different speckle intensities are averaged by photographic integration on the film. The film can detect only intensity, not phase.

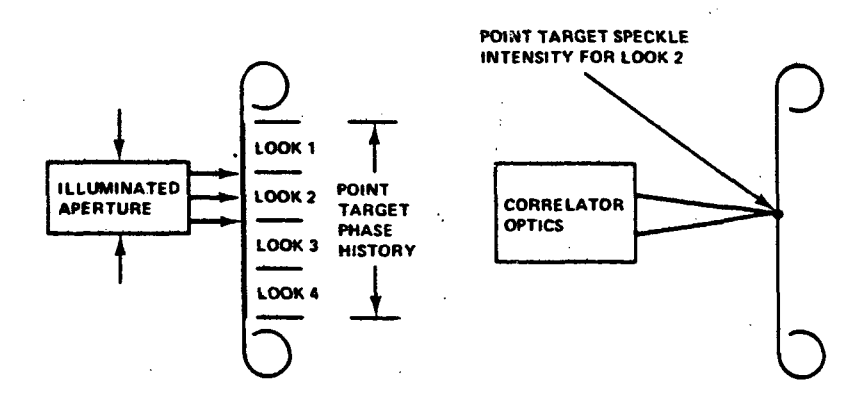


FIGURE 5.1-12 Optical Multiple-look Generation

Another technique is to illuminate the full area, in which case the spot size, i.e., the resolution, would decrease by a factor of four. Then, the output film is moved at a velocity different from the image so that the data is integrated for four cells, resulting in the same resolution as the previous technique. Instead of an average of four cells, the result is a linear integration along a four-cell length in azimuth. This process does not necessarily yield a discrete number of looks. Rather, it is a continuing process almost equivalent to an infinite number of dependent looks. If a pulsed laser were flashed exactly once per look, then exactly four looks are obtained. However, there is an improvement because the integration is continuous as opposed to an averaging of four separate cells.

Figure 5.1-13 shows a more detailed drawing of the correlator. The laser beam goes through a beam expander and a spatial filter primarily to produce a high quality plane wave. The signal film is moved past the beam, and the two spherical lenses, which are the transformer and re-transformer, can be considered as comprising a single one-to-one telescope. The telescope relays the image after it is filtered in both range and azimuth, weighted, and corrected for range migration, and relays that to the output where cylindrical optics of the azimuth telescope

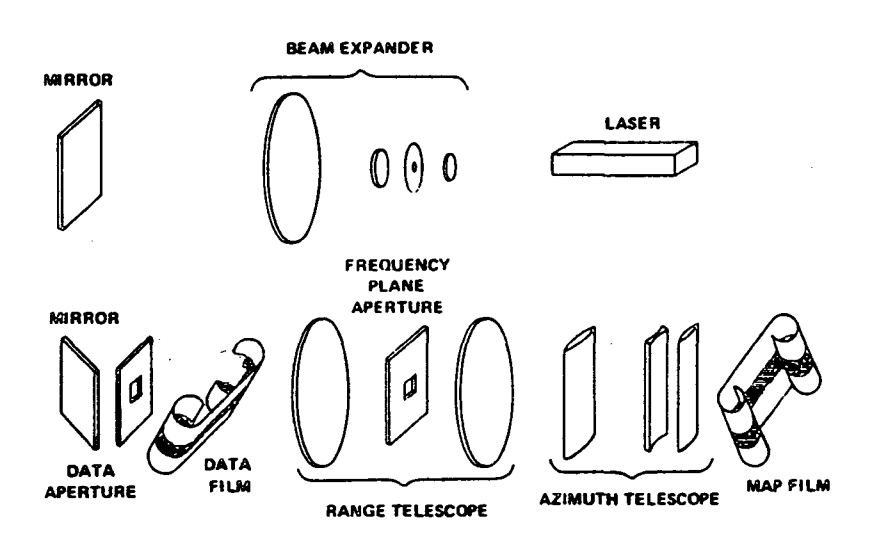


FIGURE 5.1-13 Tilted Plane Correlator

then operate on the data to bring the range and azimuth focal points into coincidence so that they are focused on the imaged film.

Normally, the signal film is stretched by some factor in azimuth; therefore, the cylindrical lenses also perform an additional function of obtaining a one-to-one aspect ratio in range and azimuth.

The range migration correction can be done perfectly at only one range to the target. The correction increasingly degrades the data with increasing distance from the center. Therefore, the data probably has to be processed in more than one range swath to prevent the degradation of the resolution by the correction. If all the data were processed in one swath with just one correction, the resolution would be degraded at the beginning and the end of the swath. The number of corrections required varies with the latitude of the data area because of the Earth's rotation. Correction in four sections is sufficient to correct for a 100 km swath to maintain a 25 m resolution for all latitudes. [8]

Synthetic Aperture Radar systems proposed, for the 1990's are currently under investigation by a number of NASA centers, contractors, and a few of the larger universities throughout the U.S. The primary focus is on data processing because of the impact on present data systems, i.e., Seasat-A SAR, and more importantly the effect on future systems by the volume of imagry to be generated by free-flyers (automated payloads) and Spacelab in the future.

During the period from August 1975 to May 1977, NASA sponsored numerous workshops to define future technology requirements for sensing and detection from space, user needs, and projected NASA missions. As a result of these workshops, a major thrust into three particular areas has been proposed: 1) provide a ten-fold increase in mission output through improved sensing accuracy, resolution, and spectral range by 1985; 2) reduce information system cost by 1 to 2 orders of

**REV. NO.: 2** 

REV. DATE: 31 Jan 1978

magnitude through extensive integration of sensor and on-board processing technology by 1985; and 3) provide the capability for near real-time, low-cost global
surveys through multipurpose. all-weather, active/passive microwave systems by 1990
[6] [11]. Current activities which support these goals will be addressed in the
remainder of this section.

Synthetic Aperture Radar systems perceived for free-flyer applications in the 1990's will include a digital processing capability. Free-flyers will be particularly useful in monitoring the dynamic features of our environment, such as sea state, soil moisture, biological growth, etc. These applications rely on timeliness of the image product so that near real-time processing and subsequent transmission to an appropriate site represents a highly desirable system capability. [1i]

Several NASA contractors and commercial companies are active in developing hardware and software for ground digital processing and limited on-board (aircraft) processing [7] [8].

The Jet Propulsion Laboratory (CIT) has proposed an effort to develop a stand-along real-time SAR digital data processor capable of producing 4-look, 25 resolution with 20 km swath width imagery utilizing Seasat-A digital raw data with an architecture such that it eventually could be used on spacecraft. Real-time production of 100 km swath width imagery will be required by 1990.

Figure 5.1-14 is a functional diagram of a digital processor. The analog to digital unit converts the analog signal from the data link to a digital format. Data corresponding to a swath interval is stored at a real-time rate in a buffer and transferred at a continuous lower rate to the digital recorder. The data is processed as a two-dimensional array as indicated in Figure 5.1-15. In the correlation process, the locus of points that the trace will go through in memory will follow a curved path.

REV. NO.: 2 REV. DATE: 31 Jan 1978

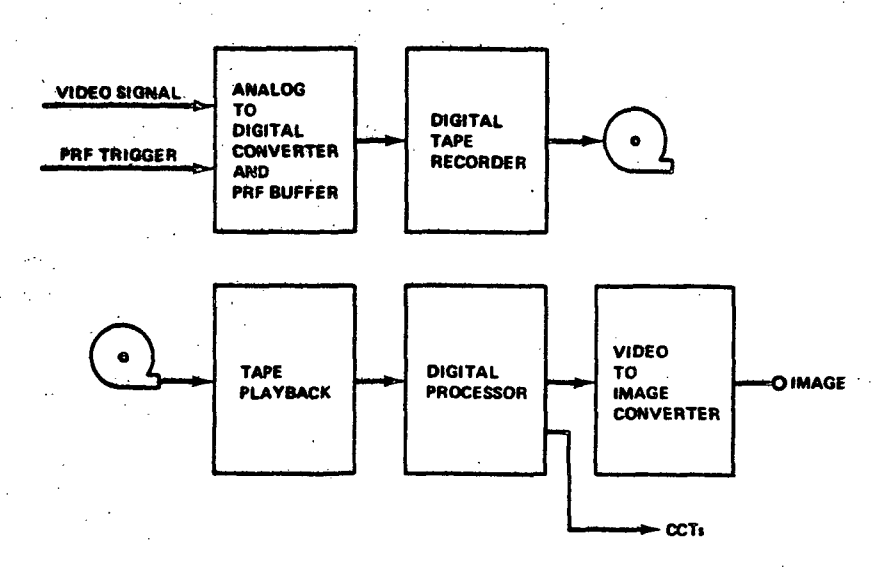


FIGURE 5.1-14 Digital Processor Functional Diagram

The azimuth correlation path depends on the range from the antenna to the correlation point and on the antenna boresight angle to the zero doppler line. Each image resolution cell has a unique correlation path and correlation function so that it is necessary to preserve the data as the correlation is made.

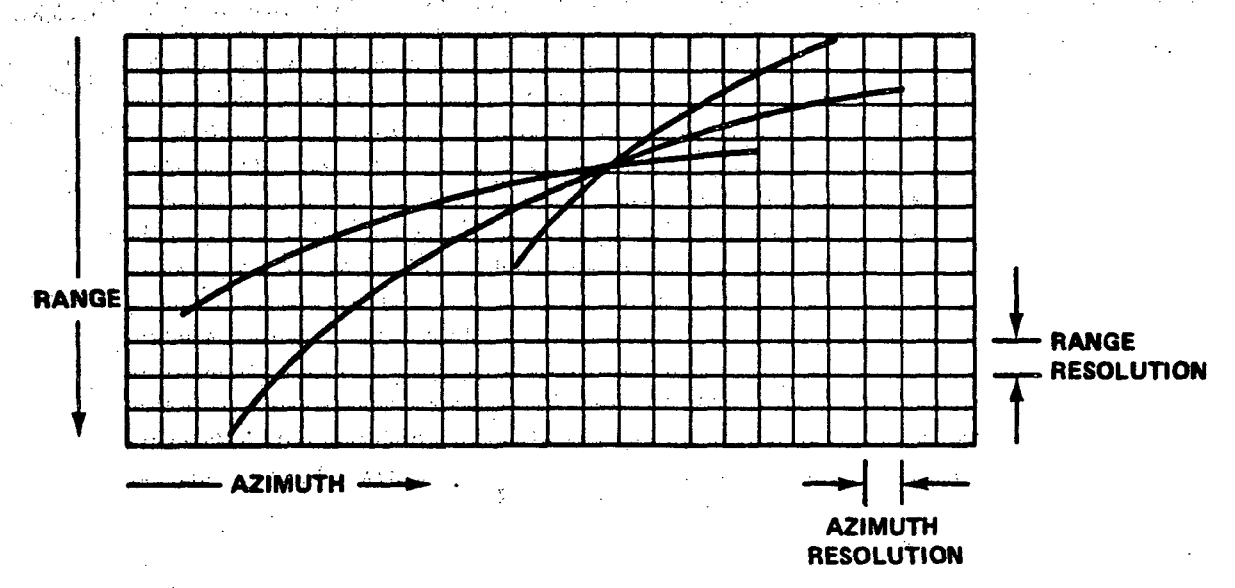


FIGURE 5.1-15 SAR Digital Data Processing

The procedures involved in digital processing are shown in Figure 5.1-16. Range compression may be accomplished before (as shown) or after azimuth compression.

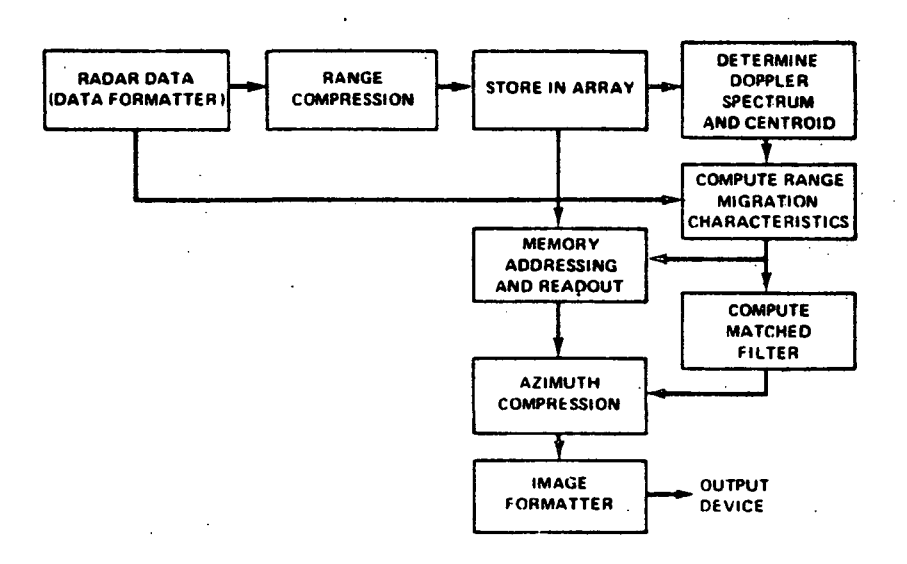


FIGURE 5.1-16 SAR Data Processing Flow

Table 1 lists the requirements for the processor if the data were processed for four separate looks and then added together. The assumptions made are: 1) 6 bits are required after range compression; 2) computation of 10 doppler spectra at 10 locations is sufficient to determine the centroid; 3) there is a 32 point interpolation accuracy between data points; 4) the matched filter has 5-bit accuracy.[8] memory consists of a very large array. Addressing is determining which element from the array will be pulled out for operations. Addressing has to be done with sufficient precision for interpolation within 1/32 of a sample between one data sample and the next. It has not been determined yet exactly what interpolation accuracy is required, but early indications are that a 32-point interpolation is The items that take a large amount of memory are the signal more than required. array, which stores about 10<sup>8</sup> bits, and the range migration correction. Although the range migration correction data is about one order of magnitude higher than the signal array, the number of operations is determined primarily by the azimuth compression, where 6.4 x  $10^{10}$  additions are needed to do one second of data. image formatter for this system has a fair amount of memory because the entire

TABLE 1 Requirements for SAR Digital Processor, Four Separate Looks

Element	Dynamic range, bits/sample	Input rate for 1:1 output, bits/s	Number of data-element, bits	Number of operations per second
Formatter	5	1.1 x 10 <sup>8</sup>	6.69 x 10 <sup>4</sup>	$2.2 \times 10^{7}$ $3.29 \times 10^{3}$ -16 KFFT
Range compression	6	1.1 x 10 <sup>8</sup>	8 x 10 <sup>4</sup>	$1.65 \times 10^8 - x$ $8.2 \times 10^7 - +$
Signal array	y 6	$2.34 \times 10^8$	$1.17 \times 10^8$	2.34 x 10 <sup>8</sup> Xfers
Memory addressing	31	••• • • • • • • • • • • • • • • • • • •	<b></b>	1.6 x 10 <sup>10</sup> Xfers 100-4 KFFT
Spectral analysis	6	1.98 x 10 <sup>6</sup>	4.8 x 10 <sup>4</sup>	$2.4 \times 10^6 - x$ $1.2 \times 10^6 - +$
Range- migration correction	31		1.2 x 10 <sup>9</sup>	3.88 x 10 <sup>7</sup> Xfers
Matched filt	ter 5	3.88 x 10 <sup>8</sup>	3.88 x 10 <sup>8</sup>	3.88 x 10 <sup>7</sup> look ups
Azimuth compression	9.	$^{-1.9} \times 10^{11}$	$4.25 \times 10^5$	$6.4 \times 10^{10} - x$ $3.2 \times 10^{10} - +$
Image formatter	11	$1.75 \times 10^8$	2 x 10 <sup>8</sup>	$8 \times 10^{7} - x$ 5.9 x $10^{7} - +$

image has to be stored for three-quarters of the synthetic aperture length. As the phase history of the tree comes in to the signal array, the first image begins to form. When one quarter of it passes through, an entire image for one look has already been generated. Now, that entire image needs to be stored while the remaining three quarters of the phase history is processed into the other three looks. Although this poses a memory problem, the number of operations for the image formatter is quite low.

Table 2 gives the processor requirements when the data is processed at full resolution and then four lines are added together to achieve the four looks. First of all, the image formatter is no longer necessary to store entire images. However, in azimuth compression, it is necessary to operate over four times as large an area for each image. If all the operations in this table were added together for the full resolution processing, the total data storage would be about  $2 \times 10^9$  bits as opposed to the four-look storage, which is only about  $1 \times 9^9$  bits.

Although the number of thousand-point transforms (KFFT) is the same, the number of transfers is more for the four solution method.

The growth of space-borne systems has been less dramatic than that of ground-based systems. Characteristics of some current or developmental space-borne computers are shown in Table 3, and projections are shown in Table 4. The progress in LSI technology and system architecture has made possible the design of on-board processors with high throughput rates. With the emphasis on the Shuttle program and the anticipated large volume of data collected onboard a spacecraft, NASA has contracted the General Electric Company to develop a processor for on-board real-time data processing applications. The GE processor employs a pipeline arrangement to perform arithmetic functions at a speed of 250 nsec. per function, with expectations to halve it to 125 nsec. The operational data rate is 100 megabits per second.

TABLE 2 Requirements for SAR Digital Processor,
Full Resolution
(pixel size - 8-m range, 5-m azimuth)

Element	Dynamic range bits/sample	Input rate for 1:1 input-output	Data number of elements MIG, bits	Number of operations per sec
Formatter	5	1.1 x 10 <sup>8</sup> /sec	6.69 x 10 <sup>4</sup>	2.2 x 10 <sup>7</sup>
Range compression	(5 in) <u>≻</u> 6 out	1.1 x 10 <sup>8</sup> bits	8 x 10 <sup>4</sup>	$3.29 \times 10^{3}$ -16 KFFT $1.65 \times 10^{8}$ -x $8.2 \times 10^{7}$ -+
Signal array	<u>≥</u> 6	234 M bits	$4.68 \times 10^{8}$	2.34 x 10 <sup>8</sup> replace
Memory addressing	31		· · · · · · · · · · · · · · · · · · ·	6.39 x 10 <sup>10</sup> Xfers
Spectral analysis	6	1.98 x 10 <sup>6</sup> bits	4.8 x 10 <sup>4</sup>	$100 - 4 \text{ KFFT}$ $2.4 \times 10^6 - x$ $1.2 \times 10^6 + +$
Range- migration correction	31	, <del></del>	1.2 x 10 <sup>9</sup>	3.88 x 10 <sup>7</sup> transfers
Matched filte computation	er 5	3.88 x 10 <sup>8</sup>	3.88 x 10 <sup>8</sup>	3.88 x 10 <sup>7</sup> look ups
Azimuth compression	11	7.66 x 10 <sup>11</sup>	1.3 x 10 <sup>5</sup>	$2.56 \times 10^{11} - x$ $1.28 \times 10^{11} - +$
Image formatting	11	2.13 x 10 <sup>8</sup>	5.2 x 10 <sup>5</sup>	$7.76 \times 10^{7} - x$ $3.88 \times 10^{7} - +$

REV. NO.: 1 REV. DATE: 30 Sept 1977

TABLE 3 Current or Developmental Spaceborne Computers

Type	Word Length (bits)	Add Time (µS)	Multiply Time (μS)	Memory Cycle Time (µS)	Memory Capacity (Words)
IBM 4Pi/EC	32	5	10	2.5	16K/132K
Bunker Ramo BR1018	18	6	28	1.0	4K/131K
CDC 469	16	2.4	10.4	1.6	0.5K/64K
Honeywell HDC-701	12	2.4	10.8	0.6	4K/16K

TABLE 4 Projections of Spaceborne Computers

Year Gate Delay (ns)		Add Time (ns)	Multiply Time (ns)	Memory Cycle Time (ns)
1975	• -	2,400	10,800	600
1980	4-6	100	770	100
1985	1.5-2	22-30	400-320	50
1990	0.8-1.5	12-22	170-320	20

With the development of space-qualified microprocessors, expected by 1980, the trend will be to decentralize the on-board computing. Individual processors will be used to replace hardwired logic in more and more of the instruments and subsystems. This form of distributed computing is comparable to the current Earth-based federated computer systems in which processors are dedicated to performing largely independent functions but can intercommunicate via data buses. Distributed computer configurations using identical microprocessors will offer increased capability at a lower cost in both hardware and software.

REV. NO.: 1 REV. DATE: 30 Sept 1977

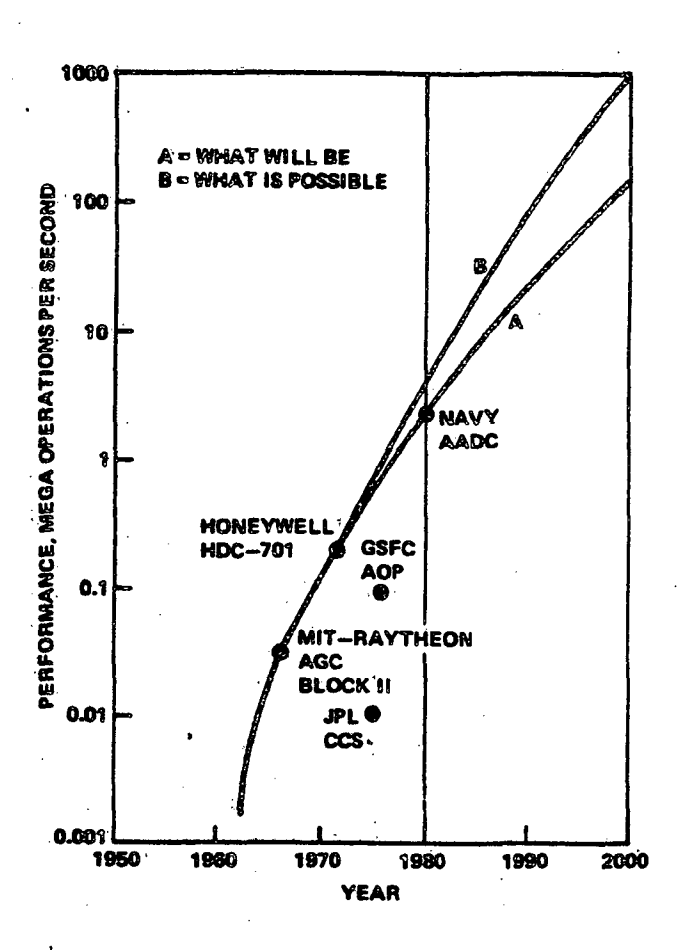


FIGURE 5.1-17 Performance of Spaceborne Computers

The use of a single, highly complex and expensive computer to perform a large number of computing tasks has been characterized by high costs in software development, verification and simulation. With a network of identical processors, all performing largely independent functions and operating at less than their full capacity, the software can be developed on an independent function-by-function basis using common software tools at a substantial reduction in effort and complexity.

The distributed computer system also offers an increase in overall system reliability. The loss of a single processor would not cause a complete system

failure as it would in a centralized computer system. Simple block redundancy would also be more easily implemented on a selected basis. The application of more complex forms of system architecture to provide higher levels of fault tolerance, as in the JPL STAR computer, is not expected to occur until the late 1990's. Control Data Corporation (CDC) has developed a processor which will handle range migration corrections and interpolations but not multiple look functions. CDC is currently operating an on-board (aircraft) computer which provides partial, or pre-processing of raw SAR data.

Other commercial companies working on SAR digital processing include Westinghouse (Baltimore, Md.), and Goodyear, Aerospace Div. Though both are presently concentrating on ground processing, their efforts are centered around handling small resolution elements (i.e.,  $5 \times 7$  meter) under conditions of large swath widths ( $50 \times 100 \, \mathrm{km}$ ).

The use of Charge Coupled Device (CCD) transverse filters provides a very powerful computational tool in the implementation of the correlators required in a SAR processor. [12] Texas Instruments, Inc., has built and tested a laboratory feasability breadboard, and an aircraft engineering model of a modular processor capable of analyzing SAR image data. The CCD filters utilized in these experiments are four-phase surface channel devices having split electrode weighting.

The achievement of high range resolution implies the use of wideband chirp signals for a pulse compression radar. The use of a surface wave device range chirp correlation filter is an alternative capable of accommodating the required bandwidths. However, the time windows commensurate with the achievable range resolution are typically tens of nanoseconds, and are difficult to handle with A/D conversions and digital techniques.

The use of a modular processor concept in which each module processes on the order of 200 range cells, makes it possible to sample the radar video at a high

REV. NO.: 2 RE

rate during a small time window corresponding to the module's swath width once each Pulse Repetition Interval (PRI). The number of samples to be stored is the number of samples required to cover the swath plus the number of bits in the range correlator. While the input sampling rate is constrained by Nyquist considerations, the output data rate is constrained by the PRI making time expansion of the video possible in order to reduce the processor module's data rate to one commensurate with CCD transversal filter operation. Subsequent processing speeds may easily be handled with present CCD technology. Another advantage of such a buffering technique is that radar data from an appropriate range swath may be recorded on a conventional instrumentation tape recorder having a few hundred kilohertz bandwidth.

In order to form a 200 x 200 element picture with this breadboard, a TI 960A computer with 28K memory used in conjunction with a 1,100,000 word disk memory and a nine-track, 800-BPI magnetic tape unit were used. The simulated radar echo pulses were transferred from the tape to the disk. The simulated radar bursts correspond to radar returns from a swath of interest at sequential azimuthal locations. By recirculating this sequence of bursts to the breadboard while sliding the azimuth read-in time window across the swath time, a complete picture can be processed an azimuth column at a time. To reconstruct the picture, the output of the azimuth correlator is digitized and stored in memory. The memory can then be used much as a scan converter to refresh a CRT display.

The time required to process a 200 x 200 element picture is 1 1/3 hours due to the long azimuth correlation time. Real-time processing could be accomplished by expanding the system to 200 azimuth correlators.

Improvements in SAR processors may be expected in the areas of improved resolution, multiple look imagery, focusing, motion compensation, and wider dynamic range.

Software development for image processing is still in the preliminary stage.

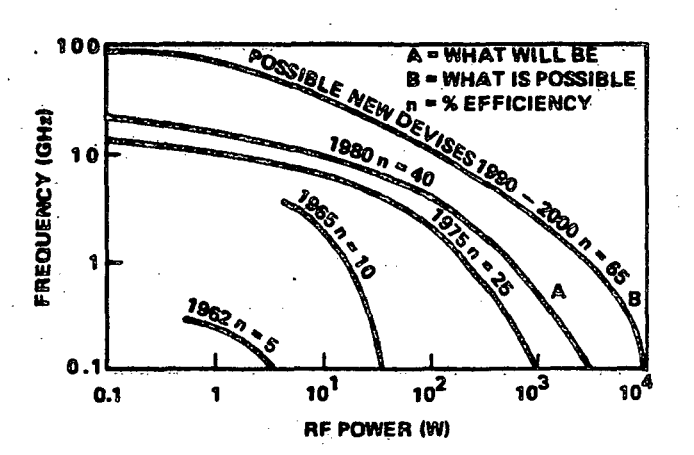
Goodyear's Sapphire Program nearly meets current requirements but lacks the

REV. NO.:

capability of correcting for range migration. Of the possible algorithm candidates which may be utilized only two support a moderately complex processor, these are: 1) the maximum likelihood algorithm; and 2) the table look-up algorithm. former is a statistical procedure based on the probability density function of the data. For the case of Gaussian data, which is a valid model for microwave imagery of the earth's surface, only first and second order statistics are required. A system based on this approach is designed by calculating these statistics from data samples of known classes and then assuming that all data from the same class have these same statistics. This approach seems well suited to large area seastate data processing. The table look-up algorithm essentially stores in a large table (computer memory) all possible outcomes of the data and associates with each possible outcome one of the classes associated with each of the possible values of the input data. Subsequent data are then classified by using the data point to address the memory to look up the classification. Both algorithms require a significant amount of computation, mainly additions, multiplications and comparisons. The table look-up algorithm requires a much smaller amount of computation but significantly more memory.

The wavelength of SAR transmitters is a subject of prime concern not only as a function of reflection from the illuminated phenomenon but also from the standpoint of power consumption and reliability. The Seasat-A SAR is an L-band system ( $\lambda \simeq 23 \, \mathrm{cm}$ ) and allows use of solid state amplifier components such as TRAPATT (Trapped Plasma Avalanche Triggered Transit) and IMPATT (Impact Avalanche Transit Time) devices. For applications requiring shorter wavelengths such as Ku-band for ocean windfields the current state-of-the-art demands klystrons or TWT's. Both of these devices require higher operating power and offer lower reliability than the longer wavelength solid state devices. Figures 5.1-18 and 5.1-19 illustrate the projected advances in solid state and TWT amplifiers. [6]

REV. NO.: 2



ORIGINAL PAGE IS OF POOR QUALITY

FIGURE 5.1-18 Solid-State Power-Frequency Characteristics

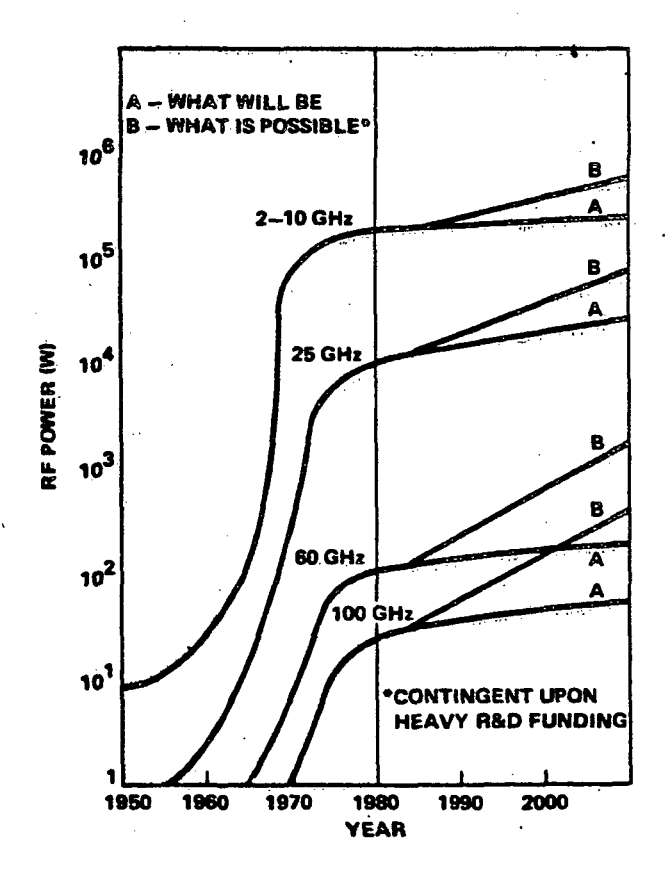


FIGURE 5.1-19 TWT RF Power

REV. NO.: 1

**REV. DATE: 30 Sept 1977** 

During the next decade, continued development of present microwave solidstate devices will increase their frequency and power capabilities and lower their
noise figures. As we have learned from the past, however, technology is an everevolving phenomenon and it can be expected that the present solid-state concepts
will give way to newer and better ones. Bulk effects will be discovered which will
increase solid-state power performance. Even now, traveling-wave effects are being
found and explored for higher solid-state gain. Low-loss matched front ends are
required for improved performance of both active and passive microwave systems.
Integrated microwave circuits can achieve this goal by eleminating cables, connectors, matching elements, and discrete components which degrade overall system
performance. Integration also implies miniaturization, which results in better
thermal stability. Feasibility demonstrations of advanced, space qualified frontend hardware are scheduled for September 1980. [10] [14]

Multiple frequency band SAR operation is a realty now (i.e., aircraft and ground tests) and is already planned for Shuttle applications in the 1980's. [10] Multiple frequency, dual polarization, and decreasing resolution size are the main drivers behind current antenna design. The chronology for multipurpose radar imagers will initially be Shuttle sorties, and will ultimately be used operationally on longer duration earth orbiting platforms.

SAR antenna design represents a particularly active area in the development of future sensors. User agencies have needs for high-resolution, wide-swath imagery. Present antennas cannot meet these needs, especially in the L- and Kuband region. Currently under investigation are deployable, large, electrically steered phased arrays. A combination of antenna elements with distributed active devices can provide low-noise passive and high-power active capability. An initial study of phase array antennas will be completed June 1979, followed

5.1.33

by a hardware feasibility study in 1980, and flight feasibility tests in September of 1981. [10] Paralleling this effort is a planned (1982), agriculturally oriented Shuttle Imaging Radar (SIR) employing a dual frequency SAR. [14] Scientists at the Remote Sensing Laboratory, University of Kansas, are currently gathering ground truth information with a vehicle mounted SAR in support of future SAR configurations. [6] The Space-borne Imaging Radar scheduled for 1979 is a geology experiment utilizing a modified (look angle) Seasat-A SAR.

REV. NO.: 2

## SYNTHETIC APERTURE RADAR LIST OF ACTIVE CONTRIBUTORS

Bill Carls
Manager, Seasat-A SAR Ground Data Processing
Jet Propulsion Laboratory
California Institute of Technology
4800 Oak Grove Dr./Pasadena, Ca. 91103
(213) 354-3386

Dr. John W. Rouse, Jr. Director, Remote Sensing Center Professor, Dept. of Elec. Engr. Texas A&M University College Station, Texas 77843 (713) 845-5422

Dr. David S. Simonett Professor of Geography, USC at Santa Barbara Santa Barbara, Ca. (805) 961-2344

Rolando Jordon
Group Supervisor
Space Radar and Microwave Radiometry Section
Jet Propulsion Laboratory
California Institute of Technology
4800 Oak Grove Dr./Pasadena, Ca. 91103
(213) 354-4442

Dr. Charles Elachi Principle Investigator for Shuttle Imaging Radar Planetology and Oceanography Section Jet Propultion Laboratory California Institute of Technology 4800 Oak Grove Dr./Pasadena, Ca. 91103 (213) 354-5673

Dr. Robert K. Moore Remote Sensing Laboratory Space Sciences Building, Irving Hill Drive University of Kansas Lawrence, Kansas 66045 (913) 864-4836

Dr. Fawaz Ulaby Remote Sensing Laboratory Space Sciences Building, Irving Hill Drive University of Kansas Lawrence, Kansas 66045 (913) 864-4836

REV.DATE: 30 Sept 1977

Dr. H. C. McDonald
Department of Geology
University of Arkansas
Fayetteville, Arkansas 72701
(501) 575-3355

REV. NO.: 1 REV. DATE: 30 Sept 1977

## SYNTHETIC APERTURE RADAR POOR QUALTY

- [1] Kovaly, John J., "Synthetic Aperture Radar," AR Tech House, Inc., Dedham, Massachusetts, 1976.
- [2] Klauder, et. al., "The Theory and Design of Chirp Radars," The Bell System Technical Journal, Vol. 39, No. 4, July 1960.
- [3] Brown, W. M. and Procello, L. J., "An Introduction to Synthetic Aperture Radar," IEEE Spectrum, Vol. 6, No. 9, pp. 52-62
- [4] Liutz, Joeseph, Jr. and Simonett, D. S., "Remote Sensing of Environment," Addison-Wesley Publishing Co., Reading, Massachusetts, 1976.
- [5] Harger, Robert O., "Synthetic Aperture Radar Systems, Theory and Design," Academic Press, New York, 1970
- [6] Sensors Workshop Summary Report
- [7] Jones, R. A., and Preston, K., Jr., <u>Digital Simulation and Processing Applied to Coherent Imaging System</u>, <u>TEEE Transactions</u>
  Systems, Vol. CAS-22, No. 3, March 1975, pp. 293-303.
- [8] Seasat-A Data Processing for a SAR from a Earth-Orbiting Spacecraft, Published by JPL from a presentation by Rolando Jordan and Thomas Bicknell, April 23, 1976, JPL 622-8.
- [9] Satellite On-Board Processing for Earth Resources Data, Summary Report, Contract NAS 2-8327, AMES Research Center, October 1975.
- [10] The JPL Microwave Program, An outline of a presentation to NASA Headquarters, February 11, 1977.
- [11] Personal communication with Dr. Rolando Jordan, Dr. Charles Elachi, and Mr. Bill Carls at JPL, and Dr. David Simonett at USC (Santa Barbara), September 1977.
- [12] Bailey, W. H., et. al., "A Synthetic Aperture Processor Using CCD Signal Processing Techniques," Conference on Charge-Coupled Device Technology and Applications, November 30 December 2, 1976, Sponsored by NASA & JPL, JPL SP 43-40, pp. 21-27.
- [13] "A Forecast of Space Technology 1980-2000," SP-387, January 1976.
- [14] Remote Sensing Instrument Performance Data Sheets, JPL-624-2, 1977.

5.1.37

### SYNTHETIC APERTURE RADAR BIBLIOGRAPHY

- (1) Sherwin, C. W., et. al., "Some Early Developments in Synthetic Aperture Radar Systems," <u>IRE Transactions on Military Electronics</u>, April 1962.
- (2) Curtona, L. J., et. al., "On the Application of Coherent Optical Processing Techniques to Synthetic Aperture Radar," Proceedings of the IEEE, August 1966.
- (3) Brown, William M., "Synthetic Aperture Radar," IEEE Transactions on Aerospace and Electronic Systems, March 1967.
- (4) Rhodes, W. T., Digital Processing of Synthetic Aperture Optical Imagery, Optical Engineering, Vol. 13, No. 3, May/June 1974, pp. 267-274.
- (5) Active Microwave Workshop Report, NASA SP-376, Lyndon B. Johnson Space Center, 1975.
- (6) Kirk, J. C., Jr., "A Discussion of Digital Processing in Synthetic Aperture Radar," IEEE Transactions on Aerospace and Electronic Systems, Vol. AES-11, No. 3, May 1975, pp. 326-337.
  - (7) Buss, D. D., Collins, D. R., Bailey, W. H., and Reeves, C. R., "Transversal Filtering Using Charge Transfer Devices," <u>IEEE Solid State Circuits</u>, SC-8, April 1973, pp. 134-146.
  - (8) Bailey, W. H., Eversole, W., Holmes, J., Arens, W., Hoover, W., McGehee, J., and Ridings, R., "CCD Applications to Synthetic Aperture Radar," <u>Proc. of CCD Applications Conference</u>, San Diego, October 1975, pp. 301-308.
  - (9) Hewes, C. R., "A Self Contained 800 Stage CCD Transversal Filter," <u>Proc. of CCD Applications Conference</u>, San Diego, October 1975, pp. 309-318.
- (10) Cook, C. E., and Bernfeld, M., Radar Signals: An Introduction to Theory and Applications, New York: Academic Press, pp. 152, 1967.
- (11) Bailey, W. H., Buss, D. D., Hite, L. R. and Whatley, M. W., "Radar Video Processing Using the CCD Chirp Z Transform," Proc. of CCD Applications Conference, San Diego, October 1975, pp. 283-290.
- (12). "A Forecast of Space Technology 1980-2000," NASA SP-387, January 1976.
- (13) Bremar, J. W., "Hardware Technology in the Year 2001," Computer, December 1976, p. 31.

REV. NO.:

- (14) Julinssen, J. E., "Magnetic Bubble Systems Approach Practical Use," Computer Design, October 1976, p. 81.
- (15) "Space Shuttle Advanced System/4Pi Prototype Input/Output Processor (IOP) Functional Description, IBM File No. 74-A31-016, October 25, 1974.
- (16) Hodges, D. A., "Trends in Computer Hardware Technology," Computer Design, February 1976, p. 77.
- (17) OAST Space Theme Workshop, Vol., V., April 26-30, 1976.
- (18) Advanced Scanners & Imaging Systems for Earth Observations, NASA SP-335, December 11-15, 1972.
- (19) "Satellite On-Board Processing for Earth Resources Data," Wintek Corporation, October 1975, N-76-16592.

CFOPOOR QUALITY

REV. DATE: 30 Sept 1977

RFV. NO.: 1

## SYNTHETIC APERTURE RADAR ILLUSTRATION CREDITS

Figure No.	Page	Reference	Page
5.1-1	5.1-3	[3]	52
5.1-2	5.1-4	[4]	54
5.1-4	5.1-7	[3]	54
5.1-5	5.1-9	[4]	251
5.1-6	5.1-10	[4]	252
5.1-7	5.1-12	[4]	254
5.1-8	5.1-14	[3]	61
5.1-9	5.1-16	[3]	60
5.1-10	5.1-17	[8]	4-3
5.1-11	5.1-17	[8]	4-6
5.1-12	5.1-18	[8]	4-14
5.1-13	5.1-19	[8]	4-15
5.1-14	5.1-22	[8]	4-19
5.1-15	5.1-22	[8]	4-21
5.1-16	5.1-23	[8]	4-23
5.1-17	5.1-28	[13]	3-84
5.1-18	5.1-32	[13]	3-43
5.1-19	5.1-32	[13]	3-43
SIR(8)	5.1-46	[14]	AM-2-14-4

#### RSDH DATA SHEET

SHEET	1	OF	4
-------	---	----	---

(1) SENSOR NAME, ACRONYM: SEASAT-A Synthetic Aperture Radar - SAR

(2) DISCIPLINE: Earth and Ocean Physics (3) SUBDISCIPLINE: Ocean Dynamics

#### (4) APPLICATION AND OBJECTIVE:

The SAR is put into near polar earth orbit and earth-oriented to obtain microwave imagery at 1275 MHz of the sea surface. This data is to be conveyed to ground stations in real time. The object is to discern the length and direction of ocean waves, the size, location and speed of sea ice, oil spill and coastal features.

(5) HERITAGE/KEY PERSONNEL: The only satellite-borne SAR flown prior to 1976 was the Apollo Lunar Sounder Experiment. It produced profiles on the lunar sub-surface at 5, 15 and 150 MHz.

Instrument Rep: Frank T. Barath (JPL) 213-354-5431 or Frank Schutz 213-354-5392

#### (6) SENSOR DEPLOYMENT:

The SEASAT-A satellite, bearing the SAR is to be launched to attain a near-polar orbit of 108° inclination and altitude of 790 km. The period will be approximately 100 minutes resulting in 14 1/2 orbits per day. This yields complete ocean coverage in 12 hours.

(7)

#### SENSOR CHARACTERISTICS

#### (7A) CAPABILITIES AND CONSTRAINTS OF THE SENSOR TO ACQUIRE THE MEASURED PARAMETER:

Using an antenna measuring 10 m (azimuth) x 2 m (elevation) the SAR receives reflected radiation from a swath of 100 km width, starting 250 km off nadir. Data is transmitted directly to ground via S-band link, video pass band is 2-21 MHz. No on-board storage is provided due to high data rates. The average on-time is 10.85 min. over each of the following STDN: Alaska, Goldstone, Rosman, Madrid and Orroral.

#### (7B) ACTIVE SOURCE CHARACTERISTICS (FOR ACTIVE SENSORS):

The swath is illuminated by 1275 MHz microwave pulses of 32 microsecond duration occurring at 1400 pps. The transmitter is operated at a peak power level of 800 watts. Azimuth compression ratio is 155:1. Range compression ratio is 576:1. Transmitter operates in 4 modes: standby, on, operate, calibrate. Mode is selectable by ground command.

#### (7C) DETECTOR MEASUREMENTS CHARACTERISTICS:

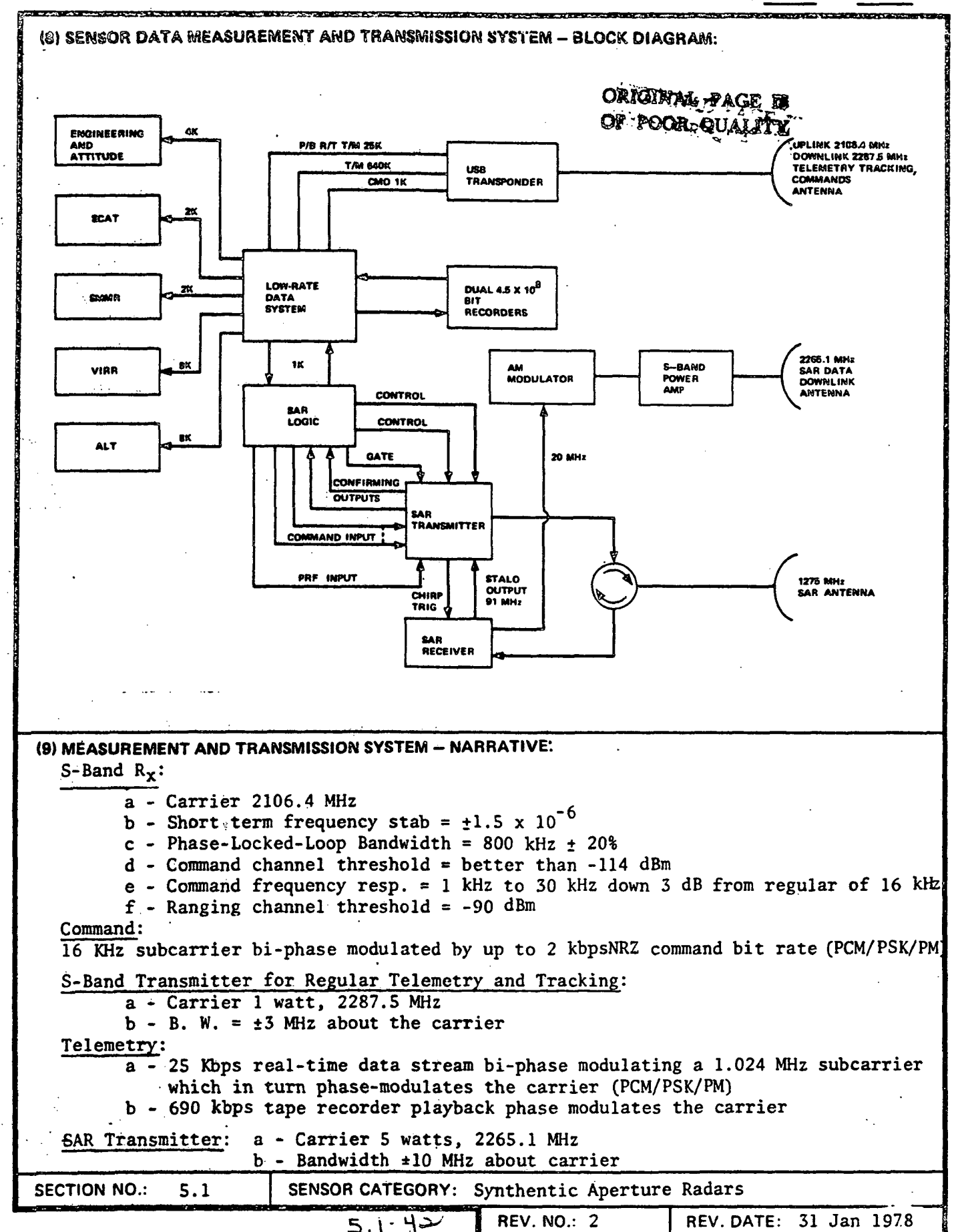
Spatial resolution of the system is 25 m. System noise figure is 2 dB.

5.1-41

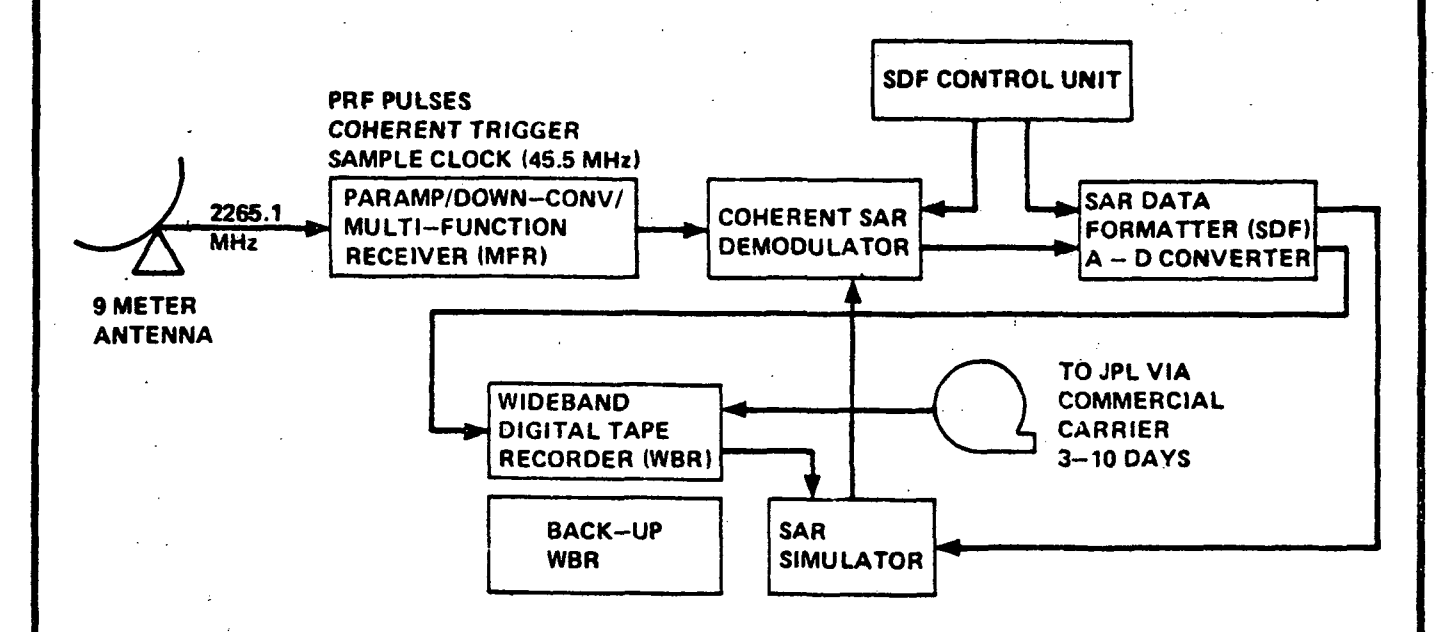
SECTION NO.: 5.1

SENSOR CATEGORY: Synthentic Aperture Radars

REV. NO.: 2



#### (10) SENSOR DATA RECEPTION AND PROCESSING - BLOCK DIAGRAM:



STDNS process the following Data Streams for SEASAT-A;

- 1 Low-rate real-time telemetry (32 kbps max.)
- 2 Low-rate playback telemetry (640 kbps min., 800 Kbps max.)
- 3 SAR Analog (2-21 MHz)
- 4 Command data (1-2 kbps)
- 5 Range/Range rate tracking data

Output of the Demodulator consists of the following:

- (a) Analog radar return signal 2-21 MHz,
- (b) Pulses occurring at the PRF of the SAR sensor,
- (c) A coherent trigger signal which is coincident with the desired leading edge of the radar return signal.
- (d) A sampling clock which is coherent with SAR sensor timing and equal to half the SAR sensor STALO frequency (i.e., approximately 45.5 MHz).

#### (11) RECEIVING AND PROCESSING - NARRATIVE:

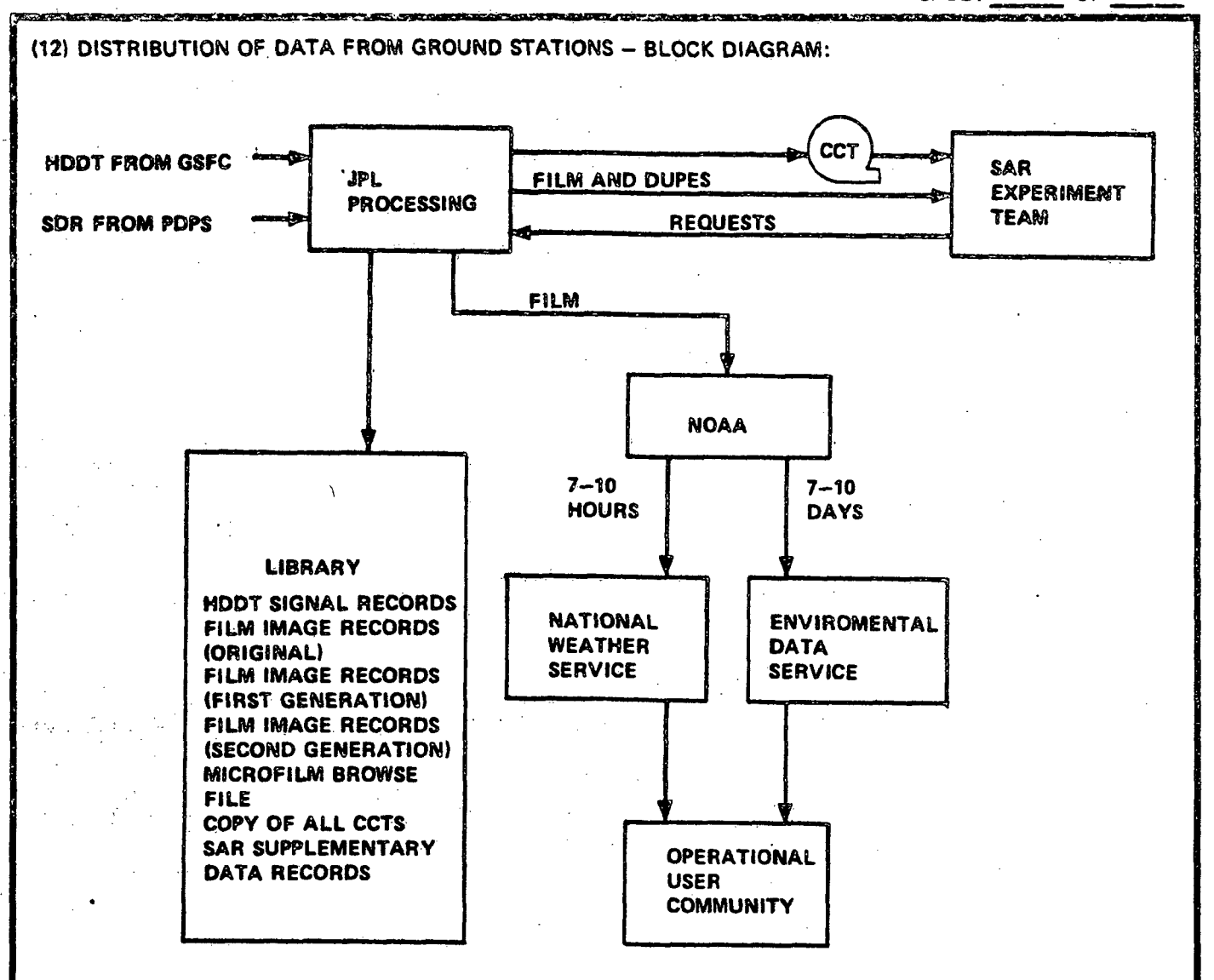
Recorded information includes (in addition to raw radar return):

- a Frame synchronized low rate real-time telemetry,
- b Predicted operational orbit information from tracking data processor,
- c Universal time tag of the coherent trigger signal, accurate to within 1 millisecond and containing day of year information,
- d The PRF/STC delay words which are extracted from the real-time data stream and used to set-up the demodulator, and
- e Configuration status of the ground station equipment, including STDN I.D. and operational parameters of the demodulator and ADC.

5.1.43

SECTION NO.: 5.1 | SENSOR CATEGORY: Synthemic Aperture Radars

REV. NO.: 2



#### (13) DATA DISTRIBUTION - NARRATIVE:

The optically processed film supplied by JPL will not be fully corrected geometrically or radiometrically. These films will be provided in strips covering 30 to 50 km of the radars' 900 km swath. Photo mosaics are created by matching appropriate film strips.

**SECTION NO.:** 

5.1

SENSOR CATEGORY:

Synthentic Aperture Radars

5.1-44

REV. NO.: 2

#### RSDH DATA SHEET

SHEET 1 OF 4

(1) SENSOR NAME, ACRONYM: Shuttle Imaging Radar (SIR)

(2) DISCIPLINE: Earth Observations (3) SUBDISCIPLINE: Land Monitoring

#### (4) APPLICATION AND OBJECTIVE:

The SIR is a synthetic aperture imaging radar which will utilize a spacecraft platform. The purpose of the SIR will be to gather image data at microwave frequencies for application to a variety of earth observation studies planned for the Space Shuttle.

#### (5) HERITAGE/KEY PERSONNEL:

Principle Investigator: Dr. K. Krishen, NASA-JSC 512-483-6287

#### (6) SENSOR DEPLOYMENT:

The SIR will be deployed by the Shuttle (sortie) and will have a variable orbit from 200 to 400 km at inclinations of 90°. The SIR will be designed for 7-day sortie missions with a useful life of approximately 5 years with refurbishment. The engineering model is planned for 1981 and the operational model is projected for 1982.

(7) • SENSOR CHARACTERISTICS

#### (7A) CAPABILITIES AND CONSTRAINTS OF THE SENSOR TO ACQUIRE THE MEASURED PARAMETER:

The SIR will transmit horizontal or vertical polarized power at X- and L-band frequencies and receive the backscatter data with dual-polarized, dual frequency antennas. The returned signals are received, amplified, and converted to digital format for later conversion to Image data. On board monitor functions are also provided.

#### (7B) ACTIVE SOURCE CHARACTERISTICS (FOR ACTIVE SENSORS):

Traveling Wave Tubes (TWT) provide the X-band (10 GHz) and L-band (1 GHz) microwave energy. Simultaneous transmission in the form of a pulse (15-25µs) with a repetition rate of 1200-1880 kHz allow nearly identical swaths to be illuminated for correlation after the returns are processed. Four different antennas are used for X-band transmission providing horizontal and vertical polarization at 25° off nadir. A beam width of 38° results in a total X-band coverage of 7° to 60° off nadir. Scanning is provided through vehicle motion. Two L-band antennas are sited at (TBD) of nadir with a beam width of (TBD).

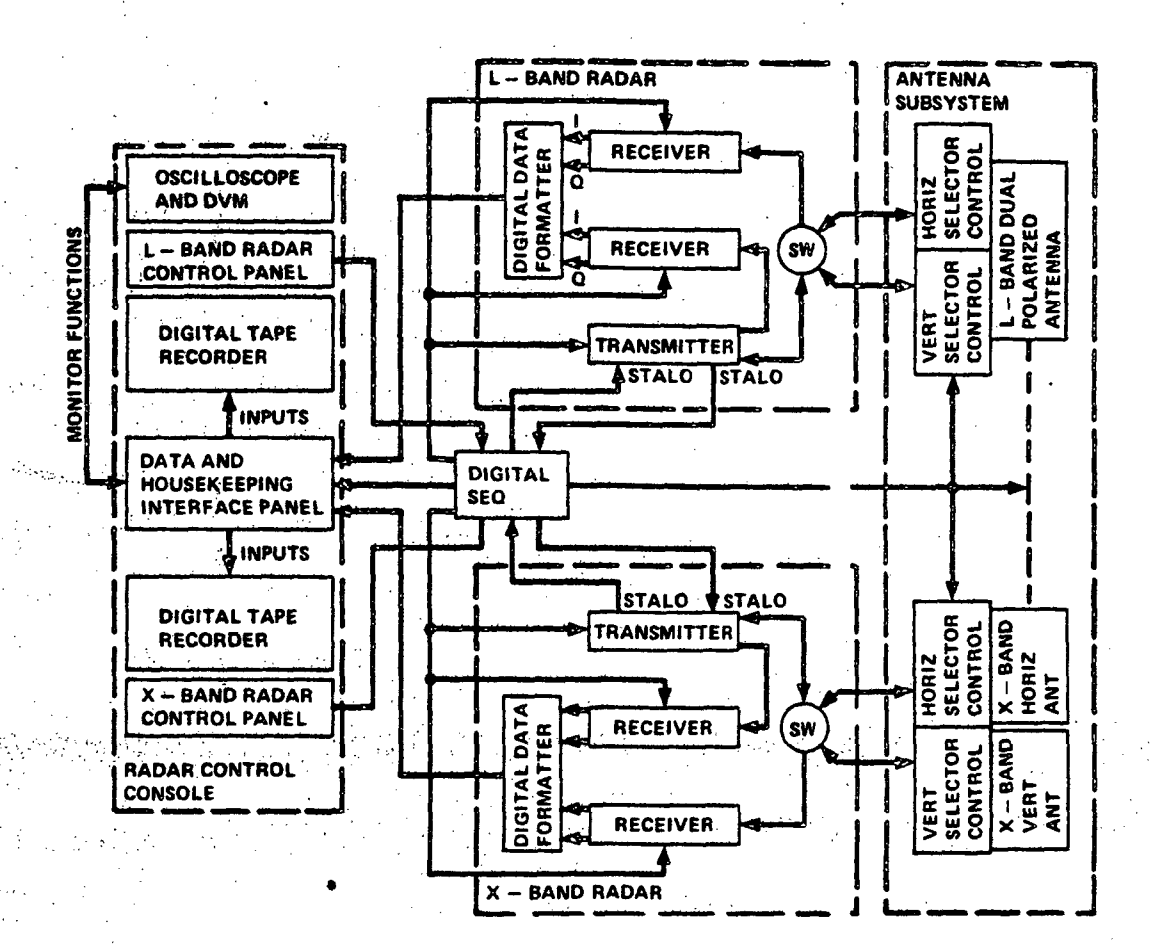
#### (7C) DETECTOR MEASUREMENTS CHARACTERISTICS:

Receivers for both bands are similar. The sequence in processing the microwave return is: pre-amplification, single conversion super-heterodyne, and pulse compression (4000:1 ratio) with range gates. Noise temperatures are 1100° and 1600°K and noise figures are 2:5 and 4 for L and X band respectively. Bandwidth for either receiver is >35 MHz (TBD) and dynamic range is >50 dB (8 bit conversion).

5.1-45

SECTION NO.: 5.1 SENSOR CATEGORY: Synthetic Aperture Radars

#### (8) SENSOR DATA MEASUREMENT AND TRANSMISSION SYSTEM — BLOCK DIAGRAM:



#### (9) MEASUREMENT AND TRANSMISSION SYSTEM - NARRATIVE:

Data will be digitized on-board and stored on magnetic tape (240 Mbps tape recorder in development).

5.1-46

SECTION NO.:

5.1

SENSOR CATEGORY:

Synthetic Aperture Radars

REV. NO.:

### **DATA SHEET**

:	SHEET	- 3	OF	4

(10) SENSOR DATA RECEPTION AND PROCESSING - BLOCK DIAGRAM:

Not Applicable.

#### (11) RECEIVING AND PROCESSING - NARRATIVE:

Data is stored on tape on-board and will be returned to ground via Shuttle. Correlation with other image data will be accomplished by ground processing.

5.1.47

SECTION NO .:

5.1

SENSOR CATEGORY: Synthetic Aperture Radars

REV. NO.:

SENSOR CATEGORY: Synthetic Aperture Radars SECTION NO .: 5.1 REV. NO.: 2

# SENSOR CATEGORY TABLE OF CONTENTS AND REVISION CONTROL SHEET

	_			T	
SENSOR NAM OR	E	NUMBER OF	PAGE	EFFECTIVE	
OTHER ENTRY		PAGES			REV. NO.
Section 5.2 Table of	Contents	1	5.2-i	31 JAN 78	2
Introduction to Altim	eters	17	5.2-1 · 5.2-2	30 JUN 77 30 JUN 77	0
			5.2-3 5.2-4	30 JUN 77	0
·	,	·	5.2-5	30 JUN 77	0
		*	5.2-6 5.2-7	30 JUN 77 31 JAN 78	0 2
	,		5.2-8 5.2-9	31 JAN 78 30 JUN 77	2 0
			5.2-10 5.2-11	30 JUN 77 30 JUN 77	0
·			5.2-12 5.2-13	31 JAN 78 31 JAN 78	2 2
			5.2-14 5.2-15	30 SEPT 77 30 SEPT 77	1
			5.2-16 5.2-17	30 SEPT 77 30 SEPT 77	1
Radar Altimeter (ALT)	, SEASAT-A	4	5.2-19	31 JAN 78	2
ganderi me orbjeker prince (i 20	The state of the s		5.2-20 5.2-21	31 JAN 78	$(x, x, y, \frac{2}{2}, x, y, y, y)$
·			5.2-22	31 JAN 78	2
•			•		
	.•				
,	·				
·			`		
					·
				•.	
				٠.	
SECTION NO.: 5.2	SENSOR CATEGORY				
	5.2·i	REV. NO.:	2 RI	EV. DATE: 31	Jan 1978

This page intentionally left blank.

REV. NO.:

REV. DATE: 30 June 1977

## Section 5.2 INTRODUCTION TO ALTIMETERS

The current state-of-the-art in altimetry takes the form of a microwave radar. In all activities to date, the role of altimetry has been visualized to include detection of dynamic ocean features (tides, waves, currents, etc.) or mapping of permanent mean ocean surface topography (geoid). Also, subsurface geological features, known to affect the ocean geoid, have been affirmed with the Skylab altimeter and could result in new applications of altimetry for bathymetric positioning of underwater topographic features. [1]

Data collection techniques, while limited to nadir viewing, provide accurate global mapping in the range of centimeters for altitude and meters for wave height. The precision with which geophysical units are inferred, however, is dependent on ground support systems and techniques such as laser tracking, ephemeris data, ground truth, orbit calibration, etc.

Initial experiments in altimetry relied on short-pulse (or pulse-limited) techniques to achieve required range resolution. This technique is described below. With the evolution of satellite measurement systems a new method of resolving range for sea state information developed called chirp radar. The result of this method is an effective compression of the transmitted pulse width. This technique is also described, along with further explication relating to a specific sensor program.

An orbiting microwave altimeter transmits a pulse with an effective spatial length that is short compared to typical wave heights (e.g., less than 0.5 m). As the pulse interacts with waves beneath the satellite, it is scattered back toward the satellite by specular points on the larger gravity waves. The short pulse is "stretched" temporarily by the ocean waves, and the degree of this stretching is a

**REV. DATE: 30 June 1977** 

0

direct measure of the mean heights of the waves at the suborbital point.

The radar cross section can be expressed as a function of the height of the radar pulse interaction region, as shown in equations (1) and (2). From specular-point theory, backscattered strength from N specular points is

$$\sqrt{\sigma_B} = \sum_{t=1}^{N} \pi g_i e^{f(2k_0 z_i \cos \theta)}$$
 (1)

where:

g; = curvature at the ith specular point

Z; = height of the ith specular point above mean surface

k = radar wave number

 $\theta$  = angle of incidence from vertical

When equation (1) is squared, written as a distribution over height, and averaged, it becomes

$$\int_{0}^{4} \hat{\eta}^{\circ} (Z) = \pi \int_{0}^{\infty} n(Z,g)g \, dg \qquad (2)$$

where  $\eta^{\circ}$  (Z) is the average backscatter cross section per unit area per unit height increment at height Z, and  $\eta(Z,g)$  is the average number of specular points per unit area for heights between Z and Z+dZ and for Gausian curvature between g and g+dg.

The physical illustration of a radar pulse of spatial width  $\Delta Z$  cos  $\theta$  = (ct)/2 advancing over the ocean is shown in Figure 5.2-1. If this model is used, and it is assumed that a symmetric Gaussian distribution of sea-wave heights exists, the expression in equation (3) is obtained for the average radar cross section of the sea as a function of time. Radar altimeter power return (H  $\ll$  a) is

$$G^{2}\sigma(t) = \sqrt{\pi}^{3} \frac{Hx}{s^{2}} \exp \left[ \left( \frac{t}{t_{s}} \right)^{2} - \frac{2t}{t_{s}} \right] \left[ 1 - \phi \left( \frac{t}{t_{s}} \right) - \frac{t}{t_{p}} \right]$$
 (3)

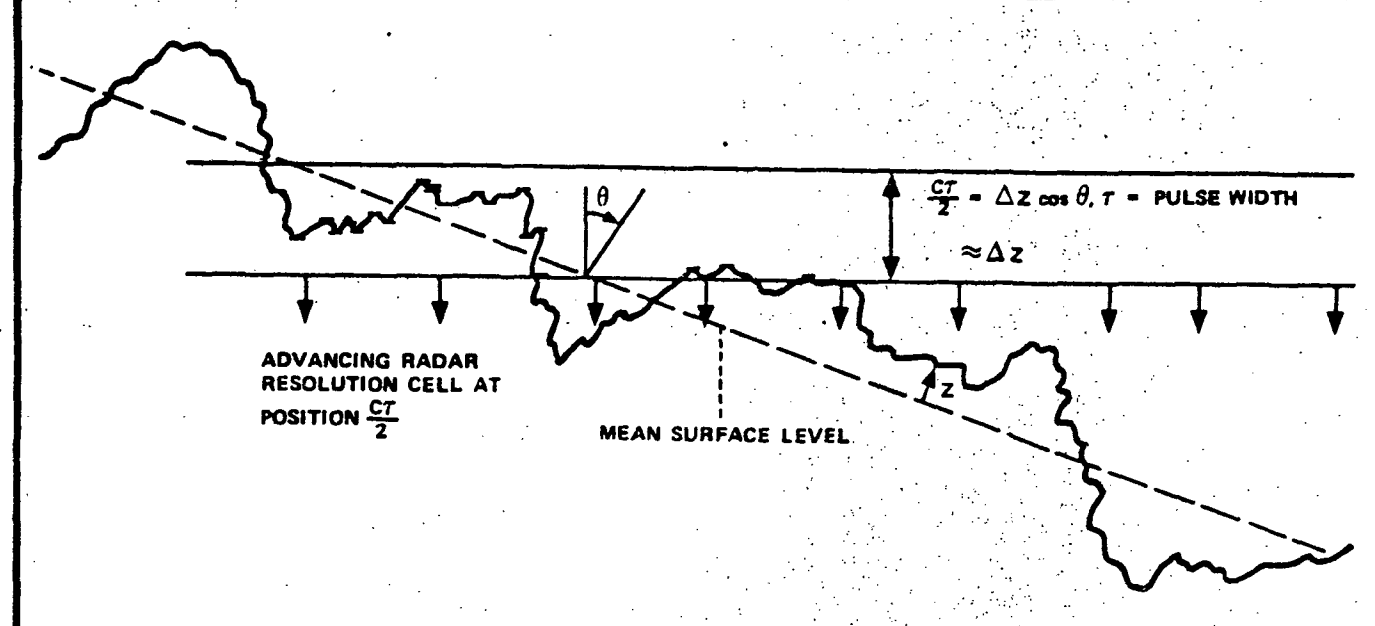


FIGURE 5.2-1 Physical Illustration of Specular Point Scatter (Specular Points are Highlighted)

#### where:

G = antenna gain as a function of time

σ(t) = average radar cross section as a function of time

H = height of the radar altimeter

a = "radio" radius of the earth

 $s^2$  = total slope

 $x_{\omega} = (c\tau) / [4(1n \ 2)^{1/2}]$ 

 $t_p = [2(x_\omega^2 2h^2)^{1/2}]/c$ 

 $t_s = (2H^2 \Psi_e^2)/e$ 

 $1/\Psi_e^2$  = [(8 ln 2)/ $\Psi_B^2$ ] + (1/s<sup>2</sup>), where  $\Psi_e$  and  $\Psi_B$  are shown in Figure 5.2-2

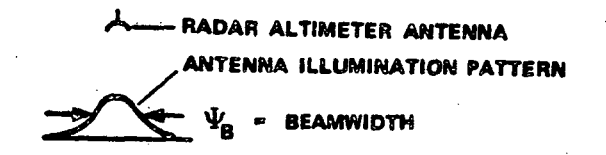
 $h^2$  = mean-square sea wave height

 $\phi(x)$  = error function of argument x

Two constants  $t_p$  and  $t_s$  appear in this model.  $t_s$  is much larger than  $t_p$ ; this defined as the "pulse limited" mode of the average radar cross section as a function of time in equation (3) is as shown in Figure 5.2-3. The slope of the leading edge of the signal is a function of the significant seawave heights  $H_{1/3}$  at the sub-

REV. NO.: 0 REV. DATE: 30 June 1977

ORIGINAL PAGE IS OF POOR QUALITY orbital point. This portion of the signal is the one that must be used to extract "sea state."



EDGE OF EFFECTIVE SPECULAR SCATTERING
AREA & (COMBINATION OF ANTENNA ILLUMINATION PATTERN AND
ANGULAR DISTRIBUTION OF REQUIRED SPECULAR SCATTERERS)

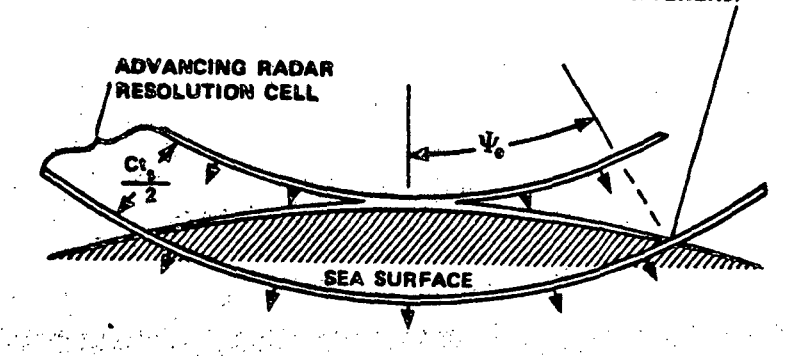


FIGURE 5.2-2 Interpretation of Altimeter Model Constant  $t_S$ .

The constants  $t_p$  and  $t_s$  have simple geometric interpretations that help to explain the nature of the received signal. As shown in Figure 5.2-4,  $t_p$  represents the amount that the incident signal (propagating vertically downward) gets stretched by ocean waves of height h. The constant  $t_s$  is a measure of the time that the radar echo is being received from the sea, as shown in Figure 5.2-2. In the pulse-limited mode ( $t_s \ll t_p$ ), this return will be received from a spherically advancing resolution cell as long as (1) there are specular points with slopes large enough to backscatter, and (2) the antenna beamwidth is great enough to permit illumination of the sea. For pulse-limited operation, the length of the trailing edge of the pulse shown in Figure 5.2-3 is essentially  $t_s$ .

Because the information on significant sea-wave height for pulse-limited altimeter operation is contained in the slope of the leading edge, one way of

REV. NO.: 0

REV. DATE: 30 June 1977

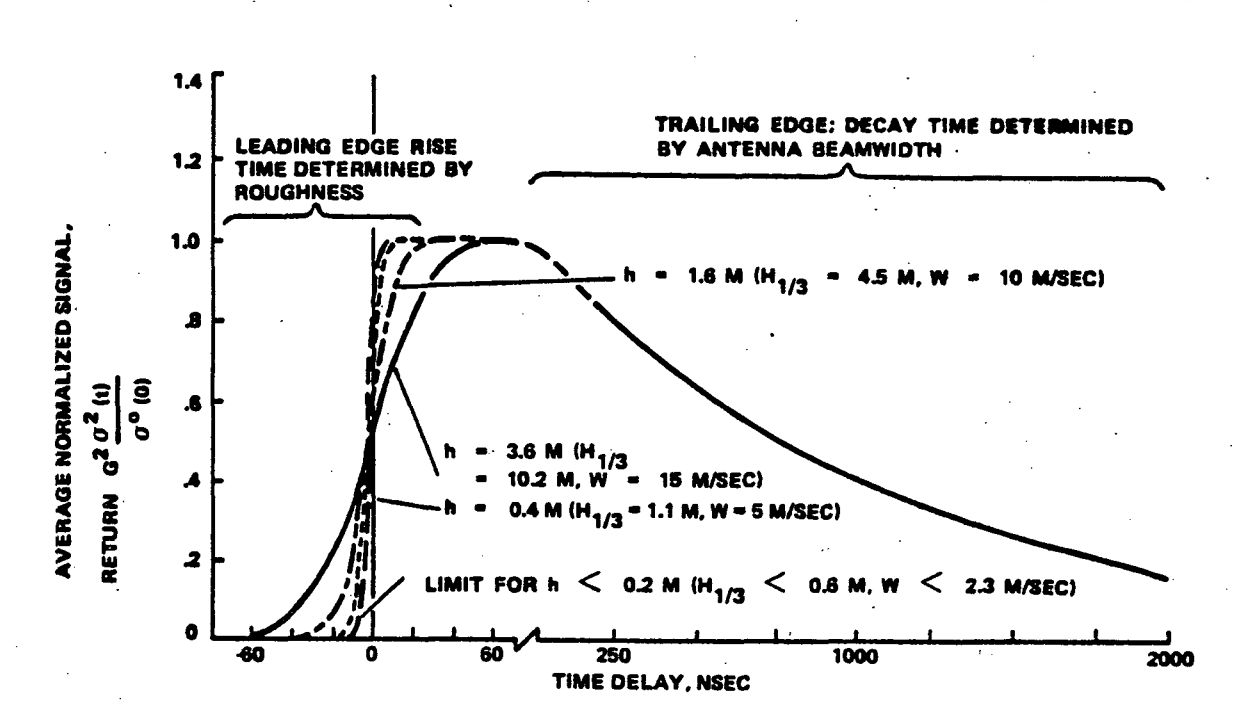


FIGURE 5.2-3 Average Radar Cross Section as a Function of Time (Where  $H_{1/3}$  is Significant Wave Height and W is Windspeed)

retrieving the height distribution information is to differentiate (as a function of time) the averaged leading edge. This derivative is then essentially a pulse that is directly proportional to the ocean-wave height probability density function. This effect is shown in Figure 5.2-5, in which a more realistic height distribution that the symmetric Gaussian function is now used. Oceanographers have known that, for greater wave heights, the height probability density function is skewed toward

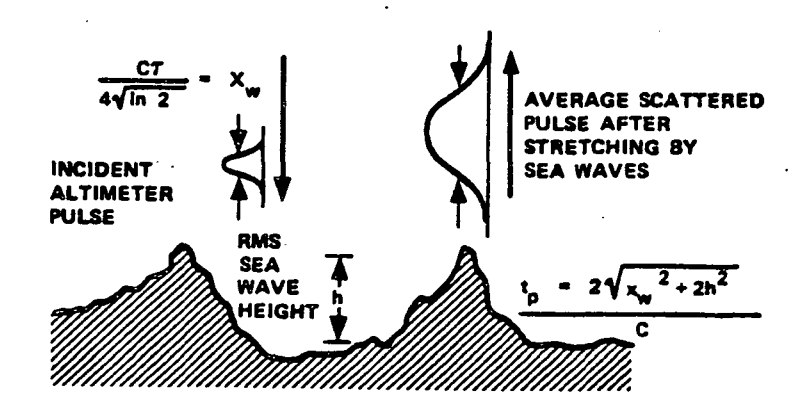


FIGURE 5.2-4 Interpretation of Altimeter Model Constant  $t_{D}$ 

REV. NO.: 0 REV. DATE: 30 June 1977

heights above the mean plane. This skewness can be described by a parameter  $\delta$ , which can be as high as 0.4. Hence, the upper graphs in Figure 5.2-5 show wave probability density functions (with and without skewness) for various wave heights. The lower graphs show the time derivative of the averaged leading edge of the received signal for a 10-nsec transmitted pulse (in the absence of noise). This signal, for greater wave heights, is stretched in direct proportion to the width of the height probability density function. However, note that when the height density function is skewed (dashed curve), the radar return is also skewed, but in the opposite direction. This has been observed experimentally, where the radar "centroid" of the measured altimetry return appears to move toward the troughs and away from the wave crests. The theoretical model explains this shift and can be used as a correction to quantitatively determine the error factor introduced by wave skewness for the purpose of determining the mean sea position.

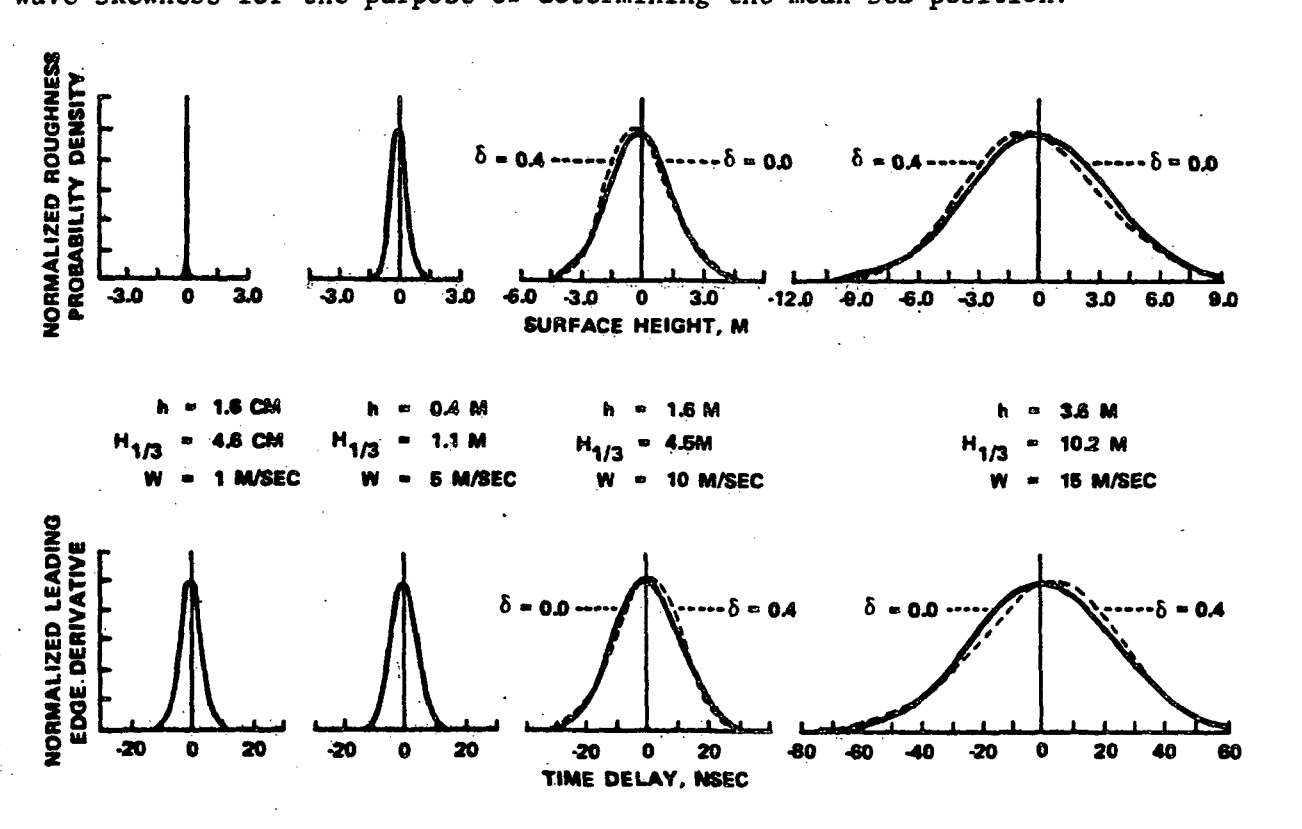


FIGURE 5.2-5 Wave Probability Density Functions

REV. NO.: 0 REV. DATE: 30 June 1977

The specular-point model, and its extension to radar altimetry, therefore, adequately explains the interaction mechanism with the sea and can permit both the design of the sensor and the interpretation/extraction of sea-wave height information from the received signal.

Results from recent experiments (i.e., AAFE) have shown that a more efficient way of measuring sea state may be attained with a chirp radar system. A chirp system allows a S/N improvement by transmitting a relatively long pulse, but retains the characteristics of the pulse limited system through pulse compression. A detailed analysis of this technique is given by [2], with only a cursory description provided below for the sake of continuity.

It is the broad frequency content, or bandwidth, of a short radar pulse that accounts for its high resolution capabilities. It follows, as a consequence of Fourier analysis, that a long pulse of constant carrier frequency contains a narrow bandwidth and, therefore, possesses poor resolution properties. However, the spectrum of this long signal can be significantly broadened by introducing modulation. To utilize the transmitting device efficiently, this modulation must take the form of frequency modulation (FM). By this method one can introduce the frequency spread characteristics of a short pulse within the envelope of a longduration signal. The linearity of a radar system permits one to realize the potential of this shorter pulse by a suitable phase equalization in the radar receiver. Darlington's model for such a system is illustrated in Figure 5.2-6. The transmitted signal consists of a sequence of adjacent pulses each possessing a unique carrier frequency,  $f_n$  (see Figure 5.2-6). To realize the short pulse potential, one imagines that the received signal is passed through a network possessing a delay versus frequency character, as illustrated in Figure 5.2-6. Although the frequency f, is the first to be received, it is just this frequency that is delayed the long-

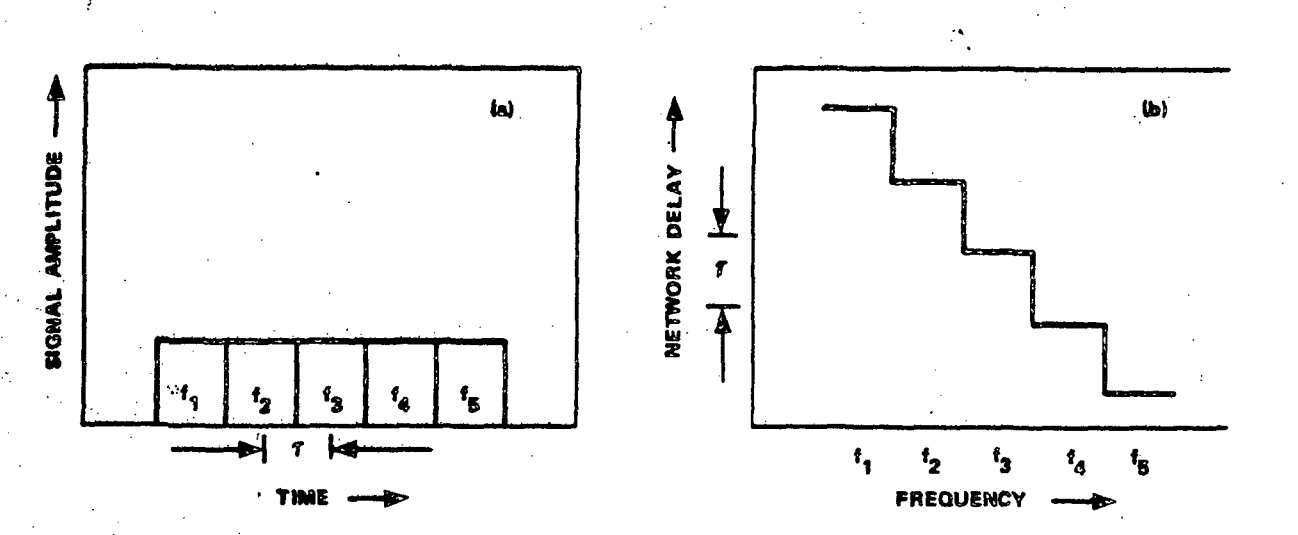


FIGURE 5.2-6 (a) Model Chirp radar signal composed of five adjacent pulses each possessing a unique frequency. (b) Suitable delay equilizer for the signal in (a). The output of this network is qualitatively a pulse of increased amplitude with a pulse width of  $\tau$  seconds. The network is illustrated for the particular case where fn  $\tau$  f<sub>n+1</sub>.

est amount by the network. In this manner each pulse of distinct carrier frequency is made to "wait" until the highest-frequency component arrives, whereupon all the short pulses emerge simultaneously. Thus following the delay equalization, the original signal of Figure 5.2-6(a) will be compressed in time, and, by energy conservation, the collapsed signal will be necessarily increased in amplitude.

For several practical as well as theoretical reasons the signal chosen for the Chirp system is characterized by a <u>linear</u> frequency modulation, as illustrated by Figure 5.2-7. This important case consists of a rectangular envelope of T seconds duration [see Figure 5.2-7(a)]. Within this envelope the instantaneous frequency is modulated in a linear manner covering a band of frequencies  $\Delta$ , centered at a frequency  $f_0$  [see Figure 5.2-7(b)]. Figure 5.2-7(c) schematically illustrates a signal in a limiting form of the one illustrated in Figure 5.2-6(a). A suitable delay-equalizing network for the signal with linear FM is given, therefore, by a limiting form of the equalizer in Figure 5.2-6(b). The delay characteristic of this limiting network is shown in Figure 5.2-8(a). This response envelope is given analytically by the absolute value of D [(sin  $\pi\Delta t$ )/( $\pi\Delta t$ )] and is illustrated in

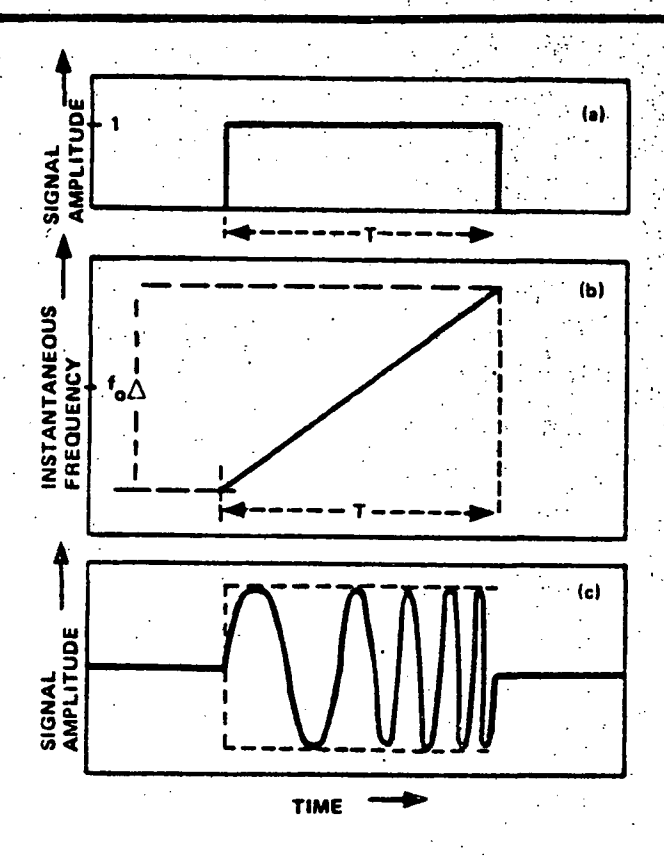


Figure 5.2-7 (a) Ideal envelope of actual Chirp signal, of  $\tau$  seconds duration and chosen to be of unit amplitude. (b) Instantaneous frequency vs. time characteristic of Chirp signal; a band of frequencies,  $\Delta$ , centered at  $f_0$  is linearly swept during the pulse duration. (c) Schematic diagram of a signal having the properties indicated in (a) and (b).

Figure 5.2-8(b). In this expression, D, called the dispersion factor, is defined by the product  $T\Delta$  and represents a parameter of fundamental significance. The collapsed pulse width,  $\tau$ , is of the order of  $I/\Delta$ . Consequently, there has been a pulse width reduction given by the ratio  $T/\tau \approx T\Delta = D$ , and a signal amplification given by  $(D)^{1/2}$ .

A typical state-of-the-art pulse compression ratio is 1000:1. That is, the effective pulse width of the received signal is  $\frac{1}{1000}$  of the transmitted pulse width.

Figure 5.2-9 shows schematic geocentric relations of the various surfaces associated with satellite altimetry. TM is the raw altimeter range which has to be corrected for laboratory instrumental calibration, electromagnetic effects,

REV. NO.: 0 REV. DATE: 30 June 1977

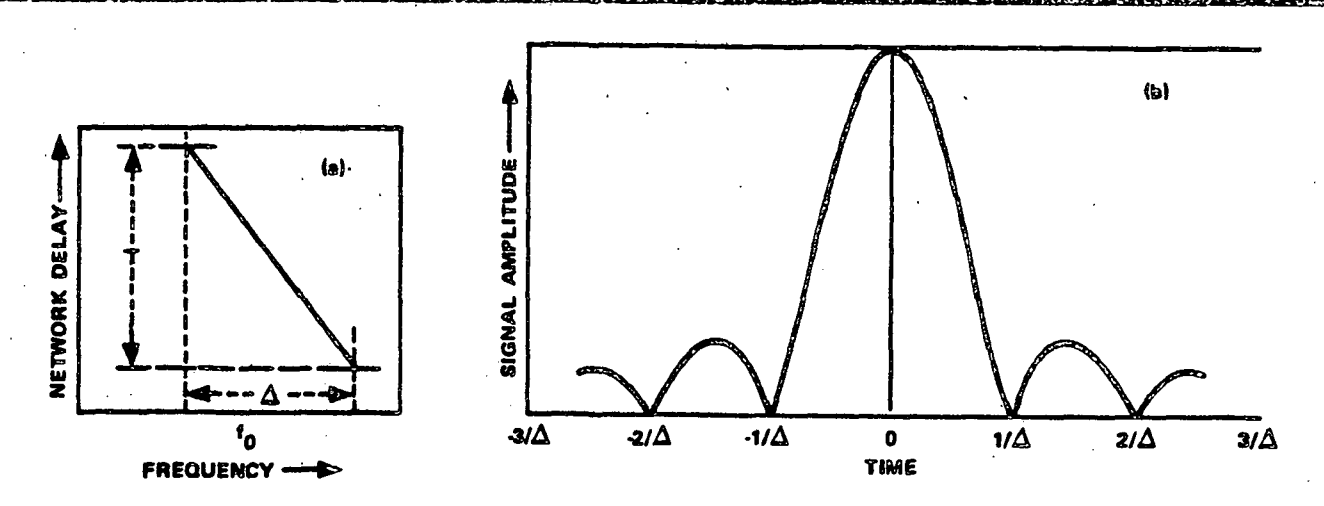


FIGURE 5.2-8 (a) Network delay vs. frequency characteristic suitable for phase equalization of the Chirp signal in Fig. 2; ideally, this network is chosen to have a flat loss characteristic. (b) Envelope of output response from the network in (a); this pulse now has a pulse width about  $1/\Delta$  and an amplitude increase given by  $\sqrt{D}$ , where  $D = T\Delta$  is called the dispersion factor.

sea state, and periodic sea surface influences to give TS. S represents the non-periodic "sea level." CT and CE, the geocentric radii of the altimeter and E, its subsatellite point on the reference ellipsoid, are computed from satellite tracking information. EG is the absolute geoidal undulation to be computed from this investigation, while SG is the quasi-stationary departure of the mean instantaneous sea surface from the geoid - the "undisturbed" mean sea level. It can be seen from the Figure 5.2-9, that the required geoidal undulations are given by

$$EG = ET - TM - MS - SG$$

where, MS represents the sum of the calibration constants and the orbit uncertainties, if any. SG represents the deviation of the surface to which the measurement is made from the geoid. Since we do not have any information on SG which is not considered to vary significantly over the length of profiles corresponding to different submodes of observations, the sum (MS + SG) is considered as the calibration constant.

The geoid to be determined must be in absolute position or geocentric (i.e., centered at the earth's center of mass) and have correct scale, shape and

**REV. NO.:** 0

REV. DATE: 30 June 1977

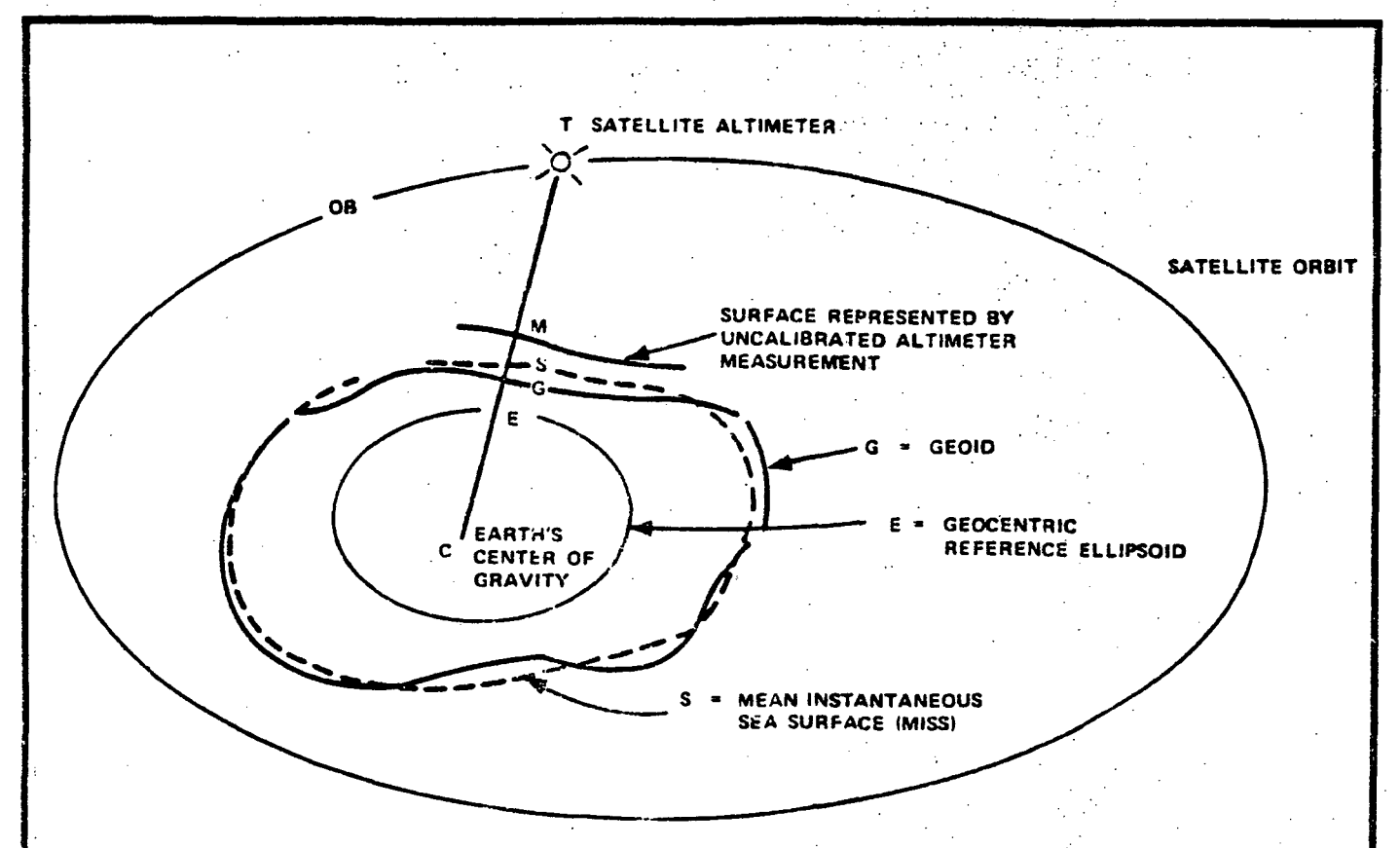


FIGURE 5.2-9 Schematic Geocentric Relations of Surfaces
Involved in Satellite Altimetry

orientation in order to meet the goals of geodesy and also make contributions to the solution of problems in earth gravity modeling, geophysics, oceanography, etc. Correctness of shape depends on the precision of the altimeter and, in theory, absolute centering and orientation are dependent on the satellite orbit ephemeris. The correctness of geoid scale requires that the orbit ephemeris and the altimeter either have no biases or systematic errors, or that such biases and systematic errors must be known to an accuracy better than the error tolerance of the geoid to be computed. Currently and for some time to come, these two scalar conditions cannot be met because of unknown systematic errors or biases in tracking station geocentric coordinates, the earth's gravity model, the tracking systems and the altimeter itself. There is, therefore, a need for other sources of scale and orientation control. Such a need can be satisfied by the use of terrestrial marine

REV. NO.: 0 REV. DATE: 30 June 1977

geodetic data to obtain scale and orientation control in the computation of the marine geoid (i.e., the geoid in the ocean areas) from satellite altimetry.

Three types of terrestrial geodetic parameters are required for this scale and orientation control: (1) the best available estimates of the figure of the earth in terms of the size and shape of a reference ellipsoid, (2) geoid heights referenced to this ellipsoid, and (3) maring geodetic controls. The first two of these are required as a priori inputs to provide a coarse scale. The third serves as benchmarks establishing the fine scale and misclosure errors. This is akin to leveling practice on land. Satellite altimetry is simply geodetic leveling from space. [3]

Measurement features and atmospheric parameters which must be addressed to both calibrate the altitude measurements and to verify the sea state measurement capability are satisfied through ground truth inputs. The term "ground truth" originated in the field of aerial photography, and if applied strictly, means direct "in situ" data taken for verification of remote measurements. For satellite applications, the definition has been extended to encompass all reference data (including remote sensing by aircraft and, in some cases, even other satellites)[4].

The Skylab S-193 experiment proved the worth of space-borne altimetry while the follow-on GEOS-3 experiment provided the necessary hardware experience to gather accurate altimetry data on a global basis. The SEASAT-A Altimeter should provide the degree of accuracy required for a global ±lm geoid determination. Benefits derived from an accurate geoid model include; (1) adjustment of the North American Datum, used for surveying, mapping, engineering operations, navigation, and resource development, (2) the extension of control points and determining their three-dimensional coordinates to offshore areas as well as the determination of national and international marine boundaries, (3) accurate knowledge of absolute

deflection of the vertical at sea, which could provide the orientation for all national datums [5].

Other applications which would benefit from a more accurate geoid include gravity field, mean sea level, and plate tectonics and ocean trench determination.

The SEASAT follow-on (B) will probably include an on-board Maximum Likelihood Processor (MLE) for near real-time processing with formatted and corrected geophysical units as an output [6].

### ALTIMETERS LIST OF ACTIVE CONTRIBUTORS

W. F. Townsend Seasat-A ALT Instrument Rep. Directorate of Applied Science Wallops Flight Center Wallops Island, Virginia 23337 (804) 824-3411, Ext. 405

C. L. Purdy
Directorate of Engineering
Radar Systems Section
Wallops Flight Center
Wallops Island, Virginia 23337
(804) 824-3411, Ext. 449

J. A. Dunne Seasat-A Ocean Experiments Manager Jet Propulsion Laboratory Pasadena, Cal. 91103 (213) 354-6904

Al Loomis
Planetology and Oceanography Section
Jet Propulsion Laboratory
Pasadena, Cal. 91103
(213) 354-2046

Dave Lame
Mission Control & Computing Center
Jet Propulsion Laboratory
Pasadena, Cal. 91103
(213) 354-4469

Bill Brence Directorate of Operations Project Management Section Wallops Flight Center Wallops Island, VA 23337 (804) 824-3411, Ext. 386

### ALT IMETERS

#### REFERENCES

- [1] Matthews, R. E., ed., "Active Microwave Workshop Report," Working Group Meeting at JSC, July, 1974, pp. 220-221 & 174-177.
- [2] Klauder, J. R., Price, A. C., Darlington, S., and Albersheim, W. J. "The Theory and Design of Chirp Radars," The Bell System Technical Journal, XXXIX (July, 1960), 746-752.
- [3] "The Application of Skylab Altimetry to Marine Geoid Determination," Battelle Columbus Labs., NASA Contract No. NAS9-13276, (July, 1975), pp. (1-2)-(1-3) § (6-4)-(6-6).
- [4] "GEOS-C Ground Truth Program Description Document," NASA Wallops Flight Center, (March, 1975), pp. (1-1) & (4-49).
- [5] Miller, L. S., Brown, G. S., "Engineering Studies Related to the GEOS-C Radar Altimeter," Applied Science Associates, Inc., (May 1974), p. 33.
- [6] Nagler, R., MSFC, "SEASAT-B Feasibility Study (Phase A)," (Dec. 1975).

**REV. NO.:** 1 | **REV. DATE:** 30 Sept 1977

### **ALTIMETERS**

#### BIBLIOGRAPHY

- (1) Leitao, C. D. and Purdy, C. L., <u>Wallops GEOS-C Altimeter Preprocessing</u>
  Report, Wallops Flight Center, Contract No. NAS6-2173, February 1974.
- (2) Mourad, A. G., Gopalapillai, S., Kuhner, M., and Fubara, D. M., The Application of Skylab Altimetry to Marine Geoid Determination, Battelle Columbus Labs, Final Report, Contract No. NAS9-13276, July 1975.
- (3) Brooks, L. W. and Dooley, R. P., <u>Technical Guidance and Analytical</u>
  <u>Services in Support of SEASAT-A</u>, <u>Technology Services Corp.</u>, Final Report,
  <u>Contract No. NAS6-2447</u>, April 1975.
- (4) McGoogan, Joseph J., Miller, Lee S., Brown, Gary S., and Hayne, George S., "The S-193 Radar Altimeter Experiment," Proceedings of the IEEE, Vol. 62, No. 6, June 1974.
- (5) Greenwood, Arthur J., Nathan, Alan, Neumann, Gerhard, Pierson, Williard J., Jackson, Frederick C., and Pease, Thomas E., "Radar Altimetry from a Spacecraft and Its Potential Applications to Geodesy," Remote Sensing of Environment, Vol. 1, 1969, pp. 59-70.
- (6) Greenwood, Arthur J., Nathan, Alan, Neumann, Gerhard, Pierson, Williard J., Jackson, Frederick C., and Pease, Thomas E., "Oceanographic Applications of Radar Altimetry from a Spacecraft," Remote Sensing of Environment, Vol. 1, 1969, pp. 71-80.

REV. NO.: 1 REV. DATE: 30 Sept 1977

## ALTIMETERS ILLUSTRATION CREDITS

Figure No.	Page	Reference	Page
5.2-1	5.2-3	[i]	175
5.2-2	5.2-4	[1]	175
5.2-3	5.2-5	[1]	176
5.2-4	5,2-5	[1]	176
5.2-5	5.2-6	[1]	177
5.2-6	5,2-8	[2]	749
5.2-7	5.2-9	[2]	750
5.2-8	5.2-10	[2]	751
5.2-9	5.2-11	[3]	1-3

This page intentionally left blank.

REV. NO.:

REV. DATE: 30 Sept 1977

SHEET 1 QE

(1) SENSOR NAME, ACRONYM:

Radar Altimeter, ALT

(2) DISCIPLINE: Earth and Ocean Physics

(3) SUBDISCIPLINE: Ocean Dynamics

### (4) APPLICATION AND OBJECTIVE:

The SEASAT-A Altimeter will survey the earth's oceans for the purpose of measuring significant wave heights and mean sea level, and to detect tides, currents and storm surges in support of global forecasting. Additional correlative data will allow a precise orbital measurement and refinement of the geoid model.

(5) HERITAGE/KEY PERSONNEL: The SEASAT-A Altimeter is the result of the Skylab-S193 and GEOS-3 experiments in altimetry. The most notable efforts in aircraft altimetry measurements from the sea surface are the AAFE-Wallops/NRL experiments.

Experiment team leader-Dr. Sam Smith/NWL; Inst. rep.-W. F. Townsend/Wallops

### (6) SENSOR DEPLOYMENT:

The SEASAT-A satellite bearing the ALT is to be launched to obtain a mean circular orbit with a 108° inclination, mean altitude of 790 km and approximate ground speed of 6.6 Km/sec. An orbital period of 104 minutes results in 14 orbits/day. Seven orbits are required for complete (mission) ocean coverage.

(7)

#### SENSOR CHARACTERISTICS

### (7A) CAPABILITIES AND CONSTRAINTS OF THE SENSOR TO ACQUIRE THE MEASURED PARAMETER:

The ALT employs a nadir viewing parabolic dish antenna to illuminate and receive energy from a circular area on the sea surface with an effective radius of 1.6 to 12 km dependent on sea state. All altimeter data will be recorded. Playback data becomes the source of data records for the low rate telemetry link as the satellite passes over selected tracking stations (STDN). Correlative data from the other 4 SEASAT-A sensors in addition to sea truth data and precise orbital information from laser tracking sites are necessary to reduce the ALT data to accurate geophysical units (i.e., waveheight, altitude).

### (7B) ACTIVE SOURCE CHARACTERISTICS (FOR ACTIVE SENSORS):

A frequency synthesizer drives the SAW dipersive delay line in the transmitter section producing a short pulse of the required shape and frequency spectrum. This FM pulse is applied to the modulator and up-converted, and finally to the TWT. The resultant transmitted energy takes the form of a 5.2 µs burst with a 13.5 GHz carrier frequency modulated at 100 MHz/us. Peak power is 2 Kw and the pulse repetition frequency is 1031 Hz. The antenna is a circular, parabolic reflector type providing 39.5 dB effective gain and 1.6° beam width.

### (7C) DETECTOR MEASUREMENTS CHARACTERISTICS:

Receiver bandwidth is ± 160 MHz centered at 13.5 GHz with an allowable inband noise level ≥ -82.75 dBm. For an average backscatter coefficient of 6 dB (min), the signalto-noise ratio is approximately 13 dB. Following RF, IF, and AGC stages, the return signal is compressed (1000:1), then segmented by range gates into aquisition, plateau, altitude, and noise video, then sampled at a 20 MHz rate. A 10 bit A/D converter provides the required 60 dB resolution.

SECTION NO.: 5.2 **SENSOR CATEGORY:** 

Altimeters

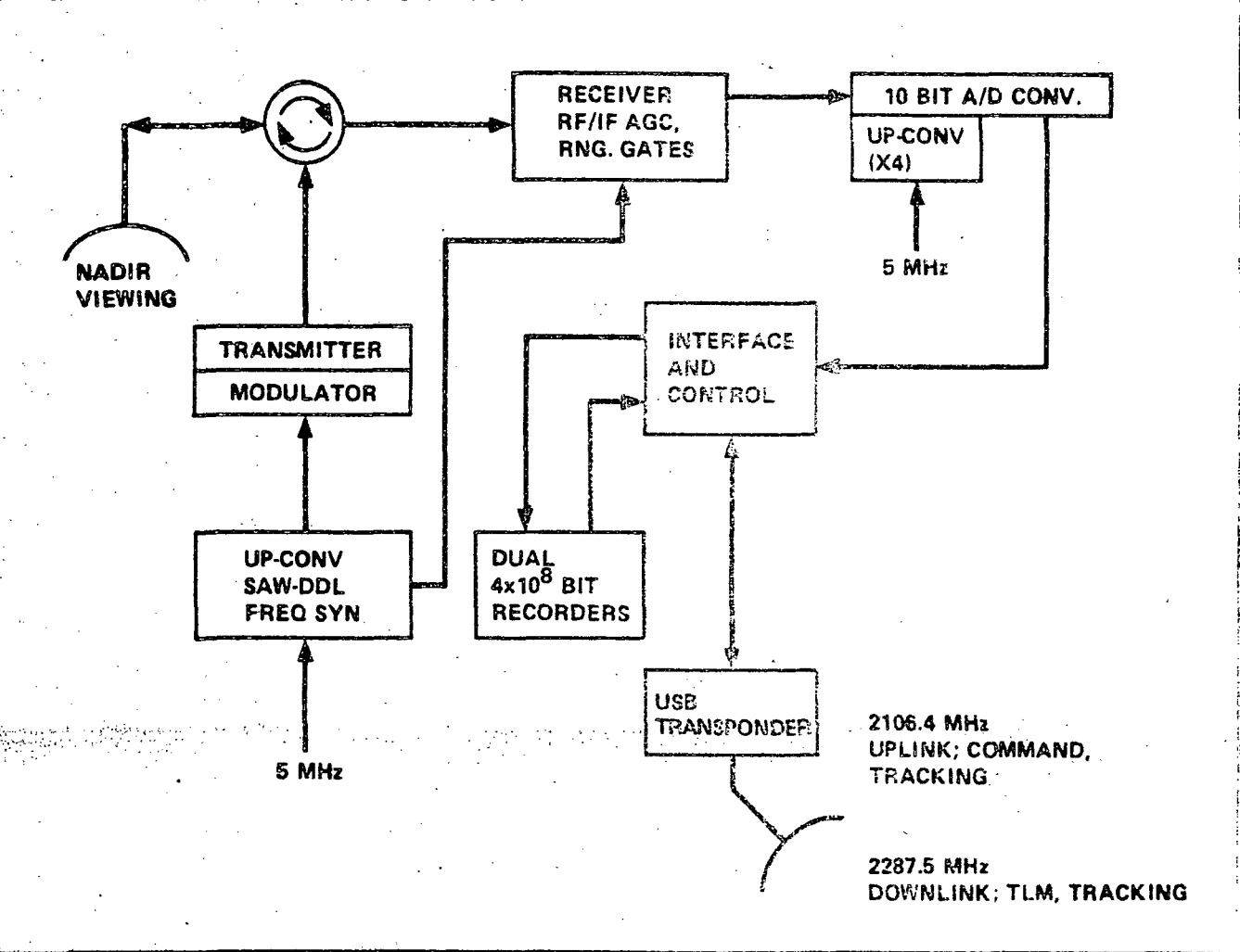
Preceding page blank

REV. DATE: 31 Jan 1978

5.2.19

REV. NO.: 2

### (8) Sensor data measurement and transmission system — block diagram.



### (9) MEASUREMENT AND TRANSMISSION SYSTEM - NARRATIVE:

The leading edge of the impulse response corresponds to the integral of the specular point density. During processing the half power point measures altitude, and an estimate of wave height is obtained by measuring the rise time of the leading edge. A/D conversion provides an average data rate output of 8 kbps. The normal tape utilization will be to record data in a forward direction and to playback in reverse. Data will be restored to the forward direction on the ground. The downline telemetry carrier power is 1 watt with a bandwidth of ±3 MHz. During real-time transmission, a 1.024 MHz subcarrier is bi-phase modulated at 25 kbps. The sub-carrier then phase modulates the carrier. In the playback mode, the carrier is phase modulated at a rate of 690 kbps.

5.2.20

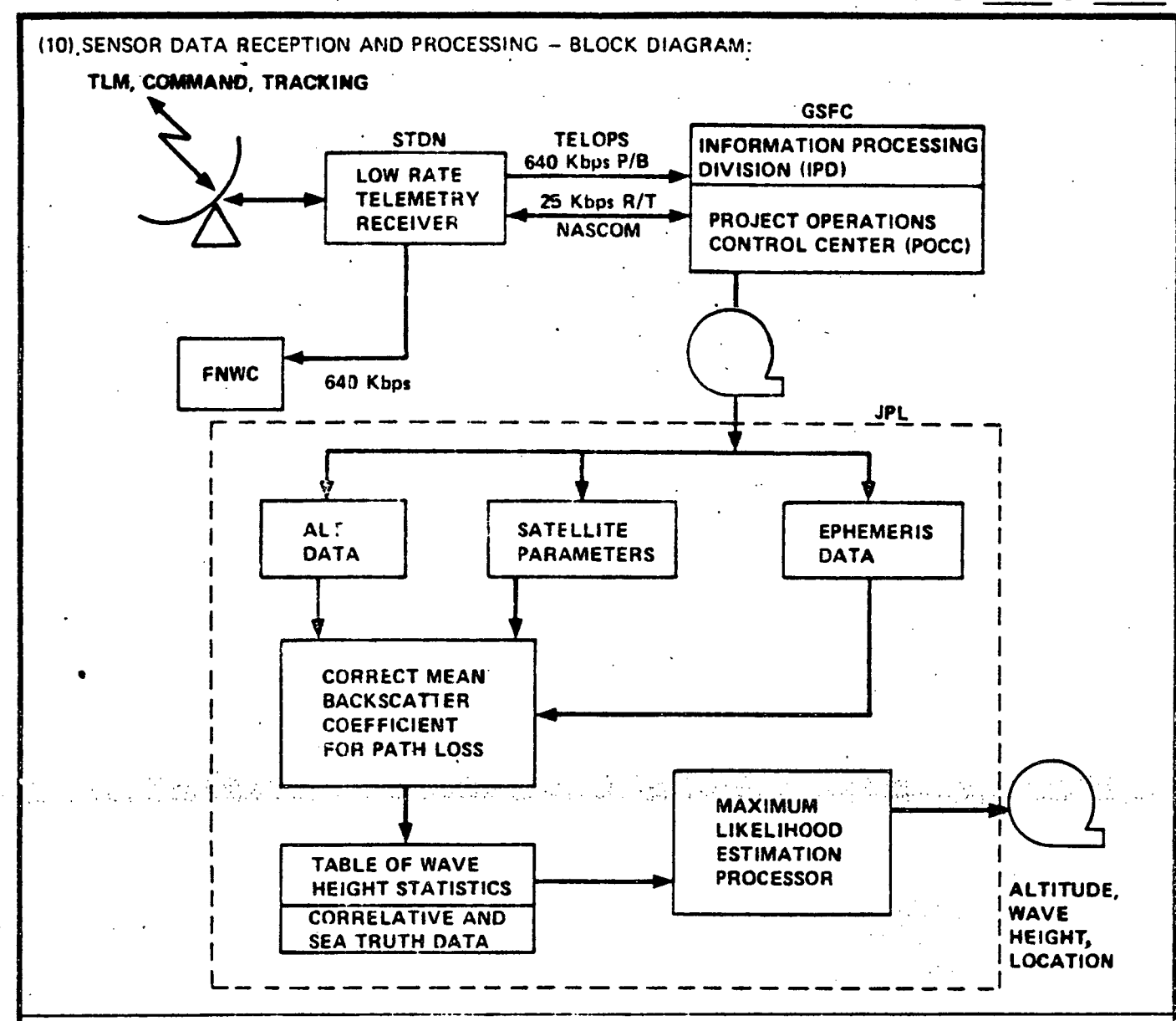
SECTION NO .:

5.2

SENSOR CATEGORY: Altimeters

REV. NO.: 2

REV. DATE: 31 Jan 1978



### (11) RECEIVING AND PROCESSING - NARRATIVE:

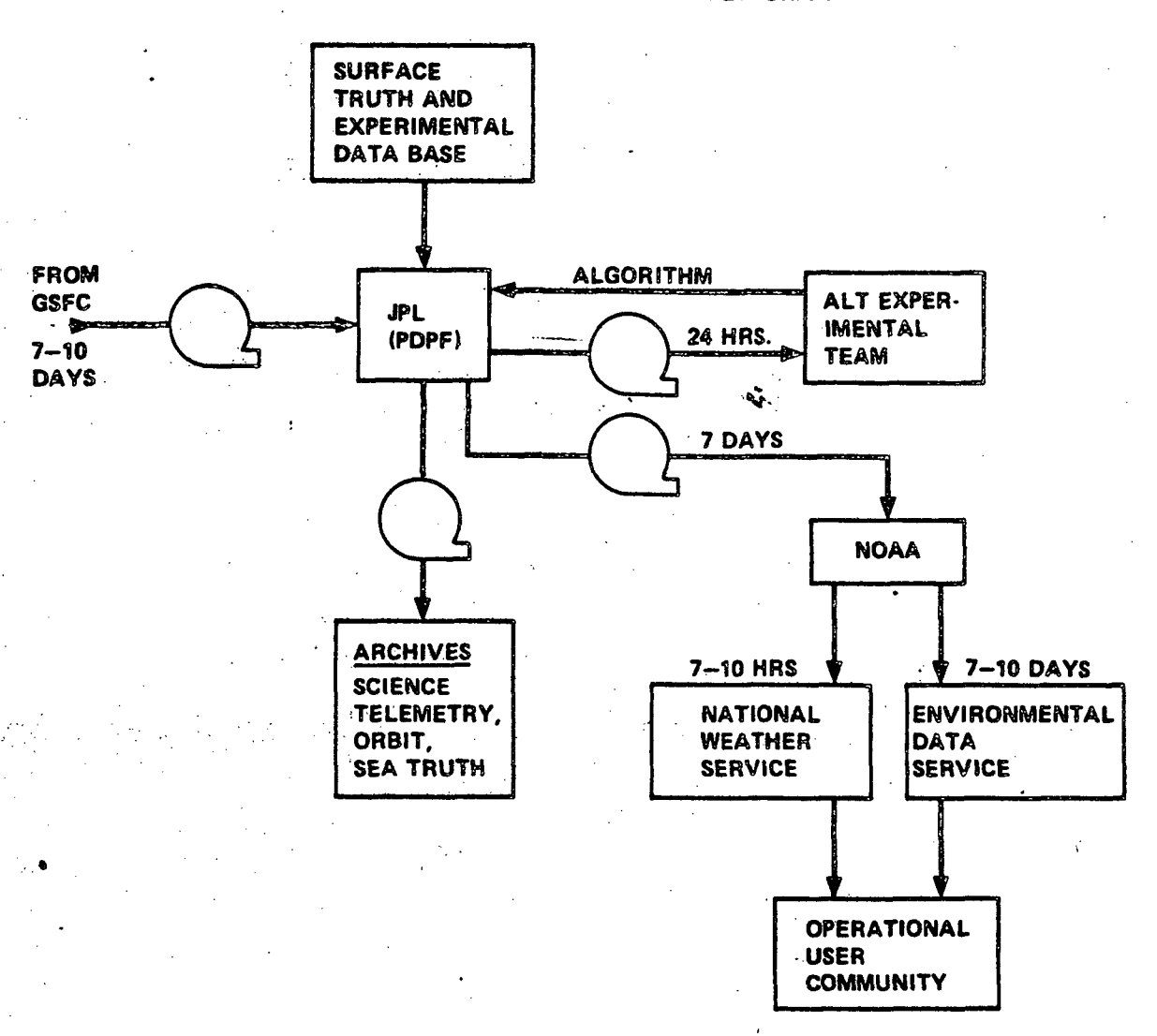
Low rate telemetry is received by the Satellite Tracking Data Networks (STDN) at 640 kbps (P/B). The IPD will construct a Master Data File in time-order as generated by the satellite. A daily data package is sent to JPL. The PDPF at JPL will produce a single processed data record in geophysical units (ie., wave height, altitude, etc.).

#### Expected Performance:

Parameter	Altitude	Significant Waveheight	Backscatter
Range	761-858 km	1-20 m	-85 ≤ σ ≤ -20 dBm
Accuracy	68% within ±10 cm	0.5 m or ±10%	±1 dB

SECTION NO.: 5.2 SENSOR CATEGORY: Altimeters

### (12) DISTRIBUTION OF DATA FROM GROUND STATIONS - BLOCK DIAGRAM:



### (13) DATA DISTRIBUTION - NARRATIVE:

JPL receives edited and time-smoothed TLM data from GSFC. The 4 primary functions of the Project Data Processing Facility (PDPF) are:

- (a) produce an Experimental Data Record for each team,
- (b) produce supplementary data for each experiment (i.e., sensor earth located footprint, engineering data, etc.),
- (c) produce a single processed data record in geophysical units for each experiment, i.e., altitude, wave height, etc., and
- (d) produce validated algorithms to independent raw data users (e.g., FNWC).

5.2.22

SECTION NO.: 5.2 SENSOR CATEGORY: Altimeters

## SENSOR CATEGORY TABLE OF CONTENTS AND REVISION CONTROL SHEET

SENSOR NAME OR	NUMBER OF	PAGE	EFFE	EFFECTIVE	
OTHER ENTRY	PAGES	NUMBER	REV. DATE	REV. NO.	
,					
Section 5.3 Table of Contents	1	5.3-i	31 JAN 78	2	
Introduction to Scatterometers	15	5.3-1	31 JAN 78	2	
		5.3-2 5.3-3	31 JAN 78 31 JAN 78	2	
		5.3-4 5.3-5	31 JAN 78 31 JAN 78	2 2 2 2 2	
		5.3-6 5.3-7	31 JAN 78 31 JAN 78	2 2 2	
	. ·	5.3-8 5.3-9	31 JAN 78 31 JAN 78	2 2	
. •	, 1 ·	5.3-10 5.3-11	30 SEPT 77 30 JUN 77	1 0	
		5.3-12 5.3-13	31 JAN 78 30 SEPT 77	2 1	
•		5.3-14 5.3-15	30 SEPT 77 30 SEPT 77	1 1	
SEASAT-A Microwave Scatterometer	4	5.3-17	31 JAN 78	2	
		5.3-18 5.3-19	31 JAN 78 31 JAN 78	2 2	
Berliner Control of the Control		5.5-20	31 JAN 78	2 <b>2</b>	
		·		•	
·				٠	
			·		
•					
•				•	
ECTION NO.: 5.3 SENSOR CATEGOR	Y: Scatteromo	ters	<u></u>	<del></del>	

This page intentionally left blank.

REV. NO.:

0

REV. DATE: 30 June 1977

### Section 5.3 INTRODUCTION TO SCATTEROMETERS

Active microwave sensors have been used to measure range, reflection or scattering coefficient and shape of the returned pulse from various objects or scenes. The ability with which a scene or object scatters incident microwave energy can be assessed by measuring the radar-scattering cross sections at various frequencies, polarizations and incident angles. A microwave scatterometer is a special-purpose radar that is used to quantitatively measure the target reflectance or scattering cross section. Long-pulse and continuous-wave scatterometers have been used to measure the scattering signatures of rough surfaces such as terrain or the ocean. The quantity of interest is the radar-backscatter coefficient, which is the backscatter power per unit area normalized for antenna gain, range loss and the transmitted power.

Ocean waves may be defined as undulations of the surface with time scales in the range from 10 ms to 25 sec., corresponding to wave lengths in the range from 0.5 cm to 1000 m, respectively. These are subclassified as (1) gravity waves, with time scales in the range of 0.1 to 25 sec., length scales from 2 cm to 500 m and heights to 30 m, and (2) capillary waves, with time scales in the range from  $10^{-1}$  to  $10^{-2}$  sec., length scales from 0.5 to 2.0 cm, and heights of less than 1.0 cm. Ocean waves are random, and a time record of the ocean-surface displacement in a storm region may contain wave periods in the entire range indicated. Far from a storm center, waves become more organized as the longer waves propagate more rapidly out of the region. Long waves occurring away from storm centers are referred to as swells. Long waves approaching a coastline are influenced by the drag of the bottom and become shallow-water waves. Wave energy is eventually dissipated through breaking in an active near-shore area called the surf zone.

REV. DATE: 31 Jan 1978

REV. NO.: 2

Wave energy is also dissipated offshore through viscous effects and by breaking, which is evidenced by the presence of whitecaps.

Capillary waves have been traditionally investigated by theoreticians and experimentalists with academic interests. More recently, and with the onset of microwave instruments as remote sensors, capillary waves have attracted more attention from a more practical point of view. The roughness of the sea is interrupted by the density and structure of capillary waves, which respond to windspeed.

Capillary spectrum components are readily related to the radar wavelength by the Bragg scattering condition that the radar return from adjacent crests of the most important ocean components add in phase. This leads to the condition:

$$\Lambda \sin \theta_i = n \lambda/2 \tag{1}$$

where  $\Lambda$  = ocean wavelength (component of spectrum)

 $\lambda$  = radar wavelength

 $\theta_{i}$  = angle of incidence (from local vertical)

The first order perturbation theory shows results only for n=1, although intuitively one might expect higher order "Bragg resonances" also to be important. At an incident angle of 30° this means that the "Bragg wavelength" for the ocean is the same as the probing radar wavelength. Consequently, the Bragg wavelengths at that angle are, for the frequencies considered here, in the capillary region of the ocean wave spectrum.

Measurements taken to date reveal the following information about the dependence of the backscattering cross section from the ocean on windspeed:

- (1) A range of radar wavelengths exists for which backscatter is primarily dependent on surface windspeed and relatively insensitive to large-scale roughness.
- (2) Backscatter at or near the vertical (0° incident angle) monotonically decreases with increasing windspeed.

- (3) Backscatter from incident angles greater than 20° (nominally) from the vertical, monotonically increase with increasing windspeed.
- (4) The upwind, downwind and crosswind viewing directions give different values for backscatter cross sections and are sensitive to windspeed.

A representation of these features of ocean backscatter as a function of windspeed and incident angle for 2-3 cm wavelength radar illumination is shown in Figure 5.3-1. For windspeeds less than 1 m/sec, essentially no sensible

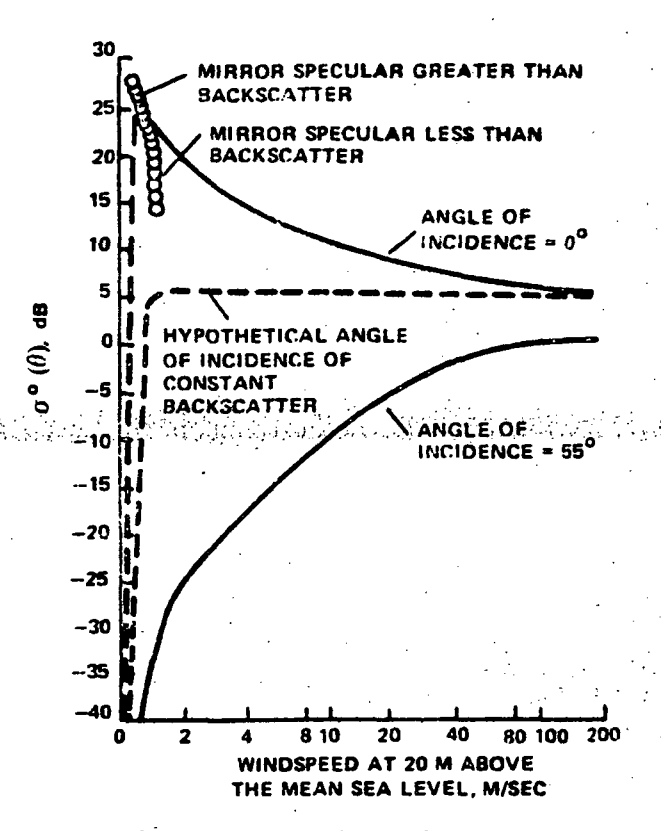


FIGURE 5.3-1 Representation of Approximate Magnitude of Backscatter Cross Section from the Ocean at 2- to 3-cm radar wavelengths

backscatter is seen at any angle of incidence; the strong radar return at 0° is from specular mirror reflection (shown as dotted line). As the windspeed increases toward 2 m/sec, patches of roughness begin to appear on the surface where turbulent gusts of the surface exceed the threshold for wind-to-water coupling. The small

capillary waves generated by these gusts produce some backscatter at all angles of incidence with very rapid rates of change of backscatter as compared to windspeed. The local slope of the curves at high windspeeds shows that extremely accurate measurements of the backscatter must be made to sense a small range of backscatter values. Alternatively, the local slopes at low windspeeds show that less accurate measurements are required to sense small percentage changes.

Backscatter measurement sensitivities with respect to windspeed and direction are shown in Figure 5.3-2. An interesting observation is that the upwind-downwind

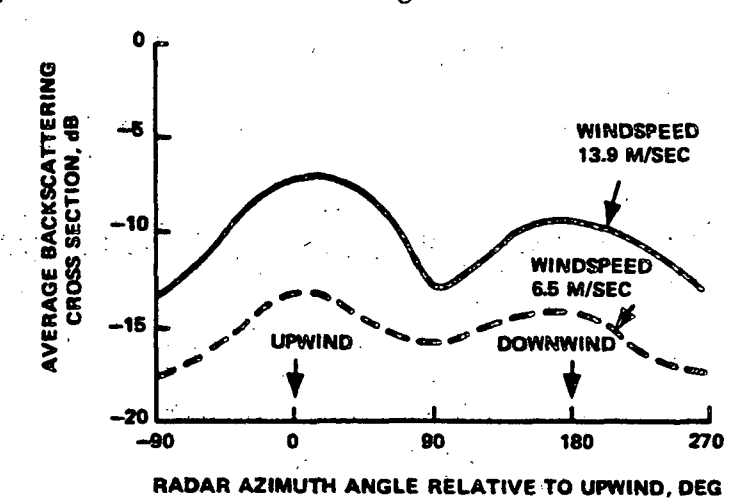


FIGURE 5.3-2 Langley Research Center Values of σ° Compared to Wind Heading (Vertical Transmit/Vertical Receive Polarization; Incident Angle of 40°)

dependency was predicted and explained more than 20 years ago at NRL, assuming specular points as the backscatter mechanism and wave tank measurements of the probability distributions of surface facets as compared to windspeed. However, the crosswind dependency was not predicted so that with perfect instrumentation (that is, no error in the backscatter measurement but no knowledge of the viewing direction) a radar cross-section data spread of many decibels will be obtained.

For example, in Figure 5.3-2, a 6-dB spread exists upwind to crosswind at a 13.9 m/sec windspeed, 40° incident angle, with an average backscatter coefficient over

all wind heading angles of -10 dB, whoreas, at 6.5 m/sec windspeed, the average is approximately -15.5 dB, with an upwind-to-crosswind spread of 4 dB.

This problem can only be solved either by knowing the viewing direction with respect to wind directions or by viewing the surface from enough different directions so that the upwind, downwind, and crosswind curves can be obtained as input data. [1]

Scatterometer resolution at angles away from vertical is given by

Resolution = 
$$R\phi_o \left(\frac{c\tau}{2\sin\theta}\right)$$
, (2)

where R is the slant range,  $\theta_0$  is the beam width in the cross-track direction,  $\tau$  is the pulse duration, and  $\theta$  is the 5 dB beam width along track. The expression in equation (2) is not appropriate at nadir, however, and may be determined by pulse duration rather than beam width. The radius of surface illumination corresponding to pulse duration at Vertical is given by

$$r = (cth)^{1/2} \tag{3}$$

The SEASAT-A Scatterometer (see data sheet) represents the current state-of-the-art in measuring ocean backscatter with a microwave radar. The SASS design, deployment, and data handling to infer wind vectors will be discussed as an example of current techniques.

In concept two radar measurements at different azimuths are sufficient to determine the ocean surface wind vector; however, the near sinusoidal scattering characteristic often yields multiple wind vector solutions from these radar measurements. These multiple solutions are approximately equal in speed but different in direction. Frequently, the quadrant of wind direction can be determined from conventional meteorological data and/or satellite obtained cloud mosaics, thereby providing a means for selecting the correct solution.

5. 3·5

REV. NO.: 2

REV. DATE: 31 Jan 1978

To infer wind vector from satellite radar measurements requires both forward and aft looking antennas to obtain data of two azimuth angles for each resolution cell. An optimum implementation uses antenna beams, each oriented 45° relative to the sub-satellite track, to provide observations which are separated in azimuth by 90° (Figure 5.3-3). The time between illumination of a given resolution cell by the forward and aft beams depends on the cells position along the fan beam illumination. Thus, the scatterometer must be designed in order to make the forward and aft beam cells cross at the same geographic site. Each resolution cell (50 km) must have two footprints on it, (not required at the same time, however) giving  $\sigma^{\circ}$  data at azimuth angles 90° apart.

The Doppler cells along the fan beam are adjacent so that the cross track grid spacing (center-to-center) can be kept to 50 km and the along-track grid spacing is set at 50 km by the scatterometer digital controller.

The resolution cell size is larger than the doppler cell size due to the smearing of the cell caused by satellite motion during the measurement period. The Doppler cell size is determined by the antenna beamwidth  $(1/2^{\circ})$  and Doppler bandwidth of the filters.

Resolution cell size is also controlled by the orientation of the doppler lines within the beam illumination which varies along the beam (Figure 5.3-3). For the inner cells (low incidence angles) the Doppler line is oriented approximately 45° to the central beam axis. For the outer cells (high incidence angles), the orientation is about 13° with respect to the beam central axis. The Doppler bandwidths are designed so that the 50 km x 50 km resolution cell size requirement is satisfied over the primary measurement zone (~25° to ~55°). At angles beyond 55°, Doppler bandwidths are held constant so the resolution cell size does increase slightly beyond the 50 km limit.

5.36

REV. NO.:

REV. DATE: 31 Jan 1978

In addition to the 12 Poppler cells needed for wind determination, three more will be used for  $\sigma^{\circ}$  measurements near nadir (0°, 4°, 8° incidence angle). This completes the complement of angles required to develop a data library of  $\sigma^{\circ}$  as a function of incidence angle (0° to 65°) for the full range of ocean surface conditions. From these data one can determine whether geophysical parameters other than local winds affect the scatterometer measurements and as a result establish more definitive design boundaries (by optimizing incidence angle, polarization, wind speed measurement range, etc.) for future scatterometers.

One of the more important questions concerning every remote sensor is whether or not it is operating properly. Extensive in-flight house-keeping data are being provided routinely by the scatterometer in addition to planned subsystem level and system level performance validation and diagnostic activities.

An array of three land-based receivers is planned to verify transmitter performance as well as the antenna gain and pattern shape. This technique was used on the Skylab RADSCAT experiment and it offers the only means of evaluating the transmitter and antenna on a subsystem basis. For diagnostic purposes, the SEASAT-A scatterometer can be operated in a radiometric mode (transmitter inhibited) in order to isolate the receiver for performance verification. Two test conditions are possible in this mode: (1) antenna not deployed and looking into deep space with a target brightness temperature ~5°K and (2) antennas deployed and looking at the ocean surface with a target brightness temperature ~125 - 175°K. A 5°K target offers high sensitivity for verification of antenna and receiver losses and VSWR. Receiver losses and noise temperature stability can be monitored throughout the mission, independent of the internal calibration source, by using the radiometric mode with the sea surface as a target. There are certain minimum requirements that must be met in order to certify the scatterometer as an operational

REV. DATE: 31 Jan 1978

REV. NO.:

instrument after it is placed in orbit. During the one year period, aircraft underflights are required so that direct comparisons can be made between a well calibrated ( $\pm 0.5$  dB) aircraft scatterometer and the satellite scatterometer. Direct comparison of aircraft and satellite  $\sigma^{\circ}$  data will be used as an absolute calibration of the satellite scatterometer thus removing any fixed biases from the data. Long term instrument stability characteristics will be determined from periodic comparison of aircraft and satellite  $\sigma^{\circ}$  values.

It has been demonstrated with extensive aircraft data that  $\sigma^{\circ}$  measured at 8° to 12° incidence angle is relatively insensitive to ocean surface roughness and wind conditions. Consequently, long and short term stability information, independent of aircraft underflights, will be gathered routinely using data from the 8° "near nadir" Doppler cell.

The quality of the SEASAT-A scatterometer data can be further evaluated using measurement results from other sensors on the satellite. Altimeter  $\sigma^{\circ}$  data, for example, can be compared with the scatterometer nadir data to reveal bias in either instrument and the time variation of these biases. Secondly, Scanning Multifrequency Microwave Radiometer (SMMR) data may be useful for correlation with scatterometer data during high wind speed measurements.

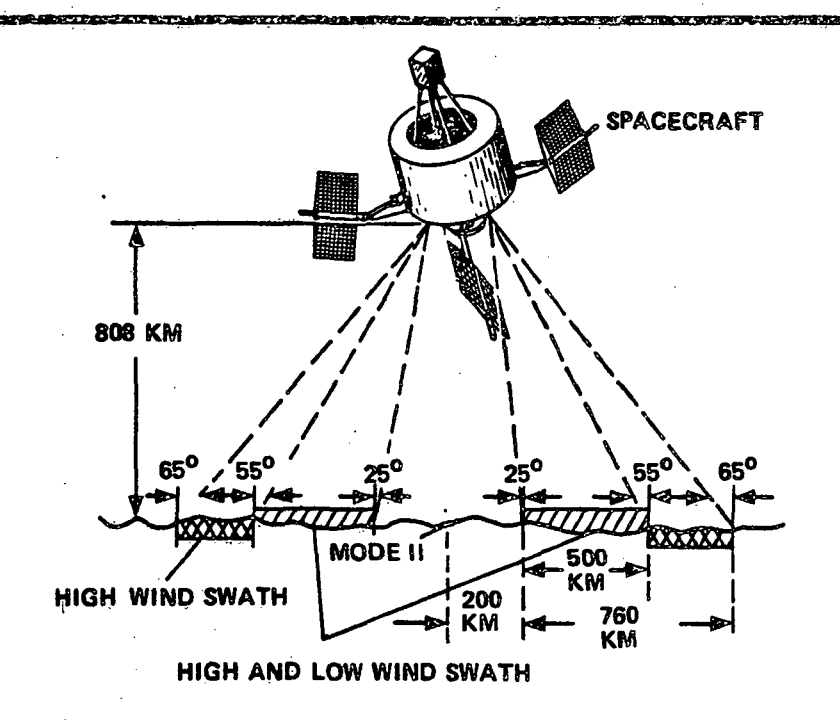
The software for inverting raw scatterometer data to  $\sigma^{\circ}$  and for converting  $\sigma^{\circ}$  to wind vector must also be validated under all measurement conditions. Figure 5.3-4 is a flow diagram showing the steps necessary in this process. This processing is conveniently separable into the conversion of raw data to scattering coefficient and the conversion of  $\sigma^{\circ}$  to geophysical units (wind vector), which allows each to be designed and evaluated independently.

Prior to launch the scatterometer will be calibrated in terms of the ratio of received power to transmitted power,  $P_{\rm R}/P_{\rm T}$ ; thus, the first step is to convert

raw data to  $P_R/P_T$  using pre-flight calibration information. Satellite parameters such as attitude, ephemeris data and various instrument and physical constants are used to determine cell locations on the earth, range, cell length, incidence angle, and antenna look angle. This information along with pertinent housekeeping data are used to determine antenna gain and are inputs for calculating  $\sigma^{\circ}$  and RMS error for use in the geophysical algorithm.

The first step in converting a  $\sigma^{\circ}$  matrix to a wind vector map is to use both the visible/infrared and microwave radiometric data from other SEASAT-A sensors to make a path loss correction to the values of  $\sigma^{\circ}$ . Conversion to wind vector will be accomplished using algorithms that have been developed using several theoretical approaches with each algorithm being evaluated during the mission. These initial values will contain aliases caused by the multi-valued relationship between  $\sigma^{\circ}$  and wind speed and direction. Several methods for removel of these aliases and the generation of wind fields are being considered. [3] [6]

The future of microwave scatterometers (through the 1980's) will probably be dependent on the performance and data quality of the SEASAT-A SCAT. Although radar techniques are well established, laser scatterometers are currently being investigated as an alternative. The latter technique relies heavily on an accurate goold model (e.g., ±10 cm) and state-of-the-art spacecraft attitude control and measurement, which are exactly the expected achievements of the SEASAT-A SCAT.



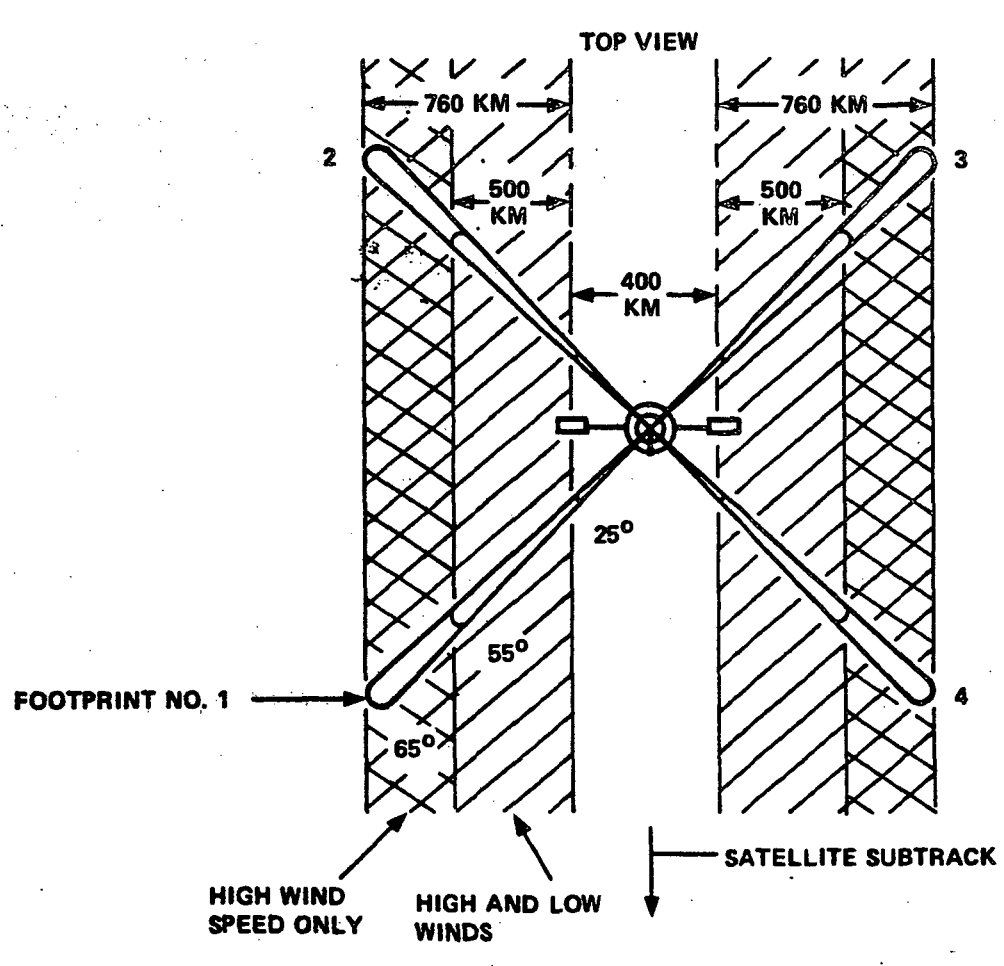


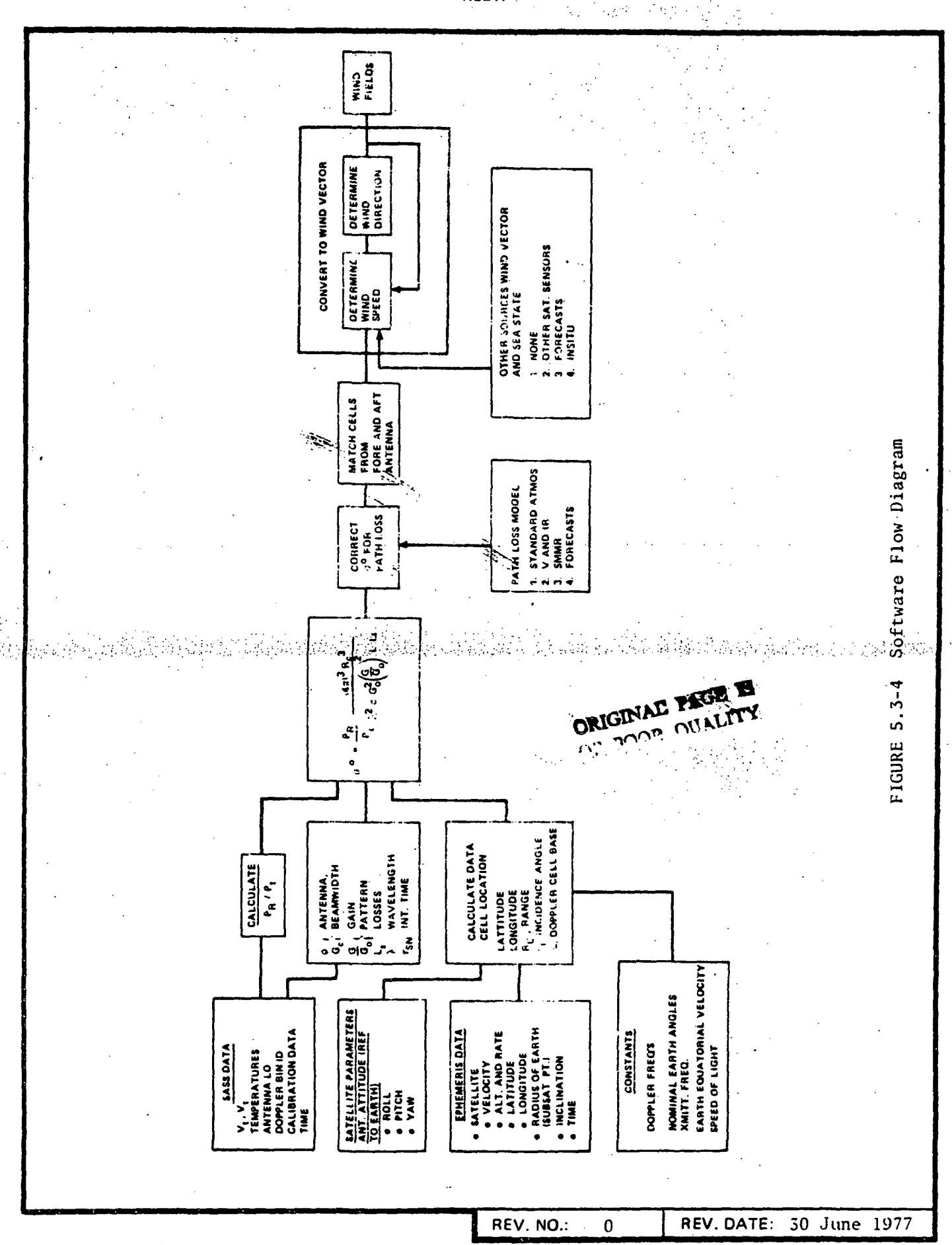
FIGURE 5.3-3 Scatterometer Fan Beam Geometry

5.3.10

REV. NO.:

1 <

REV. DATE: 30 Sept 1977



### SCATTEROMETERS LIST OF ACTIVE CONTRIBUTORS

Anthony J. Spear Seasat-A Project, Sensors Manager Jet Propulsion Laboratory Pasadena, Cal. 91103 (213) 354-4524

Dr. W. L. Grantham
FID, Microwave Remote Sensing Section
Langley Research Center
Hampton, Va. 23665
(804) 827-3631

Dr. W. Linwood Jones FID, Microwave Remote Sensing Section Langley Research Center Hampton, Va. 23665 (804) 827-3631

Dr. John Price Hydrology and Oceanography Branch Goddard Space Flight Center Greenbelt, Maryland 20771 (301) 982-4951

William J. Plant Ocean Sciences Division Naval Research Laboratory Washington, D. C. 20375 (202) 767-2060

### SCATTEROMETERS REFERENCES

- [1] Matthews, Richard E., ed., "Active Microwave Workshop Report," Report of a Working Group Meeting at JSC, (July 1974) pp. 182,223-225, 376.
- [2] "An Operatonal Satellite Scatterometer for Wind Vector Measurements over the Ocean," NASA Technical Memorandum, March 1975.
- [3] Grantham, W. L., "SEASAT-A Satellite Scatterometer," Memorandum-Proceeding Publication in IEEE (April 1977).
- [4] Schuler, "An Experimental Study of a Pulse Compression Scatterometer System," <u>IEEE Trans. Antennas and Propagation</u>, Vol AP-25, No. 1, January 1977, pp. 140-145.
- [5] "SEASAT-A Definition Phase End-to-End Data System Functional Description," NASA Final Report, June 1974.
- [6] Price, J. C., "The Nature of Multiple Solutions for Surface Wind Speed over the Oceans from Scatterometer Measurements," NASA-GSFC, July 1975.

The Market Mary Control of the September 1999

REV. NO.: 1 REV. DATE: 30 Sept 1977

#### **SCATTEROMETERS**

### **BIBLIOGRAPHY**

- (1) McCandless, S. W., and Cardone, V. J., "Seasat-A Oceanographic Data System and Users," Presented at the I.A.F. 27th Congress, Anaheim, CA, October 10-16, 1976.
- (2) Daley, J. C., "Wind Dependence of Radar Sea Return," J. Geophys. Res., Vol. 78, No. 33, pp. 7823-7833, November 1973.
- (3) Krishen, K., "Correlation of Radar Backscatter Cross Sections with Ocean Wave Height and Wind Velocity," J. Geophys. Res., Vol. 76, pp. 6528-5639, September 1971.
- (4) Claassen, J. P., Fung, H. S., Moore, R. K., and Pierson, W. J., Jr., "Radar sea return and the RADSCAT satellite anemometer," presented at the 1972 IEEE Int. Conf. Engineering in the Ocean Environment, Newport, R.I. September 1972, IEEE Publ. 72 CHO 660-1 OCC.
- (5) Moore, R. K., et al, "Simultaneous Active and Passive Microwave Response of the Earth The Skylab RADSCAT Experiment," in Proc. 9th Symp. Remote Sensing of the Environment, Ann Arbor, Michigan, 1974.
- (6) Jones, W. L., Schroeder, L. C., and Mitchell, J. L., "Aircraft Measurements of the Microwave Scattering Signature of the Ocean" IEEE Trans.

  Antennas Propagat./IEEE Journal of Oceanic Engineering, Special Issue on Radio Oceanography, January 1977.
- (7) Skolnik, M. I., <u>Radar Handbook</u>, New York: McGraw Hill, 1970, Ch. 25, pp. 25-16-25-24.
- (8) Ruck, G. T., Barrick, D. E., Stuart, W. D., and Krichbaum, C. K., Radar Cross Section Handbook, Vol. 2, New York: Plenum Press, 1970, Ch. 9.
- (9) Fischer, R. E., "Standard Deviation of Scatterometer Measurements from Space," IEEE Trans. Geoscience Electronics Vol. GE-10, No. 2, April 1972, pp. 106-113.
- (10) Pierson, W. J., Cardone, V. J., and Greenwood, J. A., "The Applications of Seasat-A To Meteorology," City Univ. of New York Tech. Report, August 1974.
- (11) Cook, A. C., Fayman, D. L., Holtzman, J. C., Moore, R. K., Sobti, A., and Spencer, W., "Measurement of Microwave Antenna Patterns from the Orbiting Spacecraft," in Proc. 1974 Int. IEEE/AP-S Symp. Digest, Atlanta, GA, June 1974, IEEE Publ. 74 CHO-857-3 AP, pp. 51-53.
- (12) Moore, R. K., and Pierson, W. J., "Worldwide Oceanic Wind and Wave Predictions Using a Satellite Radar-Radiometer," <u>Journal of Hydronautics</u>, Vol. 5, No. 2, pp. 52-60, April 1971.

## SCATTEROMETERS ILLUSTRATION CREDITS

Figure No.	Page	Reference	<u>Page</u> 224	
5.3-1	5.3-3	[1]		
5.3-2	5.3-4	[1]	225	
5.3-3	5.3-10	[2]	Fig. 14	
5.3-4	5.3-11	[3]	Fig. 9	

REV. NO.: 1 REV. DATE: 30 Sept 1977

This page intentionally left blank.

REV. NO.: 1

REV. DATE: 30 Sept 1977

# RSDH ORIGINAL PAGE IS DATA SHEET OF POOR QUALITY

SHEET 1 OF 4

(1) SENSOR NAME, ACRONYM: Microwave Scatterometer, SCAT

(2) DISCIPLINE: Earth and Ocean Physics (3) SUBDISCIPLINE: Ocean Dynamics

### (4) APPLICATION AND OBJECTIVE:

The SEASAT-A Satellite Scatterometer (SASS) provides a periodic and spatially distributed measurement of the radar backscatter coefficient (power return) for the determination of wind speed and direction (i.e., wind vector) at the sea surface. Wind vectors are a key parameter for improved weather forecasting, hazard warnings, ocean pollution monitoring, and navigational routing and scheduling.

(5) HERITAGE/KEY PERSONNEL: The functional design of the SASS is the result of 4 major experimental efforts, these are: (a) AAFE RADSCAT, LaRC, (b) 13.3 GHZ SCAT, JSC, (c) SEA CLUTTER STUDY, NRL, (d) S-193, SKYLAB;

Exp. Team Leader - W. L. Grantham, LaRC 804-827-3631

### (6) SENSOR DEPLOYMENT:

The SEASAT-A Satellite, bearing the SASS is to be launched to obtain a near circular orbit of 108° inclination and mean altitude of 794 km. The orbital period is 104 minutes resulting in approximately 14 orbits per day. Seven orbits are required for complete ocean coverage.

(7) SENSOR CHARACTERISTICS

### (7A) CAPABILITIES AND CONSTRAINTS OF THE SENSOR TO ACQUIRE THE MEASURED PARAMETER:

The SASS employs 4 dual polarited, for beam, stick antennas. The primary measurements swath is 500 km wide beginning 200 km off the satellite sub-track. Sequential antenna addressing provides orthogonal footprint crossings to the right, left, fore, and aft. These star-like patterns define 100 m grid spacing and 50 m resolution Doppler cells with incident angles of 25° to 55°. Sea State Information is supplied from 3 resolution cells at and near nadir from side lobes generated by each antenna pattern. Also, a high winds swath  $(55° \le 0) \le 65°$  though less accurate provides additional data and increases the effective coverage to over 1500 m.

### (7B) ACTIVE SOURCE CHARACTERISTICS (FOR ACTIVE SENSORS):

The measurement swath is illuminated with a 5 ms burst of microwave energy at a repetition rate of 40 Hz. The transmitted power, 100 W peak at 14.6 GHz is applied sequentially with appropriate polarization to 4 stick antennas. The illumination pattern is  $25^{\circ}$  x  $0.5^{\circ}$  directed  $42^{\circ}$  off nadir and aligned  $45^{\circ}$  across the satellite sub-track. Side lobes from the four stick arrays provide sea state information near nadir.

### (7C) DETECTOR MEASUREMENTS CHARACTERISTICS:

Received RF energy from the proper antenna is directed to a preamplifier, band pass filter, and first conversion mixer. The resulting IF signal is fed to the SASS processor consisting of 15 band-pass poppler filters, square-law detectors, DC amplifiers and signal integrators. Antenna gain is 32 dB with an efficiency of 48%. Receiver band is 14.6 GHz ± 250 MHz. In-band noise is less than -155 dBm in any 2.5 kHz band within 14.6 GHz ± 1 MHz.

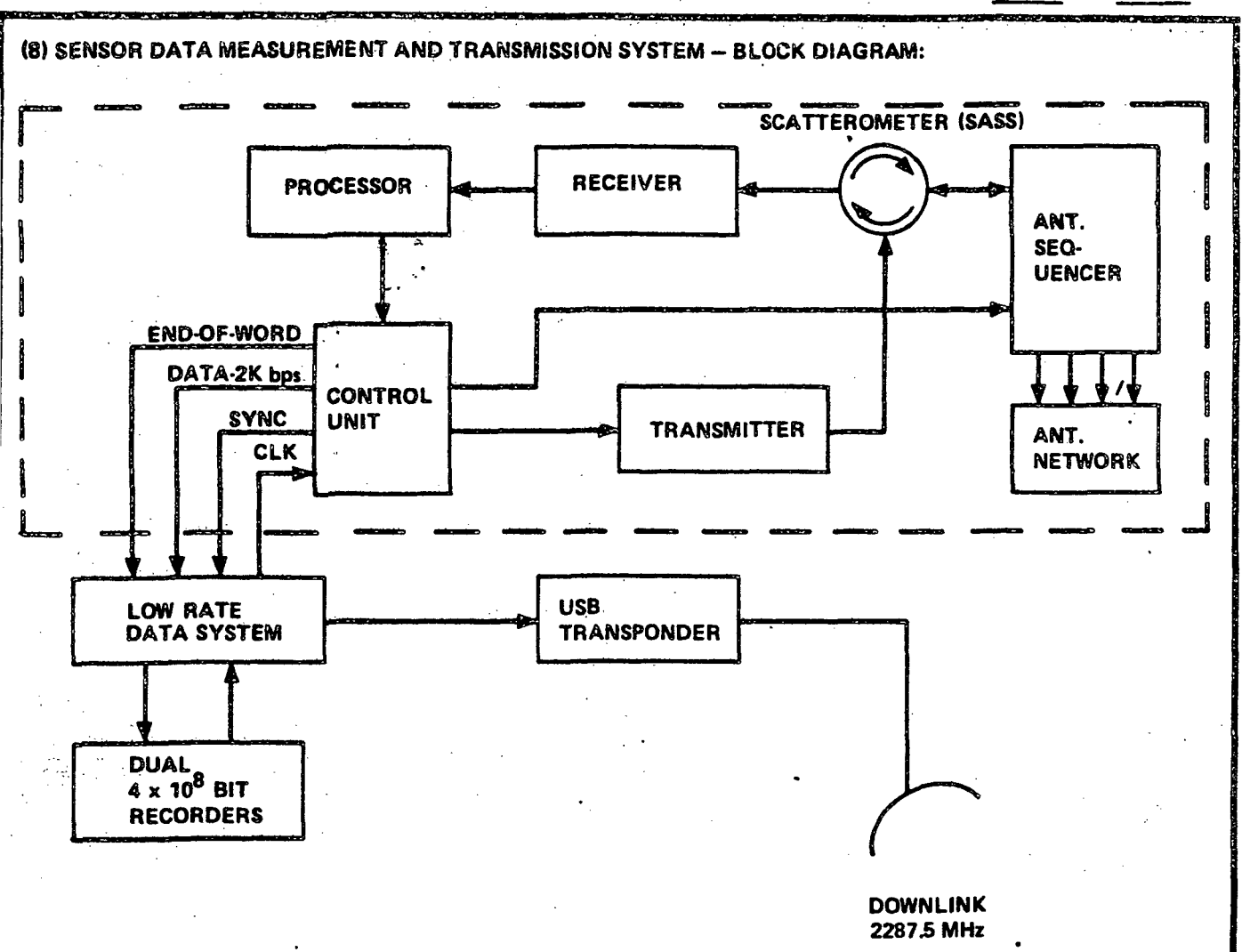
Preceding page blank

SECTION NO.: 5.3 SENSOR CATEGORY: Scatterometers

**REV. DATE**: 31 Jan 1978

5.3-17

**REV. NO.:** 2



### (9) MEASUREMENT AND TRANSMISSION SYSTEM - NARRATIVE:

### S-Band Transmitter for Regular Telemetry and Tracking:

- a Carrier 1 watt, 2287.5 MHz
- b B. W. =  $\pm 3$  MHz about the carrier

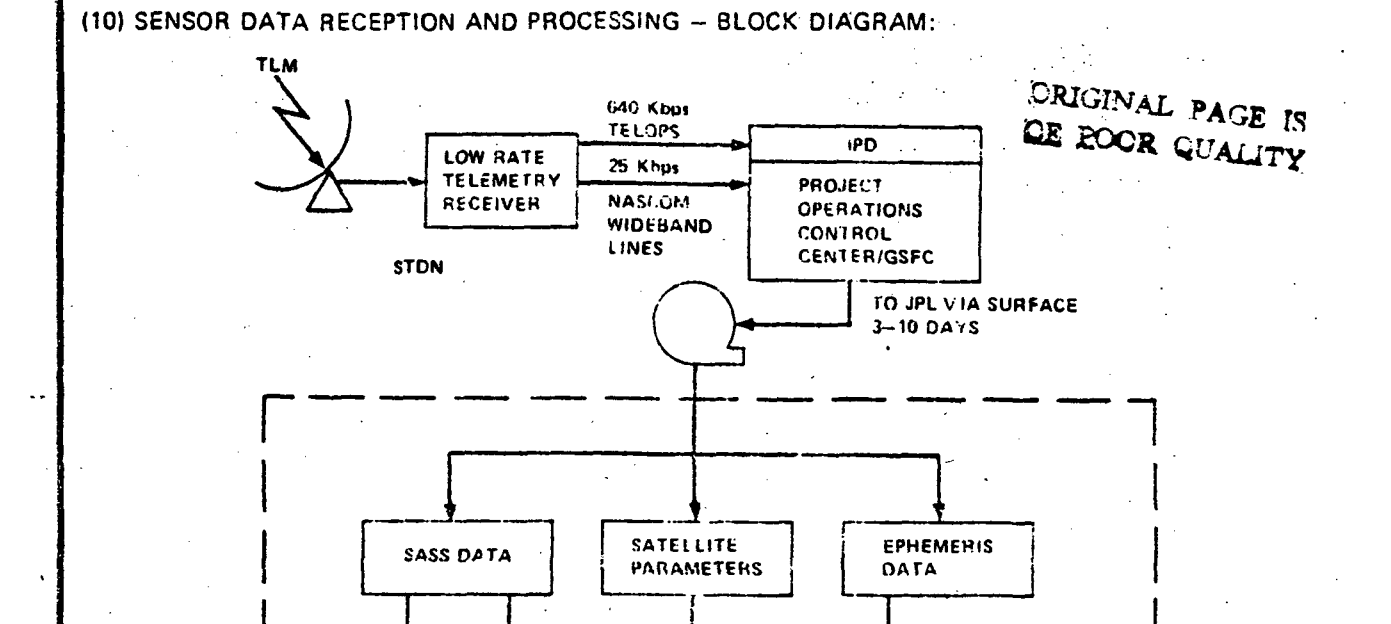
### Telemetry:

- a 25 kbps real-time data stream bi-phase modulating a 1.024 MHz subcarrier which in turn phase-modulates the carrier (PCM/PSK/PM)
- b 690 Kbps tape recorder playback phase modulates the carrier

5.3-18

SECTION NO.: 5.3 SENSOR CATEGORY: Scatterometers

REV. NO.: 2 REV. DATE: 31 Jan 1978



CALC. DATA

CONSTANTS:

EXP. DATA

CONVERT TO WIND VECTOR

PATH LOSS MODEL

DETERMINE

DIRECTION

WIND

SEA TRUTH AND

### (11) RECEIVING AND PROCESSING - NAPRATIVE:

CORRECT MEAN

BACKSCATTER

FOR PATH LOSS

COEFFICIENT

MATCH CELLS

AFT ANTENNA

FROM FORE AND

The STDN sites receive Low-Rate playback TLM data at 640 at 800 kbps during contact periods. Received TLM data is retransmitted to 1PD at GSFC via TELOPS. IPD will preprocess the TLM data to produce time-smoothed and quality-checked telemetry. A master data file is constructed on a daily basis and sent to JPL via surface delivery.

DETERMINE

WIND

SPEED

5.3.19

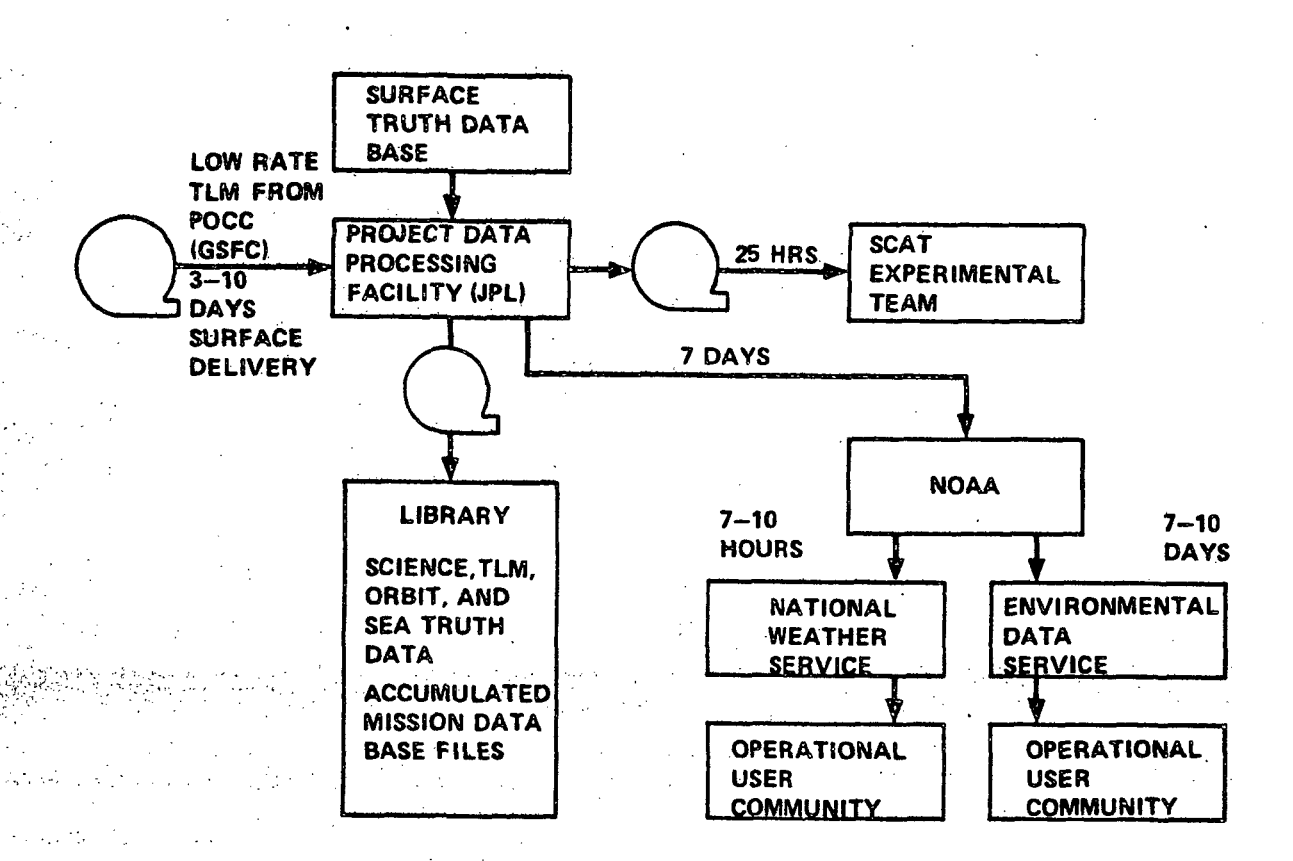
SECTION NO.: 5.3 | SENSOR CATEGORY: Scatterometers

REV. NO.:

REV. DATE: 31 Jan 1978

WIND VECTOR

### (12) DISTRIBUTION OF DATA FROM GROUND STATIONS - BLOCK DIAGRAM:



### (13) DATA DISTRIBUTION - NARRATIVE:

JPL receives edited, time-smoothed TLM data from GSFC. The four primary functions performed by JPL are:

- a produce an Experiment Data Record for each team,
- b produce supplementry data for each experiment (i.e., sensor earth located footprint, engineering data),
- c produce a single processed data record in geophysical units for each experiment, i.e., wind speed/direction, surface temperature, etc., and
- d produce validated algorithms to independent raw data users (e.g., FNWC).

SECTION NO.: 5.3 SENSOR CATEGORY: Scatterometers

# SENSOR CATEGORY TABLE OF CONTENTS AND REVISION CONTROL SHEET

SENSUR NAME OR		NUMBER	24.05	EFFE	CTIVE
OTHER ENTRY		OF PAGES	PAGE NUMBER	REV. DATE	REV. NO.
Section 5.4 Table of Co	ontents	1	5.4-i	31 July 78	3
Introduction To Laser R	tadars .	13	5.4-1 5.4-2 5.4-3 5.4-4 5.4-5 5.4-6	31 July 78 31 July 78 31 July 78 31 July 78 31 July 78 31 July 78 31 July 78	3 3 3 3 3 3 3
	·		5.4-7 5.4-8 5.4-9 5.4-10 5.4-11 5.4-12 5.4-13	31 July 78	3 3 3 3 3 3
LIDAR (APL-I)		5	5.4-15 5.4-16	31 July 78 31 July 78	3 3
	e t		5.4-17 5.4-18 5.4-19	31 July 78 31 July 78 31 July 78	3 3 3 3
Laser Altimeter/Profilom Experiment (OP-06-S) and Spaceborne Laser Ranging System (OP-16-5)		િંદુ હ <b>ેલ 5</b> એફ સ્ટ્રો	5.4-21 5.4-22 5.4-23 5.4-24 5.4-25	31 July 78 31 July 78 31 July 78 31 July 78 31 July 78	3 3 3 3 3
 		l <u>.</u>			
L .	•	<b> </b>		·	
I				·	
	_				
	5.4				

REV. NO.: 3

This page intentionally left blank.

REV. NO.: 3.

#### Section 5.4

# INTRODUCTION TO LASER RADARS (LIDAR)

Until recently, optical remote sensing has been restricted only to passive techniques in which either radiation emitted or attenuated by the target has been measured in order to provide signature information. However, recent progress in the development of more rugged and stable lasers, suggest the use of laser radar as tools to actively probe the environment.

The laser radar or LIDAR is similar to a microwave radar, but operates at optical wavelengths generated by a pulsed laser. The LIDAR has several unique features which make it useful and practical as a remote sensing instrument.

Among these are the ability to operate independently of external signal sources, to operate at night covertly, to operate in spectrally narrow wavelength bands, to eliminate shadowing and to allow one to modulate or code the radiation. The laser light can be emitted in very short pulse of high energy and thereby good spatial resolution is obtained. The high pulse energy permits coverage of long distances, and the high energy density of the laser beam offers the possibility of realizing the Raman-lidar. The laser light is monochromatic which makes it possible to eliminate background light by narrow band filters in the receiver. It can be well collimated which gives angular resolution and reduction of background light by use of narrow receiver lobe. The low divergence of the laser beam permits the tracking of comparatively small objects.

Various remote sensing techniques are currently used, proposed and/or under study, depending on the specific applications, the nature of the optical effect or process utilized, the spectral range, the type of laser as a radiation source and the relative positions of the radiation source and the detector. Laser radars as applied to the hydrosphere, can be used to provide

shallow-water bathymetric measurements, to detect and identify oil slicks, to detect algae, to measure and track subsurface currents and to measure water turbidity. As applied to the atmosphere, the laser radar can be used to study the composition, structure and dynamics of the atmosphere. The optical effects that may be utilized include emission, absorption, Raman scattering, fluorescence, and elastic scattering of the Rayleigh and Mie types depending on the wavelength of the incident radiation and the nature of the target. The spectral range extends from the near ultraviolet to the infrared. The lasers can be either fixed frequency or tunable frequency, and they can operate either in the C-W output mode or in the pulsed output mode. The fixed frequency lasers include the chemical lasers, gas lasers and the solid state lasers. Tunable frequency lasers include the organic dye lasers, parametric oscillators, semiconductor diode and spin-flip Raman lasers, harmonic generation and frequency mixing, bulk semiconductor laser (optically pumped), and high-pressure gas lasers (electron . beam pumped). The position of the radiation source relative to the detector classifies the system as single-ended active or doubled-ended active. In the single-ended active system, the radiation source and the detector are located together and backscattered radiation is measured. In the double-ended active system, the radiation source and the detectors are on opposite sides of the target and the attenuation of the laser beam by the target is measured.

## PRINCIPLE OF OPERATION

Optical remote sensing using lasers is based on the principle that photons interact with atoms, molecules and particles to produce various types of optical effects depending on the wavelength of the incident radiation and the nature of the target. A laser beam is emitted from a transmitter, scattered back by

certain media and measured in a receiver. From the signal received, one is able to make a statement on the backscattered medium (target).

Basically, a LIDAR system consists of a pulsed laser transmitter, a telescope receiver, detector(s) and data system to record the backscattered light as a function of distance or range. Examples of various applications will be discussed here.

Laser altimeters and other ranging devices can operate on the phasing principle or upon pulse time of travel. Both have their equivalent. The phasing principle is illustrated by Figure 5.4-1 where the output of a solid state or gas CW laser is amplitude modulated at some frequency  $f_1$ . Absorption type modulators are common in gas lasers due to the difficulty of direct (current) modulation. With solid state (injection) lasers, common practice is to simply modulate the current through the laser diode. The output of the laser is propagated at the velocity of light in the medium and a wave of length  $\lambda$  characteristic of  $f_1$  is generated in space. The laser's energy is reflected off a target located at "A". A corner cube reflector is normally used as a target because of its capability to reflect a beam of light back to its origin. The returned beam, detected in the receiving optics, produces an electrical signal  $\mathbf{S}_{\mathbf{1}}$ . The output of the laser is sampled and produces signal S<sub>2</sub>. The differences between S<sub>1</sub> and S<sub>2</sub> are in amplitude (which is compensated for) and in phase which is proportional to the distance (D) between the laser and the reflector. If D changes by an amount smaller than  $\lambda$ , the change can be read directly on the phase meter. However, if D is longer than  $\lambda$ , an ambiguity exists which can be resolved by determining the phase between two other  $S_1$ ,  $S_2$  signals at some other frequency  $f_n$ . Normally, phase measurements at four different frequencies are used in calculating "D" technique is often called tone ranging.

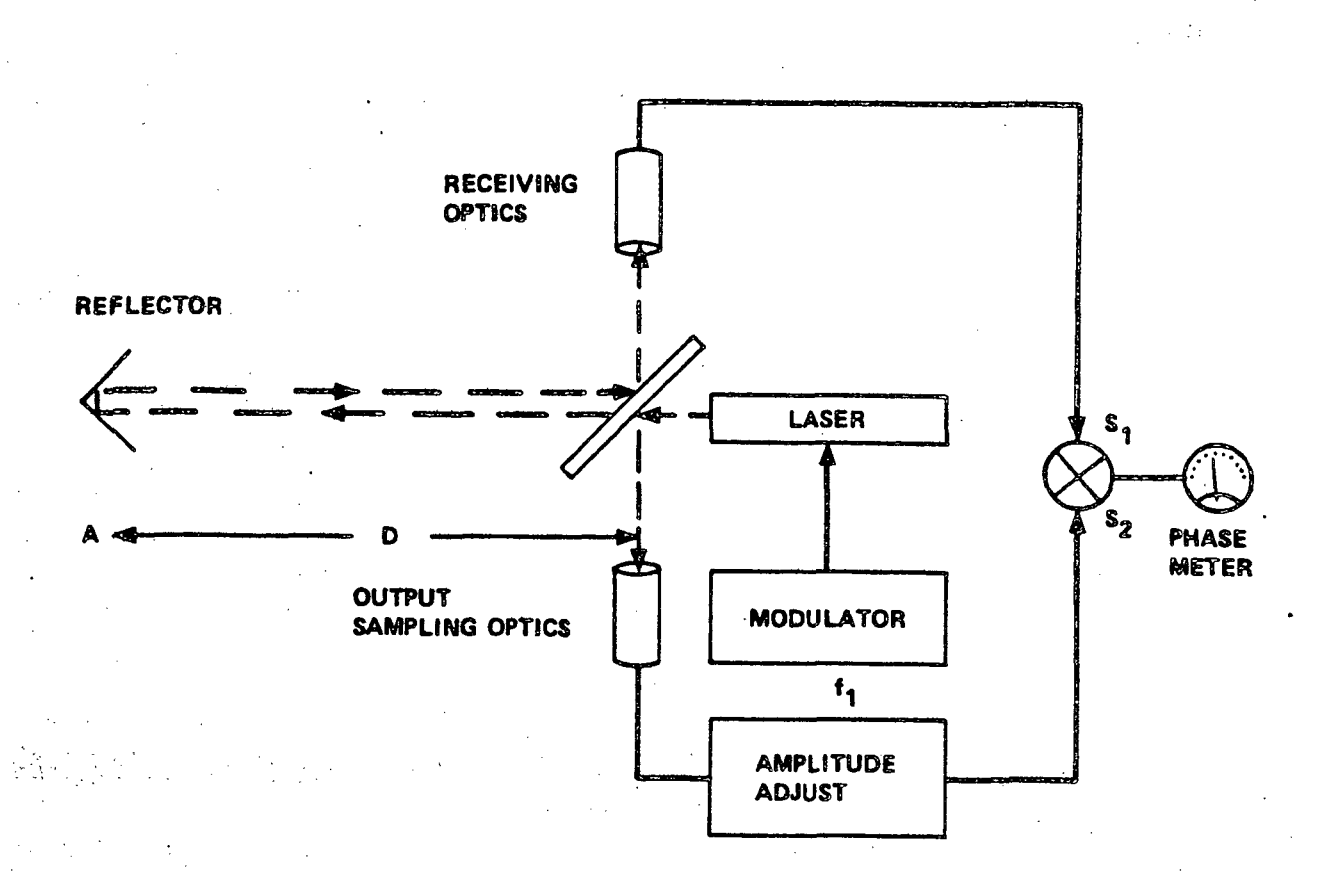


FIGURE 5.4-1 Laser Ranger (Laser)

A second ranging technique is illustrated by Figure 5.4-2 where a short pulse is emitted from a ruby or similar laser. The output is again sampled and this trigger starts a counter totalizing the pulses produced by an oscillator. The laser output reflects off the target at "A" and is detected in the receiving otpics where it stops the counter, thereby completing one determination of "D". The frequency of the oscillator driving the counter can be selected so that the number of pulses counted during the time of flight of the laser output pulse (to the target and back) numerically corresponds to the distance D in centimeters or other units.

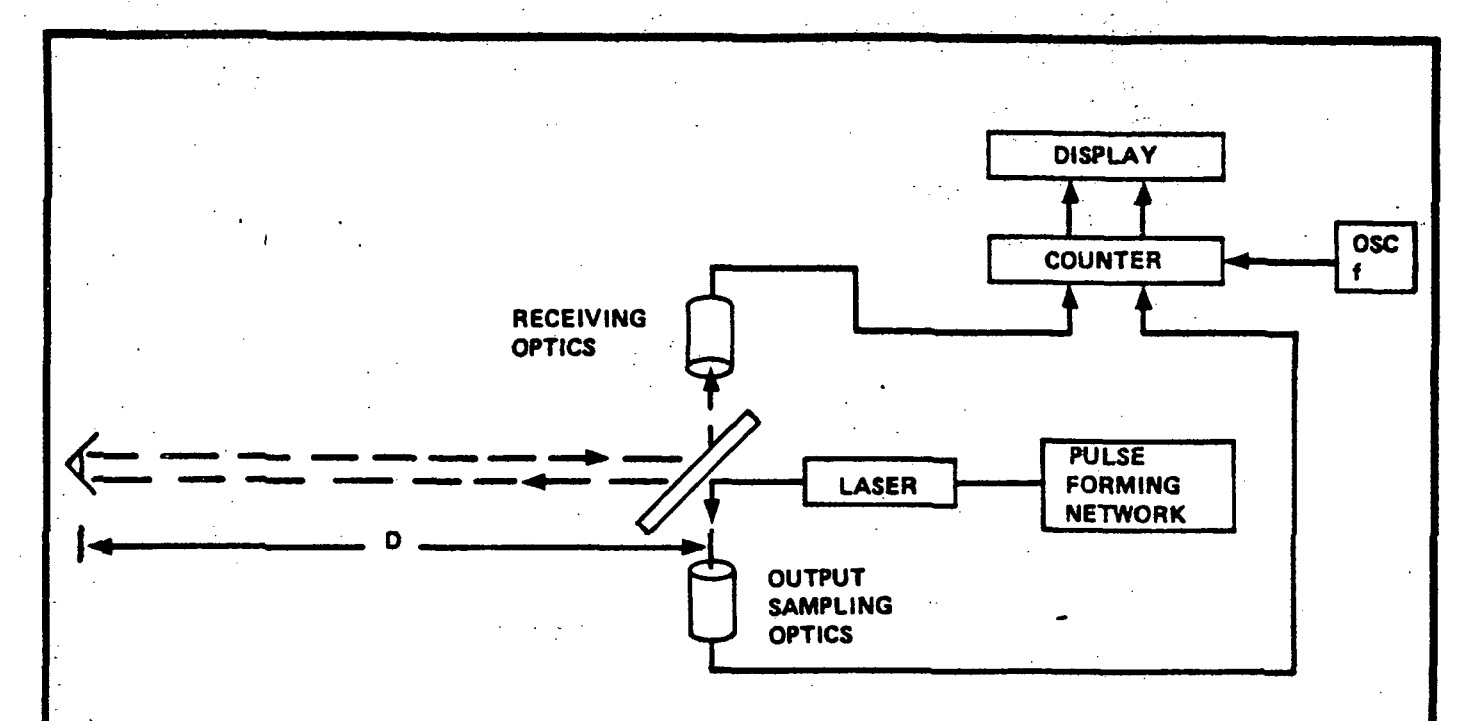


FIGURE 5.4-2 Laser Ranger (Time of Flight)

Owing to the shortness of the wavelength, pulses produced by lasers can be physically very short, which leads to good resolution of target position. Rangers of either type can be made accurate to within one or two centimeters in several kilometers. For these reasons, laser rangers have been used for determining the distance from the earth's surface to extraterrestial bodies like the moon and other satellites. In these experiments, the laser is mounted on the earth and the cornercube reflector is mounted on the satellite. Laser rangers have also been selected for use in earthquake detection schemes where they would be used in connection with a satellite to measure the motion of the plates making up the Earth's crust.

Another form LIDAR can take is essentially a scatterometer as shown in Figure 5.4-3. Here, energy emitted by the laser reacts with the medium through which it passes. The radiation thus produced is monitored at the laser site for such things as polarization rotation, backscattered radiation intensity and wavelength. Depending upon the nature of the interaction of the laser output radiation with the

medium and/or the target, the radiation received might not be the same wavelength as that emitted by the laser. There are basically two interaction phenomena of interest, florescence and Raman scattering.

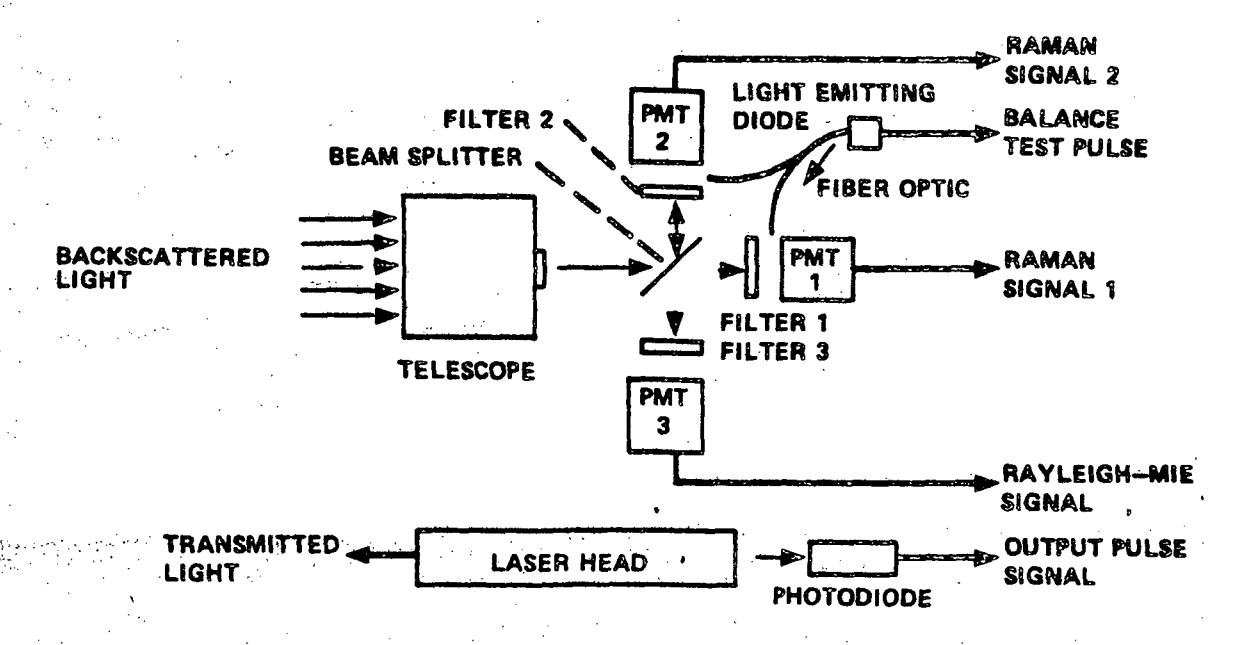
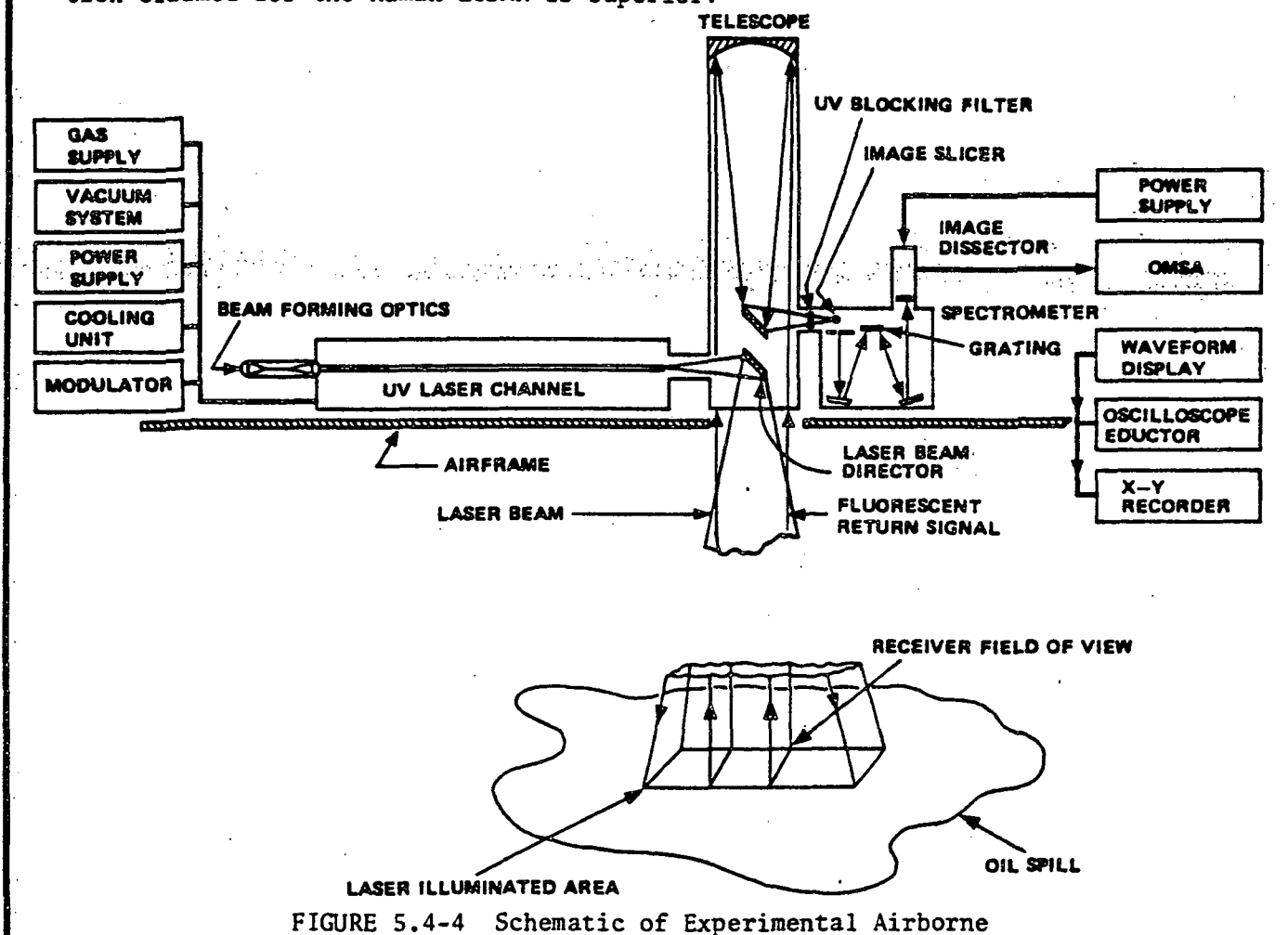


FIGURE 5.4-3 Optical Design Schematic

Florescence occurs when the laser light reacts with the surface in such a way that radiation is re-emitted at a wavelength significantly different from that of the laser. This characteristic is being employed and practical, experimental sensors have been built to detect the florescence of oil on water. This florescence has an output signature characteristic of the type of oil and the implication is that it will be possible to develop oil spill detectors capable of classifying the type oil involved. As an example, in one such experiment a N<sub>2</sub> laser emitting at 3370 Angstroms excited twenty-nine different grades of oil into florescence at wavelengths ranging from 4000 to 6000 Angstroms. An example of this kind of system is shown in Figure 5.4-4 [3]. In the configuration shown, the support systems required for operation, the power requirement, size and complexity make it difficult to imagine this evolving into spacecraft borne system.

A variation of the system described above is the Raman LIDAR. These have been developed [1] to monitor air temperature and the turbidity of water. The application to air temperature measurement can be conducted along a horizontal path (unlike a VTPR) but it lacks advantages which would obviate the VTPR. Temperature accuracy and vertical height range of measurements made by LIDAR are inferior to vertical temperature profiling radiometers but the spatial resolution claimed for the Raman LIDAR is superior.



**REV. NO.:** 

31 July 1978

REV. DATE:

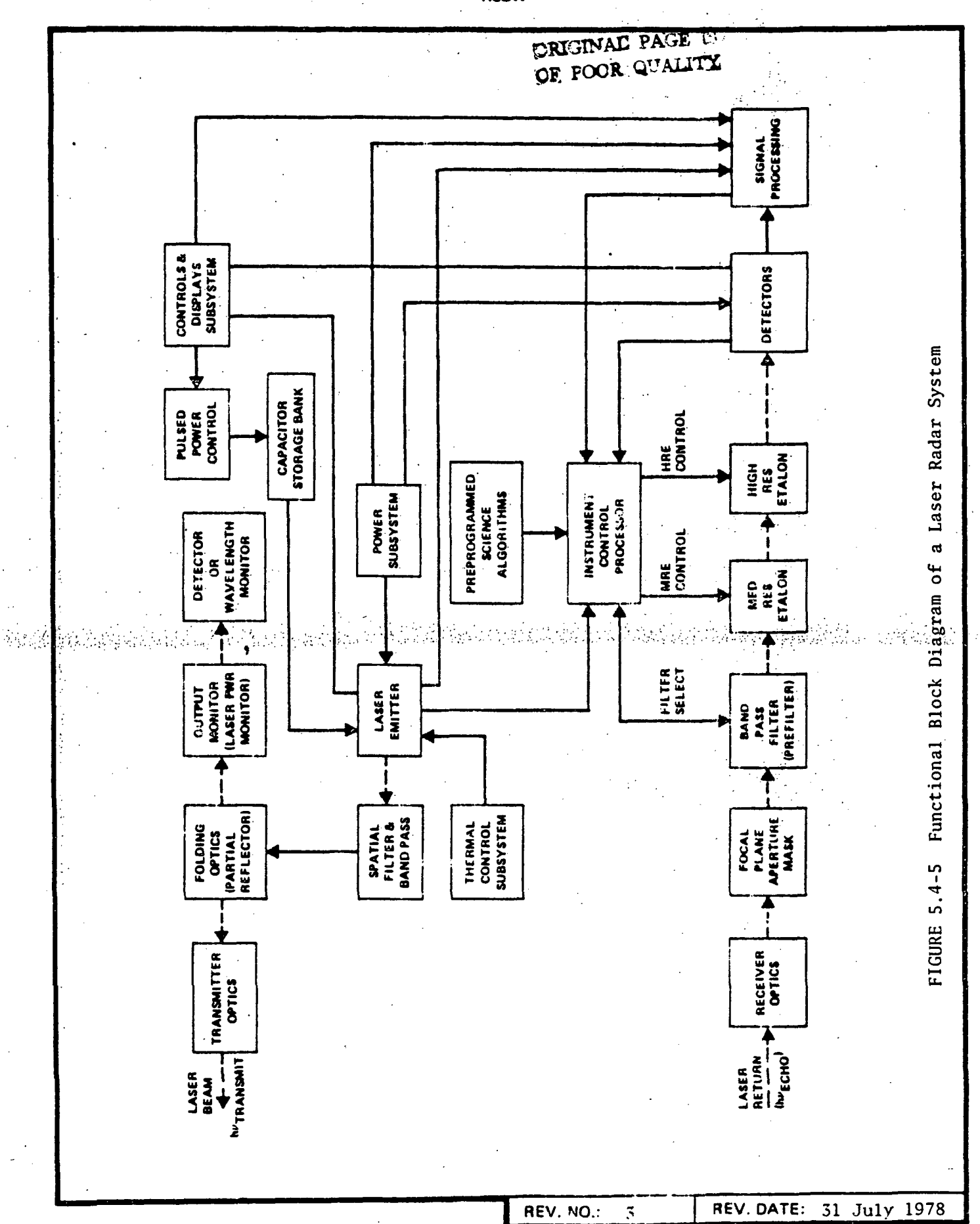
Laser Remote Sensing System

The LIDAR system for atmospheric monitoring, shown in Figure 5.4-5 uses a doubled [5] narrow band frequency tuned laser pumped by a doubled Nd:YAG laser. The laser emits a monochromatic, high power and highly collimated beam of low divergence. The beam goes to the folding optics where it is reflected to the transmitter optics for further collimation. A portion of the laser beam goes through the folding optics to the laser power monitor.

The pulsed high power laser beam, after being spatially filtered, is focused onto a narrow column of the atmosphere by the transmitter optics. Molecules and aerosols absorb and/or scatter this radiation (i.e. the emitted laser pulses undergo Mie scattering, Rayleigh scattering, Raman scattering and resonance Raman and/or resonance fluorescence). A portion of the light is scattered back from the atmosphere and is collected by a receiving telescope which is coaxial or adjacent to the transmitter.

The collected backscattered light is focused at a field of view-limiting aperture, then passed through a narrow band filter (to reject unwanted stray light of different wavelengths) and then through a narrowband interference filter to a fast response radiation detector(s).

The detector(s) transform the received photons into photoelectrons. The output signal (photoelectrons) is processed in an analog fashion or by the pulse counting technique depending on the level strength of the returned signals. The strong signals are processed in the analog fashion in which the photoelectrons are amplified, filtered, fed into a two sample hold and then into a highly stable analog-to-digital converter (ADC). The digitalized output of the ADC is transferred into a 16-bit register. The weak returns can be processed using pulse counting techniques in which the photoelectron are amplified, discriminated, pulse shaped and fed into two 8 bit counters and then into a 16-bit register.



A range bin clock activated by a laser-has-fired pulse transferred the contents of the 16-bit register into a shift-register storage buffer at intervals corresponding to 250 m of lidar range. After sufficient time has elasped for acquisition of all return-signal data, the shift register will be clocked into the experiment computer through a RAU or through a High Rate Multiplexer. The scientific data from the LIDAR is based on the time when the pulse returns (i.e., time delay between transmitted and received pulses), the amplitude of the return pulse and the pulse width.

The signal obtained from the LIDAR system is a time history of the interaction of the transmitted light pulse as it propagates through the atmosphere. By knowing the speed of light in the atmosphere, the time history of the backscattered radiation can be converted to distance, and thus the LIDAR can be used to measure the spatial distribution of the scattering media in the atmosphere. The light backscattered by the atmosphere will have spectral characteristics representative of the gas from which it is scattered. The characteristics of these spectra, line center, width and intensity lead directly to the determination of motion, temperature and abundance of the scattering species. By analyzing the spectra as a function of the transit time (i.e. time delay between transmitted and received pulses) various altitude regions will be explored.

REV. NO .:

# LASER RADARS LIST OF ACTIVE CONTRIBUTORS

Dr. Charles L. Korb
Mail Code 941.0
Building 22, Room 308
Goddard Space Flight Center
Greenbelt, MD 20771
(301) 982-6233

Dr. Edward J. Hurley
Mail Code 941.0
Building 22, Room 308
Goddard Space Flight Center
Greenbelt, MD 20771
(301) 982-6233

Dr. W. L. Barnes Mail Code 941.0 Building 22, Room 390 Goddard Space Flight Center Greenbelt, MD 20771 (301) 982-4117

Dr. Robert T. Menzies Mail Code 183B-365 Jet Propulsion Laboratory-CIT Pasadena, CA 91103 (213) 354-3787

Michael S. Shumate
Mail Code 183B-365
Jet Propulsion Laboratory-CIT
Pasadena, CA 91103
(213) 354-2016

Dr. M. Patrick McCormick Mail Code 475 Langley Research Center Hampton, VA 23665 (804) 827-1110, Ext. 3426

Dr. T. A. Coney Dept. Physics Drexel University Philadelphia, PA 19104 (215) 895-2732

REV. NO.:

# LASER RADARS REFERENCES

- [1] Coney, T. A. and Salzman, J. A., "Remote Measurement of Atmospheric Temperatures by Raman LIDAR" Proceedings of the Ninth International Symposium on Remote Sensing of Environment, Vol. I, pp. 445-451.
- [2] Shieves, T. C., et al, "Remote Measurements of Water Pollution With LIDAR Polarimeter" Ibid, Vol. III, pp. 1695-1708.
- [3] Fantasia, J. F. and Ingrao, H. C., "Development of an Experimental Airborne Laser Remote Sensing System for the Detection and Classification of Oil Spills" Ibid, Vol III, pp. 1711-1745.
- [4] Kung, R. T. V. and Itzkan, I., "A New Concept for the Remote Measurement of Oil Florescence Converdion Efficiency" Proceedings of the Tenth International Symposium on Remote Sensing of Environment, Vol. I, pp. 231-241.
- [5] AMPS Instrument Functional Requirements, AMPS Task Team NASA, MSFC, February 1976, pp I-1 1-9.

# LASER RADAR ILLUSTRATION CREDITS

Figure No.	Page	Reference	Page
5.4-3	5.4-6	[1]	445
5.4-4	5.4-7	[3]	1721

This page intentionally left blank.

REV. NO.: 3

(1) SENSOR NAME, ACRONYM: LIDAR (APE-01)

(2) DISCIPLINE: Atmospheric Sciences

(3) SUBDISCIPLINE: Atmospheric Monitoring

#### (4) APPLICATION AND OBJECTIVE:

The laser radar is designed to determine atmospheric winds, temperature profiles and constituent abundances by measuring the Doppler shift, width and intensity of the back-scattered LIDAR returns. These measurements are important to provide information concerning the dynamics, structure and composition of the atmosphere. It will be also used to determine cloud top altitudes, cirrus cloud reflectivities and thickness, and vertical profiles of atmospheric aerosols using backscatter LIDAR returns.

(5) HERITAGE/KEY PERSONNEL: At present only simple versions of this sensor exist, which are the outgrowth of military airborne laser designator technology coupled to laboratory demonstrated dye laser tuning technology. Exp. Team Leaders: M. Chanin, CNRS, France G. Fiocco Laborotorio Plasma Spazio, Italy, G. Swenson, NASA, MSFC, R.D. Hake, SRI

#### (6) SENSOR DEPLOYMENT:

The laser radar is tentatively scheduled to be launched in 1981 as part of the Spacelab, into a circular orbit, at altitude 250-275 km and inclination between 38-57 degrees. It will be hard mounted to the pallet with its optical axis parallel to the orbiter Z-axis.

(7)

#### SENSOR CHARACTERISTICS

# (7A) CAPABILITIES AND CONSTRAINTS OF THE SENSOR TO ACQUIRE THE MEASURED PARAMETER:

The laser radar includes fixed, multiwavelength and tunable emitters operable at UV, VIS and IR wavelengths, 1 mrad FOV, high resolution dispersive elements, 1 m diameter receiver, narrow band filters, photomultiplier tubes and photodiode detectors, signal processing and electronics. It can operate day or night and preferably no moon at night. The sensor will be oriented either at the nadir or 45° to the nadir. A total of 18 hours of operation will be allowed due to power constraints.

#### (7B) ACTIVE SOURCE CHARACTERISTICS (FOR ACTIVE SENSORS):

The laser radar transmits a short burst (<  $2\mu s$  pulse width) of collimated, monochromatic energy (1J) at a 1 to 10 Hz repetition rate. The spectral width is <.01 nm. Power efficency is 0.1 to 1%, and beam divergence is 1 x  $10^{-4}$  radians.

(7C) DETECTOR MEASUREMENTS CHARACTERISTICS: The detectors will measure the intensity of the backscattered lidar signals. They can be either photomultiplier tube (PMT) or photodiode depending on the wavelength of the incoming signal. The PMT is used when the incoming photon is in the UV or visible, with 20% quantum efficiency (QE) at 530 nm, 2% QE at 1060 nm, sensitivity 5 counts/sec and dynamic range from less than 1 photon per second to  $10^3$  photon per sec. When the incoming light is in the IR, the photodiode is used, with sensitivity >10  $\mu$ w/cm², dynamic range from less than 1  $\mu$ w/cm² to greater than 1 kw/cm². Possible IR detectors are the InS (1000-3000 nm) InSb (2000-2500 nm), Hg Cd Te (7000-14000 nm), Pb Sn Te (2000-12000 nm). Data generated is digital and is approximately 5.4 Kbps.

5.4-15

Preceding page blank

SECTION NO.: 5.4

SENSOR CATEGORY:

Laser Radar

REV. DATE: 31 July 1978

REV. NO.: 3

#### (8) SENSOR DATA MENSURAL AND TRANSMISSION SYSTEM - BLOCK DIAGRAM: ORBITER **SPACELAB** LIDAR ANALOG MEASUREMENT COUNTING MEASUREMENT MASS ADC (RESOLUT 0-8 BITS) (RESOLUTION DISPLAYS EXPERIMENT MEMORY COMPUTER UNIT KEY8OARDS 64K BPS PCMMU EXPERIMENT INPUT/OUTPUT REGISTER UNIT MCC COROLLARY DATA DATA TIMING (STATE VECTOR ETC.) 36 8118 INPUT **50M BPS** HIGH HIGH RATE Ku BAND RATE 2M BPS PROCESSOR MULTIPLEXER DATA RECORDER COMPOSITE DOWNLINK DATA SCIENCE DATA STREAM VOICE ANNOTATION EXPERIMENT B16 REGISTER RAU'S

### (9) MENSURAL AND TRANSMISSION SYSTEM - NARRATIVE:

The detector output can be either an analog signal or calibrated pulses depending whether the photon counting method is used or the parameter to be measured is the peak power.

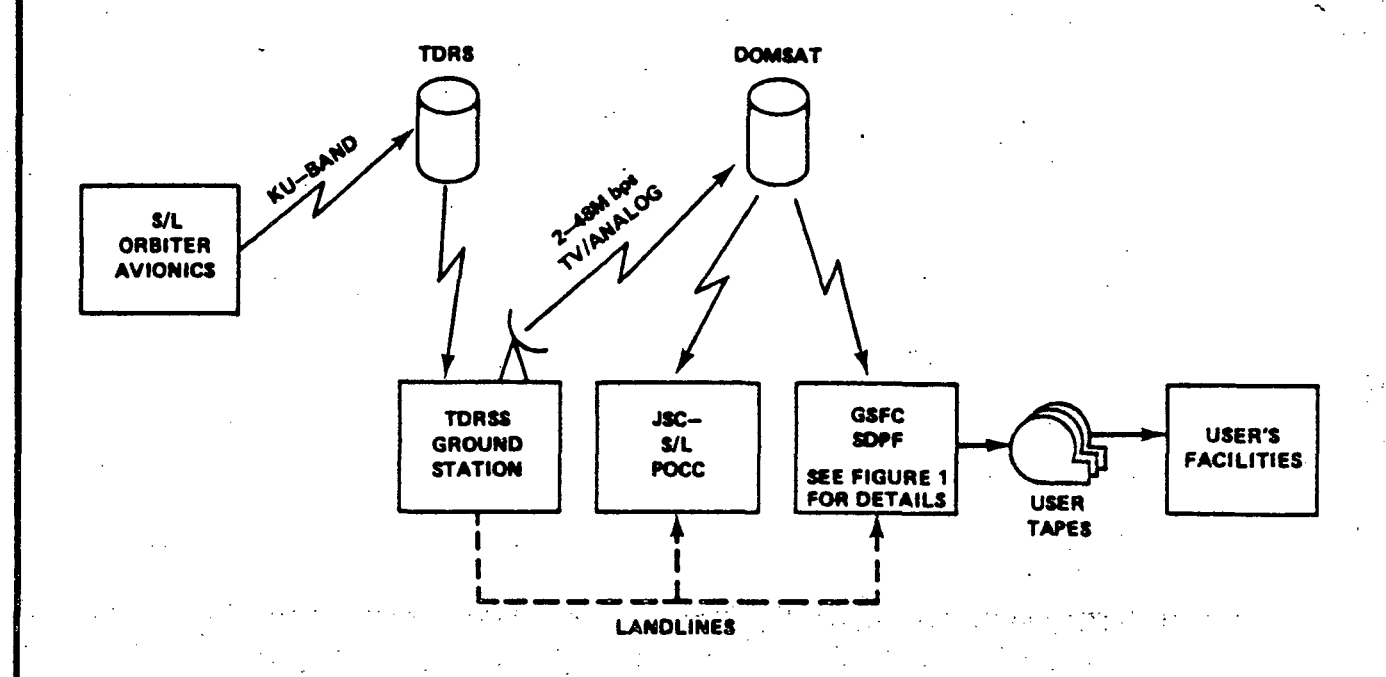
The calibrated pulses are fed into two 8-bit counters and then its contents are transferred into the 16-bit register. The signal is then routed via a buffer to the High Rate Multiplexer. The analog signal is fed into a two sample hold and then to 8 bits analog-to-digital converter. The digital output is transferred to a 16 bit register and then to the High Rate Multiplexer via a buffer. The science data, corollary data. voice and timing, form a composite data stream which is transferred to the Ku Band signal processor for downlink.

SECTION NO.: 5.4 SENSOR CATEGORY: Laser Radar

5.416

REV. NO.:

(10) SENSOR DATA RECEPTION AND PROCESSING - BLOCK DIAGRAM:



(11) RECEIVING AND PROCESSING - NARRATIVE: The Spacelab and orbiter flight data is transmitted to the TDRSS ground station via TDRS on the Ku Band. The data stream is demultiplexed inside the TDRSS ground station and outputed as follows: The high rate multiplexer wideband data stream and the video/analog 4.2 MHz data are routed to the Payload Operations Control Center (POCC) at JSC and to the Data Processing Facility (SDPF) at GSFC via the Domsat. Alternately, the low rate data is routed vialand lines to JSC and GSFC. The POCC performs the time critical payload data processing. POCC operations include monitoring, recording and demultiplexing the payload data.

The SDPF (See Figure 1 on next page) supports the non-time-critical data from the Spacelab payloads. SDPF operations include quality checking, editing, chronologically ordering and formatting of the experiment and ancillary data. It performs conversions and transformations of the ephemeris/attitudes data. SDPF contains two major systems: Spacelab Input Processing System (SIPS) and a Spacelab Output Processing System (SOPS).

(continued on next sheet)

SECTION NO.: 5.4 SENSOR CATEGORY: Laser Radar

### CONTINUATION SHEET:

# (11) continued

The SIPS performs the preprocessing functions required in SDPF. SIPS operations include data capturing, data quality monitoring, accounting demultiplexing and analog/video/voice product generation. Output products are generated by SIPS for shipment and further processing at other facilities. Their output products include: Unedited digital tapes and analog/video/voice tapes. The SOPS performs editing, time validation, formatting and digital product generation. Edited digital tapes are generated by SOP's for shipment to the principal investigators.

# ORIGINAL PAGE IN

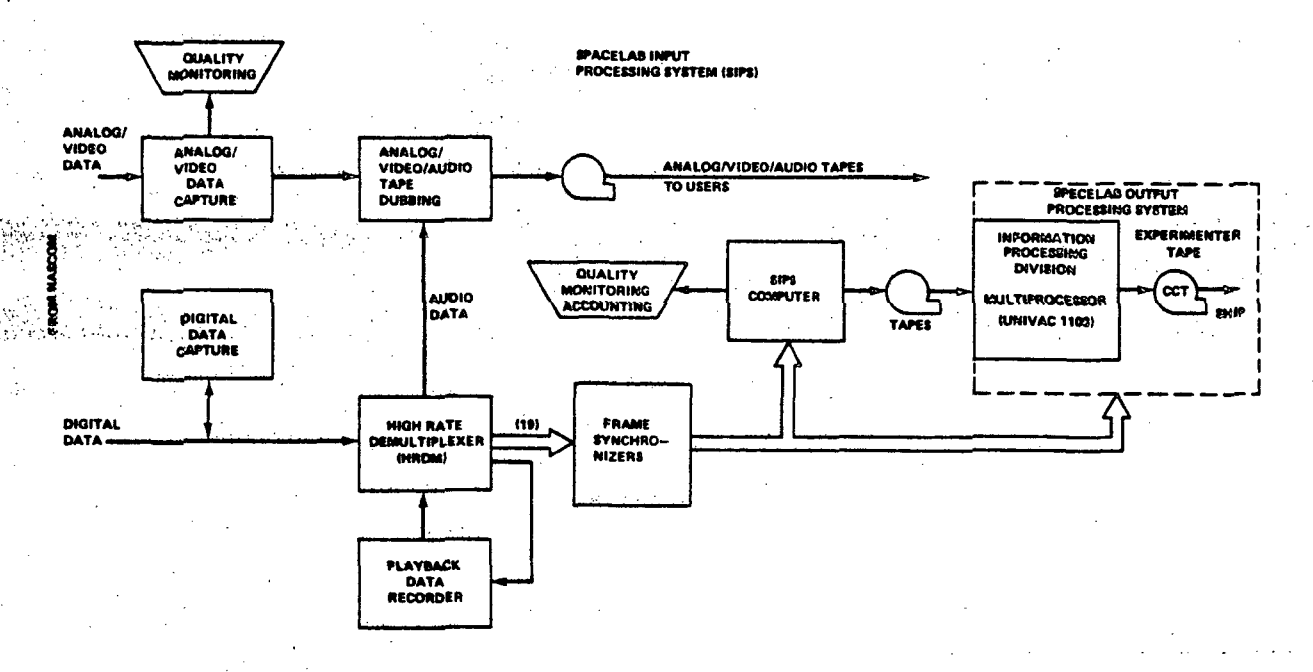
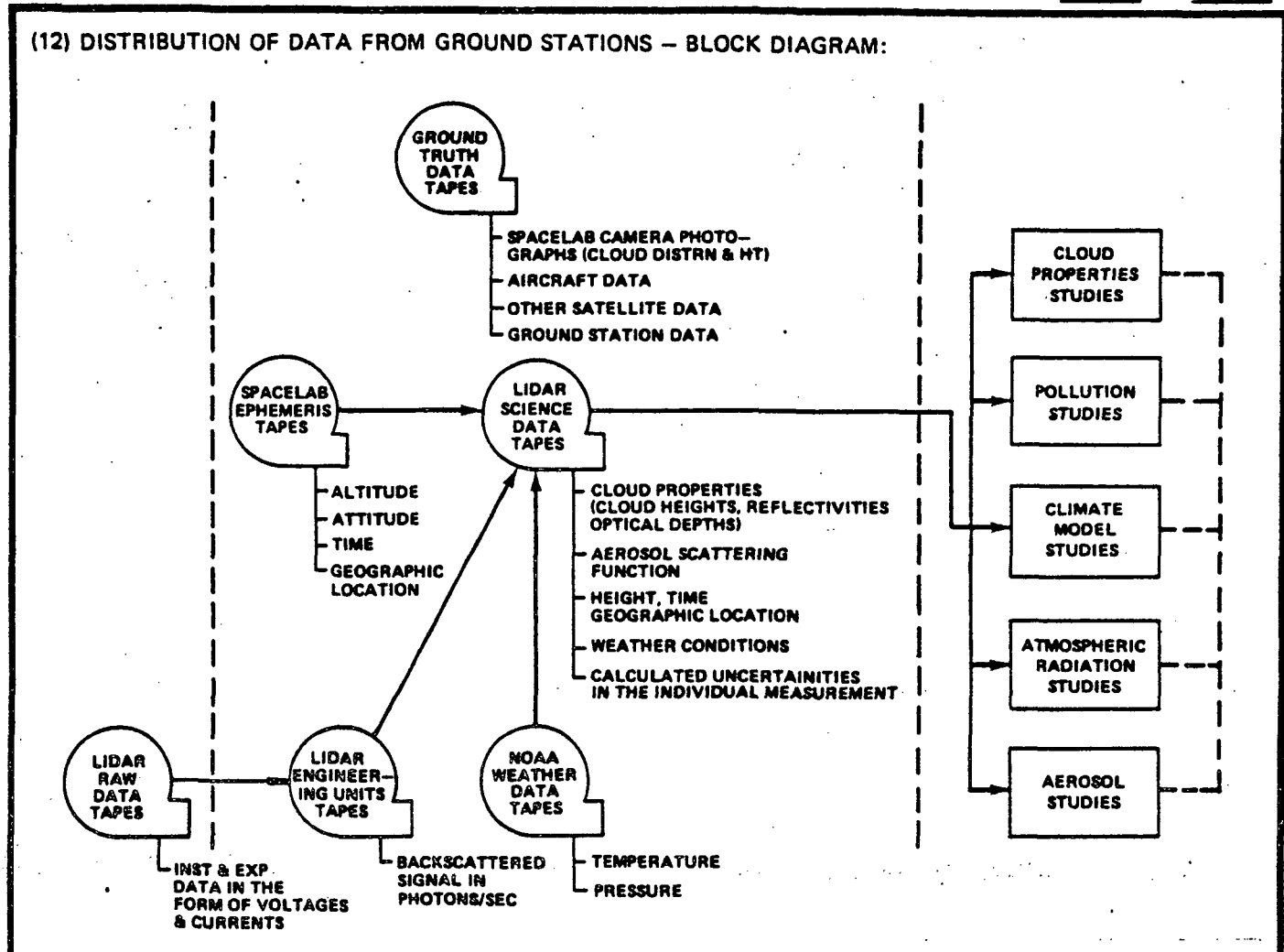


FIGURE 1 SPACELAB DATA PROCESSING FACILITY (SDPF)

5.4.18

SECTION NO.: 5.4 SENSOR CATEGORY: Laser Radar



#### (13) DATA DISTRIBUTION - NARRATIVE:

The output tapes are shipped to the Principal Investigators (PI). The PI will process the LIDAR data tapes to reduce scientific and engineering data to usable form and will then analyze the data and document the results in a form LIDAR experiment report.

The data processing and analysis program is approximately six months long. Preliminary results will be reported by LIDAR team within 90 days of the mission with final results to be published within 6 months after comparison with ground truth.

5.4.19

SECTION NO.: 5.4

SENSOR CATEGORY:

Laser Radar

REV. NO.:

REV. DATE:

31 July 1978

This page intentionally left blank.

REV. NO.: 3

# RSDH DATA SHEET

CHEET	1	05	_
SHEET	1	OF	3

(1) SENSOR NAME, ACRONYM: Laser Altimeter/Profilometer Experiment (OP-06-S)
Spaceborne Laser Ranging System (OP-16-S)

(2) DISCIPLINE: Earth & Ocean Physics

(3) SUBDISCIPLINE: Ocean Processes/Geodynamics

(4) APPLICATION AND OBJECTIVE: The laser radar is used to determine range, height or depth using backscatter LIDAR returns. These measurements are essential to provide for active sensing of directional sea state, ocean and coastal bottom topography, subsurface ocean temperature profiling, fish school detection and track, marine plankton productivity, oil and hazardous materials detection, ocean currents mapping, solid earth dynamics and earthquake events.

(5) HERITAGE/KEY PERSONNEL:

At the present there is no forerunner sensor. However there are various types of laser systems available for the precision measurement of distance. Team Leaders: Frank L. Hoge, J. T. McGoogan, NASA, WFC; M. W. Fitzmaurice, NASA, GSFC

(6) SENSOR DEPLOYMENT:

The laser radar is planned on a seven day mission in 1981, 1982, 1983 aboard the spacelab pallet. The sensor will be mounted on a pointing mount or fixed on the pallet with a gimbal mirror pointing system. It will be at an altitude of 200 Km and 50 degrees inclination.

(7) SENSOR CHARACTERISTICS

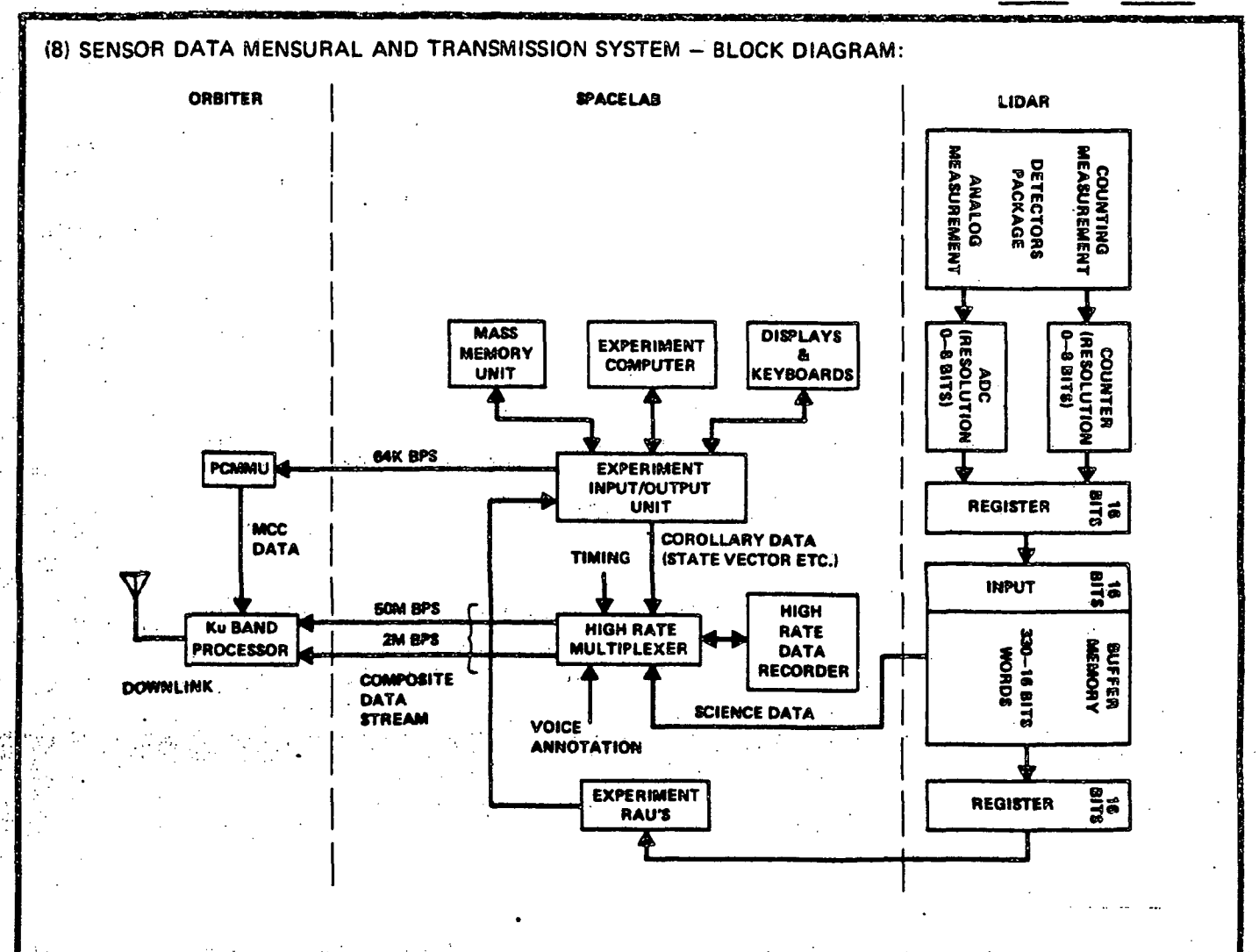
(7A) CAPABILITIES AND CONSTRAINTS OF THE SENSOR TO ACQUIRE THE MEASURED PARAMETER:
The laser radar includes fixed, multiwavelength and tunable emitters operable at UV,
Vis and IR wavelengths, 1 mrad FOV, high resolution dispersive elements, 1 m diameter
receiver, narrowband filters, photomultiplier tubes and photodiode detectors, signal
processing and electronics. The sensor requires an altitude reference system, 3-axis
Gyro Star Tracker, Global Mirror Pointing System (or Pointing Mount and a high-speed
electronic package). The sensor will be used during ocean surface darkness and will be
oriented earthward, on ocean surfaces and towards nadir (San Andres fault in Southern
California). It requires roll and pitch stabilization.

## (7B) ACTIVE SOURCE CHARACTERISTICS (FOR ACTIVE SENSORS):

The laser radar transmits a short intense, highly directional, monochromatic and well collimated flash of light operating at energies of 1 J, with 1 to 10 Hz repetiion rate, less than  $2\mu$  pulse width, spectral width from 10 pm to 1 pm, efficiency from 0.1 to 1% and  $10^{-4}$  rad beam divergence.

(7C) DETECTOR MEASUREMENTS CHARACTERISTICS: The detectors will measure the intensity of backscattered LTDAR signals. They can be either photomultiplier tube (PMT) or photodiode depending on the wavelength of the incoming signal. The PMT is used when the incoming photon is in the UV or visible, with 20% quantum efficiency (QE) at 530 nm, 2% QE at 1060 nm, sensitivity 5 counts/sec and dynamic range from less than 1 photon per second to  $10^3$  photon per sec. When the incoming light is in the IR, the photodiode is used, with sensitivity >10  $\mu$ w/cm , dynamic range from less than 1  $\mu$ w/cm to greater than 1 kw/cm . Possible IR detectors are the InS (1000-3000 nm) InSb (2000-25000 nm), Hg Cd Te (7000-14000 nm), Pb Sn Te (2000-12000 nm) Data generated is digital and is approximately 54.4 Kbps.x

SECTION NO.: 5.4 SENSOR CATEGORY: Laser Radar Preceding page blank



## (9) MENSURAL AND TRANSMISSION SYSTEM - NARRATIVE:

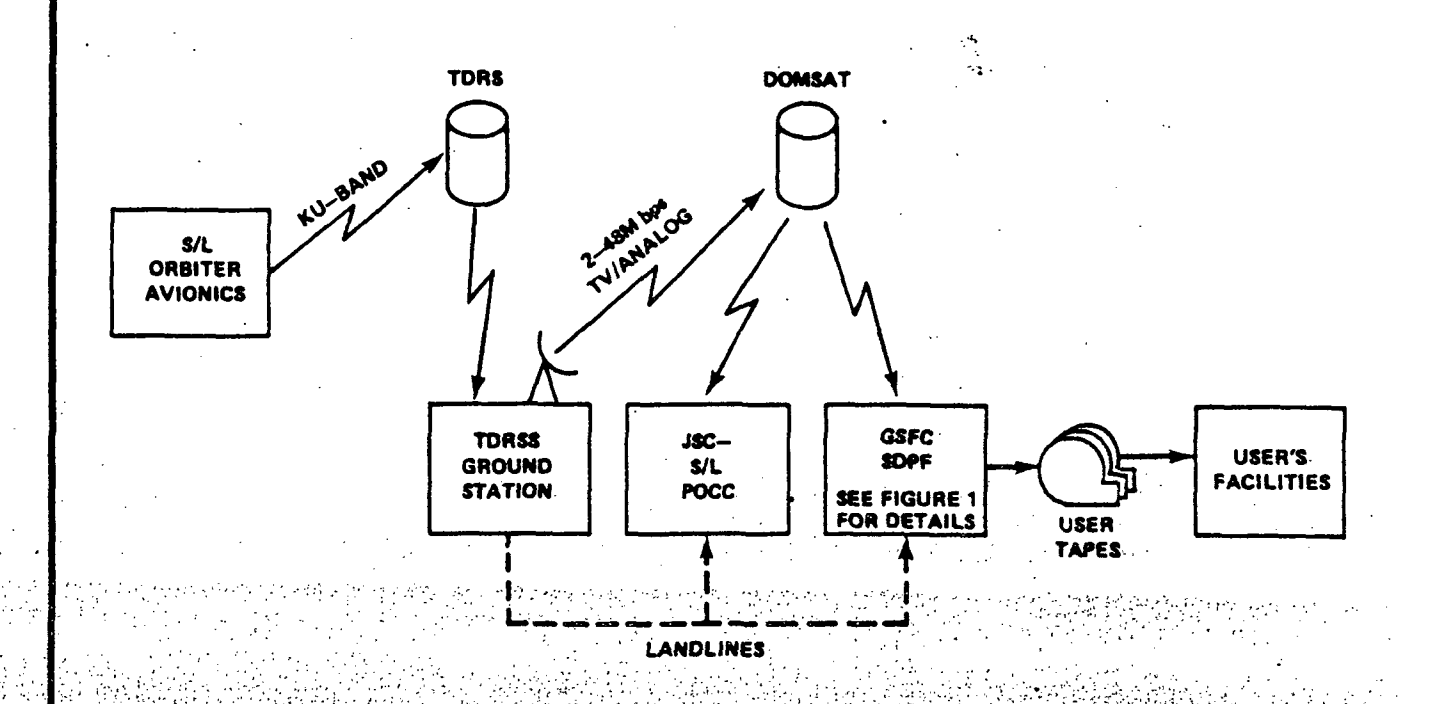
The detector output can be either an analog signal or calibrated pulses depending whether the photon counting method is used or the parameter to be measured is the peak power.

The calibrated pulses are fed into two 8-bit counters and then its contents are transferred into the 16-bit register. The signal is then routed via a buffer to the High Rate Multiplexer. The analog signal is fed into a two sample hold and then to 8 bits analog-to-digital converter. The digital output is transferred to a 16 bit register and then to the High Rate Multiplexer via a buffer. The science data, corollary data, voice and timing, form a composite data stream which is transferred to the Ku Band signal processor for downlink.

SECTION NO.: 5.4 SENSOR CATEGORY: Laser Radar

REV. NO.: 3 REV. DATE: 31 July 1978

(10) SENSOR DATA RECEPTION AND PROCESSING - BLOCK DIAGRAM:



(11) RECEIVING AND PROCESSING - NARRATIVE: The Spacelab and orbiter flight data is transmitted to the TDRSS ground station via TDRS on the Ku Band. The data stream is demultiplexed inside the TDRSS ground station and outputed as follows: The high rate multiplexer wideband data stream and the video/analog 4.2 MHz data are routed to the Payload Operations Control Center (POCC) at JSC and to the Data Processing Faculity (SDPF) at GSFC via the Domsat. Alternately, the low rate data is routed via landlines to JSC and GSFC. The POCC performs the time critical payload data processing. POCC operations include monitoring, recording and demultiplexing the payload data.

The SDPF (See Figure 1 on next page) supports the non-time critical data from the Spacelab payloads. SDPF operations include quality checking, editing, chronologically ordering and formatting of the experiment and ancillary data. It performs conversions and transformations of the ephemeris/attitudes data. SDPF contains two major systems: Spacelab Input Processing System (SIPS) and a Spacelab Output Processing System (SOPS).

(continued on next page)

SECTION NO .: SENSOR CATEGORY: Laser Radar 5.4 REV. NO.: **REV. DATE:** 31 July 1978 5.4.43

#### **CONTINUATION SHEET:**

# (11) continued

The SIPS performs the preprocessing functions required in SDPF. SIPS operations include data capturing, data quality monitoring, accounting demultiplexing and analog/video/voice product generation. Output products are generated by SIPS for shipment and further processing at other facilities. Their output products include: Unedited digital tapes and analog/video/voice tapes. The SOPS performs editing, time validation, formatting and digital product generation. Edited digital tapes are generated by SOP's for shipment to the principal investigators.

DRIGINAL PAGE IS OF POOR QUALITY

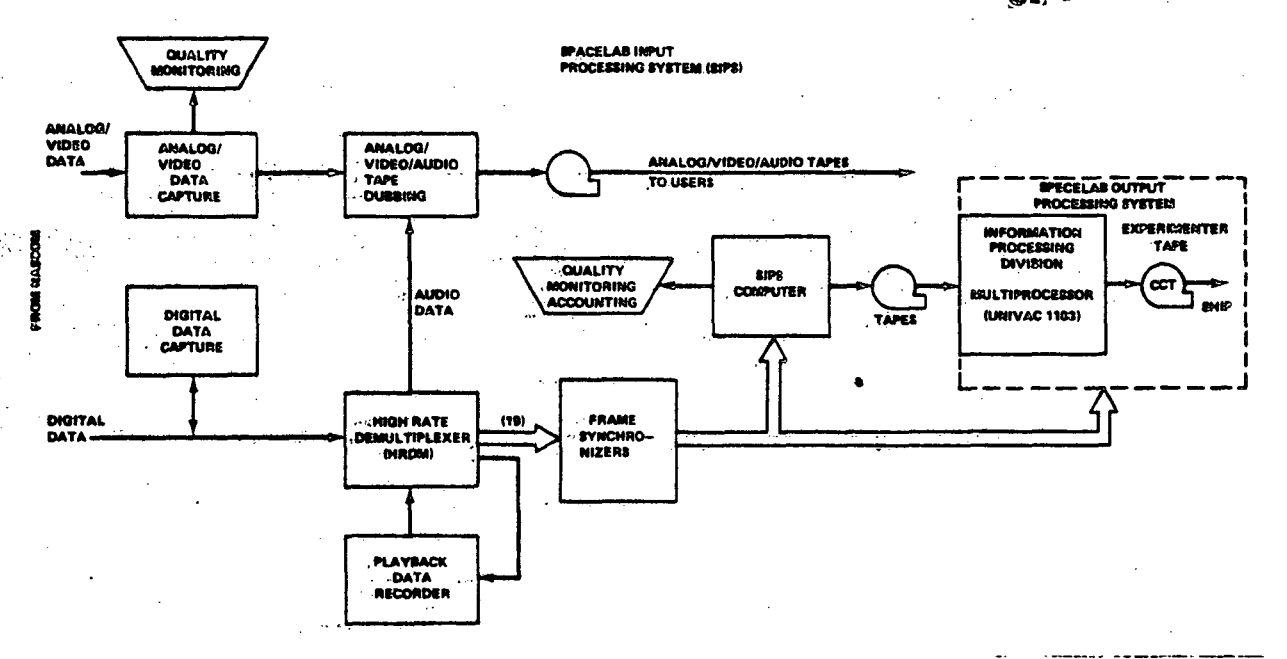


FIGURE 1 SPACELAB DATA PROCESSING FACILITY (SDPF)

5.4-24

SECTION NO.: 5.4 SENSOR CATEGORY: Laser Radar

#### (12) DISTRIBUTION OF DATA FROM GROUND STATIONS - BLOCK DIAGRAM: TRUTH DATA SPACELAB CAMERA PHOTOGRAPHS AIRCRAFT DATA OTHER SATELLITE DATA GROUND STATION DATA LIDAR SPACELAR SFA & OCEAN SCIENCE EPHEMERIS STUDIES TAPES DATA INTENSITY VERSUS TIME & RANGE ALTITUDE EARTH ATTITUDE DEPTH DYNAMICS/ TIME PROCESSES RANGE STUDIES GEOGRAPHIC LOCATION HEIGHT, TIME GEOGRAPHIC LOCATION WEATHER CONDITIONS CALCULATED UNCERTAINITIES IN THE INDIVIDUAL MEASUREMENT LIDAR NOAA LIDAR WEATHER ENGINEER RAW DATA ING UNITS TAPES TAPES TAPER BACKSCATTERED TEMPERATURE INST & EXP SIGNAL IN DATA IN THE PRESSURE PHOTONS/SEC FORM OF VOLTAGES & CURRENTS

### (13) DATA DISTRIBUTION - NARRATIVE:

The output tapes are shipped to the Principal Investigators (PI). The PI will process the LIDAR data tapes to reduce scientific and engineering data to usable form and will then analyze the data and document the results in a form LIDAR experiment report.

The data processing and analysis program is approximately six months long. Preliminary results will be reported by LIDAR team within 90 days of the mission with final results to be published within 6 months after comparison with ground truth.

5.4.25

SECTION NO.: 5.4 | SENSOR CATEGORY: Laser Radar

This page intentionally left blank.

REV. NO.: 3

# SENSOR CATEGORY TABLE OF CONTENTS AND REVISION CONTROL SHEET

SENSOR NAME OR	NUMBER OF	PAGE	EFFE	CTIVE
OTHER ENTRY	PAGES	NUMBER	REV. DATE	REV. NO.
Section 5.5 Table of Contents	1	5.5-i	31 JUL 78	3
Introduction to Multispectral and Mapping Cameras	13	5.5-1 5.5-2	31 JAN 78 31 JAN 78	2
		5.5-3 5.5-4	31 JAN 78 31 JAN 78	2 2 2
		5.5-5 5.5-6 5.5-7	31 JAN 78 30 SEPT 77 30 SEPT 77	2 1 1
		5.5-8 5.5-9 5.5-10	30 SEPT 77 31 JAN 78 30 SEPT 77	1 2 1
		5.5-11 5.5-12 5.5-13	31 JAN 78 31 JAN 78 30 SEPT 77	2 2 1
Metric Camera	5	5.5-15 5.5-16	31 JUL 78 31 JAN 78	3 2
		5.5-17 5.5-18 5.5-19	31 JAN 78 31 JAN 78 31 JAN 78	2 2
Earth Terrain Camera (S190B)	34.42 <b>6</b> 25.43	5.5-21 5.5-22 5.5-23 5.5-24	31 JUL 78 31 JUL 78 31 JUL 78 31 JUL 78	3 3 3 3
		5.5-25 5.5-26	31 JUL 78 31 JUL 78	3 3
Multispectral Photographic Facility (S190A)	6	5.5-27 5.5-28 5.5-29 5.5-30 5.5-31 5.5-32	31 JUL 78 31 JUL 78 31 JUL 78 31 JUL 78 31 JUL 78 31 JUL 78 31 JUL 78	3 3 3 3 3 3
Optical Bar Panoramic Camera (S163)	5	5.5-33 5.5-34 5.5-35 5.5-36 5.5-37	31 JUL 78 31 JUL 78 31 JUL 78 31 JUL 78 31 JUL 78	3 3 3 3 3
5.5-1				

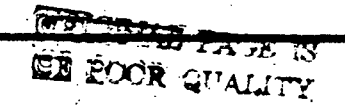
REV. NO.: 3

REV. DATE: 31 JUL 1978

This page intentionally left blank.

0.: 1

**REV. DATE:** 30 Sept 1977



## Section 5.5

# INTRODUCTION TO MULTISPECTRAL AND MAPPING CAMERAS

The uniqueness of the perspective offered by aerial photography has made it useful for planning purposes for a very long time. The first aerial cameras were borne aloft by balloons before the invention of the airplane and the progress of aerial reconnaissance and that of aerial platforms have been in parallel since the first of this century. Techniques for interpreting and correcting aerial imagery, the equipment and personalities involved in the acquisition and utilization of it have all developed around film and the camera. The roots of remote sensing are found in the photographic technology. Photographic imagery and at least some visual interpretation techniques are presently useful and will probably continue to be useful in remote sensing for some time. Photographic emulsion, deposited uniformly upon a stable backing material is in no uncertain sense a valid remote sensor. Film alone has the capability to directly correlate the geometry of a subject with its radiance. This capability makes film a reasonably dense storage medium which, together with the variety and complexity of surface-based film imagery analysis equipment now in use, are the reasons for considering cameras in this handbook.

The intention of this section is to identify in capsule form the major aspects of a photographic remote sensing system so that the user of the handbook could broadly determine the tools likely to be available to him in any given application, the limits of the capabilities of these tools and the literature that will lead to more detailed information. Discussions of the fundamentals of optics and photo-chemistry are available elsewhere and will not be dealt with. Techniques vary widely from one application to another and the degree of success

REV. NO.: 2

REV. DATE: 31 Jan 1978

reported in the literature ranges over a broad scale. Therefore, recommendations of methods are not made.

Cameras used on spacecraft are for the most part variations of those developed for aircraft use. Some aerial cameras that are in use in 1977 are changed little from the mid-1930's versions of the same cameras. The variety used in space flight includes small hand-held 70mm cameras and larger types, mounted to the spacecraft, using large film formats. The Earth Terrain Camera (framing camera) used on Skylab, for example, was referred to as the S190B experiment and was basically a high-performance reconaissance camera. The 46-cm focal length lens was chromatically corrected over the extended wavelength range of 0.40 to 0.90 microns. The shutter was a bidirectional focal plane with speeds of 1/100, 1/140 and 1/200 second. Taking into account the subtrack velocity of the vehicle, a shutter speed of 1/200 second allowed "smear" of the image which was large compared to the lens-film combination resolution capability of up to 180 lines/mm. (This translates to a ground resolution of six meters for that particular mission.) The method used to compensate for this smear was to rock the entire camera body and lens cone about a pivot at a rate which would cause the film to move at the same rate as the image. This is called rocking-camera forward motion compensation (FMC). Characteristics common to this group of framing cameras are high resolution and low geometric distortions. Table 1 summarizes the capabilities of representative cameras and Table 2 lists compatable lenses.

Another kind of function which cameras perform is spectroradiometry. In this usage, more than one image is formed with all images normally being the same size. The light forming each of the images comes from spectral bands selected by filters. One method of forming a multiplicity of images is to use a number of cameras, all boresighted together with matched lenses. An alternative is to use one camera

REV. DATE: 31 Jan 1978

150

Ķ

¥.

Pan-X

Pan-X

Pan - X, Plus X

40,45,45, 45

AWAR, 1000:1 (ξρ/mm) Film

60\*,65\*,85\*,85\*, 50

eras	HLT 548	nc, Hycon lunar topographic	11.4 x 11.4 60 64 456 calibrated w/camera	0.8 rocking camera 1.7 - 175 mrad/sec NA
Frame Aerial Camo	Model 500	J.A. Maurer, Inc. Hycon recon	11.5 x 11.5 76 NA NA NA	0.2 pulse movable film 76 - 230 NA
1 Representative 13 cm Reconnaissance - Frame Aerial Cameras	KS - 72C1	Hycon day/night recon (H,1) day recon (J,K)	11.5 x 11.5 150 std., 76 process 130 1200 std., 600 process standard & pro- cessing casettes	0.167 minimum moving film 2.5 - 305
tative 13	KA - 748	Hycon recon	11.5 x 11.5 61 60 480 removable	1.0 & 0.25 moving film 2.5 & 102
1 Represent	KS - 878	Chicago-Aerial Ind. recon	11.5 x 11.5 150 60,100,130 1,200 cassettes	0.17 moving film 2.5 - 305 2%
TABLE	KA - 76A	Chicago-Aerial InJ. recon	11.5 x 11.5 30,76 130,100 210,600 cassettes	0.17 auto moving film 3.8 - 274 2% average
	Camera	Manufacturer Primary Use	Film Length (m) 30,76 Base Thickness(µm) 130,100 Frames/Roll 240,600 Mugazine cassettes	Cycle Time (sec) 0 FMC Type m FMC Rate(um/sec) 3 FMC Error

	<del></del>	٠	ئري د	1 Park 1	·		
14°8' × 14°8'	1/50, 1/200, 1/1,000	focal plane (bi-directional)	90	rigid flange	clock, day count	manual	vacuum platen 42,1 AMAR is 75 Ap/min on 3414 film distortion allOopm
length varies w/focal length	1/200 - 1/8,000	focal plane	17 with film	NA	clock, frame- counter	auto, remote	will accept magazines w/7cm film
							:
41°6' x 41°6' varies w/focal	1/1,000,1/2,006 1/100-1/3,000 day	focal plane-day intralens-night	31,30,35,35	fixed (ii, I) stabalized (J,K)	binary ADAS, fixed	auto	"day/night version **day version
41°6' x 41°6	1/1,000,1/2,0	focal plane	4	hard	none	manual	
varies w/focal length	1/60 - 1/3,000	focal plane	33,32,32,40	hard	CRT, frame counter, fixed data	auto, internal	*10,45,60,60 on Plus-X, respectively **@1/4,5 **150,305,460 mm lenses respect- ively
varies w/focal length	1/60 - 1/3,000	focal plane	25,25,32,28 maximum	ARN-7A,8A,9A, 1A-215A,216A fixed or stabilized	CRT (MIL-STD-782) CRT, frame counter, fi	auto, internal	Single camera body w/inter- changeable lens cones equivalent to KA-SuA,-51A,
Angular Coverage varies w/focal length	Shutter Speed (sec)	Shutter Type	Weight (kg), w/o Film & Mount	· Nount(s)	Outa Aunotation	, Exposure Control auto, internal	. Renarks

5.5.3

REV. DATE: 31 Jan · 1978

TABLE 2 Representative Compatible Lenses as Indicated for 13 cm Reconnaissance Frame Aerial Cameras--Listed in Table 6-14

		•					rrection			/mm) 69 Pan-X
	KS - 72C1	A-D	150	2.8 - 22	0.5 - 0.7	Red	yes w/correction filter	yes	NA	AWAR (&p/mm) 1,000:1 49 69 Plus-X Pan-X MX641, Y=1.5 2:1 36 Plus-X
	KA - 76A	Pasar P.O.	150	2.8 - 6.7	0.4 - 0.9	W12, W25	yes	yes	ou	
KA = 76A.	KS - 87B	Pasat/Aerogat P.O./C.P. Goertz Amer.	80	4.5 - 11	0.4 - 0.9	W12, W25	yes	yes	ou	
# ( )	which used	Name Manufacturer(s)	Focal Length (mm)	f/No. Range	Wavelength Range (µm)	Filters	Can be Used w/Normal Color Film?	Can be Used w/IR Color Film?	Change of Focus Required for IR Color Film?	Remarks

body with a number of lenses forming separate images on a single piece of film. The multiple camera scheme has the advantage offered by the flexibility of being able to select an optimum film/filter combination for each camera to achieve the desired results. One disadvantage is that small differences in shutter actuation time from one camera to another will reduce the degree of registration that can be realized. An example of a multispectral camera put together from off the shelf components is the S065 experiment on Apollo 9. This unit consisted of four conventional Hasselbland 2 1/4" x 2 1/4" (70mm) cameras equipped with 80mm fL lenses and Wratten filters. These were attached to a ring which was then mounted in-flight to a hatch window in the command module. Experiment S065 took the first multiband pictures of earth on film from space. Ground resolution of the equipment varied between 50 and 125 meters depending upon the band. A state-of-the-art example of a multispectral camera of this type is the Itek Multispectral Photographic Facility (MPF) built for NASA's S-190A experiment. It consists of six cameras, taking imagery in non-overlapping optical bands. Its performance characteristics are summarized in Table 3.

Still another form of multispectral camera is one where a multiplicity of identical lenses (usually four or more) are mounted together on a common lens board. In conjunction with a common focal plane shutter, they expose multiple images on a single piece of film. Filters placed in front of each lens assign spectral coverage to each lens. One advantage of this arrangement is that the fast transit time of the shutter minimizes differences in time of occurrence and duration of exposure of various images. Also, since images appear together on the same sheet of film, then except for dimensional changes in the film (which should be small) the images have fixed relative positions and can be registered. Characteristics of two such cameras are summarized in Table 4.

5.5.5

**REV. NO.:** 2 | **REV. DATE:** 31 Jan 1978

TABLE 3 Design Specifications for S190A Multiband Camera for Skylab

DRIGINAL PAGE IS OF POOR QUALITY

Area imaged 150 x 150 Km from 5.35 Km altitude f number (minimum) 2.8 Focal length 150 70 sas Base thickness 60 um or 100 um Image distortion 0.01% Registration All bands registered to <12 um Image plane irradiance Uniformity hetter than 28% including any vignetting effects Optical axes all fall within a cone of 1 are min full angle Boresighting " Repetition rate 1 frame per 2 sec Stop openings Waterhouse stops at 1/2 stop increments from f/2.8 to f/16 securate to ±1.5% Forward motion Error 51

compensation Shutter speeds 2.5, 5, and 10 ms accurate to 5% with ±2.5% repeatability. Six shutters syn-Chronized to 4 ms

Wavelengths bunds (µm)*	Film Number	Ground Resolution m/line pair**
0.50 - 0.60	3414	20
0.60 - 0.70	3414	20
0.70 - 0.80	2424	110
0.80 - 0.90	2424	110
0.50 - 0.88	-3443	95
0.40 - 0.70	S0-242	30

Films used for remote sensing purposes include both black and white and color. In both types, films are available with response extended into the infrared region of the spectrum up to approximately 1.0 micrometer wavelength. Photographic response to wavelengths longer than this is normally not possible because the lower energy of the radiation fails to bring about the chemical changes in the Imagery at the far-infrared wavelengths beyond about 1 micrometer can be accomplished using a scanner. (See section on Imaging Spectroradiometers.) Films are distinguished by defining the following group of variables:

- (1) packaging
- (2) sensitivity
- (3) grain size

5.5-6.

Six other filters can be provided for selecting different wave-length hands in addition to those specified here. Estimate: not part of NASA specifications. Note that film 3414 was not used on S190A. It is listed here to indicate roughly what could be obtained if the system is used in future

- (4) spectral response
- (5) backing material
- (6) chemistry of development

DE POOR QUALITY

- (7) resolution
- (8) size

TABLE 4 Multispectral Aerial Cameras

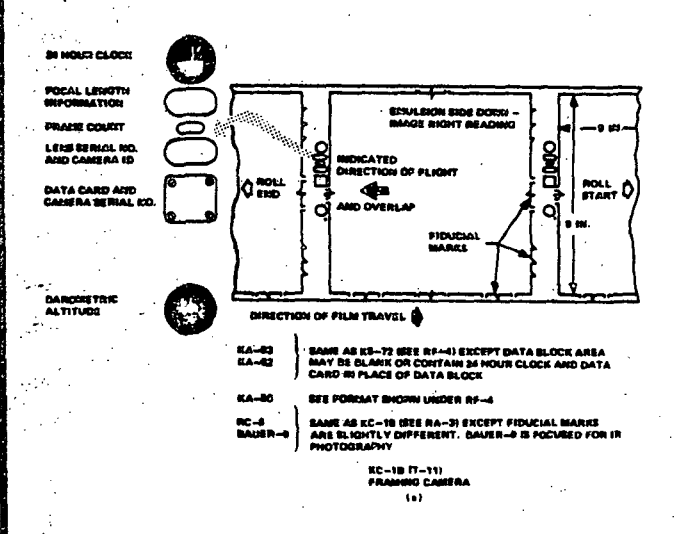
Camore Hamufocturer Primary use	Mndel 11 Spectral Data multispectral	Mirk 1  25 
Format (cm) Film length (m) Rase thickness (µm) Framen/Roil Magazine	8.9 g 8.9 76 100 188 A-SA or A-9	8.9 x 8.9 76 100 300 A-SA
Cycle time (sec) FMC Type FMC Rate (mm/sec) FMC Frree	2.0 moving film 2.5 - 700	2.6 NA NA
AWAR, 1,000:1 (tp/mm)	45*	NA
Film Processing Type of measurement	2424 NA Laboratory	NA NA
Compatible lenses Hanufacturer(s) Focal length (mm) f/No. Range Havelength Range (um)	Laboratory Kenotar Schneider 150, 100 2.8 - 16 4 bands	Renotar Schneider 150, 100 2.8 - 15 4 bands
Filters	forty available	0.4-0.7 M478, 0.47-0.59 VSB, 0.59-0.69 WZS,
Can be used w/normal cotor flim?	700 (12) (13) (14) (15) (15) (15) (15) (15) (15) (15) (15	0.74+ una+ yes
color file? Changes of focus required for IR	NA.	NA
color film? Angular coverage	varios w/focal length	varies w/focs1 longth
Shutter Speed (sec)	1/25 - 1/33 or 1/150 - 1/330	1/150 - 1/350 (A). 1/350 - 1/800 (B)
Shutter Type-	1/350 = 1/800 focal plane	focal plane (2 types: A,S)
Weight (kg), w/o film and Hount	43	26
Mount	A+A,-11,-11A,-27, -27A	A-8,-11,-11A,-27, -27A
(Into Ammotation	NA	HA.
Intervalemeter	yos	external
Exposure Control	NA	MA
Roturks		modified K-22 Camera w/4 lens 24-cm fits
	*Peak	*interference filters block iR to 3 bunds

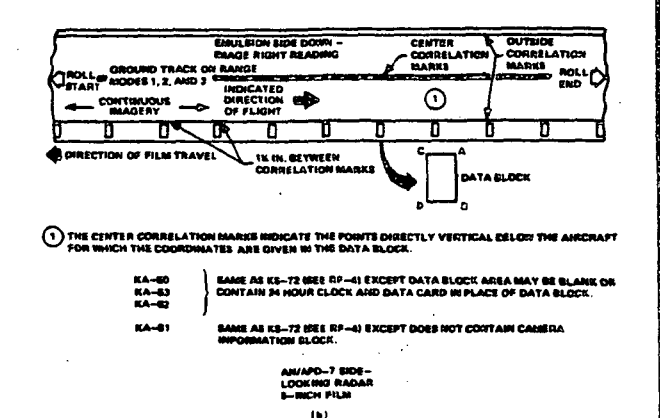
With this many variables, a detailed discussion of the subject is beyond the scope of this handbook. For details of items one through seven, the reader is referred to Reference [3]. Some of the film formats in use in cameras as well as some other remote sensors are shown in Figure 5.5-1. For more information on formats, see Reference [4].

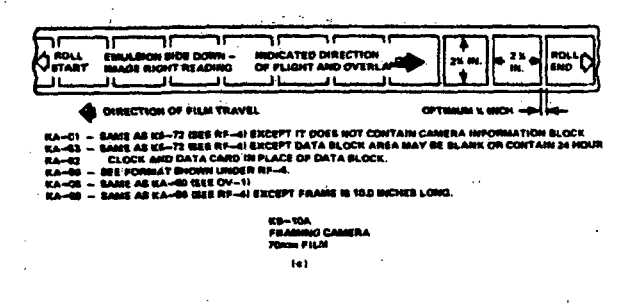
5.5.7

REV. NO.: 1 REV. DATE: 30 Sept 1977

# ORIGINAL PAGE IS OF FOOR QUALITY







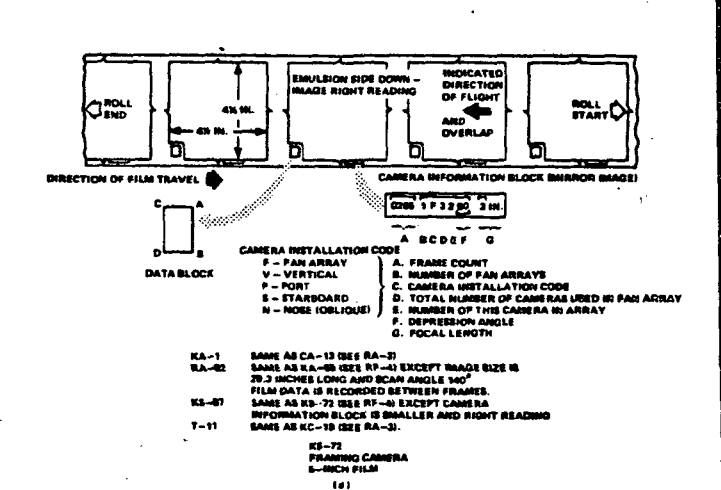


FIGURE 5.5-1 Sensor Film Formats

REV. NO.: 1 REV. DATE: 30 Sept 1977

Optical filters can be of either the pass-band or stop-band variety depending upon whether their function is to pass or block selected radiation. These two types may be implemented by an absorption or interference phenomenon. Included in the absorption filters are colored glass filters (Coming, Schott, Baird atomic) and Wratten (Kodak) filters.

Colored glass filters can be produced by ions in true solution or by submicroscopic crystals suspended in the glass melt. Wratten filters are actually
a dried gelatin stained with an organic dye and laquered for protection. Frequently,
these are mounted between layers of protective glass. The two types have relatively
broad bandpass characteristics. These filters are in wide use for color separation
in the visible wavelengths and for color correction in both the visible and invisible portions of the spectrum. Absorption filter characteristics are elaborately
depicted in references [5], [6], [10] and [12].

Interference filters consist of a transparent substrate covered with alternate layers of dielectric of different indexes of refraction. The layers are vacuum deposited and operate on the principle of the Fabry-Perot interferometer. They have the electrical analogy of a filter where the number of stages of the filter is equivalent to the number of layers of dielectric. These filters are selective by reflecting unwanted radiation. They are typified by narrow bandpasses and steep skirts. Interference filters are frequently built with a total passband of only 50 angstroms. The reflection phenomenon is produced by reinforcement by adjusting the spacing of the dielectric to a specific relationship with the wavelength of light to be passed. When the incident light is not normal to the surface, the spacing of the dielectric becomes improper for the design wavelength. The result is that off-axis light sees a "detuned" filter, one not operating at the intended wavelengths. Temperature also tends to "de-tune" interference filters.

REV. NO.: 2 REV. DATE: 31 Jan 1978

Most filters, absorption type and interference type, pass radiation outside the prescribed passband. These spurious outputs can be surpressed with another filter used in combination to eliminate the unwanted radiation. Other types of auxillary lenses are (1) antivignetting filters which are used with particular lenses to even out the light distribution in the image plane and (2) Polarization filters which are used to remove some of the effect of haze by discriminating against the naturally polarized component in sunlight.

In addition to the manual visual interpretation of photographs, there is a large demand for machine processing. In this process, a measurement is made of the density of the transparency and the coordinates of the measurement are correlated with it. This can be done manually one point at a time or a conversion to video can be made using a flying-spot scanner or a television camera. Once the conversion is made to video, the data can be treated as high resolution video and such operations as the following can be performed:

- (a) density slice
- (b) false color
- (c) edge enhancement
- (d) reverse polarity
- (e) contrast enhancement
- (f) gray level conversion
- (g) horizontal and vertical measurements
- (h) change magnification
- (i) cursor

To digitize multispectral records, more than one transparency must be scanned.

This can be done with a separate video camera for each transparency. However, the geometric distortions in the rasters must match in order to preserve the registration.

**REV. NO.:** 1 REV. DATE: 30 Sept 1977

An alternative is to utilize a flying-spot scanner where a raster is generated on a CRT with good spot definition and short phosphor decay time. The image of the raster is focused upon the transparencies to be analyzed by using beam splitting mirrors. A photomultiplier tube behind each transparency picks up the video for that particular channel. In this way, geometric distortions present in the raster will be projected equally to each transparency.

Visual multispectral image reconstruction can be accomplished using an additive color combiner. A projector is used to project each transparency onto a screen and the images are registered spatially. Filters are placed in front of each projector and the intensity of each projector's output is adjusted to produce the desired effect. Multispectral photographs where all records appear in the same piece of film simplify the registration problem from one image to the next since the relative positions of the images are fixed.

REV. NO.: 2 REV. DATE: 31 Jan 1978

#### References

#### MULTISPECTRAL & MAPPING CAMERAS

- [1] Liutz, Joseph Jr. and Simonett, David, Remote Sensing of Environment, Addison Wesley Publishing Company, Reading, Massachusetts, 1975.
- [2] Reeves, R. G., (ed.), Manual of Remote Sensing, American Society of Photogrammetry, Falls Church, Virginia, 1975.
- [3] "Kodak Data for Aerial Photography" Publication No. M-29, Eastman Kodak Company, Aerial Reconnaissance and Mapping Markets, Rochester, N.Y.
- [4] Reconnaissance Reference Manual 1973, Reconnaissance Laboratory McDonnell Aircraft Company, St. Louis, Mo.
- [5] "Kodak Filters for Scientific and Technical Uses" Publication No. B-3H, Eastman Kodak Company, Rochester, N.Y.
- [6] "Color Filter Glasses" Corning Glass Works, Corning, N.Y.
- [7] "Optical Filter Design Guide and Catalog" Infrared Industries, Inc., Waltham, Mass.
- [8] Catalog, Promfret Research Optics, Inc., Stanford, Conn.
- [9] "Thin Film Coatings on Glass" Schott Optical Glass, Inc., Duryea, Pa.
- [10] "Color Filter Glass from Schott" Schott Optical Glass, Inc., Duryea, Pa.
- [11] "Interference Filters from Schott" Schott Optical Glass, Inc., Duryea, Pa.
- [12] "Optical Filters" Baird-Atomic, Inc., Systems Components Division, Bedford, Mass.
- [13] "Manual of Color Aerial Photography" American Society of Photogrammetry, Falls Church, Va., 1968.

5.5.12

REV. NO.: 2

REV. DATE: 31 Jan 1978

# MULTISPECTRAL AND MAPPING CAMERAS ILLUSTRATION CREDITS

Figure No.	Page	Reference	Pages
5.5-1	5.5-8	[4]	10, 12, 13 & 16

5.5.13

REV. NO.: 1 REV. DATE: 30 Sept 1977

This page intentionally left blank.

REV. NO.:

REV. DATE: 30 Sept 1977

- - 14

#### RSDH DATA SHEET

SHEET	1	OF	5

(1) SENSOR NAME, ACRONYM: Metric Camera (EOE-1)

(2) DISCIPLINE: Earth Observations

(3) SUBDISCIPLINE:

Land Use

## (4) APPLICATION AND OBJECTIVE:

The Metric Camera is designed to produce small scale maps from space photographs and to test the capability of cartographic mapping and map revision from these photographs at scales 1:50000, 1:100000 and smaller with respect to topographic and thematic data.

#### (5) HERITAGE/KEY PERSONNEL:

The Metric Camera is presently available and is essentially a stock Zeiss Model RMK 30/23 Photogrametric camera. Minimum modifications are presently studied. Exp. Team Leader ESA

#### (6) SENSOR DEPLOYMENT:

The Metric Camera will be aboard Spacelab -1, planned for launch in December 1980, at altitude 250 kilometers and 57 degrees inclination. The camera will be placed inside the module, and on a suspension mount under the optical window. Pointing direction is local vertical to within ±1 degree.

(7)

#### SENSOR CHARACTERISTICS

## (7A) CAPABILITIES AND CONSTRAINTS OF THE SENSOR TO ACQUIRE THE MEASURED PARAMETER:

The Zeiss RMK 30/23 Camera utilizes a TOPAR A lens having a focal length of 305 mm and aperatures of f/5.6, f/8 and f/11. The maximum lens distortion within the 23 cm X 23 cm film format is 3  $\mu$ m. Angular coverage is  $56^{\circ}$  across the diagonal and  $41^{\circ}$  on each side. Uniformity of scene illumination in the focal plane is controlled by lens design and by anti-vignetting filters to within one-half f stop over the entire visible range and into the near infrared. No further compensation is necessary when changing film from panchromatic to infrared. Three magazines will be carried on

(78) ACTIVE SOURCE CHARACTERISTICS (FOR ACTIVE SENSORS): N/A. 7(A) Continued: board. Photomission planning calls for strip targets ranging in length from 1800-2300 km. 80% overlap is planned. A total of 1650 exposures will be produced of points of interest in all facts of the earth where sun angles between 15° (for desert areas) and 68°. Film emulsions used in any one strip will be the same throughout the strip because changing films requires a change of magazine and filter. The mounting shown in Figure 1 allows nadir viewing ±1°.

#### (7C) DETECTOR MEASUREMENTS CHARACTERISTICS:

Filter, emulsion and film base selections have not been made at this writing but it is reasonable that types 3443 and 2445 represent the type that will be employed. Forward Motion Compensation is not used in the RMK 30/23. Consequently, shutter speeds will be limited to 1/500 sec or faster. With a ground track velocity of 7.7 km/sec, image smear during shutter opening, combined with the resolution of the lens/20 m with the slower shutter speeds. Automatic exposure control is incorporated. Exposure sequence timing is shown in Figure 2.

Preceding page blank

SECTION NO.: 5.5 | SENSOR CATEGORY: Multispectral and Mapping Cameras

REV. NO.:

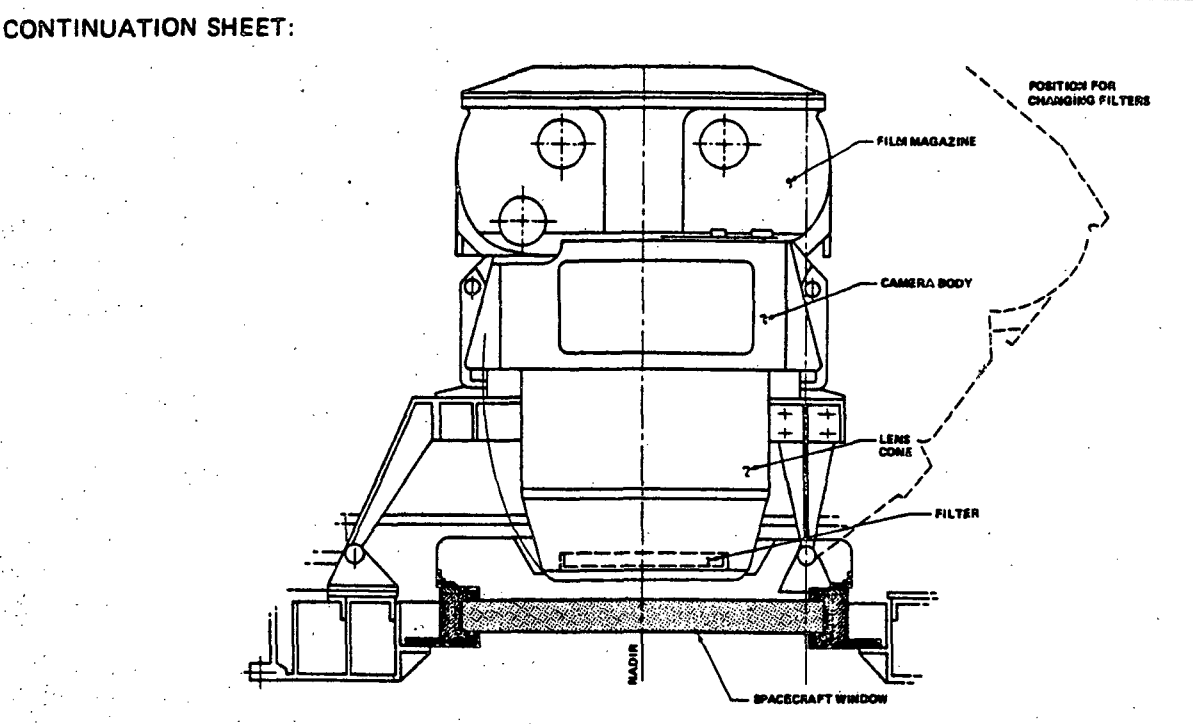
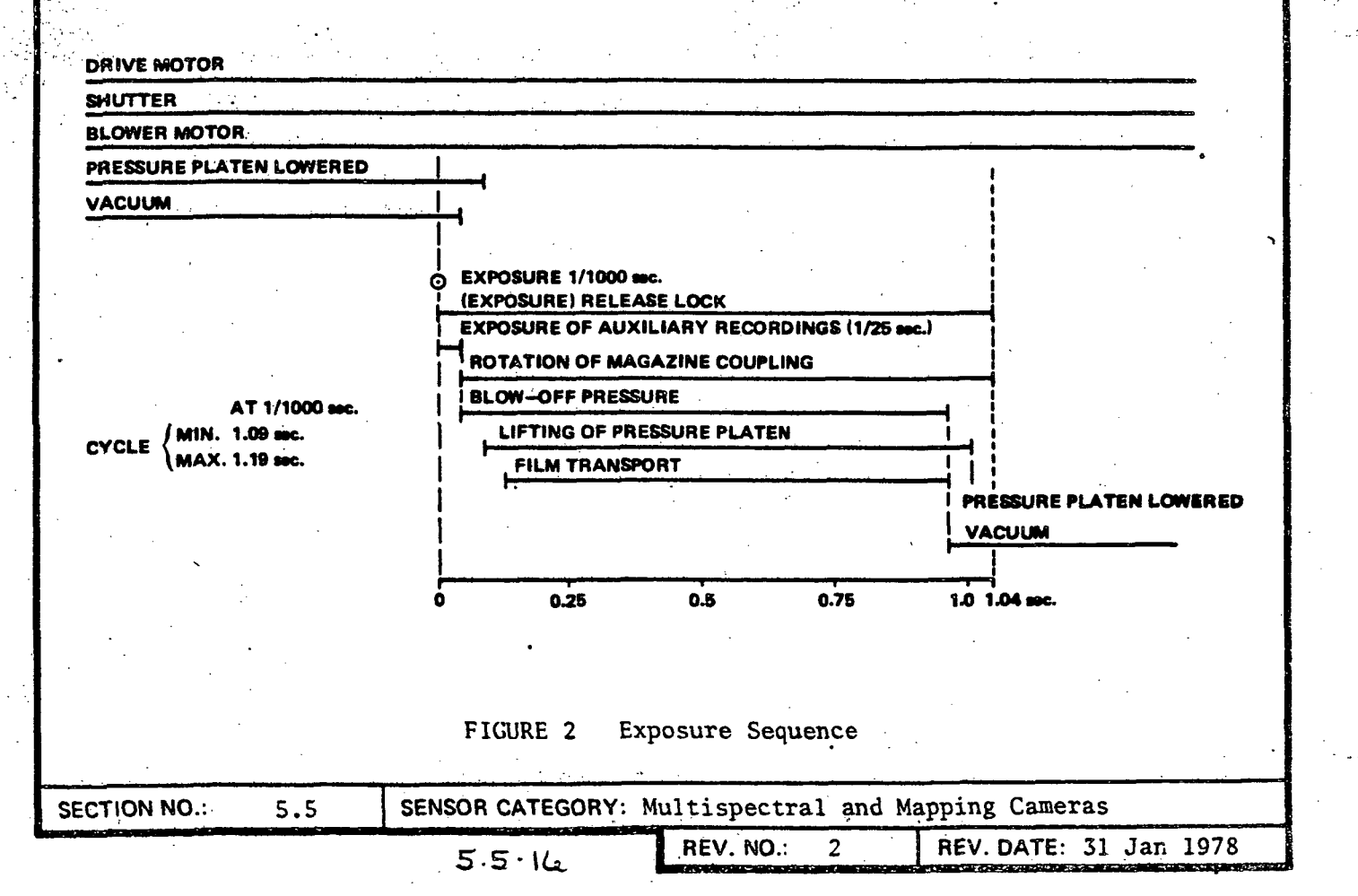
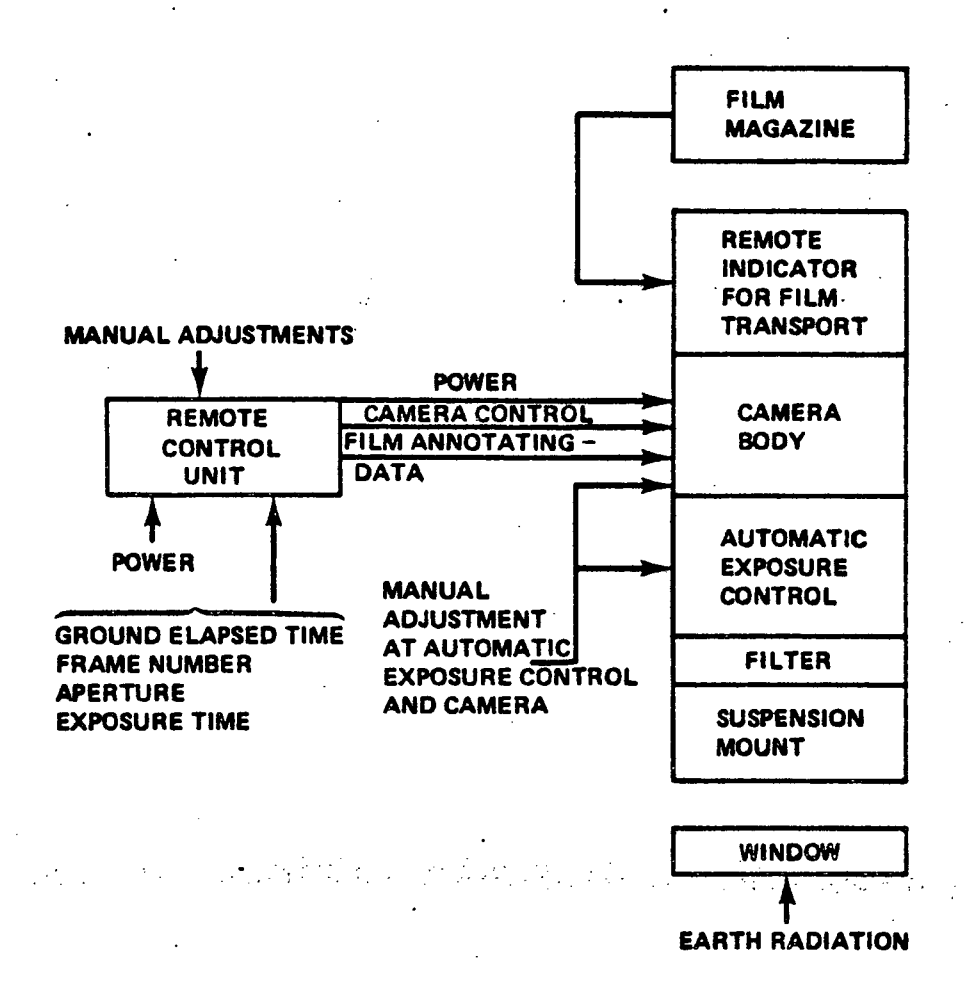


FIGURE 1 Metric Camera Mount



#### (8) SENSOR DATA MEASUREMENT AND TRANSMISSION SYSTEM -- BLOCK DIAGRAM:



#### (9) MEASUREMENT AND TRANSMISSION SYSTEM - NARRATIVE:

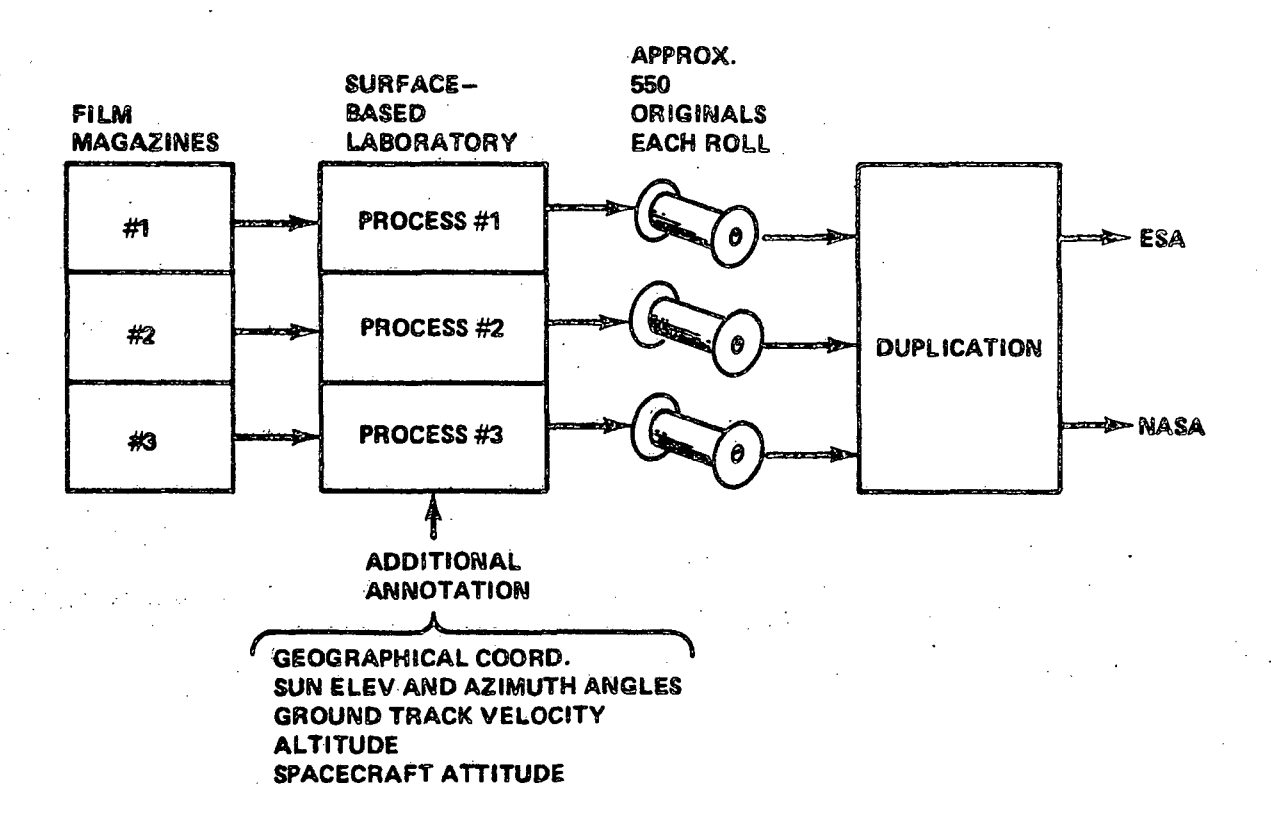
Sensor output is in the form of a latent image on photographic film. This film is returned to the surface for processing. No data is downlinked but voice recordings are coordinated with sequences.

5.5-17

SECTION NO.: 5.5 SENSOR CATEGORY: Multispectral and Mapping Cameras

REV. NO.: 2 REV. DATE: 31 Jan 1978

## (10) SENSOR DATA RECEPTION AND PROCESSING - BLOCK DIAGRAM:



#### (11) RECEIVING AND PROCESSING - NARRATIVE:

Film types have not been selected. Processes 1.2 and 3 may not be identical.

5.5.18

SECTION NO .:

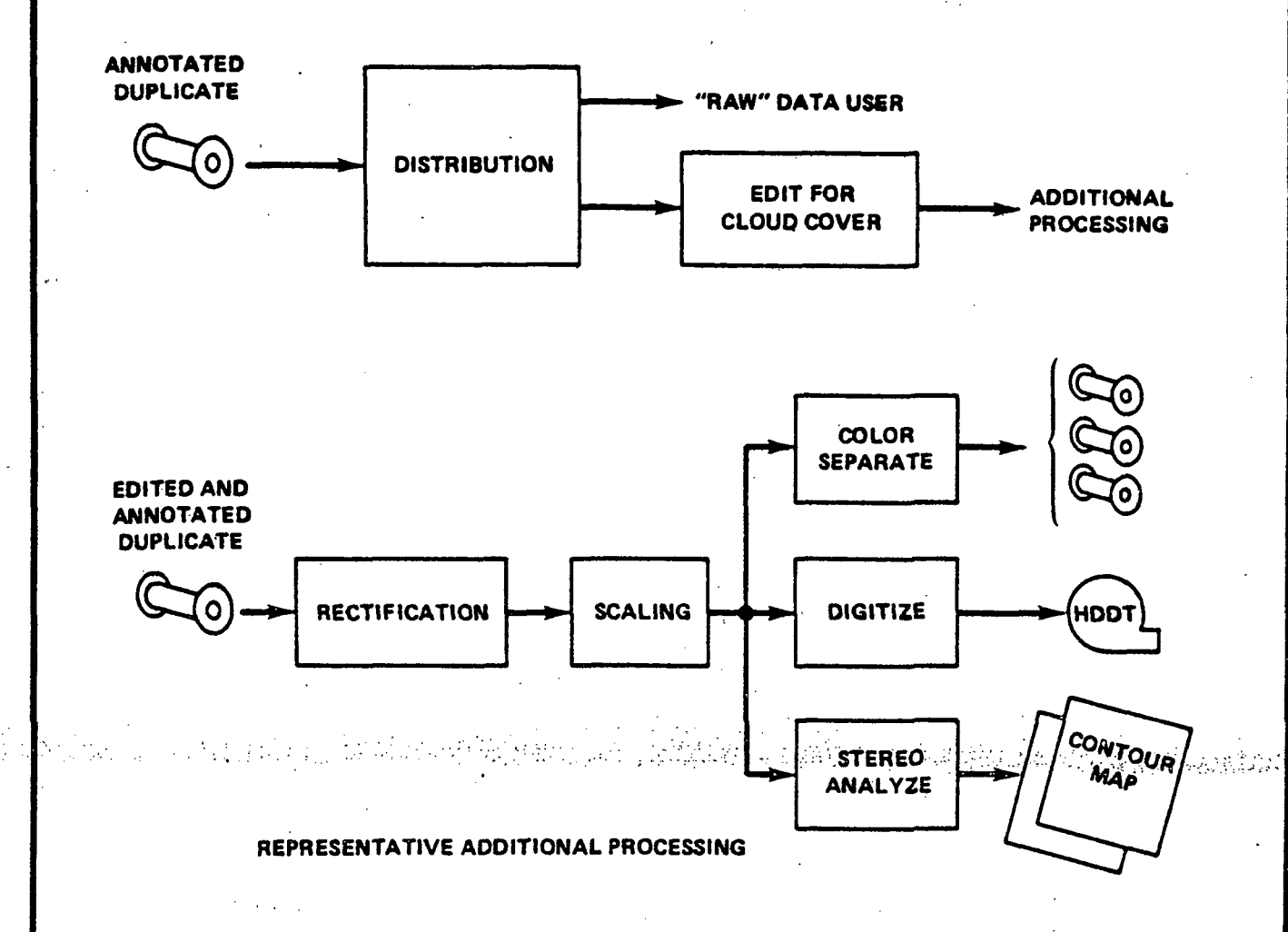
5.5

SENSOR CATEGORY: Multispectral and Mapping Cameras

REV. NO.: 5.5

REV. DATE: 31 Jan 1978

## (12) DISTRIBUTION OF DATA FROM GROUND STATIONS - BLOCK DIAGRAM:



#### (13) DATA DISTRIBUTION - NARRATIVE:

The stated purpose of the metric camera on the Spacelab-1 mission is proof of concept for mapping purposes. Plans for additional distribution beyond that objective are incomplete.

5.5.19

SECTION NO.: 5.5

SENSOR CATEGORY: Multispectral and Mapping Cameras

REV. NO.: 2

REV. DATE: 31 Jan 1978

This page intentionally left blank.

REV. NO.: 2 REV. DATE: 31 Jan 1978

### **RSDH DATA SHEET**

SHEET 1 OF 0	SHEET	1	OF	6	
--------------	-------	---	----	---	--

(1) SENSOR NAME, ACRONYM: Earth Terrain Camera (S190B)

(2) DISCIPLINE: Earth Observations

(3) SUBDISCIPLINE:

Land Use

#### (4) APPLICATION AND OBJECTIVE:

The Earth Terrain Camera (ETC) is designed to provide high resolution photographs of land areas that can be used for urban and regional planning and for the revision of maps with scales of 100,000 to 10,000,000.

#### (5) HERITAGE/KEY PERSONNEL:

The ETC is the same camera flown on Skylab. The only required modification will be the addition of pressurized housing. Team Leader TBD, NASA, JSC.

#### (6) SENSOR DEPLOYMENT:

The ETC is tentatively proposed to fly as part of the Shuttle Mission No. 4. will be rigidly fixed on the pallet. It will be operated from 443 Kilometers (239 nautical miles) altitude and 48 degrees inclination and it will point towards the nadir with pointing accuracy nadir ± 2 degrees.

(7)

#### SENSOR CHARACTERISTICS

#### (7A) CAPABILITIES AND CONSTRAINTS OF THE SENSOR TO ACQUIRE THE MEASURED PARAMETER:

The ETC is a mapping camera and is equipped with a f/4 lens with a focal length of 45.7 centimeters (18 inches). Its field of view of 14.2 degrees across flats providing ground coverage of about 111 kilometers (60 nautical miles) square surface coverage. The camera compensates for spacecraft forward motion through programmed camera rotation. Sequence photography rates of 0 to 25 frames per minute are possible, thus providing up to 85% overlap between frames providing stereo photography. Shutter speeds are selectable at 5, 7 and 10 milliseconds with a curtain velocity 292 cm/sec continued on next page

(7B) ACTIVE SOURCE CHARACTERISTICS (FOR ACTIVE SENSORS):

N/A

#### (7C) DETECTOR MEASUREMENTS CHARACTERISTICS:

The FTC uses 12.7 centimeters (5 inches) film of 2.6 mil base supplied in cassettes of approximately 450 frames each. Total film capacity is 12.7 cm x 61 m (5 inches x 200 feet) thin base. The picture size (format) is 11.4 x 11.4 cm (4.5 x 4.5 inches). The camera is designed to use the following film types and filters combinations:

(continued on next page)

Preceding page blank

SENSOR CATEGORY: Multispectral and Mapping Cameras SECTION NO.: 5.5

REV. NO.: 3

## HSUH DATA SHEET

SHEET	2	OF	6
JUELI	_	UF	

#### **CONTINUATION SHEET:**

#### (7B) continued

(115 inches/seconds). Photographs of the land areas will be obtained in the summer hemisphere when the sun elevation angle is greater than 30 degrees, and in the winter hemisphere when the sun elevation is greater than 20 degrees and cloud coverage of less than 30 percent.

#### (7C) continued

Film	Film Type	Wavelength	Wratten Filter No.
S0242	Aerial Color High Resolution	0.4-0.7 μm	Neutral
EK3414	Black and White	0.5-0.7 μm	W-12
EK3400	High Definition Aerial Black and White	0.5-0.7 μm	W-12
EK3443	Aerochrome IR, Color	0.5-0.88	W-12

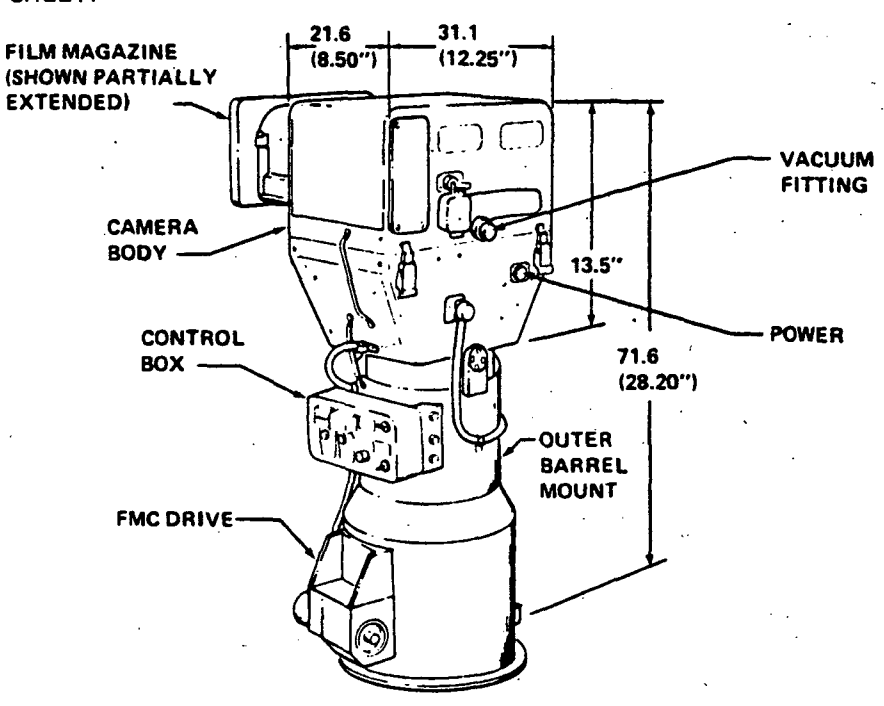
The expected ground resolution for the proposed film and filter combination will vary from 10 meters to 46 meters (37 feet to 150 feet).

SECTION NO.: 5.5 SENSOR CATEGORY: Multispectral and Mapping Cameras

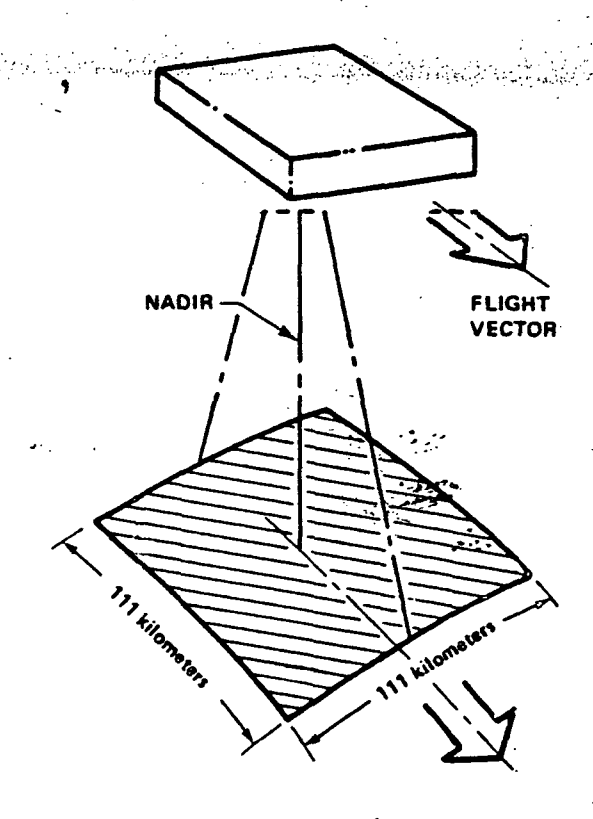
5.5.32

REV. NO.:





Earth Terrain Camera (S190B)

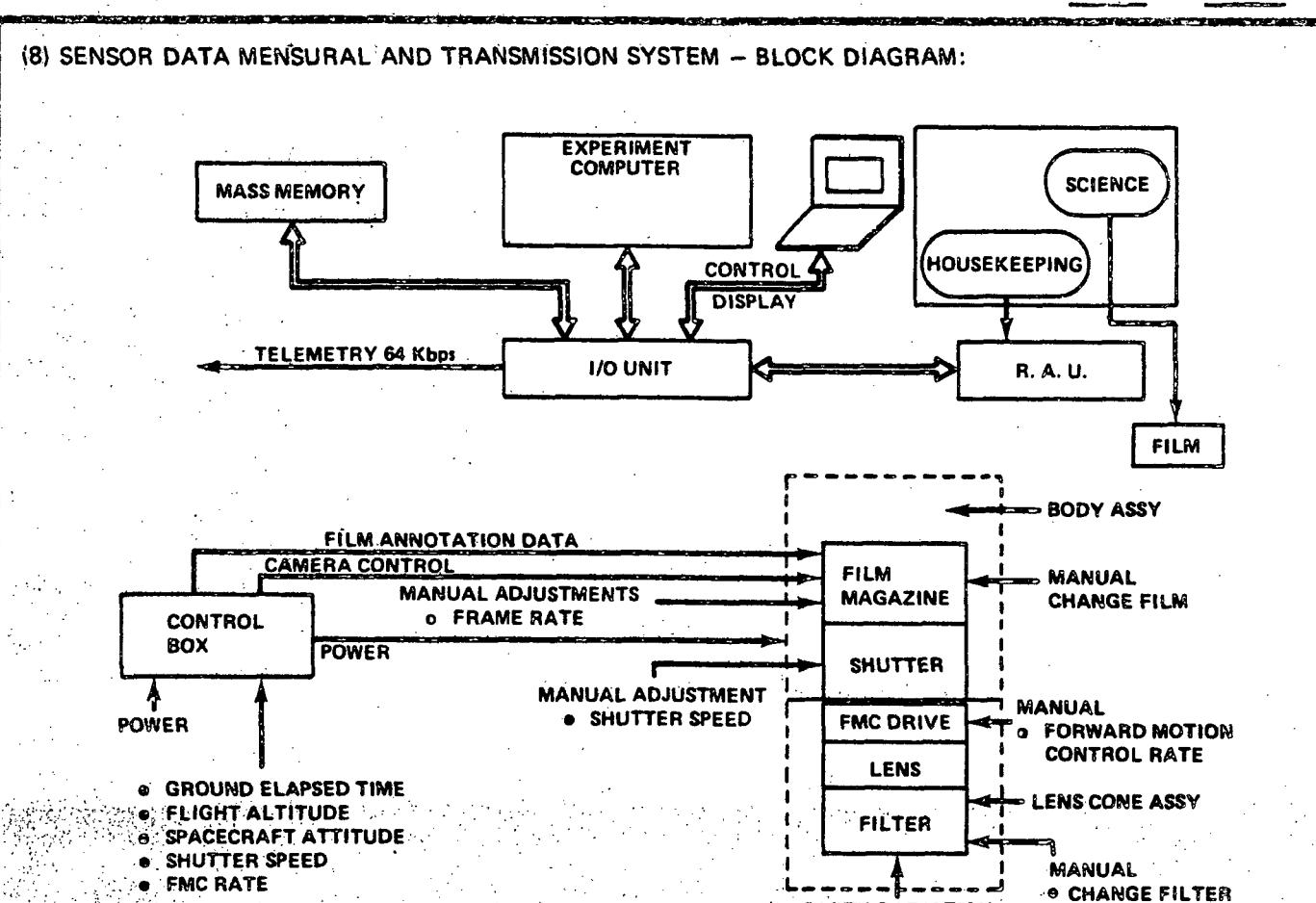


ETC (S190B) Ground Trace

SECTION NO.: 5.5 | SENSOR CATEGORY: Multispectral and Mapping Cameras

5.5.13

REV. NO.: 3



#### (9) MENSURAL AND TRANSMISSION SYSTEM - NARRATIVE:

Sensor output is in the form of a latent image on photographic film. The film is returned to the surface for processing. Housekeeping analog and digital data are downlinked. Voice recordings are coordinated with sequences.

SECTION NO.: 5.5

SENSOR CATEGORY:

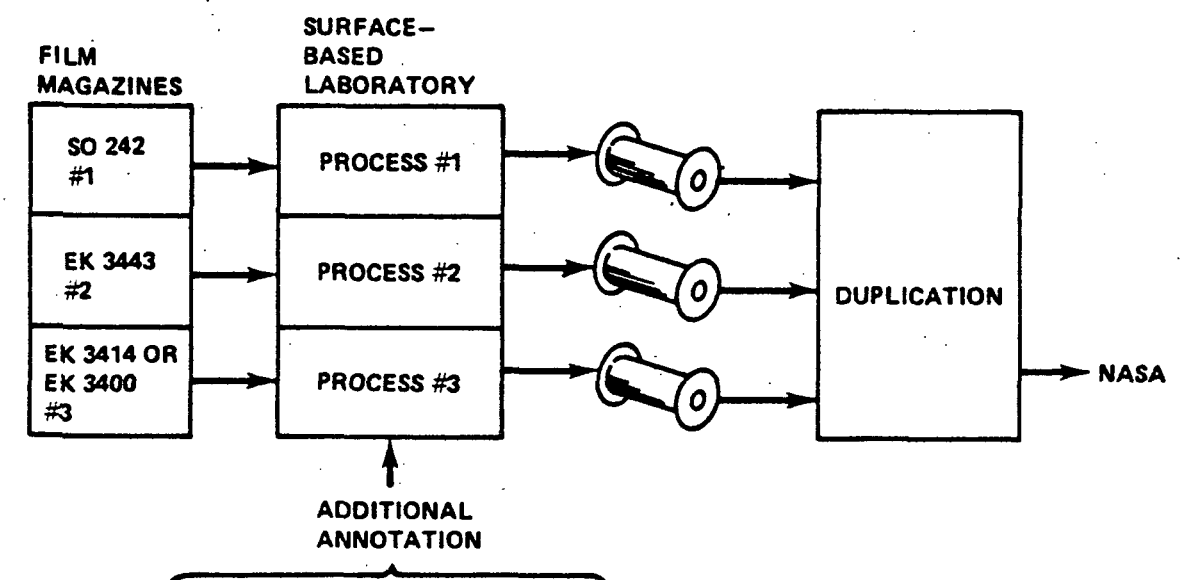
Multispectral and Mapping Cameras

**EARTH RADIATION** 

5.5.24

REV. NO.: 3

## (10) SENSOR DATA RECEPTION AND PROCESSING - BLOCK DIAGRAM:



GEOGRAPHICAL COORD.
SUN ELEV AND AZIMUTH ANGLES
GROUND TRACK VELOCITY
ALTITUDE
SPACECRAFT ATTITUDE

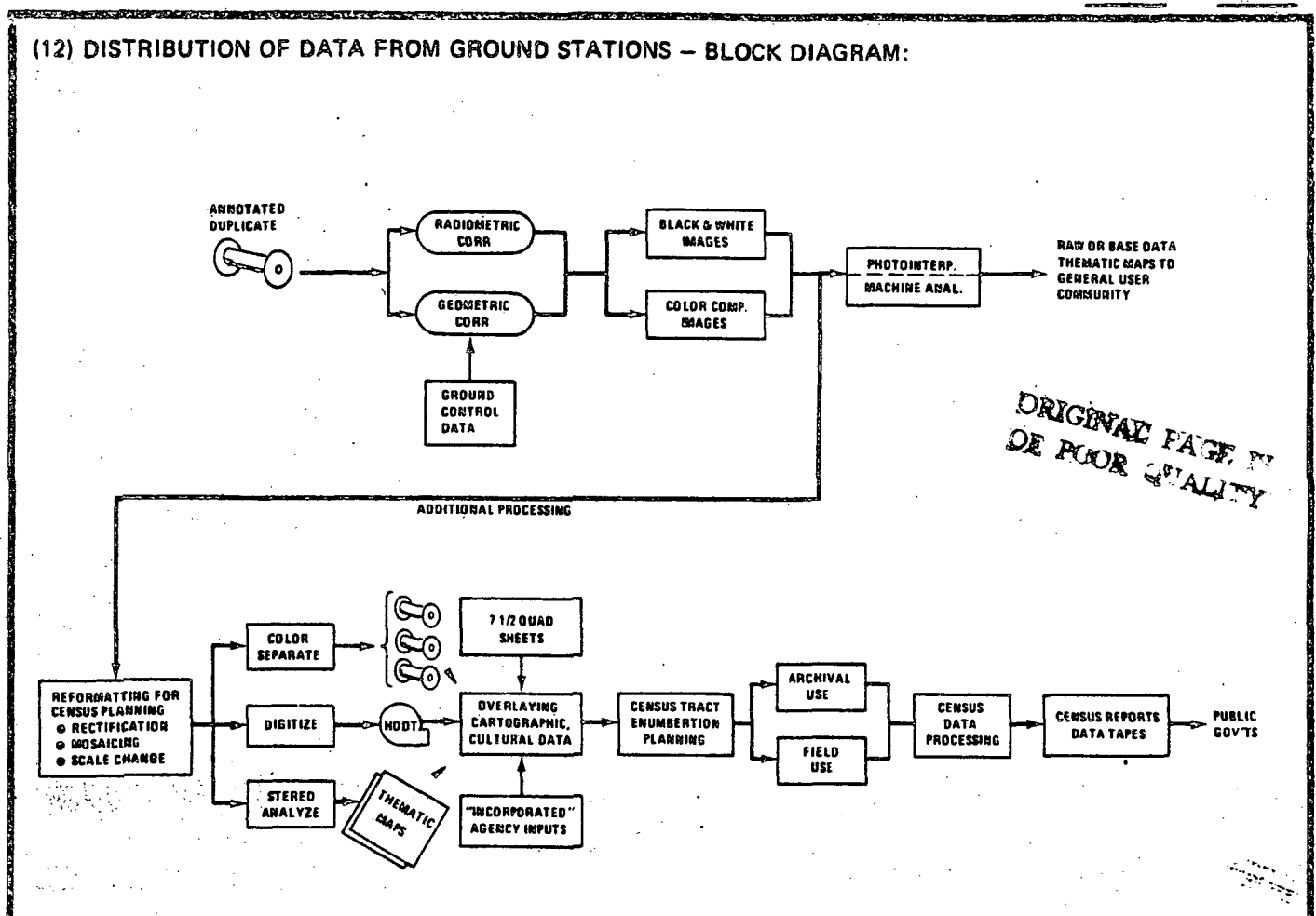
#### (11) RECEIVING AND PROCESSING - NARRATIVE:

The film will undergo initial processing, sensitometry and densitometry testing, screening and quality control, preparation of screening masters, annotation and duplication.

5.5.25

SECTION NO.: 5.5 | SENSOR CATEGORY: Multispectral and Mapping Cameras

REV. NO.: 3



#### (13) DATA DISTRIBUTION - NARRATIVE:

The annotated duplicates are subjected to both radiometric and geometric corrections which becomes the raw or base data and is used primarily by the USGS. The Bureau of Census requires further processed outputs. The black and white and color composite maps at 1:24,000 scale are generated. Cultural data is superimposed on the thematic maps from which the census tract scenarios and enumeration plans are derived. The completion of the flow includes the actual census field work and the issuance of standard census data products.

5.5.26

SECTION NO.: 5.5 SENSOR CATEGORY:

Multispectral and Mapping Cameras

**REV. NO.: 3** 

## RSDH DATA SHEET

SHEET 1 OF 6

(1) SENSOR NAME, ACRONY	M: Multispectral Pho	otographic Facility (S190A)
(2) DISCIPLINE: Earth Obse	ervations	(3) SUBDISCIPLINE: Land Use
(4) APPLICATION AND OBJECTHE Multispectral Photograph multispectral photograph planning.	graphic Facility (MPI	F) is designed to obtain precision can be used for urban and regional
	190A camera flown on cal length from 15 ce	Skylab. Two modifications are being pro- entimeters to 33 centimeters and the addition TBD, NASA, JSC
rigidly fixed on the pa will be operated from 4	llet with its long and 43 kilometers (239 na	art of Shuttle Mission No. 4. It will be as parallel to the velocity vector. It autical miles) altitude, 48 degrees inclinath pointing accuracy nadir ± 2 degrees.
(7)	SENSOR CHA	RACTERISTICS
The MPF consists of an cameras with synchroniz simultaneously photogr 15.24 centimeters (6 in degrees across flats pr meters (90 miles by 90 Data can be taken in di	array of six precise ed shutters and indi aphs the same area, ches) focal length foviding a square covmiles) from the altiscrete spectral band	R TO ACQUIRE THE MEASURED PARAMETER:  ly matched and boresighted 70 millimeter vidual film magazines and filters that each viewing a different wavelength. The /2.8 lenses have a field of view of 21.2 erage of about 166 kilometers by 166 kilotude of 443 kilometers (239 nautical miles). s from 0.4 to 0.9 micrometers by varying mes can vary from 1/400 to 1/100 seconds,
(7B) ACTIVE SOURCE CHARA		
(7C) DETECTOR MEASUREME	NTS CHARACTERISTICS:	
mately 400 frames each.	Photographic forma	a 4-mil base in cassettes holding approxi- t size is 70 millimeters by 70 millimeters designed for the following bandwidth/film
		(continued on next page)
SECTION NO.: 5.5	SENSOR CATEGORY:	fultispectral and Mapping Cameras
	ا جه سرند	REV. NO.: 3 REV. DATE: 31 July 1978

#### **CONTINUATION SHEET:**

## (7A) continued:

and framing overlap up to 88 percent can be achieved. The resolution of this camera will vary from 21 meters on the visible color image to 58 meters on three longer wave images. Photographs of the land areas will be obtained in the summer hemisphere when the sun elevation angle is greater than 30 degrees and in the winter hemisphere when the elevation is greater than 20 degrees. The cloud coverage is less than 30 percent.

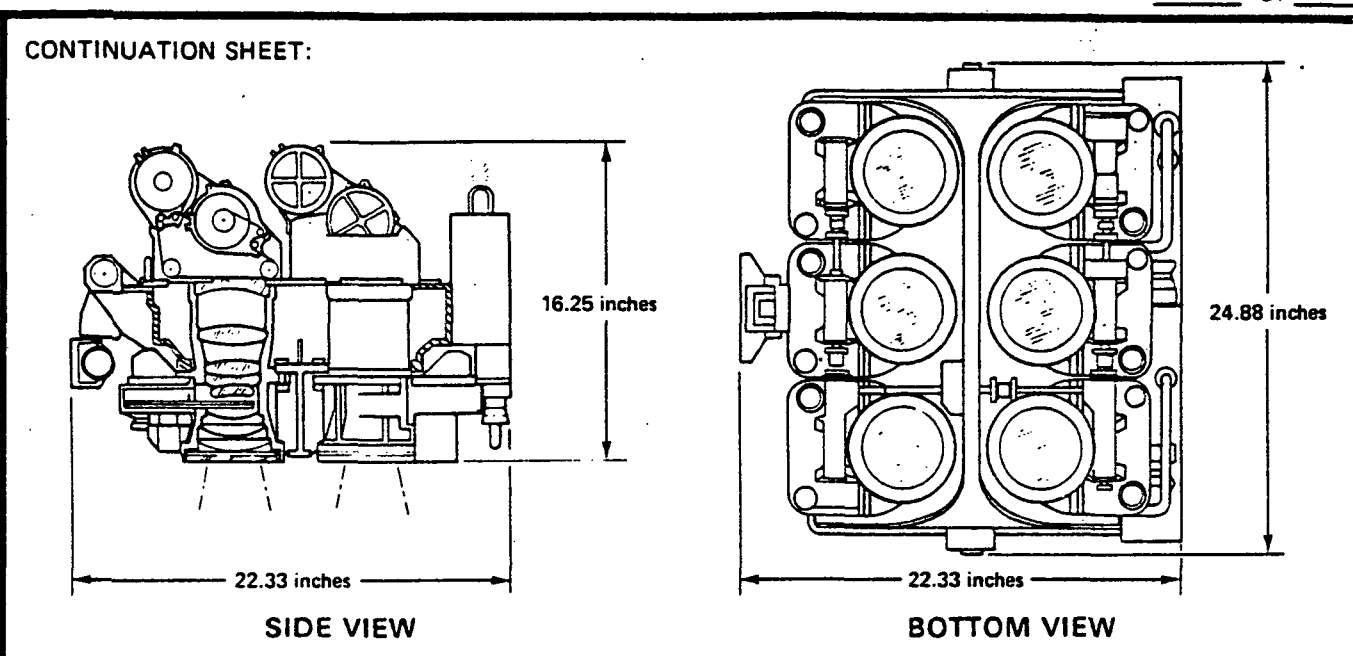
## (7C) continued

Camera	Wavelength (Micrometers)	Film	Туре	Filter
1	0.7-0.8	IR Aerographic Black & White (B&W)	EK2424	CC
2	0.8-0.9	IR Aerographic Black & White (B&W)	EK2424	DD
3	0.5-0.88	Aerochrome IR Color	EK3443	EE
4	0.4-0.7	Aerial Color (high resolution)	S0242	FF
5	0.6-0.7	PANATOMIC-X Aerial B&W	EK3400	ВВ
6 W	0.5-0.6	PANATOMIC-X Aerial B&W	EK3400	AA

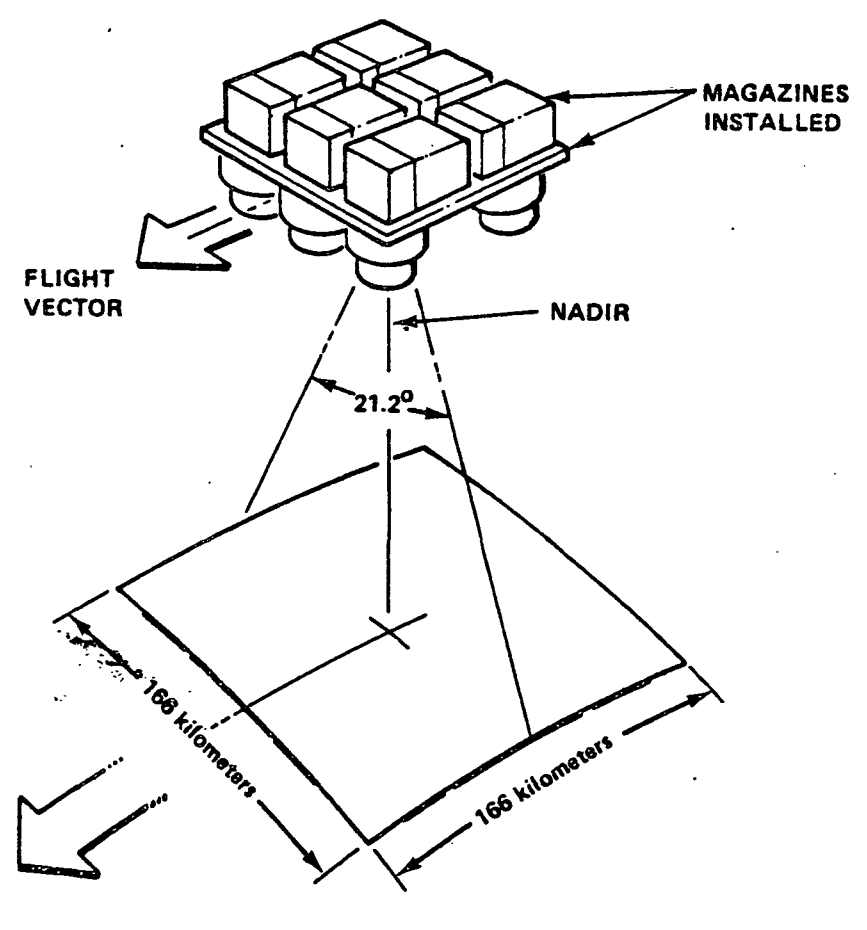
5.5.28

SECTION NO.: 5.5 SENSOR CATEGORY: Multispectral and Mapping Cameras

REV. NO.: 3



Multispectral Photographic Facility (S190A)



MPF Ground Coverage

5.5.29

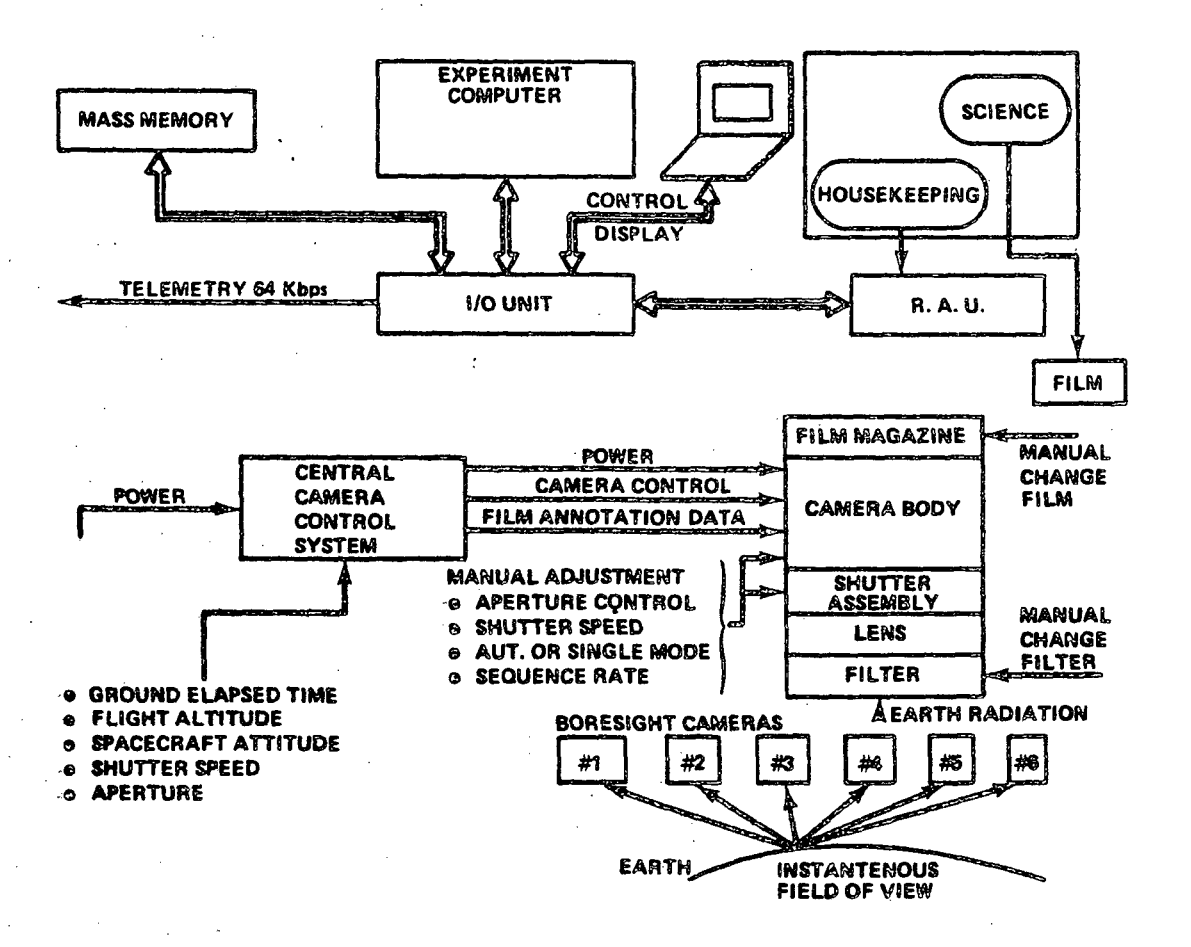
SECTION NO.: 5.5

SENSOR CATEGORY:

Multispectral and Mapping Cameras

REV. NO.: 3

## (8) SENSOR DATA MENSURAL AND TRANSMISSION SYSTEM - BLOCK DIAGRAM:



#### (9) MENSURAL AND TRANSMISSION SYSTEM - NARRATIVE:

Sensor output is in the form of a latent image on photographic film. The film is returned to the surface for processing. Housekeeping analog and digital data are downlinked. Voice recordings are coordinated with sequences.

5.5.30

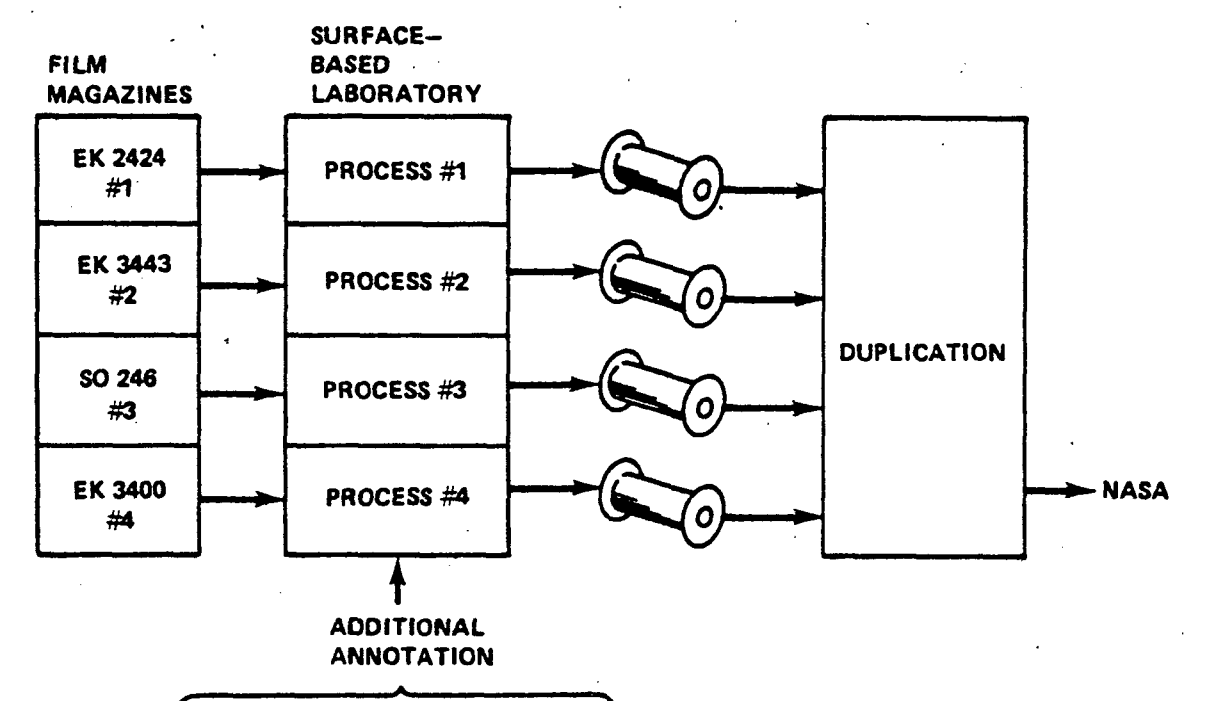
SECTION NO.: 5.5

SENSOR CATEGORY:

Multispectral and Mapping Cameras

REV. NO.: 3

#### (10) SENSOR DATA RECEPTION AND PROCESSING - BLOCK DIAGRAM:



GEOGRAPHICAL COORD.
SUN ELEV AND AZIUMTH ANGLES
GROUND TRACK VELOCITY
ALTITUDE
SPACECRAFT ATTITUDE

## (11) RECEIVING AND PROCESSING - NARRATIVE:

The film will undergo initial processing, sensitometry and densitometry testing, screening and quality control, preparation of screening masters, annotation and duplication.

5.5.31

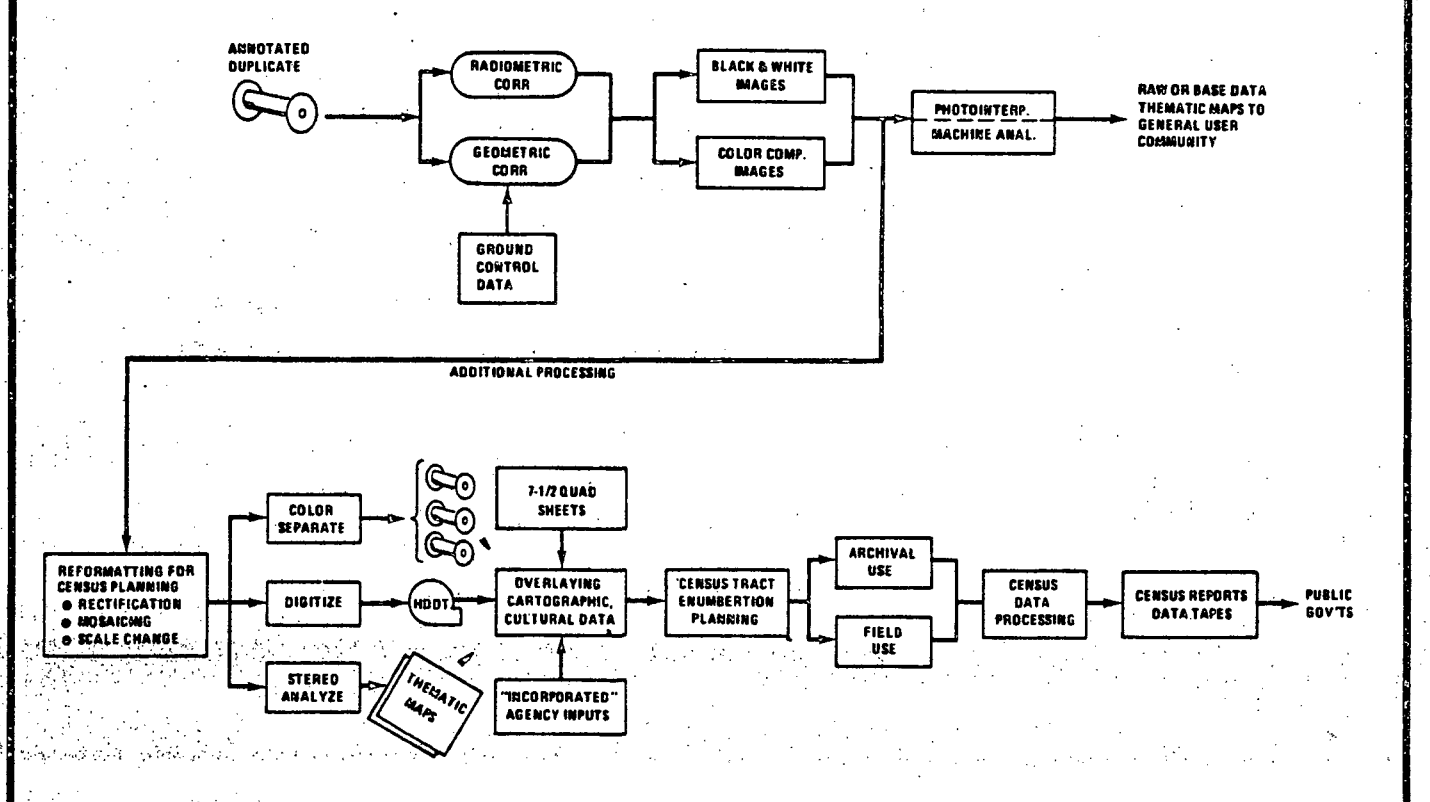
SECTION NO.: 5.5

SENSOR CATEGORY:

Multispectral and Mapping Cameras

REV. NO.: 3

## (12) DISTRIBUTION OF DATA FROM GROUND STATIONS - BLOCK DIAGRAM:



#### (13) DATA DISTRIBUTION - NARRATIVE:

The annotated duplicates are subjected to both radiometric and geometric corrections which becomes the raw or base data and is used primarily by the USGS. The Bureau of Census requires further processed outputs. The black and white and color composite images are subjected to rectification, mosaicing and scale changes where thematic maps at 1:24,000 scale are generated. Cultural data is superimposed on the thematic maps from which the census tract scenarios and enumeration plans are derived. completion of the flow includes the actual census field work and the issuance of standard census data products.

5.5.3ン

SENSOR CATEGORY: SECTION NO .: 5.5 Multispectral and Mapping Cameras

REV. NO.:

•	SHEET OF 5
(1) SENSOR NAME, ACRONYM: Optical Bar Pano:	ramic Camera (S163)
(2) DISCIPLINE: Earth Observations	(3) SUBDISCIPLINE: Land Use
(4) APPLICATION AND OBJECTIVE:	
The Optical Bar Panoramic Camera (OBPC) is a and/or monoscopic photographs of land areas areas, identification and location of new ho	designed to obtain high quality stereoscopic that will allow delineation of all urban omes, streets and roads.
	·
(5) HERITAGE/KEY PERSONNEL: The proposed OBPC is an existing Apollo came to operate in the external environment. Team Leader: TBD, NASA, JSC	era designed with heaters and insulation
(6) SENSOR DEPLOYMENT:	
	part of the Shuttle Mission No. 4. It will be operated from 443 kilometers (239 nautical It will be pointed towards nadir.
(7) SENSOR CHAI	RACTERISTICS
centimeters (24 inches). The shutter is a shutter. The design includes V/h sensing, tion and gaseous nitrogen supply for the fi cross track strips by rotating the lens aro images produced cover a field of view 1.88 degrees 46 minutes) along track. The mode	ining a f/3.5 lens with a focal length of 61 scanning focal plane, variable slit-width automatic control, forward motion compensalm transport. The camera takes panoramic and an axis parallel to the flight path. The radius cross track and 0.188 radians (10)
(78) ACTIVE SOURCE CHARACTERISTICS (FOR ACTIVE every 3.5 seconds. Exposure time varies fr	
Photographs of the land areas will be obtain sun elevation angle is greater than 30 degree elevation is greater than 20 degrees. The	ned in the summer hemisphere when the ees and in the winter hemisphere when the cloud coverage will be less than 30 percent.

## (7C) DETECTOR MEASUREMENTS CHARACTERISTICS:

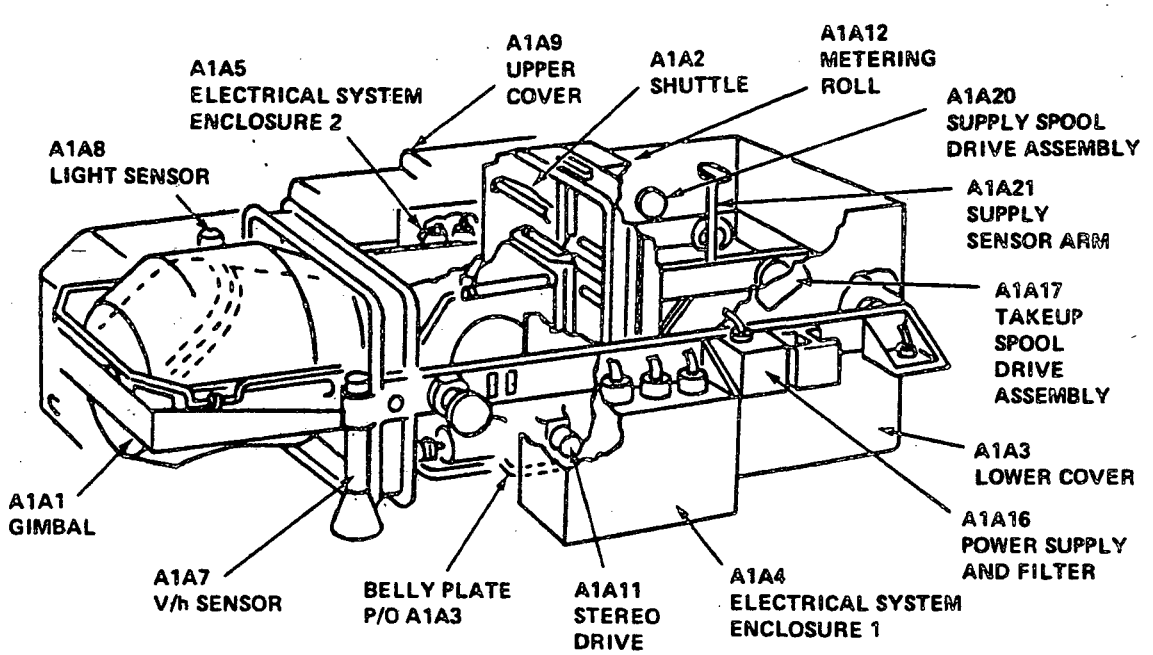
The OBPC uses 12.7 centimeters (5 inches) film, EK 3414, Black and White. The film cassettes contain 1650 frames. Total film capacity is 165 meters (6,500 feet) of thin base. The format is 11.4 by 127.7 centimeters (4.5 x 50.26 inches). The ground resolution is 50 feet.

<u> इ.5⋅33</u>

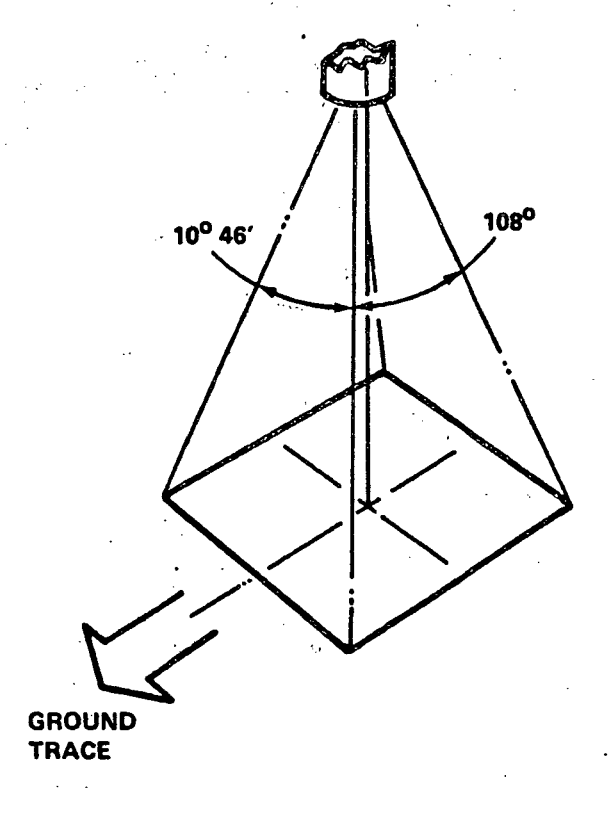
SECTION NO.: 5.5 | SENSOR CATEGORY: Multispectral and Mapping Cameras

REV. NO.: 3





Optical Bar Panoramic Camera (OBPC)-(S163) Illustrations



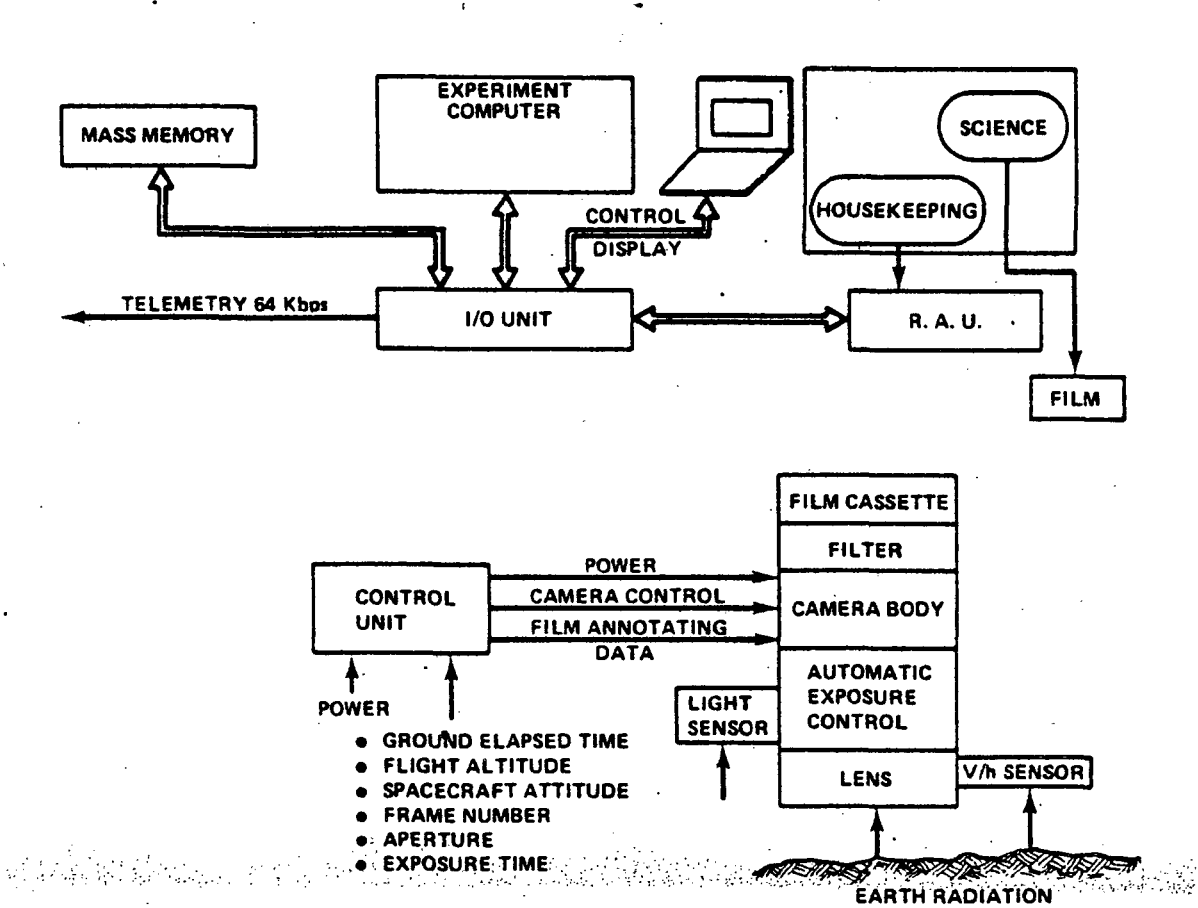
5.5.34

SECTION NO .: 5.5 **SENSOR CATEGORY:** 

Multispectral and Mapping Cameras

REV. NO.:

#### (8) SENSOR DATA MENSURAL AND TRANSMISSION SYSTEM - BLOCK DIAGRAM:



#### (9) MENSURAL AND TRANSMISSION SYSTEM - NARRATIVE:

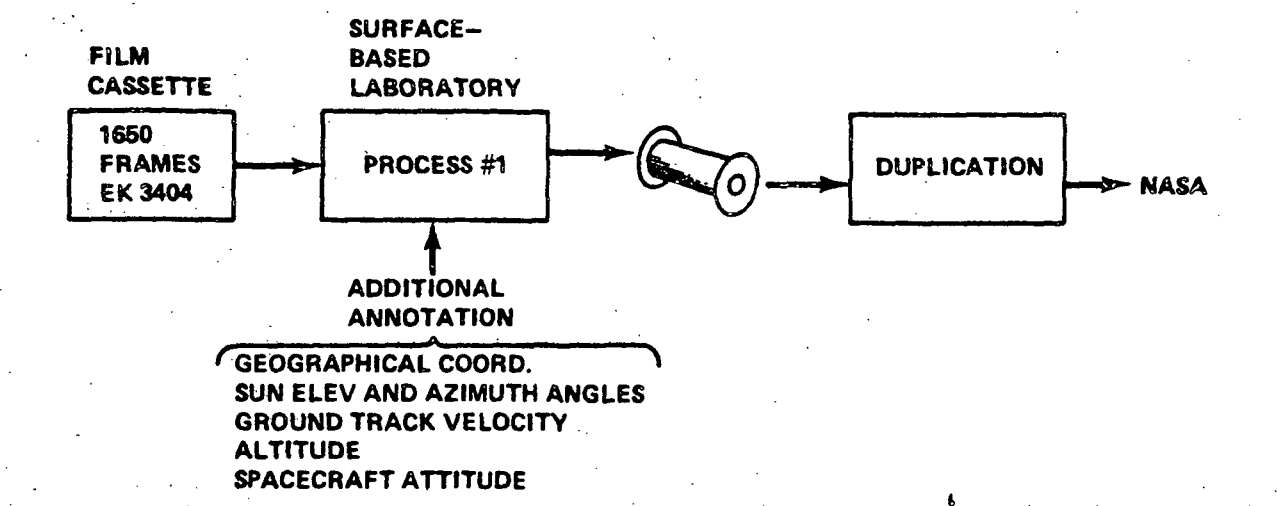
Sensor output is in the form of a latent image on photographic film. The film is returned to the surface for processing. Housekeeping analog and digital data are downlinked. Voice recordings are coordinated with sequences.

5.5.35

SECTION NO.: 5.5 SENSOR CATEGORY: Multispectral and Mapping Cameras

REV. NO.: 3 REV. DATE: 31 July 1978

## (10) SENSOR DATA-RECEPTION AND PROCESSING - BLOCK DIAGRAM:



## (11) RECEIVING AND PROCESSING - NARRATIVE:

The film will undergo initial processing, sensitometry and densitometry testing, screening and quality control, preparation of screening masters, annotation and duplication.

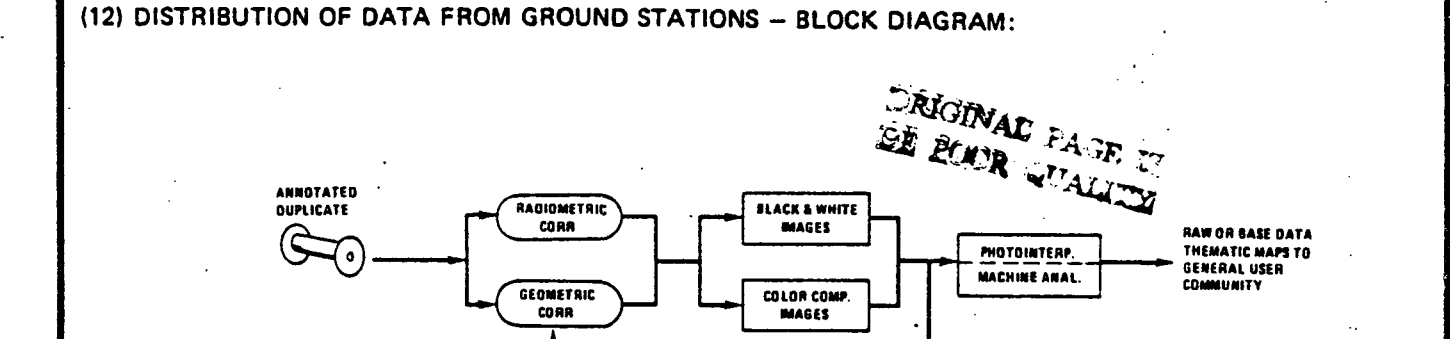
5.5.36

SECTION NO.: 5.5 SENSOR

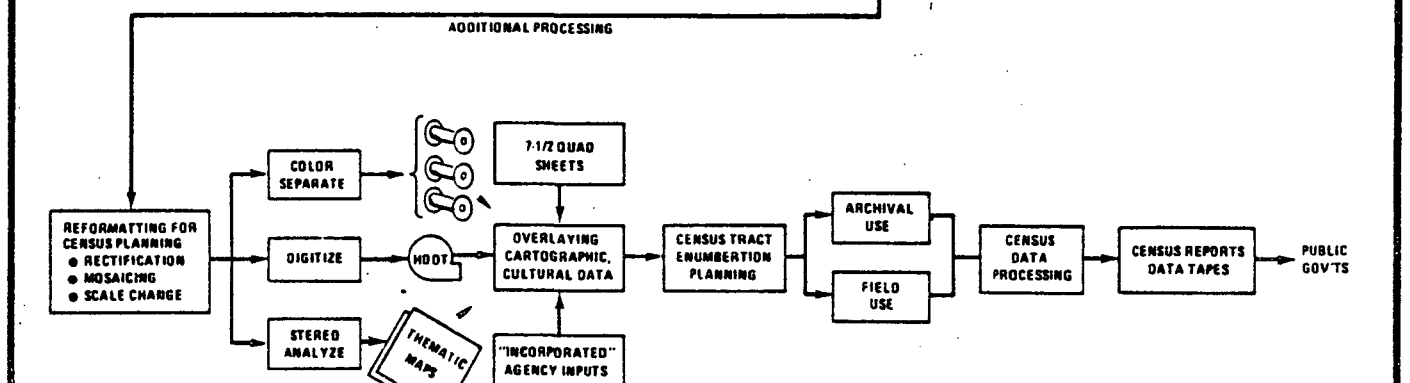
SENSOR CATEGORY:

Multispectral and Mapping Cameras

**REV. NO.: 3** 



GROUND



#### (13) DATA DISTRIBUTION - NARRATIVE:

The annotated duplicates are subjected to both radiometric and geometric corrections which becomes the raw or base data and is used primarily by the USGS. The Bureau of Census requires further processed outputs. The black and white and color composite images are subjected to rectification, mosaicing and scale changes where thematic maps at 1:24,000 scale are generated. Cultural data is superimposed on the thematic maps from which the census tract scenarios and enumeration plans are derived. The completion of the flow includes the actual census field work and the issuance of standard census data products.

5.5.37

SECTION NO.: 5.5

**SENSOR CATEGORY:** 

Multispectral and Mapping Cameras

REV. NO.: 3

This page intentionally left blank.

REV. NO.: 3

## SENSOR CATEGORY TABLE OF CONTENTS AND REVISION CONTROL SHEET

SENSOR NAM OR	Ε .	NUMBER OF	PAGE	EFFE	CTIVE
OTHER ENTR	Y	PAGES	NUMBER	REV. DATE	REV. NO.
Section 5.7 Table of C	ontents	2	5.7-i 5.7-ii	31 JAN 78 31 JAN 78	2 2
Introduction to Imagin radiometers	g Spectro-	43	5.7-1 5.7-2 5.7-3 5.7-4 5.7-5 5.7-6 5.7-7 5.7-8 5.7-9 5.7-10 5.7-11 5.7-12 5.7-13 5.7-14	30 JUN 77 30 JUN 77 30 JUN 77 31 JAN 78 30 JUN 77 31 JAN 78 31 JAN 78	0 0 0 2 0 2 2 2 2 2 2 2 2
			5.7-14 5.7-15 5.7-16 5.7-17 5.7-18 5.7-19 5.7-20 5.7-21 5.7-22 5.7-23 5.7-24 5.7-25	31 JAN 78 31 JAN 78 30 JUN 77 30 JUN 77 31 JAN 78 31 JAN 78 30 JUN 77	0 0
			5.7-26 5.7-27 5.7-28 5.7-29 5.7-30 5.7-31 5.7-32 5.7-33 5.7-34	31 JAN 78 30 JUN 77 30 JUN 77 31 JAN 78 30 JUN 77 31 JAN 78 30 SEPT 77 31 JAN 78 30 SEPT 77	0 2 0 0 2 0 2 1 2 1
			5.7-35 5.7-36 5.7-37 5.7-38 5.7-39 5.7-40 5.7-41 5.7-42 5.7-43	30 SEPT 77 30 SEPT 77 31 JAN 78	1 1 1 1 1 1 1 1 2
Thematic Mapper (TM)		4 .	5.7-45 5.7-46 5.7-47 5.7-48	31 JAN 78 31 JAN 78 31 JAN 78 31 JAN 78	2 2 2 2 2
SECTION NO.: 5.7	SENSOR CATEGORY	: Imaging	Spectroradio		

## SENSOR CATEGORY TABLE OF CONTENTS AND REVISION CONTROL SHEET

SENSOR NAME OR	NUMBER OF	PAGE	EFFE	CTIVE
OTHER ENTRY	PAGES	NUMBER	REV. DATE	REV. NO.
Visible Infrared Spin-Scan Radio-	13	5.7-49	31 JAN 78	2
meter (VISSR)	1	5.7-50	31 JAN 78	2
		5.7-51	31 JAN 78	
		5.7-52	31 JAN 78	2
	<b> </b> '	5.7-53	31 JAN 78	.2 2 2
		5.7-54	31 JAN 78	2
	ļ	5.7-55	31 JAN 78	
	l· .	5.7-56	31 JAN 78	2
	1	5.7-57	31 JAN 78	2 2 2 2
		5.7-58	31 JAN 78	
		5.7-59	31 JAN 78	2
		5.7-60	31 JAN 78	2 .
		5.7-61	31 JAN 78	2
Very High Resolution Radiometer	5	5.7-63	31 JAN 78	2
(VHRR)		5.7-64	.31 JAN 78	2
	1	5.7-65	31 JAN 78	2
en e		5.7-66	31 JAN 78	2
		5.7-67	31 JAN 78	2
Heat Capacity Mapping Radiometers	8	5.7-69	31 JAN 78	. 2
(HCMR)		5.7-70	31 JAN 78	2
Charles of March 1 and the second		5.7-71	31 JAN 78	2
		5.7-72	31 JAN 78	2 2 2 2 2
		5.7-73	31 JAN 78	2
		5.7-74	31 JAN 78	2
		5.7-75	31 JAN 78	2
		5.7-76	31 JAN 78	2
Coastal Zone Color Scanner (CZCS)	6	5.7-77	31 JAN 78	2
	,	5.7-78	31 JAN 78	-2
	,	5.7-79	31 JAN 78	2
		5.7-80	31 JAN 78	2 2
		5.7-81 5.7-82	31 JAN 78 31 JAN 78	2
		3.7-82	31 DAN 76	
Advanced Very High Resolution	4	5.7-83	31 JAN 78	2
Radiometers (AVHRR)		5.7-84	31 JAN 78	2
		5.7-85	31 JAN 78	2
		5.7-86	31 JAN 78	2
Large Earth Survey Telescope (LEST)	6	5.7-87	31 JAN 78	2
		5.7-88	31 JAN 78	2
	!	5.7-89	31 JAN 78	
		5.7-90	31 JAN 78	2 2 2
		5.7-91	31 JAN 78	
*		5.7-92	31 JAN 78	2
		<u>,</u>		
SECTION NO.: 5.7 SENSOR CATEGORY	: Imaging S	Spectroradion	eters	
5.7· ii	REV. NO.:		EV. DATE: 31	Jan 1978

# Section 5.7 INTRODUCTION TO IMAGING SPECTRORADIOMETERS

The classification of Imaging Spectroradiometers includes nonphotographic imagers which monitor reflected solar radiation in more than one region of the spectrum simultaneously through one optical system. Contrast this with (for example) Multiband Return Beam vidicon. Rather than use film as the radiation detecting mechanism, light sensitive electronic devices such as diodes, photovoltaic cells or photomultiplier tubes are used. The outputs of the detectors are transmitted in combination with synchronization pulses so that the viewed image can be reconstructed at a remote point.

Imaging spectroradiometers usually takes the form of a multi-spectral scanner and are used in those applications where: (1) orbital motion of the spacecraft can provide scan along-track, (2) a number of well-defined spectral bands is to be monitored, (3) high radiometric uniformity over the viewed area is desirable, (4) a wide field of view is desired, (5) radiation into the infrared spectrum is to be monitored. The broad spectral coverage and good spectral and spatial resolution of imaging spectro-radiometers makes them attractive for applications where a phenomenon can be recognized by its reflected or emitted radiation. Typical applications include (1) mapping of geophysical features, (2) crop inventorying, (3) hydrological surveys, (4) mineral resource searches, (5) urban population pattern studies, (6) land-use classification, and (7) location of marine life.

The output of most imaging spectroradiometers consists of a video voltage with synchronization for each of the optical passbands being used. These video signals are not at standard TV rates, owing to the fact that the inertia terms in electro-mechanical scanners will not allow the fast TV line rates. Moreover, the high resolution capability of this type scanner would make data rates excessive

REV. NO.: 0 REV. DATE: 30 June 1977

if standard TV line rates were used. It is convenient to convert the detector outputs from analog to digital and multiplex them if transmission over a distance is required. Currently, signal to noise ratios can support digital quantization to the six-bit level.

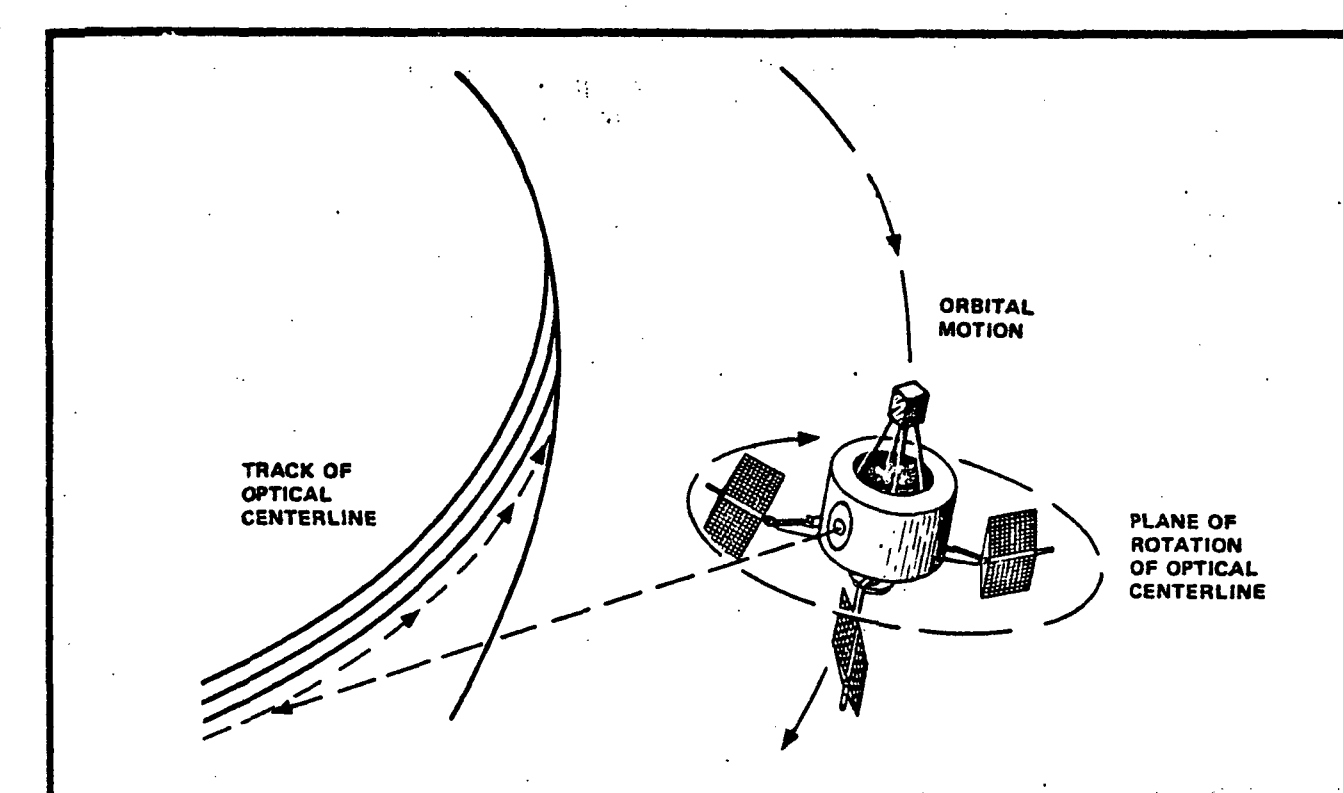
No clear separation exists between the development of imaging spectroradiometers and the development of imaging electro-optical scanners. The later dates back into the late nineteen twenties and includes early television experiments. For our purposes, little additional insight is to be gained by going back further than late 1959, when the first earth observation instrument to return usable data from space was flown on Explorer 7. Since then, thirty-six instruments, of twenty different designs, which can be classified as imaging radiometers with mechanical scanning, have flown on twenty different orbital missions.

The basic imaging spectroradiometer is exemplified by the spectroradiometers aboard the early TIROS (2 through 7) and NIMBUS (1, 2 and 3) flights except that separate imaging optics were used for each spectral band. These instruments, called Medium Resolution Infrared Radiometers (MRIR), were relatively simple and are useful for illustration purposes.

They are of two basic styles. The earlier units, those that flew on TIROS two through seven, contain no scanning mechanism whatsoever, as they were designed for use on a spin-stabilized spacecraft, where the spin provided the cross-track scan while line advancement is provided by orbital motion. The Nimbus MRIR, on the other hand, is similar in layout to the earlier spin-scan instruments, but since it was installed on a three-axis stabilized spacecraft, a scanning mirror was added to provide cross-track scan. Line advancement is still provided by orbital motion (see Figure 5.7-1).

5.7.2

REV. NO.: 0 REV. DATE: 30 June 1977



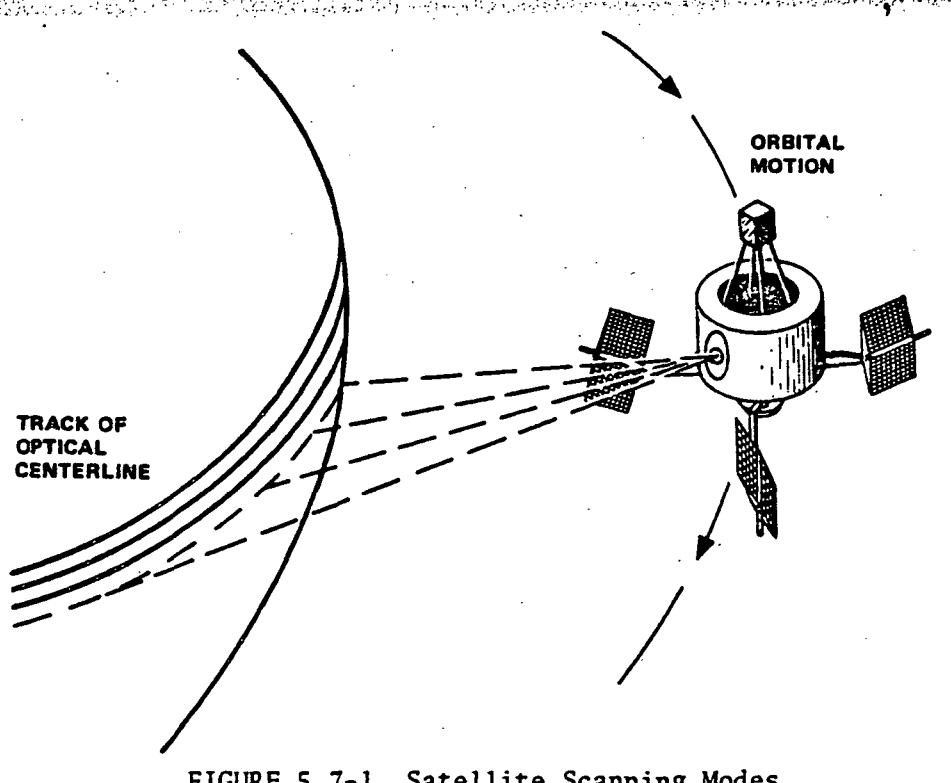


FIGURE 5.7-1 Satellite Scanning Modes

5.7.3

REV. NO.:

**REV. DATE: 30 June 1977** 

Figure 5.7-2 is an idealized and simplified pictoral diagram of the early

Tiros radiometers. The centerline of the instrument is installed parallel to the

center of rotation of the spacecraft. A flat mirror deflects the optical center
line of the imaging optics to a path orthagonal to the axis of rotation. Radiation

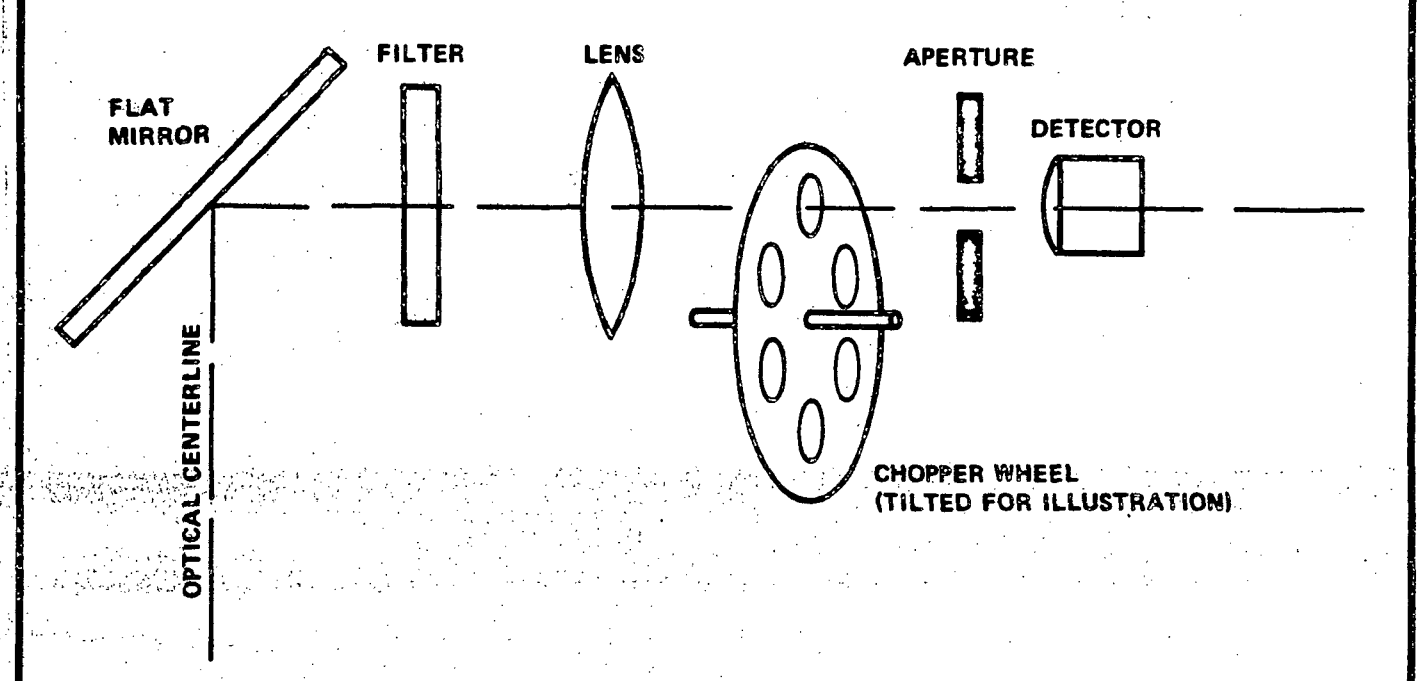


FIGURE 5.7-2 Early Tiros Radiometer Schematic

enters the radiometer via the mirror and is focused by the individual objective into an aperture, which defines the size of the "instantaneous field of view" (IFOV). The aperture allows only the imaged radiation which falls within the clear diameter of the aperture to pass to the detector and be registered as an output voltage. The Ground Resolution Element (GRE), or smallest feature which can be isolated on the surface of the earth, is directly related to the size of this aperture and the Equivalent Focal Length (EFL) of the imaging lens system by the "lens makers formula." [1] Image - object relationships are illustrated in Figure 5.7-3.

REV. NO.: 2 REV. DATE: 31 Jan 1978

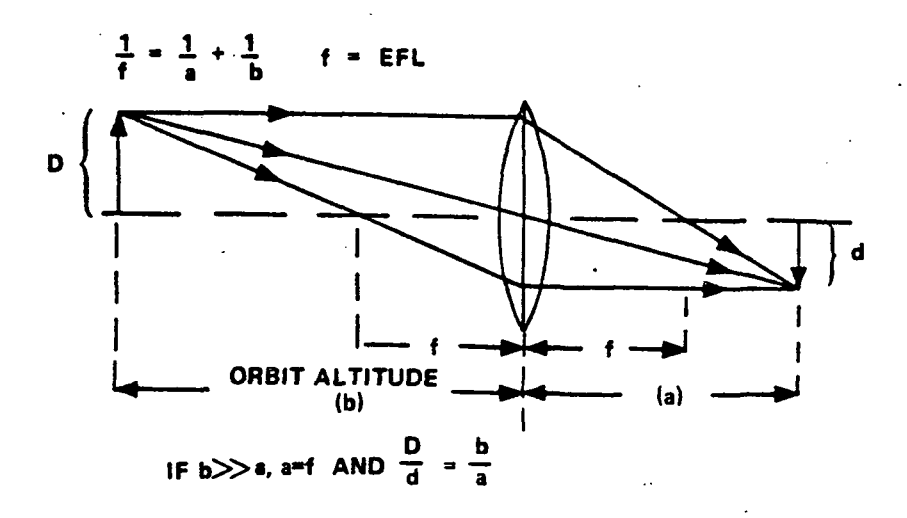


FIGURE 5.7-3 Image - Object Relationships

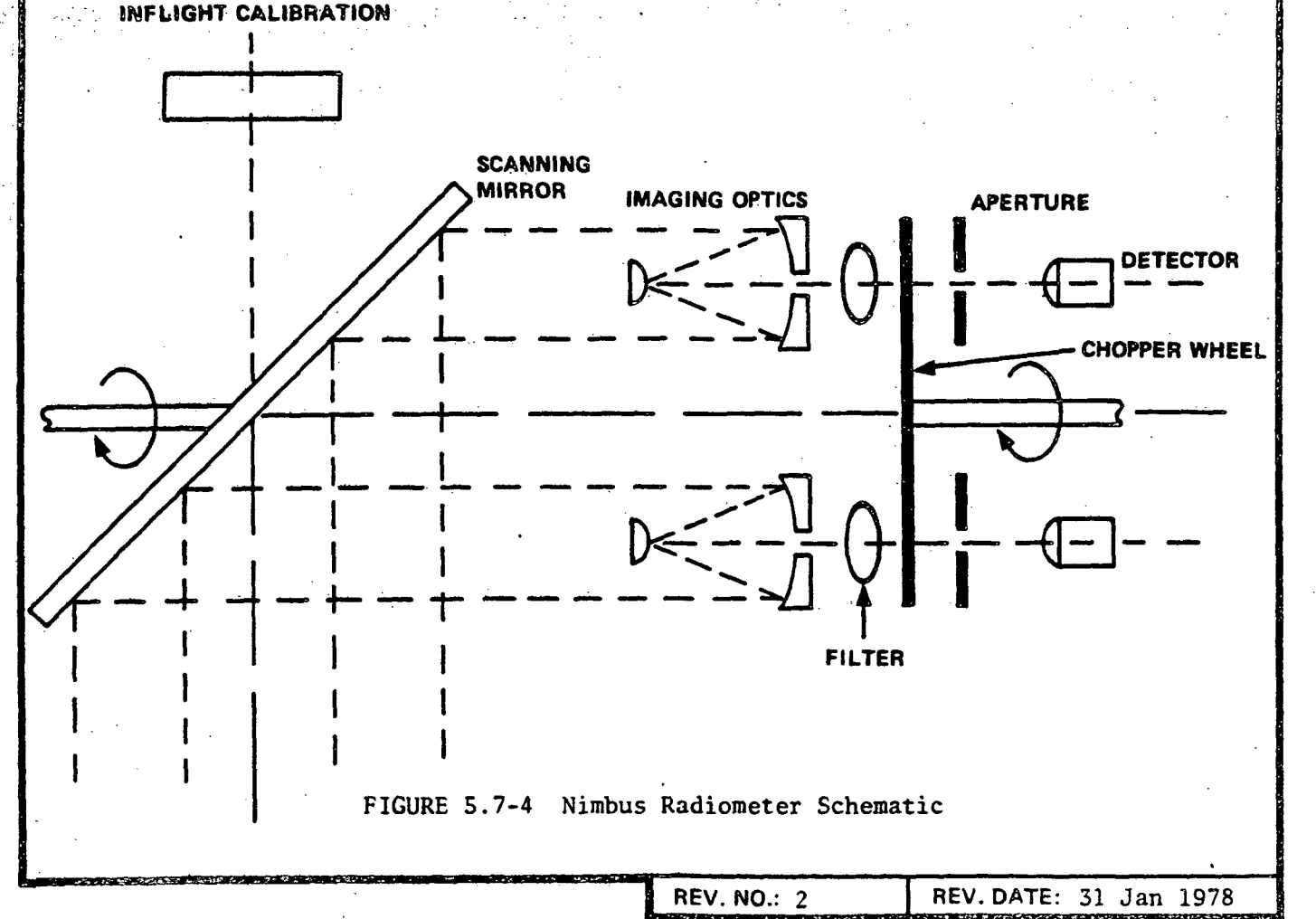
One convenient way to look at the IFOV and the GRE is to regard the GRE as the projection onto the earth of the image of the limiting aperture. It is evident from the sketch that for uniformly illuminated fields, as the diameter of the aperture is increased, more light falls on the detector, increasing sensitivity but decreasing spatial resolution. The optimum selection of the aperture diameter will be determined by the light gathering capacity of the imaging system (objective diameter) and the type of detector used. A filter is used in this illustration to limit the spectral bandpass of radiation allowed to be imaged. Since the incoming radiation is normal to the plane of the filter, an interference type filter [2] [3] could be employed for good spectral resolution. These filters can be made quite selective. Other types of filters, such as color filters, can be employed or the spectral response limits of the detector itself can be used to define the spectral resolution. See the section on Multispectral and Mapping Cameras for more references on filters.

The chopper wheel alternately switches the radiation entering the detector from scene radiation to the light level (or temperature) of the chopper disc. The detector output correspondingly swings between a level defining scene radiation

REV. NO.: 0 REV. DATE: 30 June 1977

level and a near-zero level. Successive amplifier stages can be A-C coupled and can, therefore, have higher stable gains and lower noise figures than would be possible with D.C. coupling. D.C. restoration can be used for calibration if shutter irradience (temperature) is known. On early Tiros flights, there was no on-board radiometric calibration per se, but as the optical centerline of the radiometer was rotated around to the "back side" of the sweep, it was pointed away from earth into deep space, and the resulting detector output was taken as representing a zero level. On the later Nimbus flights, the wideband radiation of the sun itself was used as an in-flight reference.

Figure 5.7-4 illustrates that the radiometers aboard Nimbus flights were similar in principle to the Tiros radiometers except that a scanning mirror SUN REFERENCE FOR



rotating at 8RPM, placed in front of the 1.7 inch diameter individual Cassagrain objectives was used to sweep the optical centerline of the system. The axis of rotation of the mirror was alligned parallel to the spacecraft velocity vector. In both of these instruments, the outputs of the detectors are digitized and recorded on tape recorders for delayed playback.

Spectroradiometers of advanced design include the Landsat Multispectral Scanner (MSS) and the Thematic Mapper. These sensors differ from earlier designs in numerous ways, as shown by Figure 5.7-5. A nutating mirror provides cross-track

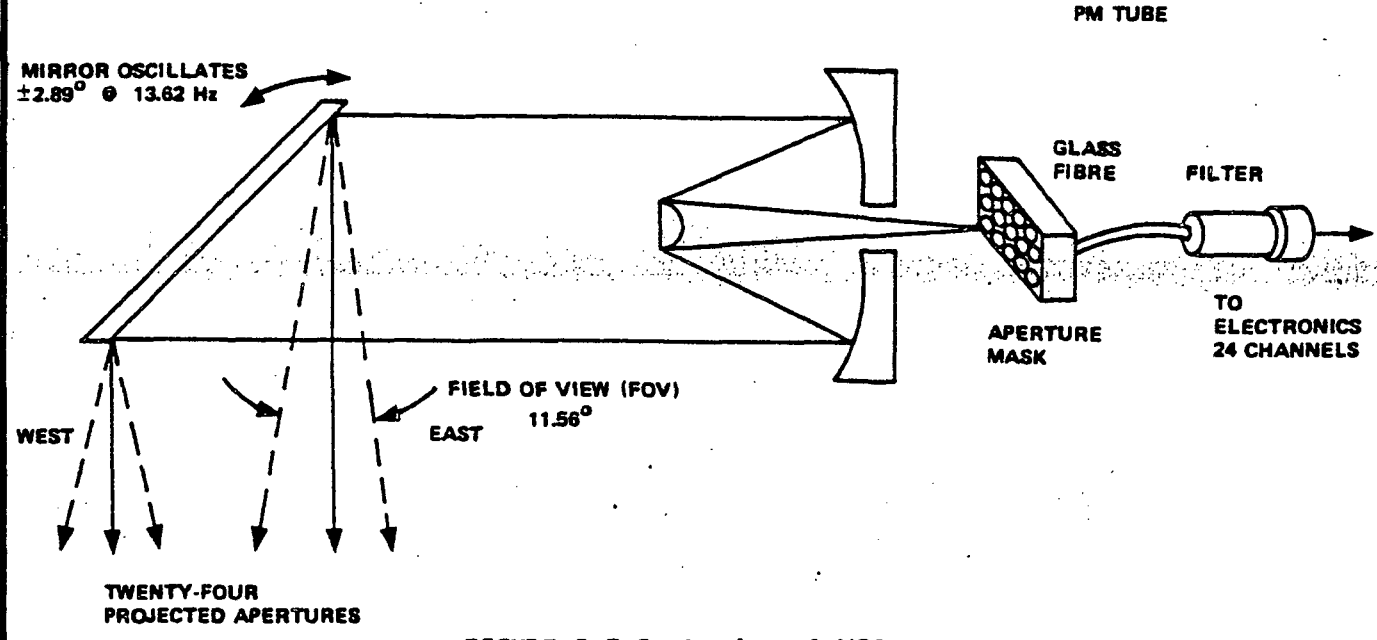


FIGURE 5.7-5 Landsat-1 MSS

scan while orbital motion provides the along-track component. In the case of Landsat-1, the mirror's frequency of oscillation is 13.62 Hz, and the amplitude is  $\pm 2.89^{\circ}$ . This yields a field of view of  $11.56^{\circ}$ , which form an altitude of 925 km, translates to a cross-track swath width of 925 km x Sin  $11.56^{\circ}$  = .2 x 925 = 185.4 km, which is the published swath width. As the mirror deflects the optical centerline across the swath, in half the period of oscillation (1.2 x 1.13.62 = 36.7 milli-

REV. NO.: 2 | R

seconds) the spacecraft generating a subsatellite track traveling at 6.47 km/sec, skews the sweep by an amount equal to:

$$\frac{1}{2} \times \frac{6.47 \text{ km/sec}}{13.62 \text{ Hz}} = 237 \text{ meters}$$

on the second half of the mirrors oscillatory cycle, (retrace) an additional equal skew is introduced, such that during a single oscillatory cycle of the mirror, the along-track advancement is 474 meters. To improve the along-track resolution, six adjacent cross-track lines are scanned simultaneously as shown in Figure 5.7-6. In this way the along-track dimension of each line is:

$$\frac{474}{6} = 79 \text{ meters}$$

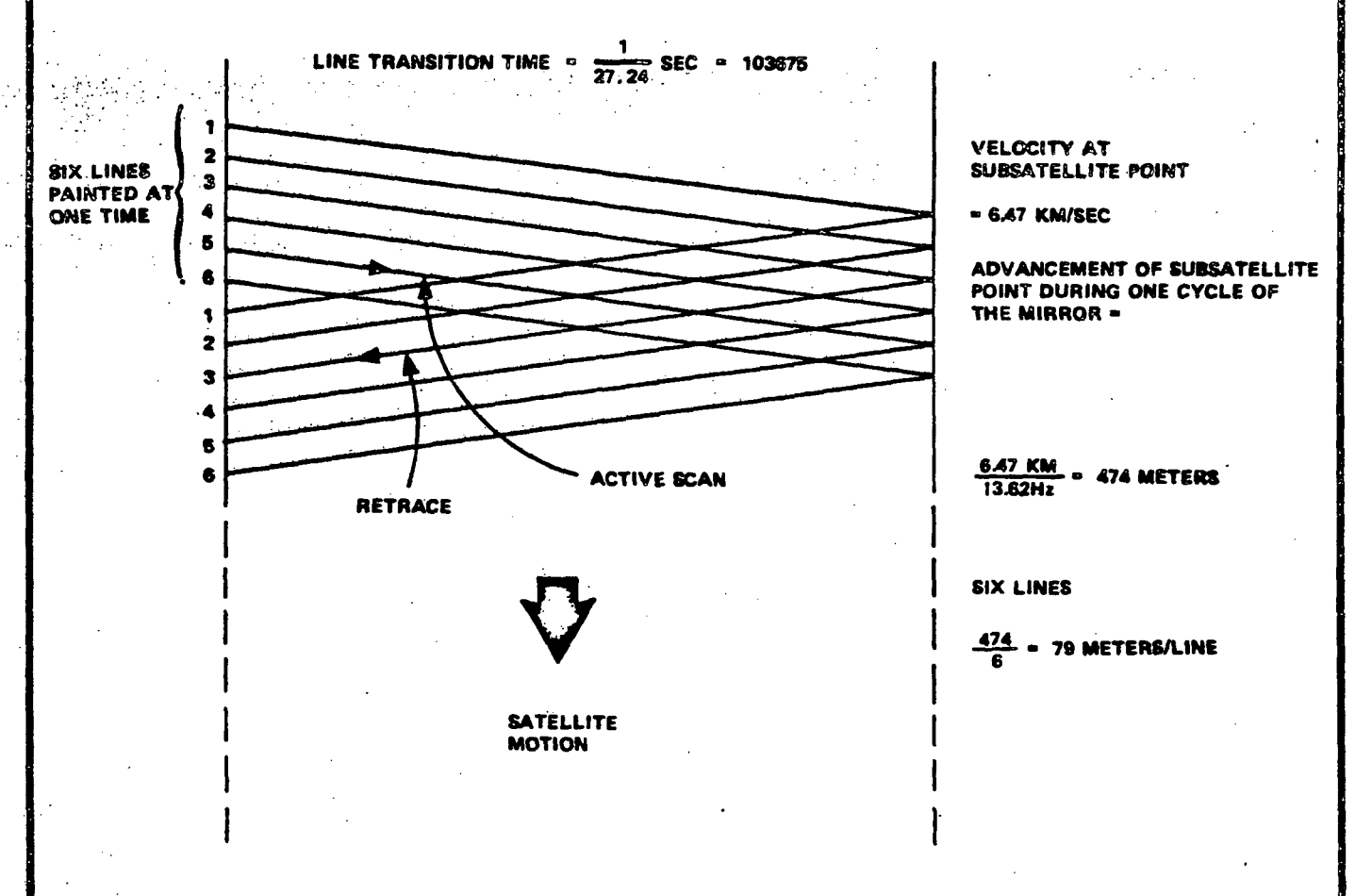


FIGURE 5.7-6 Landsat Scan Pattern

5.7.8

**REV. NO.: 2** 

The aperture mask is arranged so that the apertures of the six detectors devoted to each spectral band project onto earth as shown in Figures 5.7-6 and 5.7-7. Each additional spectral band being monitored through the MSS requires another six detectors if the same spatial resolution is to be maintained. For any band, fewer than six detectors can be used if the along track dimension of the aperture is changed accordingly. For example, in Landsat C, a thermal band is added, extending spectral response to include 10.4 to 12.5 µm. Only two detectors (which are cooled by passive coolers) are used. The apertures for their detectors are three times the size of the apertures for the other four channels and, consequently, the ground resolution element for this band is 240 meters rather than 80 meters. The apertures for the various spectral bands are arranged as shown in Figure 5.7-7 for the Landsat MSS. Fibre optics couple the radiation falling on the aperture mask to the detectors.

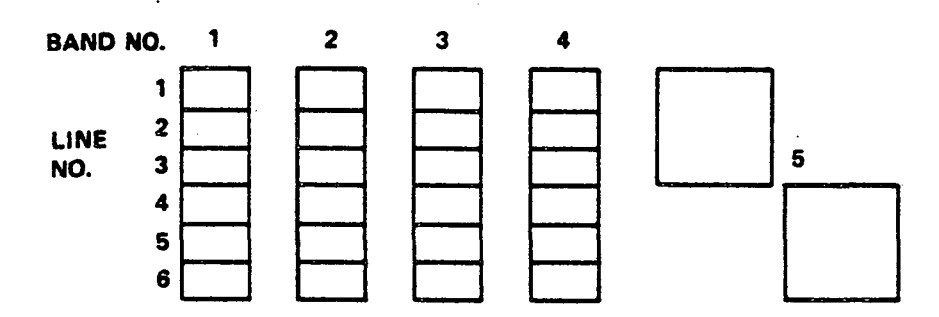


FIGURE 5.7-7 Aperture Mask

As Figure 5.7-7 implies, there is one detector required for each line generated in each band. In the case of Landsat C, twenty-six detectors are utilized.

Analog to digital conversion and multiplexing are required to organize these outputs into an intelligent format. When choosing the parameters of the A-D converter, one method for insuring that all available information is contained in the output is to choose the sample rate such that there is more than one sample per picture element (Pixel). For example, if the aperture mask dimensions are such that the

5.7-9

**REV. NO.:** 2 **REV. DATE**: 31 Jan 1978

fundamental pixel size is 80 meters square on the ground and a single line is 185 km in length, there are  $\frac{185 \times 10^3}{80}$  = 2300 elements per line, generated at a rate of 6 lines per 37.7 milliseconds =  $\frac{2300 \times 6}{.0377}$  = 366,048 elements per second per band and with four bands the pixel rate is 4 x 366,048 = 1,464,192 pixels per second. If we set the sample rate at 1 1/2 samples per pixel, then the sample rate is 1,464,192 x 1.5 = 2,196,288 samples per second. If the digital quantization is six bits, the bit rate is 2,196,2-8 x 6 - 13.2 x  $10^6$  bits per second for a system like that in Landsat 1 and 2.

A significant measure of the quality of a mechanical scanner is the repeatability and predictability of the scan produced by the oscillating mirror. This quality determines the band-to-band registration and geometric fidelity which, together with amplitude resolution and spatial resolution, describe the performance of an imaging spectro-radiometer.

Band-to-band registration is a statement of the ability of an instrument to successively position field stop apertures associated with one band so that they spatially agree with the field stops of other bands in order to bring each area on the earth's surface under the scrutiny of all bands. Spectral signature analysis with an imaging spectro radiometer is dependent upon the capability of the instrument to achieve good band-to-band registration.

Geometric fidelity is the accumulated errors of six sources which contribute to the distortion of the image. Scan linearity errors, caused largely by torque produced in the scan mirror support pivots, are systematic and can be compensated out. The remainder of the geometric errors, random cross-scan jitter, scan-to-scan repeatibility, scan start and scan end variation, sampling uncertainty and detector alignment are uncontrolled but relatively small and together constitute a total error in Landsat 1 and 2 of only twenty-six meters.

REV. NO.: 2 REV. DATE: 31 Jan 1978

Electronically self-scanned detector arrays will influence future designs by removing the restrictions imposed by some of the mechanical properties of instruments which now use oscillating mirrors. Included in this type of array are both hybrid arrays of individual detectors and the batch-processed Charge-Coupled-Devices (CCDs) on silicon. CCD's now include built-in sequential interrogation circuits and several hundred individual sensor diodes with center-to-center spacings of the order of 25 microns used with an optical system equivalent to that aboard Landsat-2, even current CCD array designs yield cross-track resolutions of 25 meters. We can project that with a 185 km swath, such an array would be required to have

$$\frac{185 \times 10^3}{25}$$
 = 7.4 x 10<sup>3</sup> diodes

and would be  $7.4 \times 10^3 \times 25 \times 10^{-6} = 18.5$  cm in length. Mercury-Cadmium Telluride detector arrays with elements on 100-micron centers are currently available. Such arrays would function in the 10-12 micron region of the spectrum and could yield spatial resolutions of 100 meters with current technology.

Arrays of detectors function as "push-broom" scanners where the along-track motion is provided by orbital motion and the cross-track scan is accomplished by sequentially addressing the detectors in the array. Multiband coverage could be obtained by providing one detector array per band. The fast scan rates which are realizable with diode arrays will obviate the requirement to scan more than one line at a time.

Folded reflective optical systems are in universal use and will probably continue to be. Folded systems like the Dall-Kirkham are uniformly responsive to broad spectra because the incoming radiation does not pass through any material except the atmosphere. The optical surfaces are usually silvered and have high reflectivity over wide optical bands. Another feature of folded systems which makes

them attractive is their compact dimensions and resulting stiffness and ruggedness and ease of thermal compensation. The state of optical fabrication technology is such that the accuracy of curve generation achievable in these telescope designs does not represent a limiting factor in resolution. The primary mirror in the Landsat 1 and 2 MSS is 22.5 cm in diameter. Other instruments are planned with objectives up to one meter diameter.

### 5.7.1 GROUND PROCESSING

In a discussion of the demand on a data system, one must consider not only the capability of the sensor to generate streams of data at given bit rates but one must also consider the kind of job that the sensor together with its data system is being called upon to do. In the current programs involving Landsat type missions, the emphasis is upon vegetation analysis, timeliness of data, frequent coverage and precise data registration and overlay for analytical purposes. The applications of the data are in the area of:

- · Monitoring world-wide food productivity
- · Mapping agricultural land use
- · Monitoring rangelands
- · Surveying forest resources
- · Managing critical watersheds
- · Detecting land-use changes
- · Oil/Mineral exploration

If we assume that these applications are basic and that the needs placed upon data systems of the future will continue to be of the kind of need now planned to satisfy mission requirements, then we can depict a representative ground system. The system illustrated is not necessarily tied to any particular program but is written around the Thematic Mapper [4]. It incorporates basic features which are

REV. NO.: 2 REV. DATE:31 Jan 19 8

common to all multiband high-resolution imaging systems. A top-level functional diagram of a representative ground system is presented in Figure 5.7-8. The five major subsystems included are the Data Input Subsystem (DIS), the Central Data Processing Facility (CDPF), the Product Generation and Dissemination Facility (PGDF) the Data Management Subsystem (DMS), and the Agriculture Utilization Subsystem (AUS) Each of these subsystems is briefly described below.

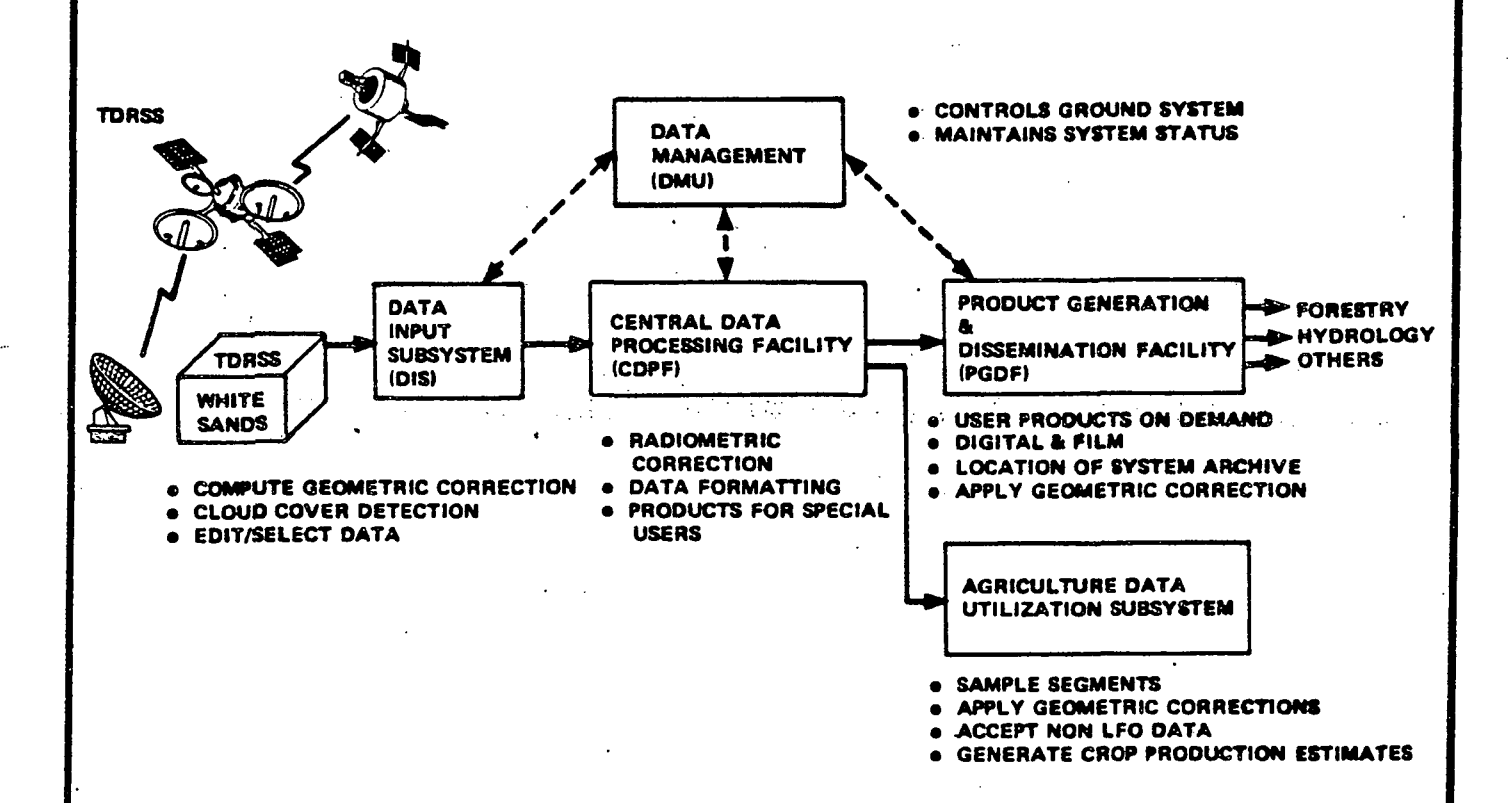


FIGURE 5.7-8 Ground System Functional Diagram

The Data Input Subsystem (DIS) receives data from the TDRSS via dedicated cable interconnection. In the early 1980's, these rates are expected to be of the order of 135 Mbps. Later, as resolution is improved, rates may go to 400 Mbps. The prime functions of the DIS are to record the raw input data, to perform cloud cover detec-

REV. NO.: 0 REV. DATE: 30 June 1977

tion and scene editing and to compute geometric correction matrices on a per swath basis.

The Central Data Processing Facility (CDPF) receives edited data from the DIS and performs standard operations to all data. These operations include radiometric correction and data reformatting to a band-interleaved-by-line (BIL) format.

The Product Generation and Dissemination Facility (PGDF) is the main interface between the ground system and general users. This facility provides imagery data, in either digital tape or film format, to users on demand. The data, which may be geometrically corrected to various map projection systems or enhanced as requested by the user, is available in a variety of sizes, formats, and media. The PGDF also houses and manages the system archive.

The Data Management Subsystem (DMS) provides the central point of control and data base management for the ground system. Its prime functions include management of user demand, the system archive, system communications and system redundancy. The DMS also maintains system status, production statistics, operations logs and administrative services.

The Agriculture Utilization Subsystem (AUS) receives data directly from the CDPF and performs those operations necessary to produce world crop production forecasts on a periodic basis. The operations to be performed include geometric correction, sample segment extraction, multispectral analysis and areal and statistical analyses. It is included here as part of the ground system because it represents the first major user.

Details of these major functions are delineated in the following paragraphs.

5.7.14

REV. NO.: 2 RE

### 5.7.2 DATA MANAGEMENT UNIT

The Data Management Unit provides the central point of control and data base management in the Data Processing Facility design. The Data Management Unit is interfaced to the Demand User Subsystem, Archive Management Subsystem, Communication Management Subsystem, Redundancy Management Subsystem and the Operations Control Center as shown in Figure 5.7-9. The DMS accepts user produce demand requests from the Demand User Subsystem, issues archive retrieval requests to the Archive Management Subsystem and generates processing schedules for the Product Generation and Dissemination Facility (PGDF). The DMS maintains the Data Processing Facility configuration table in its database and is updated by the Redundancy Management Unit in the event of any system anomaly. The Communication Management Subsystem offloads the DMS from the front-end communications handling functions associated with the DIS, CDPF, and PGDF. The Archive Management Subsystem which consists of the Multiple Archive Station Communication Units (ASCU's) allows the DMS to monitor the generation of all digital tape products and to identify and track the processing of the HDDTs, HDTs and CCTs throughout the system.

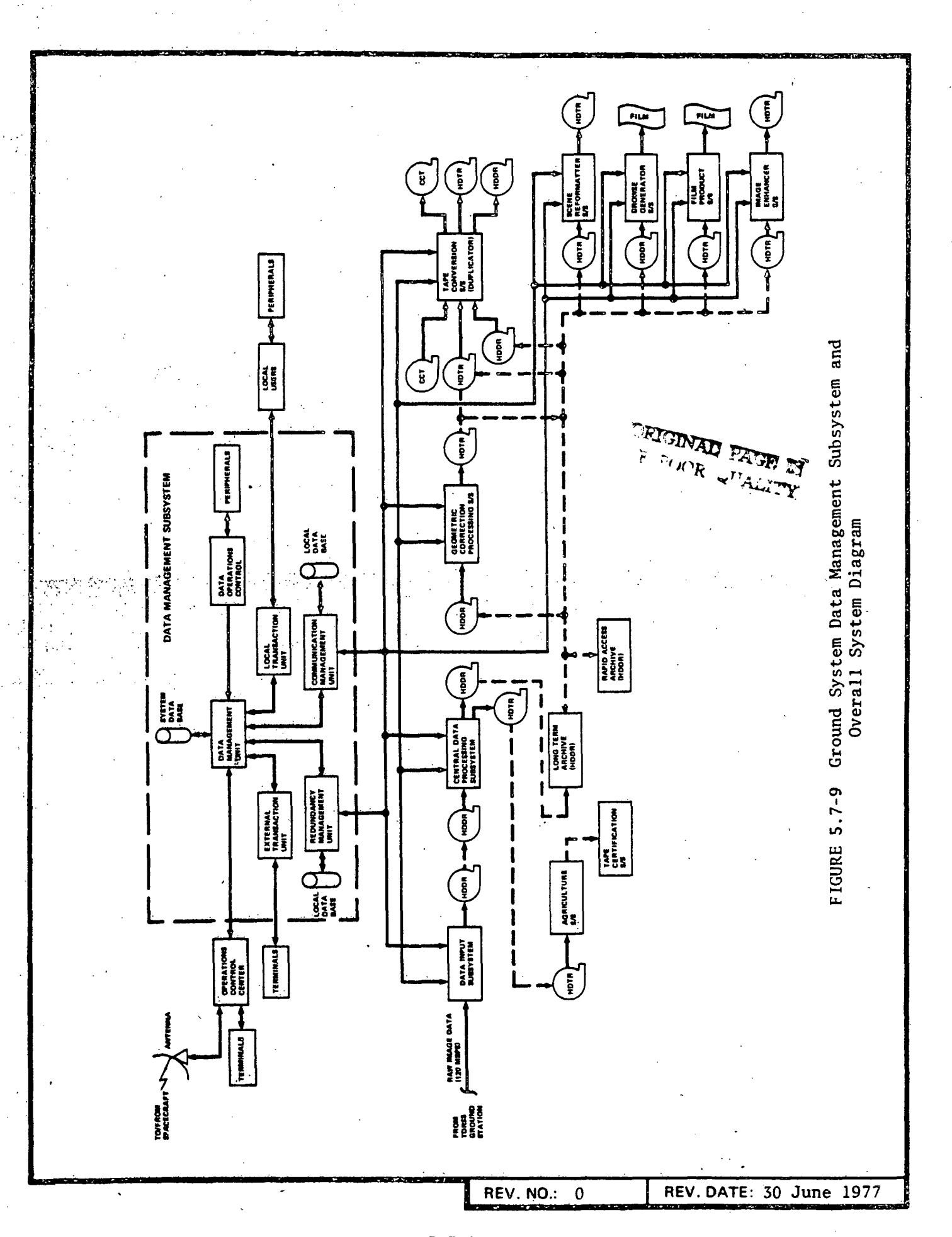
The DMS accepts predicted ephemeris data from the OCC and routes the data to the Swath Correlator Unit via the Communications Management Unit. The DMS receives Geometric Correction information and cloud cover statistics form the DIS on a periodic basis and generates the header information and editing schedules utilized in the CDPF. Radiometric correction coefficient tables are routed to the Radio-Metric Correction Control Interface Unit on a per scene basis via the Communications Management Unit.

The Data Management Unit also served as a general housekeeping, management and accounting facility within the ground system. It maintains system status and an up-to-date inventory of system spares. Production statistics and operations logs

2 | REV. DATE: 31 Jan 1978

REV. NO.:

5.7.15



are computed and maintained for the entire ground system and are available on a continuous basis to system operators. Finally, the Data Management Unit is used to assist in administrative services such as accounting, payroll, benefits, management reports, trend analysis, etc.

#### 5.7.3 DEMAND USER SUBSYSTEM

The Demand User Subsystem provides the primary interface from the DMS to the outside world. The Demand User Subsystem consists of the Local Transaction Unit and their associated peripherals and data links. The Local Transaction Unit and the External Transaction Unit both function as front-end processors or transaction concentrators which accept remote or local terminal inputs, then format and issue product or service requests to the DMS. The Local Transaction Unit supports a number of output devices utilized by the administrative services office to monitor the operation of the ground system.

### 5.7.4 ARCHIVE MANAGEMENT SUBSYSTEM

The Archive Management Subsystem provides the capability to monitor the generation of archive tapes, automatically identify and track each individual tape, request tape retrieval from the archive, and issue instructions to tape unit operators. The Archive Management Subsystem consists of a network of interrelated processors and functions within the ground system. The key elements include the Data Management Unit, Communication Management Unit, Archive Station Communication Units (ASCU) Tape Scheduler Unit, Tape Certification Subsystem and the tape archive. The DMS monitors the generation of tapes via the Tape Scheduler Unit and the Archive Station Communication Unit.

5.7.17

### 5.7.5 COMMUNICATION MANAGEMENT SUBSYSTEM

The Communication Management Subsystem is the front-end transaction processor in the ground system. It interfaces directly with the Data Management Unit, Redundancy Management Unit and all processing units in the DIS, CDPF, and PGDF including the Geometric Correction Subsystem, the Tape Duplication Subsystem, the Tape Reformatter Subsystem, the Browse Generator Subsystem, the Film Generation Subsystem and the Image Enhancement Subsystem. The Communication Management Unit provides command and data distribution functions in response to transfer requests from the DMS. All incoming interunit messages to the DMS are buffered, formatted and routed to the DMS for processing. Additional functions include down-line loading for the ground system, system safing in the event of Data Management Unit failure and alternate interunit routing of failure messages to the Redundancy Management Unit in the event of Redundency Management Unit link failures.

#### 5.7.6 REDUNDANCY MANAGEMENT UNIT

From a reliability standpoint, the most critical area in the ground system is the Data Input Subsystem (DIS), since the data stream from the TDRSS is continuous and uninterrupted. A failure of equipment here would result in data loss which cannot be made up.

In examining the DIS, it is seen that data flow from subsystem input to tape is straightforward from input, through patch panel, to the appropriate HDDR,\* and onto tape.

Status from the other subsystems is supplied to the Redundancy Management
Unit through the Communications Management Unit and the databus. Although no actual

5.7.18

REV. NO.: 2 | REV. DATE: 31 Jan 1978

<sup>\*</sup>There are two types of high data recorders, HDDR is used to refer to the 120 Mbps (42 track) recorder and HDTR is used to refer to the 20 Mbps (14 track) recorder.

switching of data results, the Redundancy Management Unit can direct the Communications Management Unit to halt a processing operation due to failures or equipment malfunctions which are detected.

### 5.7.7 THE DATA INPUT SUBSYSTEM (DIS)

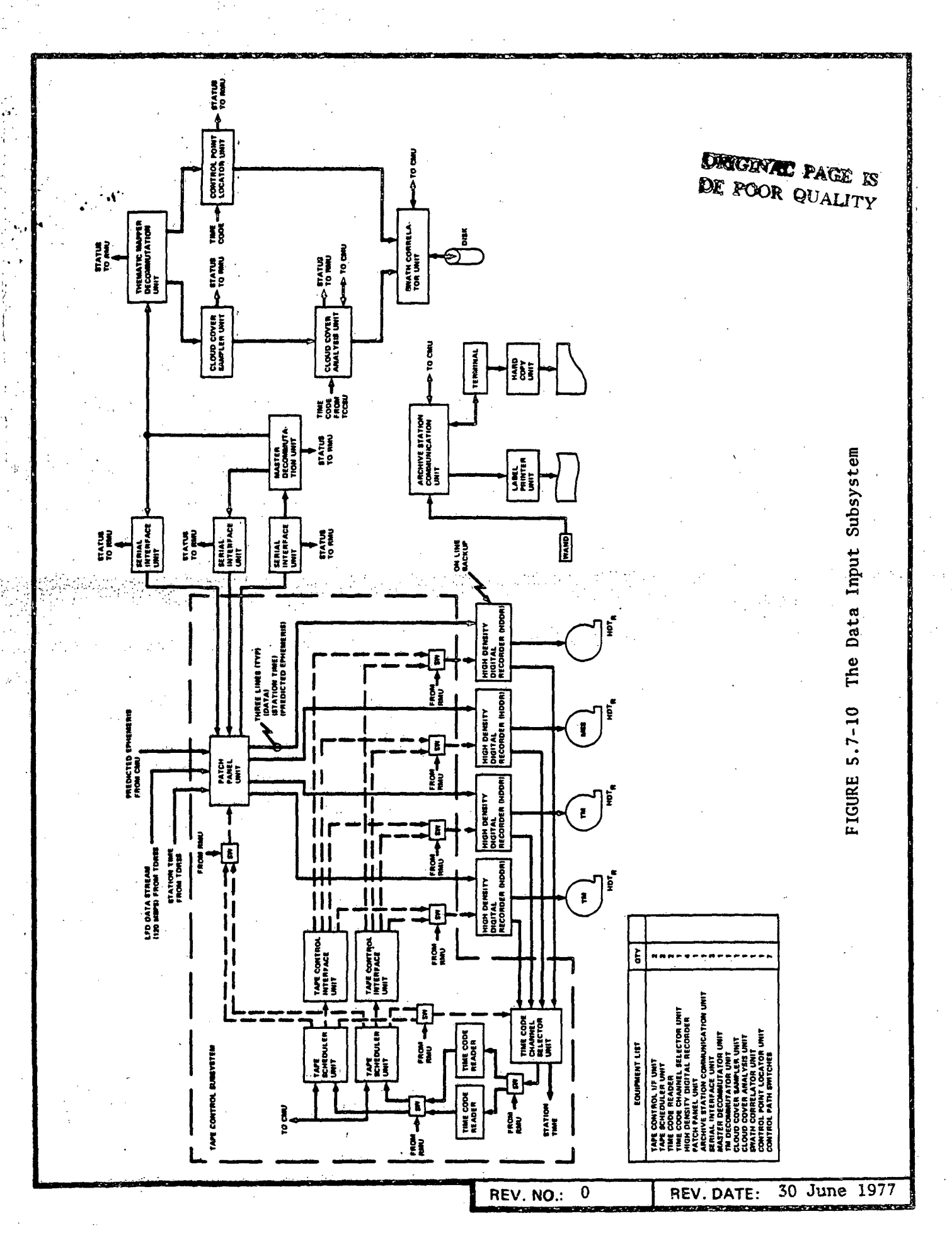
The Data Input Subsystem receives and records data from TDRSS, generates cloud cover statistics, locates control points, and provides information to the Communications Management Unit regarding status of input data. Figure 5.7-10, The Data Input Subsystem, is a block diagram of this subsystem.

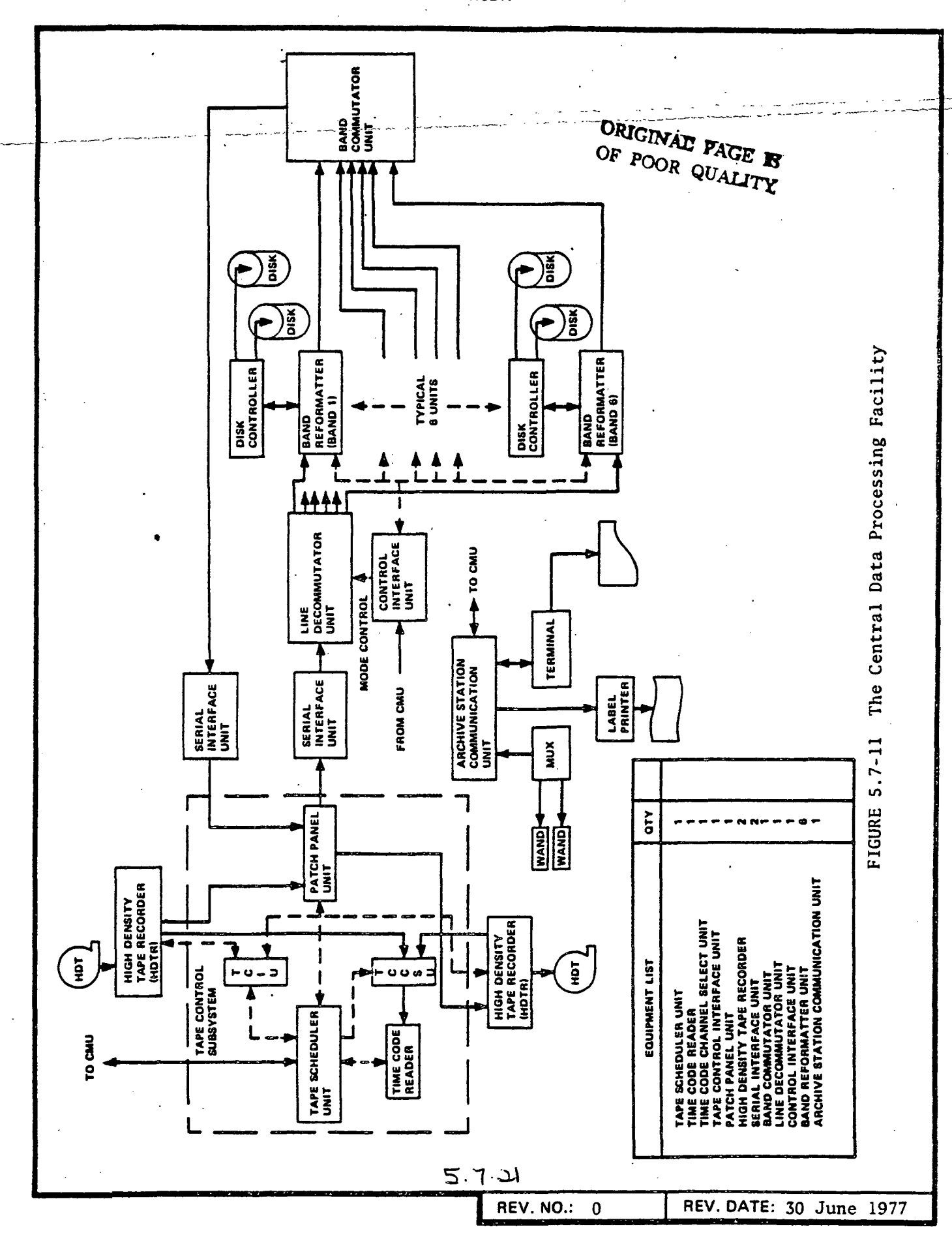
### 5.7.8 THE CENTRAL DATA PROCESSING FACILITY (CDPF)

The Central Data Processing Facility (CDPF) accepts input data on High Density Digital Tapes (HDDT), converts the serial bit stream to 8-bit types in a Serial Interface Unit (SIU) and performs data reformatting in the Lin Commutator Unit changing the data format from band-sequenced-by-detector to band-interleaved-by-line. This rearranged data is then processed in the Radiometric Corrector Unit which utilizes the standard radiometric correction algorithms developed by NASA.

The radiometrically corrected data then drives a Video Terminal Unit (VTU) for operator observation, and another SIU which converts the 8-bit back into a 12 Mbps data flow. These data are routed back through the Patch Panel Unit (PPU) to another High Density Digital Tape Recorder (HDDR).

Signal flow for the above can be observed in Figure 5.7-11, The Central Processing Data Facility. Other elements of the subsystem are relatively straightforward, operating at data rates of 15 Mbps. The radiometric correction is done in a "pipeline" fashion which eliminates the rather extensive system timing problem which would be formidable otherwise.





# 5.7.9 THE PRODUCT GENERATION AND DISSEMINATION FACILITY (PGDF)

## 5.7.9.1 GEOMETRIC CORRECTION SUBSYSTEM

The basic, working part of this subsystem is the Geometric Corrector Unit.

The balance of the units comprising the subsystem are simply interface devices with this unit.

Information flow through the Geometric Correction Subsystem begins with the input tape being played back on the High Density Recorder (HDDR) as shown in Figure 5.7-12. Data and time code information are input to the Tape Control Subsystem, providing commands to the Patch Panel Unit, the recorders and back to the Communication Management Unit. The serial data stream is converted to 8-bit bytes in the Serial Interface Unit and the data is then ready to enter the Geometric Correction Unit.

#### 5.7.9.2 TAPE DUPLICATION SUBSYSTEM

The Tape Duplication Subsystem, shown in Figure 5.7-13, accepts data input in HDDR or HDTR system tape media and converts it to suitable input to the Magnetic Tape Units for the Generation of Computer Compatible Tapes (CCT). The Tape Duplication Subsystem can also duplicate the original HDDR or HDTR input tape, or duplicate a CCT. Control of the subsystem comes from the Communication Management Unit and is based upon copy requests submitted from various users.

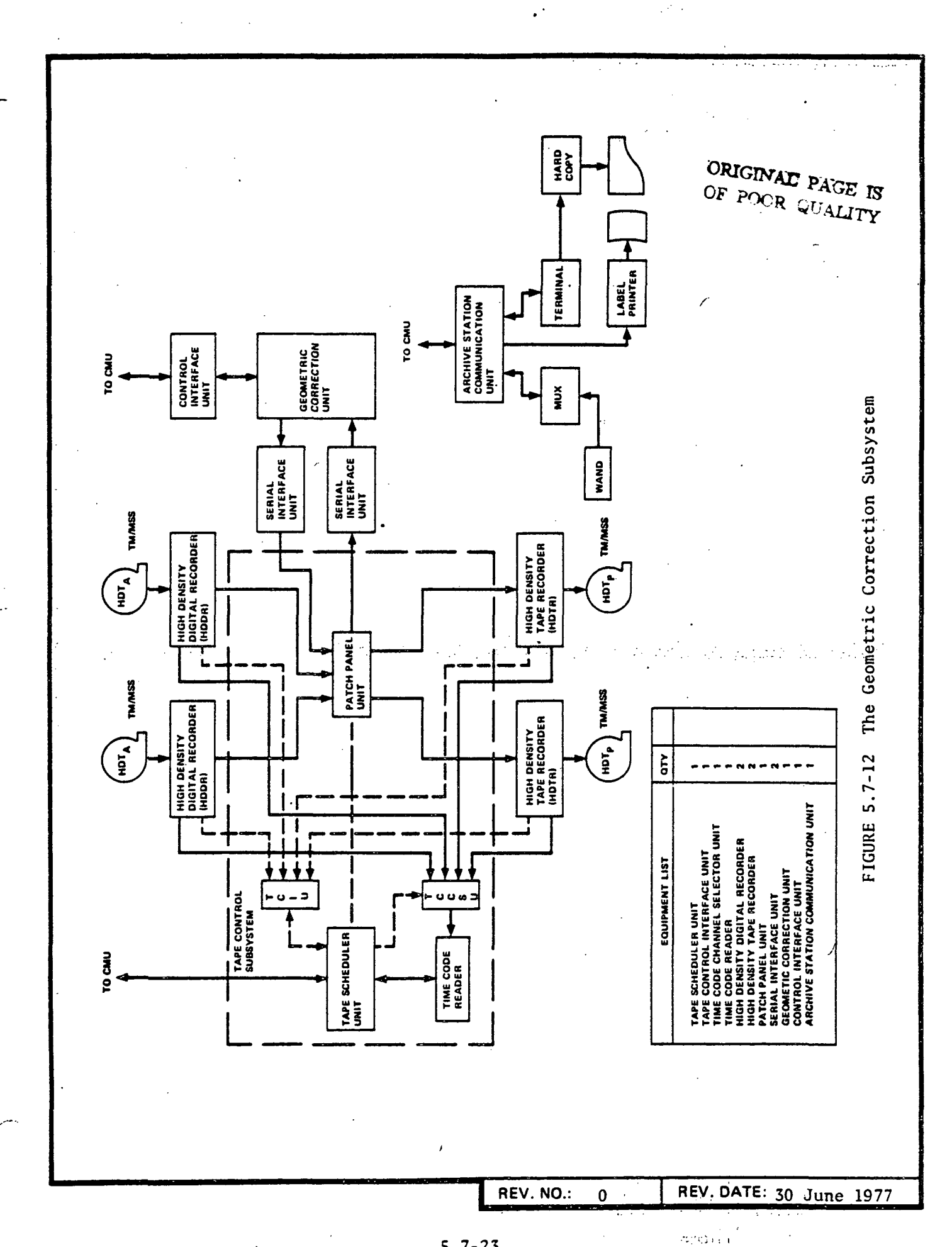
### 5.7.9.3 TAPE REFORMATTER SUBSYSTEM

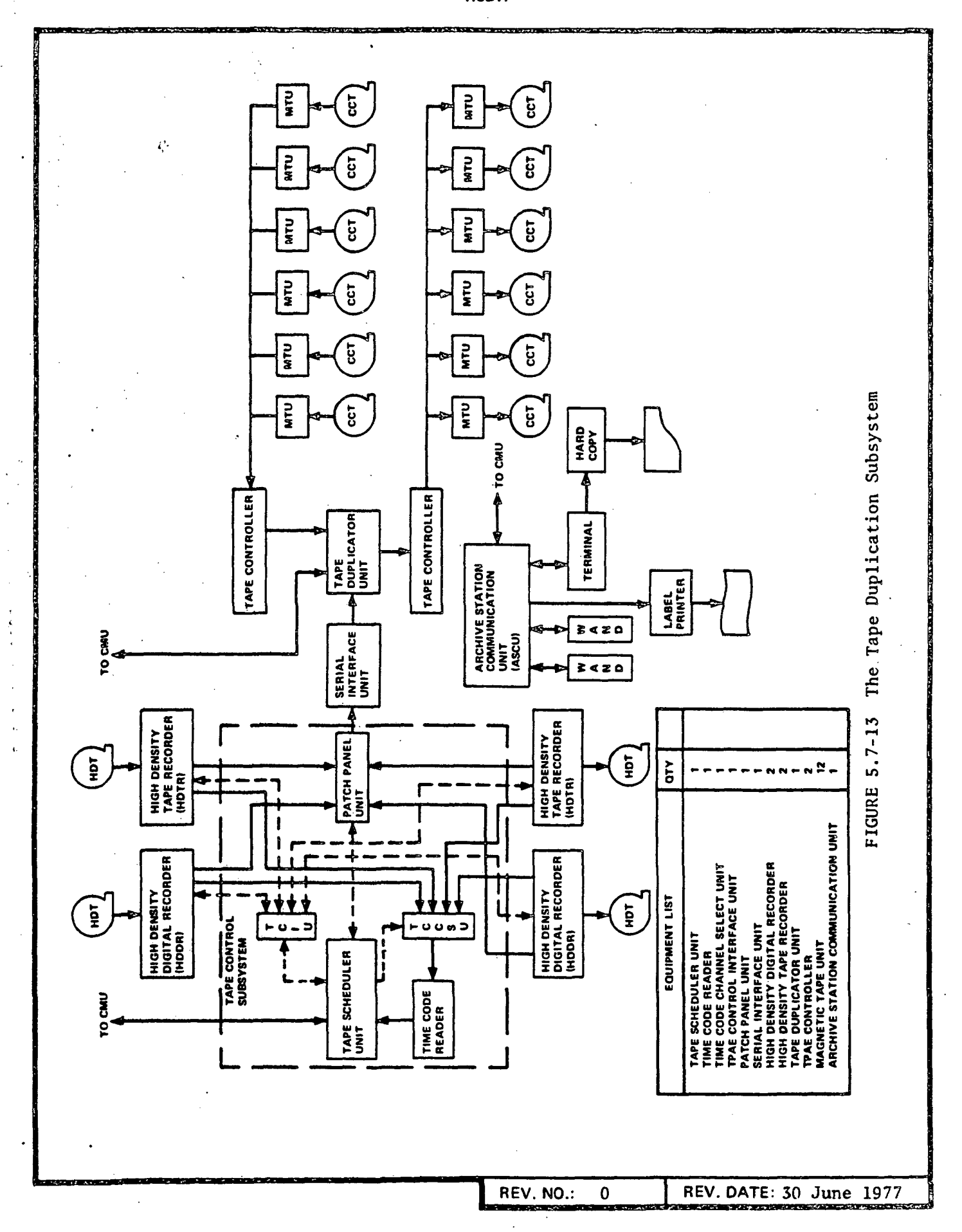
Data input and output from the Tape Reformatter Subsystem is controlled by the Tape Control Subsystem under instructions received from the Communication Management Unit, as shown in Figure 5.7-14.

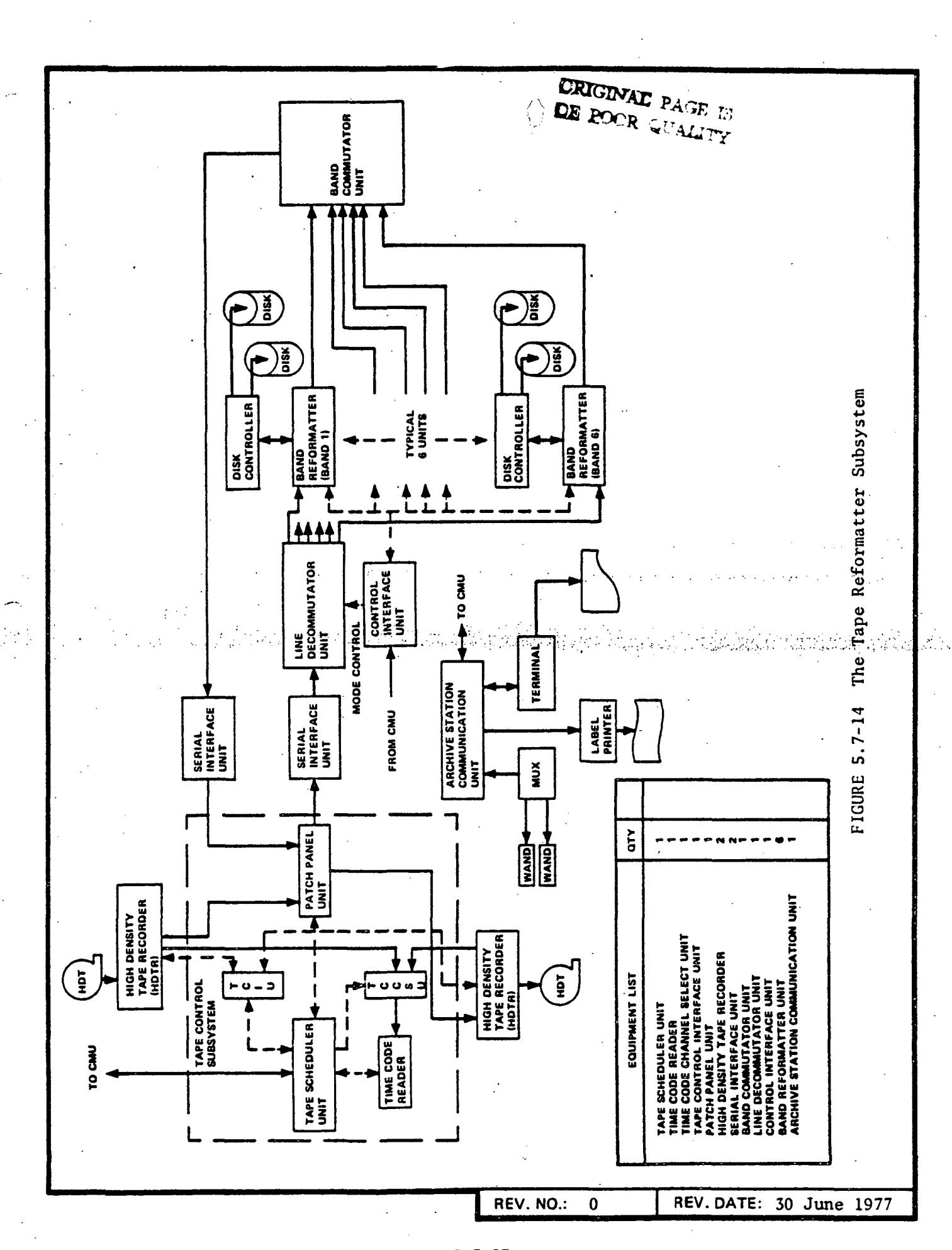
Input data after routing in the Tape Control Subsystem is processed by a Serial

Interface Unit and then fed into the Line Decommutator Unit. This unit separates

REV. NO.: 2







band interleaved data (interleaved line-by-line) to separate lines in each band. Each band output is then stored on disc, and output to the Band Commutator Unit in a band-sequential format. The Band Commutator Unit recommutates the data, which passes through another Serial Interface Unit, converting the data back into serial format. It then re-enters the Tape Control Subsystem and is recorded on an HDTR.

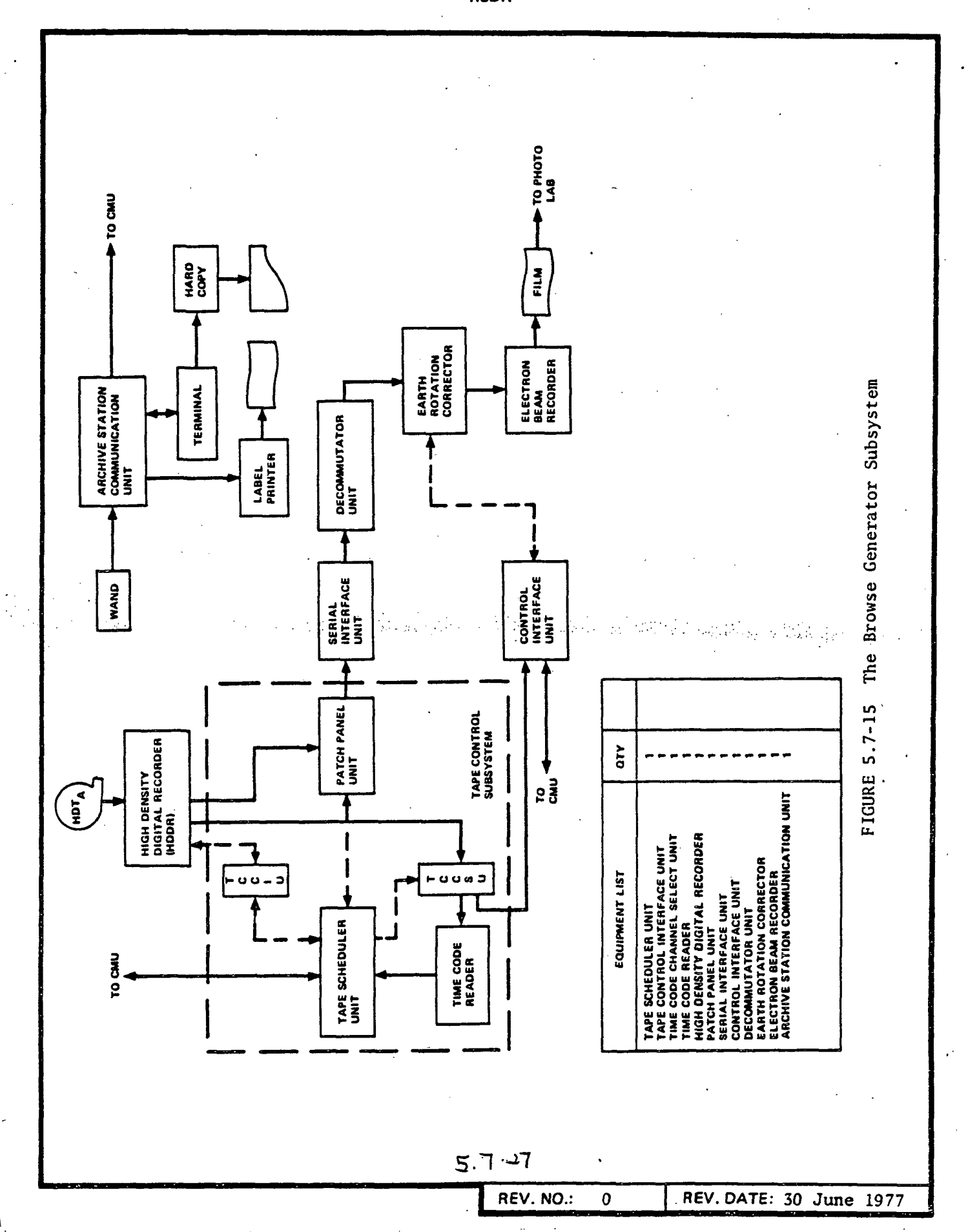
### 5.7.9.4 BROWSE GENERATOR SUBSYSTEM

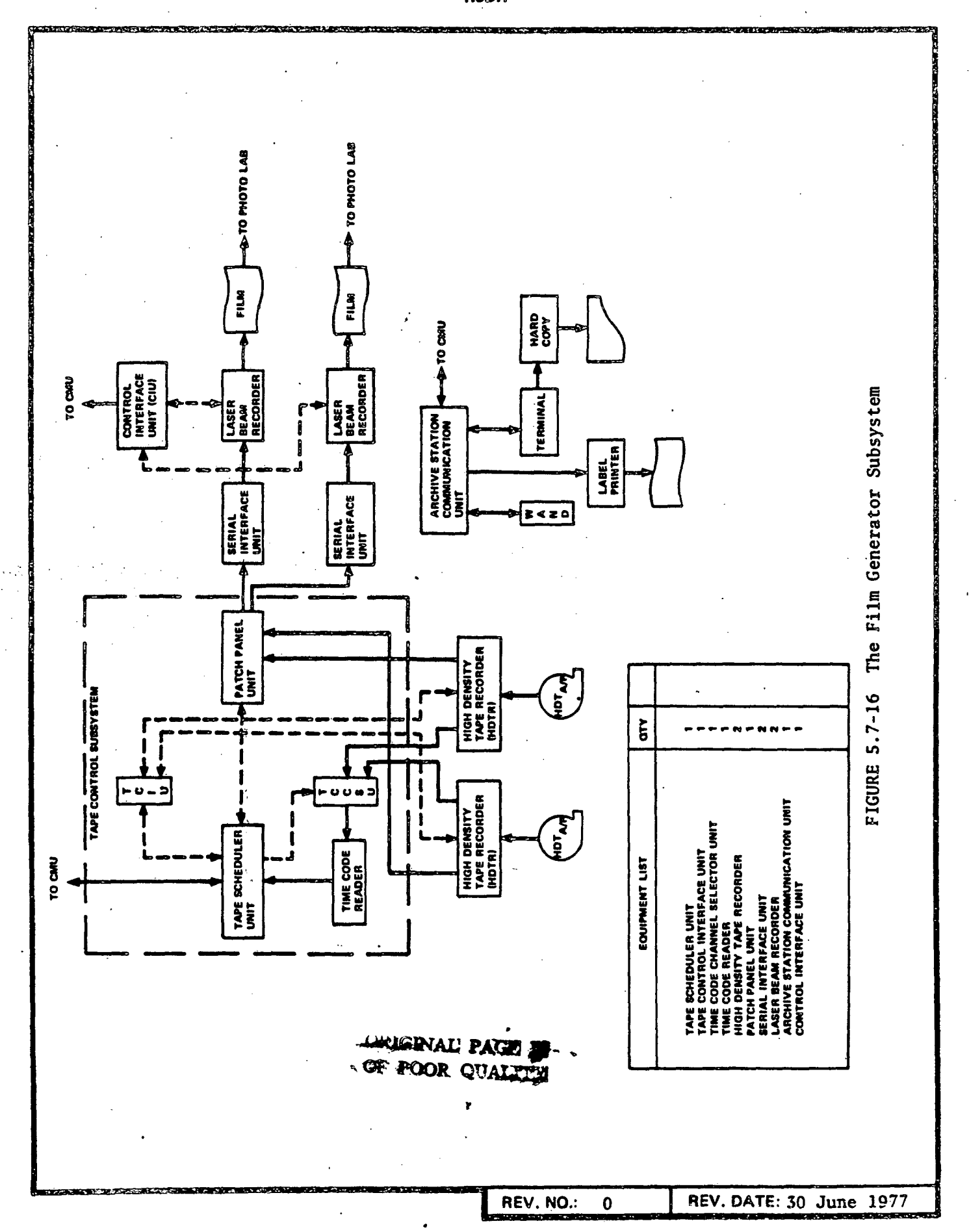
The Browse Generator Subsystem converts tape recorded data to photographic film images, corrected for each rotation effects and outputs them for scene quality assessment and generation of scene "shopping lists". Data input to Browse Generation Subsystem is through a Tape Control Subsystem which provides interactive/control from the Communications Management Unit as shown in Figure 5.7-15. Serial output data from the HDDR is routed through a Serial Interface Unit, where it is converted to 8-bit bytes, and through a decommutator in order to select pixels from the desired spectral band. Spacecraft location is provided by Communications Management Unit to a Central Interface Unit which establishes the amount of correction required for earth rotation. The data is then modified to correspond to this, and converted to latent film imagery by the Electron Beam Recorder.

### 5.7.9.5 THE FILM GENERATOR SUBSYSTEM

The Film Generator Subsystem accepts data tapes as input and processes them under Communications Management Unit control into latent image output (See Figure 5.7-16). Input data is routed through a Serial Interface Unit where it is converted into 8-bit bytes. This data provides the driving signal to a Laser Beam Recorder which produces high quality, high resolution latent imagery on photographic film. Annotation of the imagery with sensor, satellite, time and other information is also provided to the recorder.

REV. NO.: 2 REV. DATE: 31 Jan 1978





All operational commands to the Film Generator Subsystem originate in the Communications Management Unit and are started when the input tape reel label is read by the band input device in the Film Generator Subsystem's Archive Station Communication Unit.

### 5.7.9.6 THE IMAGE ENHANCER SUBSYSTEM

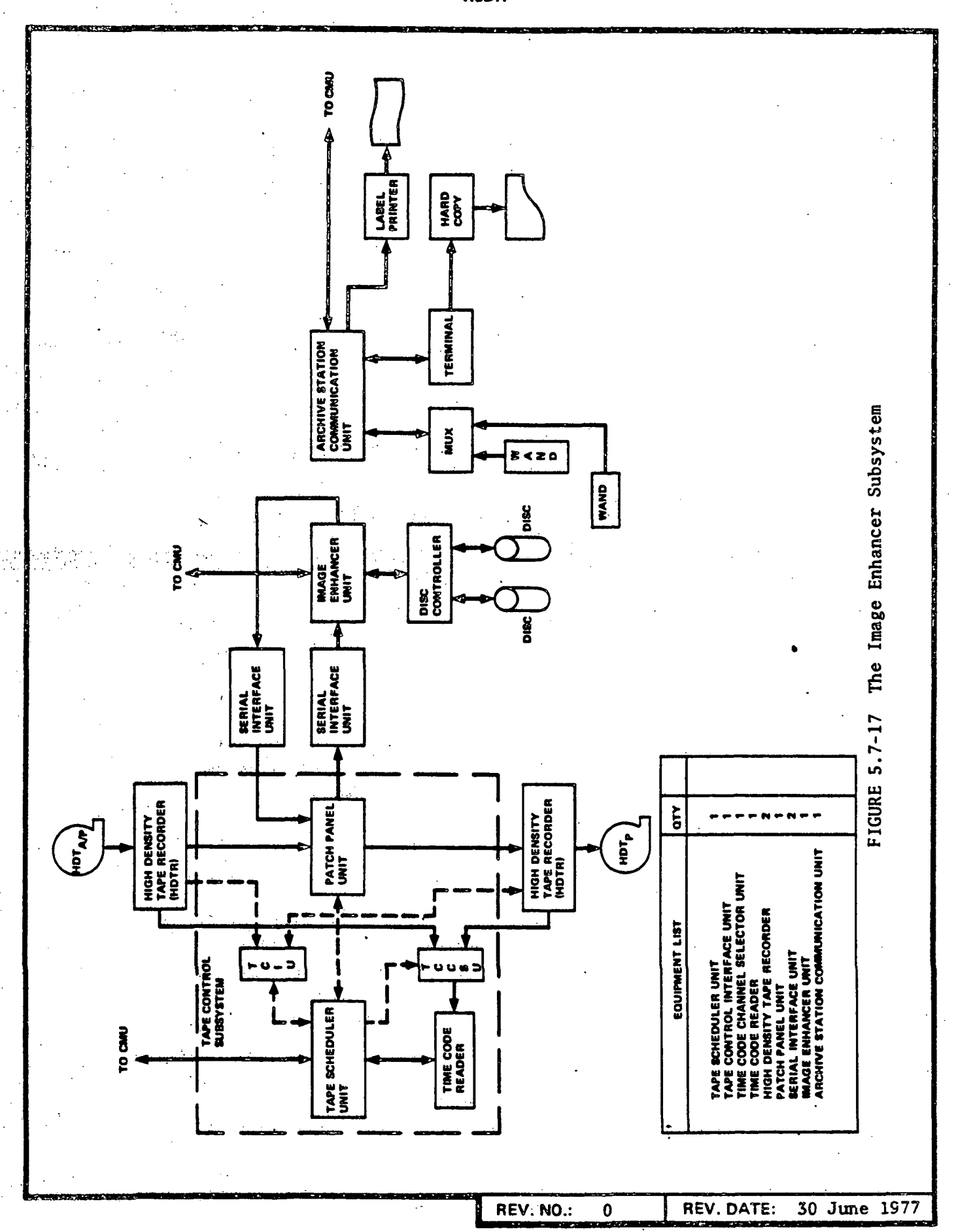
The Image Enhancer Subsystem provides the capability to perform image enhancements for non-standard image products. The subsystem is shown in Figure 5.7-17.

Typical of the class of enhancements are "gamma compensation," "level slicing" and digital filtering. Requests for special enhancement products are handled by the DMS in a manner similar to normal product requests, in that requests are received by the Data Management Unit from the Local Transaction Unit or the External Transaction Unit. The Data Management Unit then schedules the processing and issues a tape retrieval request to the archieve via the proper Archive Station Communication Unit. Once the archival input tape is mounted and registered, the Data Management Unit will issue a process request to the Image Evaluation Subsystem and monitor the status of the output tape product.

### 5.7.10 FUTURE SENSOR

The configurations of imaging spectroradiometers that have already flown, including such conspicuous examples as the four band MSS and virtually every radiometer designed for wavelengths shorter than 20 µm, has been some form of coaxial reflector, predominantly cassegrain, where the primary is concave and secondary in convex. Depending upon requirements, these take the form of Dall-Kirkham or Ritchey-Chretien designs. Nothing that is planned for flight during the eighties suggests any significant departure from this practice. The largest earth-oriented design being developed for use up to 1990 is the Large Earth Survey

REV. NO.: 2 REV. DATE: 31 Jan 1978



Telescope (LEST) which has a diameter of 1.5 meters. Beyond that, there are spaceoriented instruments that are up to 2.4 meters in diameter. The weights associated
with these two satellites are 3300 kg and 9500 kg, respectively, and one can see a
rough correlation between weight and mirror area in this one example. Due to
fabrication complexities induced by weight limitations, it is probably reasonable
to expect that we will not see earth-oriented optical systems appreciably larger
than 1.5 meters until the 90's.

Apertures as large as that on the Thematic Mapper (40 cm) have been objectspace scanned. That is, scanning is accomplished by an oscillating diagonal mirror interposed (at 45°) between the entrance aperture of the telescope and the object. There is a strict requirement for flatness of this mirror as it oscillates as well as for linearity of motion and low induced vibrations. The smaller dimension of the eleptical diagonal mirror is equal to the diameter of the primary mirror and the other axis is 1.414 times as large. The problems obviously magnify as the diameter of the primary increases. Considering the technology in other areas, it is probable that these large aperture telescopes will utilize something other than a mirror for scanning object space. One alternate method is pushbroom scanning which has the prerequisite that there be one detector for each pixel in a scan line. [9] These detector's IFOV's are "swept" through the image space electronically by sequentially addressing each detector in turn. This line of detectors is then caused to scan the object by spacecraft attitude control or by spacecraft orbital motion. Figure 5.7-18a illustrates the former while 5.7-18b illustrates the latter.

The diode arrays that will be used for these pushbroom scanners are in some cases monolythic arrays of many hundreds of diodes, each coupled to a common bus through a switch. These arrays are commonly referred to as Charge Coupled Devices (CCD) owing to the electronic technology associated with the switch. CCD detector

**REV. NO.:** 2

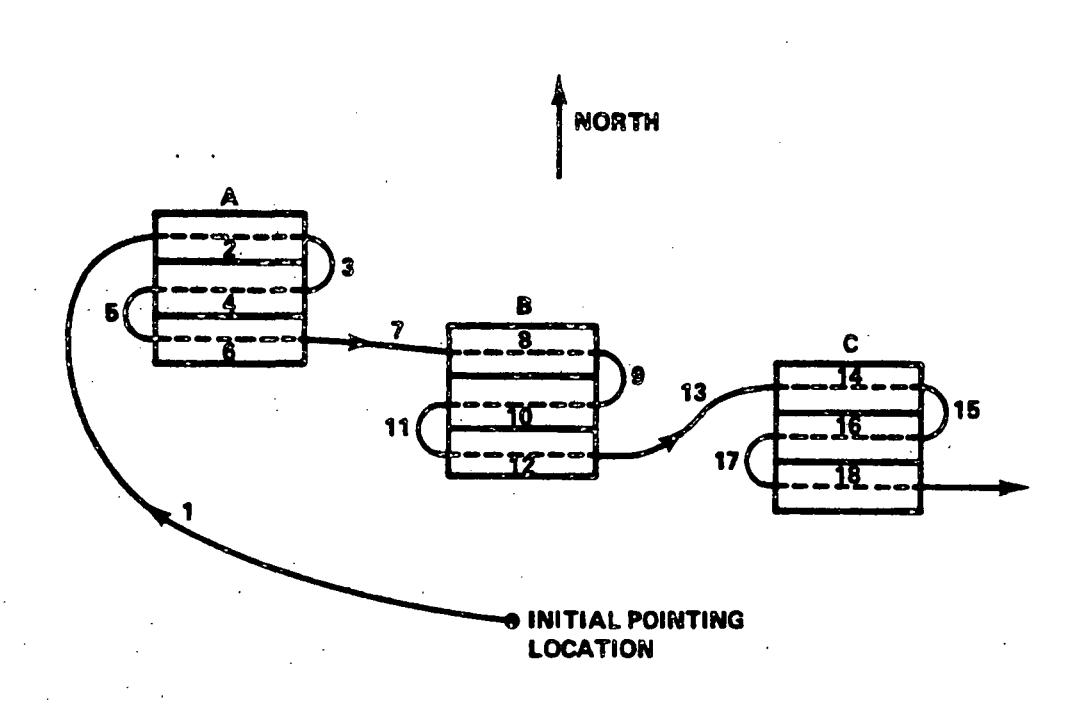


FIGURE 5.7-18a Example of Object Space Scan by Satellite Attitude Control

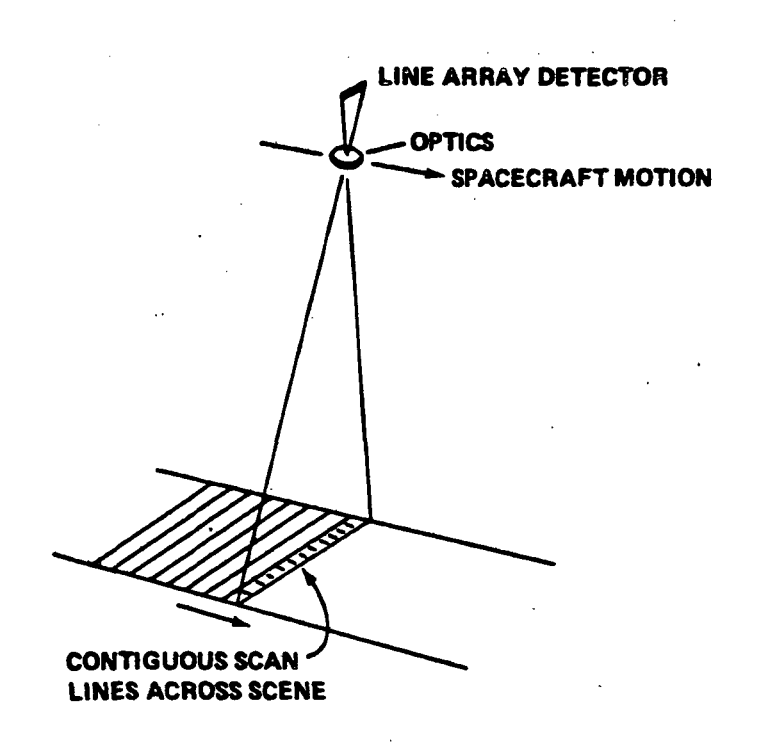


FIGURE 5.7-18b Example of Object Space Scan by Spacecraft Oribtal Motion

REV. NO.: 1 REV. DATE: 30 Sept 1977

arrays meeting 1980 requirements are essentially available for wavelength bands from 0.4 to 1.0 µm, but will not be available for bands above 1 µm for 2-3 years. Fairchild has made 1728 element monolithic silicon arrays using a buried channel structure and a distributed floating gate amplifier that are capable of NES values below 100 electrons. Monolithic CCD arrays for the infrared bands at wavelengths longer than 1 µm are not available at present for the configurations required for mid 1980 because monolithic structures fabricated in narrow bandgap semi-conductor material are not well developed. However, there is considerable work on hybrid arrays where discrete HgCdTe and PbSnTe elements are "hardwired" to a silicon CCD. Hughes-Santa Barbara is fabricating InSb arrays for the 1.0-5.5 µm region and has achieved near BLIP performance on a developmental 8-element array cooled to 77°K. Honeywell recently received a contract from GSFC to develop 9-element hybrid arrays using both photoconductive and photovoltaic HgCdTe detectors coupled to buried channel CCD registers. A tentative specification defining detector requirements was submitted to Honeywell to determine if hybrid IR-CCD detectors meeting SEOS-LEST requirements would be available in 2-3 years. Their conclusion based on current work at Honeywell and Hughes-Santa Barbara is that detectors better than these requirements would be available during the nineteen eighties.

Detector size available near term is 15 µm for Silicon and 30 µm for IR detectors. If primary mirror diameters stay under 1.5 meters and system speed is F5 or better, focal lengths of the order of 7 meters can be expected. With a geosynchronous altitude of 35,000 km, 15 µm detector size and 7 m focal length, the ground resolution that can be obtained is 75 meters. The same parameters applied to a telescope deployed in a Landsat-like orbit yields ground resolutions of 1.5 meters. We can say that a Landsat-like future orbiter carrying an advanced pushbroom scanner would have its resolution limited by political rather than technical factors.

REV. NO.:

Current and projected user needs are indicating requirements of up to twenty spectral bands. Only about half these bands would be required for any specific application of the data so that it may be possible to economize on downlink bandwidth requirements in this way. "Scene noise" or random variation of radiance values is larger than ±.5%. Therefore, it appears that for earth-oriented observations radiance quantitizations above the eight-bit level would be superfluous. With these limitations, data rates for any coverage desired can be calculated.

REV. NO.: 1 REV. DATE: 30 Sept 1977

### LIST OF ACTIVE CONTRIBUTORS

### Marvin E. Bauer

Program Leader

Crop Inventory Systems Research Laboratory for Applications of Remote Sensing Purdue University West Lafayette, Indiana 47906

317-749-3052

Ralph Bernstein

Senior Engineer, Manager of Advanced Image Processing Department IBM Corporation, Federal Systems Division, 18100 Frederick Pike Gaithersburg, Maryland 20760 301-840-6291

## Frederick C. Billingsley

Group Supervisor, Earth Resources Image Processing Jet Propulsion Laboratory 4800 Oak Grove Pasadena, California 91103

### Byron P. Blair

Professor

Crop Ecology, Agronomy Dept, and LARS
Purdue University, Lafayette, Indiana 47907
317-749-2052

### Peter A. Castruccio

President, Ecosystems International, Inc. P. O. Box 225
Gambrills, Maryland 21054
301-987-4974

# Charles F. Cheeseman, Jr.

Manager, Mission and Applications Program General Electric - Space Division, P. O. Box 8661 Valley Forge, Pennsylvania 19101 s15-962-4728

### William C. Draeger

Principal Applications Scientist - Agriculture Technicolor Graphic Services, Inc. South Dakota Operations - EROS Data Center Sioux Falls, South Dakota 57198 605-594-6511

#### Donald H. Ebert

Head of Systems Engineering Group Bendix Aerospace Systems Division

**REV. NO.:** 1 REV. DATE: 30 Sept 1977

3300 Plymouth Road Ann Arbor, Michigan 48107 313-665-7766

### Jon D. Erickson

Head, Information Systems and Analysis Department and Senior Research Engineer Environmental Research Institute of Michigan
P. O. Box 618
Aqn Arbor, Michigan 48107
313-483-0500

# Robert H. Haralick

Associate Professor of Electrical Engineering Remote Sensing Laboratory Space Technology Building University of Kansas Lawrence, Kansas 66045

### Roger M. Hoffer

Professor of Forestry, and Leader, Ecosystems Research Program, LARS Dept. of Forestry and Natural Resources
Purdue University
West Lafayette, Indiana 74906
317-749-2052

# Roger A. Holmes

Dean, College of Engineering University of South Carolina Columbia, South Carolina 29208 803-777-4177

### Warren A. Hovis Jr.

Associate Chief, Earth Observations Systems Division NASA, Goddard Space Flight Center, Code 940 Greenbelt, Maryland 20771 301-982-6465

## D. Alexander Koso

Director of Research and Engineering Honeywell Incorporated Radiation Center 2 Forbes Road Lexington, Massachusetts 02173 614-862-6222

## Norman P. Laverty Senior Staff Engineer

TRW Systems Group One Space Park Redondo Beach, California 90278 213-535-2036

**REV. NO.: 1** 

REV. DATE: 30 Sept 1977

Donald S. Lowe
Deputy Director
Infrared & Optics Division
Environmental Research Institute of Michigan
P. O. Box 618
Ann Arbor, Michigan
313-483-0500

Stanley A. Morain
Manager Remote Sensing Center
University of New Mexico
Albaquerque, New Mexico 87131
505-277-3622

James D. Nichols
Director
Remote Sensing Research Program
260 Space Sciences Laboratory
University of California
Berkeley, California 94721
415-642-2351

Virginia T. Norwood
Senior Scientist
Space and Communications Group
Hughes Aircraft Company
P. O. Box 92919
Los Angeles, California 90009
213-648-1666

Andrew E. Potter
Chief, Research, Test, and Evaluation Branch
Earth Observations Division, TF3
NASA Johnson Space Center
Houston, Texas 77058
713-483-2071

John W. Rouse, Jr.
Director, Remote Sensing Center
Professor, Department of Electrical Engineering
Texas A & M University
College Station, Texas 77843
713-845-5422

Vincent V. Salomonson
Branch Head
Hydrology and Oceanography Branch
Goddard Space Flight Center, NASA Code 913.0
Greenbelt, Maryland 20771
301-982-6481

**REV. NO.:** 1 REV. DATE: 30 Sept 1977

J. Ralph Shay
Assistant Dean of Research
Oregon State University
Corvallis, Oregon 97331
503-754-3451

David S. Simonett
Professor of Geography, University of California
Santa Barbara, California
805-961-2344

Bruce W. Steiner
Administration 1002
Bureau of Standards
B-312, Meteorology
Washington, D.C. 20234

Philip H. Swain

Program Leader for Data Processing & Analysis Research
Laboratory for Applications of Remote Sensing
Purdue University, 1220 Potter Drive
West Lafayette, Indiana 47906
317-749-2052

Frederick J. Thomson
Research Engineer
Environmental Research Institute of Michigan
P. O. Box 618
Ann Arbor, Michigan 48107
313-483-0500

Stephen G. Ungar
Space Scientist
NASA Goddard Institute for Space Studies
2880 Broadway
New York, N.Y. 10025
301-474-5603

Sam S. Viglione
Manager, Earth Information Sciences
McDonnell Douglas, Building 28
5301 Bolsa Avenue
Huntington Beach, California 92647
714-896-5165

Craig L. Wiegand
Soil Scientist and Technical Advisor
for Remote Sensing, USDA ARS
P. O. Box 267
Weslaco, Texas

REV. NO.: 1 REV. DATE:

William H. Wigton
Mathematical Statistician
United States Department of Agriculture
Statistical Reporting Service
Washington, D. C. 20250

REV. NO.: 1

**REV. DATE: 30 Sept 1977** 

## IMAGING SPECTRORADIOMETERS REFERENCES

- [1] Fundamentals of Optics, Jenkins and White, McGraw Hill Book Co., 1957, p. 51.
- [2] Ibid, p. 284.
- [3] See references 7, 8, 9, 11 and 12 in "Multispectral and Mapping Cameras" this handbook.
- [4] LANDSAT D Data Processing Facility Study (General Electric) N77-13495, November 22, 1976.
- [5] Brister, C. L., Central Processing and Analysis of Geostationary Satellite Data, March 1975.
- [6] Corbell, R. P., Callahan, C. J., Kotsch, C. J., The GOES/SMS Users Guide, November 1976.
- [7] Hussey, J. W., "The Geostationary Environmental Satellite System," <u>EASCON '74 Proceedings</u>, 1974.
- [8] Requirements Concept Design for Large Earth Survey Telescope for SEOS, Final Report, Goddard Space Flight Center, April 1975.
- [9] Proceedings of the Conference on Charge-Coupled Device Technology, NASA OAST & JPL, December 1976, JPL SP 43-40.
- [10] Advanced Scanners and Imaging Systems for Earth Observations, NASA SP-335, 1973.
- [11] Smith, S. R., (NASA) Applications Explorer Missions (AEM): Mission Planners Handbook (NASA TM-X-69906), May 1974.
- [12] The NIMBUS-G Sensor Systems: A Preliminary Description, GSFC-X-430-74-72 (Rev. 2), July 1976.
- [13] NIMBUS-G Sensor Interface Requirements (NASA-GE), September 1973.
- [14] Remote Sensing Instrument Performance Data Sheets, JPL-624-2, 1977.

#### IMAGING SPECTRORADIOMETERS

## Thematic Mapper BIBLIOGRAPHY

- (1) LANDSAT D Position Determination and Correction Study (General Electric) N77-13496, November 22, 1976.
- (2) LANDSAT D User Data Processing Study (General Electric) N77-13493, November 22, 1976.
- (3) LANDSAT D Data Transmission and Dissemination Study Final Report (General Electric) NASA-CR-144827, November 22, 1976.
- (4) LANDSAT D Local User Terminal Study Final Report (General Electric) N 77-15086, October 1976.
- (5) GSFC Specification Thematic Mapper System and Associated Test Equipment, GSFC No. S-726-9, May 1976.
- (6) GSFC Specification Thematic Mapper Interface Control Document, GSFC No. S-720-1, May 1976.
- (7) LANDSAT D Thematic Mapper Technical Working Group Final Report, NASA CR-147413, Lyndon B. Johnson Space Center JSC-09797.
- (8) Resource and Environmental Surveys from Space With the Tehmatic Mapper in the 1980's, National Academy of Sciences National Research N77-11508, October 1976.
- (9) Proceedings Conference on Charge-Coupled Device Technology and Applications, NASA (JPL) N77-17263 through N77-17290, December 1976.
- (10) Ground Data Handling for LANDSAT D. Goddard Space Flight Center, N77-13686, November 1976.
- (11) An Emperical Study of Scanner parameters LARS Information Note 110976, Laboratory for Applications of Remote Sensing, Purdue University, West Lafayette, Indiana, 1976, N77-13389.

## Very High Resolution Radiometer BIBLIOGRAPHY

- (1) Fortuna, J., Hombrick, L., The Operation of the NOAA Polar Satellite System, November 1974.
- (2) Remote Sensing Instruments Performance Data Sheets, JPL Document 624-2 (Draft).
- (3) Earth Observing Sensors, Systematics General Corporation, May 1976.

**REV. DATE:** 30 Sept 1977

1 .

## Visible/Infrared Spin-Scan Radiometer BIBLIOGRAPHY

- (1) Hummer, Robert F., "Earth Observation from Geostationary Orbit," In Proceedings of the Society of Photo-Optical Instrumentation Engineers, Vol. 62, Modern Utilization of Infrared Technology, August 1975.
- (2) Brister, C. L., Central Processing and Analysis of Geostationary Satellite Data, March 1975.
- (3) NOAA, The Federal Plan for Meteorological Services and Supporting Research: Fiscal Year 1977.
- (4) Corbell, R. P., Callahan, C. J., Kotsch, W. J., RADM, USN, <u>The GOES/SMS User's Guide</u>, November 1976.
- (5) Cook, A. K., "The 18 Minute Miracle," NOAA, January 1974.
- (6) Hussey, J. W., "The Geostationary Environmental Satellite System," EASCON '74 Proceedings, 1974.

REV. DATE: 30 Sept 1977

REV. NO.: 1

# IMAGING SPECTRORADIOMETERS ILLUSTRATION CREDITS

Figure No.	Page	Reference	Page
5.7-8 through 5.7-17	5.7-13 through 5.7-30	[21]	4-2 through 4-19
VISSR(Fig. 1)	7	[2]	3
VISSR(10)	14	[2]	15
VISSR(Fig. 3)	11	[4]	35
VISSR(12)	15	[7]	493
VISSR(Tb1.1)	17	[5]	138
5.7-18a	5.7-32	[8]	103
5.7-18b	5.7-32	[10]	312
HCMR (8)	5.7-70	[11]	5-9
HCMR (Fig. 1)	5.7-71	[11]	5-11
HCMR (12)	5.7-74	[11]	5-15
CZCS(Fig. 1)	5.7-79	[12]	11
CZCS(8)	5.7-80	[12]	6
CZCS(10)	5.7-81	[13]	1-3
AVHRR (8)	5.7-84	[14]	VIR-1-9-4

This page intentionally left blank.

REV. NO.: 1

**REV. DATE:** 30 Sept 1977

#### RSDH DATA SHEET

CHEET	1	ΩE	4	
SHEET	_	OF	•	

(1) SENSOR NAME, ACRONYM: LANDSAT-D Thematic Mapper - TM

(2) DISCIPLINE: Earth Observations

(3) SUBDISCIPLINE: La

Land Monitoring

#### (4) APPLICATION AND OBJECTIVE:

The EOS-A Thematic Mapper is a multispectral high resolution scanner capable of fulfilling the observational requirements of the EOS program, i.e., improved land use, water resources and food supply/distribution/management by imaging filtering and detecting reflected solar radiation from the surface of the earth in several spectral bands simultaneously through the same optical system.

#### (5) HERITAGE/KEY PERSONNEL:

LANDSAT MSS, Oscar Weinstein (GSFC), (301) 982-4108

#### (6) SENSOR DEPLOYMENT:

The observatory will complete 14 6/17 orbits per day in a circular, sun synchronous, near-polar orbit at an altitude of 705 km aboard a 3 axis stabilized spacecraft. The local solar time at the north-to-south equatorial crossing is to be  $\pm 30$  hrs.

(7)

#### SENSOR CHARACTERISTICS

## (7A) CAPABILITIES AND CONSTRAINTS OF THE SENSOR TO ACQUIRE THE MEASURED PARAMETER:

Area scanned is 185 Km swath width centered at nadir. Ground resolution element for the first five bands is 30 m and 120 m for band 6. Radiometric measurements of these elements are made to within 0.5% of F.S. radiance and quantitized to an 8-bit level. Line rate is TBD/sec. TBD lines are scanned simultaneously with scan efficiency of TBD. A low data rate mode ("night only") of 15 Mbps is available wherein band 6 only is utilized. Maximum data rate is 120 Mbps including overhead, telemetry and calibration information and including bits for a future seventh band of 30 m resolution. Dummy band 7 data is included in the data stream even before band seven is added.

(7B) ACTIVE SOURCE CHARACTERISTICS (FOR ACTIVE SENSORS):

ELTING PAGE BLANK NOT FINE

N/A

#### (7C) DETECTOR MEASUREMENTS CHARACTERISTICS:

Bands are defined as follows:

Units are micrometers: Band 1: .45-.52, Band 2: .52-.60, Band 3: .63-.69, Band 4: .76-.90, Band 5: 1.55-1.75, Band 6: 10.4-12.5. Square wave modulation response for Bands 1-5 is 35% for 30 m targets and for 120 m targets in Band 6.

Silicon diodes used as detectors in Bands 1-4. And mercury cadmium telluride detectors for Bands 5 and 6, cooled to the region of 100°K by radiative cooler.

5 7.45

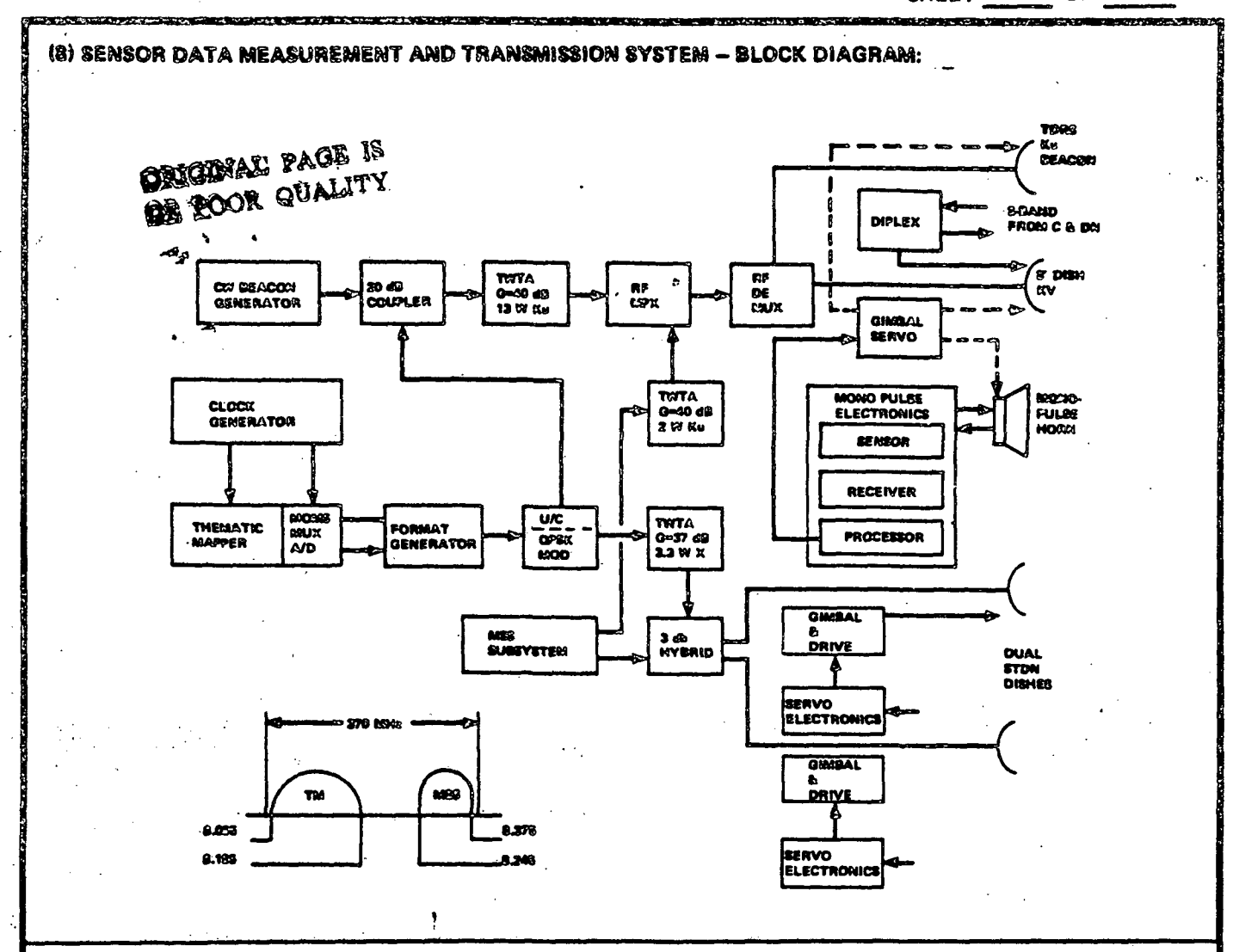
**SECTION NO.:** 

5.7

SENSOR CATEGORY: Imaging Spectroradiometers

Preceding page blank

REV. NO.:



#### (9) MEASUREMENT AND TRANSMISSION SYSTEM - NARRATIVE:

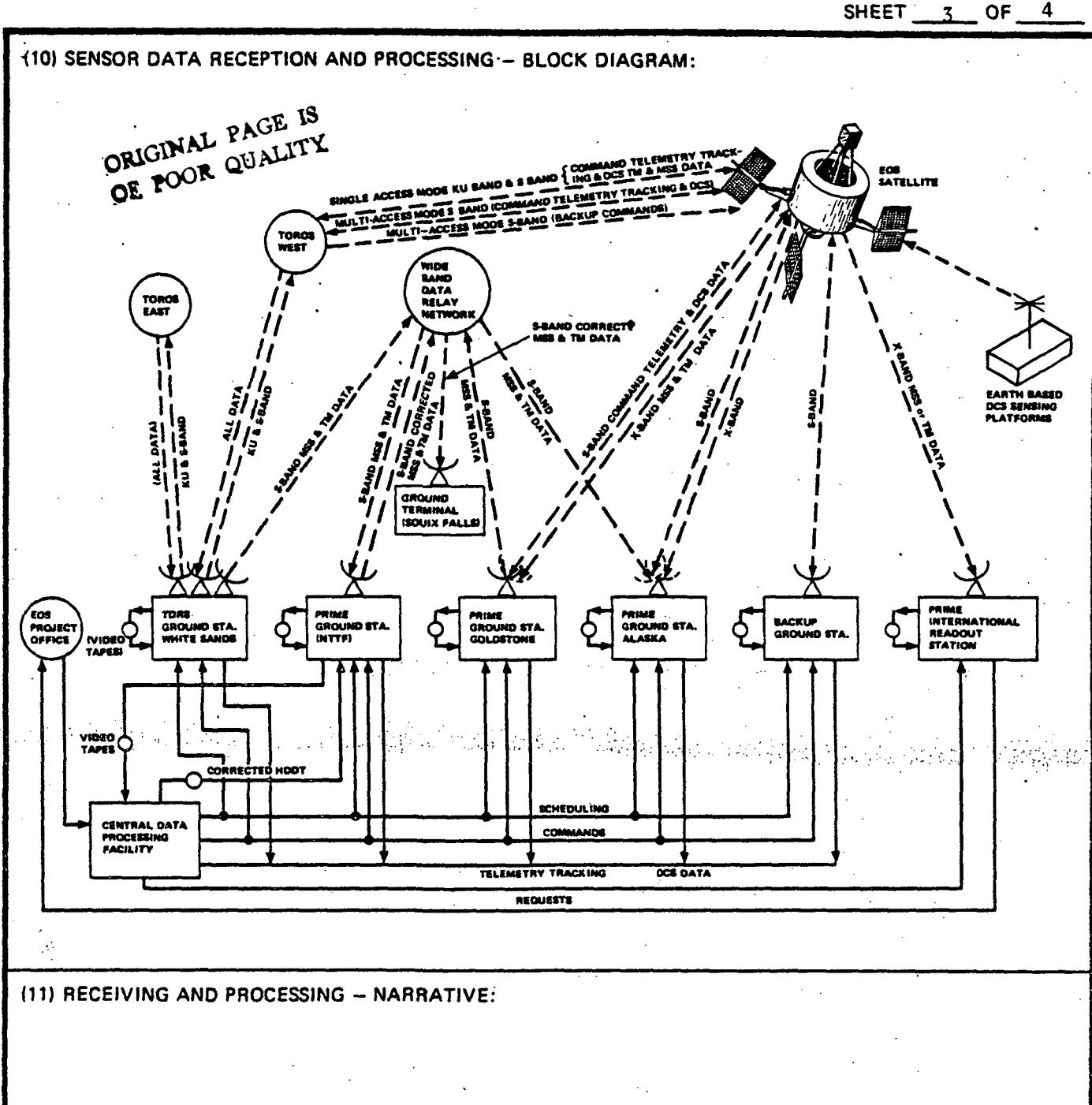
The EOSA Wideband Communication Subsystem accepts, processes and transmits data in real time from the TM and a MSS. Three independent spacecraft-to-ground RF links are provided. A link via TDRSS which gives extra-continental coverage and two identical STDN links for TM and MSS. Four antenna subsystems are employed. The TDRSS antenna provides an S-band T/R feed via the diplexer shown; a wideband transmit only feed at Ku coaxial with the S-band feed; a monopulse tracking horn with electronics for pointing the 8-foot furlable reflector and a broad beam CW beacon source.

SECTION NO.: 5.7 | SENSOR CATEGORY: Imaging Spectroradiometers

5.7.46

REV. NO .:

Z

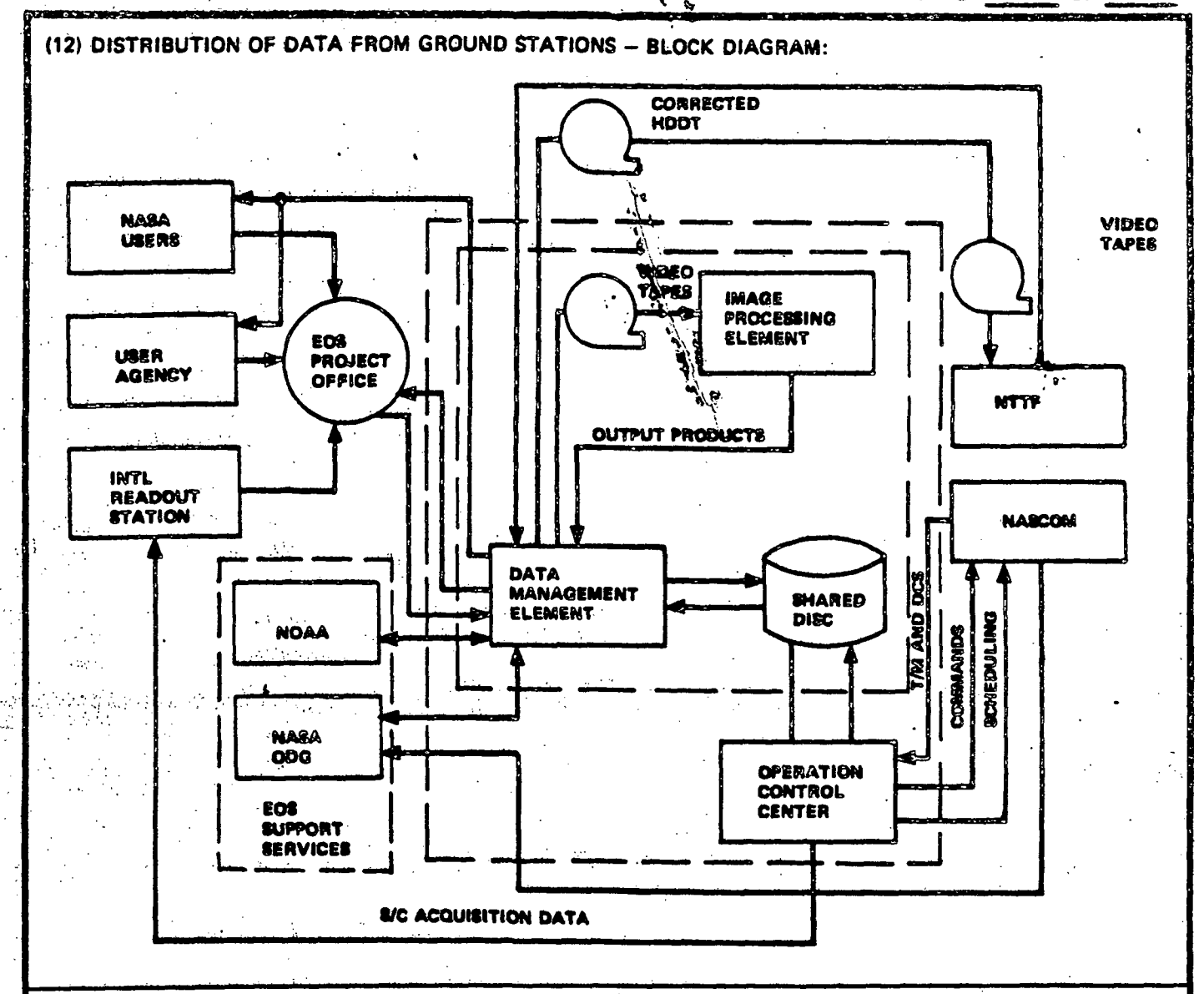


This section intentionally left blank.

5.7-47

SECTION NO .: 5.7 SENSOR CATEGORY: Imaging Spectroradiometers

> REV. DATE: 31 Jan 1978 REV. NO.:



## (13) DATA DISTRIBUTION - NARRATIVE: Data Operations within the CDPF:

- (a) provide geometric and radiometric correction,
- (b) convert all data to HDDT,
- (c) convert HDDT to imagery as required.
- (d) convert HDDT to CCT's as required,
- (e) annotate imagery with alphanumeric data per location code, grey scale image quality and cloud assessment,
- (f) provide extractive processing for selected themes,
- (g) generate one band of all imagery from each SEASOP for catalog purposes,
- (h) establish and maintain catalog of processed imagery.

Note: Radiometrically corrected tapes are geographically corrected by the CDPF using  $\frac{\sin x}{x}$  resampling to space oblique mercator projection. Tapes are also available with geographic correction data included but not applied.

SECTION NO.: 5.7 SENSOR CATEGORY: Imaging Spectroradiometers

5.7-48 REV. NO.: 2 REV. DATE: 31 Jan 1978

#### RSDH DATA SHEET

CIICCT	1	OE	13	
SHEET	-	()F		

(1) SENSOR NAME, ACRONYM: Visible-Infrared Spin-Scan Radiometer (VISSR)

(2) DISCIPLINE: Earth Observations (3) SUBDISCIPLINE: Atmospheric Monitoring

#### (4) APPLICATION AND OBJECTIVE:

The VISSR provides visible and IR images of the earth from geosynchronous orbit. Since the instrument is stationary relative to a point on the earth's surface, the instrument observes movement of weather across the earth.

(5) HERITAGE/KEY PERSONNEL: Advanced Technology Satellite (ATS) Multicolor Spin Scan Cloud Camera (MSSCC)

Instrument Rep.: Larry Rouzer (GSFC) (301) 982-6114 Ground Systems: Ed Bisone (GSFC) (301) 982-4581

#### (6) SENSOR DEPLOYMENT:

The VISSR is designed for geosynchronous orbit on a spin stabilized satellite (100 rpm) (SMS and GOES). Instruments are currently in operation on SMS-2, GOES-1. Launches are planned in June, 1977 (GOES-2) and January, 1978 (GOES-3). Attitude is maintained to within .1° with a stability of .5 arc sec. maximum.

(7) SENSOR CHARACTERISTICS

(7A) CAPABILITIES AND CONSTRAINTS OF THE SENSOR TO ACQUIRE THE MEASURED PARAMETER:
The Spin of the satellite provides on W-E scan of the earth. On each scan, 8-scan
lines of visible data and 1-scan line of IR data are collected. Following each scan,
the field of view is stepped to the next southerly adjacent set of scan lines. The
full earth disk or any portion may be scanned as directed by ground command. 19.93
minutes is required for full scan and scan return. Each visible channel has an IFOV
of .021 x .025 mrad. (.9 km at satellite subpoint) and the IR has a IFOV of .192 mrad
(8 km). There is a 20% underlap in the FOV of the adjacent visible scans. Scan limits
are ±10° of the subpoint, 1821 latitude steps are required for a full earth scan.

(7B) ACTIVE SOURCE CHARACTERISTICS (FOR ACTIVE SENSORS):

N/A

(7C) DETECTOR MEASUREMENTS CHARACTERISTICS: The visible channel detector consists of eight S-20 photo multiplier tubes (PMT) arranged in a linear array, and sensitive to radiation on the .55 to .75 micron range. Each PMT is .025 x .021 milliradians. The dynamic range is 3-80% Albedo. Calibration is by direct solar illumination via prisms designed to provide 50% Albedo. Signal bandwidth is 210 kHz.

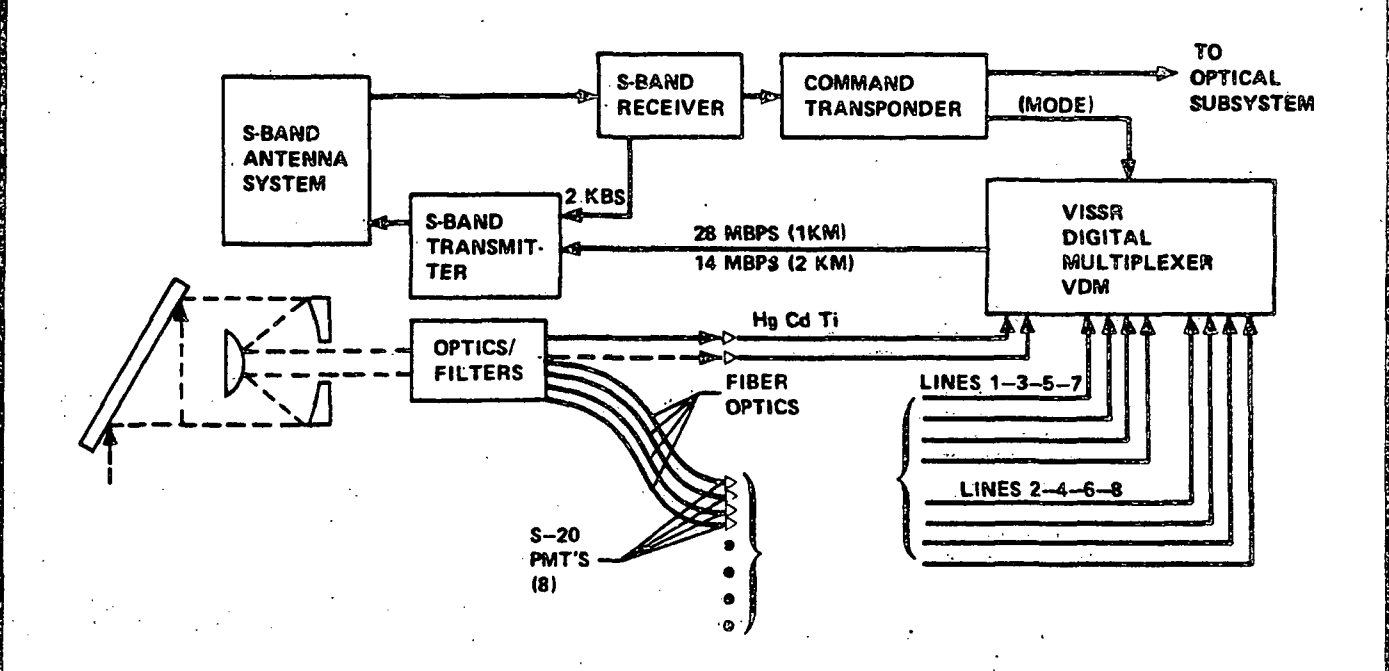
The IR detectors (2) are HgCdTe, cooled to  $95^{\circ}$ K. The noise equivalence radiance is  $1 \times 10^{-5}$  watt cm<sup>-2</sup> sterad. Each detector is 192 radians x 192 radians and measures thermal radiance with 10.5 to 12.6 micron range. Lenses send the same IFOV to both detectors simultaneously.

SECTION NO.: 5.7 | SENSOR CATEGORY: Imaging Spectroradiometers

REV. DATE: 31 Jan 1978

REV. NO.: 2

## (8) Sensor data measurement and transmission system — block diagram:



## (9) MEASUREMENT AND TRANSMISSION SYSTEM - NARRATIVE:

The Ritchey-Chretien Telescope (Aperture = 16 inch, focal length = 114.7 inch) focuses the visible radiance onto 8 filter optical cords that are incident upon the 8 PMT detectors. The .06 x .06 mm dimensions of the fiber form the visible band field stops. The IR bands are filtered and routed by lenses to each of the HgCdTe detectors. The video analog output of all detectors is routed to the VISSR Digital Multiplexer (VDM). The VDM sequentially samples the inputs, sampling each visible line every 2 microseconds and each IR line every 8 microseconds. The samples are multiplexed and converted to digital values, 6 bits for each visible band value and 8 bits for each IR value.

The VDM operates in either of two modes, as commanded by the ground station. Mode 1 multiplexes all eight visible line outputs into the output stream. Mode 2 averages adjacent visible lines before converting to digital values and reduces the data rate to 14 Mbps from the 28 Mbps of Mode 1. Track and hold logic within the VDM holds the signal level of a sample constant while it is converted to digital format. The values are merged with a scan line identifier, sun pulse data (calibration) and synchronization data for each scan line. The formatted (continued on next page)

SECTION NO.: 5.7

SENSOR CATEGORY:

Imaging Spectroradiometers

5.750

REV. NO.:

#### (9) continued

output for Mode 1 is shown in Figure 1 (below). All data is immediately transmitted to ground, there is no buffering nor on board recording. The data is collected, processed as just described and transmitted to ground during the time that the earth is in view  $(\pm 10^{\circ})$  of the subpoint) which is about 5% of each scan.

Commands from the ground can select the mode 1 or 2, focus the optical system, select the scan volume to be viewed. The starting of each scan frame requires a command from the ground.

16 bits 12 bits 8 bits 20 bits

FIGURE 1: VISSR Data Output Sequence [2]

SECTION NO.: 5.7 SENSOR CATEGORY: Imaging Spectroradiometers

 $(IR_1)$   $(VIS_1)$  - - -  $(VIS_8)$ 

--- Word 5 ----

. etc. to Word 3822

#### RSDH DATA SHEET

SHEET	4	OF	13
-------	---	----	----

(10) SENSOR DATA RECEPTION AND PROCESSING - BLOCK DIAGRAM:

See Block Diagram on Sheet 10.

## (11) RECEIVING AND PROCESSING - NARRATIVE:

The Wallops Island Command Data Acquisition Station receives the 28 Mbps or 14 Mbps data stream transmitted by the satellite. The signal is transformed into machine readable bits by a four phase Demodulator/Demultiplexer and transferred to the Synchronizer-Data Buffer (S/DB). Within the S/DB, the IR and visible data are separated. The visible data is calibrated to adjust for the bias, etc., of each detector, sampled and placed in an output buffer. The output data can be sampled at equal time intervals or equal angle intervals. Three interpolation methods are provided to maintain the selected resolution regardless of the sampling method chosen. Similarly, special purpose hardware samples and interpolates the IR data. A GTE TEMPO computer adjusts each IR response for individual detector characteristics and uses a lookup table to convert the raw data to temperature. Corrections are inserted for spacial alignment of sensors and satellite spin rate flunctuations.

(continued on next page)

SECTION NO.: 5.7

41.5

SENSOR CATEGORY:

Imaging Spectroradiometers

REV. NO.: 2

#### (11) continued.

The data is entered into an output buffer along with auxiliary information giving spacecraft status and housekeeping data. The added information includes an Earth locator gridding for IR data. The gridding is a 9th bit that indicates whether a contrasting spot (boundry) is to be set in this location.

The data resolution can be changed as commanded. The available resolutions are:

Visible Data

.9 km (Mode A)

1.9 km (Mode B)

3.7 km (Mode C)

IR Data

8 x 4 km (Normally Chosen)

8 x 8 km (Mode D and NESS Find

Line)

The 8 x 4 IR data is output in all modes, including D. The two IR channels can be averaged or individually selected. The IR data is formatted by special computers and sent to the Satellite Field Service Sites (SFSS) and to the Central Data Distribution Facility (CDDF).

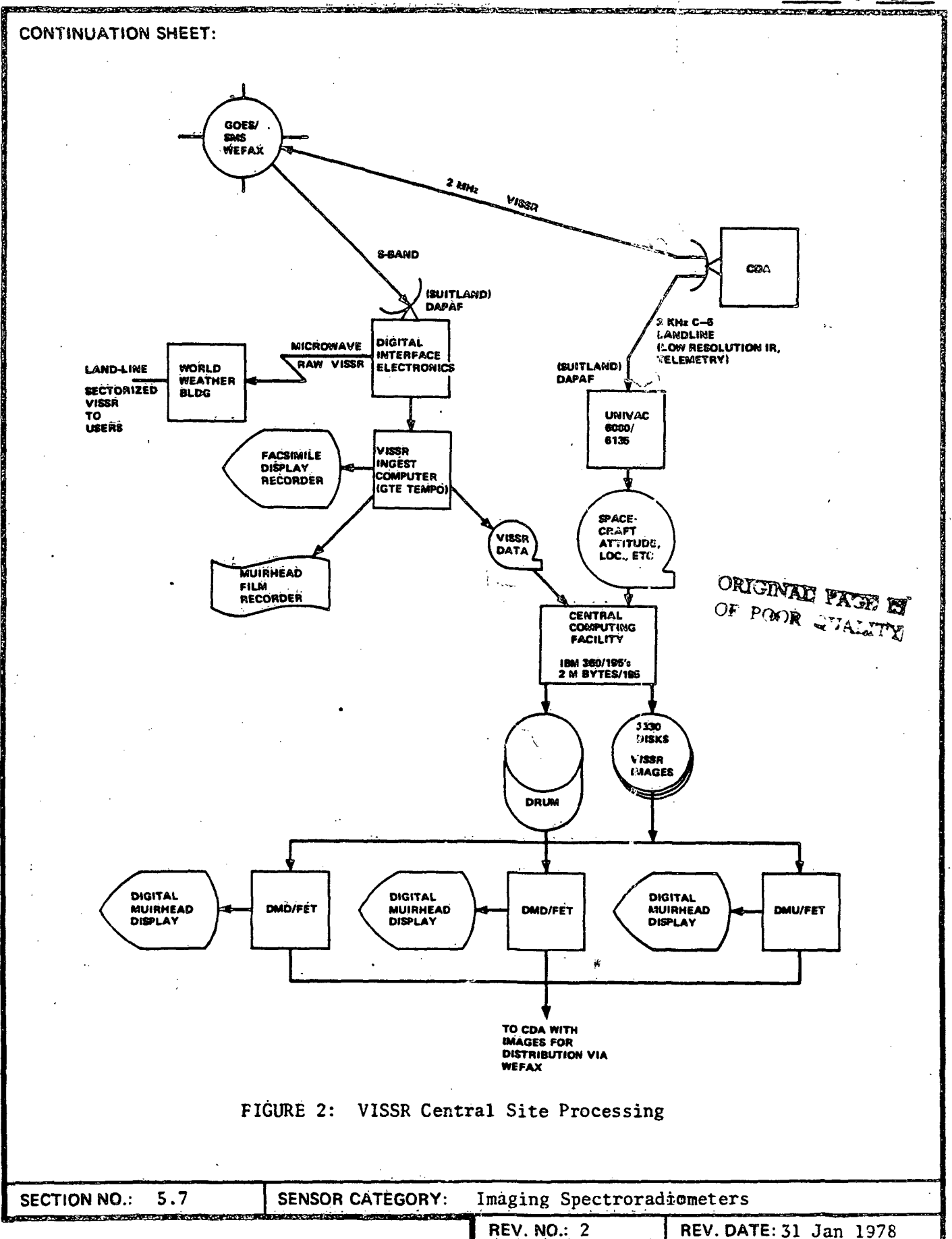
The CDA retransmits the processed data at 2 MHz, to the NESS facility at Suitland (Figure 2) via the satellite. The NESS facility relays the data via microwave to the Central Data Distribution Facility (CDDF) in the World Weather Building (WWB) at Marlow Heights, MD. In normal operation, the WWB receives a full disk image every 30 minutes over the microwave link and sectorizes, enhances (if requested) and transmits the images to the Satellite Field Service Sites. Each of 18 spectral purpose digital electronic units called Sectorizers extract, from the received, high resolution, "full disc" images, two data sections of specified geographical areas (sectors) at resolutions of .9, 1.9 or 3.7 km (See Figure 3). In normal operation, seven of the .9 km sectors or 4 of the 1.9 km sectors cover the continuous 48 states. A 3.7 km resolution sector covers the Western U.S., Alaska & Eastern Pacific. These sectors plus one sector covering Puerto Rico are generated every 30 minutes, unless the satellite is commanded to a special scan mode to monitor severe weather in a given area. Each sector includes grid information inserted at the CDA. The sectorizers require about 9 minutes to receive the data and then 17 minutes to process and transmit it. This time span is within the 30 minute spacecraft imaging interval. Numerous sectorizes are located at the CDDF and are controlled from a central console and automated Both visible and the equivalent IR data may be sectorized. full disk IR provided to the SFSS;s from the CDA's bypasses the sectorizers.) IR data is normally used when visible data is not available (night).

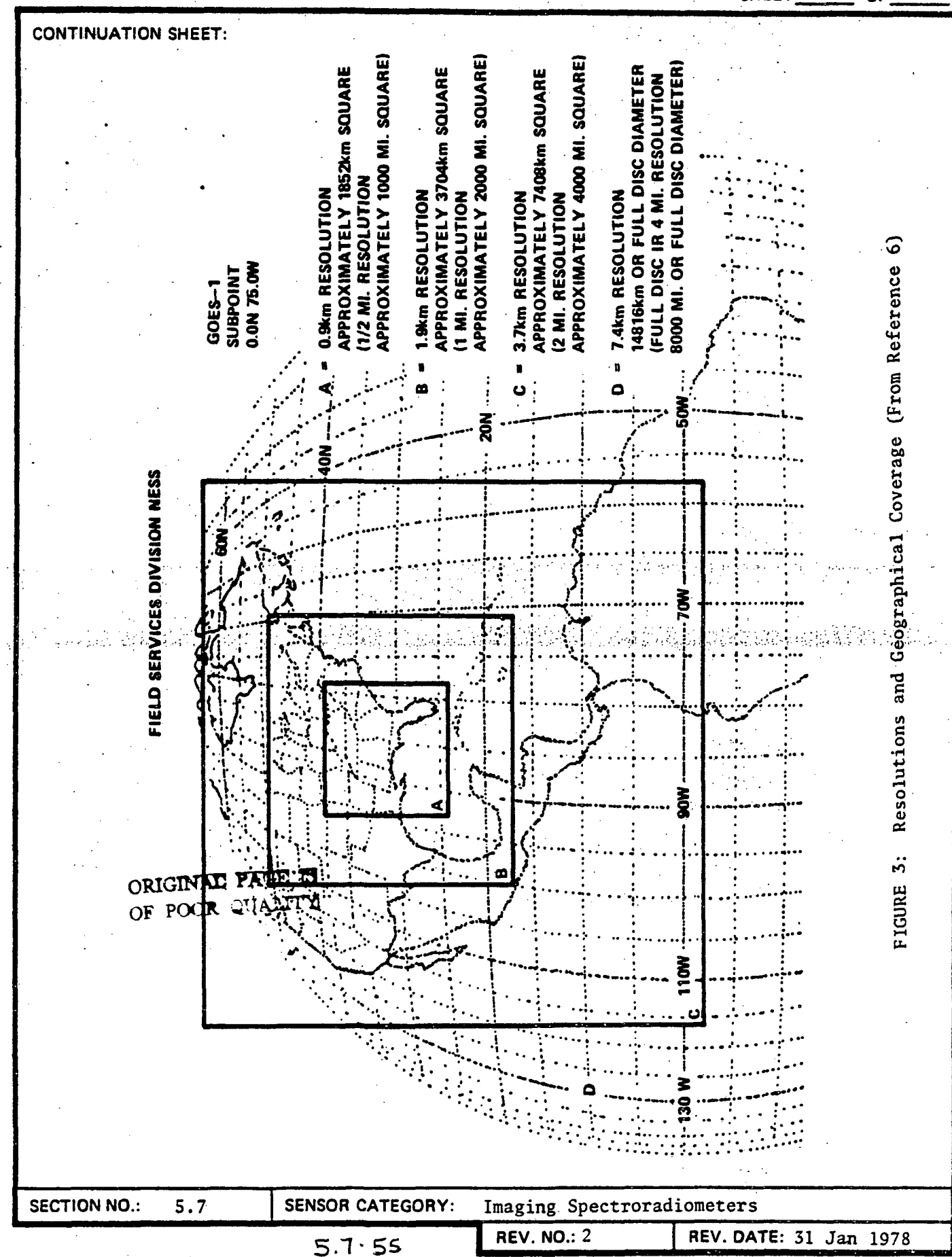
The CDDF photographic laboratory provides sequences of negatives of the images produced on modified photorecorders, as film loops, showing the motion of the weather. A PDP-8 minicomputer and 16 mm camera system are used to generate the film loops. The 8 km IR and 4 km visible image sequence are used. Each loop

(continued on next page)

SECTION NO.: 5.7

Imaging Spectroradiometers SENSOR CATEGORY:





#### (11) continued

includes 6 images taken as a 2 1/2 hour period. The first and last frames are repeated 20 times and each intermediate frame is displayed twice.

Upon request, the sectorizers can enhance an image to emphasize selected features. The procedure implements an enhancement curve which re-assigns grey scale values to increase the contrast between small temperature variances in a selected range. Normally, the temperature magnitude is represented by 256 values of grey scale. Small changes in temperature cannot be distinguished on displays. By reassigning the magnitude values associated with selected features in a manner that increases the grey scale differences between values, the brightness contrast between the values is increased. The specific magnitudes assigned (enhancement curves) are defined to be proportional to the temperatures in the ranges associated with the features being enhanced. Currently 13 operational enhancement curves are maintained. Applications currently include enhancement of cloud images at specific altitudes, hurricane development, snow melt images and coastal upwelling.

In addition to being transmitted to the WWB, the VISSR data is transferred within the NESS facility to the VISSR Ingest Computer (VIC) where all IR data and selected portions (sectors) of visible data are transferred at various resolutions to tape. The IVC can then read the data from tape, reformat it, and transmit it to a facsimile device or to a Muirhead Film recorder. The tape is taken to the 360/195 for further processing. (Full earth 8 x 4 km IR images are always present on the tape.)

At the 360, the data are mapped into either polar stereographic or Mercator maps (option) using the following procedure. Picture elements are located on the earth by using the time, scan line number, sample number and spacecraft location and attitude data to calculate the image's latitude and longitude. Currently each 16th sample of each 16th scan line is located for the 4 or 8 km resolution that is being mapped. This requires 15,000 locators to be processed and uses 20 seconds of CPU time on the 360/195. (Over 40 minutes would be required to locate each sample.) IR and visible data are mapped identically (visible data is expanded to 8 bits). A map storage buffer array of 11.25 mesh per degree (8 km resolution) is The located samples are used to assign each raw data sample mesh coordinates by interpolating its position between the located samples. The interpolating algorithm has been highly optimized to provide efficient mapping. The current mapping program requires 425,000 bytes of main memory and usually requires about 1.25 minutes of CPU per image. The output map consists of 1302 1913 array of picture elements (full disk). The data is placed on disk for use in building the output products.

(continued on next page)

SECTION NO.: 5.7 SENSOR CATEGORY: Imaging Spectroradiometers

5.7-56

REV. NO.:

 $<sup>^{1}</sup>$ For 1 km data, resolutions are 1 km for 1/8 of earth, 2 km for 1/2 of earth or 4 km for all of earth. For 2 km, resolution is 2, 4, 8 km for 1/2 or all of earth.

(11) continued.

Total processing for each frame requires about 10 minutes. This local 360 processing is used for research and other non-operational processing. The major operational data is provided through the microwave link to the CDDF at the World Weather Building.

5.7.57

**SECTION NO.:** 

5.7

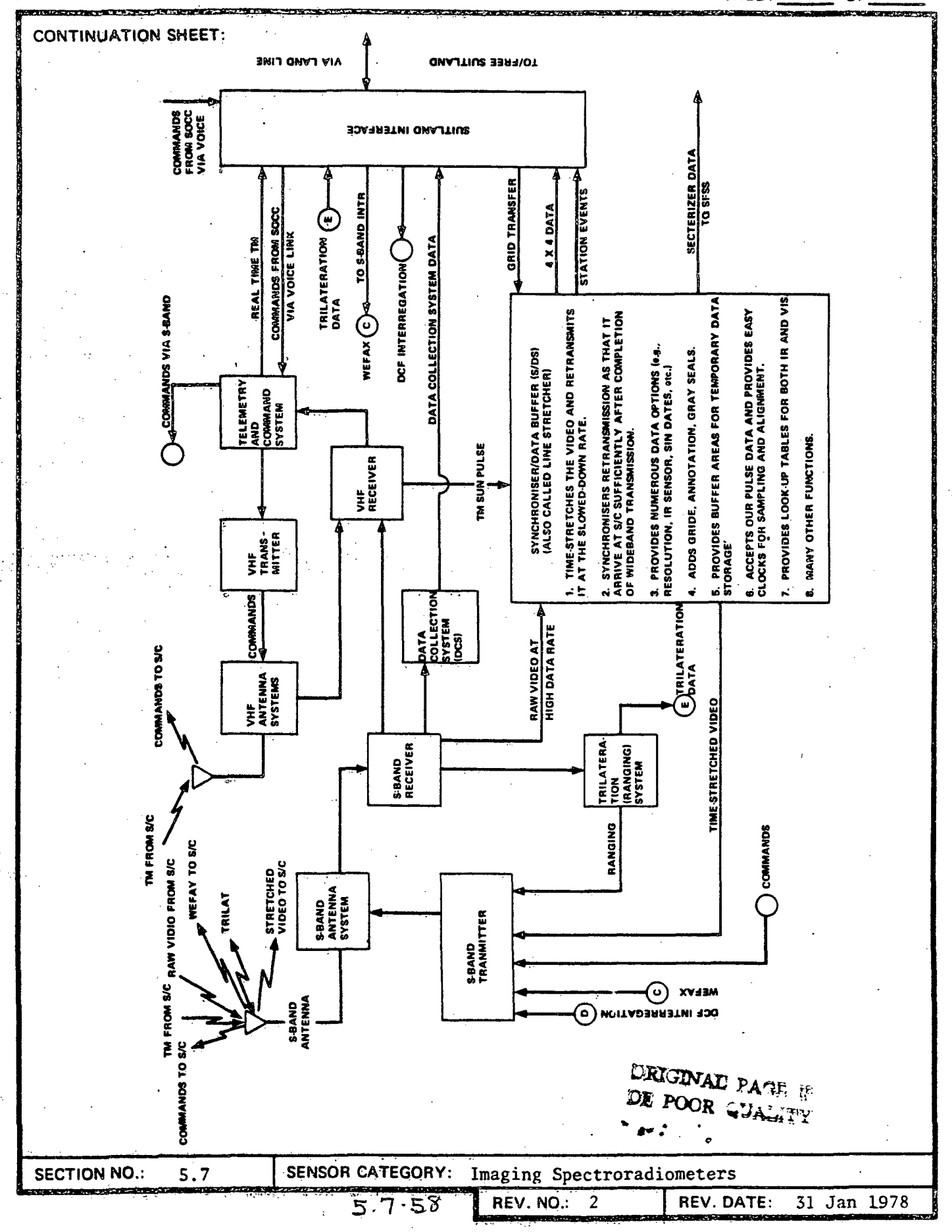
SENSOR CATEGORY:

Imaging Spectroradiometers

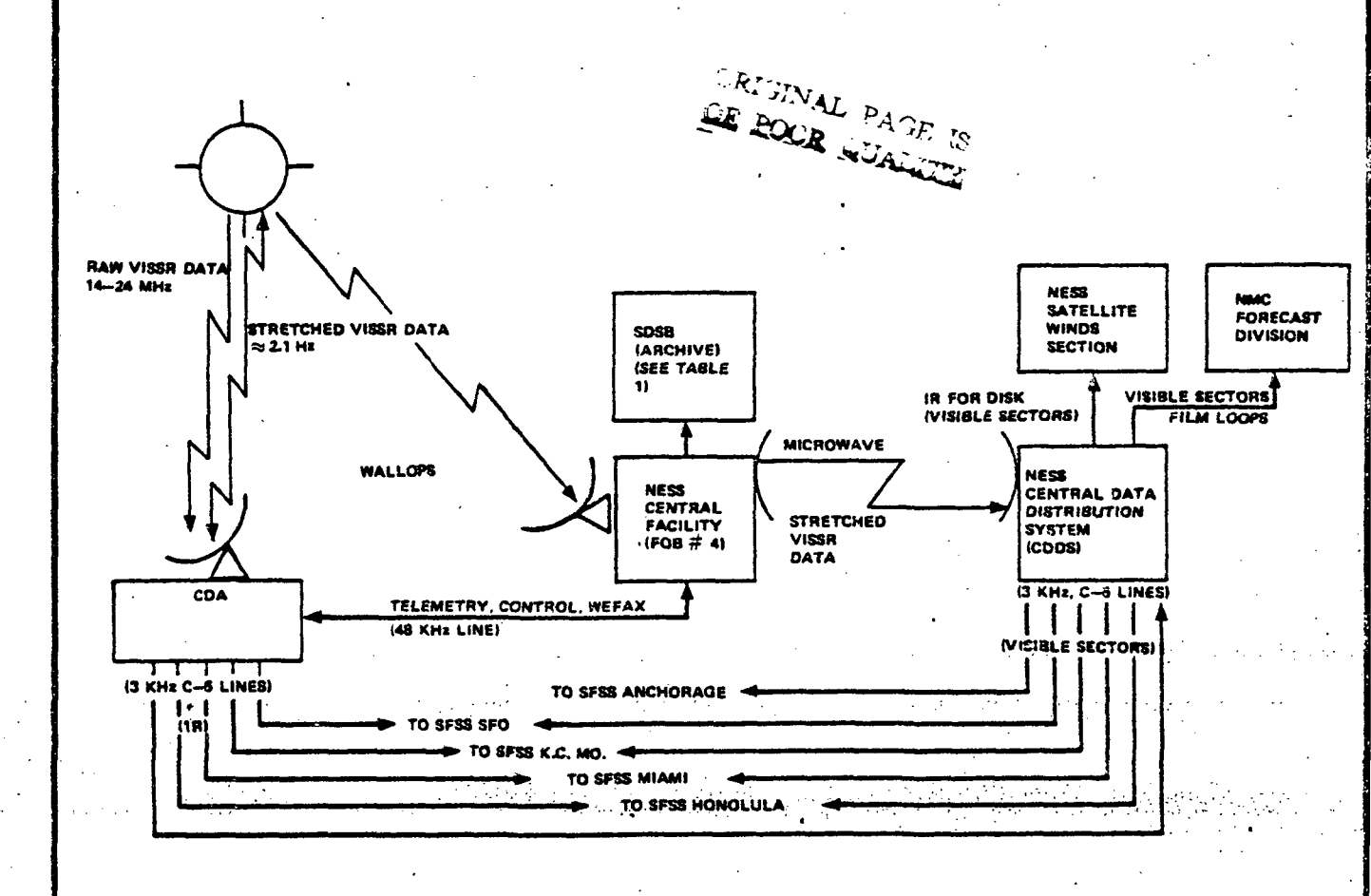
REV. NO.: 2

REV. DATE: 3

31 Jan 1978



## (12) DISTRIBUTION OF DATA FROM GROUND STATIONS - BLOCK DIAGRAM:



#### (13) DATA DISTRIBUTION - NARRATIVE:

Each SFSS has its own set of regularly received sectors from the 12 standard sectors that are routinely provided. In addition, each SFSS has two floater sectors that can be centered at any requested point on the earth disk. (Ref. 6 provides a detail definition of the sectors available at each SFSS.)

Full disk IR data and sectorized images are available to VISSR users. The IR, unsectorized, image data is transferred directly to the Satellite Field Service Sites (SFSS) where the data is forwarded to the appropriate Weather Forecast Service Offices. The unmapped images are transmitted each 30 minutes or more often in case of severe weather. 1500 mi<sup>2</sup> sectors are transmitted to each corresponding SFSS. The transmission of a single sector requires a dedicated C-5 telephone line. Each SFSS must be connected to the CDDF by a number of C-5 lines in order to receive multiple sectors each 30 minutes. Each SFSS has photorecorders to allow redisplay of an image. While discussing its interpretation with the WSFO. This same data is available to any user that taps into the system at an SFSS (GOESTAP) via a C-5 full duplex line. (continued on next page)

SECTION NO.: 5.7

SENSOR CATEGORY:

Imaging Spectroradiometers

5.7.59

REV. NO.: 2

### (13) continued

The CDDF photographic laboratory provides sequences of negatives of the images produced on modified photorecorders, as film loops, showing the motion of the weather. Each day, two film strips are generated for each VISSR and 15 film loops for wind traction. These are archieved. The data distributed by the VISSR is listed in Table 1.

The NESS Satellite Winds Section is supplied with images to evaluate wind magnitude and direction. A Man-Machine-Interactive Processing System (MMIPS) is used to determine wind velocity and altitude for three synoptic times per day (0000z, 1200z, and 1800z). The information is used to prepare synoptic analysis and forecasts for the Global Telecommunications System. Two special sectorizers and four digital Muirhead devices are dedicated to the Winds processing. Inputs are received each 30 minutes.

A C-5 land-line link from the NESS Central Facility to the CDA is used to transmit control and image data. The control data is used at the CDA and consist of such items as grid points, spacecraft commands and CDA operational commands. The image data consists of processed images that are transmitted by the CDA via the satellite WEFAX capability to users with modified (to receive S-Band) APT receiving stations. The satellite WEFAX capability is available only when the VISSR is not acquiring data. Currently eight 10-minute time slots of WEFAX data are made daily. The data products available by this link include 8 km resolution IR and visible data. This year, plans are to expand this service to provide 6 hour repetitive IR coverage and 12 hour visible coverage of the full earth disk. This coverage would require 12-Tcm minute time slots daily.

The Satellite Data Services Branch of the Environmental Data Services National Climatic Center must archieve VISSR data. Table 1 (on the next page) identifies the products that are archieved and the volume of data involved for each product.

5.7.60

SECTION NO.: 5.7

SENSOR CATEGORY:

Imaging Spectroradiometers

CONTINU	CONTINUATION SHEET:									
	Remarks	EDS/NESS review before disposal	EDS/NESS review before disposal	Indefinite review after I year retention at NESS	Retained 1 month by SFSS, further retention to be determined	Retained at SFSS or WSFO 3 months, then deposited with cooperating universities for library use			·	Plans are for future storage of images of full disk at full resolution on mass storage device
	Film (F) or Paper Print (P)	Ľ.,	<u></u>	Ľ.	Œ,	ír.	<b>(1.</b>	N/A	N/A	N/A
VISSR Image Archive	Retention Time at SDSB	5 yrs.	5 yrs.	0pen	oben .	3 mos.	Open	Indefinite (5 years)	٠.	Open
TABLE 1 VISSR 1	Total Pieces per year	35,040	11,700	11,700	102,000	133,000	730	208,050 Vectors (12 Tapes @1600 BPI)		Unknown
TABI	Quantity per day per Satellite	48	32	32	280	d 364 ·	2	570 Vectors	12 Pictures (2 Tapes)	Unknown
	Q Format	Full Disk	Full Disk	Quarter Disk	Variable Size and Location	Designated Sectors	Unknown		89°Latx 99°Long	SIR Unknown
	Spatial Resolution (km)	œ	4		1 and 2	1 and 2	Unknown )	See Text	<b>&amp;</b>	
	Sensor Channel	IR Images	VIS Images	VIS Images	VIS Images	VIS Images	l6mm Movie Strips (15 meter)	Wind Vectors (Magnetic Tape)	Images (Magnetic Tape)	Images
SECTION	NO.: 5.	, 7	SE	NSOR (	CATEGORY	': Imaging	Spectrors	adiometers	<del></del> 3	
		•		_		55			<del> </del>	

5.7.61

**REV. NO.:** 2

#### RSDH DATA SHEET

				A	
				CHEET	AL.
				ance i	XJr.
(P) (出ても 1:10 fm (2:2A) (A) (F) (F) (*****************************	PARTESIAN CHAIRMAN PROCESS OF THE PROPERTY OF THE PARTE O	The second of the second of the second	the first transmitted with and entirent of constant the bound to the entire of the professional districts.		

CONTINUATION SHEET:

This page intentionally left blank.

SECTION NO.: 5.7 SENSOR CATEGORY: Imaging Spectroradiometers

REV. NO.: 2 REV. DATE: 31 Jan 1978

#### RSDH DATA SHEET

SHEET 1 OF 5

(1) SENSOR NAME, ACRONYM: Very High Resolution Radiometer (VHRR)

(2) DISCIPLINE: Earth Observations (3) SUBDISCIPLINE: Atmospheric Monitoring

#### (4) APPLICATION AND OBJECTIVE:

The VHRR provides day and night high resolution images in the visible and infrared spectrum. It is designed for use mainly with local stations for real-time read-out of the images. Applications are related to cloud images and sea surface temperature studies.

#### (5) HERITAGE/KEY PERSONNEL:

Instrument Rep.: A. Martin Eiband (GSFC) (301) 982-5981

#### (6) SENSOR DEPLOYMENT:

Near Polar Orbit, sun synchronous at altitude of 1464 km, the sensor is designed for 3-axis earth stabilized orbit (i.e., the spacecraft rotates about pitch axis once/orbit so that the instrument is always pointed toward earth). Pitch attitude is maintained within  $\pm 1/2^{\circ}$ . The VHRR is currently deployed aboard the ITOS/NOAA series of satellites.

(7) SENSOR CHARACTERISTICS

#### (7A) CAPABILITIES AND CONSTRAINTS OF THE SENSOR TO ACQUIRE THE MEASURED PARAMETER:

The sensor scans cross track at 400 scans per minute. The IFOV for both the IR and visible channels is .87 km at subpoint and 1.33 km at the scan limits. Scanning of the full earth is provided except at the equator where 320 km gaps occur between successive orbits. The scanning mirror revolves 360° so that the earth is in view about 1/3 of the time. The VHRR S/N degrades when both visible and IR channels are active, so the current NOAA series uses two instruments viewing the earth alternately: one measuring in the IR channel and the other in the visible channel. The system gathers 69.8131 IFOV's per millisecond while observing the earth.

(7B) ACTIVE SOURCE CHARACTERISTICS (FOR ACTIVE SENSORS):

N/A

6.3

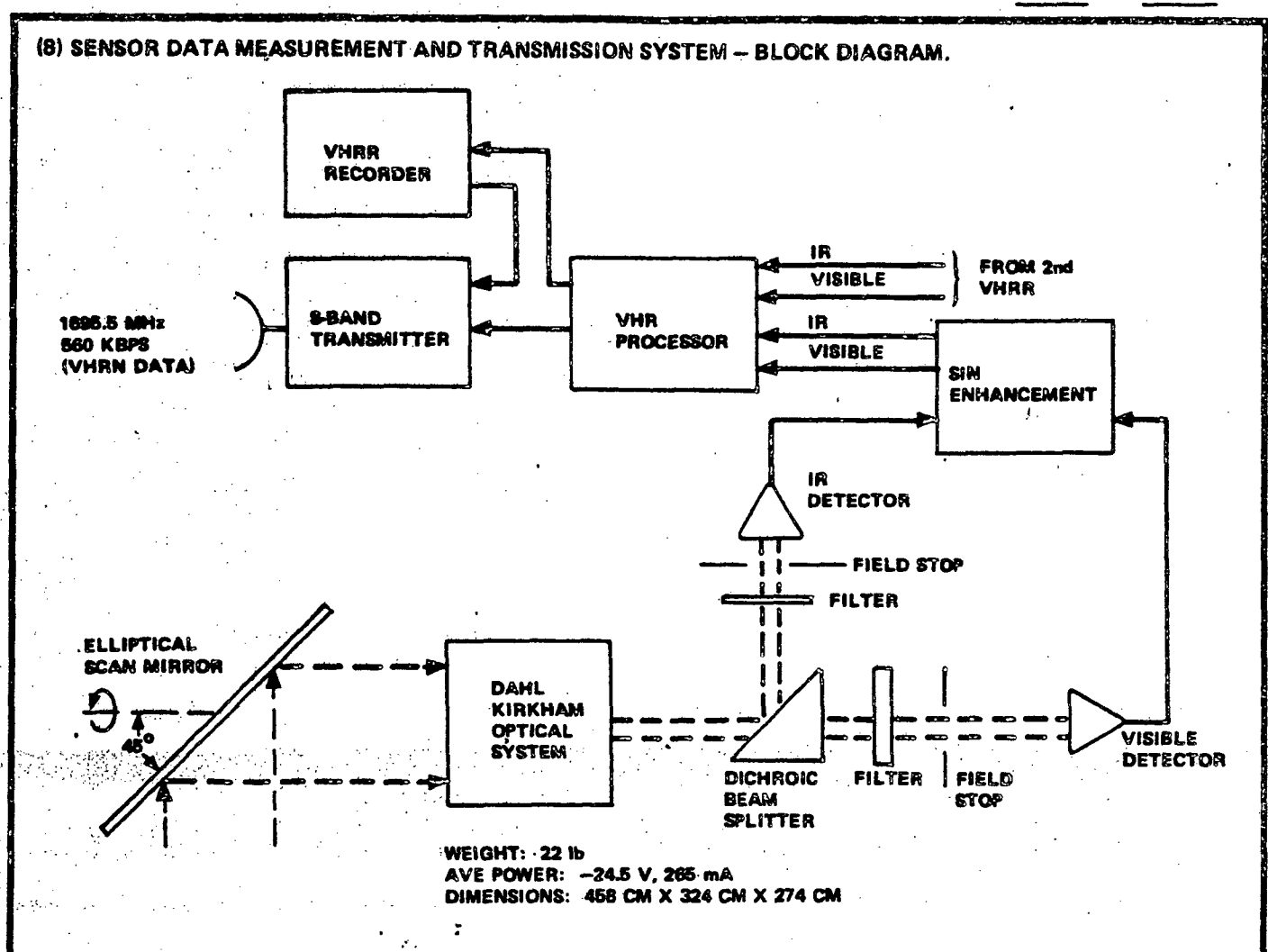
(7C) DETECTOR MEASUREMENTS CHARACTERISTICS: Two detectors are used: a mercury-cadinum-tellerude detector in the IR channel (10.5-12.5 microns) and a Silicon Photo Diode in the visible channel (.6-.7 microns). The Noise Equivalent Differential Temperature (ΝΕΔΤ) for the HgCdTe is .5 (at 300°K) to 2.0° (at 185°K) with only one channel active, and degrades to 4°-25° with both channels active on a single instrument. The operating temperature of the HgCdTe detector is 105°K. The detector size of both detectors is .6 milliradians. On each scan, the zero output level is set while the instrument is viewing space. The output of the VHRR is the difference between the radiating target and space. Once per orbit an on-board target is illuminated for calibration purposes.

SECTION NO.: 5.7 SENSOR CATEGORY: Imaging Spectroradiometers

Preceding page blank

5.7.63

REV. NO.:



#### (9) MEASUREMENT AND TRANSMISSION SYSTEM - NARRATIVE:

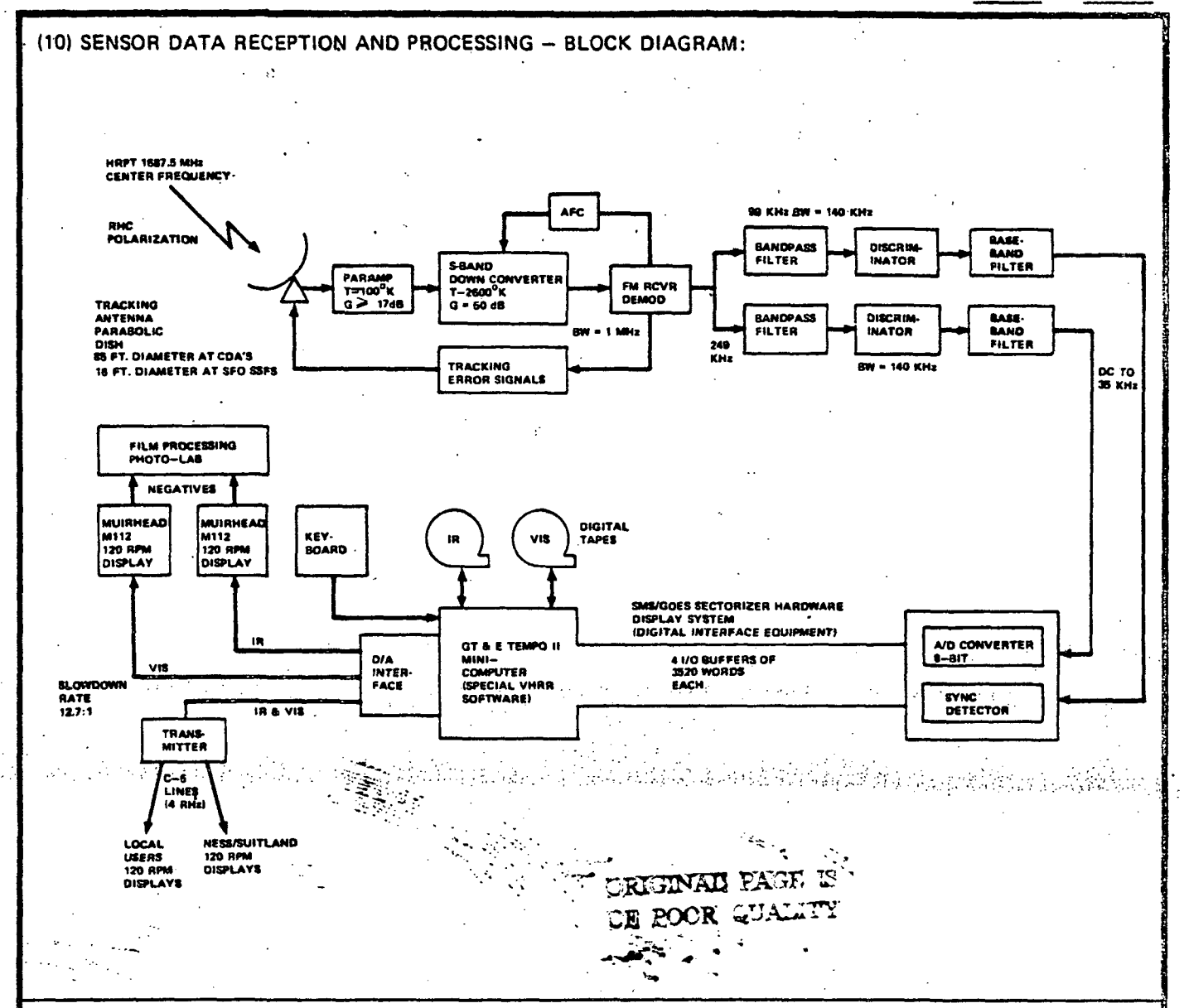
The scan mirror rotates at 400 rpm. In current configurations, two instruments are used to maximize S/N ratio. One is 180° out of phase with the other. The first instrument views earth with its IR sensor active, and while it is viewing space the second instrument views earth in the visible spectrum. Ground Commands allow either channel (or both) to be active in either instrument. Normally, output is transmitted directly to ground. Under control of ground supplied commands up to 8 minutes of data may be recorded. The recorder is played back at the record speed.

The VHRR can be programmed by ground commands to provide image data for a full orbit or for selected segments (8 per orbit) of a full orbit.

Data collection rate is approximately 70,000 samples (IFOV's) per second per channel during the time the earth is in view. This gives a data rate equivalent to 1.1 Mbps of information. (The information remains in analog form until it is converted at the receiving station.) The information is buffered and the necessary buffering and merges the data streams from IR and visible channels of the two instruments.

SECTION NO .: SENSOR CATEGORY: 5.7 Imaging Spectroradiometers REV. NO.: 2 REV. DATE: 31 Jan 1978

5.7-61



#### (11) RECEIVING AND PROCESSING - NARRATIVE:

High Resolution Picture Transmission (HRPT) Receiving Stations have been implemented by NOAA at each CDA (Gilmore Creek, Alaska and Wallops Island, Va.) and at the NESS San Francisco Field Service Station. The recorded data is played back at the CDA's. While the playback transmission is in progress, the signal strength is degraded so that stations with smaller antenna and less sophisticated systems cannot receive data. (HRPT stations can be built by any user that so desires.) The receiving stations are capable of continuous autotrack down to 5° of the horizon. The input signal is processed to maximize S/N and converted to 8-bit digital values. All values at the NOAA sites are saved on digital tape as shown in (10) above.

Approximately 66 ms of data is generated each scan (for both IR and visible data) at 1.1 Mbps. The data is received in the input buffers at 7,040 bytes per scan. Four I/O buffers are used, giving a total of nearly 30,000 bytes of buffers. The

(continued on next page)

SECTION NO.: 5.7 | SENSOR CATEGORY: Imaging Spectroradiometers

REV. NO.: 2

#### (11) continued

data is packed, telemetry information is added and the results (5,340 byte per scan for both IR and visible data) is written to tape. The number of samples per line is adjusted by averaging so that when the image is displayed, the horizontal scaling will equal the vertical scaling (250 IFOV's per inch). The two digital tapes (1600 bpi) can hold up to 17.5 minutes of data which is sufficient to record one full pass of maximum duration.

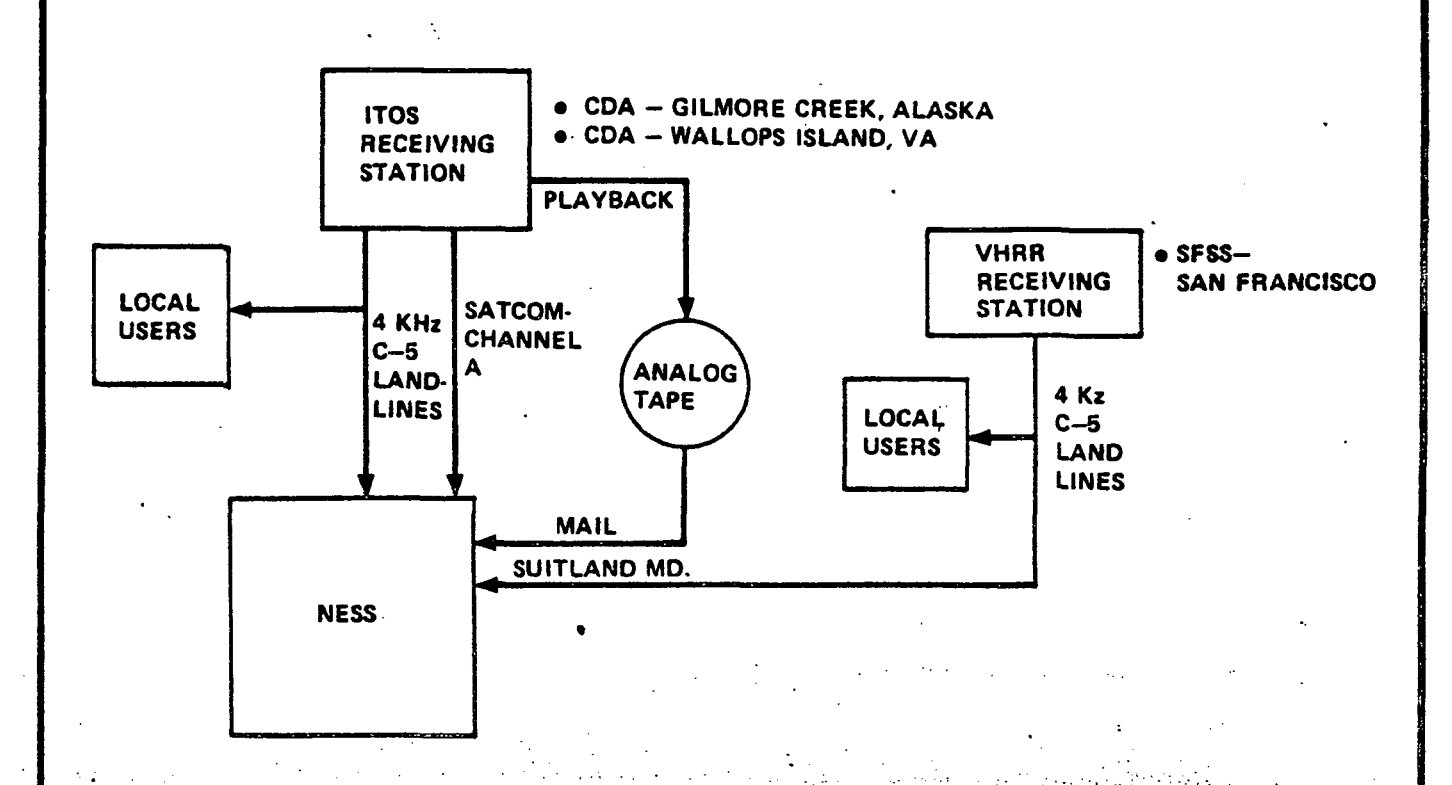
Following the satellite pass, the tapes are played back simultaneously for display and transmission to the central site. The Murhead M112 displays provide 2500 lines in the vertical dimension and the horizontal spacing is scaled equal to the vertical. The image, plus up to 100 lines of tabular display data, is fed through a D/A interface to the display and the C-5 line transmitter. The tabular data includes orbit and time identification, and HRPT label.

About six-minutes of data is displayed in each image. Each image is centered at the satellite subpoint and displays an area about 2,580 km on a side. 30 minutes of processing is required for each 6 minutes of received data. The 8-bits of magnitude provide for 256 shades-of-grey to be displayed.

The Wallops, VA and the SFO SFSS stations receive five passes per day and the Gilmore Creek Alaska station receives eight. The central NOAA facility at Suitland provides the HRPT stations with satellite orbit characteristics, satellite command schedules and overlay map guides.

The HRPT stations are designed to allow growth to more advanced sensors and more elaborate processing in the future.

SECTION NO.: 5.7 **SENSOR CATEGORY:** Imaging Spectroradiometers (12) DISTRIBUTION OF DATA FROM GROUND STATIONS - BLOCK DIAGRAM:



(13) DATA DISTRIBUTION - NARRATIVE: The images are transmitted from the CDA's to the NESS Central Data Distribution Facility and to local users. The VHRR is used only for research and no general distribution of the data is normally made. Transmission to the CDDF is:

- a via an analog tape transmitted through the mail (raw data) and injested on the Image Information, Inc. High Resolution Image Processing at CDDF,
- b over channel A of the SATCOM lines at 8:1 slowdown (normally not used because of the load it places on the lines),
- c recorded at Wallops Island and playback through the ATS digitizer at a 4:1 slowdown through 48 kHz digital lines to the ATS digital picture terminals, and
- d via 4 kHz C-5 land-lines.

At the CDDF, the images can be viewed on several available display terminals and film transparencies can be produced on the Digital Murhead Display (DMD). The data is used for research purposes and is not further distributed.

SECTION NO.: 5.7 SENSOR CATEGORY: Imaging Spectroradiometers

REV. NO.: 2 REV. DATE: 31 Jan 1978

	RSD DATA S		SHEET	OF
CONTINUATION SHI	ET:		Bear whomether return to the second	
				·
			·	
•				
	This page intention	ally left blank.		•
		4. 3 F		
			• •	
	· ·			•

**REV. NO.:** . 2 **REV. DATE**: 31 Jan 1978

Imaging Spectroradiometers

SENSOR CATEGORY:

SECTION NO.: 5.7

#### RSDH DATA SHEET

SHEET	1	OF	8

(1) SENSOR NAME, ACRONYM: Heat Capacity Mapping Radiometer (HCMR)

(2) DISCIPLINE: Earth Observations (3) SUBDISCIPLINE: Land Monitoring

#### (4) APPLICATION AND OBJECTIVE:

The purpose of the HCMR is to conduct a thermal mapping experiment with high spatial resolution in an orbit optimized for Earth resources sensing rather than meteorological sensing. Measurements of surface temperature will be made during successive day and night passes for determination of surface temperature variation.

(5) HERITAGE/KEY PERSONNEL: Similar to the High Resolution Surface Composition Mapping Radiometer (HRSCMR) which has already been developed for NIMBUS-E.

Project Scientist - Dr. W. A. Hovis

#### (6) SENSOR DEPLOYMENT:

The Heat Capacity Mapping Mission (HCMM) will place the HCMR into a 600 km circular sun synchronous orbit with a nominal 2:00 p.m. ascending node. A six-month minimum operational lifetime is planned. The launch vehicle will be a Scout-F launched from the Western Test Range(WTR). The HCMM launch is planned for the second quarter of 1978.

(7) SENSOR CHARACTERISTICS

#### (7A) CAPABILITIES AND CONSTRAINTS OF THE SENSOR TO ACQUIRE THE MEASURED PARAMETER:

The HCMR will have a small instantaneous geometric field of view, less than  $1 \times 1$  milliradians, high radiometric accuracy and a wide enough swath coverage on the ground so that selected areas are covered within the twelve-hour period corresponding to the maximum and minimum of temperature observed. The sensor will operate in two channels, 10.5 to 12.5 micrometers (IR) and 0.8 to 1.1 micrometers (visible). The visible channel is matched to the LANDSAT MSS Band 4.

(7B) ACTIVE SOURCE CHARACTERISTICS (FOR ACTIVE SENSORS):

Not Applicable

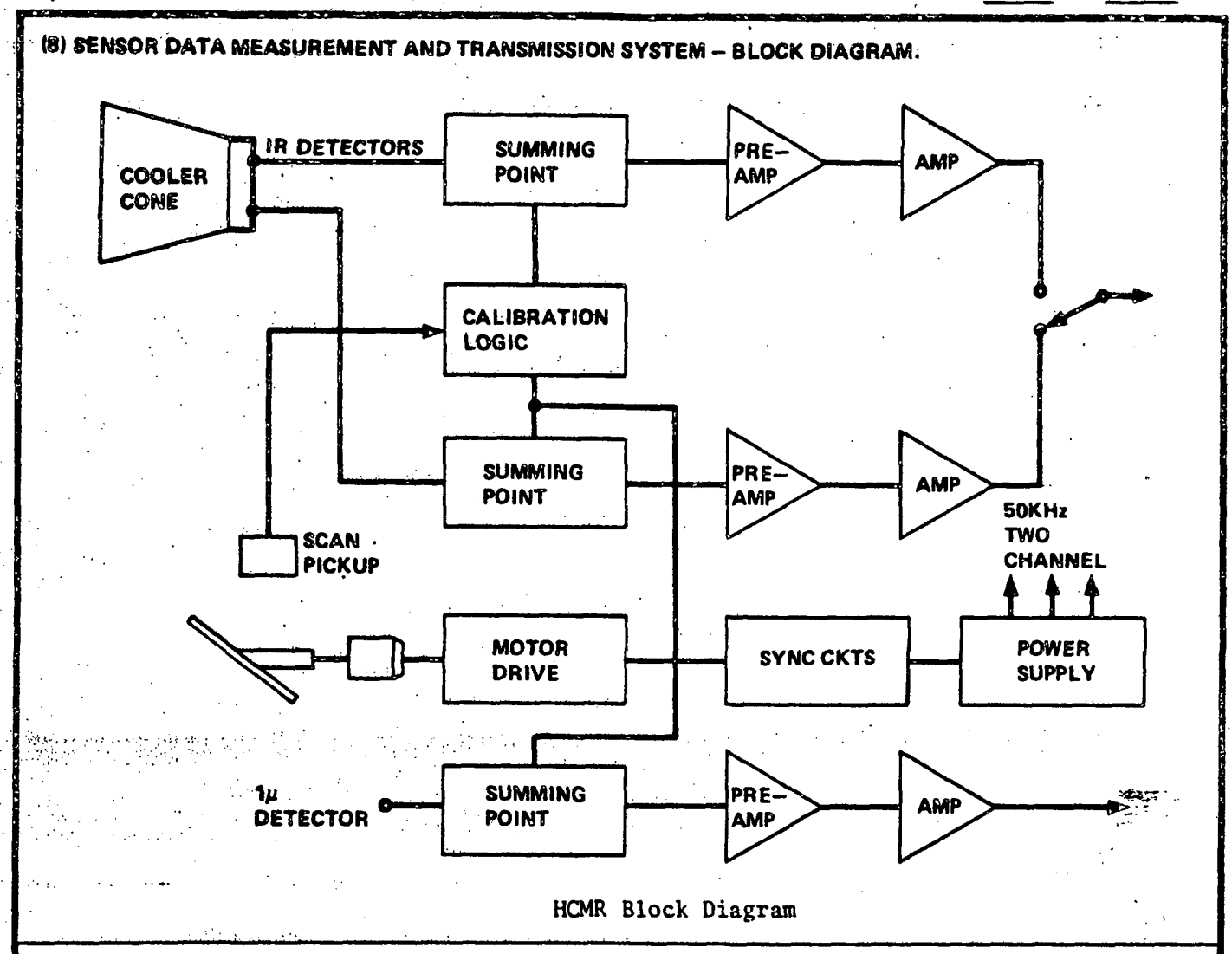
#### (7C) DETECTOR MEASUREMENTS CHARACTERISTICS:

The visible channel optics consist of a long wavelength-pass (>0.8µm) interference filter, a parabolic focusing mirror and an uncooled silicon photo diode. The two 10.5 and 12.5 IR channels are provided by inserting a second beam splitter in the reflected beam of the first. The two beams are focused onto the HaCdTe detectors using germanium lenses. Final focusing and spectral trimming is accomplished by germanium band pass filter and germanium aplanats located at the detectors.

SECTION NO.: 5.7 SENSOR CATEGORY: Imaging Spectroradiometers

Preceding page blank 5.7.69 REV. NO.: 2 REV. DATE: 31 Jan 1978

53



#### (9) MEASUREMENT AND TRANSMISSION SYSTEM - NARRATIVE:

The HCMR is comprised of four major subassemblies mounted in a common housing. These subassemblies are:

- · Scan Mirror and Drive
- · Optics
- · Electronics
- · Radiant Cooler

The scan mirror drive assembly provides cross-course scanning of the instantaneous field of view with reference to the subsatellite ground track. The optical sub-assembly provides increased ground resolution and spectral definition of the three channels. The electronics subassembly contains the data amplifiers and housekeeping telemetry and formats the analog sensors data such that it is compatible with the HCMR data system. The radiant cooler subassembly provides detector operating temperatures of approximately 115°K.

Scan Drive Subassembly

The scanner design uses an elliptically shaped plane mirror set at 45° to the axis. The scan mirror is fabricated from berythium and is Kanogen coated. The mirror (continued on next page)

SECTION NO.: 5.7 SENSOR CATEGORY: Imaging Spectroradiometers

REV. NO.: 2 REV. DATE: 31 Jan 1978

### (9) continued

is driven by an 80-pole Schaeffer motor which is synchronized to the space-craft two-phase clock. Angular momentum compensation of the scan mirror is provided by a separate motor driving a compensation mass. Scan mirror position is monitored once each revolution by a magnetic pick-up.

Optics Subassembly

The optical subassembly (see Figure 1) is catadioptric collecting with an afocal reflecting telescope. The telescope is a modified Dall-Kirkham configuration which reduces the optical beam from an eight inch to a one inch diameter. Spectral separation is provided by a dichroic beam splitter positioned in the collimated beam from the secondary mirror which acts as a folding mirror for the 10.5 to 12.5 micrometer band and transmits energy at shorter wavelengths. The electronic and radiant cooler subassemblies are discussed in information cell #11.

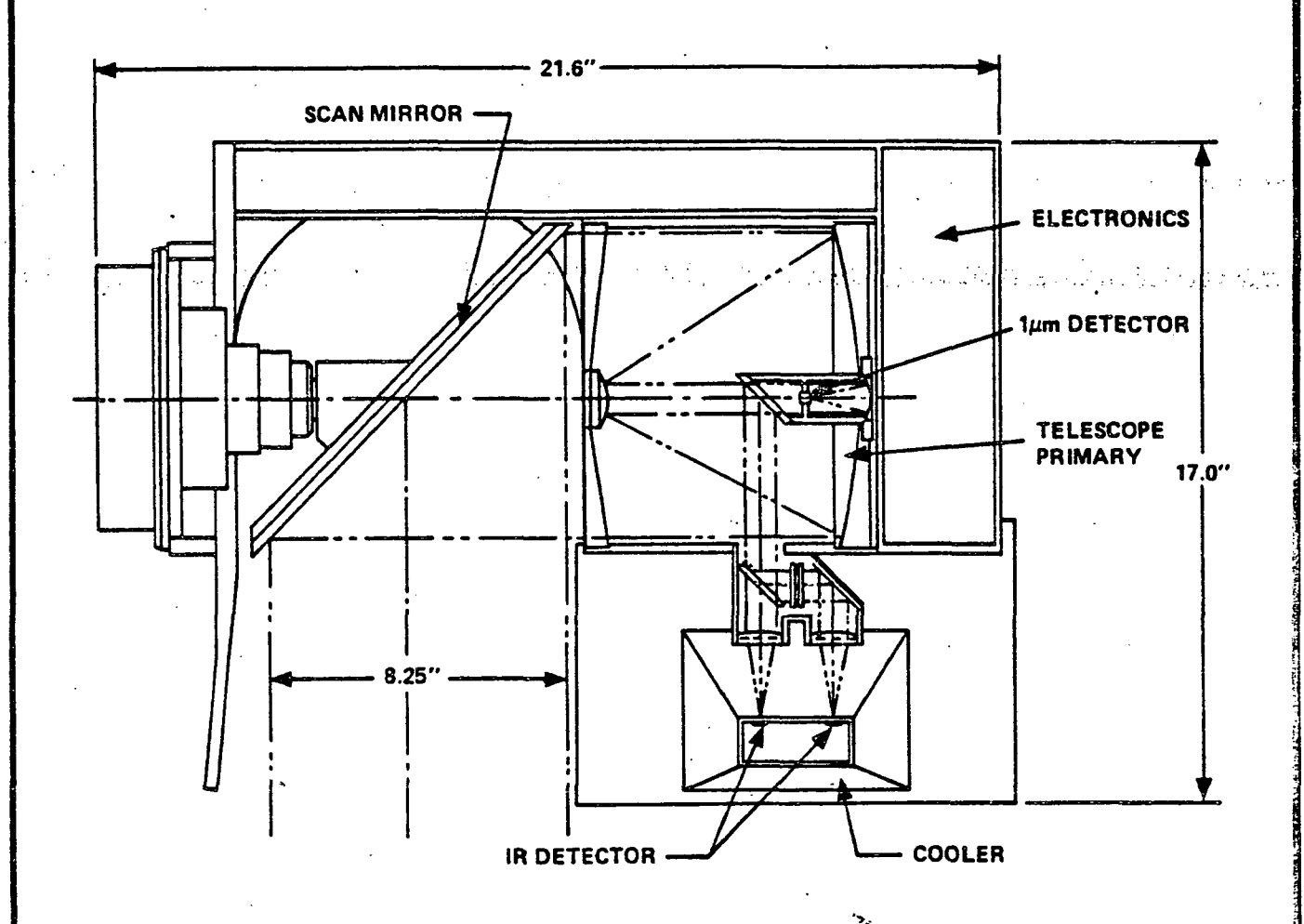


FIGURE 1 HCMR Optics Subassembly

SECTION NO.: 5.7 SENSOR CATEGORY: Imaging Spectroradiometers

5.7.71

REV. NO.:

(10) SENSOR DATA RECEPTION AND PROCESSING - BLOCK DIAGRAM:

See information cell #8.

#### (11) RECEIVING AND PROCESSING - NARRATIVE:

Electronic Processing

The detectors produce a small AC electrical signal which is proportional to the difference in radiant energy between the scene and space. The electrical signals from the detectors are amplified in each video amplifier to a level required for processing. Each video amplifier contains a low noise preamplifier, video filter and postamplifier. A space clamping technique is also used which establishes the DC zero level once every rotation of the scanner by clamping the output to zero when viewing cold space and holding this level for the duration of the scan. The overall video amplifier gain will be such that the highest energy scene will produce a 6-volt output signal. Calibration signals consisting of a 6-step staircase waveform will be inserted at the amplifier input as well as at the amplifier output on every scan line to provide constant calibration and complete assessment of the amplifier performance. At the amplifier output, synchronizing pulses are also gated in along with the output calibration to make up the composite (continued on next page)

SECTION NO.: 5.7

SENSOR CATEGORY:

Imaging Spectroradiometers

**REV. NO.: 2** 

### (11) continued

video. Output buffer amplifiers with unit gain and low output impedance are used for the output interface to the data system.

The calibration circuitry consists of an accurate, stable digital-to-analog converter which will generate a staircase of six one-volt steps for insertion at the amplifier input and output.

## Radiant Cooler

The radiant cooler is designed to cool the patch to 110°K. The patch will be controlled in temperature to 115°K by a temperature control circuit which monitors temperature with a thermistor and supplies heat to the patch.

5.7.73

SECTION NO .:

5.7

SENSOR CATEGORY:

Imaging Spectroradiometers

REV. NO.:

REV. DATE: 31

31 Jan 1978

#### (12) DISTRIBUTION OF DATA FROM GROUND STATIONS - BLOCK DIAGRAM: HCMR ANALOG **ANALOG TAPES ARRIVED AT** TAPES RECORDED **GSFC** AT GRND STATIONS **ANALOG TAPES** ARRIVED AT HCMM CONTROL CENTER HCMM/HCMR Analog Data Flow HCMR SURVEY **PICTURES PRODUCED** HARD PRELIMINARY **SELECTED TAPES** COPY **ANALYSIS OF** PROCESSED ON PIX **HCMR DATA** FIS ANALOG TAPES **MASTER DATA** TO IPD WITH TAPES TO INSTRUCTION SIOUX FALLS HARD COPY IPD DIGITIZING **DIGITAL TAPE** CONTOUR LINE MAKES **PROCESSING** PLOTS. DIGITAL TAPES COLOR PIX, ETC

## (13) DATA DISTRIBUTION - NARRATIVE:

Data will be collected in real time only, when the spacecraft is within the range of one of the stations equipped to receive HCMM data. Stations presently equipped are Rosman, N.C., Mojave, California, Gilmore Creek, Alaska, Honeysuckle, Australia and Madrid, Spain. Data will be collected in analog form only. Data tapes will be mailed to GSFC in all cases and some direct recording at GSFC can be accomplished using the wide band link from Rosman to GSFC.

Data will be collected at each station for every pass where the station is operating and where cloud cover is not so extensive as to cover 70% to 80% of the area that would be seen.

Pictures from each data pass will be produced directly from the analog tapes to determine if the data quality is sufficiently good to merit digitization and further processing. The analog pictures will be made on the EIS machine where a

(continued on next page)

SECTION NO.: 5.7 SENSOR CATEGORY: Imaging Spectroradiometers

Zing Sing opposite the control of th

5.7-74

REV. NO.:

#### **CONTINUATION SHEET:**

#### (13) continued

black and white positive and negative are made simultaneously at a rate of three minutes per frame. In no case will a station pass result in more than three frames.

The black and white positives will be scanned to determine if the data is of good quality and the cloud cover sufficiently small to merit further processing. The negatives from this uncalibrated picture will be washed and stored for possible further use.

The positive survey pictures will be utilized to prepare instructions for the digitization line in the Information Processing Division (IPD). Instructions normally contain the tape register number, the number of the tracks containing the data of interest and the start and stop time from he spacecraft time code recorder on the tape. The tapes and the instructions for processing will be transported to the digitization facility in the event that the survey picture facility and the digitization line are not co-located.

Digitization of the analog data will be carried out with the digitization line established for the Nimbus 5 Surface Composition Mapping Radiometer (SCMR). The data will be digitized in the format utilized for the SCMR so that the software developed for the SCMR can be utilized.

The digitized data will be processed first into thermal maps utilizing the instrument internal calibration for thermal calibration and the spacecraft altitude and attitude information to correct the data to a uniform scale and grid the data. Based on past Nimbus experience, it is estimated that 20 to 25 usable frames of data will be acquired each day. The processed data will be converted into calibrated imagery in the facilities of the Information Processing Division.

Duplicates of the processed tapes will also be produced in the facilities of the Information Processing Division. With the exception of scale correction, this may be necessary because of the non-circular orbit possible with a Scout launch, software for all operations up to this point already exists.

Processing for thermal inertia mapping will require registration of data from overlapping orbits from a day and night overpass of the same area. The scale correction and location gridding already applied will be utilized as the first step in registration. Since the day and night orbits will cross at an angle of approximately 30° one of the two scenes will be rotated to coincide with the other. Software for this operation will be developed in cooperation with the Information Processing Division. The registered frames will be processed with an algorithm to extract thermal intertia from the temperature measurements and the daytime albedo measurements. From the 20 to 25 frames of useful data per day an estimated 2 pairs will be sufficiently cloud free and occur in an area where thermal inertia measurements will be of use.

(continued on next page)

SECTION NO.:

5.7 SENSOR CATEGORY:

Imaging Spectroradiometers

CHEET	8	OE	8
SHEET	O	OF	0

#### CONTINUATION SHEET:

### (13) continued

The processed thermal inertia data will be produced to provide imagery and magnetic tapes. The imagery will be produced in black and white with gray scale annotation. Annotation will also include gridding and the times at which the frames were taken. Data tapes will be duplicated for the primary users in the IPD facilities. Further duplication will be carried out at a data depository.

### Data Dissemination

Processed data in the form of pictures or magnetic tapes will be sent to the EROS Data Center, Sioux Falls, S.D. Distribution of the data to investigators other than at GSFC or the USGS will take place through the Data Center.

SECTION NO.: 5.7 | SENSOR CATEGORY: Imaging Spectroradiometers

REV. NO.: 2

(1) SENSOR NAME, ACRONYM: Coastal Zone Color Scanner (CZCS)

(2) DISCIPLINE: Earth Observations (3) SUBDISCIPLINE: Ocean Monitoring

### (4) APPLICATION AND OBJECTIVE:

The CZCS is a passive imaging, scanning, visible/infrared, spectroradiometer. Its' purpose is to gather radiometric data to map chlorophyll concentration, sediment distribution, gelbstoffe (yellow substance) concentration as a salinity indicator, and temperature of coastal waters and the open ocean.

Similar to Nimbus-5 Surface Composition Mapping Radiometer (5) HERITAGE/KEY PERSONNEL: (SCMR).

CZCS Applications Scientist--Dr. Warren A. Hovis--(301) 982-6465

#### (6) SENSOR DEPLOYMENT:

The CZCS is one of nine (9) sensors aboard Nimbus-G, scheduled for launch in October 1978. Nimbus-G will operate in a sun-syncronous, circular orbit at an altitude of 955km and 100° inclination. Mission lifetime is scheduled for one year and CZCS duty cycle is 30%.

(7)

#### SENSOR CHARACTERISTICS

### (7A) CAPABILITIES AND CONSTRAINTS OF THE SENSOR TO ACQUIRE THE MEASURED PARAMETER:

The CZCS has six (6) spectral bands, five(5) sensing reflected solar energy and one sensing thermal emission. Four of the five reflectance solar bands have their dynamic range set for water targets and will saturate over most land scenes. The fifth band (700-800nm) has the same spectral location as band 6 of the Landsat MSS and its dynamic range is set for land targets. Band 6, centered at 11.5µm, will measure the temperature of coastal waters and ocean currents over the range of 270-305°K, and with the same spatial resolution as the reflectance bands. (continued on next page)

#### (7B) ACTIVE SOURCE CHARACTERISTICS (FOR ACTIVE SENSORS):

Not Applicable

#### (7C) DETECTOR MEASUREMENTS CHARACTERISTICS:

The detectors for bands 1-5 are silicon photodiodes. The thermal emission detector (band 6) is a Mercury Codmium Teluride (HgCdTe) photoconductor. Interference filters provide the spectral selectivity shown in Table 1. Reflected solar energy and thermal radiation are collected and focused on the detector assembly with Cossegrain objective system with a clear aperture of 17.8cm and a focal length of 71cm Calibration measurements:

(continued on next page)

SENSOR CATEGORY: Imaging Spectroradiometers **SECTION NO.:** 5.7

REV. NO.: REV. DATE: 31 Jan 1978

### CONTINUATION SHEET:

### 7(A) continued

Swath width for all bands is ± 800 km about the nadir. The distance between sub-orbital tracks is 490 km at the equator and the orbit repeats at six day intervals so that a particular scene might be viewed in passes on three successive days. At higher latitudes successive day coverage is greater than at the equator. The scan parameters and view axis geometry are illustrated in Figure 1 (Sheet 3).

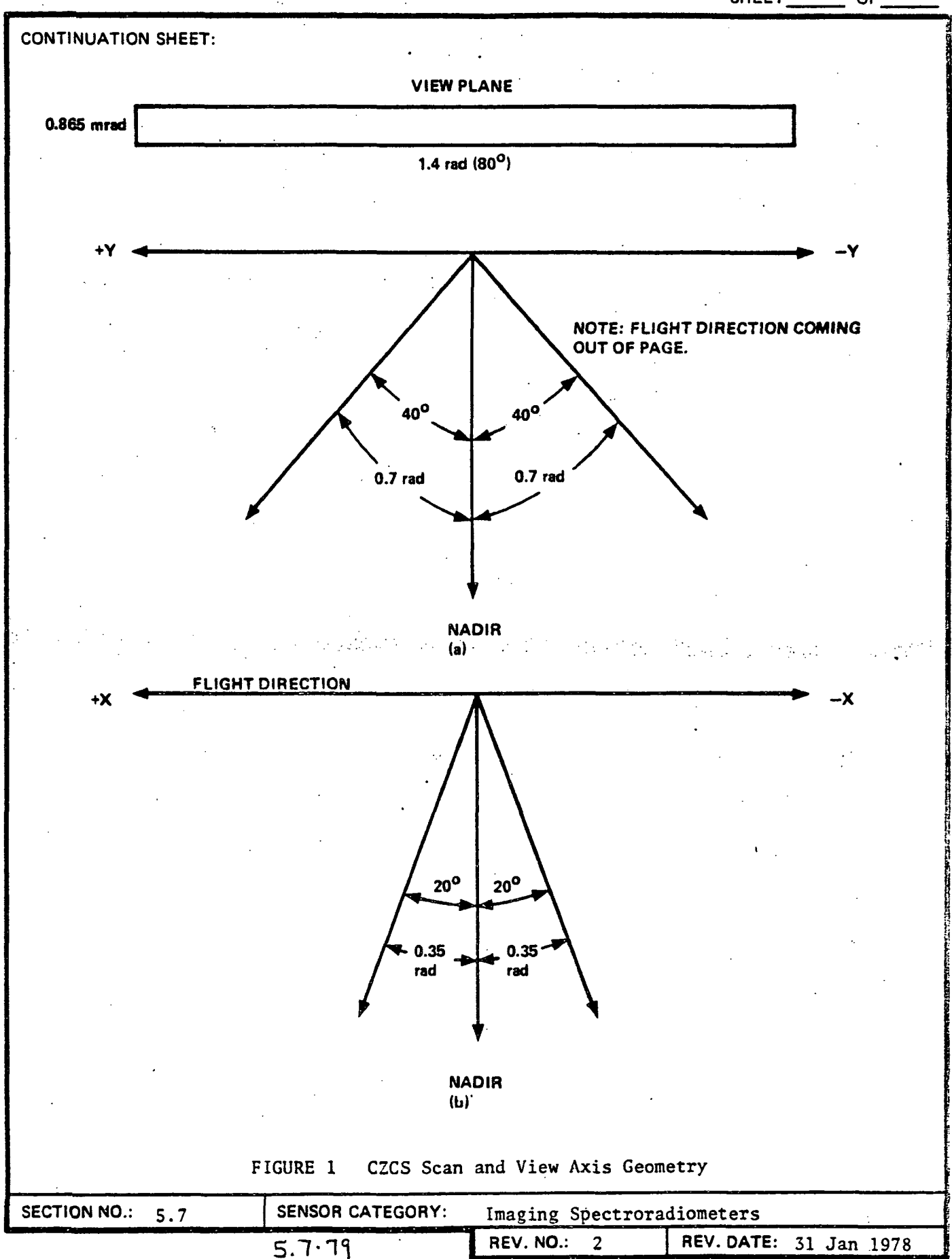
### 7(C) continued

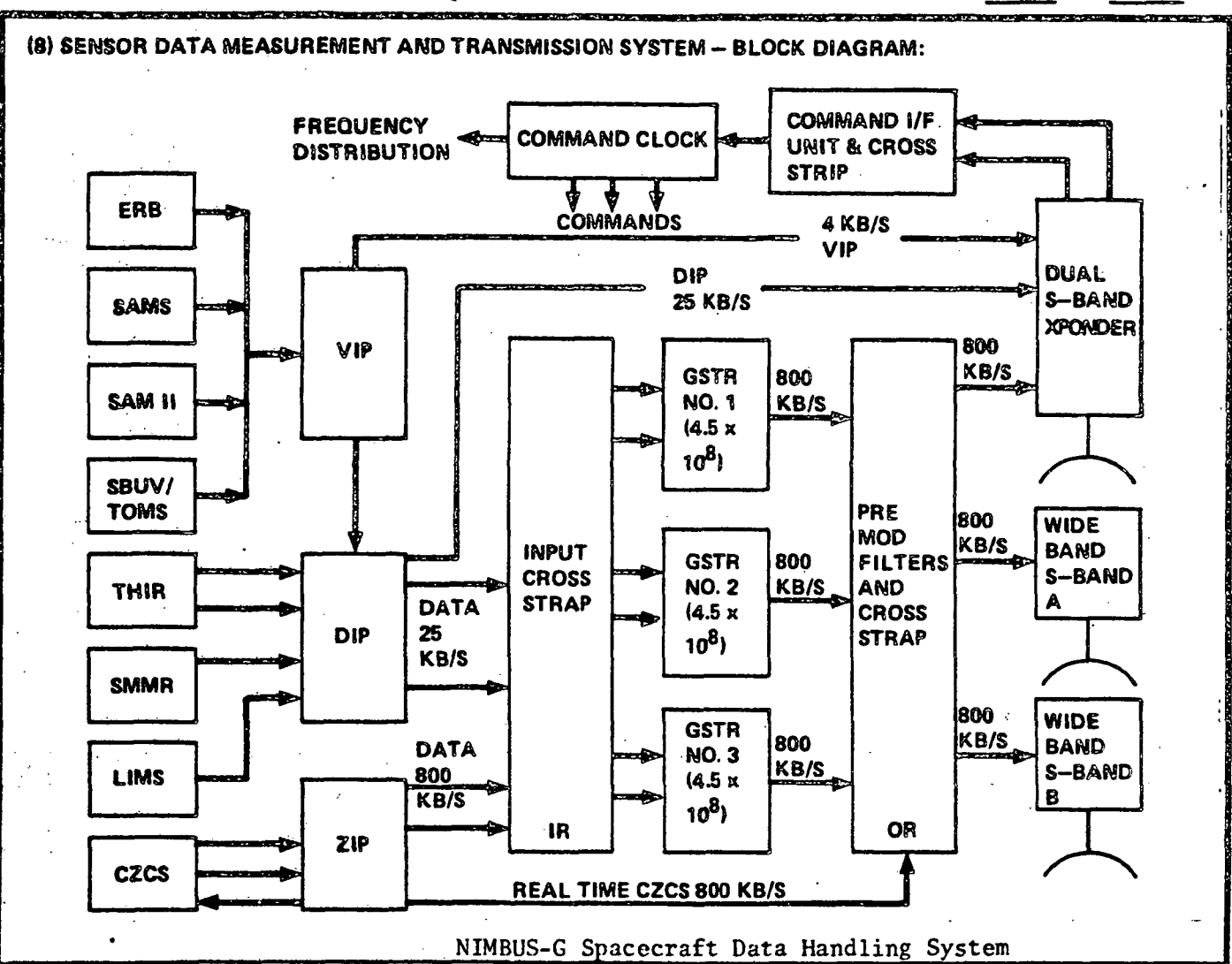
Table 1
SPECTRAL CHARACTERISTICS

Band No. 1		2	3	4	5	6
Bandwidth (nm)	443±10	520±10	550±10	670±10	750±50	1150±1
Accuracy (%)	.4	.4	.4	.4		
Sensitivity [mw/(cm²svµm)]	11.46	7.64	6.21	2.86		
NEP (1)	2.1x10 <sup>-11</sup>	1.7x10 <sup>-11</sup>	1.5x10 <sup>-11</sup>	1.2x10 <sup>-11</sup>	1.5x10 <sup>-10</sup>	(2) 1.3x10 <sup>-12</sup>
Spectral Parameters Observed		Chlorophyll Correlation		Chlorophyll Absorption	Surface Vegetation	Surface Tempera- ture

- (1) NEP Noise Equivalent Power (dimensionless quantity)
- (2) Band 6 shall have a noise equivalent temperature difference (NETD) of 0.25°K or better at 270°K.

SECTION NO.: 5,7	SENSOR CATEGORY:	Imaging Spectrorad	iometers
	5.7.78	REV. NO.: 2	REV. DATE: 31 Jan 1978





#### (9) MEASUREMENT AND TRANSMISSION SYSTEM - NARRATIVE:

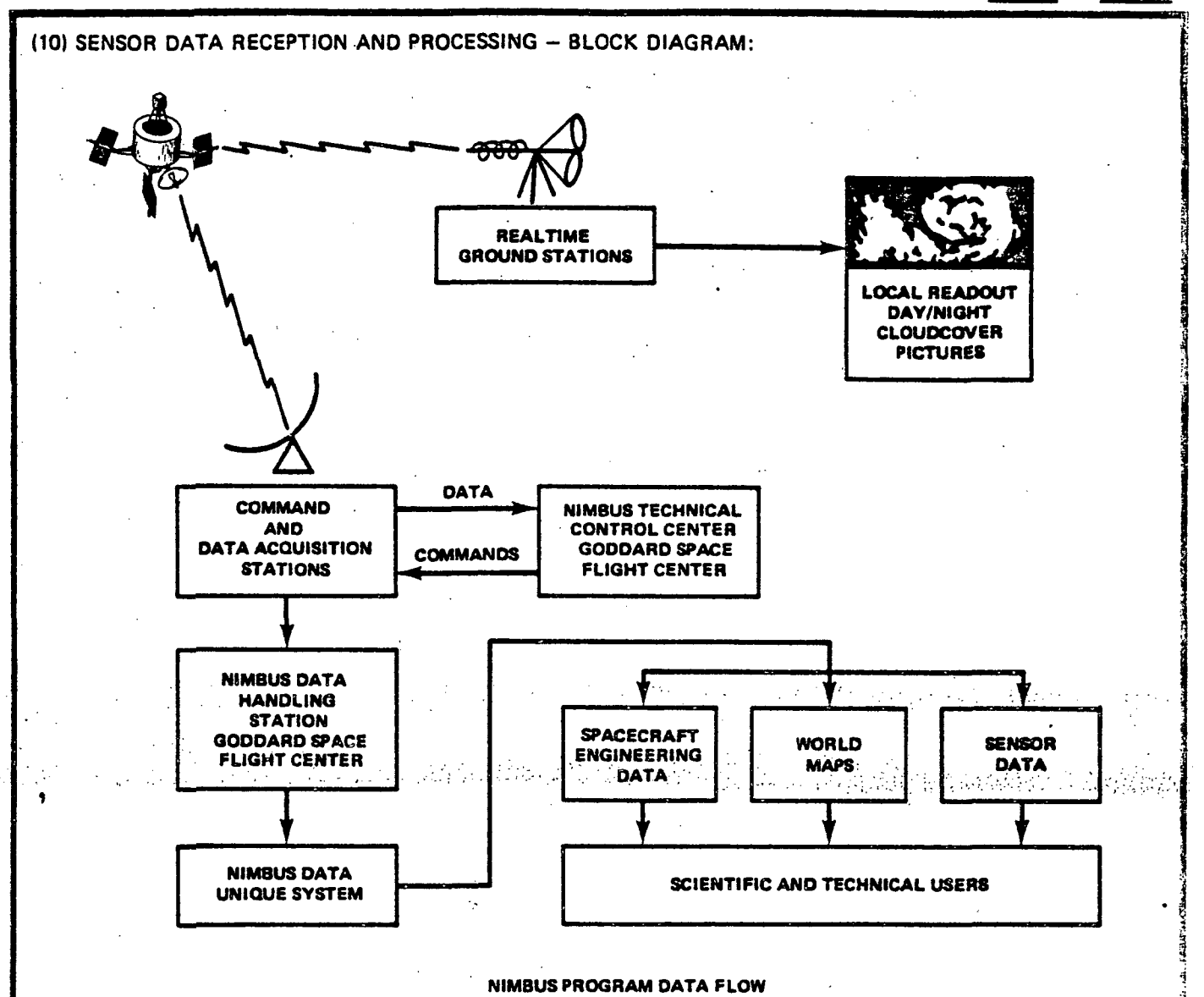
The high data rate ocean color sensor data (800kbs) are processed and stored for a portion of the orbit (approximately 10 minutes). Input and output cross-strapping provides alternate signal routing in the event of failure of a tape recorder or transmitter. The routing of CZCS data through the NIMBUS-G onboard system is illustrated in the block diagram above.

The ZIP is part of the data processor subsystem (DAPS), which is the primary communication system for observatory data. The ZIP is a special purpose processor for handling CZCS sensor data. In general, the ZIP multiplexes the six channels of CZCS digital radiometric data, removes nonsensible data, gates-in calibration and synchronization data, and compresses the resulting output to a rate compatible with the spacecraft tape recorders and S-band transmission system.

Separate ground data handling equipment will be used to process or display VIP, and CZCS data for evaluation purposes.

SECTION NO.: 5.7 SENSOR CATEGORY: Imaging Spectroradiometers

REV. NO.: 2 REV. DATE: 31 Jan 1978



### (11) RECEIVING AND PROCESSING - NARRATIVE:

The data from CZCS will be received via the NIMBUS Program Data Flow, illustrated above, and will be processed with algorithms developed from field experiment data to produce maps of chlorophyll absorption.

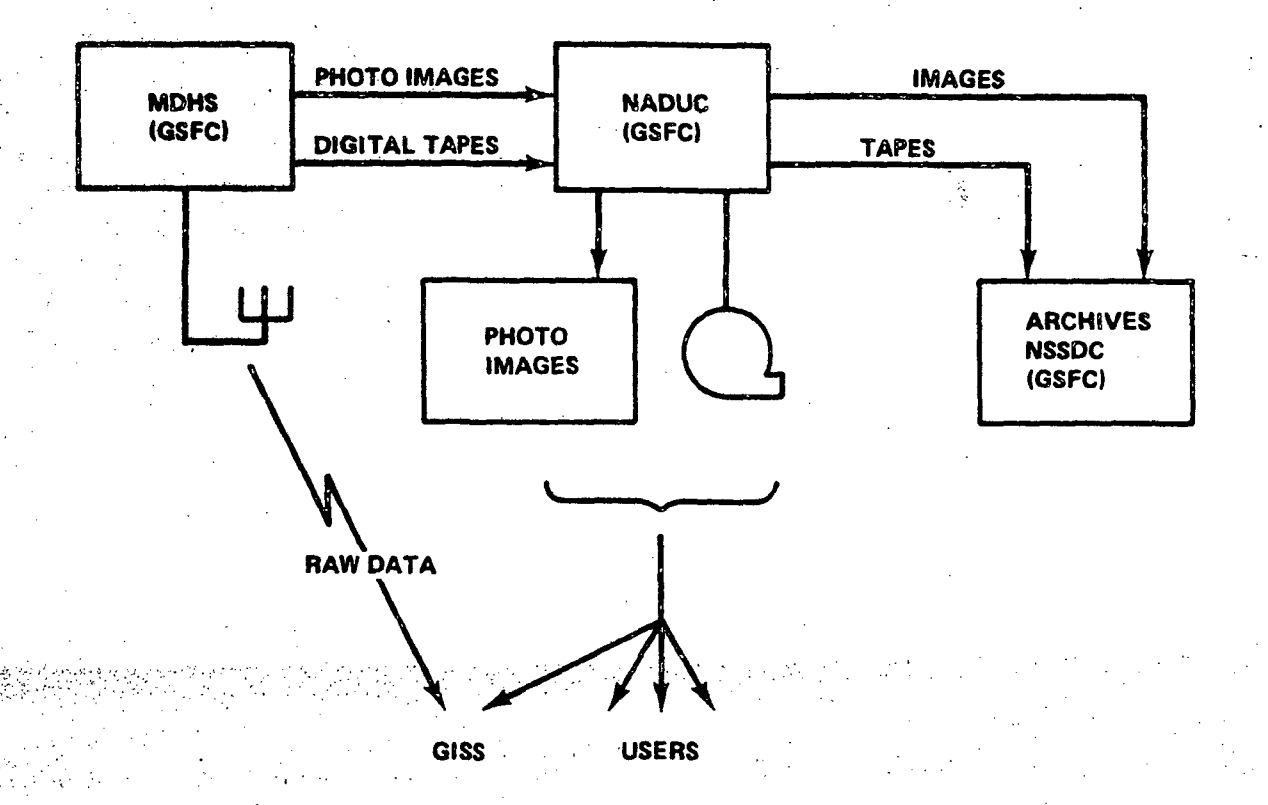
SENSOR CATEGORY: SECTION NO .: 5.7

Imaging Spectroradiometers

5.7.81

REV. NO .:

### (12) DISTRIBUTION OF DATA FROM GROUND STATIONS - BLOCK DIAGRAM:



#### (13) DATA DISTRIBUTION - NARRATIVE:

NIMBUS Program Data is distributed by the NADUC at GSFC. The following functions are generally performed for NIMBUS data users:

- · Accounts for and distributes experiment data processed by the MDHS
- · Processes all photographic data through to archival products
- Reproduces and distributes photographic data to NASA-approved users
- · Provides special technical services to the experimenters and data users
- · Maintains a complete photographic data reference file

SECTION NO.: 5.7 SENSOR CATEGORY: Imaging Spectroradiometers

REV. NO.: 2 REV. DATE: 31 Jan 1978

### RSDH DATA SHEET

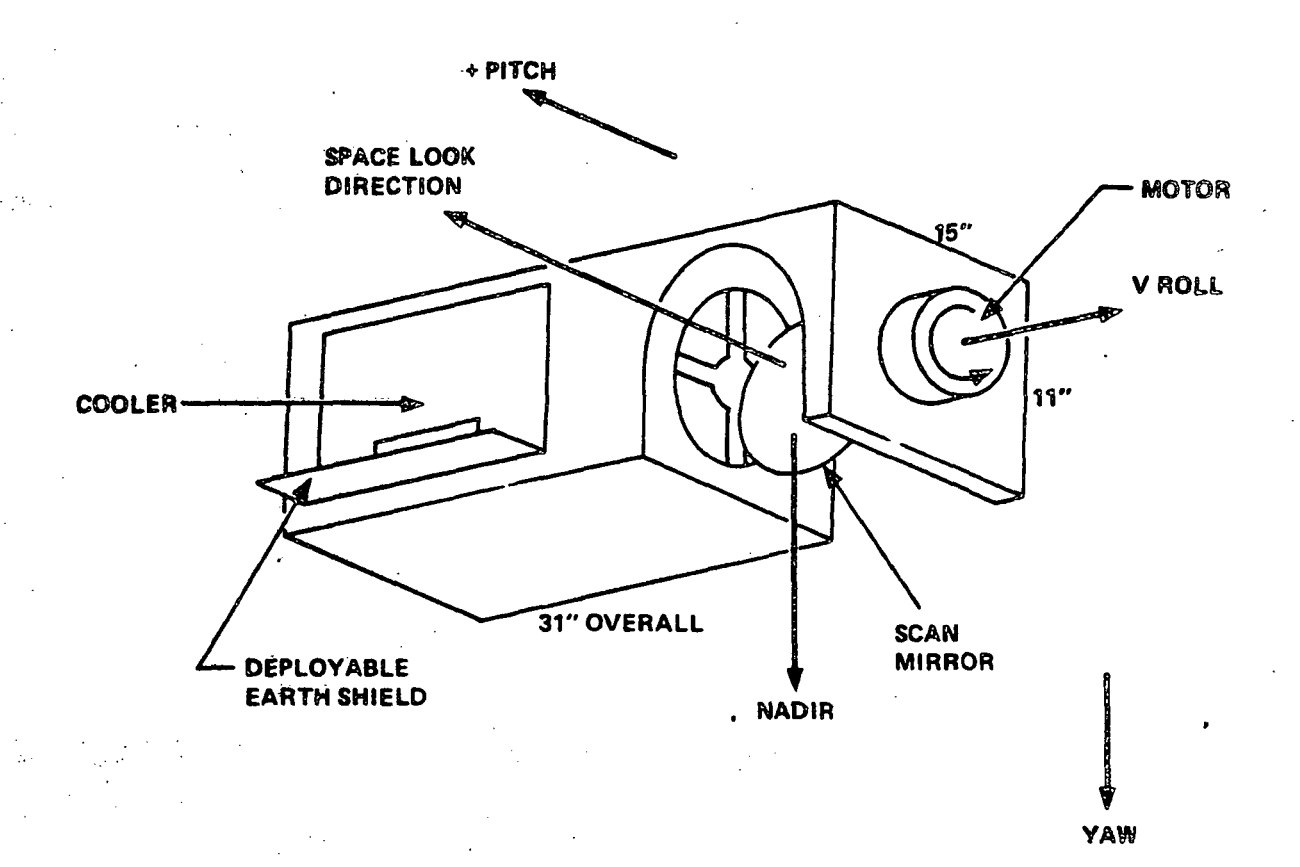
CULET 1 OF A					
	4	)F	1	ET	SHE

			SHEET 1 OF 4
(1) SENSOR NAME, ACRONYM	: Advanced Very High	n Resolution Radio	meter (AVHRR)
(2) DISCIPLINE: Earth Obse			Atmospheric Monitoring
(4) APPLICATION AND OBJEC	TIVE:		·
	ing high resolution	radiometry for de	l have night and day termining sea surface
(5) HERITAGE/KEY PERSONN The AVHRR is an exte	· -	own on ITOS missi	ons.
Principal Investigat	or: Dr. A. Arking,	TIROS Office, GSF	C
(6) SENSOR DEPLOYMENT:			
The AVHRR is to be d first quarter of 197 sun-synchronous, 98.	8. The AVHRR will b	e deployed at an a	ed for launch during the altitude of 830 km in a 100 minutes.
(7)	SENSOR CHA	RACTERISTICS	
scope. The various	channels are separat etectors utilize HgO	ed with dichroncis	front of a common tele- s and defined with filters cooling. The visible
(7B) ACTIVE SOURCE CHARA	CTERISTICS (FOR ACTIVE	SENSORS):	
Not Applicable.			
			•
	hannels as follows: 4) 10.5 - 11.5µm. T 3mrad² and a scan ra	he AVHRR will have te of 360 RPM. Du	, (2) 0.72 - 1.0µm, e an Instantaneous Field uty cycle will be con-
·			
SECTION NO.: 5.7	SENSOR CATEGORY: In	naging Spectroradio	ometers

5.7-83

**REV. NO.:** 2

### (8) SENSOR DATA MEASUREMENT AND TRANSMISSION SYSTEM - BLOCK DIAGRAM:



### (9) MEASUREMENT AND TRANSMISSION SYSTEM - NARRATIVE:

IR channels look at on-board calibration target built into instrument. No onboard visible calibration targets are provided. High and low resolution downlinks are provided. Data averaging done on spacecraft for low resolution information.

**SECTION NO.:** 

5.7

SENSOR CATEGORY: Imaging Spectroradiometers

5.7.84

REV. NO.:

#### RSDH DATA SHEET

SHEET 1 OF 6

(1) SENSOR NAME, ACRONYM: Large Earth Survey Telescope (LEST)

(2) DISCIPLINE: Earth Observations

(3) SUBDISCIPLINE: Land/Atmospheric Monitoring

### (4) APPLICATION AND OBJECTIVE:

LEST is a conceptual future system for providing multispectral imagery, atmospheric sounding and data collection for earth resources and meteorological applications. Since from its synchronous orbit position, the LEST maintains a constant position with respect to earth, sites of interest may be viewed on command, continuously or repeatively. NOTE: All information refers to the "Full Up" configuration.

(5) HERITAGE/KEY PERSONNEL: This is a conceptual design and bears little resemblence to anything in existance. Elements of the design are found in the Space Telescope and the Thematic Mapper. Detailed planning is incomplete. Diagrams shown here are representative only. Milt Ritter, GSFC 301/982-4382.

#### (6) SENSOR DEPLOYMENT:

Deployed into geostationary orbit (35.9 x  $10^3$  km) over the equator at  $105^\circ$  West longitude. LEST is the primary sensor on the Synchronous Earth Observation Satellite (SEOS), planned for a mid-1980's launch by either Titan IIIe or Shuttle/ Tug Combination.

(7)

#### SENSOR CHARACTERISTICS

#### (7A) CAPABILITIES AND CONSTRAINTS OF THE SENSOR TO ACQUIRE THE MEASURED PARAMETER:

The telescope used with the detector system is a 1.4 meter diameter f/1.5 Cassegrain having a primary constructed of ultra low expansion (ULE) material, using eggcrate techniques. Telescope pointing and E-W scan is provided by spacecraft motion produced by control moment gyro (CMG). N-S scanning is accomplished by pushbroom arrays in three different focal planes: f/5 for visible f/2 for two of the near-IR bands and f/1.3 for the far IR and one of the near-IR bands. In all, 22 bands are provided with simultaneous operation in up to ten bands. Switchable filters are

(7B) ACTIVE SOURCE CHARACTERISTICS (FOR ACTIVE SENSORS): N/A 7(A) Continued: provided to allow operation in alternate modes; e.g., Earth Resources and Meterological. Ground resolution element size for visible bands is 100 meters and 1000 meters for thermal bands. A non-imaging 23-channel atmospheric sounder is also incorporated.

### (7C) DETECTOR MEASUREMENTS CHARACTERISTICS:

Four different detector materials are utilized in linear arrays composed of discrete detectors, sequentially interrogated by integrated CCD switches or by hybrid devices. The material used for the visible band is Silicon (Si). Lead Sulfide (PbS) and Indium Antimonide (InSb) are used for the near-IR bands and Mercury Cadmium, Telluride (HgCdTe) is used for the thermal IR bands. One of the InSb arrays and the HgCdTe arrays are cooled to 110°K by passive radiative cooler. Optical bandpass is limited by filters mounted in arrays and can be selected on command.

5.7-87

SECTION NO .:

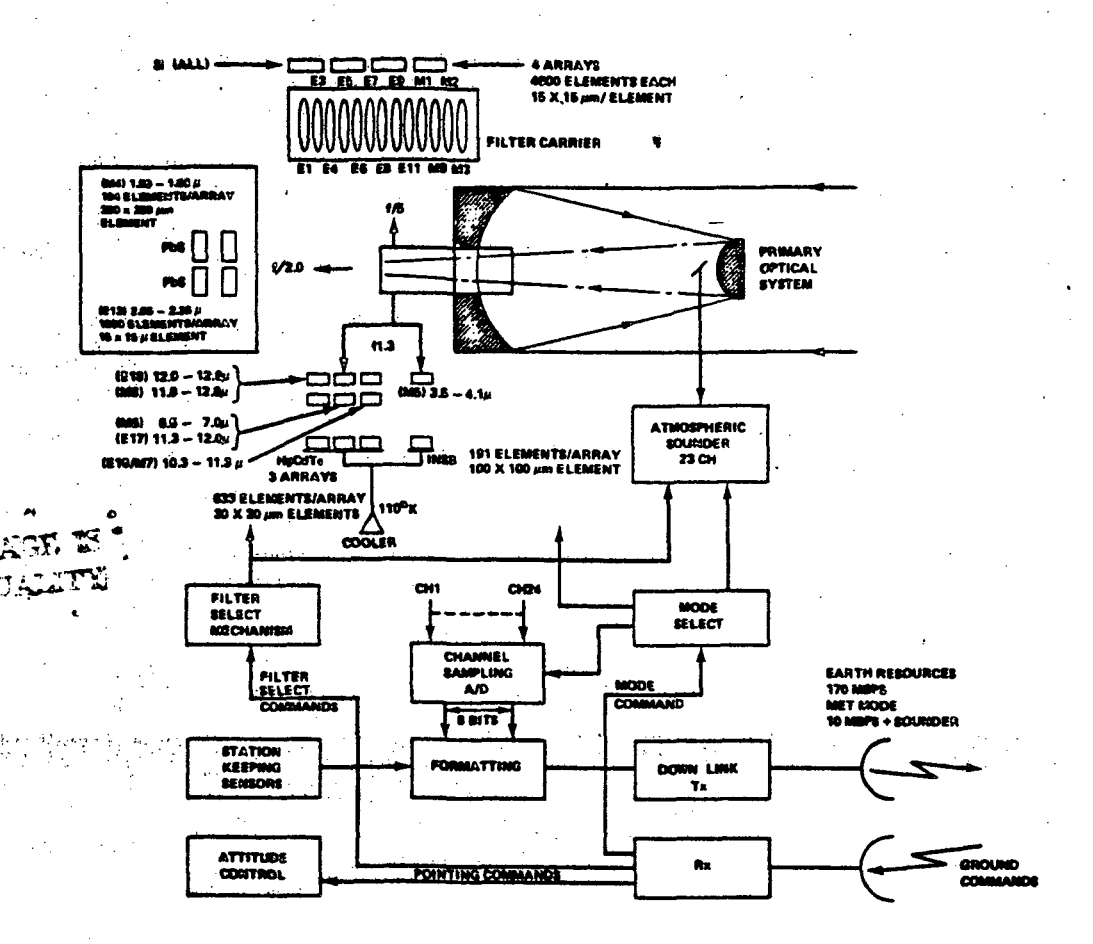
5.7

SENSOR CATEGORY:

Imaging Spectroradiometers

REV. NO.:

### (8) SENSOR DATA MEASUREMENT AND TRANSMISSION SYSTEM — BLOCK DIAGRAM:



### (9) MEASUREMENT AND TRANSMISSION SYSTEM - NARRATIVE:

The LEST combines 22 channels of imaging optics in the visible and infrared and an atmospheric sounder. For imaging, three different images are formed in different focal planes. Five different kinds of pushbroom arrays, constructed of four different detector materials, scan the images. Narrow band filters are called up by ground command as appropriate to these modes of operation: (a) earth resources, (b) meterological search, including 13-band IR sounder, (c) meterological monitor and (d) 23-band IR sounder. Not all bands are downlinked simultaneously. A maximum of 23 channels are sampled by the A-D converter. Available choices of combinations of channels along with the slew rates are summarized in Table 1.

5.7.88

SECTION NO .:

5.7

SENSOR CATEGORY:

Imaging Spectroradiometers

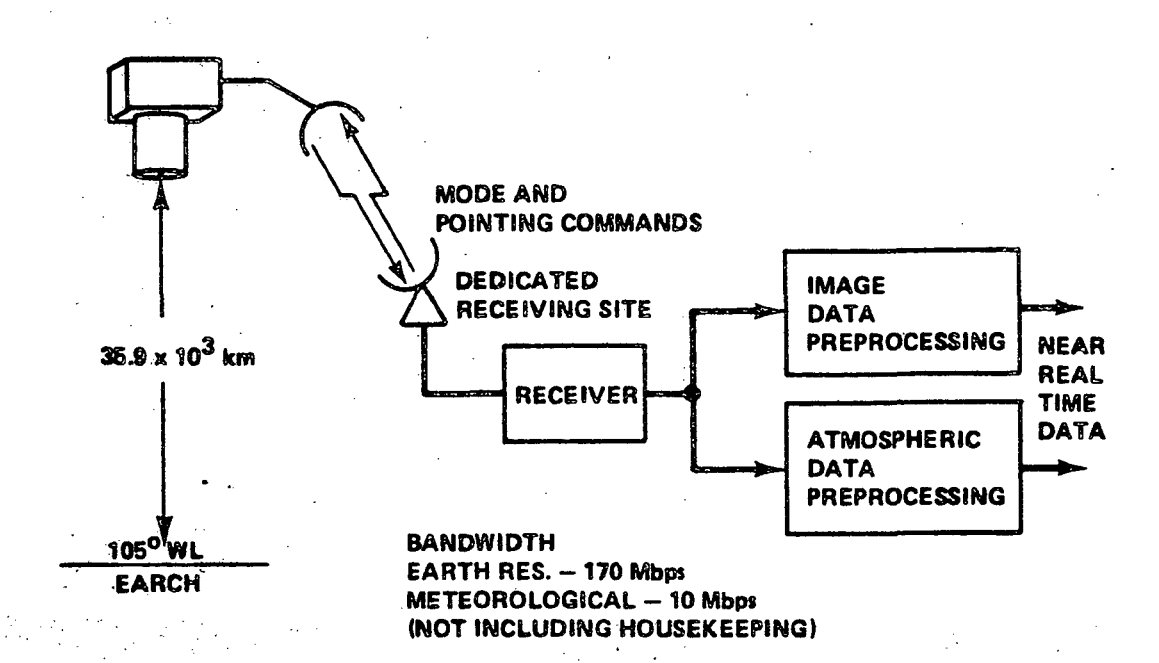
REV. NO.:

REV. DATE:

31 Jan 1978

<b>31</b>																				Sł	HE	<u> </u>	3	_	OF_	6	
	CONTINUATION	SHEE	T:	(9)	Cont	inu	ed				•					•								•			
	-0.		COOLER TO 110°K	ў. <del> —</del>			-		<del>-</del> 9	YES	YES	YES	9 9	?	<u></u>	2	9. S	7.10	ves	YES							
ri Ce	NALI FACE II OCR JAMES	¥.	SKEW RATE MR/SEC	K,N		·					-	K/X								3:1							
		METEOROLOGY (NON ITOR)	E1FOV (METERS)	N/A		-					-	N/A	2000	3	3000	300	3000	0007	1200	1200		•					
·			REQ	9.								2	<u>-</u>							YES						1	
	istics		SKEW RATE MR/SEC	N/A						-		۲,	-							<b>-</b> 0					:		•
	Characteristics	METEOROLOGY (SEARCH)	EIFOV (METERS)	N/A							-	N/A	0004	3	0009	009	0009	2,000	2400	2400		,	. •				
	Band C		REQ	શ્-							-	8 5	<u>-</u>					_		YES				•			
,	of	CES NS	SLEW RATE NR/SEC	2.2								2.2	ζ <b>~</b>							N/A							
	Summary	EARTH RESOURCES APPLICATIONS	EIFOV (METERS)	100				-	300	1000	1000	1000	<b>∀</b>			; · '	,	:	<i>:</i>	1 / N			₽÷.	,			
	-	_	REQ	-	SUNDS-	MOOA	λNV		YES.	YES	YES	YES	9 9	?	2	8	2 9	2 5	2 2	2							
	TABLE	, k	NAT'L	Si.					Si Pbs	HgCdTe	HgCdTe	НВСФТе	χ :	ភ	Si	Si	PbS	11130	HgCdTe	нвсете							
		ELEMENTS IN DETECTOR ARRA	S12E (MICRONS)	15		<del></del>	-		<del>-</del> -s	30	30	30	5 5	3 .	15	15	280	00.	R 8	3. 05							
	:		No.	4900					1960	653	633	633	1900	3	4900	4900	2 3	161	633	633	1						
			Į.	s <del></del>				->	ري در	1.3	1.3	1.3	us v	,	Ŋ	v	2 .	: :		1.3							
	·		PASS-BAND MICRONS	0.42-0.46	0.53-0.57	0.60-0.65	0.70-0.73	0.78-0.82	2.05-2.35	10.3-11.3	11.3-12.0	12.0-12.9	0.55-0.70	0.759	0.7617-	0.75-1.0	1.58-1.68	2.0.0	10.3-11.3	11.8-12.8							
			BAND	E3	ES E4	E6	E8	63	E11	E16	E17	E18	<del>=</del> =	<del></del>	¥	ξ.	¥ :	2 3	£ 5	<b>2</b>							
				V1S.	V1S.	715.	VIS.	VIS.	V.1S.	TIR.	TIR.	TIR.	V.1S.		V.1S.	V15.	NIR.	Y C	TIR	TIR.				•			
,	SECTION NO.:	5	. 7	SE	NSOF	R CA	TEG	OR	<b>Y</b> :	I	nag	in	g S	Spe	ctr	or	adi	on	net	ers							
,											RE	٧.	NO.	.:	2			R	EV	. D/	ATI	E:	31	Jan	19	78	

### (10) SENSOR DATA RECEPTION AND PROCESSING - BLOCK DIAGRAM:



### (11) RECEIVING AND PROCESSING - NARRATIVE:

The pointability of the sensor, in geostationary orbit, combined with the TIR capability, produce a high volume data generator capable of imaging phenomena in real-time in the Western Hemisphere on a continuous basis both day and night. Ground facilities capable of handling these data streams will be dedicated facilities. Pointing accuracy is ±1 km at the subpoint. Scanning is accomplished by alternate E-W, W-E scans as shown in Figure 1 (see continuation sheet 5/6).

SECTION NO .:

5.7

SENSOR CATEGORY:

Imaging Spectroradiometers

REV. NO.:

CONTINUATION SHEET: (11) Continued

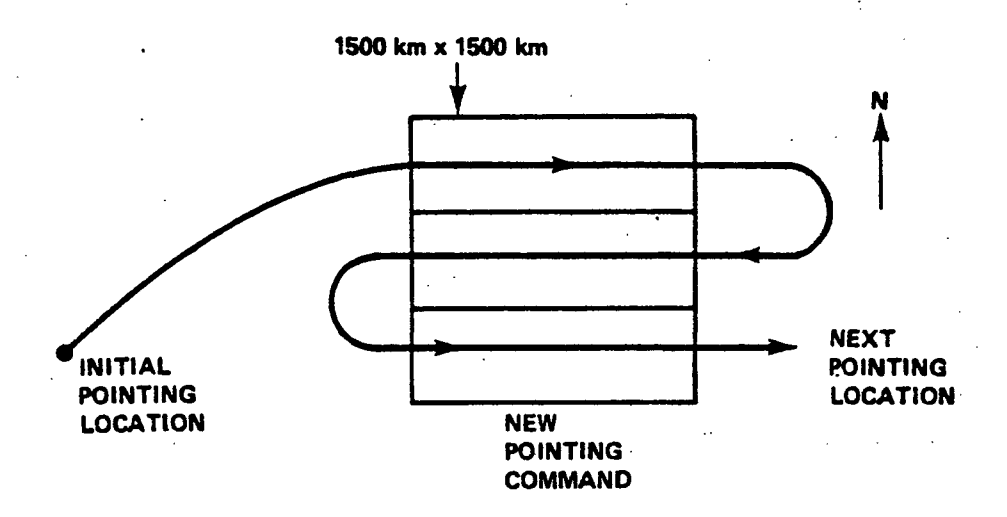


FIGURE 1 Pointing/Scanning Pattern of LEST

5.7.91

SECTION NO.: 5.7 SENSOR CATEGORY: Imaging Spectroradiometers

REV. NO.: 2 REV. DATE: 31 Jan 1978

(12) DISTRIBUTION OF DATA FROM GROUND STATIONS - BLOCK DIAGRAM:

This space intentionally left blank.

### (13) DATA DISTRIBUTION - NARRATIVE:

Planning of ground stations, image preprocessing and data product distribution is incomplete and unavailable at this time. For representative examples of the type of facilities which will be required, see the Thematic Mapper and VISSR/VAS data sheets.

5.7.92

**SECTION NO.:** 

5.7

SENSOR CATEGORY: Imaging Spectroradiometers

REV. NO .:

## SENSOR CATEGORY TABLE OF CONTENTS AND REVISION CONTROL SHEET

SENSOR NA	ME	NUMBER		EFFECTIVE					
OR OTHER ENT	RY	OF PAGES	PAGE NUMBER	REV. DATE	REV. NO.				
Section 5.8 Table of	Contents	3	5.8-i 5.8-ii 5.8-iii	31 JAN 78 31 JAN 78 31 JAN 78	2 2 2 2				
Introduction to Atmo	spheric Sounders	31	5.8-1 5.8-2 5.8-3 5.8-4 5.8-5 5.8-6 5.8-7	31 JAN 78 31 JAN 78 31 JAN 78 31 JAN 78 30 JUN 77 31 JAN 78 31 JAN 78	2 2 2 2 2 0 2 2				
			5.8-8 5.8-9 5.8-10 5.8-11 5.8-12 5.8-13 5.8-14 5.8-15	30 JUN 77 31 JAN 78 31 JAN 78 30 JUN 77 31 JAN 78 30 JUN 77 30 JUN 77 30 SEPT 77	0 2 2 0 2 0 0 0				
			5.8-16 5.8-17 5.8-18 5.8-19 5.8-20 5.8-21 5.8-22 5.8-23	30 SEPT 77 30 SEPT 77 30 SEPT 77 31 JAN 78 31 JAN 78	2 1 1 1 2 2 2 1				
			5.8-24 5.8-25 5.8-26 5.8-27 5.8-28 5.8-29 5.8-30 5.8-31	30 SEPT 77 31 JAN 78 31 JAN 78 30 SEPT 77 31 JAN 78 31 JAN 78 31 JAN 78 31 JAN 78	1 2 2 1 2 2 2 2				
Temperature/Humidity Radiometer (THIR)	Infrared	5	5.8-33 5.8-34 5.8-35 5.8-36 5.8-37	31 JAN 78 31 JAN 78 31 JAN 78 31 JAN 78 31 JAN 78	2 2 2 2 2				
Advanced Atmospheric Imaging Radar (AAS		11	5.8-39 5.8-40 5.8-41 5.8-42 5.8-43 5.8-44	31 JAN 78 31 JAN 78 31 JAN 78 31 JAN 78 31 JAN 78 31 JAN 78	2 2 2 2 2 2				
SECTION NO.: 5.8	SENSOR CATEGORY	: Atmospher	ic Sounders						
	5.8·i	REV. NO.:	2	REV. DATE: 31	Jan 1978				

## SENSOR CATEGORY TABLE OF CONTENTS AND REVISION CONTROL SHEET

SENSOR NAME OR	NUMBER OF	2005	EFFE	CTIVE
OTHER ENTRY	PAGES	PAGE NUMBER	REV. DATE	REV. NO.
		5.8-45 5.8-46 5.8-47 5.8-48 5.8-49	31 JAN 78 31 JAN 78 31 JAN 78 31 JAN 78 31 JAN 78	2 2 2 2 2
Vertical Temperature Profile Radiometer (VTPR)	6	5.8-51 5.8-52 5.8-53 5.8-54 5.8-55 5.8-56	31 JAN 78 31 JAN 78 31 JAN 78 31 JAN 78 31 JAN 78 31 JAN 78	2 2 2 2 2 2
Stratospheric and Mesospheric Sounder (SAMS)	6	- 5.8-57 5.8-58 5.8-59 5.8-60 5.8-61 5.8-62	31 JAN 78 31 JAN 78 31 JAN 78 31 JAN 78 31 JAN 78 31 JAN 78	2 2 2 2 2 2
Visible Infrared Spin-Scan Radiometer Atmospheric Sounder (VAS)	6	5.8-63 5.8-64 5.8-65 5.8-66 5.8-67 5.8-68	31 JAN 78 31 JAN 78 31 JAN 78 31 JAN 78 31 JAN 78 31 JAN 78	2 2 2 2 2 2 2
Microwave Atmospheric Sounding Radiometer (MASR)	5	5.8-69 5.8-70 5.8-71 5.8-72 5.8-73	31 JAN 78 31 JAN 78 31 JAN 78 31 JAN 78 31 JAN 78	2 2 2 2 2 2
High Resolution Infrared Radiation Sounder (HIRS)	n 4	5.8-75 5.8-76 5.8-77 5.8-78	31 JAN 78 31 JAN 78 31 JAN 78 31 JAN 78	2 2 2 2
Microwave Sounding Unit (MSU)	6	5.8-79 5.8-80 5.8-81 5.8-82 5.8-83 5.8-84	31 JAN 78 31 JAN 78 31 JAN 78 31 JAN 78 31 JAN 78 31 JAN 78	2 2 2 2 2 2
Stratospheric Sounding Unit (SSU)	. 4	5.8-85 5.8-86 5.8-87 5.8-88	31 JAN 78 31 JAN 78 31 JAN 78 31 JAN 78	2 2 2 2
SECTION NO.: 5.8 SENSOR CATEG	ORY: Atmospher: REV.NO.	<del></del>	EV. DATE: 31	Jan 1978

### SENSOR CATEGORY TABLE OF CONTENTS AND REVISION CONTROL SHEET

SENSOR NAME OR	NUMBER OF	PAGE	EFFE	CTIVE				
OTHER ENTRY	PAGES	NUMBER	REV. DATE	REV. NO.				
Scanning Multichannel Microwave Radiometer (SMMR)	5	5.8-89 5.8-90 5.8-91	31 JAN 78 31 JAN 78 31 JAN 78	2 2 2 2 2				
		5.8-92 5.8-93	31 JAN 78 31 JAN 78	2 2				
,			·					
•								
				·				
	·							
			·					
CTION NO.: 5.8 SENSOR CATEGOR	Y: Atmospher	ric Sounders						
5·8 - iii	REV. NO.:		EV. DATE: 31	Jan 1978				

This page intentionally left blank.

REV. NO.:

**REV. DATE: 30 Sept 1977** 

.

# Section 5.8 INTRODUCTION TO ATMOSPHERIC SOUNDERS

In 1959, Lewis D. Kaplan of the Massachusetts Institute of Technology wrote a paper which appeared in the Journal of the Optical Society of America in which the first suggestion was made that the temperature structure of the atmosphere could be inferred from radiation measurements. Soon after that, the literature reflected an abundant interest of some segments of the technical and scientific community in using radiation measurements made from a satellite to infer the distribution of temperature along a vertical line starting at the earth's surface and going up to 30-45 km. There is current interest in the region of the atmosphere up to 100 km. The obvious motivation for the majority of this interest is the study of weather phenomena on a world-wide basis. With rapid global coverage by satellites, the potential of studying the world-wide oceans of air currents that determine our weather is enormous. In this country and in other selected locations, measurements of the atmosphere can be made by radiosonde. It is apparent that these free-flying balloons routinely make direct, multi-parameter measurements of atmospheric properties to the 10 millibar level (> 30 km). However, on the two thirds of the globe which is covered by water and in some foreign countries, the network of sites from which radiosonde launchings are made is too course to produce the fine scale temperature reconstructions upon which numerical weather information is based. Geostrophic wind shear fields cannot be evaluated in these remote areas without the thermal gradient information. At this writing, instrument design has progressed to the point that intercomparisons of data derived from satellite and from radiosonde soundings are basically favorable. Horn et al [1] indicate that the use of these satellite data has the potential for producing significant improvement in numerical weather predictions, if the general characteristics and accuracy

REV. NO.: 2 REV. DATE: 31 Jan 1978

of the data are properly assessed. Imprudent mixing of satellite data with conventional data, it is claimed, can be counter-productive, offsetting any advantage provided by the additional data.

Many comparisons have been made [2] between satellite measurements and manual soundings. In one study, 150 pairs of radiosondes were released simultaneously within a distance of 100 km. RMS differences between pairs ranged from 1.3°C to 2.3°C in various layers between 1000 and 100 mb (SL-15000') [3]. The differences could be caused by several factors including small-scale atmospheric variability along the path of the rising balloons and minor differences in the instruments. Little significance, then, should be attached to differences between satellite soundings and radiosondes which are smaller than 2°C. On the other hand, more complete data comparisons that take into account vertical resolution and the impact of the data on models can be complicated and difficult to understand [1] [4]. It should be emphasized here that the method utilizing radiative properties does not measure specific temperatures at specific altitudes. Rather, a vertical temperature structure is inferred.

Remote soundings from satellites depend for the most part upon reradiation of solar energy by gasses which are uniformly distributed in the atmosphere. Carbon dioxide is known to be present in the atmosphere up to 30 km and uniformly mixed to within 1 or 2 percent. Its emission spectrum when viewed from above will depend only on the vertical distribution of atmospheric temperature [4]. In literature written primarily by Clark, Hilleary, Hanel, Conrath and Houghton, it has been illustrated that by 1970, the mean temperature of a 200 mb thick layer could be measured to within 2°K

The spectrum of solar radiation as it arrives at the surface of the earth is shown in Figure 5.8-1. Of the radiation which arrives at the earth's surface,

REV. NO.: 2

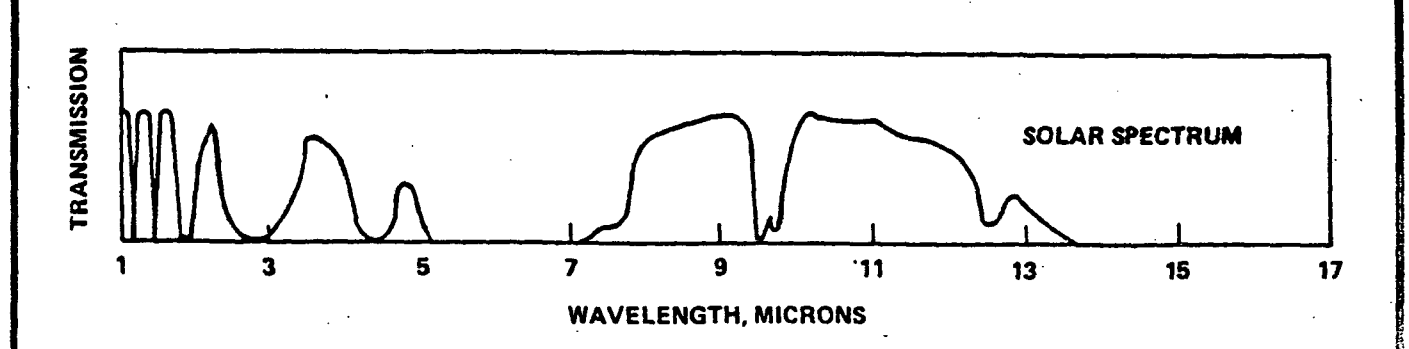


FIGURE 5.8-1 Solar Spectrum

approximately 45% is reflected back into space and 55% is absorbed by the earth to maintain its temperature. The earth acts essentially as a blackbody, and all of its emitted radiation is in the infrared and much of it in spectral regions where the atmosphere absorbs strongly. Much of it is thus absorbed by the atmosphere and is in turn re-radiated by the atmosphere in amounts depending upon the concentration and the temperature of the absorber. The absorber of interest here is CO<sub>2</sub>, the transmission characteristics of which are shown in Figure 5.8-2. As can be seen

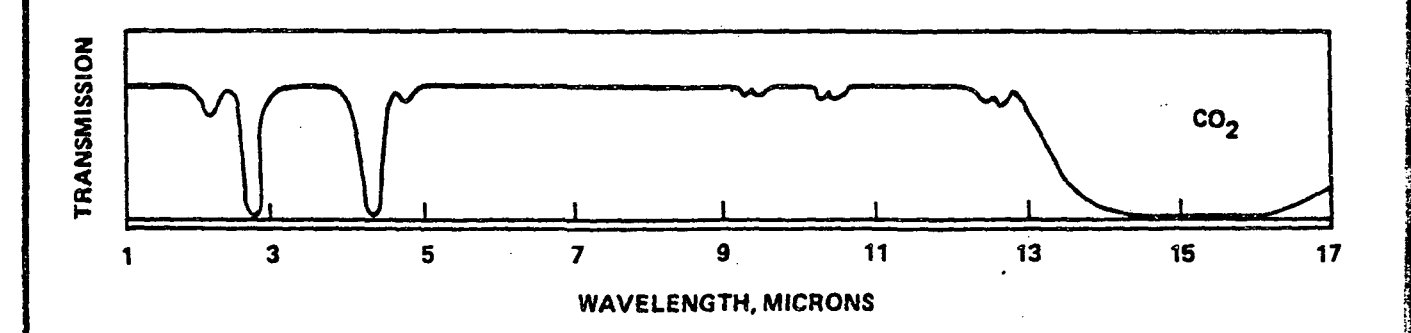


FIGURE 5.8-2 % Transmission -  $C0_2$ 

from the figure, the atmosphere is essentially opaque in a narrow band centered at about 15  $\mu$ m. As viewed by a satellite, the Earth's radiation is represented by Figure 5.8-3.

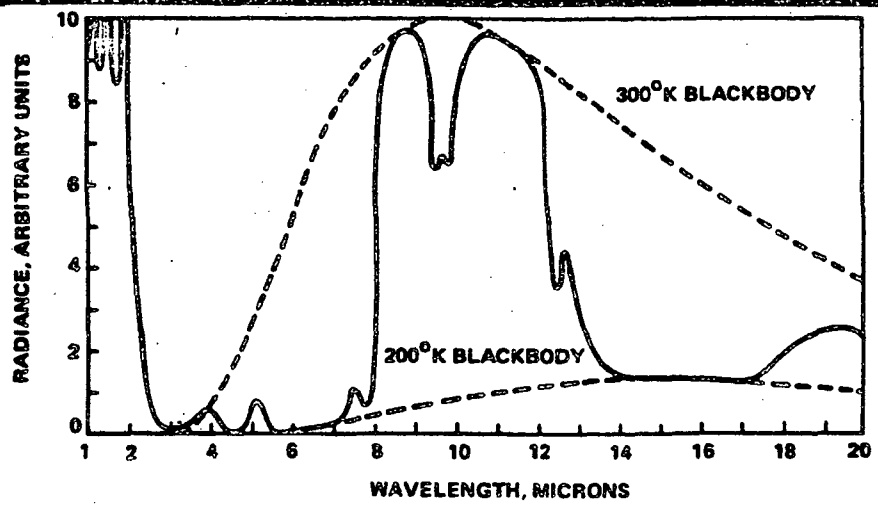


FIGURE 5.8-3 Earth's Radiation as Viewed by a Satellite

The principle upon which the inference is based can be understood by considering an atmosphere of uniformly distributed absorptive gas (in this case (CO<sub>2</sub>) which is horizontally stratified and in thermal equilibrium as shown in Figure 5.8-4.

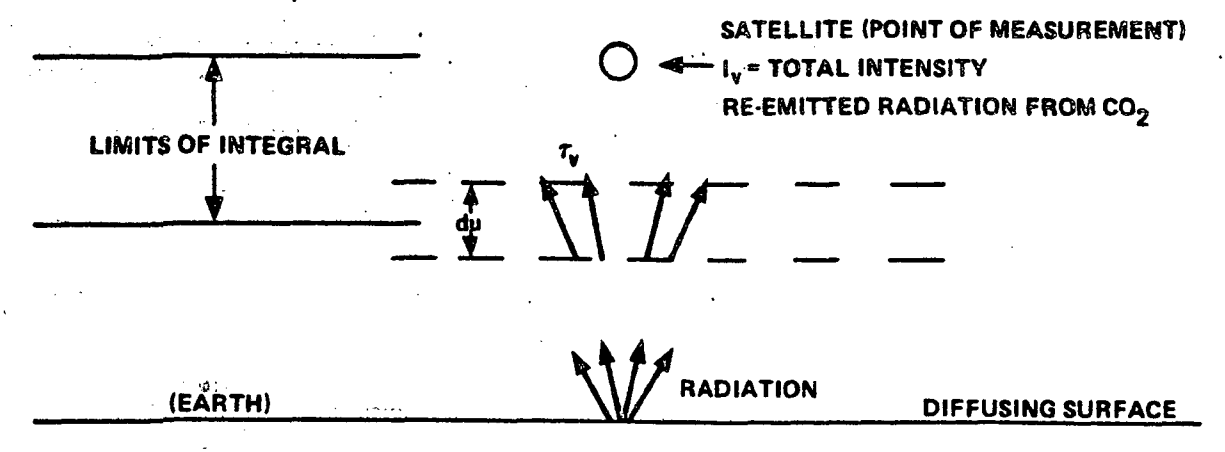


FIGURE 5.8-4 Earth Radiation and Atmospheric Absorption Viewed by a Satellite

At the spectral frequency v where the absorption coefficient is  $K_V$ , Kirchoff's Law states that the emitted intensity from the slice shown in Figure 4 in the vertical direction will be

 $K_{v}duB_{v}(T)$ 

where  $B_V$  = Planck function at frequency v and temperature T. Of this radiation, a portion  $\tau_V$  will reach the top of the atmosphere.

REV. NO.: 2 REV. DATE: 31 Jan 1978

$$\tau_{\mathbf{V}} = \exp \left(-\int K_{\mathbf{V}} d\mathbf{u}\right)$$

The limits of the integral in this expression are from the slice to the top of the atmosphere.

If we integrate over all such slices to determine the total radiation (I) at frequency v reaching the top of the atmosphere, we have:

$$I_{V} = \int B_{V}(T) K_{V} du \exp(-\int K_{V} du)$$

$$= \int_{0}^{1} B_{V}(T) d\tau_{V}$$

$$\tau_{V} = 0$$

It is convenient to use an altitude dependent variable y = -ln p where p is the pressure in atmospheres. In this case:

$$T_{V} = \int B_{V}(T) \frac{d\tau_{V}}{dy} dy$$
$$= \int B_{V}(T) K(y) dy$$

In other words,  $I_V$  is the weighted average of the blackbody intensity, the weighting function K(y) being  $\frac{d\tau_V}{dy}$ . It can be demonstrated that the radiation of a given wavelength reaching the top of the atmosphere is distributed in elevation according to a curve similar to that shown in Figure 5.8-5. In the example shown, it can be

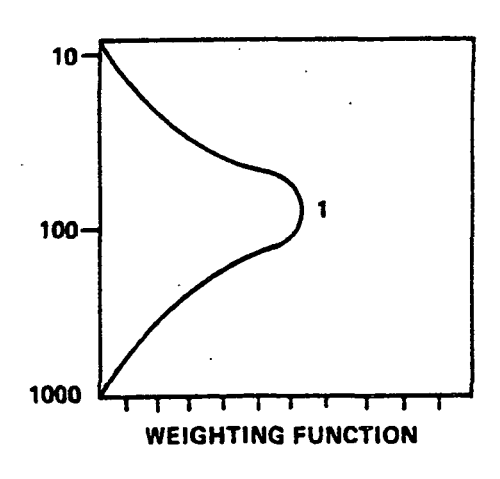


FIGURE 5.8-5 Weighting Function

REV. NO.: 0 REV. DATE: 30 June 1977

seen that the majority of the radiation of the particular wavelength reaching the top of the atmosphere originated at the 100 mb level or about 16 km. Had another wavelength been chosen, the majority of the radiation reaching the top of the atmosphere would have originated at some other altitude. To further illustrate this, refer to Figure 5.8-6. Here are illustrated the vertical distributions of radiation at six different wavelengths as viewed from the top of the atmosphere.

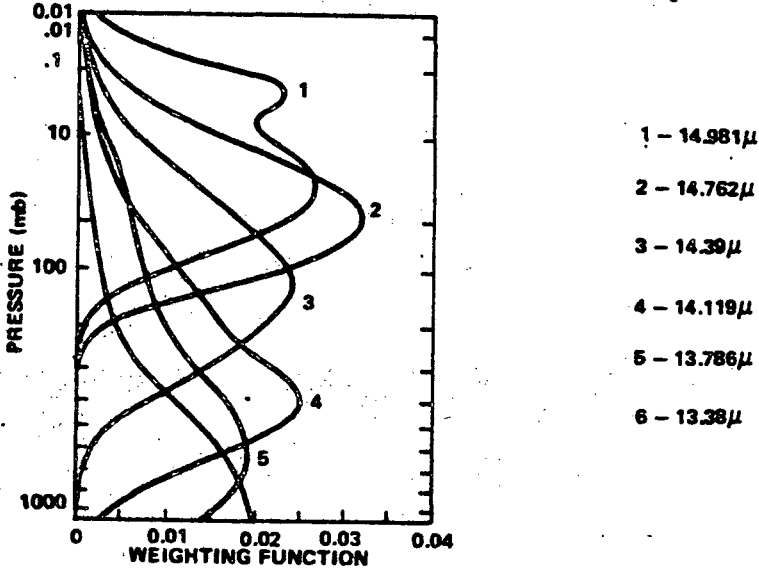


FIGURE 5.8-6 Weighting Functions at Several Wavelengths

The flux F (W Cm $^{-2}$ Sr $^{-1}$ ) incident on a radiometer sensitive to a narrow spectral interval  $\Delta$  v centered at frequency v can be related to an equivalent radiometric temperature T by the relation

$$F = Bv (T) \Delta v$$

where Bv(T) is the Planck function appropriate to frequency v and temperature T. In order that T be derived with a maximum error of 1°K, if we are dealing with CO<sub>2</sub> in the 15 µm band, F must be measured with a maximum error of about 1%. If errors are greater than these (particularly the relative errors between different spectral channels) serious degradation of the information content of the measurements will result [4].

REV. NO.: 2 REV. DATE: 31 Jan 1978

For measurements in upper atmosphere, the weighting functions must be well defined. This can be enhanced by selecting observed spectral regions where the absorption coefficient of the gas whose emission is being observed is as nearly uniform as possible.

The device for limiting the spectral input to the various detectors (filters, grating, etc.) must be reasonably narrow spectral bandwidth (of the order of 2000 angstroms). An argument can be made [5] [6] that measurements of five or six channels are required to adequately describe the atmospheric temperature profile up to 50 under cloud-free conditions, and that additional channels add little except when used to assess cloud cover, or to describe the water vapor level. In addition, the measurements made in the several channels must be acquired from the same field of view.

Objects whose temperature is above absolute zero radiate microwave energy in addition to the radiated infrared. As a result, the rationale developed above can be applied to microwave frequency as well as to optical frequencies and a set of weighting function curves similar to Figure 5.8-6 can be developed in the microwave frequencies. One band which is in use in the 60 GHz (5 mm wavelength) 0<sub>2</sub> absorption band. The advantage of using microwave is that coverage can be obtained under all weather conditions and frequency discrimination is simplified. Current remote sensors for temperature profile work are combining microwave channels and optical channels help in solving the anomolies caused by cloud cover.

An illustrative sample of a simple VTPR designed for use on early ITOS vehicles is shown diagramatically in Figure 5.8-7. It viewed earth in the nadir direction from the stabilized vehicle in eight optical channels. Six are in the 15  $\mu$ m CO<sub>2</sub> band, as described above, one channel is in the rotation band of water vapor at 5.7 microns for cloud detection and one is in the atmospheric window at 11.12

REV. NO.: 2 REV. DATE: 31 Jan 1978

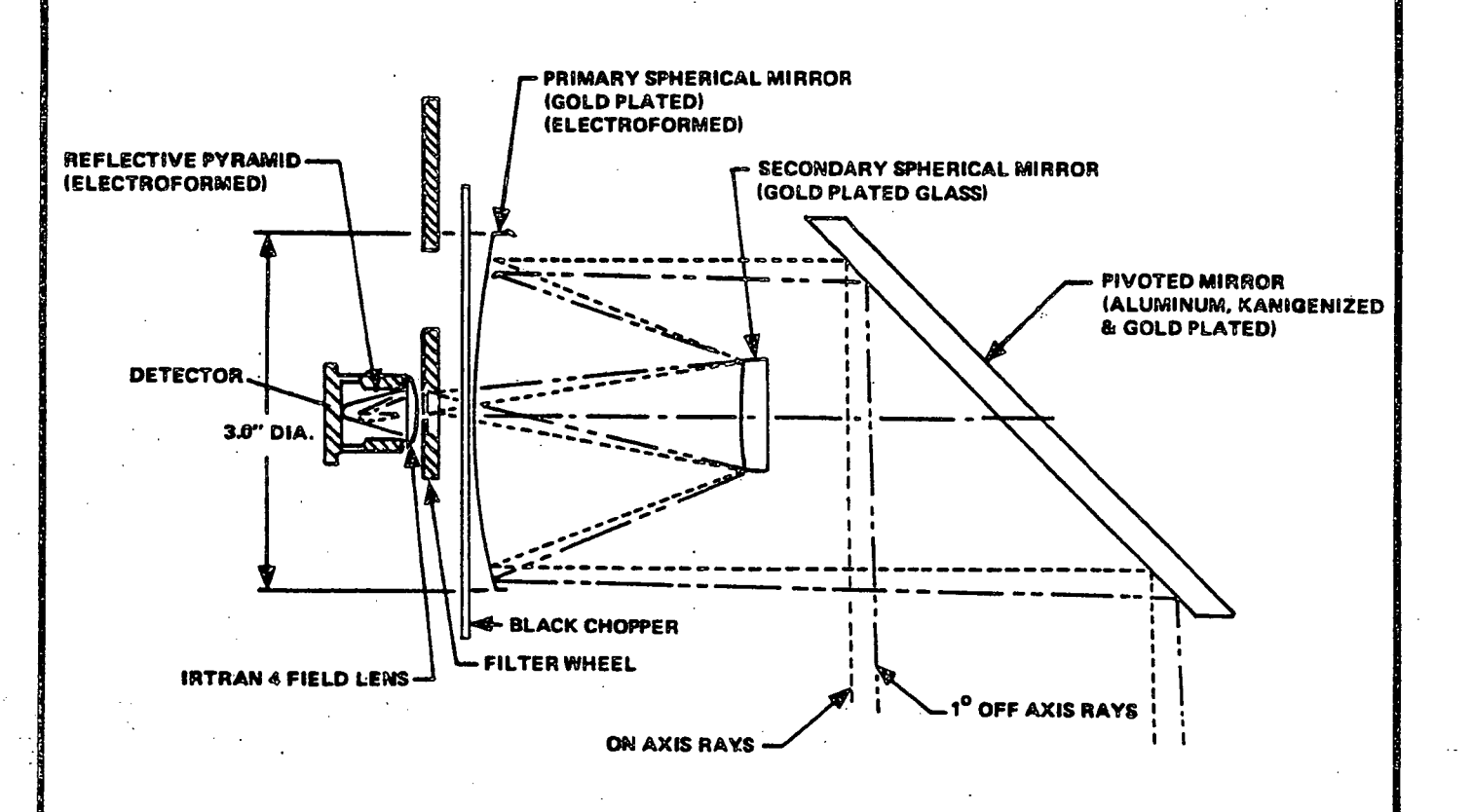


FIGURE 5.8-7 ITOS VTPR - Optical Layout

microns for detection of the surface temperature. The wavelength intervals and widths are determined by the characteristics of interference filters mounted on the rim of a wheel rotating at 60 RPM. The advantage of using the single detector and changing filters is that relative measurement accuracy between channels is a constant and detector calibration considerations are minimized. In operation, a column of the atmosphere is viewed by an f/3 folded telescope of 2.6 inch diameter sequentially through the eight filters on the wheel. A chopper wheel mounted directly in front of the detector chops the radiation at a rate which is high compared to the filter rate. The pulsating voltage thus generated at the output of the detector is transmitted to earth using digital telemetry. The field stop

REV. NO.: 0 REV. DATE: 30 June 1977

which limits the radiation arriving at the detector is sized to provide a 2.2° field of view which is scanned beneath the satellite by an oblique mirror.

Measurements are averaged over eight cycles which, together with satellite motion, gives the instrument an equivalent of 4° FOV in the along-track direction. The power consumption of this ten pound instrument is two watts. The accuracy of spectral radiance measurements is 0.5%.

Sounders can be implemented on both geosynchronous and polar orbiting satellites. Polar orbiting sounders scan cross-track to collect measurements along a line about ±700 km from nadir. The forward motion of the spacecraft provides the along-track progression of the scan. Each orbit a 1400 Km wide swath around the earth is sounded, providing total earth coverage each 12 hours. (Depending on the cross-track scan width, there may be small gaps in the coverage at the equator.) Current polar orbiting sensors are in view of each ground station for about 20 minutes of each 2 hour orbit. Future polar satellites will use geosynchronous communication satellites to lengthen communication time with ground stations. Data rates from polar orbiting sounders are less than 1000 bits per second. Geosynchronous satellites are limited by the resolution they can achieve at their high altitudes (35,000 km). However, the fact that they are stationary relative to a point on the earth allows them longer integration periods, improving the signal to noise ratio and compensating for the altitude. The determining of accurate geographic position of geosynchronous soundings requires a highly stable spacecraft with precise attitude control. Geosynchronous systems now being planned will use earth landmarks to achieve geographical locating accuracy of less than 1 km. The geosynchronous sensors have more flexible scanning capability than polar orbiters. Commands from ground allow the user to immediately look at a selected geograph ic area on the earth at a selected repetition frequency. (Coverage is limited to the

REV. DATE: 31 Jan 1978

2

earth disk in the view of the satellite.) The resolution of the satellite decreases rapidly as the sensor is scanned off the subpoint. (Maximum coverage is about 40° lat.) In general, the scanning and temporal flexibilities of the geosynchronous sensors give them an advantage when monitoring current weather development for storm warning and mesoscale forecasting, while global coverage provided by the polar orbiting satellites is valuable for synoptic weather monitoring and prediction.

Data rates produced by the sounding sensors are low compared to imaging devices. The existing polar orbiters produce about 12,700 measurements per orbit and require about 1 1/2 hours of 360/195 computer time to produce about 3000 soundings each day. With improved resolution to 25 km (which appears to be the highest resolution required by the users) the data rates and processing requirements would increase by a factor of four, still well under today's data rates for imaging radiometers. Geosynchronous satellites which have the potential for resolution finer than 25 km are probable candidates for monitoring severe storms. But as resolution is increased, integration time can be expected to increase and the data rates would decrease. The integrated signals are transmitted to the ground for processing into atmospheric soundings. Ground processing procedures for both geosynchronous and polar orbiting sounding data satellites are similar.

Figure 5.8-8 is a block diagram of the ground processing required to generate atmospheric soundings. An ingest program receives, error-checks and formats the data transmitted from the sensor. The raw data is normally recorded as it is received and the ingest system has the capability to play back the recorded data into the normal data processing paths. Most of the sounders perform calibration

<sup>&</sup>lt;sup>1</sup>The assumption is made that integration of the signal over time is performed on board the spacecraft.

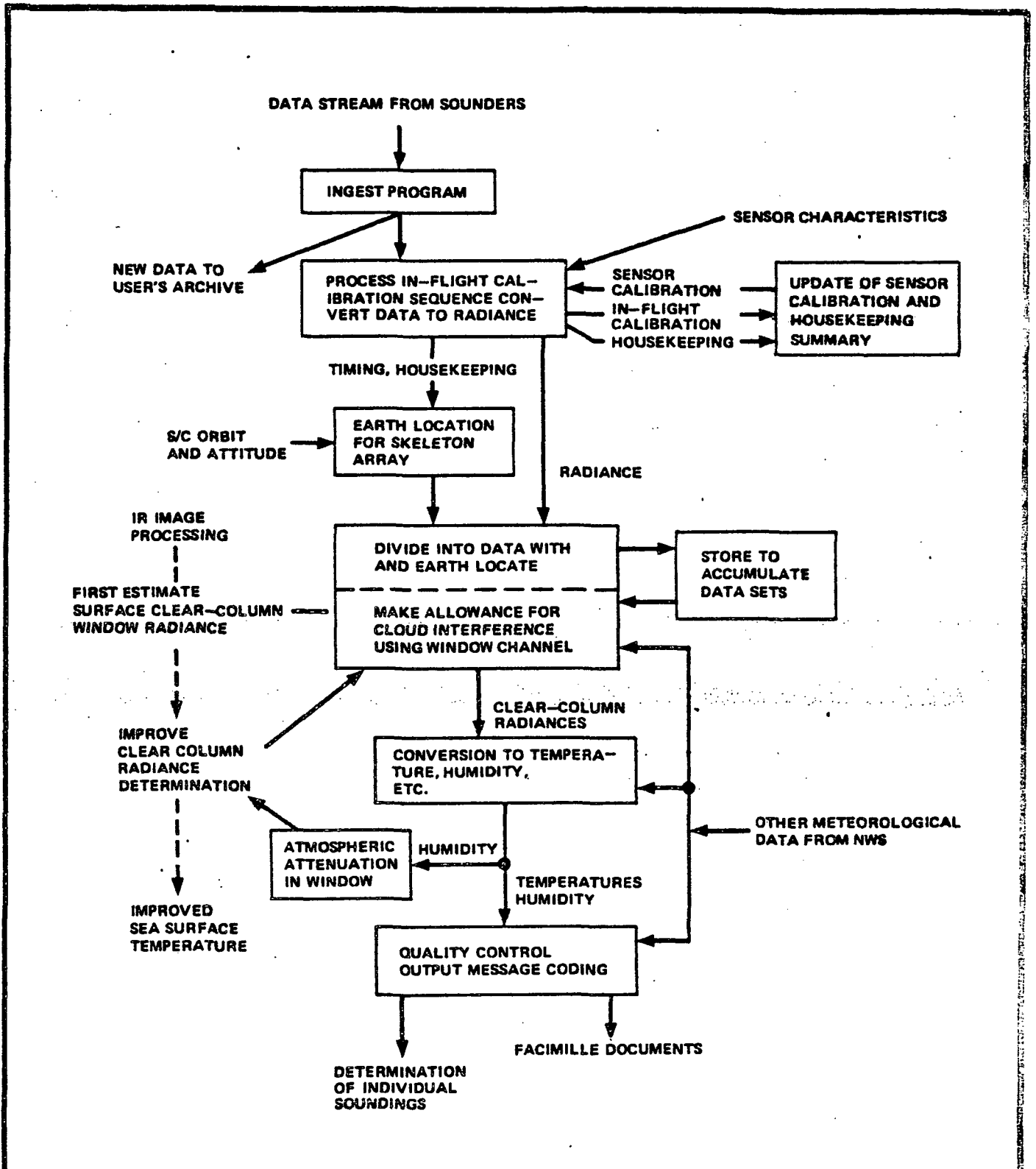


FIGURE 5.8-8 Outline data flow for analysis of sounding data. In the case of data from a polar orbiting spacecraft, orbit and attitude data will be made available from external sources.

**REV. NO.:** 

0

**REV. DATE: 30 June 1977** 

measurements at regular intervals, normally once per scan. In most cases, space is viewed to get a cold temperature measurement and an interior object is viewed to get a known warm temperature. These measurements are multiplexed into the data stream. These calibration data along with other calibration data determined before launch, are used to adjust the voltage readings for variances between detectors (detector bias) or spectral channel variations. The adjusted raw voltages more consistantly and accurately represent the actual radiation sensed by the detector sensor in each spectral band. These voltages can be converted to radiances by the application of a matrix of coefficients.

The measurements are geographically located to the earths surface using altitude and orbit parameters of the spacecraft. Normally time information is transmitted with the sounding data to allow the ground system to determine the position of the spacecraft for each measurement. For geosynchronous satellites, image data landmarks will be correlated with soundings and used to locate the satellite IFOV on the earth.

The ground processing system uses a matrix of measurements (8 x 8) to generate each sounding. The matrix smooths the reading of the individual radiance profiles and helps relieve the problem of cloud cover. Current sounders, operating in the IR spectrum, cannot penetrate solid, opaque clouds. While they can penetrate light clouds and broken clouds, the clouds will bias the radiance profile toward the cold temperature associated with their altitude. The procedure for adjusting for partial cloud cover is based on two principles:

- (1) the radiance in a column is a linear function of the cloud amount in that column (within limits), and
- (2) the magnitude of the effect of partial clouds is dependent upon and unique to spectral band.

A graph is plotted of the values of intensity (I) for a window channel vs. the intensity received in a second spectral channel from the same IFOV's. Where the the changes in intensity are due only to cloud cover variations, the plotted points will define a straight line (see Figure 5.8-9). Using a first guess temperature profile and a surface temperature measurement, the theoretic clear-atmosphere radiance is computed for the window channel. This window channel radiance defines a point on the plotted line that gives the corresponding clear-atmosphere radiance for the second spectral channel.

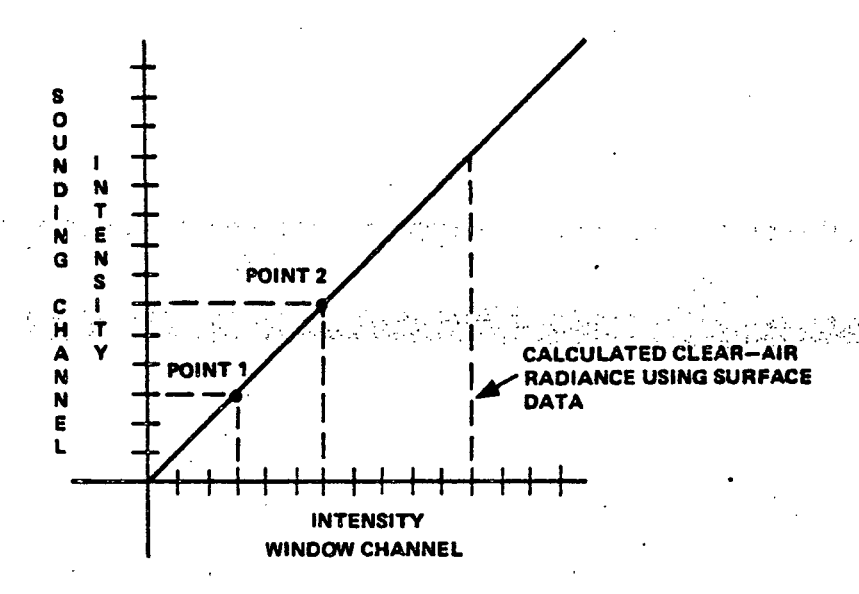


FIGURE 5.8-9 Technique for Calculating Clear Atmosphere Radiances

A second technique can be used to eliminate the need for the first guess profile values and the surface temperature. Two measurements are taken in each of two window channels and the straight line is plotted as in the previous method. For these window channels, a plot is generated of the intensities produced in each channel by identical brightness temperatures of an opaque surface. (The Planck Function values of the waves.) The point of intersection of the straight line and the Planck Function is the value corresponding to clear column measurement of the

REV. NO.: 0 REV. DATE: 30 June 1977

surface (see Figure 5.8-10). Line plots of each sounding channel vs. the window channel can then be developed and the clear column values determined for the window channel can be used to determine the clear column values on the sounding channels as in the first method.

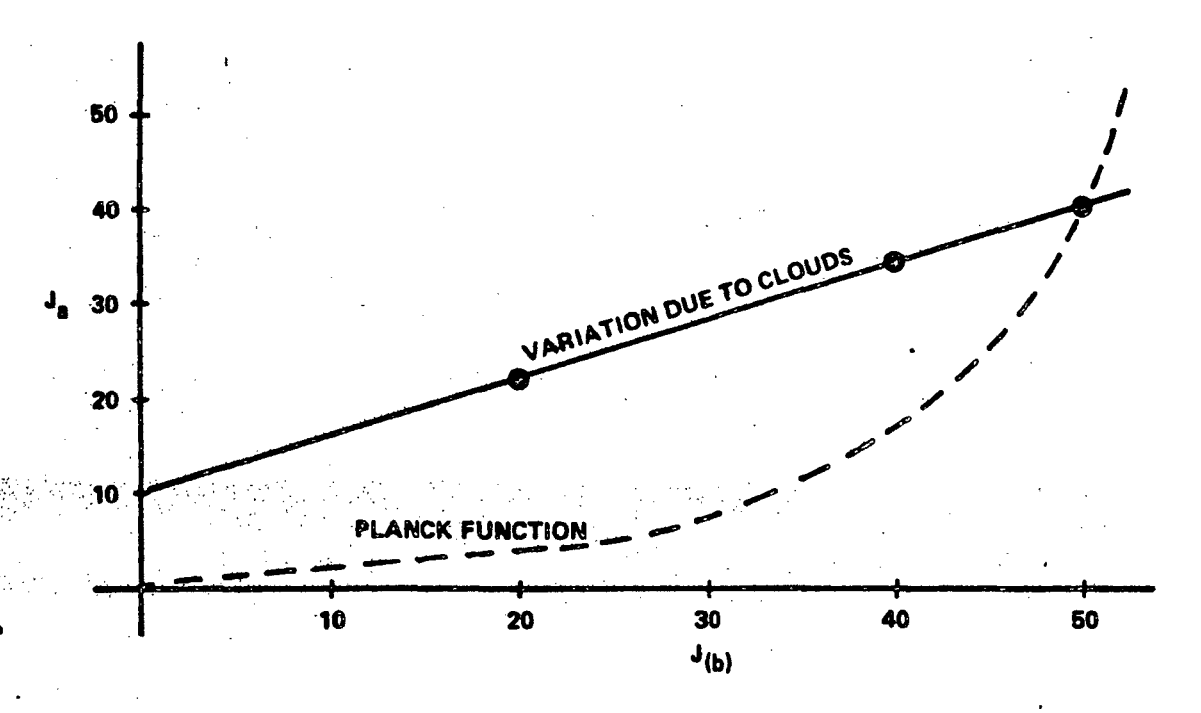


FIGURE 5.8-10 Determining Clear Column Radiance in a Window Channel

With the clear column radiances developed, the actual temperature profile can be generated. There are two basic methods for generating the profile: Regression Method and the Minimum Information Solution Method.

The Regression Method has been the most successful. Basically, a set of regression coefficients are generated by processing a number of co-located radio-sonde and satellite measurements. The radiosonde measures atmospheric temperature from which brightness temperatures are developed for fifteen levels of the atmosphere. Coincident satellite measurements in all 8 spectral channels are regressed against the brightness temperatures to achieve a 15 x 8 matrix of

REV. NO.: 0 REV. DATE: 30 June 1977

coefficients relating satellite sensed radiance to brightness temperature at 15 levels of the atmosphere. These coefficients are applied to independent satellite measurements to get the desired profile.

The Minimum Information Solution guesses at a profile, then applies the transmittance characteristics of the atmosphere against the guess to determine if the radiation generated by the guess profile is consistent with that sensed by the sounder. If not, the guess is modified and the process repeated. The first guess may come from (a) existing forecasts, (b) surface based measurements that are interpolated in time and space to the location of interest, and (c) a regression of historical data. The first guess is used to modify the transmittance functions because they are slightly temperature dependent. The transmittance functions are applied to the guess profile and integrated to the surface of the atmosphere to obtain total radiance at the top of the atmosphere. The calculated radiance is compared to the measured radiance and if the values agree within some acceptable delta, the guess profile is considered as the actual temperature profile. If the values do not agree the guess is modified and the process repeated.

This section has thus far addressed only the meteorological applications of sounders. Another major application of optical spectrographic-type instruments is in the detection of chemical constituents in the atmosphere. Several methods are presently being developed including active laser methods which will be discussed under the LIDAR section. Methods which can be covered in this section include interferometric schemes and laser heterodyne methods.

From a detailed study of the spectrum of light from a gas mixture, one can deduce: [16]

(a) Composition (what molecules are present, e.g.  $0_2$ ,  $N_2$ ,  $H_20$ ,  $CO_2$ ,  $NH_3$ ,  $CH_4$ , etc.)

REV. DATE: 30 Sept 1977

**REV. NO.:** 

- (b) Abundance (how much of each molecule, including isotopes)
- (c) Temperature
- (d) Pressure
- (e) Velocity (how fast the gas mixture producing the spectrum is moving toward or away from us)
- (f) Turbulence (how fast one part of the mixture is moving relative to another part)
  - (g) Field Strengths (magnetic or electric)

These spectra are of two basic types: (a) absorption (dark line) spectra where light passing through the mixture is attenuated at wavelengths characteristic of the gasses and (b) emission (bright line) spectra where the heated gas re-radiates light energy at wavelengths which are characteristic of the gas. Astronomers have for years made detailed studies of the spectra of light from planets to deduce the chemical composition of their atmospheres. Recently, new information and methods have changed traditional thinking about some of these measurements.

A typical spectrometer as shown in Figure 5.8-11 consists of a radiation collection means, a dispersion element such as a prism, grating or similar device for breaking up the incoming light according to wavelength and an analyzing device which could be film (except that for infrared energy will not register) or a detector. A slit is used in front of the detector to limit the spectral width of light entering the detector and thereby improves resolution. High spectral resolution is attained by narrow slits, which reduces the amount of light reaching the detector. As slit widths are reduced to increase spectral resolution, the light reaching the detector decreases and eventually cannot be separated from background radiation.

REV. NO.: 2 REV. DATE: 31 Jan 1978

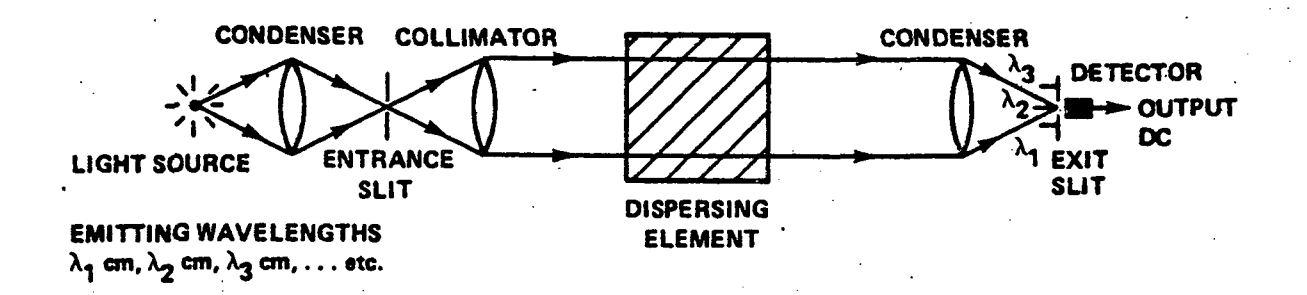


FIGURE 5.8-11 Schematic Representation of a Photoelectric Dispersing Spectrometer

An alternative which provides relief from this impasse is the Fourier Spectrometer which is shown schematically in Figure 5.8-12. It consists of an entrance aperture

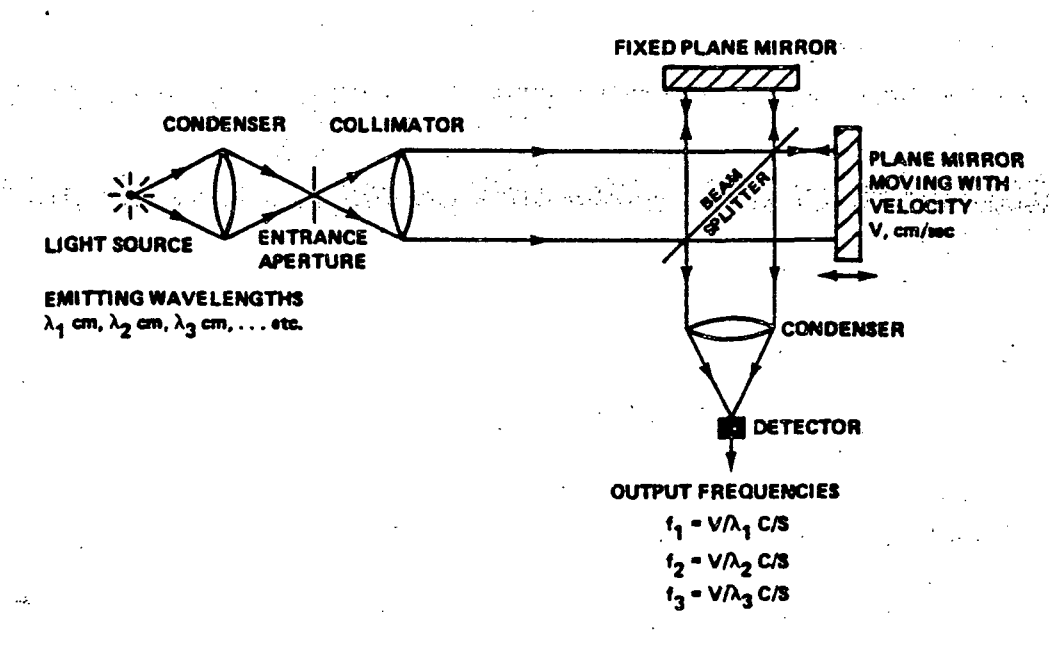


FIGURE 5.8-12 Schematic Representation of a Fourier Interference Spectrometer

and lens (or mirror) which can be large, a Michelson interferometer, a lens or mirror for condensing the radiation a circular exit aperture and a photoelectric detector.

REV. NO.: 1 | REV. DATE: 30 Sept 1977

The Michelson interferometer was the invention of A. A. Michelson, the first American Nobel Laureate. It consists of a plate which reflects half and transmits half of the incident radiation (called a beam splitter) and two flat mirrors which intercept these two beams and reflect them back to the beam splitter (see Figure 5.8-12). As a consequence of the phenomenon known as interference, the fraction of the radiation which is again reflected from, or transmitted by, the beam splitter is controlled by the difference in the distances of the two flat mirrors from the beam splitter (called the path difference). As the path difference changes, so does the relative proportion of the two beams transmitted or reflected. The transmitted fraction passes to the detector. If light of only one wavelength is incident on the system, and if one of the flat mirrors moves at a constant velocity with respect to the other, the output of the detector will vary in a periodic fashion at a rate which depends only on the wavelength and the mirror velocity. Consequently, if now two or more individual wavelengths are incident on the same system, the detector will produce periodic signals that are related to the relative wavelengths. Therefore, if we know either (a) one of the incident wavelengths, or (b) the mirror velocity, we can find the unknown wavelengths and their relative intensities. A spectrum is precisely this: a plot of wavelength against relative intensity. If the incident radiation is continuous (that is, comes from a hot body such as a tungsten filament lamp), the outgoing frequencies will also form a continuous set. By means of a Fourier Transformation (whence comes the name Fourier Spectroscopy) and a digital computer, one can produce the required spectrum. A typical output, called an interferogram, is shown in Figure 5.8-13. To overcome some of the physical difficulties of building the classic Michelson interferometer, a variation known as the "cat's eye interferometer" was developed. In the cat's eye, the flat mirrors are replaced by retroreflectors which are more tolerant to misalignment. Early models of this

REV. DATE: 30 Sept 1977

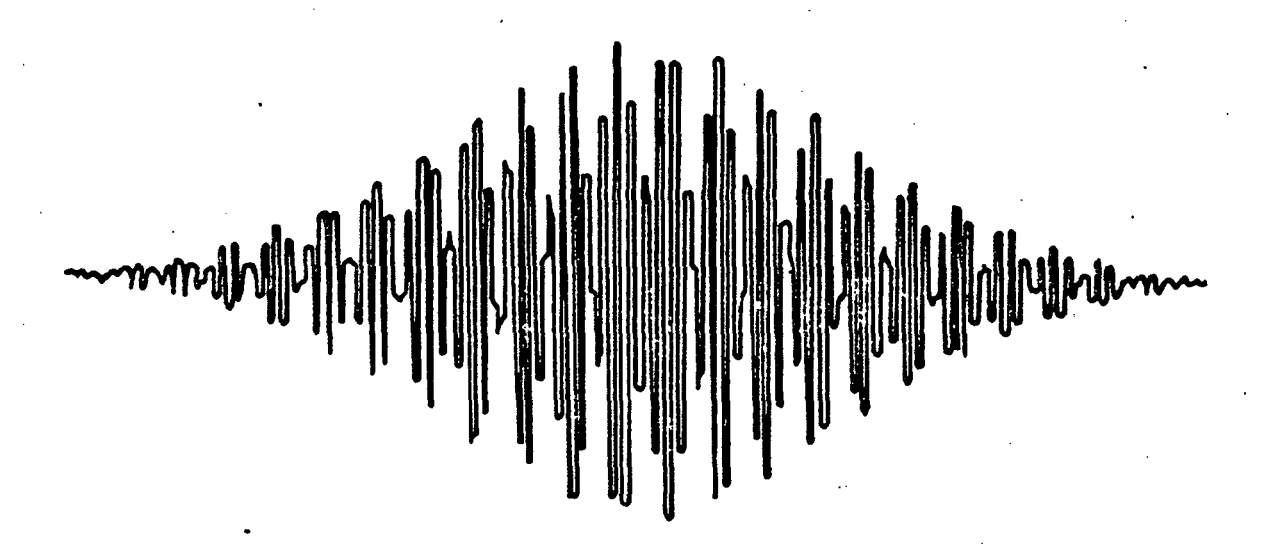


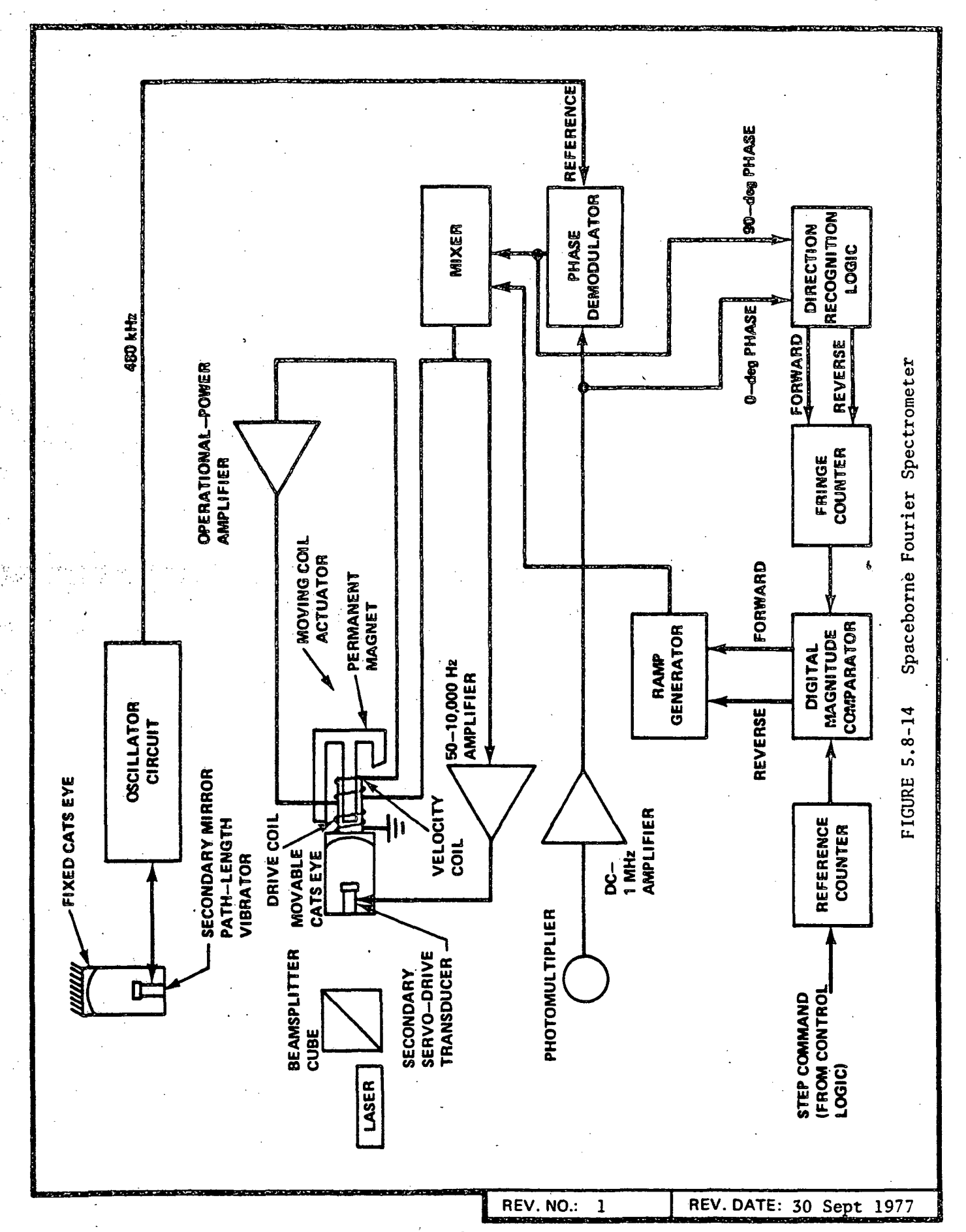
FIGURE 5.8-13 A typical output from a Fourier Spectrometer. The plot is called an interferogram and, in this case, was generated by observing a hot tungsten filament in the neighborhood of 2-2.5  $\mu$  wavelength (1  $\mu$  = 10<sup>-4</sup>cm).

were built in the late sixties at JPL. A later version, shown schematically in Figure 5.8-14 is not unlike the unit to be flown as the ATMOS instrument aboard Shuttle.

The laser which is shown in the diagram is a monochromatic source which is directed through the interferometer along with the radiation being analyzed. The effect on the laser's radiation is measured and is used to null the servo which drives the movable retroreflector.

Satellite experiments planned for the near term on Nimbus-G (1978) and AEM-B (1979) will concentrate upon measurements in the stratosphere [18]. These will include vertical profiling of stratospheric H<sub>2</sub>O, O<sub>3</sub>, oxides of nitrogen, HNO<sub>3</sub>, CO<sub>2</sub> and aerosols using atmospheric horizon viewing (limb) instruments: the Stratospheric and Mesospheric Sounder (SAMS) and the Limb Infrared Monitoring of the Stratosphere (LIMS), and the Stratospheric Aerosol Measurement Radiometer (SAM II). Also, further stratospheric O<sub>3</sub> measurements are planned for Nimbus-G: Solar Backscatter Ultra-

REV. NO.: 1 REV. DATE: 30 Sept 1977



violet (SBUV) and Total Ozone Mapping Radiometer Spectrometer (TOMS).

At this stage the NASA program plan includes a mid-term (1984) multisensor environmental monitoring satellite which will include both stratospheric and tropospheric pollution profiling measurements. The experiment definition for this major spaceborne pollution mission will be based upon the results of the near term experiments planned for Nimbus-G, AEM-B and shuttle spacecrafts, as well as upon aircraft flight programs and ground based measurements.

High resolution interferometer measurements of stratospheric trace constituents  $(0_3, CH_A, HNO_3, CO, CO_2, NO_Y)$  have been conducted from aircraft and are planned for the 1980 Shuttle-I experiment: Atmospheric Trace Molecules Observed by Spectroscopy (ATMOS) which will include, in addition, the measurement of HCl and chlorofluoromethanes (CFM). Another technique, correlation spectroscopy, reduces the effects of interfering gases by placing a sample cell containing the gas of interest (CO, HCl, N<sub>2</sub>0, SO<sub>2</sub>) in a portion of the optical path of the instrument (Gas Filter Correlation Radiometer, Correlation Interferometer). A spaceflight test of this technique as a tropospheric pollution experiment is planned for the Shuttle OFT-2: Measurements of Air Pollution from Satellites (MAPS). This will be the first tropospheric experiment from space. Another version of the gas correlation technique using two sample gas cells at different pressures (differential correlation radiometer (DCR)) is under development for operation in the sun viewing or reflected solar radiation modes. The DCR has the potential to profile twelve pollutants with much greater sensitivity to pollution concentrations close to the earth's surface. Other pollution profiling techniques being developed are limb scanning radiometers that observe in the infrared and microwave regions and a high spectral resolution technique using laser heterodyne detection in the infrared. Another future stratospheric experiment for measuring HCl, HF, CFM and others is the Halogen Occultation Experiment (HALOE) which observes solar radiation through the atmospheric limb.

Near and mid-term development efforts have concentrated upon passive sensors i.e., sensors that passively observe signals originating in the atmosphere or from the sun. Passive techniques suffer a severe fundamental limitation in vertical profile resolution and consequently vertical profile accuracy. Long term efforts will stress techniques with the potential for much higher vertical resolution and accuracy, namely: active experiments which use a laser as the radiation source or probe. Such laser experiments have the capability of making direct vertical profile measurements when operated in a pulsed radar mode, a technique known as Light Detection and Ranging (LIDAR), and using a combination of atmospheric absorption and scattering of the laser radiation called Differential Absorption and Lidar (DIAL).

Microwave sensors which will be used in the near-term and mid-term for (primarily) meteorological purposes are in an advanced state of development. Their use is expected to expand in the 1990's for measuring water vapor and liquid water. Areas of increased interest during this time will include the boundry layer of the atmosphere consisting of the first three hundred meters.

One can project that accuracies of soundings can reach the .5°C level before the 1990's and that vertical resolutions capable of being reached are described in terms of one or two meters. Opinion in the scientific community is divided on the timing of advances in on-board processing of temperature data. The thought is widely held that an on-board processor is a prerequisite to sounders which are significantly advanced over present configurations. If the assumption is made that the solution of the on-board processing problem in the next decade will allow direct transmission of profiles, an estimate of data rates using current satellite coverage can be made.

5.8.22

## ATMOSPHERIC SOUNDERS LIST OF ACTIVE CONTRIBUTORS

Dr. Jerome Eckerman Mail Code 953.0 Building 19, Room 93 Goddard Space Flight Center Greenbelt, MD 20771 (301) 982-6786

Dr. Edward J. Hurley
Mail Code 941.0
Building 22, Room 308
Goddard Space Flight Center
Greenbelt, MD 20771
(301) 982-6233

Dr. J. T. Houghton Clarendow Laboratory University of Oxford Oxford, England

Dr. James C. Shiue
Mail Code 952.0
Building 19, Room 37
Goddard Space Flight Center
Greenbelt MD 20771
(301) 982-6963

Dr. D. H. Staelin Research Laboratory of Electronics Massachusetts Institute of Technology Cambridge, Mass. 02139

Dr. Crofton B. Farmer
Mail Code 183-301
Jet Propulsion Laboratory
California Institute of Technology
Pasadena, CA 91103
(213) 354-2039

Dr. Reinhard Beer Mail Code 183-301 Jet Propulsion Laboratory California Institute of Technology Pasadena, CA 91103 (213) 354-4748 Mr. Edward J. Johnston Mail Code 168-327 Jet Propulsion Laboratory California Institute of Technology Pasadena, CA 91103 (213) 354-2645

Dr. Charles L. Korb Mail Code 941.0 Building 22, Room 308 Goddard Space Flight Center Greenbelt, MD 20771 (301) 982-6233

Dr. Barney J. Conrath Mail Code 622.0 Building 21, Room 221 Goddard Space Flight Center Greenbelt, MD 20771 (301) 982-6088

Dr. J. W. Waters Mail Code 168-327 Jet Propulsion Laboratory California Institute of Technology Pasadena, CA 91103 (213) 354-3025

### ATMOSPHERIC SOUNDERS

#### REFERENCES

- [1] Horn, Lyle H., et.al., "Intercomparisons of Data Derived from NIMBUS 5 Temperature Profiles, Radiosonde Observations and Initialized LFM Model Fields," Monthly Weather Review, Vol. 104, November 1976, pp. 1362-1371.
- [2] Smith, W. L., Woolf, H. M., Abel, P. G., Hayden, C. M., Chalfout, M., and Grody, M., Nimbus-5 Sounding Data Processing System Part 1: Measurement Characteristics and Data Reduction Procedures, Final Report, 1975, NASA Contract S-70249-AG, 68 pp.
- [3] The Performance of Space Observing Systems for the First GARP Global Experiment, GARP Working Group on Numerical Experimentation, Report No. 6, 31 pp.
- [4] Thompson, O. E., Eom, J. K., and Wagenhofer, J. R., "On the Resolution of Temperature Profile Finestructure by NOAA Satellite Vertical Temperature Profile Radiometer", Monthly Weather Review, Vol. 104, No. 2, February 1976, pp. 117-126.
- [5] Houghton, J. T. and Smith, S. D., Remote Sounding of Atmospheric Temperature from Satellites, <u>Proceedings of the Royal Society of London</u>, Vol. 320A, pp. 23-33, 1970.
- [6] Indirect Measurements of Atmospheric Temperature Profiles from Satellites: Part I, II, III, IV, V, and VI. Monthly Weather Review, Vol. 94, No. 6, June 1966, and Vol 95, No. 7, July 1967. Articles by D. Q. Work, H. E. Fleming, D. T. Hillery, E. L. Heacock, W. A. Morgan, R. H. Moore, E. C. Mangold, S. D. Soules, S. T. Womey, D. G. James, M. Wolk, F. Van Cleef, and F. Saiedy.
- [7] Jamieson, John A., et. al., "Infrared Physics and Engineering," McGraw Hill Book Co., Inc., 1963.
- [8] Goldberg, I. L., "Meteorological Infrared Instruments for Satellites," SPIE Journal, November 1970, pp. 22-31.
- [9] Block, G. F., et. al., Study of Meteorological Data Processing Methods, September 1972.
- [10] Smith, W. L., et. al., NIMBUS-5 Sounder Data Processing System, Part II, Results, July 1975.
- [11] Sissala, S., NIMBUS-6 User Guide, February 1975.
- [12] Specification ES511746A, Jet Propulsion Laboratory.
- [13] STORMSAT Ground System Study, Computer Sciences Corporation, Draft.

- [14] Chase, S. C., "Advanced Atmospheric Sounder and Imaging Radiometer (AASIR) for STORMSAT," AIAA Systems Design Driven by Sensors, October 1976.
- [15] "Study of Meteorological Data Processing Methods," GFGMS Working group report, 75N-29689, December 1972.
- [16] Beer, Reinhard, "Remote Sensing of Planetary Atmospheres by Fourier Spectrocopy," The Physics Teacher, April 1968.
- [17] "Global Survey of Atmospheric Trace Constituents and Pollutants (Final Report) to the AAFE Program and the Experiment Definition Program for Space Shuttle, January 1974 (JPL).
- [18] Hurley, Ed, unpublished Memorandum, Global Air Polution Monitoring from Earth-oriented Satellites.
- [19] Seasat-A Satellite Specification, Attachment 5A (750-59), March 1975.

REV. NO.: 2 | REV. DATE: 31 Jan 1978

## ATMOSPHERIC SOUNDERS BIBLIOGRAPHY

- (1) Chaney, L. W., Drayson, S. R., and Young, C., "Fourier Transform Spectrometer Radiative Measurements and Temperature Inversion," Applied Optics, Vol. 6, No. 2, February 1967, p. 347.
- (2) Kaplan, Lewis D., "Inference of Atmospheric Structure from Remote Radiation Measurements," <u>Journal of the Optical Society of America</u>, Vol. 49, No. 10, October 1959.
- (3) Conrath, B. J., Hanel, R. A., Kunde, V. G., and Prabhakara, C., "The Infrared Interferometer Experiment on Nimbus 3," <u>Journal of Geophysical Research</u>, Vol. 75, No. 30, October 20, 1970.
- (4) Hanel, R. A., Schlachman, B., Clark, F. D., Prokesh, C. H., Taylor, J. B., "The Nimbus III Michelson Interferometer," Applied Optics, Vol. 9, No. 8, August 1970.
- (5) Wark, D. Q., Hilleary, D. T., "Atmospheric Temperature: Successful Test of Remote Probing," Science, Vol. 165, September 1969.
- (6) Staelin, David H., 'Measurements and Interpretation of the Microwave Spectrum of the Terrestrial Atmosphere near 1-Centimeter Wavelength,"

  Journal of Geophysical Research, Vol. 71, No. 12, June 15, 1966.
- (7) King, Gilbert W., Hainer, R. M., and Cross, Paul C., "Expected Microwave Absorption Coefficients of Water and Related Molecules," <u>Physical</u> Review, Vol. 71, No. 7, April 1, 1947.
- (8) Abel, P. G., Houghton, J. T., Matley, J. B., and Williamson, E. J., "Remote Sounding of Atmospheric Temperature from Satellites III. Measurements up to 35 Km altitude with a balloon-borne Selective Chopper Radiometer," Proc. Roy. Soc. Lond. A. 320, pp. 57-69, 1970.
- (9) Abel, P. G., Ellis, P. J., Houghton, J. T., Peckham, G., Rodgers, C. D., Smith, S. D., and Williamson, E. J., "Remote Sounding of Atmospheric Temperature from Satellites II. The Selective Chopper Radiometer for Nimbus D," Printed in Great Britain, Proc. Roy. Soc. Lond. A. 320, pp. 35-55, 1970.
- (10) Vleck, J. H. Van, "The Absorption of Microwaves by Uncondensed Water Vapor," Physical Review, Vol. 71, No. 7, April 1, 1947.
- (11) Meeks, M. L. and Lilley, A. E., "The Microwave Spectrum of Oxygen in the Earth's Atmosphere," <u>Journal of Geophysical Research</u>, Vol. 68, No. 6, March 15, 1963.
- (12) Staelin, David H., "Passive Remote Sensing at Microwave Wavelengths," Proceedings of the IEEE, Vol. 57, No. 4, April 1969.

**REV. DATE: 30 Sept 1977** 

- (13) Hill, Robert M., "Microwave Spectrum of 02," Physical Review, Vol. 93, No. 4, February 15, 1954.
- (14) Barrett, A. H. and Chung, V. K., "A Method for the Determination of High-Altitude Water-Vapor Abundance from Ground-Based Microwave Observations," <u>Journal of Geophysical Research</u>, Vol. 67, No. 11, October 1962.
- (15) Vleck, J. H. Van, "The Absorption of Microwaves by Oxygen," Physical Review, Vol. 71, No. 7, April 1, 1947.
- (16) Waters, J. W., "Remote Sensing of Atmospheric Temperature Profiles with Nimbus-5 Microwave Spectrometer," <u>J. Atmospheric Sciences</u>, Vol. 32, No. 10, October 1975, pp. 1953-1969.
- (17) Farmer, C. B., "Infrared Measurements of Stratospheric Composition," Canadian Journal of Chemistry, Vol. 52, No. 8 (part 2), 1974, pp. 1544-1559.
- (18) Staelin, D. H., et. al., "Microwave Spectrometer on the Nimbus-5 Satellite: Meteorological and Geophysical Data," <u>Science</u>, December 28, 1973, Vol. 182, pp. 1339-1341.
- (19) Croom, D. L., "Stratospheric Thermal Emission and Absorption Near the 183.311 GC/S (1.64 mm) Rotational Line of Water Vapour," J. Atmospheric and Terrestrial Physics, 1965, Vol. 27, pp. 235-243.
- (20) Conrath, Barney J., "Vertical Resolution of Temperature Profiles Obtained from Remote Radiation Measurements," J. Atmospheric Sciences, Vol. 29, pp. 1262-1271, October 1972.
- (21) Gaut, Norman E., et. al., "Studies of Microwave Remote Sensing of Atmospheric Parameters," AFCRC-TR-75-0007, Airforce Cambridge Research Laboratories, August 1974.

## Temperature/Humidity Infrared Radiometer (THIR) BIBLIOGRAPHY

- (1) Sissala, J. (GSFC), The NIMBUS-G Users Guide, February 1975.
- (2) Hogan, C. (GSFC), "System Design Considerations for the NIMBUS-G Observatory Mission," AIAA System Design Driven by Sensors, October 1976.

## Advanced Atmospheric Sounding and Imaging Radar (AASIR) BIBLIOGRAPHY

(1) Chase, S. C., "Advanced Atmospheric Sounder and Imaging Radiometer (AASIR) for Stormsat," <u>AIAA Systems Design Driven by Sensors</u>, October 1976.

- (2) Advanced Scanners and Imaging Systems for Earth Observations, NASA/GSFC, December 1972.
- (3) Shank, W. E., "The Severe Storms Observation Satellite (SSOS)," Presented in Symposium on Meteorological Observations and Instrumentation, February 10-13, 1975.
- (4) Computer Sciences Corporation, Stormsat Ground System Study, (Draft).

## Vertical Temperature Profile Radiometer (VTPR) BIBLIOGRAPHY

- (1) Fortuna, J. and Harbrick, L., The Operation of the NOAA Polar Satellite System, NOAA Technical Memorandum NESS 60, November 1974.
- (2) Schwalb, A., "Modified Version of the Improved TIROS Operational Satellite, (ITOS D-G)," NOAA Technical Memorandum NESS 35, April 1972.
- (3) Johnson, K., "Information Content of the Vertical Temperature Profile Radiometer Data," NOAA-NESS, 1975.
- (4) Remote-Sensing Instruments Performance Data Sheets, JPL Document 624-2 (Draft).
- (5) The Use of Radiosonde in Deriving Temperature Soundings from the NIMBUS and NOAA Satellite Data, NESS, #PB-256-755, April 1, 1976.
- (6) Bonner, W. D., et. al., A Test of the Impact of NOAA-2 VTPR Soundings on Operational Analysis and Forecasts, NOAA-NMC, February 1976.
- (7) Hillger, D. W., Vonder Hoar, T. H., <u>Mesoscale Temperature and Moisture Fields from Satellite Infrared Soundings</u>, Department of Atmospheric Sciences, Colorado State University, May 1976.

## Stratospheric and Mesospheric Sounder BIBLIOGRAPHY

- (1) Hogan, C., "System Design Considerations for the NIMBUS-G Observatory Mission," from proceedings of AIAA Systems Design Driven by Sensors, October 1976.
- (2) Earth Observation Sensors, NASA Office of Applications, May 25, 1976.
- (3) The NIMBUS-G Sensor Systems: A Preliminary Description, GSFC, July 1976.

REV. NO.: 2 | REV. DATE: 31 Jan 1978

## Visible Infrared Spin-Scan Radiometer Atmospheric Sounder BIBLIOGRAPHY

- (1) Chase, S. C., "Advanced Atmospheric Sounder and Imaging Radar (AASIR) for Stormsat," Proceedings of AIAA Systems Design Driven by Sensors, October 1976.
- (2) Earth Observation Sensors, NASA Office of Applications, May 1976.
- (3) The Federal Plan for Meteorological Services and Supporting Research, Fiscal Year 1977, NOAA, June 1976.
- (4) <u>Information on Meteorological Satellite Programs Operated by Members and Organizations</u>, World Weather Watch, 1975.
- (5) Remote Sensing Instrument Performance Data Sheets (Draft), NASA/JPL Document 624-2, (to be published).
- (6) <u>Visible Infrared Spin-Scan Radiometer Atmospheric Sounder</u>, Santa Barbara Research Center, (unpublished memo).

## High Resolution Infrared Radiation Sounder BIBLIOGRAPHY

(1) Sissala, J., NIMBUS 6 User Guide, GSFC, February 1975.

## Microwave Sounding Unit BIBLIOGRAPHY

- (1) Fortuna, J., Harbrick, L., The Operation of the NOAA Polar Satellite System, NOAA Technical Memorandum NESS 60, November 1974.
- (2) Ludwig, G., The NOAA Operational Environmental Satellite System Status and Plans, Presented in Conference on Aerospace and Aeronotical Meteorology, November 1974.
- (3) Earth Observation Sensors, May 1976.
- (4) Notes from JPL Spec ES511746 A sent by R. Ratliff.

REV. NO.: 2 REV. DATE: 31 Jan 1978

# ATMOSPHERIC SOUNDERS ILLUSTRATION CREDITS

Figure No.	Page	Reference	Page
5.8-1	5.8-3	[7]	48
5.8-2	5.8-3	[7]	48
5.8-3	5.8-4	[7]	112
5.8-5	5.8-5	[5]	58
5.8-6	5.8-6	[4]	119
5.8-7	5.8-8	[8]	30
5.8-8	5.8-11	[15]	72
5.8-9	5.8-13	[10]	39
5.8-10	5.8-14	[10]	39
5.8-11	5.8-17	[16]	Fig. 3
5.8-12	5.8-17	[16]	Fig. 4
5.8-13	5,8-19	[16]	Fig. 5
5.8-14	5.8-20	[17]	12.
HIRS(8)	5.8-75	[11]	45
MSU(8)	5.8-80	[12]	7
MSU(Fig. 1)	5.8-81	[12]	25
THIR (Fig. 1)	5,8-34	[12]	28
THIR(8)	5.8-35	[13]	2-18
AASIR (Tb1. 1)	5.8-41	[13]	2-16
AASIR(Tb1. 2)	5.8-42	[13]	2-18
AASIR(Tb1. 3)	5.8-43	[14]	6
VAS(Tb1. 1)	5.8-66	[16]	5
SMMR (8)	5.8-90	[19]	5
SMMR (Tbl. 1)	5.8-90	[19] _	2

This page intentionally left blank.

REV. NO.:

1

REV. DATE: 30 Sept 1977

#### RSDH DATA SHEET

SHEET 1 OF 5

(1) SENSOR NAME, ACRONYM: Temperature/Humidity Infrared Radiometer (THIR)

(2) DISCIPLINE: Earth Observations (3) SUBDISCIPLINE: Atmospheric Monitoring

#### (4) APPLICATION AND OBJECTIVE:

The THIR provides images of cloud cover, measures temperature of cloud tops, land and ocean surfaces and provides information on the moisture content of the upper troposphere and stratosphere for the location of jet streams and frontal systems.

## (5) HERITAGE/KEY PERSONNEL:

NIMBUS 5, 6, G

Instrument Rep.: M. Freidman (GSFC) (301) 982-4211

#### (6) SENSOR DEPLOYMENT:

This sensor is normally deployed in a sun-synchronous orbit of 1100 km altitude with an orbital period of 107.25 min. (NIMBUS-G). Pitch and roll axis are maintained within .5 degrees and yaw axis within 1 degree.

(7) SENSOR CHARACTERISTICS

## (7A) CAPABILITIES AND CONSTRAINTS OF THE SENSOR TO ACQUIRE THE MEASURED PARAMETER;

The THIR scans cross track, using a .7 mrad. IFOV for the 11.5µ channel. The scan is continuous from horizon to horizon, but degradation in resolution at the limits of the scan limit the usable scan angle to ±37.5° from the satellite subpoint. Figure 1 (see next page) shows degradation of resolution as a function of scan angle. 48 scans are completed each minute (approximately 21% of the scan time is used for data collection over the area ±37.5°). Both spectral bands are sampled simultaneously.

### (7B) ACTIVE SOURCE CHARACTERISTICS (FOR ACTIVE SENSORS):

N/A

### (7C) DETECTOR MEASUREMENTS CHARACTERISTICS:

Two Geranium-Immersed thermistor bolometer detectors are used, one for each band. The detectors are uncooled, operating at 290°K. The field of view is defined by the field stop: .7 mrad for the 11 µm channel and 20.5 mrad for the 6.7 µm channel. Calibration measurements are taken each scan by viewing the sensor housing and space.

5.8.33

Preceding page blank

SECTION NO.: 5.8 | SENSOR CATEGORY: Atmospheric Sounders

REV. NO.: 2



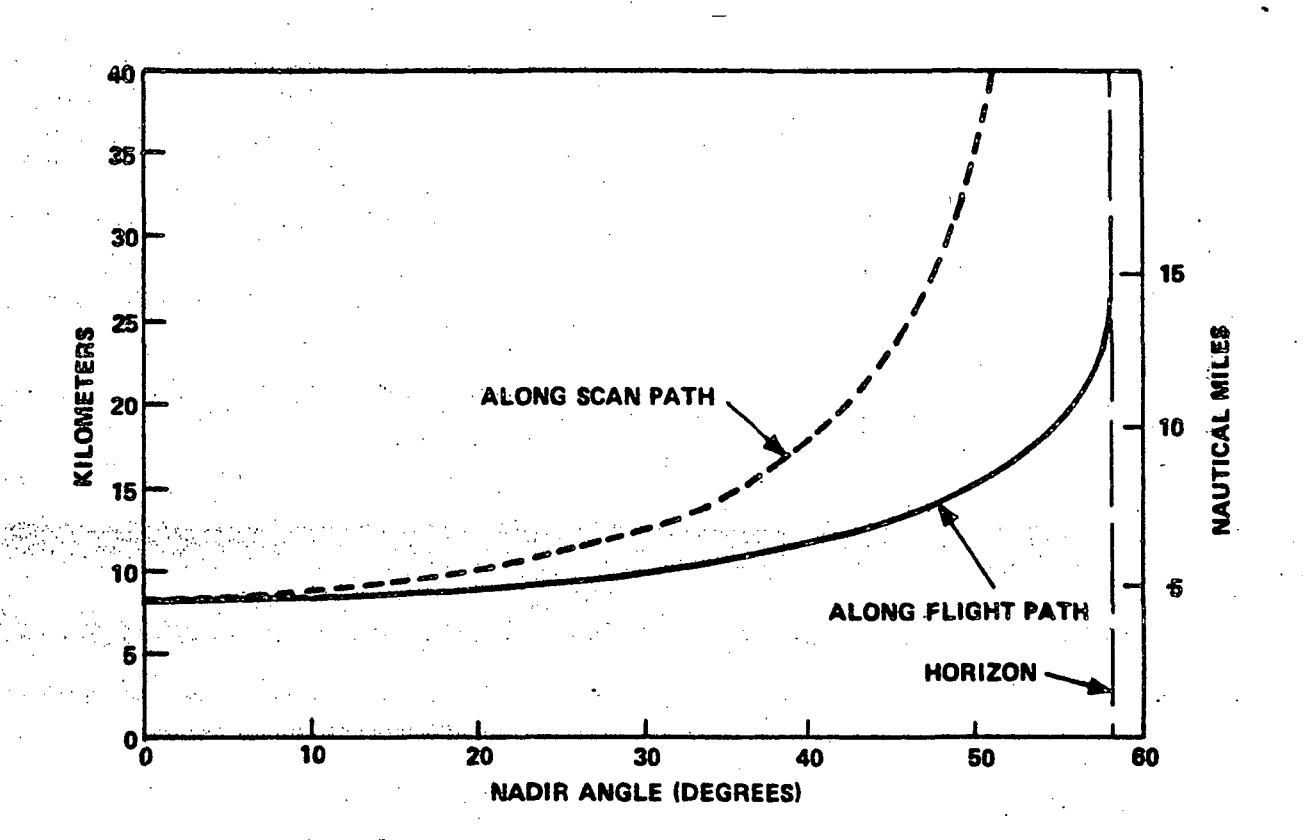


FIGURE 1 Relationship Between Nadir Angle and Ground Resolution for the THIR 11.5 µm Channel at 1100 km

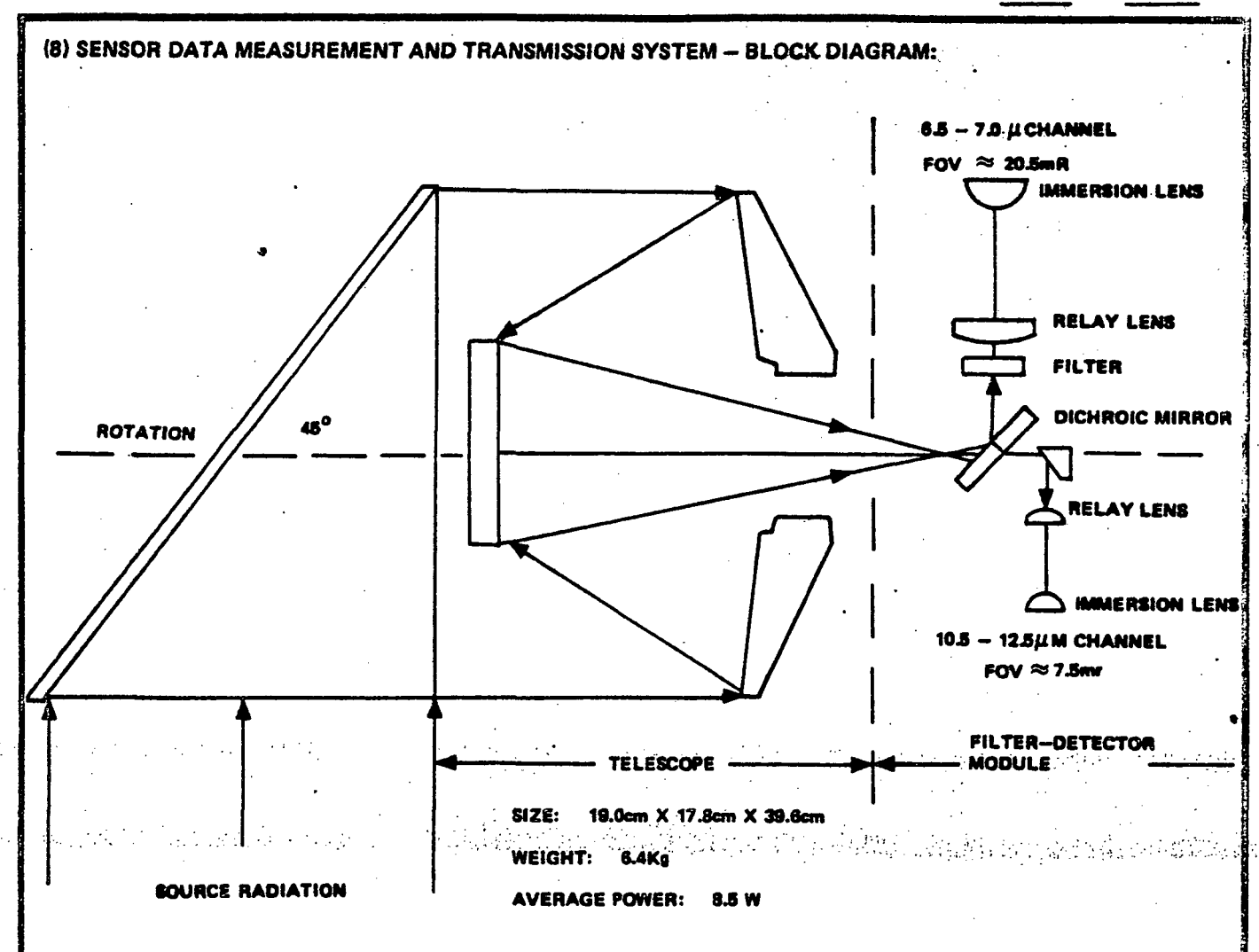
5.8.34

SECTION NO.: 5.8 SENSOR CATEGORY: Atmospheric Sounders

**REV. NO.:** 2

REV. DATE:

31 Jan 1978



## (9) MEASUREMENT AND TRANSMISSION SYSTEM - NARRATIVE:

The ellipical scan mirror rotates at 48 rpm to scan 360° in a plane perpendicular to satellite motion. The scan alternately views the sensor housing, space and earth. Calibration sequences are executed each scan during the periods that the earth is not in view. A DC restorer circuit provides a zero signal reference during the portion of the scan where the optics are viewing space. The output of the detectors is amplified and corrected to provide the required frequency response. The output voltage is routed to on-board recorder(s) or can be relayed through the geosynchronous satellite to ground stations in real time.

5.8.35

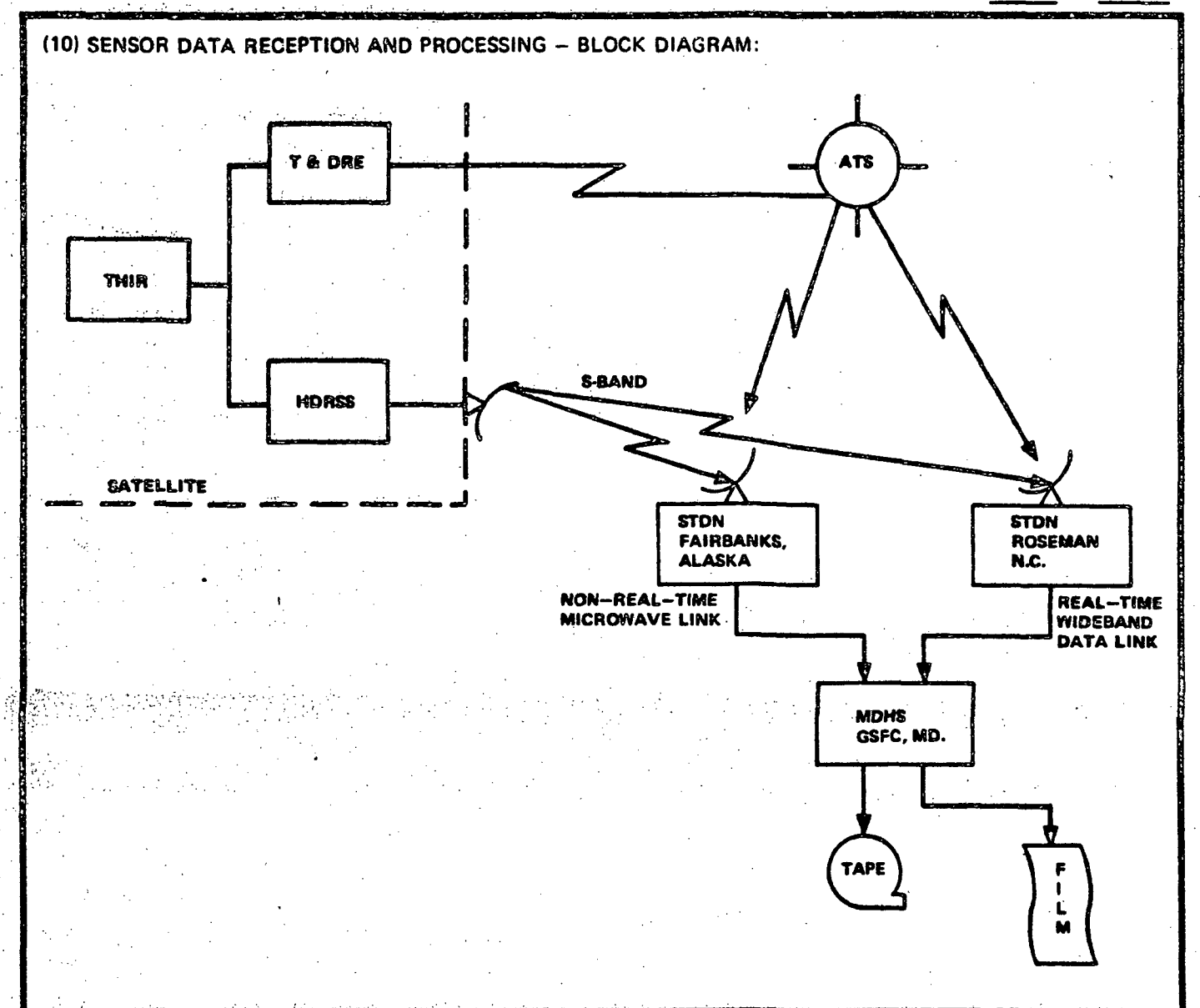
SECTION NO .: - 5.8

SENSOR CATEGORY:

Atmospheric Sounders

**REV. NO.: 2** 

REV. DATE: 31 Jan 1978.

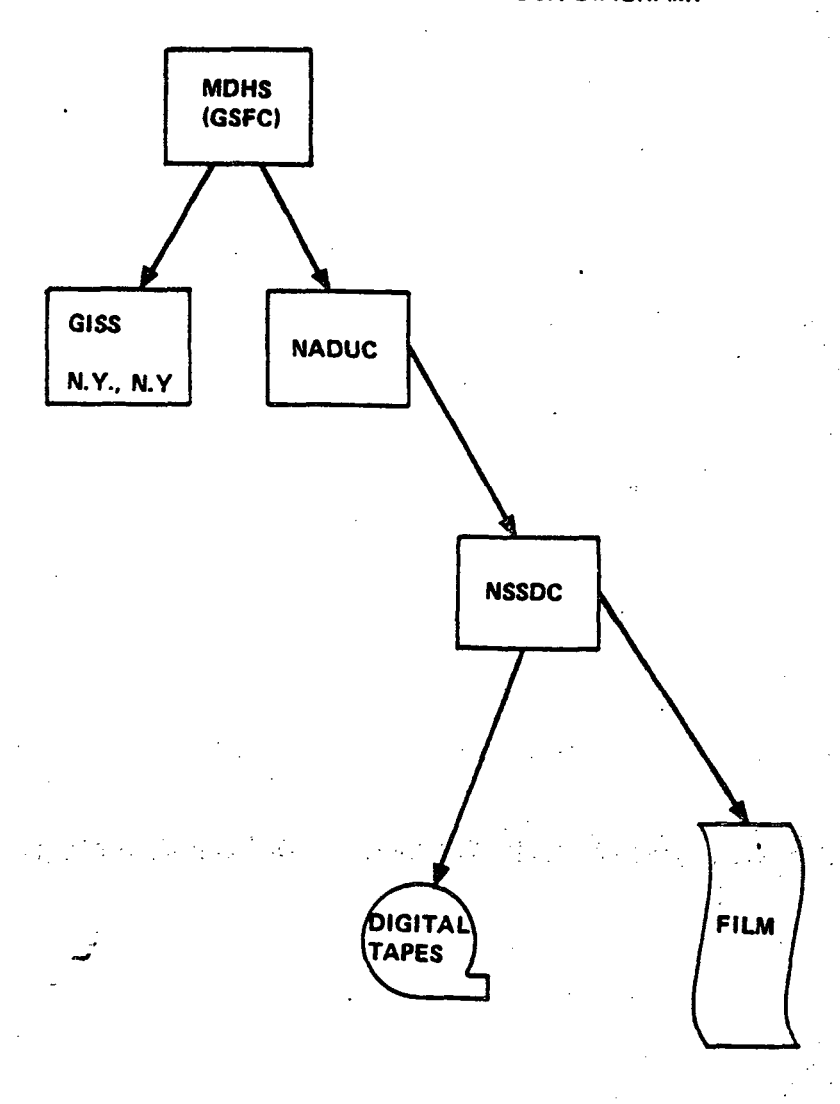


(11) RECEIVING AND PROCESSING - NARRATIVE: The information is read back from the TDRSS at 32 x the record rate. (Real-time data may be relayed via ATS to ground). The data is received at the Spaceflight Tracking and Data Network (STDN) at one of two stations as shown. At the Alaska station, the data is recorded (analog) and then transmitted to GSFC. The Roseman station transmits directly to the Meteorological Data Handling System at GSFC. The MDHS integrates the data with geographic grid marks a CDC 924 computer calculates the location of grid marks and superimposes them onto the THIR data in analog form. (No registration or correction for spacecraft attitude is performed.) The grid and THIR image are output to 70 mm filmstrips line-by-line. The THIR analog data is converted to digital and a digital tape is prepared by the CDC 924 Computer. The digital tape is processed by an IBM-360 computer which produces a NIMBUS Meteorological Radiation Tape (NMRT-THIR). This tape contains spacecraft attitude and orbital information, scanning angles, scan time, longitude and latitude, THIR data values and calibration data. (The digital data are only processed on special orders because of the expenses. Grid print maps may be produced from the digital data, showing the approximate geographic location of THIR measurements for single or multiple orbits.

SECTION NO.: 5.8 SENSOR CATEGORY: Atmospheric Sounders

REV. NO.:

## (12) DISTRIBUTION OF DATA FROM GROUND STATIONS - BLOCK DIAGRAM:



## (13) DATA DISTRIBUTION - NARRATIVE:

The MDHS distributes the THIR data to the Goddard Institute for Space Studies for use in Numerical Forecast Modeling and GARP support. The main distribution of THIR data is performed by the Nimbus/ATS Data Utilization Center (NADUC). The NADUC performs the necessary reproduction and technical services required to prepare final products from the MDHS outputs. The data products are delivered to the National Space Science Data Center (NSSDC) for archiving and delivery to selected users.

5.8-37

5.8 SECTION NO .: SENSOR CATEGORY: Atmospheric Sounders

REV. NO.: 2 **REV. DATE:** 

31 Jan 1978

#### RSDH DATA SHEET

CONTINUATION SHEET:

MONEEL			
,	SHEET	ΩE	

This page intentionally left blank.

SECTION NO.: 5.8 SENSOR CATEGORY: Atmospheric Sounders

REV. NO.: 2 R

#### RSDH DATA SHEET

	•		
SHEET	1	OF	11

(1) SENSOR NAME, ACRONYM: Advanced Atmospheric Sounding and Imaging Radiometer (AASIR)

(2) DISCIPLINE: Earth Observations

(3) SUBDISCIPLINE:

Atmospheric Monitoring

#### (4) APPLICATION AND OBJECTIVE:

Provide visible and infrared imagery and temperature and humidity soundings from geosynchronous orbit altitudes with a temporal resolution consistant with small scale weather events, (i.e., severe storms) for real-time observation and short-term storm forecasts.

(5) HERITAGE/KEY PERSONNEL: The AASIR evolved from the Visible Infrared Spin Scan Radiometer (VISSR) of GOES-A and the VISSR Advanced Sounder of GOES-D

Instrument Rep.:

Jack Over

(GSFC) (301) 982-2372

(6) SENSOR DEPLOYMENT: Planned for launch in 1982 on STORMSAT Satellite, geosynchronous 3-axis stabilized (using Multimission Modular Space Craft). Short term (8 sec) platform stability is 4.2  $\mu$ rad in pitch and roll and 25  $\mu$ rad in yaw; Long term (20 min) stability is 11  $\mu$ rad in pitch and roll and 87  $\mu$ rad in yaw. Real-time attitude must be determined to within 525  $\mu$ rad in pitch and roll and 315  $\mu$ rad in yaw. Ground location error will be reduced to less than 10 km (1 km) by using ground control points.

(7)

## SENSOR CHARACTERISTICS

## (7A) CAPABILITIES AND CONSTRAINTS OF THE SENSOR TO ACQUIRE THE MEASURED PARAMETER:

The AASIR simultaneously gathers visible and IR image data and IR temperature soundings. The scanning mirror scans in the S-N and N-S directions. The IFOV for visible data is 15.6 rad; for sounding data, 347 rad; and for IR image 125 rad. Table 1 (see Sheet 3 of 11) converts this angular value to spacial coverage at various latitudes and longitudes relative to the satellite subpoint. Scan limits and location of scan is selected by ground command by identifying the N-S scan length, number of E-W steps,

(continued on next page)

(7B) ACTIVE SOURCE CHARACTERISTICS (FOR ACTIVE SENSORS):

N/A

(7C) DETECTOR MEASUREMENTS CHARACTERISTICS: Table 3 (see Sheet 5 of 11) gives the spectral bands and Noise Equivalent Radiance for the AASIR. An array of 24 silion photodiodes detect visible image data. The detectors are arranged in a single linear array. The detector array subtends a field of view of 375 µrad. An array of three detectors provide IR image data. Each detector has a 125 µrad field of view (giving 375 µrad coverage for the array). An array of 18 detectors provide sounding data (12 HgCdTe and 6 InSb). Each detector provides a 375 µrad field of view. The sounding detectors are arranged in 3 rows of 6 detectors each, with each detector separated from the next by one IFOV. Detectors are located to an accuracy of ±0.13 cm.

SECTION NO.:

5.8

SENSOR CATEGORY:

Atmospheric Sounders

Preceding page blank

5.8.39

REV. NO.: 2

#### CONTINUATION SHEET:

### (7A) continued

and the pointing angle of the center of the frame. Table 2 (see Sheet 4 of 11) gives the identified scan option, time per frame and IFOV's (pixels) collected per frame for five examples. The time to complete a N-S scan is constant (1.29 sec) regardless of the length of the scan. Sample time is shortened as the scan length increases, reducing S-N (accuracy). The E-W or W-E scan is stepped in 4.5 mrad units at the end of each 12 N-S scans (see information cell 9).

Each N-S scan collects the following data:

- 6 lines of sounder data (3 spectral bands sampled on each scan)
- 3 lines of IR image data
- 24 lines of visible image data

Data Rate is a maximum for the full earth scan and decreases proportional to the frame size selected. (The scanning logic is described in more detail in information cell 9.)

5.8.40

SECTION NO.: 5.8 SENSOR CATEGORY: Atmospheric Sounders

REV. NO.:

**CONTINUATION SHEET!** 

TABLE 1 AASIR Ground Coverages (km x km)

			9		
ANGULAR FIELD	30117.T.A.1		LONGITUDE RELATIV	LONGITUDE RELATIVE TO SATELLITE SUBPOINT	BPOINT
OF VIEW	11001	•0	15°	30°	45°
	•0	.57 x .57	. 59 x .57	.70 x .58	.96 x .59
15 6; ad	15°	.57 x .95	.60 × .60	.70 x .6C	.96 x .62
2	30°	.58 x .70	.60 x .70	$.70 \times .71$	.95 x .72
	45°	.59 x .96	.62 x .96.	.71 x .96	.94 x .96
	0°	4.46 x 4.46	4.43 x 4.5	5.6 x 4.6	7.7 × 4.73
าวราเหล่	15°	4.5 x 4.43	4.76 x 4.8	5.63 x 4.83	7.63 x 5.76
	30°	4.6 x 5.6	4.8 x 5.63	5.66 x 5.7	7.6 x 5.76
	45°	4.73 x 7.7	4.93 x 7.7	5.73 x 7.66	7.5 x 7.66
	0.	13.4 x 13.4	14.2 x 13.5	16,8 x 13.8	23.1 x 14.2
375uRad	15°	13.5 x 14.2	14.3 x 14.4	16.9 x 14.5	22.9 x 14.9
	30°	13.8 x 16.8	14.4 x 16.9	17.0 x 17.1	22.8 x 17.3
	45°	14.2 x 23.1	14.8 x 23.1	$17.2 \times 23.0$	22.5 x 23.0
	•0	161 x 161	170 x 162	202 x 165	277 x 170
4.5mRad	15°	162 x 170	172 x 173	203 x 174	275 x 179
	30°	165 x 202	173 x 203	204 x 205	273 x 208
	45°	$170 \times 277$	178 x 277	206 x 276	270 x 276

SECTION NO.:

5.8

SENSOR CATEGORY: Atmospheric Sounders

CONTINUATION SHEET:			M	(32)1922										
	DEAV RIT	RATE/SEC	77.9 x 10 <sup>3</sup>	156 x 10 <sup>3</sup>	1 x 10 <sup>6</sup>	2.88 x 10 <sup>6</sup>	7.0 × 10 <sup>6</sup>			:				
	FULL SCAN	VISIBLE	$3.2 \times 10^3$	194 x 10 <sup>3</sup>	1290 x 10 <sup>3</sup>	$4370 \times 10^3$	168 x 10 <sup>6</sup>					1	•	-
	PIXELS PER F	IR	1.3x10 <sup>3</sup>	7.8x10 <sup>3</sup>	52x10 <sup>3</sup>	170×10 <sup>3</sup>	6.7×10 <sup>6</sup>							
ons	PI	SOUNDER	2.6x10 <sup>3</sup>	15.6x10 <sup>3</sup>	104x10 <sup>3</sup>	350×10 <sup>3</sup>	13.4×10 <sup>6</sup>							
E 2 Scan Options	TIME FOR	FULL SCAN	18 sec.	55 sec.	2.5 min.	4.7 min.	22.8 min.	٠.			• .			
TABLE	FRAME	COVERAGE												
	ANCIII AR*	COVERAGE	4.5 x 4.5	$13.5 \times 9.0$	36.0 x 22.5	$67.5 \times 70.5$	324 x 324		lliradians					
	Т	E-W x N-S	Minimum	Cloud	Mesoscale	Regional	Full Earth		* Units are Milliradians					
SECTION NO.: 5.8			CATEG	ORY	-		heric	Soun	ders					
the second section of the second section is the second section of the second section of the second section of the second section is the second section of the section of the second section of the second section of the section of the second section of the section of th	5	8.4	ک			REV.	NO.:	2	200	REV. D	ATE:	31	Jan	1978

## **CONTINUATION SHEET:**

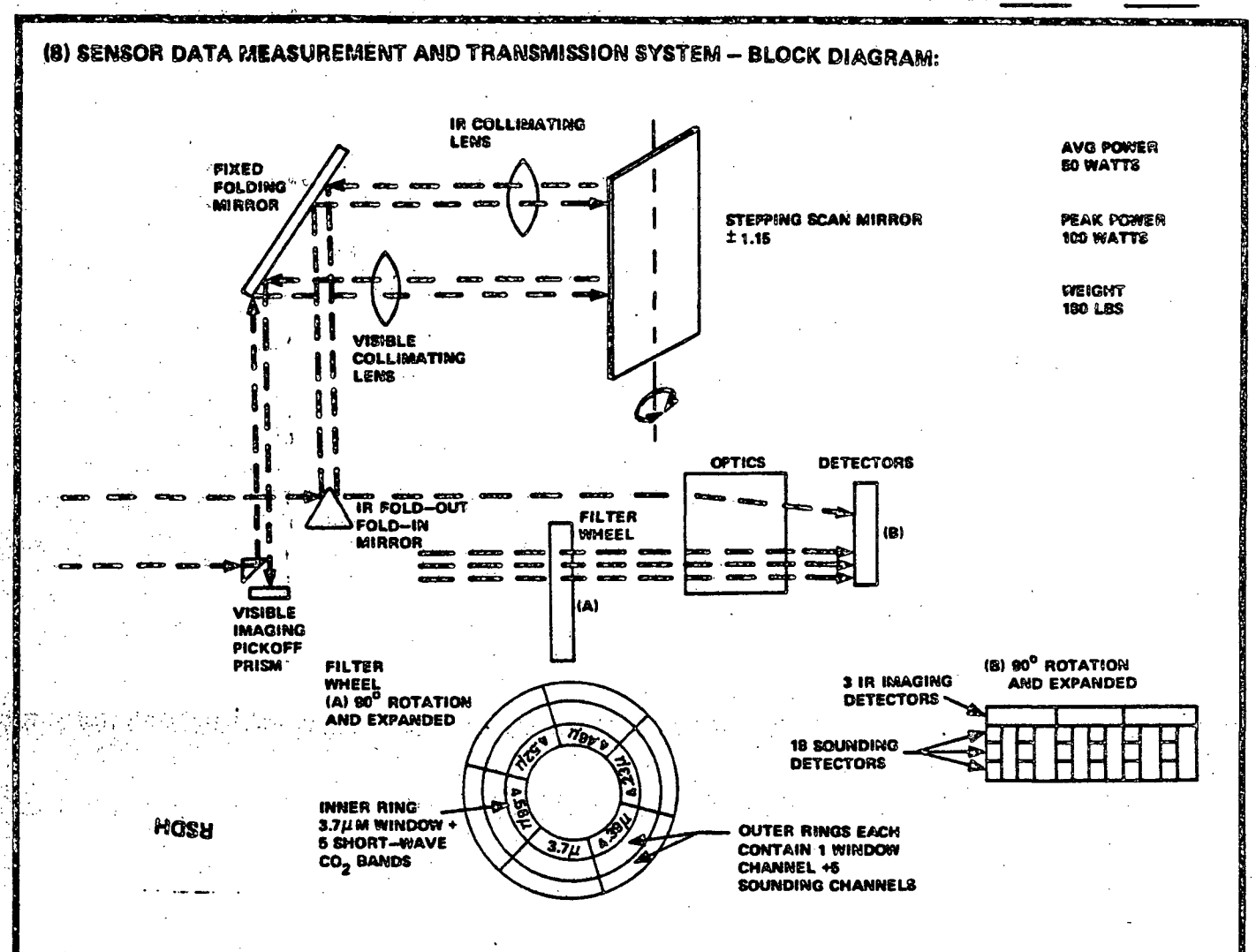
TABLE 3 Spectral Bands and Detector Noise Equivelant Radiance for the AASIR

FUNCTION	NUMBER OF CHANNELS	SPECTRAL BAND CENTER	AASIR CALCULATED NEN*
VISIBLE IMAGING	15	1.0	
IR IMAGING	3	11.1	.067
CO <sub>2</sub> SOUNDING	1	14.95	2.51
CO <sub>2</sub> SOUNDING	1	14.70	0.45
CO SOUNDING	1	14.49	0.255
CO <sub>2</sub> SOUNDING	1	14.22	0.214
CO, SOUNDING	1	13.96	0.152
CO <sub>2</sub> SOUNDING	1 · · · · · · · · · · · · · · · · · · ·	13.64	0.154
CO SOUNDING	1	13.35	0.152
CO <sub>2</sub> SOUNDING	1	12.66	0.138
CO <sub>2</sub> SOUNDING	1	4.23	0.0033
co sounding	. 1	4.39	0.0047
CO SOUNDING	1	4.46	0.0073
CO <sub>2</sub> SOUNDING	. 1	4.52	0.0073
CO <sub>2</sub> SOUNDING	1	4.56	0.0073
H <sub>2</sub> O ABSORPTION	1	7.75	0.065
H <sub>2</sub> O ABSORPTION	1	6.71	0.022
WINDOW	. 1	3.79	0.0004

<sup>\*</sup>Noise Equivelant Radiance in Units of ergs/sec -  $cm^2$  - sr -  $cm^{-1}$ 

SECTION NO.: 5.8 SENSOR CATEGORY: Atmospheric Sounders

5.3-43 REV. NO.: 2 REV. DATE: 31 Jan 1978



## (9) MEASUREMENT AND TRANSMISSION SYSTEM - NARRATIVE:

The AASIR uses a 40.6 cm diameter Ritchey-Chretian telescope. Because of heat problems associated with a 3-axis stabilized spacecraft, active focus control is provided in the IR and visible channels. The sounding spectral bands pass through a filter wheel consisting of 3 rings of filters with six filters per ring. The sounding detectors are arranged so that the outer two rings filter the signal incident on the two rows of HgCdTe sounding detectors (the top two rows in B in the block diagram) and the inner ring filters the signal on the InSb detectors. The detectors in each row are separated from the adjacent line by one line-width (375 µrad). At the end of each N-S scan, the filter wheel is advanced to the next filter. When all filters have been used (six N-S scans), the entire AASIR is stepped in the E-W direction one step (i.e., one N-S line) and six N-S scans are made observing the areas between the previous six lines. When these lines have been scanned for all filters, the AASIR is stepped in the E-W direction by eleven steps and the process is repeated for the next twelve lines.

Twenty-four lines of visible image data and three lines of IR image data are collected for each N-S sounder scan. Following each N-S scan, a separate stepping

(continued on next page)

SECTION NO.: 5.8 SENSOR CATEGORY: Atmospheric Sounders

5:8-44

REV. NO.: 2

SHEET	7	05	11	
SHEET		UF-		

### **CONTINUATION SHEET:**

### (9) continued

mirror steps the IR and visible image data two E-W steps (750 µrad). Thus, in the 12 scans necessary to sample 12 continuous sounder lines, 36 lines of IR data are sampled and 288 lines of visible data are sampled.

Each IFOV is measured twice to provide the data necessary to adjust for blur due to satellite motion. Each measurement is converted to digital form (eight bits for visible measurement, 10 bits for all others) multiplexed and transmitted to the ground station. Measurements are segmented into minor frames (estimated to be 4.5 x 4.5 rad segments) and proper synchronization, error and labeling bits are inserted at the start of each minor frame.

Calibration measurements are taken at 2 different blockbody temperatures over each scan and merged into the data stream. Maximum data rate of the sensor to ground transmission is about 7 megabits/second and is achieved for the full earth disk scan. (The maximum rate for cloud scale scan is about 1/36 the full disk.) The data rate is proportional to the rate of the N-S scan. The maximum data rate is achieved at the center of the scan and slow at scan limits to about 70% of the maximum. Filler data may be added to maintain a constant scan rate.

Ground initiated commands are provided to select the scan limits and pointing directions.

5.8.45

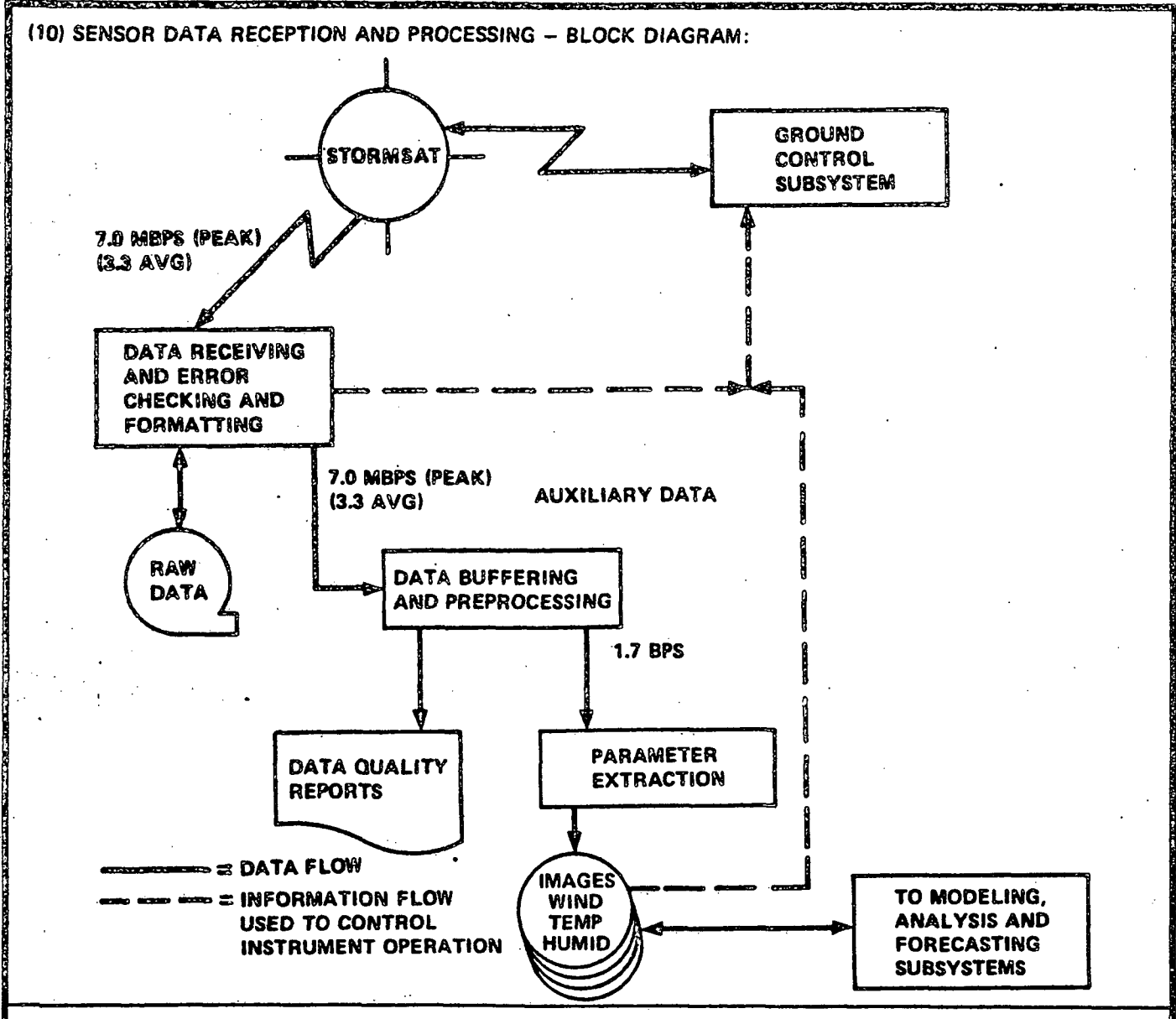
SECTION NO.: 5.8

SENSOR CATEGORY:

Atmospheric Sounders

REV. NO.:

2



#### (11) RECEIVING AND PROCESSING - NARRATIVE:

All data are transmitted in real time to Goddard Space Flight Center (GSFC). The receiving station for AASIR data must support a data input rate of at least 7 Mbps from the AASIR. The RF signal is down-converted to IF and demodulated into an encoded digital signal. Error checking bits incorporated into the input stream are monitored and removed from the signal and indications of data quality are output by the receiver. The receiver monitors the signal locating the start of a minor frame. Following frame synchronization, the data is demultiplexed and sorted by spectral band. Visible data (8-bits/Pixel) is packed 2-pixels/byte and IR and Sounder data (10 bits) is placed into a 16-bit word by zeroing leading bits. The data, "sorted" by spectral band, and some associated bits describing error rates, signal strength, etc., are output.

5.8-46 (continued on next page)

SECTION NO.: 5.8 SENSOR CATEGORY: Atmospheric Sounders

REV. NO.: 2

#### CONTINUATION SHEET:

## (11) continued

The received data must be further formatted to be usable for meteorological processing. This pre-processing must not delay data thruput. Current estimates are that all pre-processing must be completed within five minutes of the end of the scan frame. Pre-processing includes:

- (1) recording of raw data to high density analog tapes for short term storage (until the quality of processed data is known),
- (2) consolidating and formatting of a header record of ancillary data for each frame (giving attitude, location, time, etc.),
- (3) calculating of calibration coefficients from the received calibration measurements and applying those coefficients to the raw data,
- (4) using the dual measurements of each IFOV to eliminate (reduce) blur (this filtering will reduce the data rate by 50%),
- (5) converting the input sequence to be compatable with GOES,
- (6) transfering of data to the meteorological processing system.

Of the functions, the converting of the input sequence (5 above) is the most stressing. GOES instruments scan from west to east beginning with the northern most latitude and stepping south. To be compatible, the AASIR output, every other scan (i.e., the S-N scan) must be reversed, and the entire frame must be transposed for a N-S scan with E-W stepping (or W-E) to a E-W scan sequence with N-S stepping. This process requires large storage areas for full frames of data.

The planned hardware for the pre-processing system is based on the scan averaged bit rate of about 3.3 Mbps (vs. the peak rate per scan of 7.1 bps) for the full disk scan. The processing system must be able to process the data as received and will require a minicomputer in the class of PDP11-70 or Interdata 8/32 (.6 - .8 Million Operations per Second). Special processors will be used for filtering and I/O functions. About .5 x 10 bytes are required to hold a full earth scan (i.e., one N-S scan) of measurements. Current estimates allow multiple buffers for input, buffers for processing and additional buffers for output of processed data to disk. When the reduction in data volume due to filtering is included, the resulting buffer requirements are between 3 and 4 Mbytes (8 bits/byte).

A separate processor will provide transposition of the data elements to the VISSR format. Nearly 200,000 bytes of memory buffers are required. A small minicomputer would provide the necessary processing capability, but very fast I/O capability will be required to perform the transposition of data. (Disk I/O rates of 370 K bytes per second to store a full frame of AASIR data.) About 5 Mbyte of disk storage is required for each frame. To maintain this rate, a 1.2 Mbyte/sec disk is required (due to losses in head positioning, etc.) and a minicomputer (such as Interdata 8/32, LEL 32/55) that have sufficient I/O bandwidth.

(continued on next page)

SECTION NO .:

5 8

SENSOR CATEGORY: Atmospheric Sounders

### CONTINUATION SHEET:

## (11) continued

Definition of ground system requirements is still in progress at this time and the above figures are subject to change.

The parameter extraction processing consist of determining wind velocity and temperature profiles. The wind velocity is extracted by tracking the movement of clouds. An interactive mode is used in which the process is automatic, but may be controlled by the operator. Soundings are generated using the AASIR and MASR data to achieve maximum accuracy for all cloud extents. All image data may be displayed for visual analysis by the meteorologist. Special aid to enhance the image, provide selected altitude slices, etc., will be provided. All output data is buffered and used for model inputs to generate short range forecasts.

The meteorological processing hardware will include two displays and a minicomputer (PDP 11/70 class) for wind extraction and cloud analysis. A similar configuration for analysis of individual spectral images and control of sounding data processing. These computers are connected to the disk data base through redundant data base management computers.

The interactive analysis and forecasting subsystem adds two more display subsystem (i.e., 2 pan of displays and 2 minicomputers). From these displays, the forecaster may watch more crops or view any data on the memories of the other display subsystems. One of these display subsystems will be connected into the NOAA weather communication return.

Between 15 and 50 minutes of CPU time is necessary (estimate) for wind extraction on a PDP 11/70 scale computer. Sounding are expected to require about 20 minutes of CPU time for each mesoscale (1000 x 1250 km) frame (15,000 profiles per hour at 4000 operations per profile). The sounding CPU also supports image spectral analysis. The estimates for this processing is dependent on the classification techniques used.

The data base computers will require moderate minicomputer processing capabilities, but must support high I/O bandwidths (1.2 Mbytes/sec). The estimated on-line disk storage is

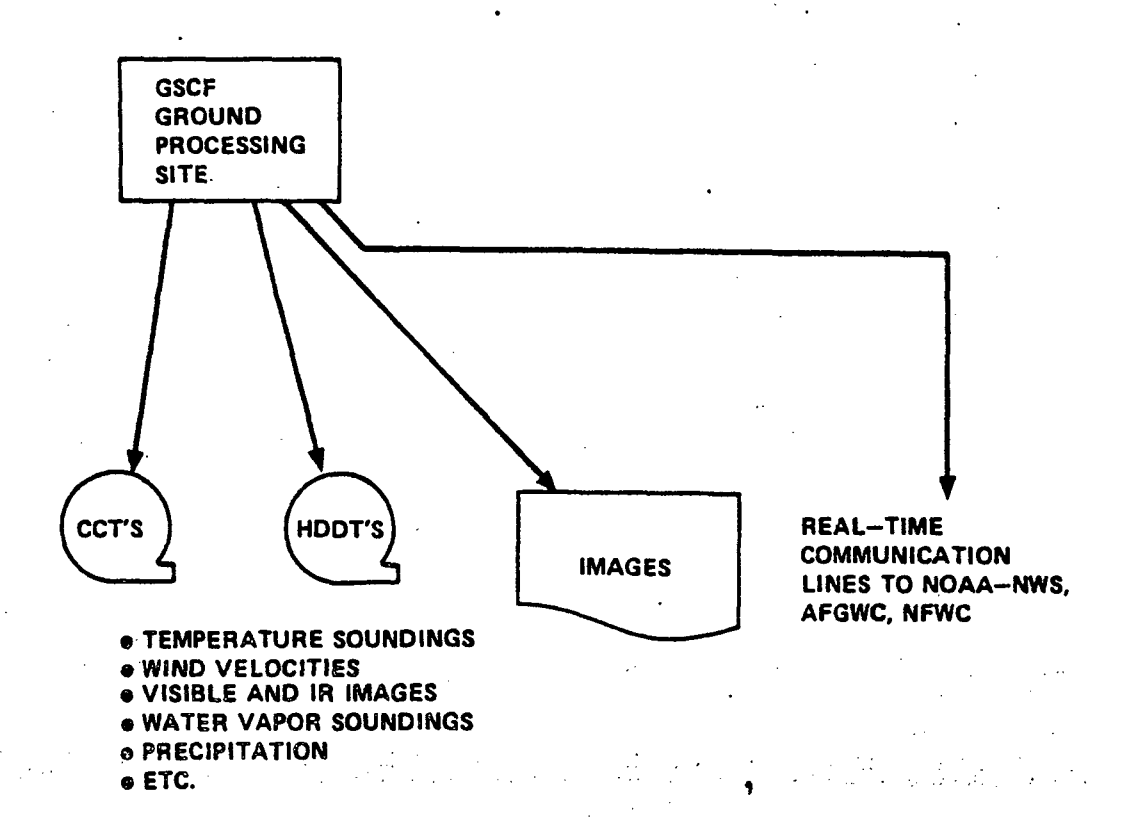
On-line image data for analysis	425 Mbytes
Meteorological Parameter Supporting	
Forecast Models	200 Mbytes
Sounding Data	225 Mbytes
Contents, coefficients, etc.	100 Mbytes
Total	1,000 Mbytes

The estimated CPU and on-line storage would provide full analysis and forecasting capabilities to GSFC.

The Ground Control Subsystem will allow meteorologists to implement pointer commands within all min of the request, and will transfer tables and coefficients required for attitude and location stabalizing by the on-board computer.

SECTION NO.:	5.8	SENSOR CATEGORY:	Atmospheric	Sounders

## (12) DISTRIBUTION OF DATA FROM GROUND STATIONS - BLOCK DIAGRAM:



#### (13) DATA DISTRIBUTION - NARRATIVE:

Data output consists of visible and IR images, and IR sounder radiances. They are provided in CCT format and as hard copy photographs. The final products of wind, temperature, water vapor, pressure and precipitation are available. The users and data distribution lines are defined at this time. Existing lines will probably be used (AFOS) for NWS and DOD distribution.

The system is designated for real-time operation (1 hour) and much of the data will be used at the data reception site. High density digital tapes will be generated.

**SECTION NO.:** 

5.8

SENSOR CATEGORY:

Atmospheric Sounders

REV. NO.:

## RSDH DATA SHEET

and the second s		J11661	VI
CONTINUIATION SHEET.			
CONTINUATION SHEET:	•		
	•		
•			
•			
		•	
•			
			i
•			Š
n			
•			
	·		
	This page intentionally left blank.	. •	
•	•		Ì
	·		
	. •		
•			
		•	
	•		
			į
			9
	•		
•		•	
		•	
•			
· J			
•	•		
•	•		. 1
	T		
SECTION NO.: 5.8	SENSOR CATEGORY: Atmospheric Sounders		
the second of th		N DATE. 71 T	1070

#### RSDH DATA SHEET

SHEET 1 OF 6

(1) SENSOR NAME, ACRONYM:

Vertical Temperature Profile Radiometer (VTPR)

(2) DISCIPLINE:

Earth Observations

(3) SUBDISCIPLINE: Atmospheric Monitoring

## (4) APPLICATION AND OBJECTIVE:

The ITOS-VTPR is used to obtain temperature and water vapor measurements at 15 altitude levels of the atmosphere (up to 30 km).

(5) HERITAGE/KEY PERSONNEL:

NOAA-3 11-06-73 (ITOS-F)

NOAA-4 11-15-74 (ITOS-G)

NOAA-2 10-15-72 (ITOS-D)

NOAA-5 11- -76 (ITOS-H)

NIMBUS-5 (NEMS) NIMBUS-6 (Adv. Atmos.

Inst. Rep.: Gary Cunningham (GSFC) (301) 982-6778 Ground Systems: A. Weberwetzki (NOAA) (301) 763-5433

Sounder)

#### (6) SENSOR DEPLOYMENT:

The ITOS satellites are launched into sun synchronous orbit at an inclination of 101.7 degrees, at an altitude of 1463 km. The satellites are 3-axis stabilized ( $< \pm 1^{\circ}$ ) and complete 12.5 orbits per day. Global coverage is provided by each satellite in 12 hours.

(7)

#### SENSOR CHARACTERISTICS

#### (7A) CAPABILITIES AND CONSTRAINTS OF THE SENSOR TO ACQUIRE THE MEASURED PARAMETER:

One complete measurement (8 bands) is completed each 1/2 second. The scanner is stepped after each measurement by 2.235 degrees, using 23 steps to cover the complete cross-track scan of 62.9 degrees. Each scan requires 11.5 sec. plus one sec. for return. Ground resolution is 59 km at the satellite subpoint. Ground coverage for each scan is approximately 1400 km. Only measurements taken over the ocean can be used.

#### (7B) ACTIVE SOURCE CHARACTERISTICS (FOR ACTIVE SENSORS):

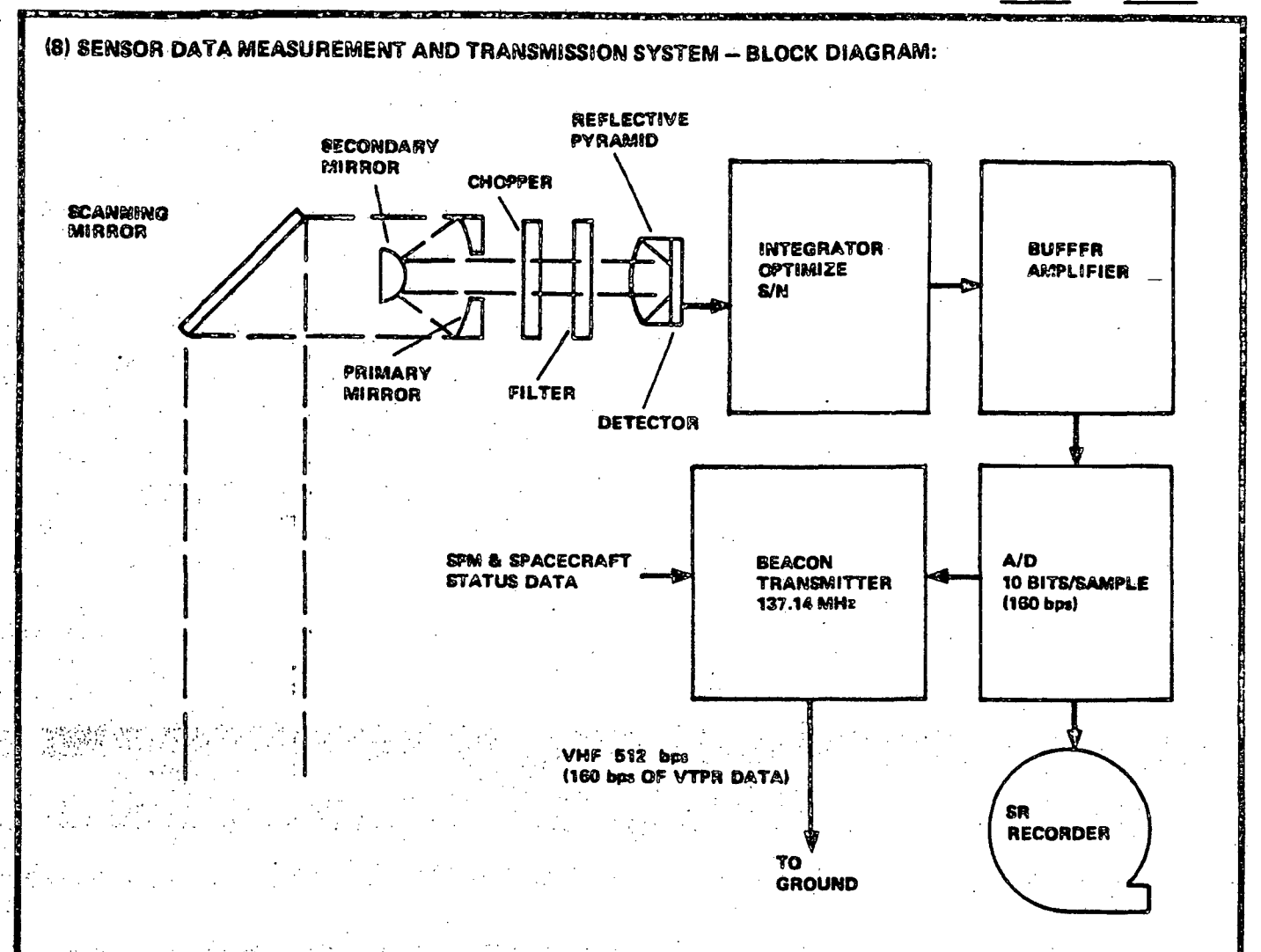
N/A

(7C) DETECTOR MEASUREMENTS CHARACTERISTICS: The VTPR measures spectral radiation in 8 bands: 12 μm, 13.8 μm, 13.4 μm, 14.1 μm, 14.8 μm, 14.4 μm, 14.97 μm, 18.7 μm. 62.5 ms are required for each band measurement, allowing one set of 8 measurements each 1/2 second. (Following the 8th band measurement, the scanner steps to the next scan cell.) The single pyroelectric detector (triglysene sulphate) has a Noise Equivalent Power of less than 1.5 x 10<sup>-10</sup> W(HZ)<sup>-1/2</sup> and operates at a temperature of 290°K (uncooled). Its effective area is 1.5 mm. The detector is modulated at 16 Hz Space (40°K) and internal black (258°K) body calibration is performed each 15 sec.

5.8.51

SECTION NO.: 5.8

SENSOR CATEGORY: Atmospheric Sounders



(9) MEASUREMENT AND TRANSMISSION SYSTEM - NARRATIVE: The VTPR uses a Cassegrain Telescope (6.6cm) with a wheel of eight filters and a single pyroelectric detector. The wheel rotates at 120 rpm, putting one filter into the field of view each 62.5 milliseconds (allowing one full measurement of 8 bands each 5 sec.). Compensation for orbital motion is achieved by using a spiral mask in the filter wheel which indexes the system field stop so as to track a spot on the earth's surface for a filter wheel sequence. The chopper is viewed for 31.25 milliseconds. The chopper and filter wheel are synchronized so that the transition between filters occurs during the chopper viewing time. Chopper frequency is 16 Hz. The filter and chopper are mounted on thermoly insulated hubs and surrounded with a black housing to control the temperature (308°K).

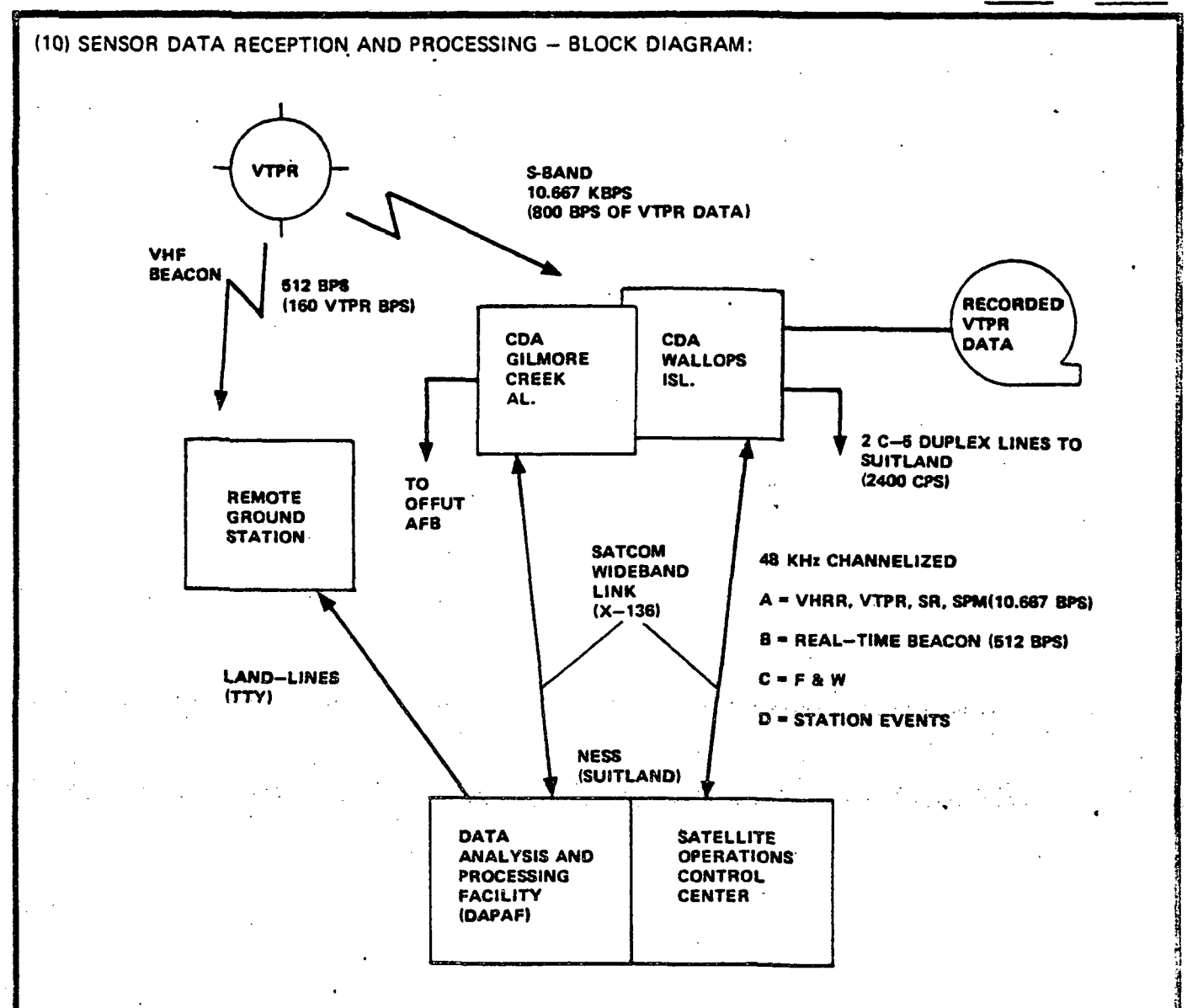
The detector is located at the truncated opening of a reflective pyramid. The detector output is shaped and equalized by an analog signal processor. The signal is maximized for S-N and converted to 10 bits digital for each measurement. The digital signal is recorded on the scanning radiometer recorder and is transmitted in real-time over the VHF link.

SECTION NO.: 5.8 SENSOR CATEGORY: Atmospheric Sounders

5.8.52

REV. NO.:

2



#### (11) RECEIVING AND PROCESSING - NARRATIVE:

The VTPR data is recorded on the scanning Radiometer Recorder as it is sensed and is also transmitted in real time over the VHF beacon link to direct ground stations on command from the CDA. The Direct Ground Station is designed to serve local users only and no further distribution of its output occurs. The NESS Central Data Distribution Facility provides satellite status, location and orbit location data to the ground site via TTY.

Direct ground stations receive the raw voltage measurement values. The user processing of VTPR data consists of three steps:

- (a) conversion of raw voltage counts to radiances,
- (b) correction (or elimination) of radiances for cloud effects,

(continued on next page)

SECTION NO.: 5.8 | SENSOR CATEGORY: Atmospheric Sounders

3 REV. NO.: 2

			٠,	
SHEET	4	OF	,	•

#### CONTINUATION SHEET:

### (11) continued

(c) conversion of the resulting clear radiances to temperature and moisture profiles.

NESS provides sets of calibration coefficients for (a) above. To correct the measurements for cloud cover (b above), NESS recommends the user select a spacial array of 8 x 8 complete measurements. The user then compares the radiance of the 11 µm window band to the Plank function value, B, at that spectral band and associated surface temperature to determine where the area is not entirely overcast. The radiance values closest to B can be considered as clear-column radiances. The regression coefficient matrix is multiplied by the clear radiance vector to get a single temperature profile vector for each array of radiance values. Normally 4 or 5 17-minute data periods can be received by a user each day. The area covered by each pass is about 1400 km wide and 5000 km long.

Two command and data acquisition (CDA) stations acquire the VTPR (and all other satellite outputs) for the central processing facilities of NOAA. (During Blind orbits, a station in France acquires and transmits VTPR data.) The CDA's operate in one of three modes as directed by the Satellite Operations Control Center (SOCC):

- a) acquire real-time direct broadcast only (APT, HRPT, Beacon-VTPR/SPM, spacecraft telemetry),
- b) acquire real-time direct broadcast and playback single orbit of VTPR data (and SR, VHRR), or
- c) acquire real-time direct broadcast and multiple orbits of VTPR data (and SR, VHRR).

The selection of mode is dependant on the orbital path of the satellite. On some orbits the VTPR does not pass over either CDA so that on the following orbit, mode C is necessary. During other orbits, the satellite passes over both stations, allowing mode A to be commanded for one of the stations.

The real-time VTPR data is multiplexed with beacon data for transmission to ground. The real-time beacon data is recorded on magnetic tape as it is received. The beacon data is demodulated, recorded on paper chart recorders, and transmitted via channel B of the SATCOM Longlines to the NESS facility at Suitland.

Up to 201 minutes of VTPR data can be recorded on the on-board recorders as controlled by ground commands transmitted via CDA's and stored on-board for execution at the specified times. The recorded data is played back, on command, at 20 x the record rate (10.667 kbps). Both SR and VTPR data are received and recorded at the CDA on a separate magnetic tape recorder (at 60 ips). Both CDA stations compensate for speed flunctuation of the NOAA recorders. The CDA amplifies and demodulates the input signals before recording. Following the satellite data acquisition, the recorded SR/VTPR data is played back and transmitted to the NESS Suitland Facility and to Global Weather Central at Offutt AFB.

(continued on next page)

**SECTION NO.:** SENSOR CATEGORY: Atmospheric Sounders 5.8

### (11) continued

The data enters the NOAA facility at the Digital Data Handling System (DDHS) of the Data Processing and Analysis Facility. The DDHS separates and formats the VTPR data for processing by a central large-scale computing facility. The DDHS is a completely redundant system. Each of the systems can operate simultaneously to process both NOAA satellites when both are over a CDA station. As the data is received, it is recorded to an analog recorder, converted to digital form and formatted for input to an EMR-6130 computer. (UNIVAC 6000 series). The EMR-6130 is a mid-scale computer, 16-bits/word with expanded I/O capabilities. The VTPR data is output to disk along with satellite time information.

There is no buffering of data before the 6130 processing. The occurance of input from the SATCOM lines interrupts the 6130 and initiates immediate processing of the data. Approximately 12,700 VTPR measurements are received each orbit, corresponding to 127,000 bits of VTPR data + the time words for each scan. This data requires a reel of 800 bpi tape for one orbit of data and two reels when a blind orbit has been encountered.

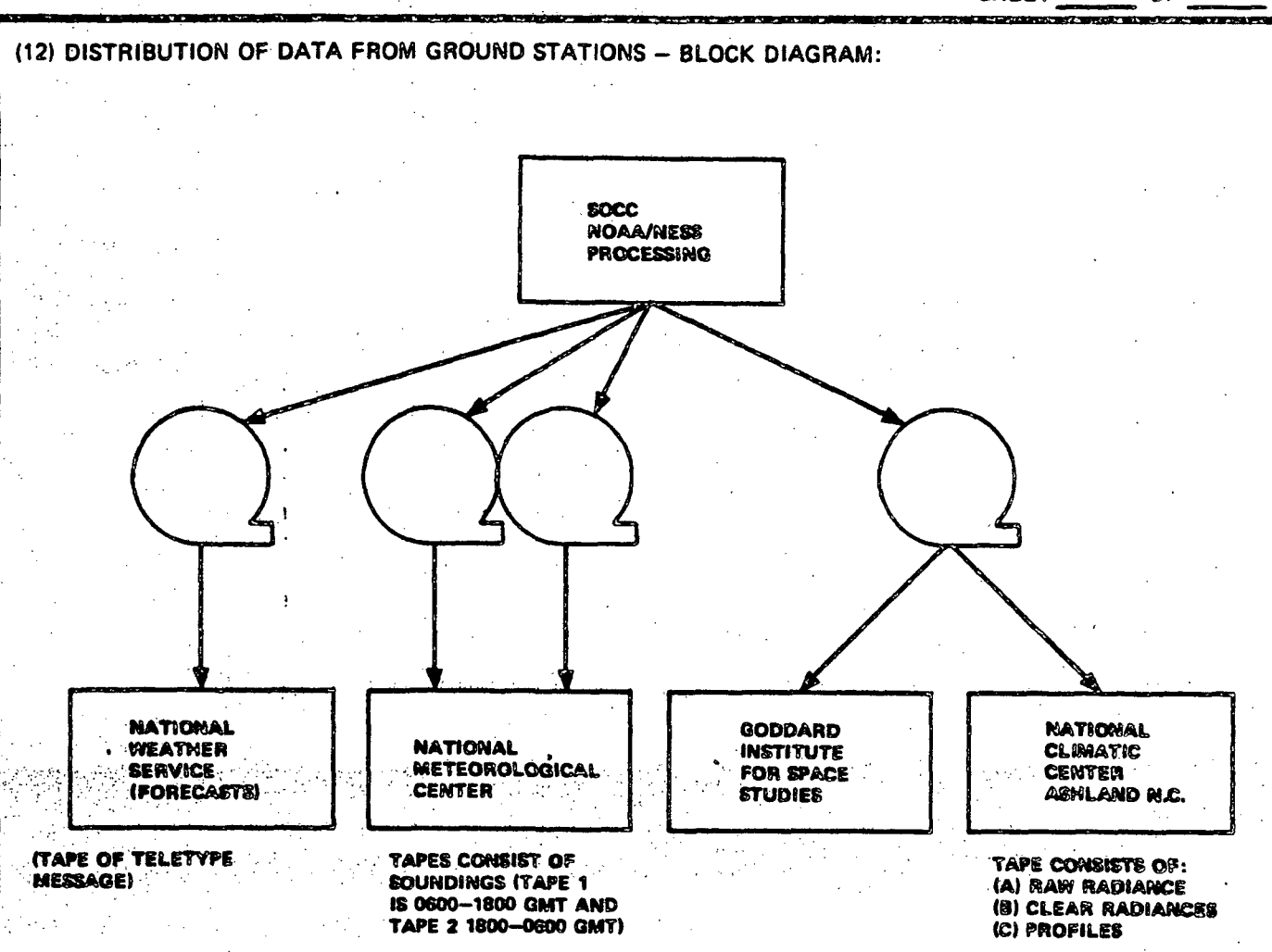
The stored values are later output to the NOAA 360-195 complex over a direct communications channel. There, the VTPR data is geographically registered to locate the position of the soundings to be developed and locate known sea-surface temperatures for associated soundings. Calibration data taken by the sensor is used to verify the status of the instrument and to compute radiance values. The window channel, surface temperature and first guess values\* of temperature and humidity profiles are used to calculate the clear radiance of the other channels for an  $8 \times 8$  array (approximately 600 km  $\times$  600 km). A single temperature sounding is generated for each array. The temperature profile is used to determine the moisture profile of the array. Soundings are generated for 15 levels of the atmosphere: 1000 mb, 850 mb, 700 mb, 500 mb, 400 mb, 300 mb, 250 mb, 200 mb, 150 mb, 100 mb, 70 mb, 50 mb, 30 mb, 20 mb, 10 mb.

The Central Computing Facility (360/195) requires about 1 1/2 hours per day to process the 152,400 daily measurements into 2,600 temperature soundings. (The exact number varies depending on cloud cover, etc.)

SECTION NO.: SENSOR CATEGORY: Atmospheric Sounders 5.8

> **REV. NO.: 2** REV. DATE: 31 Jan 1978

<sup>\* 1</sup>st Guess values for the northern hemisphere as taken from NMC forecasts.



#### (13) DATA DISTRIBUTION - NARRATIVE:

The major product is a Satellite Infrared Sounding (SIRS) that contains location, heights, temperature, and dewpoint temperature depression at levels up to 40 mb, and then contain heights and temperatures up to 10 mb. (Only data on the oceans are included.) The data are prepared at the SOCC by the National Environmental Satellite Service in various formats required by users. The NWS tape is prepared in as a teletype message. The other tapes are prepared as shown. The NWS, NMC, and GISS tapes are transmitted as each orbit of processing is completed. The tape to the NCC is transmitted weekly.

Data products developed by users that have access to direct receiving stations are not controlled or distributed by a central organization.

Soundings are transmitted twice daily via GTS of the WWW by the NMC.

SECTION NO.: 5.8 SENSOR CATEGORY: Atmospheric Sounders

REV. NO.: 2 REV. DATE: 31 Jan 1978

SHEET 1 OF 6

(1) SENSOR NAME, ACRONYM: Stratospheric and Mesospheric Sounder (SAMS)

(2) DISCIPLINE: Earth Observations

(3) SUBDISCIPLINE: Atmospheric Monitoring

### (4) APPLICATION AND OBJECTIVE:

The SAMS is used to determine temperature profile and composition of the atmosphere between the 10 km and 120 km altitude levels (i.e., the vertical concentrations of  $H_2O$ ,  $N_2O$ ,  $CH_4$ , CO and NO). The sensor will attempt to measure doppler shift of emission lines to determine the zonal wind shift in the 50-100 km region.

#### (5) HERITAGE/KEY PERSONNEL:

Instrument Rep.: Richard White (301) 982-4520

#### (6) SENSOR DEPLOYMENT:

SAMS is designed for 3-axis earth stabilized platforms in a near polar sunsynchronous orbit at an altitude of 900-1200 km. First deployment will be on NIMBUS-G (3rd quarter of 1978).

(7)

#### SENSOR CHARACTERISTICS

#### (7A) CAPABILITIES AND CONSTRAINTS OF THE SENSOR TO ACQUIRE THE MEASURED PARAMETER:

The SAMS scans in a vertical plane at right angles to the direction of spacecraft motion. The sensor will normally scan an angle of 2.6° in 32 equal steps as shown in Figure 1, but will have the ability to scan an angle of 6° to insure that the nominal scan volume can be scanned given attitude and orbit errors. Each scan position defines three 28 mrad x 2.8 mrad (100 km x 10 km) simultaneously (see Figure 2). A second integration time is required for each measurement. Scan speed, nominal scan volume and

(continued on next page)

#### (7B) ACTIVE SOURCE CHARACTERISTICS (FOR ACTIVE SENSORS):

N/A

### (7C) DETECTOR MEASUREMENTS CHARACTERISTICS:

Six detectors measure the input signal in the following spectral bands:  $4.3\mu m (CO_2)$ ,  $5.3\mu m (NO)$ ,  $2.7\mu m (H_0)$ ,  $25-100\mu m (H_0)$ ,  $5.8\mu m (N_0)$ , and  $7.6-7.8\mu m (CH_4)$ . The detectors consist of  $^24$ -Triglysene Sulphate (uncooled) 1-Lead Sulphide (cooled to  $273^{\circ} K$ ) and 1-InSb (cooled to  $160^{\circ} K$ ). Two separate signals are output by the detectors, one at 250 Hz (chopper frequency) and one at the Pressure Modulated Cell (PMC) frequency. Calibration measurements are taken by viewing space and an internal black body.

SECTION NO.: 5.8

SENSOR CATEGORY: Atmospheric Sounders

5.857

**REV. NO.:** 2

### (7A) continued

scan step size are set by ground commands. Minimum step size is 1/2 IFOV. An azimuth scan is used to measure doppler shift in the emission spectrum. The scan can begin at a minimum angle of 75° to the direction of spacecraft motion and can scan horizontally to a maximum angle of 105°. The scan is continuous with the rate of scan compensating for the velocity of the spacecraft. Scan time for the full horizontal scan is 240 seconds. The scan is under control of ground command.

5.8-58

SECTION NO .:

5.8

SENSOR CATEGORY:

Atmospheric Sounders

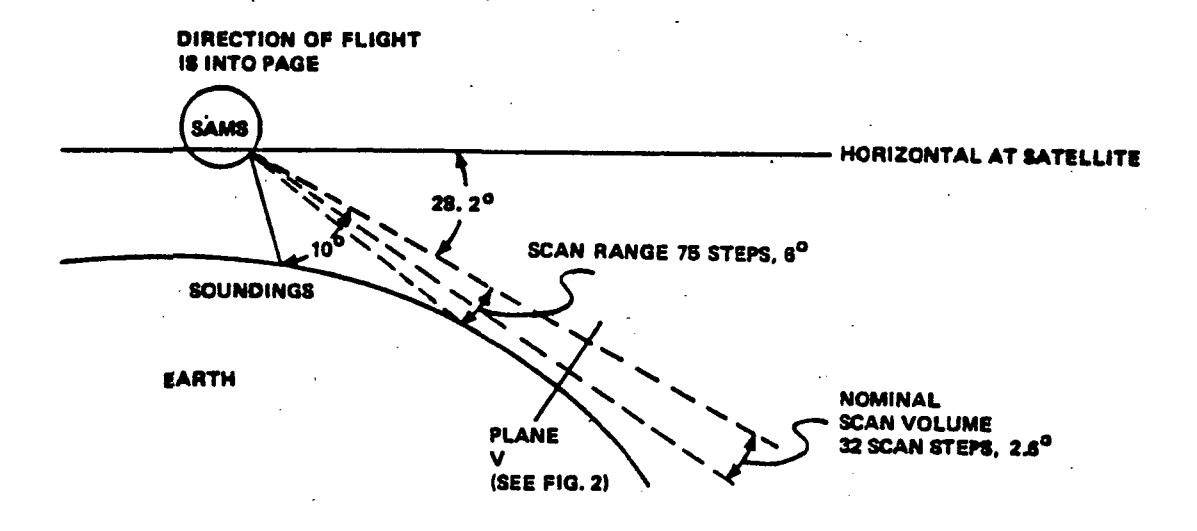


FIGURE 1 Scan Geometry

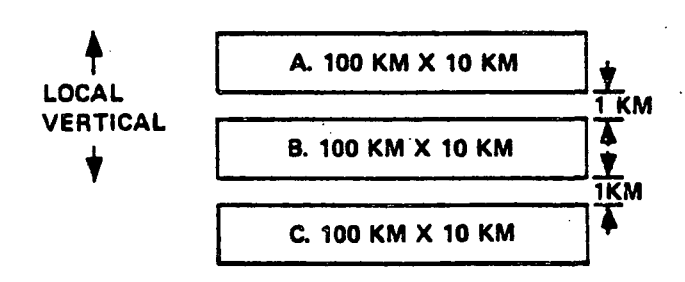


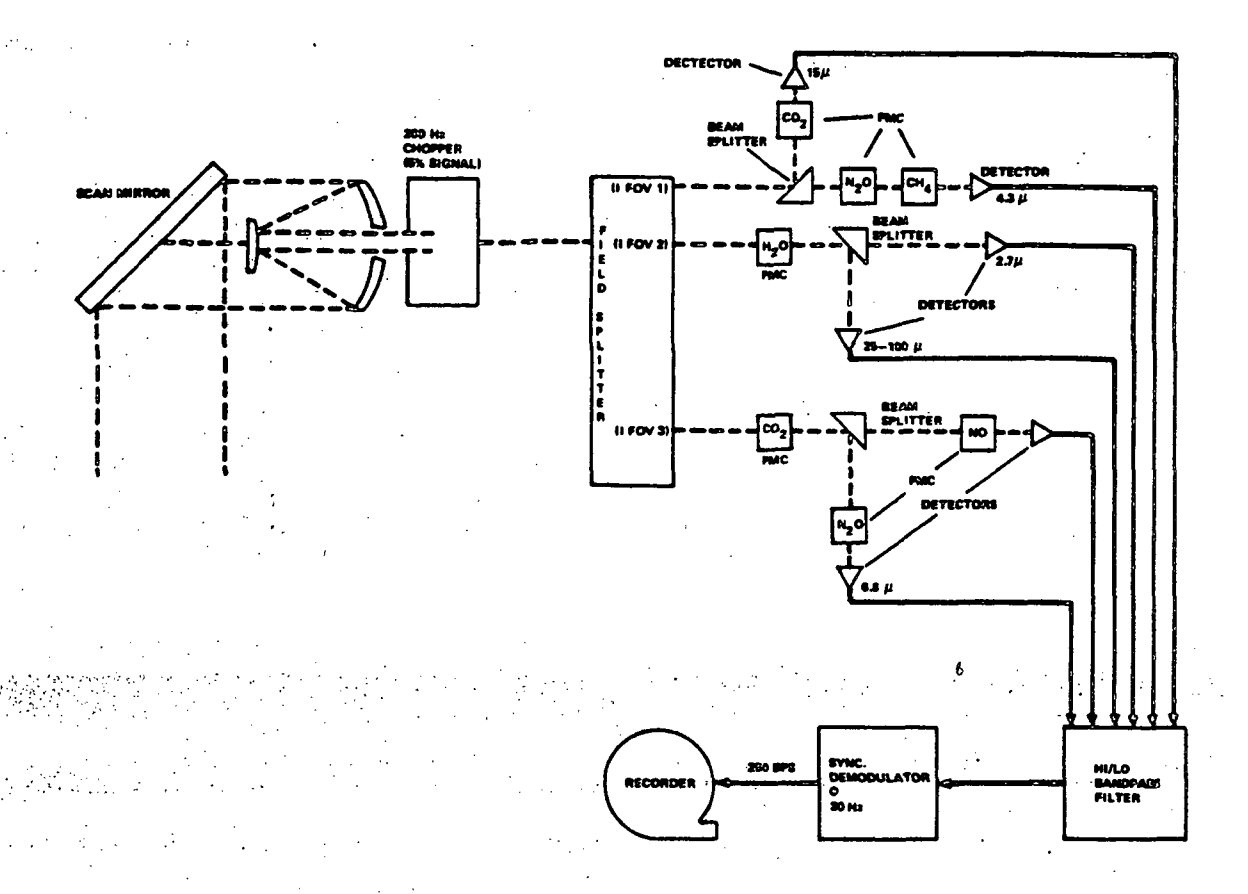
FIGURE 2 Orientation of IFOV's Viewed Simultaneously on Plane V (see Figure 1) as one scan position

SECTION NO.: 5.8 SENSOR CATEGORY: Atmospheric Sounders

5.8.59

**REV. NO.:** 2

### (8) SENSOR DATA MEASUREMENT AND TRANSMISSION SYSTEM — BLOCK DIAGRAM:



#### (9) MEASUREMENT AND TRANSMISSION SYSTEM - NARRATIVE:

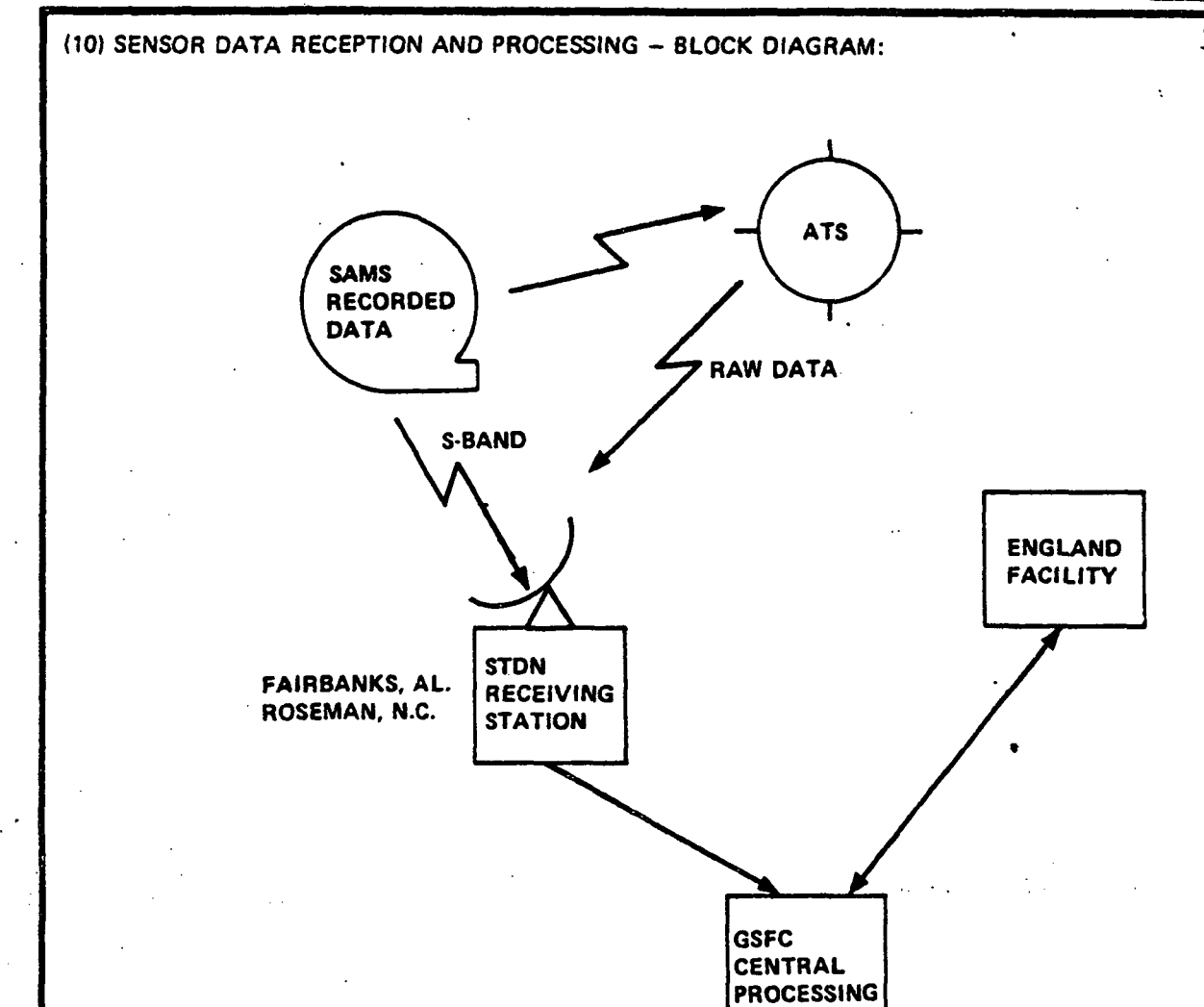
The incoming radiation is incident upon a scan mirror 202 by 185 mm. The IR input is modulated at two points to obtain two outputs from each detector. The chopper modulates 5% of the incoming signal at 250 Hz. The signal is split into 3 fields of view. These three outputs are passed through a series of Pressure Modulated Cells (PMC) and beam splitters to filter the signal so that the desired spectral band is directed to its associated detector. The PMC's are modulated at 30 Hz The output of the detectors is passed through a Hi/Lo bandpass filter and demodulated into two signals. The 250 Hz modulation gives a signal in which all spectral bands were modulated, the PCM modulation affects only the spectral range associated with the PCM. These two outputs enable emissions from interfering gases within a spectral interval to be eliminated.

Commands allow the PMC's to be selected and modulated as desired, and control the scan logic at the SAMS. 27 commands are defined.

SECTION NO .: 5.8 SENSOR CATEGORY:

Atmospheric Sounders

REV. NO.:



### (11) RECEIVING AND PROCESSING - NARRATIVE:

The SAMS data are transmitted to GSFC and then immediately transmitted to the England facility. There it is formatted and pre-processed and then returned to GSFC for processing. (The data is also processed in England.) (See THIR, Section 8 for more information.) The two separate signals output by each detector are compared to eliminate emission generated by interferring within a given spectral interval.

Zonal wind measurement is accomplished by analyzing the doppler shift introduced between the emission lines of the atmosphere (as sensed by an azimuth scan) and the absorption lines in the PMC's.

5.8.61

SECTION NO.: 5.8 | SENSOR CATEGORY: Atmospheric Sounders

REV. NO.: 2

SECTION NO .:

5.8

SENSOR CATEGORY: Atmospheric Sounders

REV.:NO.:

**REV. DATE:** 

31 Jan 1978

	RSI					
•	DATA:	SHEET	SHEET	1	OF	6
(1)	SENSOR NAME, ACRONYM: Visible Infrared Sp	in-Scan Radiometer				
(2)	DISCIPLINE: Earth Observations	(3) SUBDISCIPLINE:	Atmospheric	Monif	tori	ng
(4)	APPLICATION AND OBJECTIVE:					
	The VAS operates at Geosynchronous Altit sea surface temperature measurements, cl Earth Images for meteological use.					on.
(5)	HERITAGE/KEY PERSONNEL: The VAS is a modi Radiometer (VISSR) flown on SMS-2 and GO both, sounding capability was added to t Instrument Rep.: Larry Rouzer (GSFC) (	ES-1. The visible he VISSR to obtain	imaging is			
	SENSOR DEPLOYMENT: The VAS is designed for geosynchronous of stabilized spacecraft. Attitude is to be stability of .5 arc sec. maximum. First for 1980.	e maintained to wi	thin .1° with	ıa	_	•
(7)	SENSOR CHAR	ACTERISTICS				
(7A) CAPABILITIES AND CONSTRAINTS OF THE SENSOR TO ACQUIRE THE MEASURED PARAMETER:  The VAS depends on spin (100 rpm) of the satellite for its E-W scan and steps in the N-S direction. IR imaging has a resolution of .192 milliradians (8 km at the subpoint), visible images have a resolution of .021 x .025 milliradians (.9 km).  The sounding channels (4) have a resolution of 16 km. For soundings, multiple scans are required to integrate signals sufficiently to obtain the required S-N ratio. Multiple sets of scans are required to obtain data in all sounding channels (4 scan integrations per measurements). (For more detail on the imaging capability, (continued on next page)						
(7B	ACTIVE SOURCE CHARACTERISTICS (FOR ACTIVE	SENSORS):				
	N/A				·	
(7C	DETECTOR MEASUREMENTS CHARACTERISTICS:					
	The Visible and IR imaging detectors are VISSR data sheets). Four detectors are InSb detectors. The detectors have a fi measure radiance in the 14.7 µm through integrated to achieve required S-N. An is viewed once per scan for signal calib	added for sounding eld of view of .38 3.9 µm spectral ha onboard black body	: two HgCdTe 4 urad. Thes	e and se de	two tect	ors

SENSOR CATEGORY: Atmospheric Sounders

5.8.63

**SECTION NO.:** 

5.8

REV. NO.:

SHEET	.2	OF	6
SHEET		QF	0

### CONTINUATION SHEET:

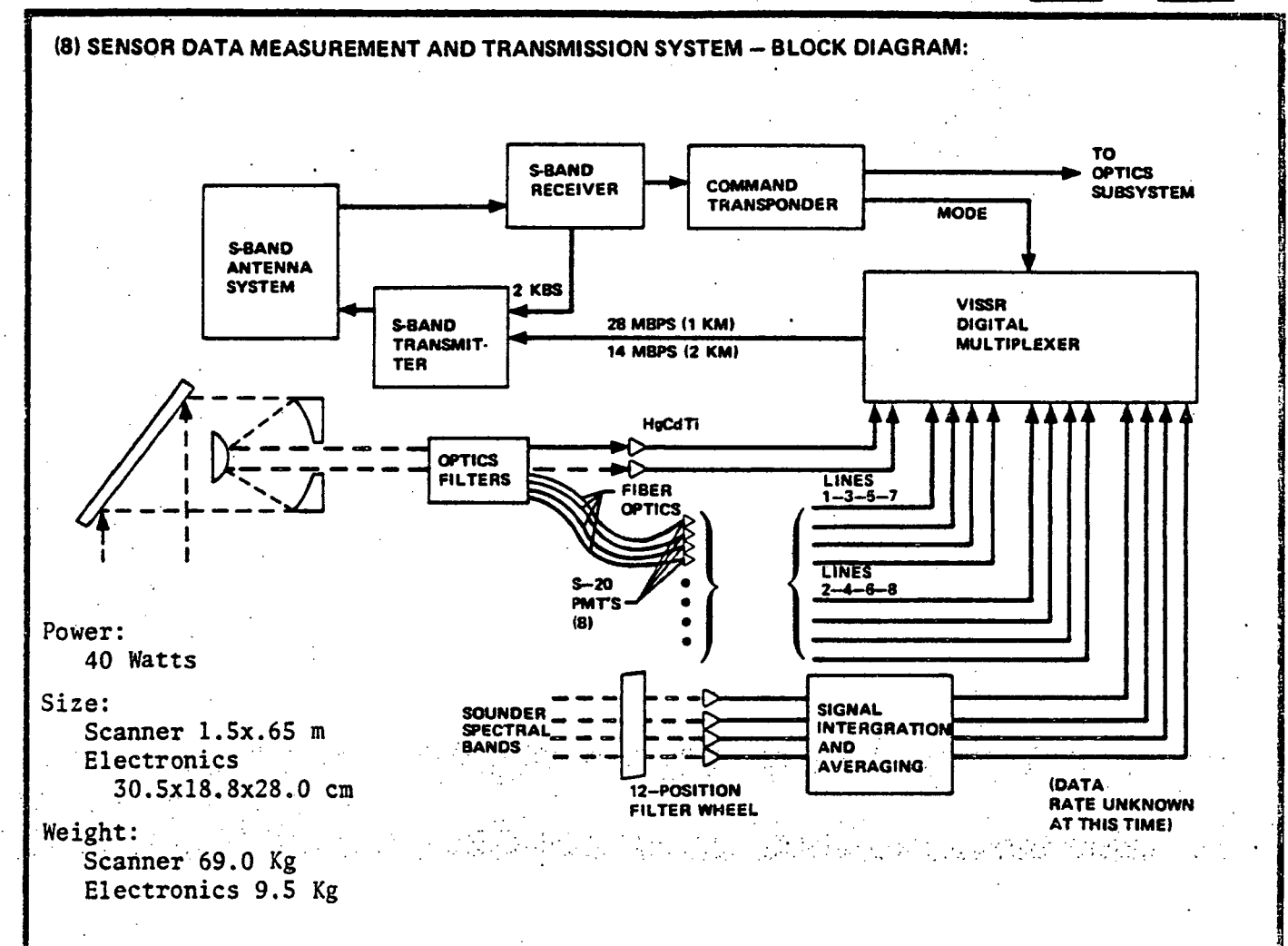
(7A) continued

see paragraph 7A of the VISSR.) Ground commands control the mode as imaging or sounding. A complete sounding requires about 150 spacecraft spans for each GLW line.

5.8.64

SECTION NO.: 5.8 SENSOR CATEGORY: Atmospheric Sounders

REV. NO.: 2 REV. DATE: 31 Jan 1978



#### (9) MEASUREMENT AND TRANSMISSION SYSTEM - NARRATIVE:

The VAS can be commanded to any one of three modes. In the "Normal VISSR" mode the measurement and processing of image data for the VAS is identical to that of the VISSR and the reader should refer to the VISSR data sheets for a description of that processing. This mode is considered a fall-back mode of operation for the satellite solar-cell-end-of-life period when power requirements must be minimized.

The "Multispectral Imaging" mode uses two of the four additional IR channels to gain additional image data. The angular pair of IR detectors (.192 mrad) produce two lines per satellite E-W scan and therefore need be active for only 1/2 the scans. Either the pair of .384 µrad InSb detectors may be activated during the unused scans. The data from each pair of detectors is used for imaging.

In the "Dwell-Sounding" mode, the filter wheel is positioned to a selected spectral band for each E-W scan. The choice of filters and the number of scans each filter is to remain in the IFOV is programmed by ground commands. Table 1 lists the spectral bonds covered by the 12 filters. Eight of these bonds can be viewed with any pair of the six IR detectors, while the other four (1, 2, 11, 12) can be viewed only with the larger IR detector. Multiple E-W line scans are required to obtain (continued on next page)

SECTION NO.: 5.8 SENSOR CATEGORY: Atmospheric Sounders

5.8 ©5. REV. NO.: 2 REV. DATE: 31 Jan 1978

### (9) continued

the necessary signal to visual ratios for some spectral bands. The sensor can be programmed to scan the E-W line from 0 to 255 times. The data is spacially averaged to obtain 30 km resolution cells. About 120 satellite spans are required to obtain the necessary number of samples for all filter positions for each scan line. The 30 km swath requires about 2.5 minutes.

The scan limits, filters, scans/filters, etc., result in 59 commands that can be passed to the sensor. The commands are programmed into VAS memory using a dedicated command line. A bit stream of 171 bits set the VAS to the desired program. Approximately 11 seconds are required for program loading.

TABLE 1 VAS Infrared Spectral Bands

				<u> </u>		
SPECTRAL BAND	υ (cm <sup>-1</sup> )	λ (μm)	∆u (cm <sup>-1</sup> )	SINGLE SAM 320°K SCENE	PLE_S/N AT TEMPERATURE	REMARKS
Brito	(Om )	(pm)	(0 )	0.192 mrad IGFOV (dB)	0.384 mrad IGFOV (dB)	
1	680	14.71	10	NA NA	28.4	.co <sub>2</sub>
2	692	14.45	16	NA	36.3	co <sub>2</sub>
2 3	703	14.22	16	31.0	37.0	co <sub>2</sub>
4	715	13.99	20	33.3	39.3	co <sub>2</sub>
5	752.	13.31	20	32.3	38.3	co <sub>2</sub>
6	2214	4.52	20	32.4	38.4	co <sub>2</sub>
7	790	12.66	20	32.6	38.6	н <sub>2</sub> 0
8	895	11.17	140	52.9*	56.6	WINDOW
9	1380	7.25	40	24.7	30.7	H <sub>2</sub> 0
10	1490	6.71	150	34.3	40.3	н <sub>2</sub> 0
11	2255	4.44	50	N.A.	38.5	CO <sub>2</sub> -InSb
	•				}	DETECTOR
12	2540	3.94	440	N.A.	47.0	WINDOW- InSb DETECTOR

\*FOR 340°K SCENE TEMPERATURE

SECTION NO.: 5.8 SENSOR CATEGORY: Atmospheric Sounders

5.8.66

REV. NO.:

			SHEET 5 OF 6
(10) SENSOR DATA RECEPTION AN	ND PROCESSING - BLOC	K DIAGRAM:	
	•		
		. *	
.*			
	•		
		•	
	•		
		*•.	. *
Image Processing is identified and processing is available.	ntical to VISSR. N able at this time.	o addition of sou	unding data reception
a p			
		The second section is the second	
1975年 · 1976年	And the following the second s		
•	* . *	and the second of the second o	જર્મ ભાગમાં જ જો તે માત્ર ભાગમાં પ્રાપ્ય માટે પ્રાપ્ય નિર્ણયો છે. જ
	•		
,			
(11) RECEIVING AND PROCESSING	- NARRATIVE		
(11) 11232.1114 7.113 1.1133233.113	, , , , , , , , , , , , , , , , , , , ,	•	
Same as (10)			
			· · · · · · · · · · · · · · · · · · ·
	<b>4</b>	8.67	
Same as (10)		. 3 ム7 mospheric Sounder	

SHEET 6 OF 6

(12) DISTRIBUTION OF DATA F	ROM GROUND STATION	S – BLOCK DIAGRA	И:	and the second s
	•			
			•	
				•
	_			
Image Processing is i at this time.)	dentical to VISSR.	(No additional	information	is available
at this time.				
				•
			•	
	•			
			•	
				•.
		* :	•	
	•		•	•
		•		
(13) DATA DISTRIBUTION - NA	RRATIVE:			
Soundings with a hor	zontal resolution	of 30 km will be	nroduced by	averaging
the 8 or 16 measurement	ents. Accuracy is to	within 13° of a	ctual atmosph	eric temper-
ature. (Further info	ormation will be pr	ovided as it bec	omes availabl	e.)
	•			
				• •
•				
			•	
				•
	•			
	•.	•		•
SECTION NO.: 5.8	SENSOR CATEGORY:	Atmospheric Sour	nders	
		REV NO · 2		31 Jan 1978

5.8.68

SHEET 1 OF 5	SHEET	1	OF	5
--------------	-------	---	----	---

(1) SENSOR NAME, ACRONYM: Microwave Atmospheric Sounding Radiometer (MASR)

(2) DISCIPLINE: Earth Observations (3) SUBDISCIPLINE: Atmospheric Monitoring

### (4) APPLICATION AND OBJECTIVE:

The MASR senses microwave emittences in the oxygen and water vapor bands for calculation of atmospheric temperature and humidity profiles in clear thru overcast conditions. The instrument is normally used with data from the AASIR to achieve necessary accuracy and resolutions for severe storm warning and forecasting.

#### (5) HERITAGE/KEY PERSONNEL:

Based on the NEMS and SCAMS in the NIMBUS Program

Instrument Rep.: Dr. James Shiue, GSFC (301) 982-6716

#### (6) SENSOR DEPLOYMENT:

Planned for launch on STORMSAT in 1982. Geosynchronous earth orbit. (see AASIR data sheet for additional description)

(7)

#### SENSOR CHARACTERISTICS

### (7A) CAPABILITIES AND CONSTRAINTS OF THE SENSOR TO ACQUIRE THE MEASURED PARAMETER:

The IFOV resolution is .7 milliradians (25 km at the satellite suppoint). MASR scans North-South and back at 290 urad/sec, collecting data (on the fly) in each direction. Following each scan, the instrument steps in the E/W or W/E direction by about .7 mrad. The scan/step logic describes an image frame. The location and size of the frame is commanded by ground signals that specify the direction of the center of the frame and the scan length and number of steps per Table 1 (next page) shows time required to scan the defined frame sizes. (continued on next page)

#### (7B) ACTIVE SOURCE CHARACTERISTICS (FOR ACTIVE SENSORS):

N/A.

#### (7C) DETECTOR MEASUREMENTS CHARACTERISTICS:

The MASR uses detectors at 16 frequencies:

- $\cdot$  8 channels for temperature soundings at 113 to 123 GHz
- · 8 channels for humidity soundings at 173 to 193 GHz

5.8.69

Atmospheric Sounders SECTION NO.: 5.8 SENSOR CATEGORY:

**REV. NO.:** REV. DATE: 31 Jan 1978 2

### (7A) continued

The MASR samples about 7 pixels/sec (700 µradians each) for each spectral bond. The pointing accuracy is 1.7 milliradians (giving a possible 60 km mis-registration with AASIR data).

TABLE 1 Scan Frame Sizes and Speeds

Frame	Angular Coverage (millirad)	Number of <u>Pixels</u>	Time for Full Frame Scan
Minimum	4.5 x 4.5	7.80	2 min
Cloud	13.5 x 9.0	4,600	11 min
Mesoscale	36.0 x 22.5	27,000	68 min
Regional	67.5 x 40.5	89,000	3.7 hours
Full Earth	324 x 324	N/A	N/A

5.8.70

SECTION NO.: 5.8 SENSOR CATEGORY: Atmospheric Sounders

REV. NO.: 2 REV. DATE: 31 Jan 1978

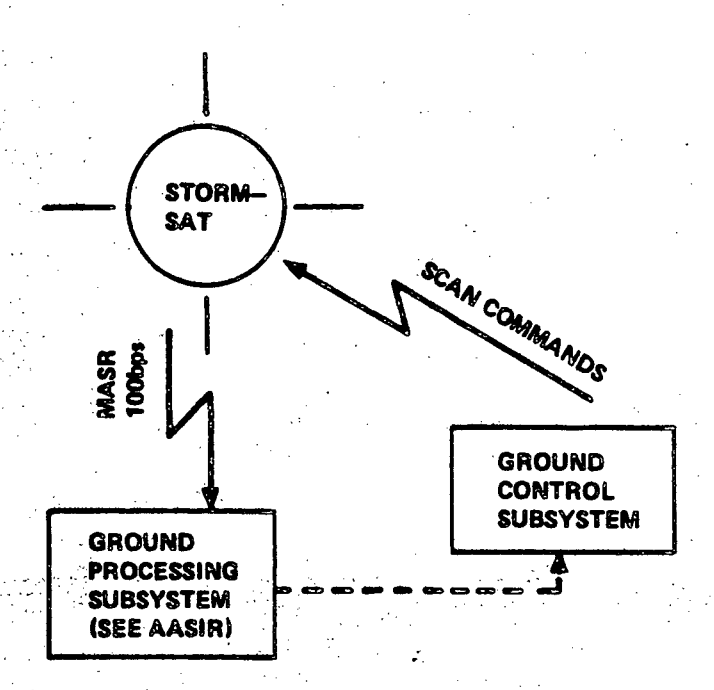
SHEET 3 OF 5

(8) SENSOR DATA MEASUREN	MENT AND TRANSMISSION ST	YSTEM — BLOCK DIAGRAM	l:
	·		
		•	
		e e	
		:	
	and an experience of		and the second s
		·	
(9) MEASUREMENT AND TRA	NSMISSION SYSTEM — NARR	ATIVE:	
ment and transmits i	n real-time to the gro	to digital values of ound station. The va	f 10 bits per measure- alues are multiplexed
with the AASIR data	before transmission.		
	•	·	
•			•
• • • • •			
		·	
·			
			,
SECTION NO.: 5.8	SENSOR CATEGORY: Ati	mospheric Sounders	

5.8.71

**REV. NO.:** 2

### (10) SENSOR DATA RECEPTION AND PROCESSING - BLOCK DIAGRAM:



### (11) RECEIVING AND PROCESSING - NARRATIVE:

The MASR data is processed as described for AASIR sounder data (see AASIR processing).

SECTION NO.: 5.8

SENSOR CATEGORY:

Atmospheric Sounders

REV. NO.:

2

SHEET 5 OF 5

12}	DISTRIBUTION	OF DATA	FROM	GROUND	STATIONS	- BLOCK	CDIAGRAM:

See AASIR Diagram

#### (13) DATA DISTRIBUTION - NARRATIVE:

The MASR data is used with AASIR data to generate the high resolution data products. See the AASIR data sheets for a description of these products and their distribution. In overcast skies, where AASIR data isn't available, the MASR provides a 2 to 3 degrees Celcius temperature accuracy, with 4 - 5 km vertical resolution and 28 km horizontal resolution at the satellite subpoint; a 10-15% relative humidity accuracy with 3-4 Km vertical resolution and 18 km horizontal resolution.

SECTION NO.:

5-8

**SENSOR CATEGORY:** 

58.73

Atmospheric Sounders

REV. NO.:

	•		
 		SHEET	OF

CONTINUATION SHEET:

This page intentionally left blank.

SECTION NO.:

5.8

SENSOR CATEGORY:

Atmospheric Sounders

REV. NO.:

REV. DATE: 31 J

31 Jan 1978

SHEET	1	OF	4
SUEEI	<u> </u>	UF.	

(1) SENSOR NAME, ACRONYM: High Resolution Infrared Radiation Sounder (HIRS)

(2) DISCIPLINE: Earth Observations

(3) SUBDISCIPLINE:

Atmospheric Monitoring

#### (4) APPLICATION AND OBJECTIVE:

The HIRS provides temperature and humidity soundings, surface temperature measurements, and cloud detection and measurement. The HIRS provides vertical temperature profile from the surface to 40 km, water vapor profile from surface to 10 km, liquid water content of clouds, pressure altitudes and amount of clouds, albedo.

(5) HERITAGE/KEY PERSONNEL:

NIMBUS V ITPR

NIMBUS VI HIRS

Instrument Rep.: E. Mundy (301) 982-2267

### (6) SENSOR DEPLOYMENT:

This sensor is designed for near-polar orbit of  $833 \pm 90$  km, Sun-Synchronous orbit. (TIROS-N)

(7)

#### SENSOR CHARACTERISTICS

### (7A) CAPABILITIES AND CONSTRAINTS OF THE SENSOR TO ACQUIRE THE MEASURED PARAMETER:

The instrument scans perpendicular to the subpoint track. There are 21 scan elements on each side of the subpoint track. Each scan element (IFOV) is 1.24° (25 km at the subpoint, 31.3 km at scan end). Each element is observed for 71 ms, with a step time of 35 ms between observations.

(7B) ACTIVE SOURCE CHARACTERISTICS (FOR ACTIVE SENSORS):

N/A

### (7C) DETECTOR MEASUREMENTS CHARACTERISTICS:

20 channels are sampled. Calibration occurs every 90 seconds. Two detectors are cooled to 120°K for IR channels. There is one uncooled SI detector for visible channel.

5.8.75

Preceding page blank

SECTION NO .:

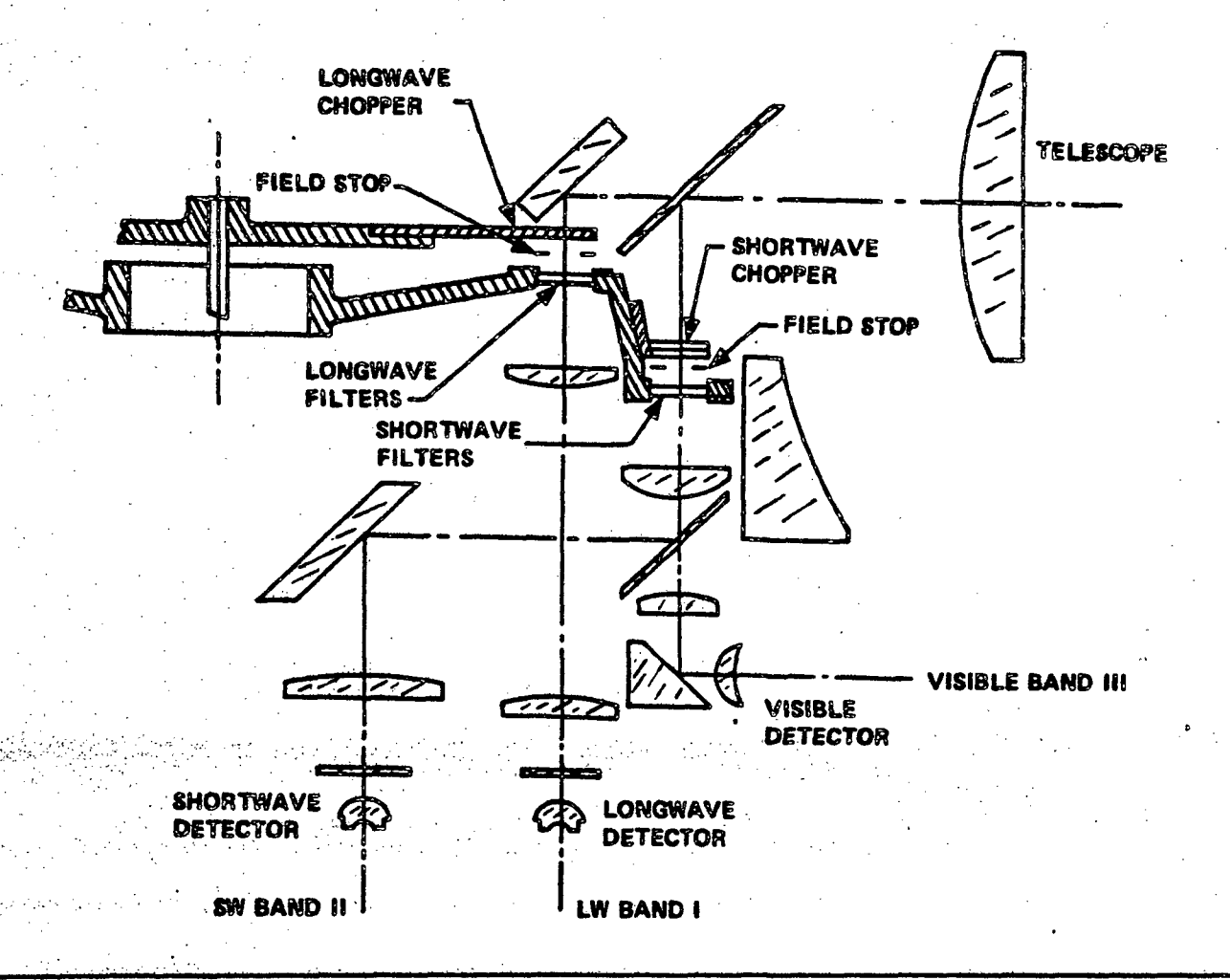
5.8

SENSOR CATEGORY:

Atmospheric Sounders

**REV. NO.: 2** 

### (8) SENSOR DATA MEASUREMENT AND TRANSMISSION SYSTEM - BLOCK DIAGRAM:



### (9) MEASUREMENT AND TRANSMISSION SYSTEM - NARRATIVE:

- Cassegrain Telescope
- 12 bit output voltage signal
- Two amplifier chains one for long wavelength IR and one for short wavelength and visible channels
- Output signal is integrated over a number of chopper waveform cycles

SECTION NO.: 5.8 SENSOR CATEGORY: Atmospheric Sounders

\_\_\_\_

REV. NO.:

SHEET \_\_\_\_\_\_ OF \_\_\_\_4

(10) SENSOR DATA RECEPTION	I AND PROCESSING - BL	OCK DIAGRAM:	•		
					·
	•		,		
See THIR	•				
		•			
		· ·			
,					
·					•
		* * * * * * * * * * * * * * * * * * * *			· · ·
			· · · · .		-
					•
/// 0505 WING AND DOGGE				,	
(11) RECEIVING AND PROCESSI	ING - NAHHATIVE:				
See THIR					~
·		•			
SECTION NO.: 5.8	SENSOR CATEGORY:	Atmospheric			
		REV. NO.:	REV.	DATE: 31 J	an 1978

#### RSDH Data sheet

(12) DISTRIBUTION OF DATA FROM GROUND STATIONS - BLOCK DIAGRAM: See THIR (13) DATA DISTRIBUTION - NARRATIVE: See THIR 5.8 SENSOR CATEGORY: SECTION NO .: **Atmospheric Sounders** 

REV. NO.:

REV. DATE:

31 Jan 1978

TA SHEET	SHEET_	1	OF_	6	

.(1) SENSOR NAME, ACRONYM: Microwave Sounding Unit (MSU)

(2) DISCIPLINE: Earth Observations

(3) SUBDISCIPLINE:

Atmospheric Monitoring

#### (4) APPLICATION AND OBJECTIVE:

Measure atmospheric temperature (0-20 km) profile through cloud cover with an absolute error of  $<2.0^{\circ}$ K rms.

(5) HERITAGE/KEY PERSONNEL:

NIMBUS 5 Microwave Spectrometer

NIMBUS 6 Scanning Microwave Spectrometer (SCAMS)

Instrument Rep.: R. Ratliff, GSFC (301) 982-2419

#### (6) SENSOR DEPLOYMENT:

TIROS-N Altitude is  $833 \pm 90$  km, sun-synchronous, near-polar orbit with a period of 101 min.

(7)

#### SENSOR CHARACTERISTICS

### (7A) CAPABILITIES AND CONSTRAINTS OF THE SENSOR TO ACQUIRE THE MEASURED PARAMETER:

Scans ±47.35° cross track, 25.6 sec/scan in 11 steps. The step angle is 9.47°, with 1.84 sec per step sampling time. Angular resolution is 7.5° (190 km at Nadir to 323 km x 177 km at scan extremes), swath width is 2320 km. The MSU scans 360P, taking data during the period it is viewing the earth, at a space calibration point, and at a microwave blackbody calibration point.

### (7B) ACTIVE SOURCE CHARACTERISTICS (FOR ACTIVE SENSORS):

N/A

### (7C) DETECTOR MEASUREMENTS CHARACTERISTICS:

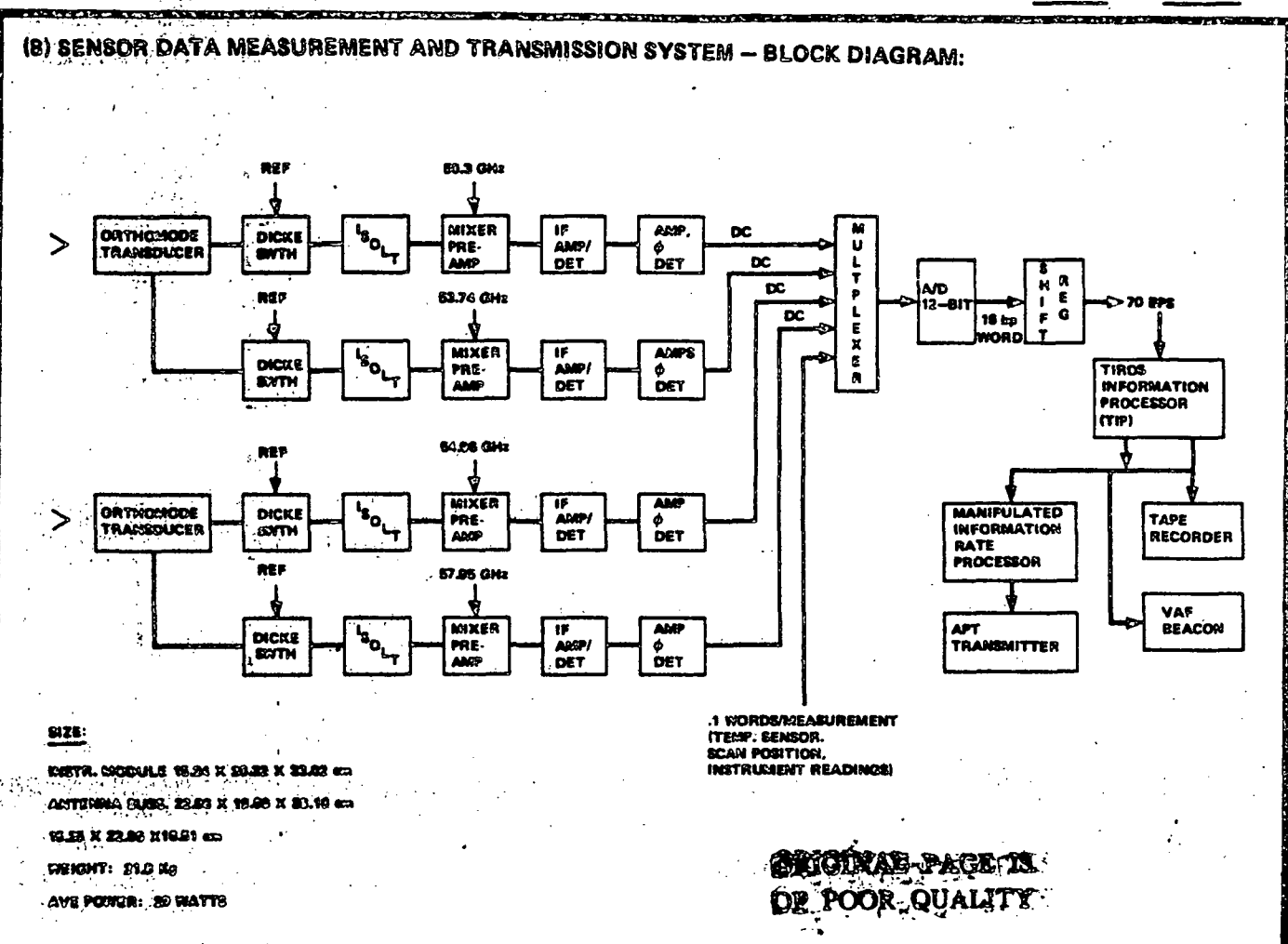
Spectral Bands: 5.96, 5.58, 5.46, 5.18 mm (check against 50.3, 53.74, 54.96, and 57.95 GHz)

4 Dicke radiometer. Noise Temperature .3°K.

"gallium arsenide diode" The sensor takes two calibration measurements per scan.

SECTION NO.: 5.8 SENSOR CATEGORY: Atmospheric Sounders

REV. NO.: 2 REV. DATE: 31 Jan 1978



(9) MEASUREMENT AND TRANSMISSION SYSTEM — NARRATIVE: The MSU takes measurements simultaneously at each frequency. Data rate is 100 bps. 12 bits per sample. and control data are output on two separate streams. Each of the 4 channels can be operated independent of the other channels. The channels are identical except for operating frequency. The DICKE switch modulates the input and reference signals at 1 kHz. The DICKE output is fed through an isolater to a mixer pre-amp. The IF output is square law detected and the detected signal is amplified and synchronously detected. The output of the synchronous detector is the difference between the ref. load and the input (antenna) signal. This signal is integrated for 1.82 sec. and then digitized by a 12-bit A/D converter, 4 bits of identification are added giving a 16-bit per word output. The output of each signal channel is formatted into a data word and multiplexed with the instrument voltage and temperature data (4 words) to form 8-16 bit words of output per measurement. The output is generated in a 40 ms period between scan positions and shifted into a 128-bit shift register. The TIP reads the shift register at a 20 word/sec rate (.4 sec to read 128 bits). The output for each scan consists of 14-8 word grc ps: 11 groups for the data measurements, 2 calibration measurements and one system zero test. The 14x8 words for a given scan is shown in Table 1. The average data rate generated by the MSU is 70 bps (8x14x16/25.6 sec/scan) In addition to the digital data, 10 analog outputs are provided each measuremer?. These are included in the spacecraft data stream as shown in Table 2.

SECTION NO.: 5.8 SENSOR CATEGORY: Atmospheric Sounders

5.2-80.

REV. NO.: 2

TABLE 1 MSU Digital Telemetry

<u> </u>	1.1	<u> </u>	r_	T.	T_1	1. 1	
INST SER NO. INDEX	T <sub>1</sub> CAL LO	Z T <sub>2</sub> CAL LO	CH 1 DATA	CH 2 DATA	CH 3 DATA	CH 4 DATA	SCAN POS. Ø SCAN COUNT
E CAL LO	T <sub>1</sub> CAL HI	T <sub>2</sub> CAL HI					POS. 1 SCAN COUNT
16 E CAL HI	ORTH 1 TEMP CH 1-2	ORTH 2 TEMP CH 3-4					31 .
24 XTAL CH 1+	L.O. CH 1 TEMP	L.O. CH 2 TEMP					39
XTAL CH 1-	L.O. CH 3 TEMP	L.O. CH 4 TEMP					47
XTAL CH 2+	DICKE LOAD CH 1 TEMP	DICKE LOAD CH 2 TEMP					55
XTAL CH 2-	DICKE LOAD CH 3 TEMP	DICKE LOAD CH 4 TEMP					63
XTAL CH 3+	TARGET 1A - TEMP CH 1-2	TARGET 1B TEMP CH 1-2					71
XTAL CH 3-	TARGET 2A TEMP CH 3-4	TARGET 2B TEMP CH 3-4		•			79
XTAL CH 4+	ANT 1 BEARING TEMP CH 1-2	ANT 2 BEARING TEMP CH 3-4					79
XTAL CH 4-	MOTOR TEMP	ENCODER TEMP					87
+S Volts	R.F. CHASSIS TEMP -Z -Y	R.F. CHASSIS TEMP -Z +Y					95
96 E ZERO	PROG TEMP +Z +X	PROG TEMP -Z -X					POS. 12 SCAN COUNT
104 +5 Volts	PROG TEMP -Z +Y	PROG TEMP -Z -X	107 CH 1 ZERO	CH 2 ZERO	CH 3 ZERO	CH 4 ZERO	SCAN POS. X SCAN COUNT

5.8-31

SECTION NO.: 5.8 SENSOR CATEGORY: Atmospheric Sounders

REV. NO.: 2 REV. DATE: 31 Jan 1978

Table 2
Analog Outputs

Temp 1	Calibration Target 1 Temp	-30° to +75°C
Temp 2	Calibration Target 2 Temp	-30° to +75°C
Temp 3	Dicke Reference Load 1 Temp	-10° to +75°C
Temp 4	Dicke Reference Load 3 Temp	-10° to +75°C
Scan Position	Antenna Position	0 - 360°
Ch 1 Data	50.30 GHz Data	0 - 350°K
· Ch 2 Data	53.74 GHz Data	0 - 350°K
Ch 3 Data	54.96 GHz Data	0 - 350°K
Ch 4 Data	57.95 GHz Data	0 - 350°K
Analog Reference		0 - 6 V

Note:

Status of the power command relays and certain functions in the scan system are monitored by spacecraft digital "B" telemetry.

5.8.82

SECTION NO.: 5.8 SENSOR CATEGORY: Atmospheric Sounders

REV. NO.: 2 REV. DATE: 31 Jan 1978

(10) SENSOR DATA RECEPTION	AND PROCESSING - B	LOCK DIAGRAM:		
•		• •		
		•		
•				
See SSU			•	:
				٠.
		•		
grand the state of		and provide a state of the state of		
	•	•	ē.	
		•		
		:· .		
(11) RECEIVING AND PROCESS	ING - NARRATIVE			
		•		
•	· 5	•		
		•		
	•	•		;
See SSU				
•				,
			<del></del>	
SECTION NO.: 5.8	SENSOR CATEGORY:	Atmospheric Sounder REV. NO.: 2		7 1070
		nev. No. 2	REV. DATE: 31	Jan 19/8

(12) DISTRIBUTION OF DATA FROM G	ROUND STATION	S – BLOCK DIAG	SRAM:	
	•		•	
	,			·
,				
See SSU				
,	•			
	•			
				·
(13) DATA DISTRIBUTION - NARRATI			······································	
(13) DATA DISTRIBUTION - NARRATI	V C.			
	•	·		: •
Coo CCII		•		•
See SSU	•			
	<b>.</b> .			
SECTION NO.: 5.8 SENSO	R CATEGORY:	Atmospheric	Sounders	
		REV. NO.: 2	REV. DATE:	31 Jan 1978

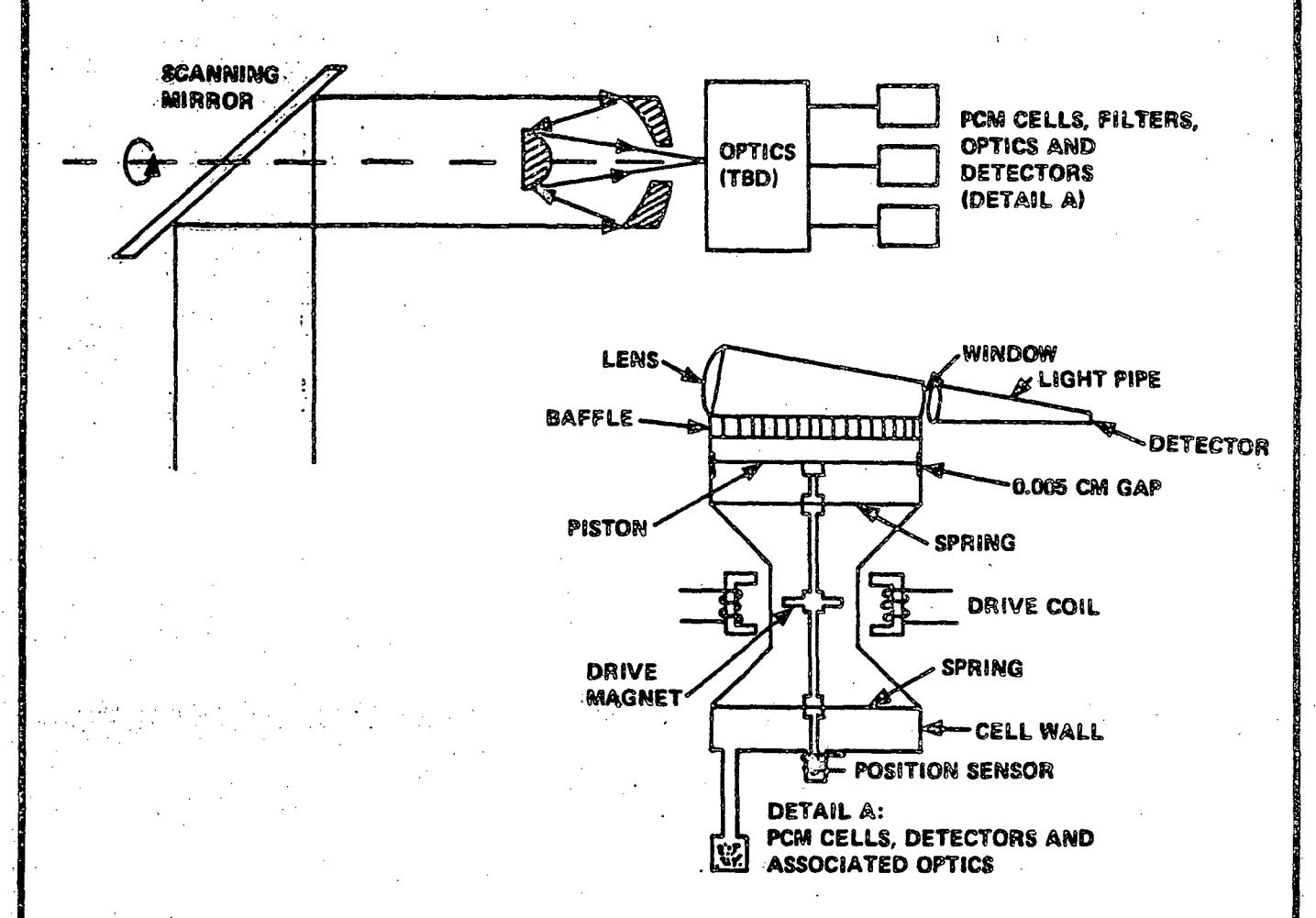
RSDH DATA SHEET SHEET (1) SENSOR NAME, ACRONYM: Stratospheric Sounding Unit (SSU) (3) SUBDISCIPLINE: Atmospheric Monitoring (2) DISCIPLINE: Earth Observations (4) APPLICATION AND OBJECTIVE: This instrument provides temperature soundings in the 25 km and 50 km altitude range. (5) HERITAGE/KEY PERSONNEL: Selective Chopper Radiometer (NIMBUS V), Pressure Modulation Radiometer (NIMBUS VI) Sensor Rep.: F. Cunningham (GSFC) (301) 982-6778 (6) SENSOR DEPLOYMENT: The SSU will operate aboard TIROS-N at an altitude of 833 km in a near-polar, sun-synchronous, circular orbit. Launch is planned for January 1978. Stability = ±.2° of local vertical. SENSOR CHARACTERISTICS (7) (7A) CAPABILITIES AND CONSTRAINTS OF THE SENSOR TO ACQUIRE THE MEASURED PARAMETER: The SSU scans ±40° to either side of nadir in 10° steps (total scan = 1474 km). Each step has a four second sampling time with 32 seconds required for the full scan. The IFOV at NADIR is 147 km (diameter); at scan end, the IFOV is 244 km x 186 km. IFOV's are separated in the along-track direction by 210 km. (7B) ACTIVE SOURCE CHARACTERISTICS (FOR ACTIVE SENSORS): N/A

### (7C) DETECTOR MEASUREMENTS CHARACTERISTICS:

The three pyroelectric detectors are uncooled at 290°K. Three channels radiances (14.9 µm for all) are directed onto each of the detectors through PMC cells modulated to three pressures: 100 mb, 36 mb, 10 mb.

SECTION NO .: SENSOR CATEGORY: Atmospheric Sounders 5.8

### (8) Sensor data measurement and transmission system — block diagram:

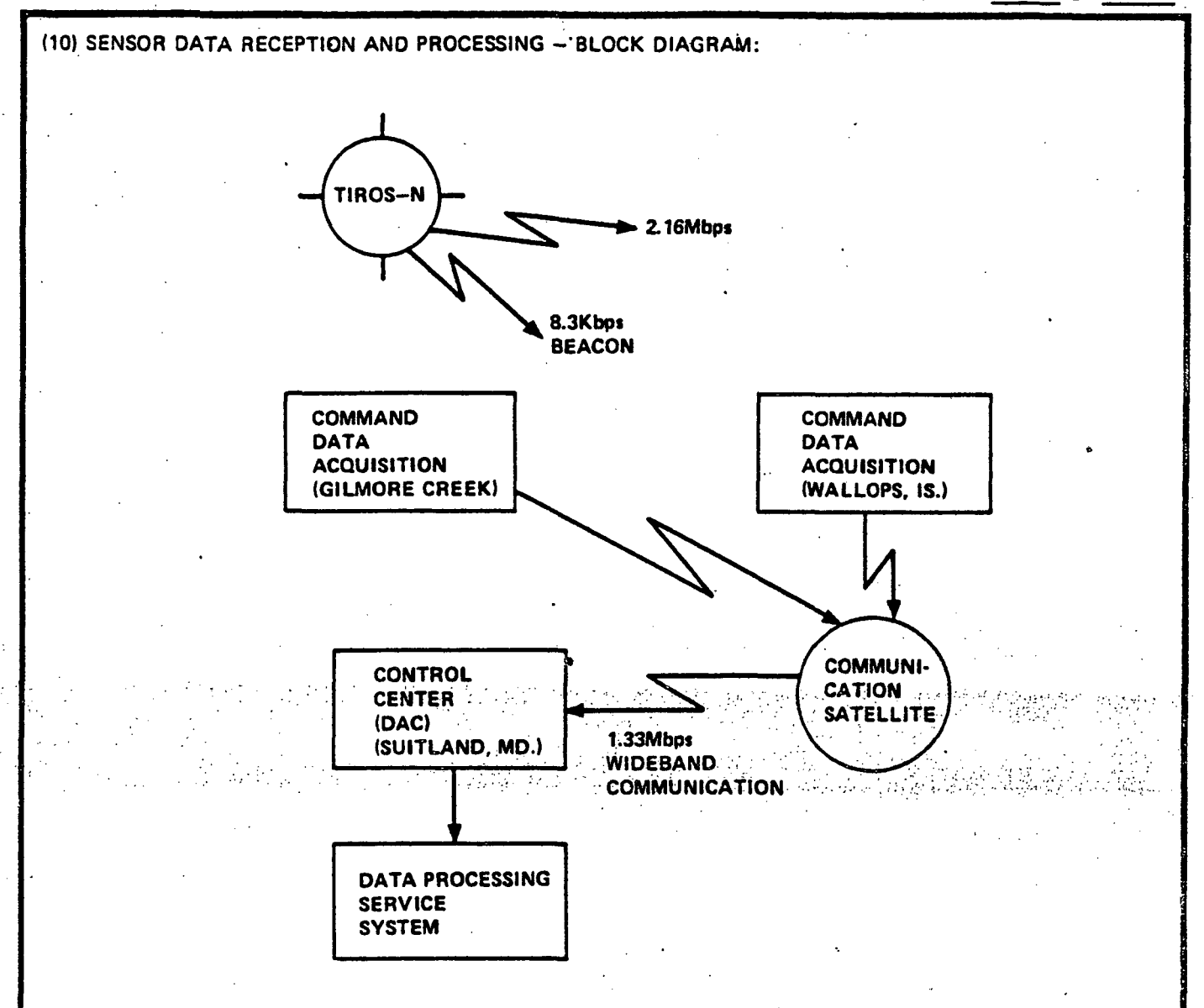


### (9) MEASUREMENT AND TRANSMISSION SYSTEM - NARRATIVE:

Data is gathered simultaneously in three channels. A mirror step-scans across the orbit track. The image from a single cassegrain telescope is directed to three separate channels, each containing a PCM cell that is pressure modulated over the selected absorption band. The voltage output of the detector is digitized into 12 bit values (16 bits are used for each value with the four leading bits zero) at 480 bits per second. The data is multiplexed with information from the high resolution radiometer (AVHRR) and recorded. The data is also transmitted in the VHF Beacon in real-time and recorded for playback to a CDA.

SECTION NO.: 5.8 - SENSOR CATEGORY: Atmospheric Sounders

REV. NO.: 2 REV. DATE: 31 Jan 1978



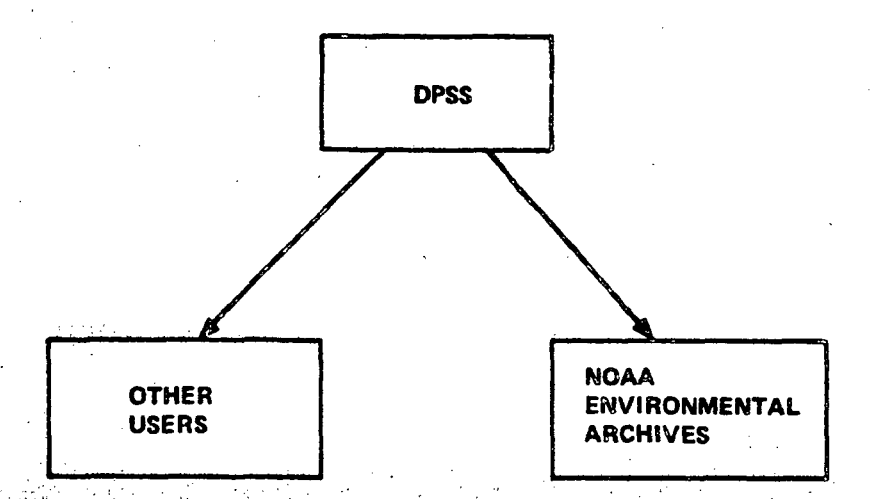
### (11) RECEIVING AND PROCESSING - NARRATIVE:

The Data Acquisition and Control Subsystem (DACS) consists of ground stations at Gilmore Creek and Wallops Island recover all the sounder sensor data from the satellite at 2.4 kbps. The data is recorded in analog recorders. Two Data General Eclipse 200 computers are used at each site. Image data is sectorized and all data is transmitted to the central control center. The central control facility at Suitland contains three Data General computers. An AMPEX teribit memory (18x10 bits) is used for rapid access on-line storage. The computers and equipment at the data acquisition stations and the control center provide space-craft and sensor control and data handling capabilities only. The central center computer format the data and transmit it to the DPSS for processing. A direct communications link connects the central center and the DPSS. The DPSS contains a PDP 11/45, SEL 32, and a IBM-360 for reduction and analyzing of ITOS data all output products are prepared at the DPSS.

SECTION NO.: 5.8 SENSOR CATEGORY: Atmospheric Sounders

REV. NO.: 2 REV. DATE: 31 Jan 1978

## (12) DISTRIBUTION OF DATA FROM GROUND STATIONS - BLOCK DIAGRAM:



### (13) DATA DISTRIBUTION - NARRATIVE:

All data products are distributed to the Environmental Data Archives (NOAA) and to selected other users as required.

SECTION NO.: 5.8 SENSOR CATEGORY: Atmospheric Sounders

REV. NO.:

### RSDH DATA SHEET

SHEET 1 OF 5

(1) SENSOR NAME, ACRONYM: Scanning Multichannel Microwave Radiometer (SMMR)

(2) DISCIPLINE: Earth and Ocean Physics (3) SUBDISCIPLINE: Ocean Dynamics

- (4) APPLICATION AND OBJECTIVE: The SMMR experiment on SEASAT-A will evaluate passive micro wave techniques for providing operationally useful ocean surface wind speed and temperature data, polar ice canopy characteristics and maps of atmospheric water vapor and liquid water over oceanic regions. The SMMR measurements will be interpreted in terms of various geophysical parameters, such as the ocean wind speed and temperature above. Microwave emission from the respective parameter has distinguishing spectral and polarization characteristics which allow the individual parameters to be measured.
  - (5) HERITAGE/KEY PERSONNEL: The SMMR (SEASAT-A) is an outgrowth of the Electronically Scanned Microwave Radiometers (ESMR), the NIMBUS-E Microwave Spectrometer (NEMS) and the Scanning Microwave Spectrometer (SCAMS) on NIMBUS E & F, and the SMMR planned for NIMBUS-G.

### (6) SENSOR DEPLOYMENT:

The SEASAT-A satellite bearing the SMMR is to be launched to obtain a mean circular orbit with a 108° inclination, a mean altitude of 790 km and approximate ground speed of 6.6 km/sec. An orbital period of 104 minutes results in 14 orbits per day. Seven orbits are required for complete (mission) ocean coverage.

(7)

### SENSOR CHARACTERISTICS

### (7A) CAPABILITIES AND CONSTRAINTS OF THE SENSOR TO ACQUIRE THE MEASURED PARAMETER:

The SMMR simultaneously measures microwave thermal emission from the Earths! atmosphere and surface with five(5) radiometer channels. Each channel measures radiation in two orthogonal linear polarizations. The radiation is collected by an offset parabolic reflector antenna with an 80cm diameter aperture which is projected normal to the direction of observation and is scanned 25 degrees to either side of the direction of satellite motion. The antenna focuses the radiation into a multifrequency feed system which is connected to the radiometer inputs.

(7B) ACTIVE SOURCE CHARACTERISTICS (FOR ACTIVE SENSORS):

Not Applicable

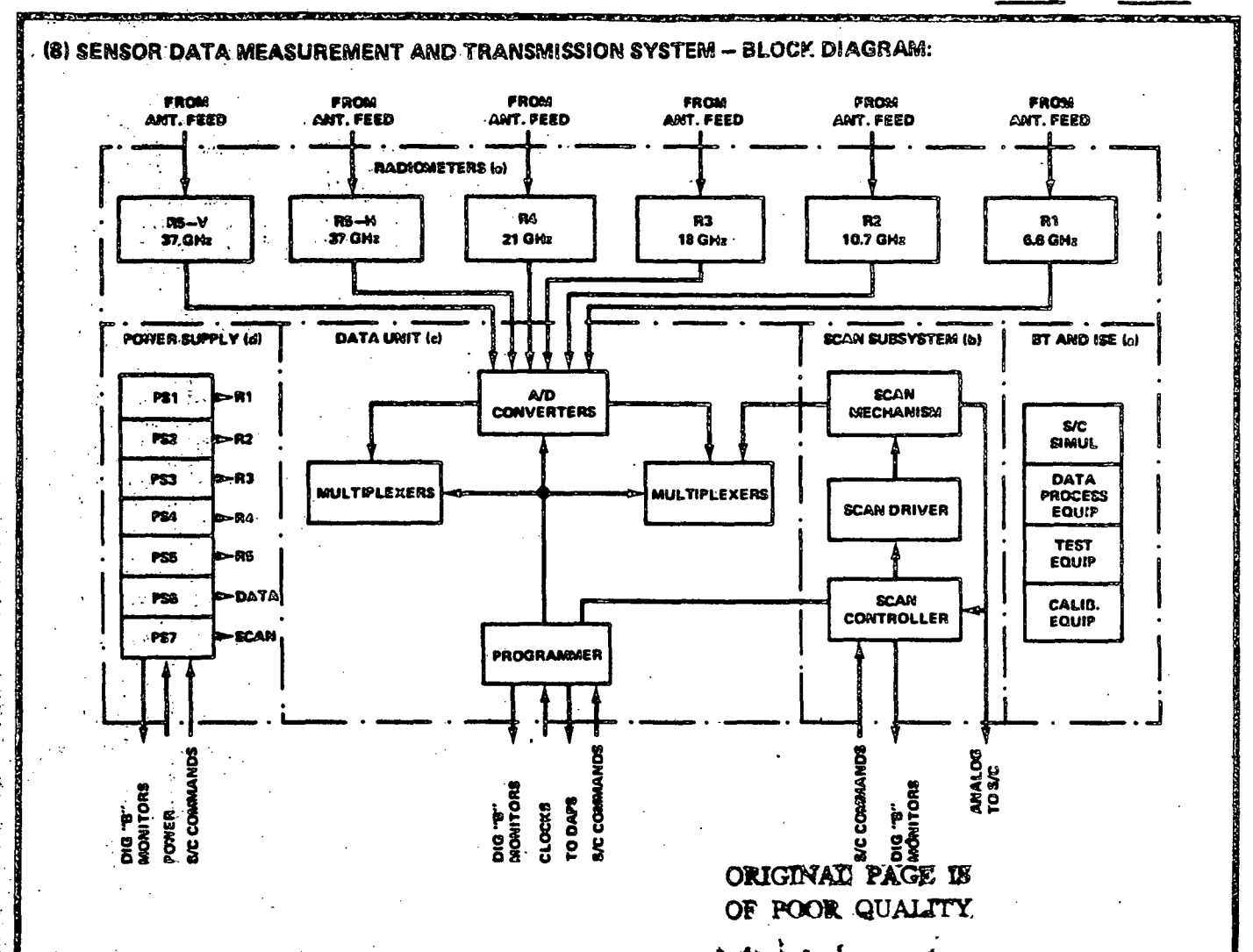
### (7C) DETECTOR MEASUREMENTS CHARACTERISTICS:

The five channels range in wavelengths from 0.8cm to 4.5cm. The frequencies, wavelengths and other characteristics are presented in Table 1 (see information cell #9) for all 5 SMMR channels. The radiometers detect, amplify and convert the received signals to digital data which is multiplexed with instrument engineering and calibration data and fed to the satellite data system.

SECTION NO.: 5.8

SENSOR CATEGORY: Atmospheric Sounders

REV. NO.: 2



### (9) MEASUREMENT AND TRANSMISSION SYSTEM - NARRATIVE:

The SMMR simultaneously measures microwave thermal emission from the earth's atmosphere and surface with five channels having the center frequencies and wavelengths as given in Table 1.

TABLE 1 Center Frequencies and Wavelengths

Channel	Frequency (GHZ)	Wavelength (cm)
1	6.60	4.5
2	10.69	2.8
3	18.00	1.7
4	21.00	1.4
5	37.0	0.8

(continued on next page)

SECTION NO.: 5.8 SENSOR CATEGORY: Atmospheric Sounders

Action Action Principle During 13

5.8.90

REV. NO.: 2

### CONTINUATION SHEET:

### (9) continued

Each channel measures radiation in two orthogonal linear polarizations. Channels 1-4 will switch between polarizations on alternate scans of the antenna beam, and channel 5 will simultaneously measure both polarizations.

The microwave thermal emission from the earth and atmosphere is collected by an offset parabolic reflector antenna which focuses this radiation into a multifrequency feed system. The feed system is connected to the radiometer inputs through orthomode transducers for separating the polarization and then through polarization, calibration and Dicke switches. The radiometers detect, amplify and convert the signals-to-digital data which is multiplexed with instrument engineering and calibration data and fed to the satellite data system for telemetry to ground.

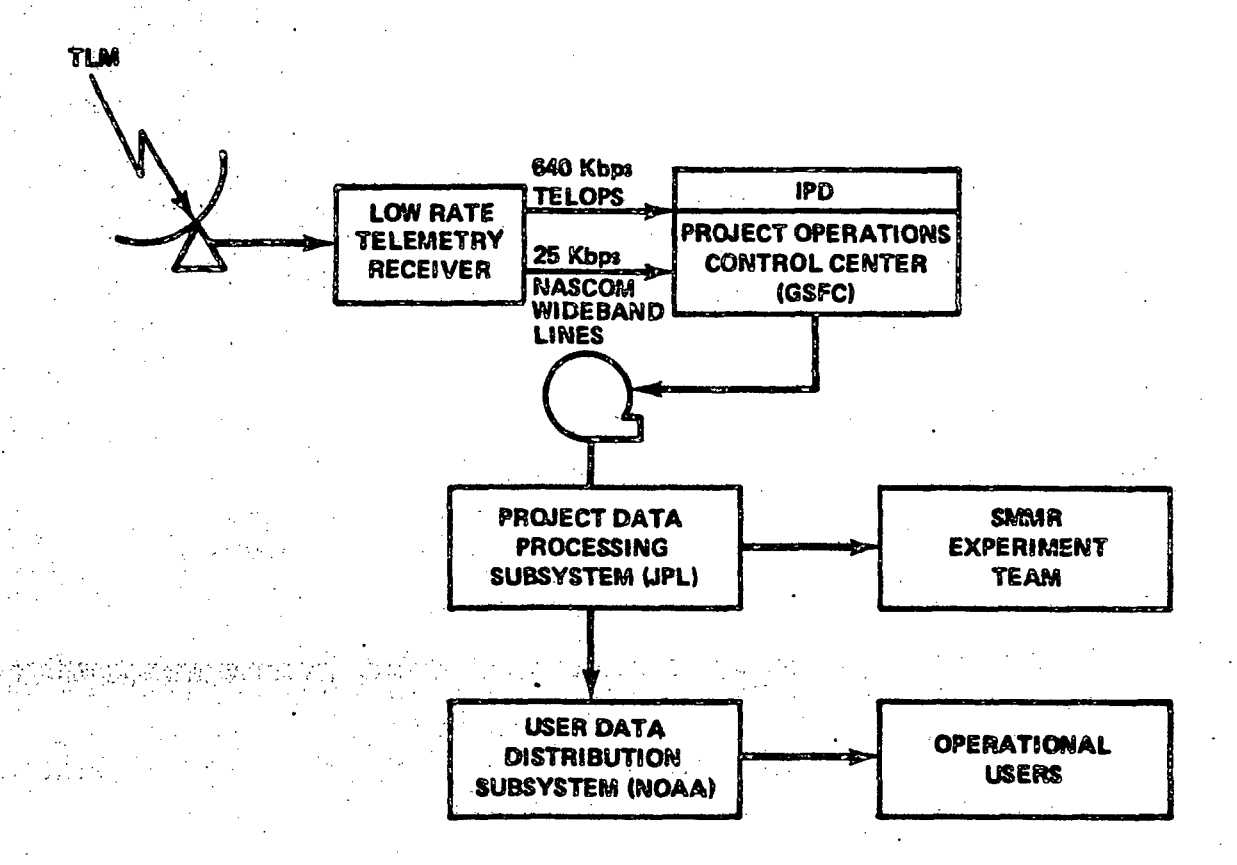
The offset parabolic antenna has an 80 cm diameter aperture measured normal to the direction of observation and is scanned 25° to either side of the direction of satellite motion. The angle of the beam with respect to nadir is maintained at 42° in order to provide a constant earth-incident angle of 50°. The beamwidth for channel 5 is 0.7° and gives a surface resolution element of 17 x 26 km. Resolutions for other channels are larger in proportion to their respective wavelengths.

The SMMR measurements will be interpreted in terms of various geophysical parameters, such as ocean surface wind speed and temperature, sea-ice boundaries and characteristics, soil moisture content, and atmospheric water content and characteristics. Microwave emission from the respective parameters has distinguishing spectral and polarization characteristics which allow the individual parameters to be measured.

SECTION NO.: 5.8 | SENSOR CATEGORY: Atmospheric Sounders

REV. NO.: 2 REV. DATE: 31 Jan 1978

### (10) SENSOR DATA RECEPTION AND PROCESSING - BLOCK DIAGRAM:



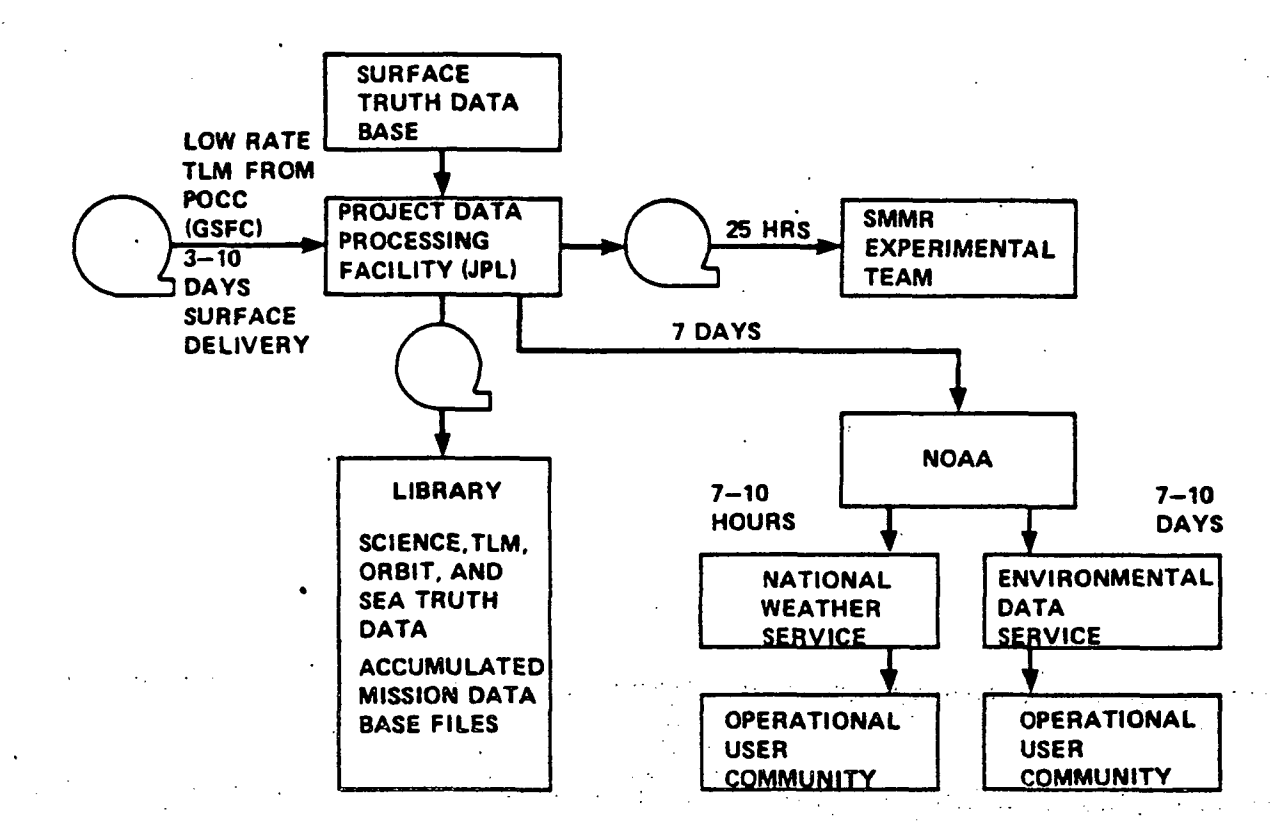
### (11) RECEIVING AND PROCESSING - NARRATIVE:

The STDN sites receive Low-Rate playback TLM data at 640 at 800 kbps during contact periods. Received TLM data is retransmitted to IPD at GSFC via TELOPS. IPD will preprocess the TLM data to produce time-smoothed and quality-checked telemetry. A master data file is constructed on a daily basis and sent to JPL via surface delivery.

SECTION NO.: 5.8 SENSOR CATEGORY: Atmospheric Sounders

REV. NO.: 2 REV. DATE: 31 Jan 1978.

### (12) DISTRIBUTION OF DATA FROM GROUND STATIONS - BLOCK DIAGRAM:



### (13) DATA DISTRIBUTION - NARRATIVE:

JPL receives edited, time-smoothed TLM data from GSFC. The four primary functions performed by JPL are:

- (a) produce an Experiment Data Record for each team,
- (b) produce supplementry data for each experiment (I.E., sensor earth located footprint, engineering data),
- (c) produce a single processed data record in geophysical units for each experiment, i.e., wind speed/direction, surface temperature, etc., and
- (d) produce validated algorithms to independent raw data users.

SECTION NO.: 5.8 | SENSOR CATEGORY: Atmospheric Sounders

REV. NO.:

2

		DATA SHEET	•	*		
					SHEET	OF
CONTINUATION SHEET:	in think in it was a subject to the little of the little o	and the state of t	A TOLD DOWN THE METERS AND A STREET WAS A	The second of	eriginate comprehensi in est est	No de la companya de la comp
					•	
		•		•		
					•	
				•		
	1					
	•				•	
		•				-
		•				•
						•
•		• .			•	
			•			
Th	is page intenti	onally left bl	lank.			•
						•
		•				
			•			
		•	: ·		•	
				•	•	•
						•
	,					
•	•		•			
,	•					
	••		•	•		
		•				
	•	•	•			
•						
•					•	
	٠.					
			•			
	•			•		•

REV. NO.:

Atmospheric Sounders

REV. DATE:

31 Jan 1978

SENSOR CATEGORY:

SECTION NO .:

5.8

## SENSOR CATEGORY TABLE OF CONTENTS AND REVISION CONTROL SHEET

Section 5.10 Table of Contents   1	SENSOR NAME OR	NUMBER OF		EFFE	CTIVE
Introduction to Field Measuring		1	1	REV. DATE	REV. NO.
Introduction to Field Measuring	· · · · · · · · · · · · · · · · · · ·				
Sensors    S.10-2   30 JUN 77   0	Section 5.10 Table of Contents	1	5.10-i	31 JAN 78	2
S.10-3   31 JAN 78   2		29			1
S.10-S   31 JAN 78   2   2   30 JUN 77   0   0   1 JUN 78   2   0   1 JUN 78   2   0   1 JUN 77   0   0   1 JUN 78   2   0   1 JUN 78    Sensors		1	1		
S.10-6   SO JUN 77   O				l .	2
S.10-8   31 JUN 77   0			B .		
S.10-8   31 JAN 78   2   2   5.10-9   31 JAN 78   2   2   5.10-10   30 SEPT 77   1   5.10-11   31 JAN 78   2   5.10-12   30 JUN 77   0   0   0   0   0   0   0   0   0					
S.10-9   31 JAN 78   2   1   1   1   1   1   1   1   1   1		•			
S.10-10   30 SEPT 77   1   1   1   1   1   1   1   1   1	•		i	1	
S.10-12   30 JUN 77   0	•		i		1
S.10-13   30 JUN 77   0	•		5.10-11		2
S.10-14   31 JAN 78   2   2   31 JAN 78   2   3   3   3   78   2   3   3   3   78   2   3   3   3   78   2   3   3   3   78   2   3   3   3   3   78   2   3   3   3   3   78   2   3   3   3   3   3   78   2   3   3   3   3   3   78   2   3   3   3   3   3   3   3   3   3					,
S.10-15   31 JAN 78   2   2   31 JAN 78   2   31 JAN 78   2   32 JAN 78   2   32 JAN 78   2   33 JAN 78   2   34 JAN 78   34			ŧ.		, ,
S.10-16   31 JAN 78   2			8		2
S.10-17   S1 JAN 78   2	•	:	3		2
S.10-19   31 JAN 78   2   31 JAN 78    and the single transport to the contract the contract to the contract the contract to the con				2	
S.10-20   31 JAN 78   2   30 JUN 77   0   5.10-21   31 JAN 78   2   5.10-23   31 JAN 78   2   5.10-23   31 JAN 78   2   5.10-25   30 SEPT 77   1   5.10-26   30 SEPT 77   1   5.10-26   30 SEPT 77   1   5.10-27   30 SEPT 77   1   5.10-28   30 SEPT 77   1   5.10-28   30 SEPT 77   1   5.10-28   30 SEPT 77   1   5.10-29   30 SEPT 77   1   5.10-29   30 SEPT 77   1   5.10-32   31 JAN 78   2   5.10-33   31 JAN 78   2   5.10-33   31 JAN 78   2   5.10-34   31 JAN 78   2   5.10-34   31 JAN 78   2   5.10-36   31 JAN 78   2   5.10-37   31 JAN 78   2   5.10-38   31 JAN 78   3					2
S.10-21   30 JUN 77   0					2
S.10-22   31 JAN 78   2	1. The transfer of the state of the second o	t in the district and finds			, <u> </u>
S.10-23   31 JAN 78   2				1	2
S.10-24   31 JAN 78   2   30 SEPT 77   1   5.10-26   30 SEPT 77   1   5.10-27   30 SEPT 77   1   5.10-27   30 SEPT 77   1   5.10-29   30 SEPT 77   1   5.10-29   30 SEPT 77   1   5.10-29   30 SEPT 77   1   5.10-32   31 JAN 78   2   5.10-32   31 JAN 78   2   5.10-33   31 JAN 78   2   5.10-33   31 JAN 78   2   5.10-34   31 JAN 78   2   5.10-34   31 JAN 78   2   5.10-36   31 JAN 78   2   5.10-37   31 JAN 78   2   5.10-37   31 JAN 78   2   5.10-37   31 JAN 78   2   5.10-38   31 JAN 78					2
S.10-26   30 SEPT 77   1			1		2
S.10-27   30 SEPT 77   1   1   30 SEPT 77   1   1   30 SEPT 77   1   1   1   1   1   1   1   1   1			T .	l .	. 1
S.10-28   30 SEPT 77   1					1
Fluxgate Magnetometer (FMAG)  4					1
Fluxgate Magnetometer (FMAG)  4					1
S.10-32   31 JAN 78   2	Eluvgato Magnetemeter (EMAC)	A			2
Rotating Gravity Gradiometer  4  5.10-34  31 JAN 78  2  5.10-35  31 JAN 78  2  5.10-36  31 JAN 78  2  5.10-37  31 JAN 78  2  5.10-37  31 JAN 78  2  5.10-38  31 JAN 78  2	Tavkare makiteromeret (Ling)	"			
Rotating Gravity Gradiometer  4  5.10-34  31 JAN 78  2  5.10-35  31 JAN 78  2  5.10-36  31 JAN 78  2  5.10-37  31 JAN 78  2  5.10-37  31 JAN 78  2  5.10-38  31 JAN 78  2	· \				2
5.10-36 31 JAN 78 2 5.10-37 31 JAN 78 2 5.10-38 31 JAN 78 2					2
5.10-36 31 JAN 78 2 5.10-37 31 JAN 78 2 5.10-38 31 JAN 78 2	Rotating Gravity Gradiometer	4	5.10-35	31 JAN 78	2
				•	2
					2
SECTION NO.: 5.10 SENSOR CATEGORY: Field Measuring Sensors			5.10-38	31 JAN /8	2 .
SECTION NO.: 5.10 SENSOR CATEGORY: Field Measuring Sensors					
SECTION NO.: 5.10 SENSOR CATEGORY: Field Measuring Sensors					
SECTION NO.: 5.10 SENSOR CATEGORY: Field Measuring Sensors	·		-		
SECTION NO.: 5.10 SENSOR CATEGORY: Field Measuring Sensors			,		
SECTION NO.: 5.10 SENSOR CATEGORY: Field Measuring Sensors	•				
	SECTION NO.: 5.10 SENSOR CATEGORY	: Field Meas	suring Sensor	:s	

5.10-i

This page intentionally left blank.

REV. NO.:

REV. DATE: 30 June 1977

# Section 5.10 INTRODUCTION TO FIELD MEASURING SENSORS

This section contains introductions to various field measuring sensors. Each introduction to a specific sensor type is addressed independently. The intent of this section is to provide a review of the principles of primary field sensors (gravity, magnetic and electric), although a more general class of sensors associated with monitoring the space environment above the ionosphere may be included.

### 5.10.1 MAGNETOMETERS

The Earth's magnetic field, when accurately known, is an important reference for navigation. Also, a global map of the Earth's magnetic field, when correlated with geological and geophysical models of the Earth's crust, can indicate magnetic anomalies (potential targets for natural resource exploration).

There are two classes of magnetometers, vector and scalar. Each performs a valuable function and will be described independently following a brief review of the characteristics of the earth's magnetic field.

A theoretical concept that has gained increasing acceptance, especially in understanding the Earth's magnetosphere, is field-line merging. At the interface between two different plasmas, regions occur in which there are basically oppositely directed fields (e.g., a northward directed field adjacent to a southward directed field) and where the field strength is weak. It is thought that plasma can flow into this neutral region from the two sides and then flow out of the region parallel to the boundary (see Figure 5.10-1). In the neutral region, the field lines can be thought of as being broken and reconnected. This mechanism can lead to a direct connection between interplanetary and planetary magnetic fields. As a consequence,

reconnected field lines leaving the Earth in the vicinity of the magnetic pole do not return to the opposite pole but are attached to field lines leading off into interplanetary space (see Figure 5.10-2).

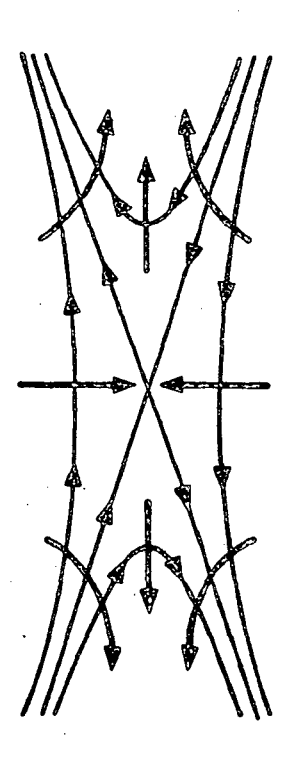


FIGURE 5.10-1 Field line merging at a neutral point. This figure is one of the earliest representations of the merging region. The thin lines represent lines of force of the magnetic field and the thick lines are the stream lines of the plasma flow. Plasma enters the region from the left and right and leaves by flowing upward and downward. The magnetic fields adjacent to the region are oppositely directed as shown by the arrows. The field lines are forced together by the inflowing plasma and the fields originating on opposite sides of the region become connected.

Studies of the Earth's magnetic field have continued at a vigorous pace, in part because the extraterrestrial field is so accessible to spacecraft and in part because of the long record of observations, which cover entire solar cycles, and the wealth of detail available. In addition, the magnetic field is a fundamental

REV. NO.: 0 REV. DATE: 30 June 1977

parameter of great significance to many other scientific investigations such as studies of trapped and precipitating particles and their interaction with various species of waves that can propagate in a plasma. There is a close correspondence between the magnetic field and large-scale electric fields which have been found to play an important role in the coupling which takes place between the interplanetary medium and the region in and above the Earth's ionosphere. As a final example, the Earth's field and its complement of trapped ambient particles represent a large number of different regimes available for study as examples of naturally occurring collisionless plasmas. One of the basic parameters used to characterize plasmas is the ratio of the thermal particle energy to the magnetic-field energy, a parameter which varies significantly from one region of the Earth's field to another.

Before the first measurements in space, the geomagnetic field had been mapped extensively using aircraft and ships and an accurate quantitative representation in terms of spherical harmonics had been derived. Currents above the Earth's surface were known to contribute fields as large as one percent of the internal field. From surface measurements, much information had been accumulated about transient irregular variations known as magnetic storms. The storms were known to be correlated with solar activity and to contain potential information about the outermost extremities of the Earth's field. It has proved difficult, however, to infer the location and nature of the currents that were causing the observed field changes, especially as their distance above the Earth increased.

The outstanding successes from the previous era were the characterization of at least the horizontal component of the currents in the high-latitude ionosphere and inferences regarding the confinement of the Earth's field by solar plasma and the existence of a ring current circling the Earth at several planetary radii.

REV. NO.: 2 REV. DATE: 31 Jan 1978

Many magnetic storms were observed to begin with an abrupt increase in the geomagnetic field and this was correctly attributed to the compression of the Earth's field by a cloud of neutral ionized gas emitted by the Sun. During the subsequent magnetic storm, a slowly varying component was identified corresponding to an essentially uniform field over the Earth's surface. The source of this field was thought to be a current loop that was somehow established at large geocentric distances during the storm and which then slowly decayed away as the storm ended.

Limited information was also available regarding the existence of relatively dense low-energy plasma at high altitudes. Lightning discharges have been shown to give rise to whistling radio signals that propagated along the lines of force of the Earth's field between conjugate points in opposite hemispheres. The dispersion that characterized these "whistlers" implied a density of 10<sup>2</sup> electrons cm<sup>-3</sup> near the magnetic equator at a distance of about  $5r_E$ . It was thought, however, that these electrons were part of a static interplanetary medium, a view which is now known to be incorrect. However, the observations correctly implied that the Earth's field was still essentially dipolelike at that distance.

One of the major achievements of space research has been the rather complete characterization of the Earth's magnetic field in space. The presence of plasma in the space surrounding Earth has a profound effect on the geomagnetic field and leads to a field configuration that is very unlike a magnetic dipole in a vacuum. The concept of frozen-in fields implies that the geomagnetic field and its trapped particles will be excluded from the space occupied by the magnetized interplanetary medium. This realization has led to the concept of the "magnetosphere," i.e., a cavity or bubble in the interplanetary medium into which the geomagnetic field is compressed. In its simplest form, the field topology would be closed with the

REV. NO.: 2

boundary, called the "magnetopause," a simple surface of revolution with the Earth's field on one side and the interplanetary medium on the other.

The actual situation is much more complicated owing to the continual outward streaming of the solar plasma at supersonic speeds to form the solar wind. Thus the proper characterization involves, not a steady state, but a quasi-stationary flow pattern. A reasonable, low-order approximation is provided by the flow of a supersonic gas past a cylinder or sphere (representing the magnetosphere). In this gas-dynamic example, a detached bow shock occurs which converts the streaming energy of the oncoming gas into internal energy and allows the gas to be deflected around the sides of the cylinder. The other essential features of the interaction are a boundary layer adjacent to the cylinder and a long wake extending downstream. The flow could be revealed by means of a snapshot showing the flow lines, although it must be recognized the medium is actually continuously in motion. The counterparts of all three of these features, including the bow shock, have been observed to be a part of the solar-wind interaction with the Earth's magnetic field.

Even the aforementioned gas-dynamic analogy is actually far simpler than the interaction of the Earth with the solar wind because, to continue the analogy, the solar wind contains a magnetic field and the cylinder is permeable. Particles, momentum, and energy can be transferred across the boundary and into the cylinder, apparently as a consequence of a direct connection between the interplanetary and planetary magnetic fields. The Earth's magnetic field apparently extends through the boundary and connects the magnetospheric plasma inside with the solar-wind plasma outside.

A further complication is the existence of processes within the magnetosphere which effectively represents sinks for the particles' momentum, and energy imparted by the solar wind. Thus some of the particles are precipitated into the atmosphere,

REV. NO.: 2 | REV. DATE: 31 Jan 1978

in part to cause the aurorae. The momentum transfer leads to an internal circulation (convection) of the magnetic field and plasma in the outermost regions of the magnetosphere. This convection is the counterpart of the external solar-wind flow around the Earth. Energy from the solar wind results in the acceleration of trapped particles to high energies as well as the production of intense currents in the ionosphere which act as dissipative loads. Thus many features of the interaction depend on the nature of the competition between external sources and internal sinks.

As a final complicating factor, the solar-wind flow is not steady but consists of strong gusts which occur several times a month in the form of fast streams. To characterize the interaction properly requires, not a snapshot, but a motion picture. The enhanced solar-wind flow associated with a stream significantly increases the transfer of particles, momentum, and energy into the magnetosphere and gives rise to major transient variations known as magnetic storms. Since the processes acting as sinks have their own, relatively long characteristic times, it is possible temporarily to store magnetic energy as well as particles inside the magnetosphere even after the solar-wind stream has passed the Earth and traveled onward into interplanetary space. The main reservoir is thought to be the long magnetotail. Eventually, however, the Earth tends to relax back to the quiet configuration during the so-called "recovery phase" of the storm.

An important aspect of the direct connection between field lines inside and outside the magnetosphere, and a phenomenon which provides evidence for the merging process, is the observation of "substorms." These are episodes of only a few hours duration involving basically the same phenomena as magnetic storms (i.e. particle energization and precipitation, the development of intense current sheets and electrojets as high latitudes, increased convention inside the magnetosphere, etc.),

REV. NO.: 0 REV. DATE: 30 June 1977

but on a smaller magnitude. The close correspondence suggests that magnetic storms are actually several substorms occurring sequentially. Observations in space have shown that substorms can be triggered simply by a random change in the direction of the interplanetary magnetic field such as to increase the prospects for field-line merging.

With the aforementioned material as a general background, it now becomes possible to describe the main features of the Earth's field in the quasi-stationary state during quiet intervals, as diagramed in Figure 5.10-2. It is convenient to

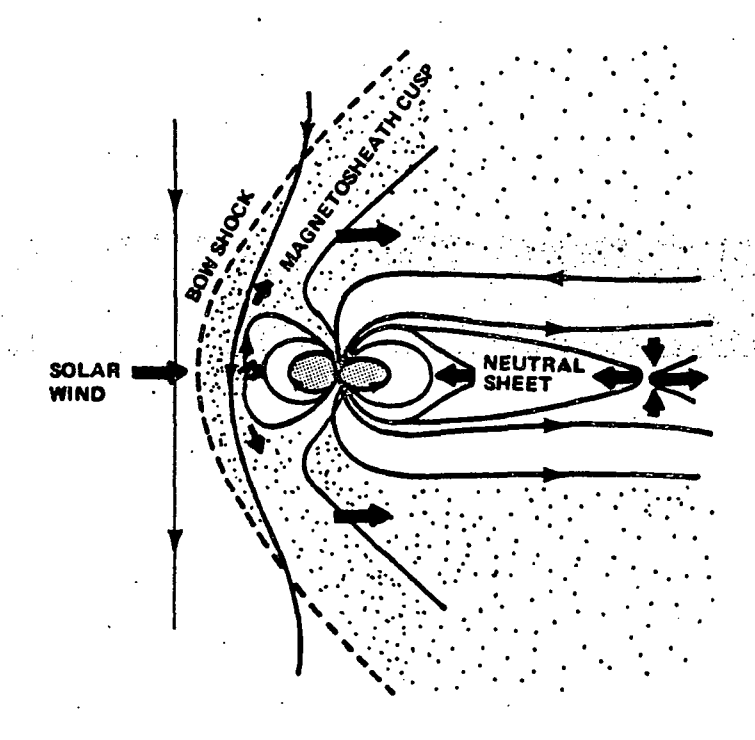


FIGURE 5.10-2 Interaction of the solar wind with the Earth's magnetosphere. The solar wind arrives from the left, crosses the detached bow shock, and proceeds into the "magnetosheath," a transition region shown here as dotted. The thin lines represent magnetic fields in a meridian plane and the heavy lines show the direction of plasma flow. Two neutral regions are shown, one on the front side of the magnetosphere and the other in the magnetic tail. The dotted region near the Earth represents the corotating magnetic field and relatively dense plasma derived from the ionosphere. An "open" field line is shown which originates in the Earth's polar region and becomes an interplanetary field line in the magnetosheath.

REV. NO.: 0 REV. DATE: 30 June 1977

describe the topology as a function of latitude, although it should be recognized that a correspondence exists between latitude and the distance at which the (closed) field lines cross the equatorial plane. Thus, at low and moderate latitudes (up to 60°), the field is dipolelike and corotates with the Earth, carrying with it the low-energy high-density plasma that represents the upward extension of the ionosphere. At latitudes between 60° and 70°, corresponding roughly to the auroral ovals in the northern and southern hemispheres, convection becomes dominant and, although the field lines are closed, their motions are no longer simply the result of the Earth's rotation. At these latitudes, the field lines are returning to the magnetosphere, after being reconnected in the tail, and are being convected sunward. At the highest latitudes, corresponding to the polar cap, the field lines are predominantly open and are being carried downstream to form the Earth's magnetic tail.

Although there are many details about which scientific opinion is still divided, some of the current physical explanations for this topology are the following. The internal convective motions are a consequence of a direct connectiong between the two fields in restricted areas of the magnetopause, called neutral regions, where the fields tend to be oppositely directed. The field lines passing near the magnetopause through such regions map back to the Earth at high latitudes. Once geomagnetic field lines become tied to interplanetary fields, they are swept downstream to form the Earth's tail, because the interplanetary field is frozen into the solar wind and the parts of the field still in interplanetary space travel anti-sunward at high velocities. The feet of these field lines are transported across the polar cap, a motion made possible by the presence of the electrically insulating neutral atmosphere below the ionosphere. Thus the field lines are conceived of as being severed at the base of the ionosphere.

REV. NO.: 2

Field lines cannot be removed from the magnetosphere indefinitely, especially since the formation of the tail leads to a configuration consisting of oppositely directed fields, which is the counterpart of the configuration on the dayside that originally led to field-line merging. It is thought that merging again takes place with the ends of the geomagnetic field and the interplanetary field once again being reconnected geomagnetic field lines takes place at slightly lower latitudes in the vicinity of the auroral zone. The observed dayside cusp is presumably the demarcation between open field lines convecting tailward and closed field lines within the ionosphere giving rise to intense electrojet currents which flow eastwest and to current sheets in which field-aligned currents either enter or leave the ionosphere.

All spacecraft have stray magnetic fields due to magnetized permeable material and to electric current flowing in the power mains and electronic subsystems. Currents flowing in solar panels can also contribute stray fields. If the stray fields were truly steady, a preflight calibration would suffice to determine the error introduced for all time. Unfortunately, spacecraft fields are typically unstable and change with time. Some of these changes are due to the magnetization of permeable material during the launch phase when the presence of the Earth's field is important together with the vibration spectrum of the launch vehicle. Changes are also probably introduced by aging and temperature variations of the permeable materials in space. Current changes due to command switching of circuits and the aging of electronic components may also contribute to changing fields. Finally, if the distance from the Sun to the spacecraft changes, the power output from solar panels will vary.

Control and reduction of stray fields impose stringent requirements on the spacecraft design. The use of permeable materials must be kept to a minimum. It

REV. NO .:

is common practice to use a long boom to place the sensors as far as practical from the spacecraft body. The design of a suitable boom is a nontrivial problem since long booms can affect the spacecraft dynamics in complicated ways. On attitude-stabilized spacecraft, boom vibrations can couple into the servosystem, while the dynamics of spinning spacecraft are significantly modified by booms. Nevertheless, instruments other than magnetometers also require booms, and considerable effort in the past decade has gone into understanding how to design an efficient boom.

From the standpoint of currents, their treatment depends upon the type of measurement to be made and on whether the spacecraft is attitude-stabilized or spinning. The effect of steady currents upon measurements on an attitude-stable spacecraft is identical to that caused by magnetized material, although the time dependence is probably far different. On spinning spacecraft, the fields due to currents rotate with the spacecraft and again appear as a quasi-steady field with the following exceptions. Currents associated with solar panels show a time dependence because of the rotation and non-constant illumination by sunlight. Consequently, in the rotating frame of the magnetometer, a ripple may appear. The harmonic spectrum of the ripple is complex and depends upon the time dependence of the illumination function. Fortunately, solar panels can be back-wired so as to reduce this effect. The use of twisted-wire pairs throughout the spacecraft is an important aid in reducing current-derived fields. The pitch of the twist is a critical parameter in the optimum reduction of stray fields. [1]

The flux-gate magnetometer, first built in 1941, has been used in the majority of space flights where particle and fields research is carried out. The principle of operation of the flux-gate is based upon a high-permeability core ariven into saturation by an oscillator feeding current through a primary vinding at a fre-

REV. NO.: 1 REV. DATE: 30 Sept 1977

quency of 5-10 kHz (Figure 5.10-3). It can be shown that in the absence of an external field (input field), the output of a secondary coil wound on the saturable core consists of a series of odd harmonics. When an external field is applied, it biases the core and the output will contain even harmonics whose amplitudes are proportional to the strength of the input field. The second harmonic is syncronously detected by comparing its phase with the second harmonic of the drive signal. Feedback is achieved by driving the saturable core with a current proportional to the detector output thereby maintaining a null condition. A triaxial sensor is assembled by placing one such element on each of three orthogonal axes. [2]

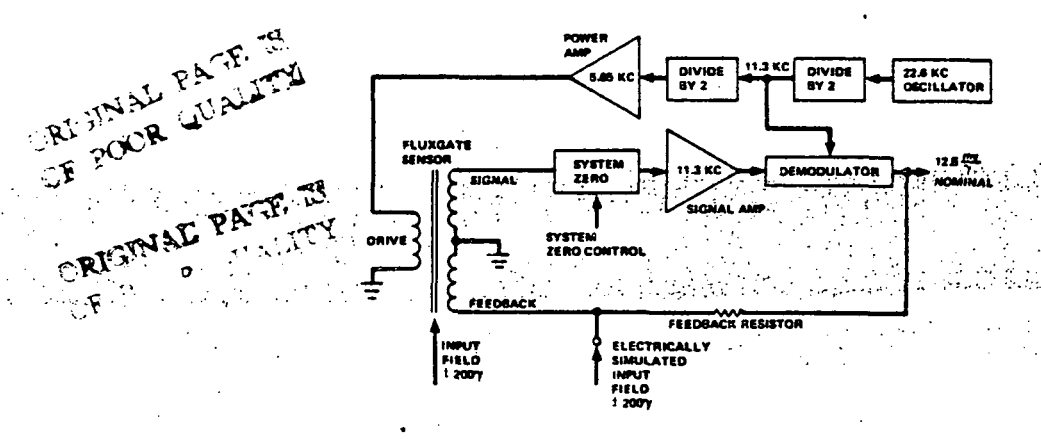


FIGURE 5.10-3 Block Diagram of a Single Axis Flux-Gate Magnetometer

Recent spaceflight magnetometers have used optical pumping of a gas in order to detect and exploit the Zeeman effect in relatively weak magnetic fields. Basically, two types of magnetometers have been flown. The rubidium-vapor magnetometer, which has been used as a scalar instrument to provide a measure of the field magnitude, and the vector helium magnetometer, which measures all three components of the field. The rubidium magnetometer has commonly been used with low-altitude earth-orbiting satellites to obtain global maps of the geomagnetic field above the ionosphere. The vector-helium magnetometer has been flown on planetary-interplanetary missions to Mars, Venus and Jupiter.

The block diagram of a representative rubidium magnetometer is shown in Figure 5.10-4. Intense radiation is obtained by a sustained radio-frequency discharge in a lamp containing rubidium. The resonance radiation (at 794.7 nm) passes through a circular polarizer and interference filter to an absorption cell containing rubidium vapor at low pressure and is then focused on a photodetector. The incident radiation optically pumps the rubidium, preferentially populating one of the ground-state magnetic levels. The induced magnetic moments cause the pumped atoms to precess about the ambient magnetic field at the Larmor frequency.

In a common configuration used on satellites, a coil is wound around the absorption cell and used to produce an oscillating field parallel to the light beam (optic axis). When the frequency of the oscillating field is equal to the Larmor frequency, a coherency is introduced that causes a variation in the transparency of the cell and hence a periodic modulation of the light intensity

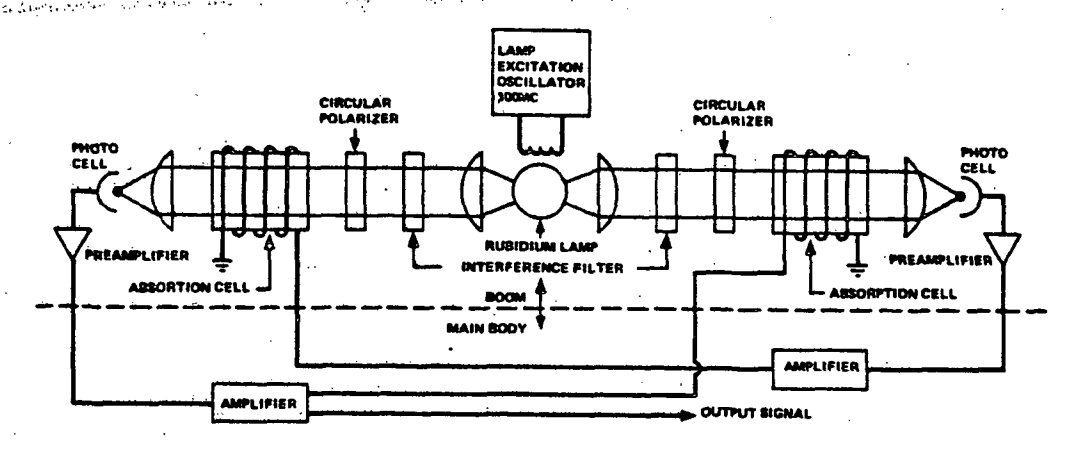


FIGURE 5.10-4 Block Diagram of a Rubidium-Vapor Magnetometer

at the detector. This effect makes it possible to feed the detector output back to the coils to form a self-oscillating magnetometer. The output is then a voltage oscillating at the Larmor frequency which is directly proportional to the scalar magnitude of the field. Dual cells are used to eliminate the ne essity of switch-

REV. NO.: 0 REV. DATE: 30 June 1977

ing the phase of the feedback signal when the sense of the field changes. signal strength is aspect dependent and the magnetometer is insensitive to ambient fields either parallel or perpendicular to the optic axis. Two independent rubidium magnetometers in a crossed configuration have been commonly used to reduce substantially the solid angle subtended by the null directions, and hence to reduce the likelihood that the magnetometer will be unable to measure the field because of an unfavorable orientation.

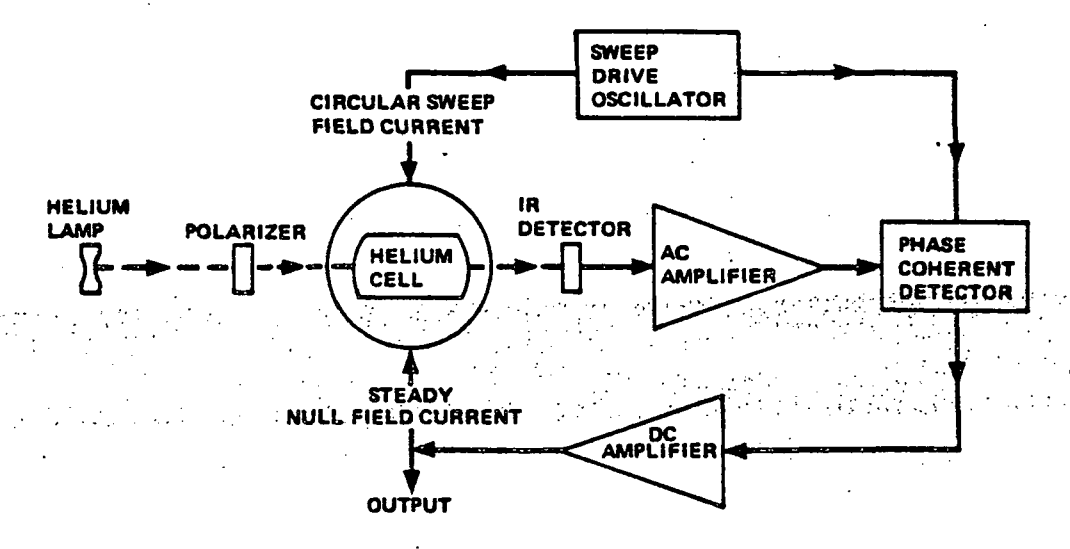


FIGURE 5.10-5 Block diagram of a vector-helium magnetometer. The circle enclosing the absorption cell is symbolic of the Helmholz coils which are driven by both an ac sweep-field and a dc feedback-field.

The vector-helium magnetometer (Figure 5.10-5) has many of the same general elements as the rubidium magnetometer. Intense radiation obtained from a heliumdischarge lamp passes through a circular polarizer, a helium-filled absorption cell, and is focused onto an infrared detector (the resonant pumping line has a wavelength of 1.08 µm). Mestable helium atoms are generated in the absorption cell by a sustained RF discharge. The triplet "ground" state of mestable helium is optically pumped by the incident resonant radiation.

**REV. DATE: 30 June 1977** 

The absorption cell is located inside a set of Helmholz coils which are used to generate a magnetic field at a frequency of a few hundred hertz rotating in the plane containing the optic axis. Since the optical-pumping efficiency depends on the angle between the magnetic field and the optic axis, the changing orientation of this sweep field causes a periodic modulation of the cell transparency and, hence, a sinusoidal variation in the detector output. Phase coherent detection is used to determine the phase shift between the detector output and the reference sweep field which is introduced when a steady ambient magnetic field is also present. Steady currents are then fedback to the Helmholz coils to null the ambient field by reducing this phase error to essentially zero. In this closedloop mode of operation, the magnetometer output consists of two voltages proportional to the feedback currents and hence to the components of the ambient magnetic field in the sweep plane. Triaxial measurements are obtained by alternating the sweep field between two orthogonal planes which intersect along the optic axis.

One of the more promising types of magnetometers, which may accelerate U.S. efforts to globally map the Earth's magnetic field, and aid in exploration of natural resources, is the double-resonance system developed by Anatole Abragam at the Laboratoire d'Electronique et de Technologie de l'Informatique (LETI) in Grenoble, France. Abragam's theory exploits the knowledge that protons have a magnetic momentum which is directly related to the ambient magnetic field. concept suggests that field variations can be monitored by measuring the proton's precession frequency--the movement of its spin axis when affected by a magnetic field. Although this principle has been researched by others, Abragam was the first to propose increasing the proton's magnetic momentum by transf rring to the protons energy from liquids containing protons and free electrons. In some liquids

REV. DATE: 31 Jan 1978

REV. NO .:

the proton's magnetic momentum can be multiplied by a factor of 4000. The French claim that their double-resonance magnetometer has a resolution of 0.01 gamma, about 100 times more accurate than conventional magnetometers. [3]

### 5.10.2 GRAVITY SENSORS

Gravimetry is the science of measuring quantities characterizing the terrestrial gravitational field. Initially, gravimetry was a section of higher geodesy, dealing with the study of methods for measuring the gravitational force and methods of applying the results of these measurements to the determination of the compression of the Earth's figure. [5] More recently, gravimetry has become one of the most effective methods of studying the interior of the earth, particularly in locating density variations near the surface which might lead to natural resource deposits. Additionally, fields such as navigation and inertial guidance, altimetry and bathymetry are supported through accurate gravity gradient and gravity anomaly surveying.

For the determination of the gravitational force it is possible to use many physical phenomena which are in some form dependent on it, such as the free fall of bodies in a vacuum, in air or in a liquid; the oscillations of a pendulum; the elongation of a spring under the action of a load; the rise of a liquid in a capillary; voltage developed as a result of force on a piezoelectric element, and others. The basic problem of gravimetry is the study of the gravitational force G, being the derivative of the gravitational potential V in the direction of the normal to an equipotential surface, passing through a given point A (Figure 5.10-6). So that one may write:

 $\frac{\sigma V}{\sigma N} = -G$ 

(1)

REV. NO.: 2 | REV. DATE: 31 Jan 1978

where the sign of G depends on the choice of the direction of the normal N. The outward direction with respect to the equipotential surface corresponds to a reduction in the gravitational force. Note that the curvature of the equipotential

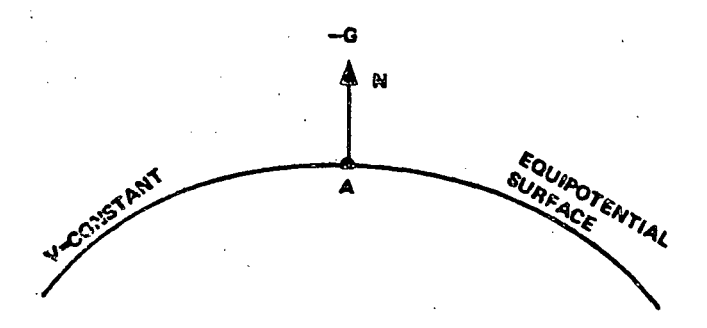


FIGURE 5.10-6

surface, hence the value of the potential V at any point on the surface (earth) changes in the course of time. The acceleration constant (g) on the terrestrial surface varies approximately 0.53% from about 978 to 983 cm/sec<sup>2</sup>, increasing from the equator towards the poles and decreasing with elevation above sea level at a rate of 300 µm/sec<sup>2</sup> per meter. [6]

One objective of geodesy is to determine the variations of the Earth's gravitational potential, which can be expressed in terms of spherical harmonics;

$$V = \frac{GM}{r} \left[ 1 + \sum_{n=2}^{\infty} \left( \frac{R}{r} \right)^{n} \sum_{m=0}^{\infty} Pnm \left( \sin \phi \right) \left[ Cnm \cos m\lambda + Snm \sin m\lambda \right]$$
 (2)

where R is the mean radius of the Earth, Pnm is the normalized Lengendre polynomial, Cnm and Snm are the coefficients of the harmonic terms, and  $(r, \phi, \lambda)$  are the coordinate positions of the instrument. [7]

The methods used for measurement of the gravitational force are historically divided into two catagories; dynamic and static. Dynamical methods are used for absolute and relative measurements. Absolute measurements are intended to determine the absolute value of the gravitational force at a point (or integrated

C-5

.REV. NO.: 2

over an area), whereas relative measurements are carried out when determining the difference  $\Delta g$  with respect to a given reference.

Static methods are used for highly accurate determination of differences of gravitational force and are limited, for the most part, to point measurements on the Earth's surface.

When measuring the variation in the horizontal plane (gradients of the gravitational force) as well as positions of the principal normal sections of the equipotential surface and curvature differences, a gradiometer relates quite well and has a predictable relationship to the second order derivatives of the gravitational potential.

The Gravity Gradiometer measures a combination of second spatial derivatives of the gravitational potential; i.e., the spatial change in acceleration. This is accomplished by utilizing proof masses to measure the small differences in acceleration between points in the satellite. [8]

The advantage of gradiometer techniques in obtaining the higher-order harmonics of the Earth's gravitational field is straightforward. Terms with increasing N correspond to small scale features on or near the surface. Although the contribution of these harmonic components to the gravitational potential is quite small, their contribution to the gravitational force gradient at point above them is a substantial fraction of the gravitational gradient of the entire earth.

The Hughes Research Lab rotating gravity gradient sensor [7] is a device for measuring the second-order gradient of the total gravity potential field. The sensor consists of a resonant cruciform mass-spring system with a tortional vibrational mode. In operation, the sensor is rotated about its tortionally

resonant axis at an angular rate  $\omega$  which is one-half the tortional resonant frequency. Gradients in the gravitational field excite the structure at twice the rotational frequency (see Figure 5.10-7). Only the differential torque  $\Delta T$  between the sensor arms is coupled to the central tortional flexture for conversion to a measurable voltage. The tortional gravity gradiometer has two significant

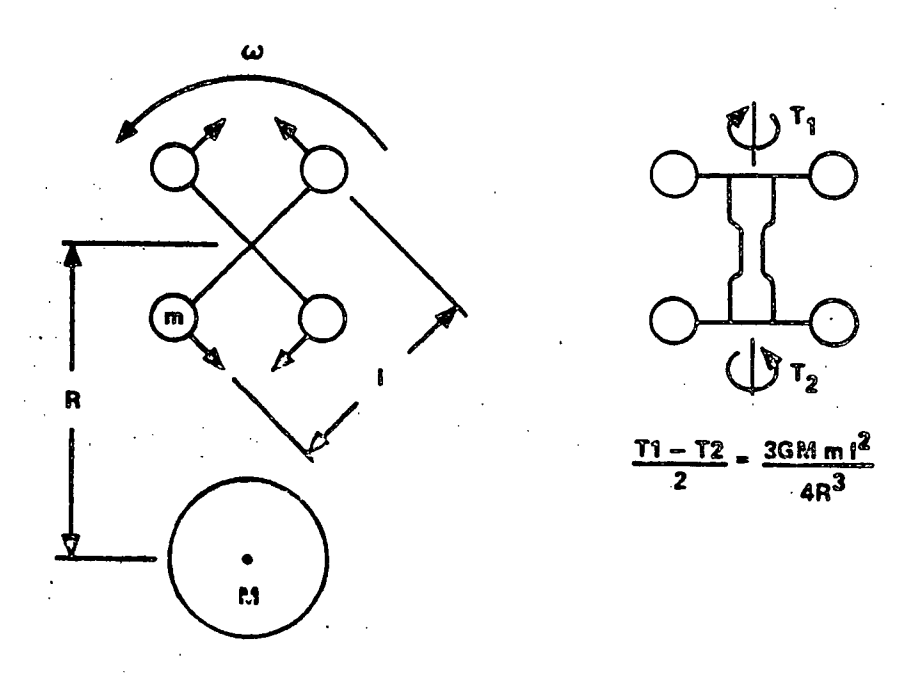


FIGURE 5.10-7 A Functional Diagram of the Hughes Research Lab Rotating Gradiometer

advantages over other gradient sensing instruments. There are no bearing noise problems, which are the primary source of difficulty in earthbound operation, and, most important, since the spacecraft is rotating along with the sensor, the gravity field of the spacecraft is stationary in the frame of reference of the sensor, hence, only the gravity gradient field of the earth is sensed.

The effective resolution of a gradiometer at an altitude of 220 is approximately 220 km. If a gradiometer were placed in a near polar orbit with

REV. NO.: 2 REV. DATE: 31 Jan 1978

suitably chosen orbital parameters, it would pass within 220 km of every point on the earth in 80 orbits, thus completely mapping the earth in 5 days (see Figure 5.10-8). The track spacing between the half arcs is approximately 250 km, so there is a good match between track spacing and swath width.

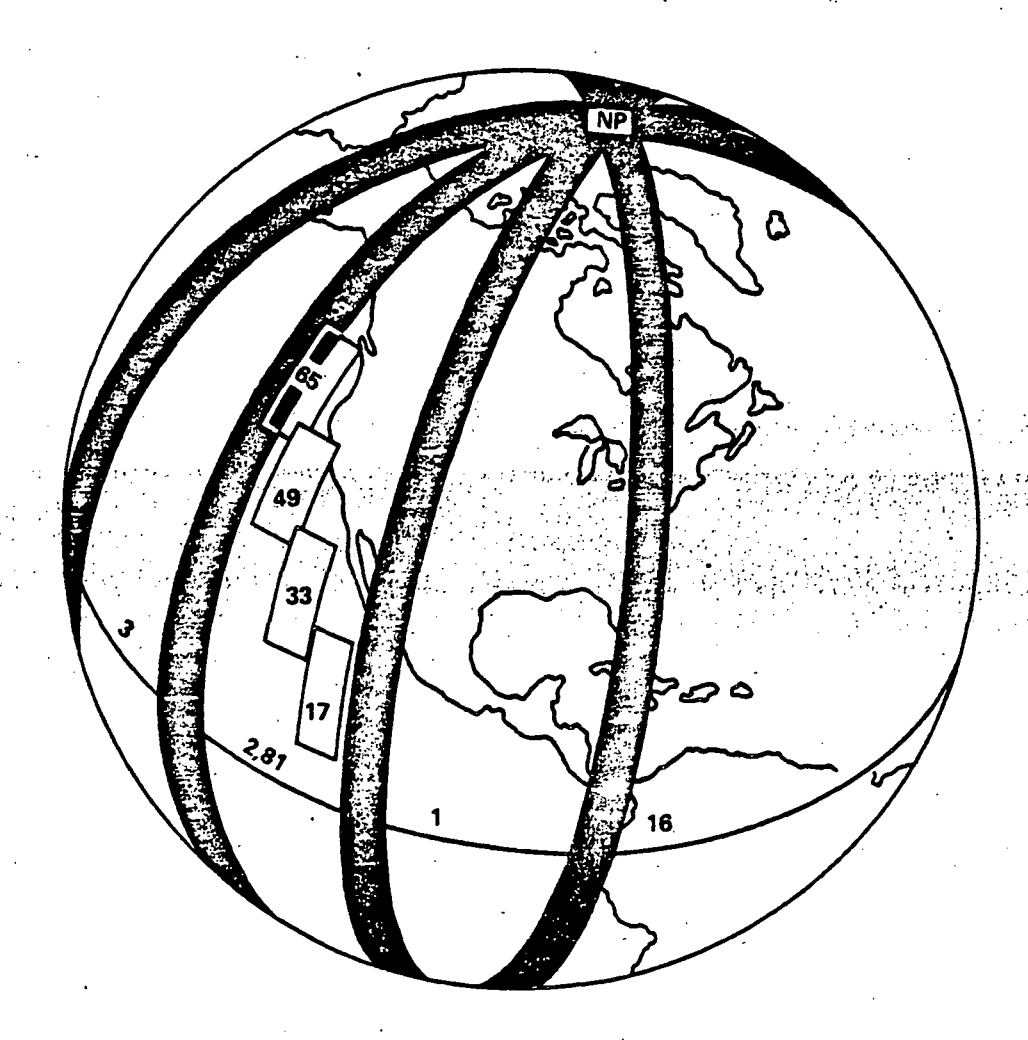


FIGURE 5.10-8 Swath Pattern of Full Coverage Orbit

This, of course, is not realizable since the orbital altitudes will decay because of drag. A more feasable approach would include an orbital lifetime of from 30 to 50 days following a 330 km launch into a polar orbit. The time spent near 320 km would be long enough to obtain good coverage of the earth at that resolution

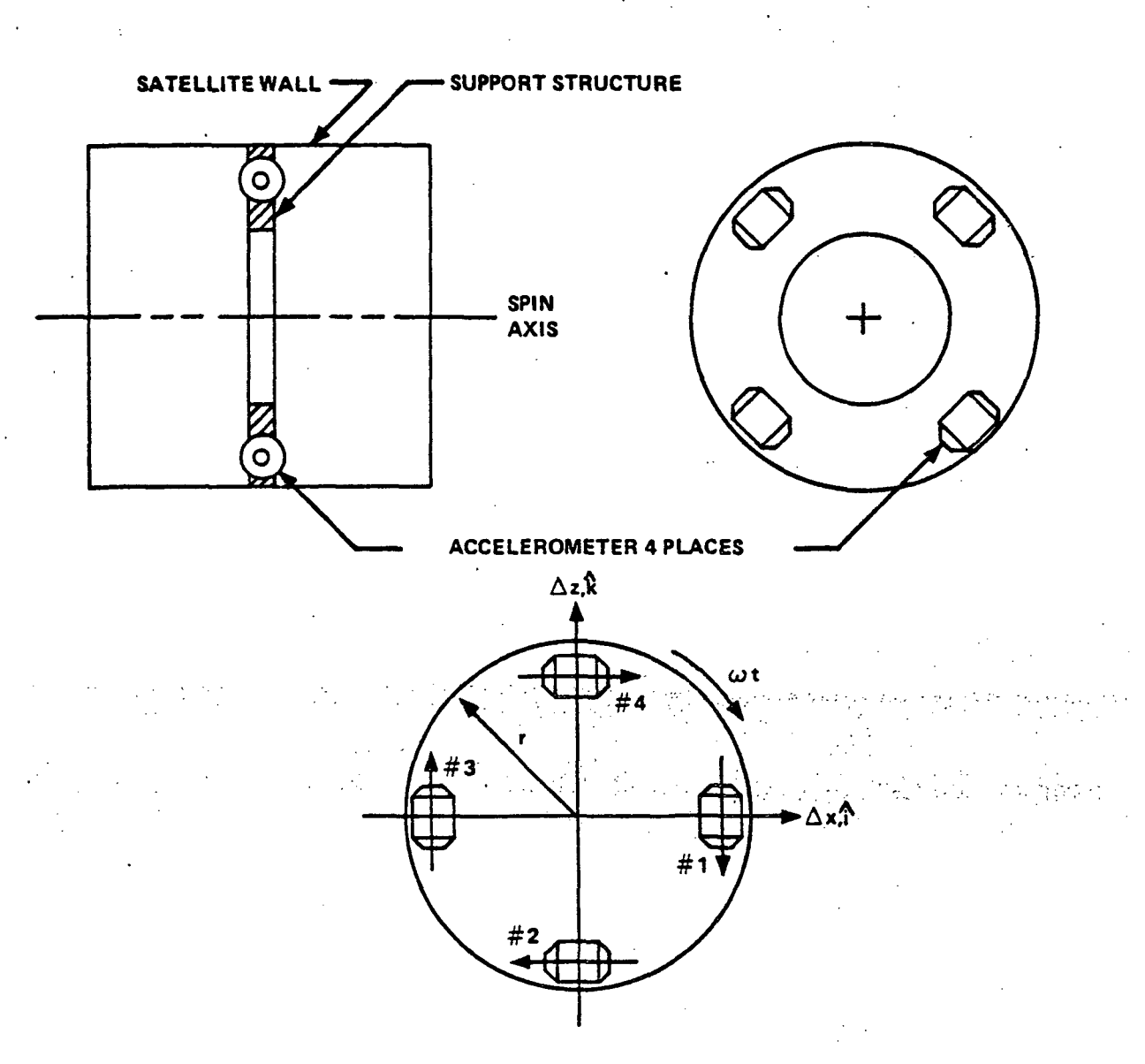
REV. NO.: 2 | REV. DATE: 31 Jan 1978

(640 km wavelength or degree 62). As the altitude decreases, the resolution would improve steadily. There would be a substantial amount of coverage near 220 km altitude with excellent resolution (440 km wavelength or degree 90), but some coverage would be lost because the track spacing at the equator of 250 km is slightly larger than the sensor resolution.

A similar type instrument may be constructed from accelerometers. A direct analogy is obvious if one thinks of an accelerometer as a proof mass sliding on a frictionless wire. Consider the Bell Aerospace instrument operating at a fixed point in a gravitational field which varies slowly with position (see Fig. 5.10-9). The proof mass is centered electronically so that a signal is produced which is proportional to the force required to maintain the proof mass at the center of the wire. Thus the signal is proportional to the acceleration relative to the accelerometer housing that the proof mass would experience if free to travel along the sensitive axis. The entire system rotates about the y axis. The acceleration due to this rotation is radial and the sensitive axes are tangential; thus no signal is produced by the satellite rotation.

The situation due to the gravitational field is different, and since the field is slowly varying, one is justified in writing a Taylor's series expansion for the gravitational potential. This must be carried to at least second order. By differentiating the Taylor's series expansion with respect to each of the coordinate axes one obtains the vector acceleration to the proof masses as a function of position (x,y,z). Substituting expressions for sinusoidal motion in the x,z-plane as a function of time, and dotting these expressions with a time variant unit vector in the direction of each accelerometer's sensitive axis (i.e., taking the vector component of acceleration in the direction of the sensitive xis), one obtains the four equations shown in Fig. 5.10-9 for the signal of each accelerometer.

REV. NO.: 2 REV. DATE: 31 Jan 1978



### ACCELERATION:

 $(V_x + V_{xz} \Delta z + V_{xx} \Delta x)^{2} + (V_z + V_{xz} \Delta x + V_{zz} \Delta z)^{2}$ 

POSI"	POSITION:		SENSITIVE AXIS:	
Δ×	Δz		î	· R
r cos ω t	-r sin ω t	#1	−sin ω t	-cos ω t
−r sin ω t	−r cos ω t	#2	−cos ω t	sin ω t
−r cos ω t	r sin ω t	#3	sin ω t	<b>cos</b> ω t
r sin ω t	r cos ω t	#4	cos ω t	−sin ω t

FIGURE 5.10-9 The Bell Aerospace Gravity Gradiometer

REV. NO.: 0 REV. DATE: 30 June 1977

The inputs to a gravity gradiometer data reduction program would be as follows: trajectory data, spacecraft engineering data, science data and the gradiometer data itself. The output of a gravity gradiometer data reduction program would be coefficients of the spherical harmonic expansion of the Earth's gravitational field.

Trajectory data will be available from the satellite tracking net observing the satellite. It will include time of acquisition and angular position at acquisition for each observation of the spacecraft by each tracking station. The trajectory data may also include range and angular position at regularly spaced time intervals throughout the period of observation of the spacecraft by the tracking station.

The spacecraft engineering data will be transmitted by the spacecraft itself and recorded at the tracking stations. It will include orientation information relative to the horizon and the sun, spin rate and temperature data useful for estimating the gradiometer scale factor. Spacecraft engineering data may also include measurement of the in-plane (relative to the spin axis) drag components acting on the spacecraft.

The science data includes all the ground truth necessary for gravity gradiometer data reduction. This includes an initial estimate of the coefficients of the spherical harmonic expansion of the earth's gravitational field, station locations for the satellite tracking net and a variety of estimates of the amplitudes of perturbations acting on the satellite trajectory. These last considerations include the effects of the sun and moon (which contribute negligibly small gradients), estimates of the atmospheric drag acting on the spacecraft, the effects of wobbles in the Earth's spin vector, relativistic effects, etc.

The gravity gradiometer data will consist of amplitude measurements at regularly spaced time intervals from a low circular polar orbit with the satellite spin vector maintained perpendicular to the plane of the orbit and the orbital altitude selected to give repeating ground tracks.

5.10.22

**REV. NO.:** 

These four types of data will be processed to obtain an improved estimate of the coefficients of the spherical harmonic expansion of the Earth's gravitational field. This involves three principle steps. First, the trajectory of the satellite needs to be estimated. Second, the gradiometer data needs to be adjusted for non-ideal effects. And third, the data needs to be integrated over a sphere to obtain harmonic coefficients. Thus, the data reduction system will follow the flow diagram shown in Figure 5.10-10.

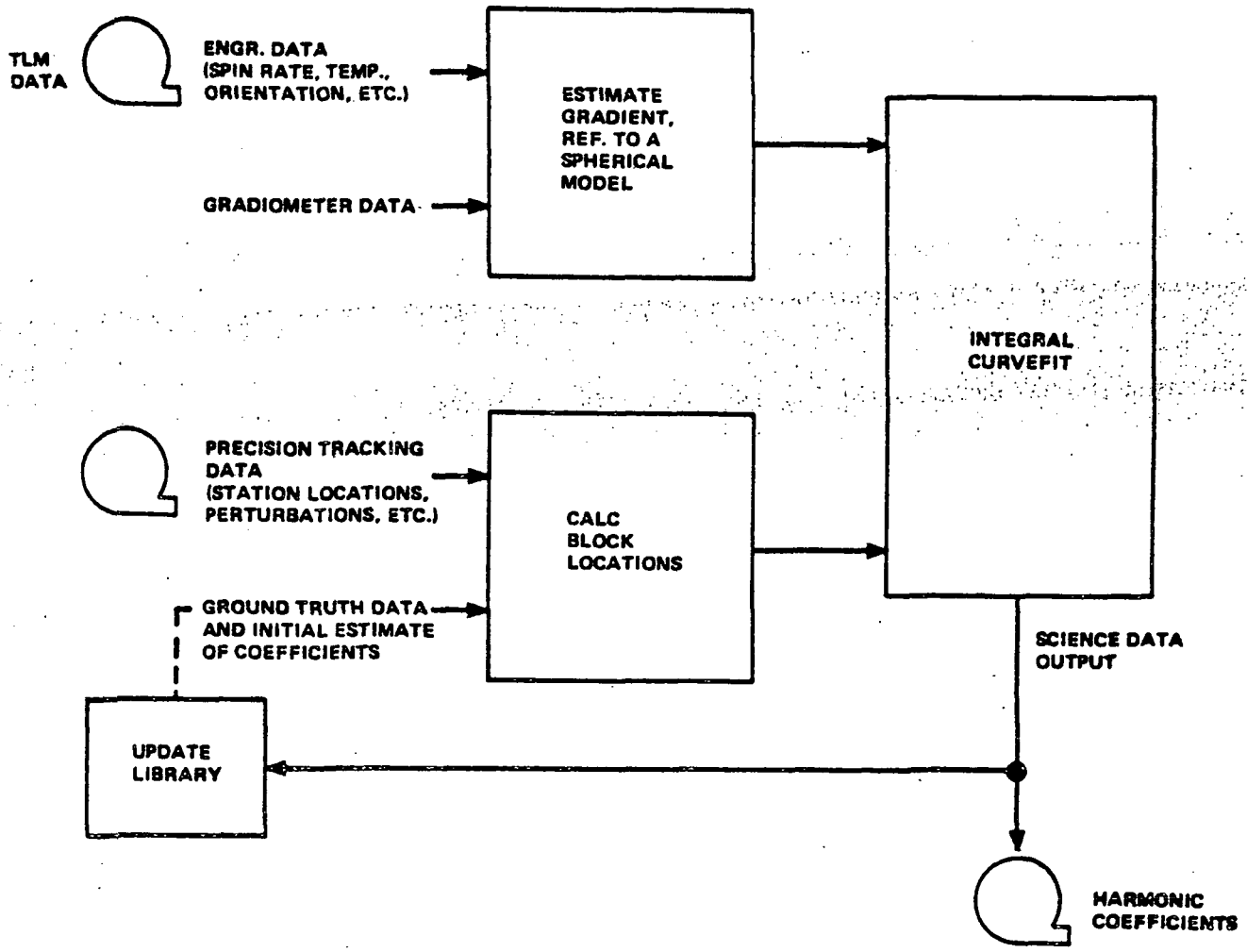


FIGURE 5.10-10 Data Reduction System Flow Diagram

There are a number of other techniques that have been proposed for obtaining gravitational data. Direct observation of long term satellite motions from the

REV. NO.: 2 REV. DATE: 31 Jan 1978

earth has been applied to calculate the gravitational field [9]. The data reduction technique used involves expressing the orbital elements as Fourier series whose coefficients are expressed as linear functions of the spherical harmonic coefficients. This is known as frequency decomposition. The accuracy of this technique is expected to improve dramatically in the next few years with the development of laser position determination.

Doppler radar or laser measurement of the range between two satellites has been proposed as a possible experiment for determining the Earth's gravitational field [10]. The range rate between an earth syncronous satellite and a low test satellite could be measured. Alternately, two low test satellites might be used, one continuously ranging the other. A recent proposal for data reduction involves parameter fitting to an assumed mass distribution on the ground [11].

A radar altimeter has been suggested for determination of the earth's gravitational field. Altimetry data contains considerable information about the gravitational field in the ocean regions where the mean surface height closely follows the geoid. This information coupled with existing surface data could be used to improve existing representations of the gravitational field [12].

**REV. NO.: 2** 

### **MAGNETOMETERS**

### LIST OF ACTIVE CONTRIBUTORS

Dr. Donald F. Adams
Professor of Mechanical Engineering
University of Wyoming
(307) 776-1121

Dr. Ulli G. Hartman Staff Scientist Ball Brothers Research Corp., TEL Gardena, Cal. 90247 (213) 327-2221

Lawrence I. Lazarow
Senior Mechanical Engineer
Ball Brothers Research Corp., TEL
Gardena, Cal. 90247
(213) 327-2221

Dr. J. Owen Maloy Staff Scientist Ball Brothers Research Corp., TEL Gardena, Cal. 90247 (213) 327-2221

George W. Mohler
Engineering Manager
Ball Brothers Research Corp., TEL
Gardena, Cal. 90247
(213) 327-2221

Dr. Mario Acuna Space Plasma Physics Branch Goddard Space Flight Center Greenbelt, Maryland 20771 (301) 982-2258

Dr. W. Harry Farthing Electrodynamics Branch Goddard Space Flight Center Greenbelt, Maryland 20771 (301) 982-5330

Dr. Edward J. Smith
Physics Section
Jet Propulsion Laboratory
Pasadena, Cal. 91103
(213) 354-2248

1

### **GRADIOMETERS**

### LIST OF ACTIVE CONTRIBUTORS

Dr. R. L. Foward Hughes Research Corporation Exploratory Studies Dept. Malibu, Cal. 90265 (213) 456-6411

Dr. Joseph Firy Applications Directorate Goddard Space Flight Center Greenbelt, Maryland 20771 (301) 982-6662

Dr. E. J. Sherry
Mission Engineering Section
Jet Propulsion Laboratory
Pasadena, Cal. 91103
(213) 354-3915

Robert J. Glaser Environmental Requirements Section Jet Propulsion Laboratory Pasadena, Cal. 91103 (213) 354-5459

Dr. A. A. Loomis
Planetology and Oceanography Section
Jet Propulsion Laboratory
Pasadena, Cal. 91103
(213) 354-6629

**REV. NO.: 1** 

REV. DATE: 30 Sept 1977

# FIELD MEASURING SENSORS REFERENCES

- [1] Smith, E. J., and Sonett, C. P., "Extraterestial Magnetic Fields: Achievements and Opportunities," <u>IEEE Transactions on Geoscience</u> Electronics, Vol. GE-14, No. 3, (July 1976), pp. 154-158.
- [2] "Vector Magnetometer Design Study: Analysis of a Triaxial Fluxgate Sensor Design Demonstrates That All Magsat Vector Magnetometer Specifications Can Be Met," <u>Ball Brothers Research Corp.</u>, Contract No. NAS 5-23661, Nov. 1976.
- [3] "Magnetometer Aids Oil-search Chances," <u>Electronics</u>, Vol. 48, No. 18, (Sept. 1975), pp. 40,42.
- [4] Stanley, J. M., Ludbey, F. C., Green, R., "An Alkali Vapour Magnetometer Using Integrated Circuits," <u>Space Science Instrumentation</u>, Vol. 1, (1975), pp. 471-492.
- [5] Shokin, P. F., "Gravimetry," Printed in Jerusalem by S. Monson, IPST Cat. No. 644, 1963.
- [6] Kattner, Wilbur T., ed., "Advances in Dynamic Gravimetry," ISA Proceedings of the Symposium on Dynamic Gravimetry, (March 1970), p. 116.
- [7] Glaser, R. J., "Gravity Gradiometer Data Reduction," Thesis for Degree of Aeronautical Engineer, California Institute of Technology, Pasadena, California, U.S.A., 1972.
- [8] Foward, Robert L., "Geodesy with Orbiting Gravity Gradiometers," American Geophysical Union, 1972.
- [9] Heiskanen, W. And Moritz, H., <u>Physical Geodesy</u>, W. H. Freeman and Company, San Fransisco, California, 1967.
- [10] Comfort, G. C., "The Determination of Gravitational Potential from the Measurement of Relative Velocity Between Satellites," Doctoral Thesis at MIT Aerospace Dept., Cambridge, Ma., June 1971.
- [11] Schwartz, C. R., "Gravity Field Refinement by Satellite to Satellite Doppler Tracking," Reports of the Department of Geodetic Science, No. 147, Ohio State University, Columbus, Ohio, (December 1970).
- [12] Rapp, R. H., "Accuracy of Potential Coefficients Determination from Satellite Altimetry and Terrestrial Gravity," Reports of the Department of Geodetic Science, No. 166, Ohio State University, Columbus, Ohio, (December 1971).

# FIELD MEASURING SENSORS BIBLIOGRAPHY

- (1) Foward, Robert L., "Review of Artificial Satellite Gravity Gradiometer Techniques for Geodesy," George Veis, ed., <u>Proceedings of the International Symposium on the use of Artificial Satellites for Geodesy and Geodynamics held in Athens</u>, May 1973.
- (2) Foward, Robert L., "Gravitational Field Measurements of Planetary Bodies with Gravity Gradient Instrumentation," <u>Astrodynamics Specialists Conference</u>, Ft. Lauderdale, Florida, August 1971.
- (3) Metzger, E. H., Jircitano, A., Affleck, C., Satellite Borne Gravity
  Gradiometer Study, Final Report, Bell Aerospace, Contract NAS 5-20910,
  March 1976.
- (4) Argentiero, P., and Garza-Robles, R., A Spacecraft-Borne Gradiometer Mission Analysis, GSFC (932), Technical Note, July 1976.
- (5) Acuna, Mario H. and Ness, Norman F., "The Pioneer XI High Field Flux-gate Magnetometer," <u>Space Science Instrumentation</u>, Vol. I, 1975, pp. 177-188.
- (6) McPherron, R. L., Coleman Jr., P. J., Snare, R. C., "ATS-6 UCLA Flux-gate Magnetomèter," <u>IEEE Trans. Aerospace and Electronic Systems</u>, Vol. AES-11, No. 6, November 1975.
- (7) Hedgecock, P. C., "Magnetometer Experiments in the European Space Research Organisations HEOS Satellites," Space Science Instrumentation, Vol. 1, 1975, 61-82.
- (8) Hess, Wilmot, H., ed., <u>Introduction to Space Science</u>, New York: Gordon and Breach, 1965, pp. 5-357.

REV. NO.: 1 REV. DATE: 30 Sept 1977

# ILLUSTRATION CREDITS FIELD MEASURING SENSORS

Figure No.	Page	Reference	Page
5.10-1	5.10-2	[1]	158
5.10-2	5.10-4	[1]	164
5.10-3	5.10-11	[1]	155
5.10-4	5.10-12	[1]	155
5.10-5	5.10-13	[1]	156
5.10-6	5.10-16	[5]	i
5.10-7	5.10-18	[6]	118
5.10-8	5.10-19	(1)	166
5.10-9	5.10-21	[7]	10

This page intentionally left blank.

REV. NO.: 1

REV. DATE: 30 Sept 1977

#### DATA SHEET

SHEET 1 OF 4

(1) SENSOR NAME, ACRONYM: (Triaxial) Fluxgate Magnetometer, FMAG

(2) DISCIPLINE: Earth and Ocean Physics

(3) SUBDISCIPLINE: Global Surveying & Mapping

#### (4) APPLICATION AND OBJECTIVE:

The vector satellite system employs 3 FMAG's which will measure the global vector magnetic field in a near earth orbit to an accuracy of approximately  $\pm$  5 gamma on a temporal and spatial basis.

(5) HERITAGE/KEY PERSONNEL: IMP. OGO. Explor

IMP, OGO, Explorer, ATS-6, Skylab

Cognizant Scientist: Dr. Joseph Siry, GSFC (301) 982-6662 Project Leader: Dr. Robert Langel, GSFC (301) 982-5600

#### (6) SENSOR DEPLOYMENT:

The FMAG's will be delivered via SHUTTLE and deployed as a system of 3 satellites in 400 km circular orbits phased 4 hours apart in local time (120° separation) and operating simultaneously for 12 months.

(7)

#### SENSOR CHARACTERISTICS

#### (7A) CAPABILITIES AND CONSTRAINTS OF THE SENSOR TO ACQUIRE THE MEASURED PARAMETER:

The Triaxial FMAG is boom mounted on a satellite that is stabilized with respect to a 3-axis earth centered coordinate system and measures the local magnetic field to an accuracy of ±5 gamma over the range of ±(15 K - 60 K) gamma.

(7B) ACTIVE SOURCE CHARACTERISTICS (FOR ACTIVE SENSORS):

N/A

R.

#### (7C) DETECTOR MEASUREMENTS CHARACTERISTICS:

The magnetic flux induced in the core by the gating field is modified by the external magnetic field which generates even harmonies on the output winding as a function of the magnitude of the external field. The discriminated second harmonic is calibrated to yield the magnitude of the field component parallel to the sensor axis, while the phase indicates the direction.

SECTION NO .:

5.10

SENSOR CATEGORY:

Field Measuring Sensors

2

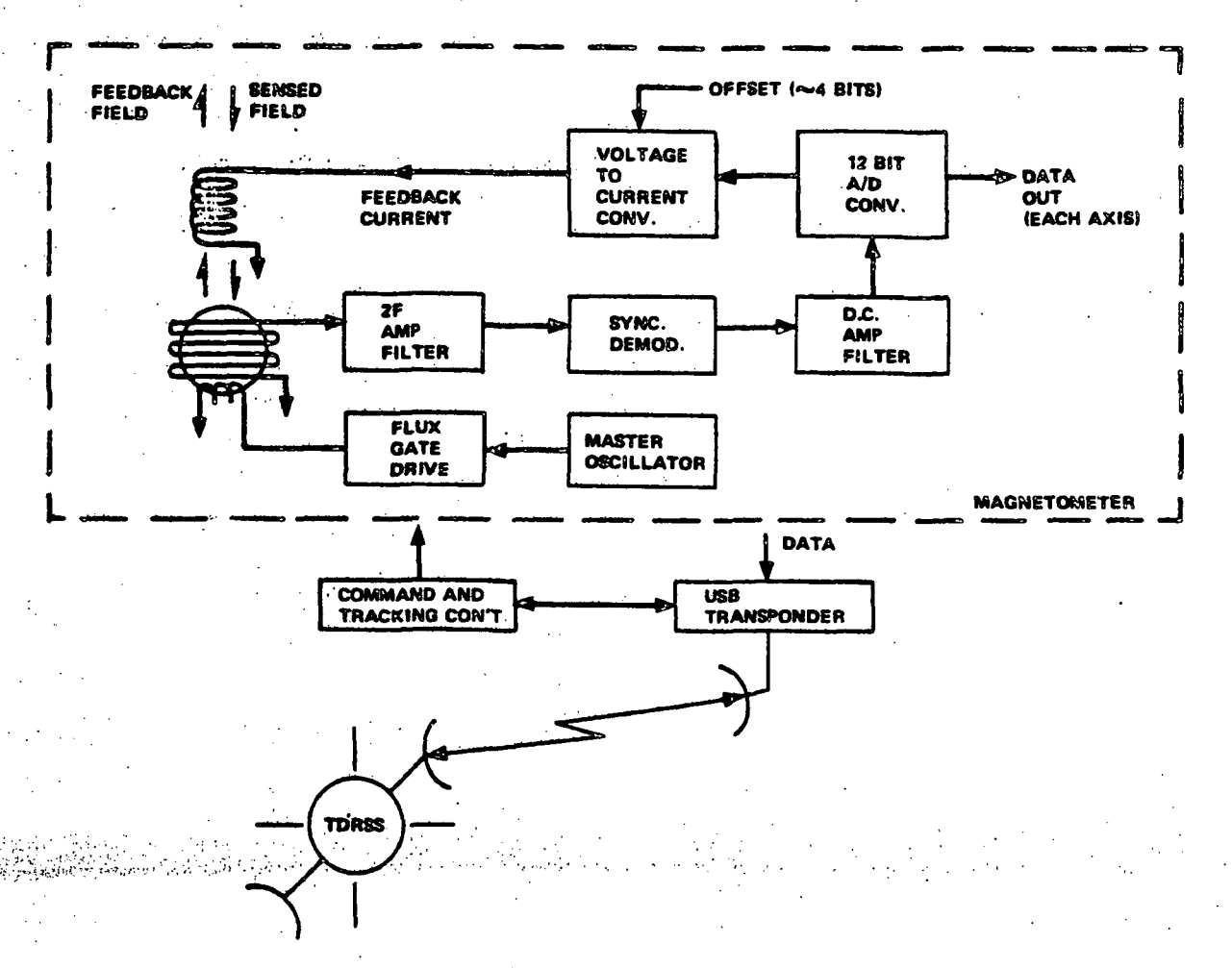
Preceding page blank

REV. NO.:

REV. DATE:

31 Jan 1978

#### (8) SENSOR DATA MEASUREMENT AND TRANSMISSION SYSTEM - BLOCK DIAGRAM.

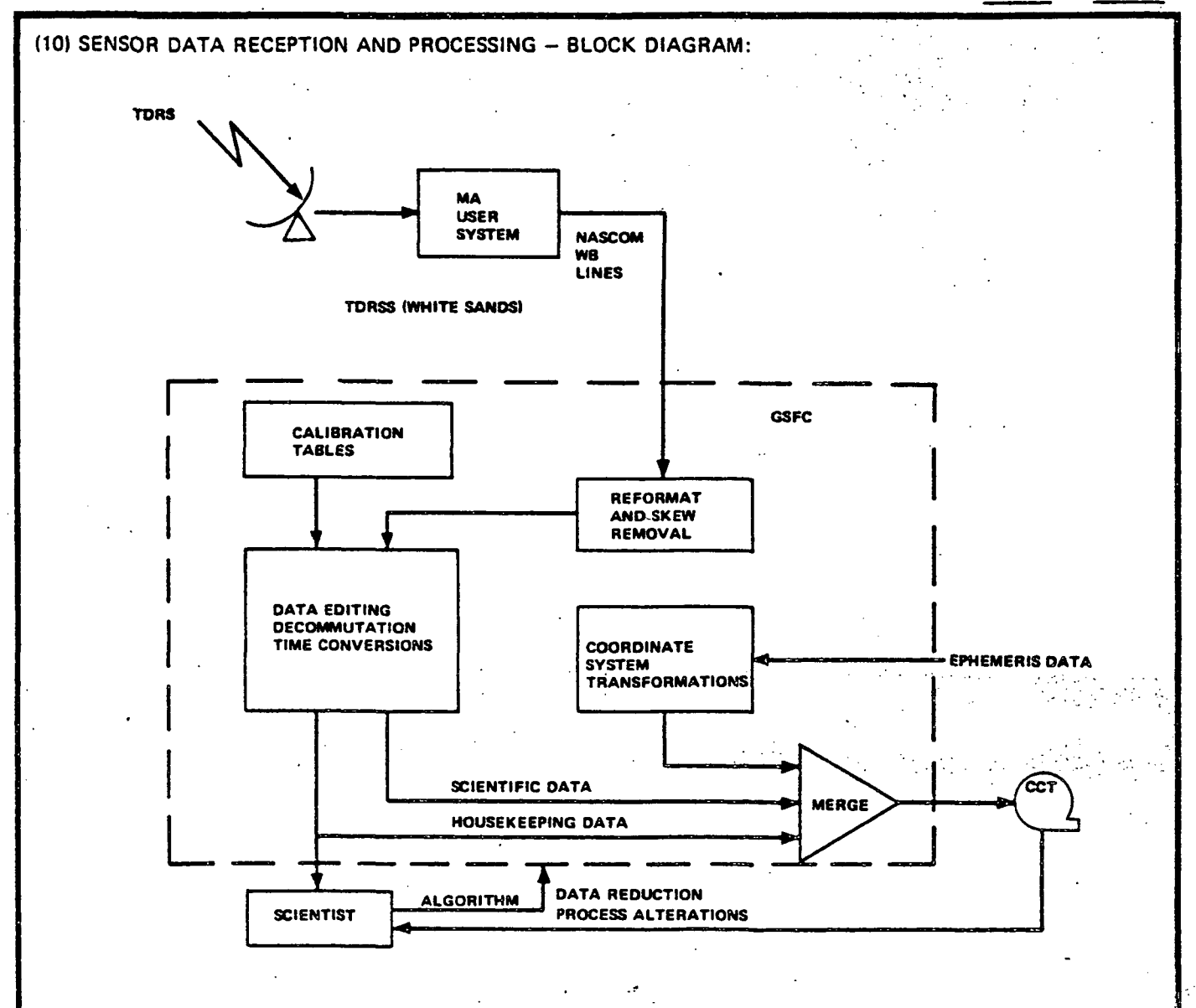


#### (9) MEASUREMENT AND TRANSMISSION SYSTEM - NARRATIVE:

The gating field is driven by a 30 kHz oscillator and drive coil. The presence of the ambient field induces asymmetry into the induction cycle when the core is saturated to maximum magnetic induction. The asymmetry is a measure of the ambient field and is detected as a second harmonic of the fundamental gating frequency. The sampling rate is 8 to 25 samples per second and provides for an approximate 600 bps data rate to the TDRS. Four bits representing an offset bias plus the 12 bit resolution from the A/D converter provide a 16 bit measurement of each axis for each sample.

SECTION NO.: 5.10 SENSOR CATEGORY: Field Measuring Sensors

REV. NO.: 2 REV. DATE: 31 Jan 1978



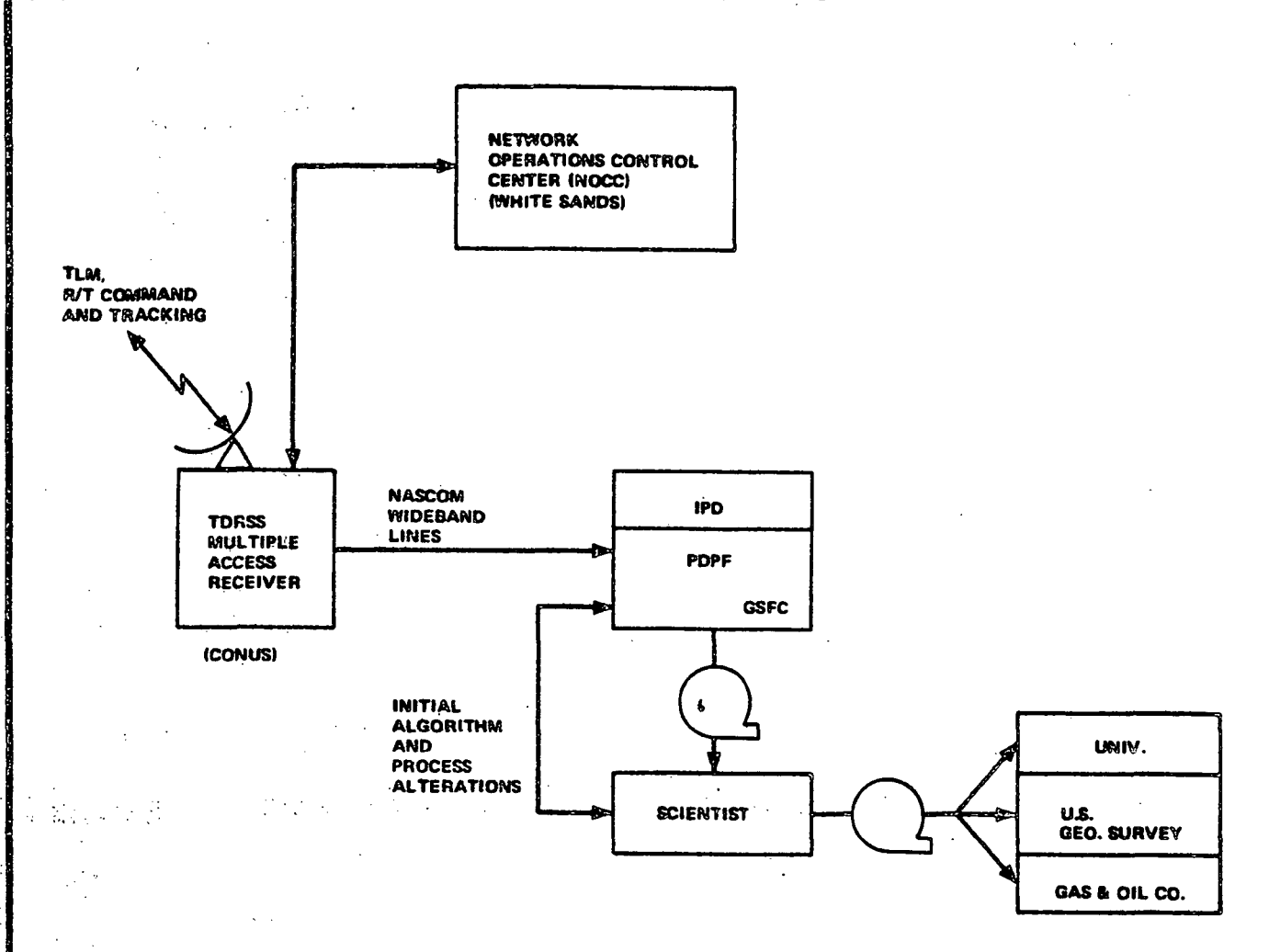
#### (11) RECEIVING AND PROCESSING - NARRATIVE:

The TDRS downlink frequency is 13.525 GHz  $\pm$  125 MHz. NASCOM wideband lines provide a  $^{56}$  kbps data transmission link from White Sands to GSFC. The cognizant scientist analyzes the housekeeping data to determine the process that must be performed on the scientific data. The calibration tables are from preflight ground calibrations for each magnetometer.

SECTION NO.: 5.10 SENSOR CATEGORY: Field Measuring Sensors

REV. NO.: 2 REV. DATE: 31 Jan 1978

#### (12) DISTRIBUTION OF DATA FROM GROUND STATIONS - BLOCK DIAGRAM:



#### (13) DATA DISTRIBUTION - NARRATIVE:

The TDRSS can provide global, real-time coverage for > 90% of each orbit. For normal operation, a 24 hour lead time is required from NOOC for periodic real-time mission requirements.

SECTION NO.: 5.10 SENSOR CATEGOR : Field Measuring Sensors

#### RSDH DATA SHEET

SHEET 1 OF 4

(1) SENSOR NAME, ACRONYM: Rotating Gravity Gradiometer, Grad (OP-02-A)

(2) DISCIPLINE: Earth and Ocean Physics

(3) SUBDISCIPLINE:

Solid Earth Dynamics

#### (4) APPLICATION AND OBJECTIVE:

The fine structure of the Earth's gravity field will be determined by flying a Gravity Gradiometer in a low earth orbit (300 km) satellite. The gradiometer, which is a rotating cruciform configured with tip masses and piezoelectric strain monitors on the arms, measures the second-order gradient of the gravity potential field. The satellite is precisely tracked and its position relates the gravity field variations to the geoid coordinates.

#### (5) HERITAGE/KEY PERSONNEL:

Cognizant Scientist - Dr. Joseph Siry, LaRC

#### (6) SENSOR DEPLOYMENT:

The Gravity Gradiometer satellite will be placed in a 300 km, near circular, polar orbit during the 1980 equinox via shuttle craft. The satellite will be spin-stabilized at 2 rps. Further attitude control and spin-speed control is accomplished with a cold gas reaction jet system.

(7)

#### SENSOR CHARACTERISTICS

#### (7A) CAPABILITIES AND CONSTRAINTS OF THE SENSOR TO ACQUIRE THE MEASURED PARAMETER:

The rotating Gravity Gradiometer moves through the gradient field sensing the field components in its plane of rotation. Samples, taken at 5 second intervals contain two signals in quadrature (sine & cosine terms). One is a measurement of the difference between two of the diagonal components, and the other measures the cross product component of the gradient tensor in the coordinate frame of the sensor. Peak performance is in the range of the 35th to 75th spherical harmonic order and term.

(7B) ACTIVE SOURCE CHARACTERISTICS (FOR ACTIVE SENSORS):

N/A

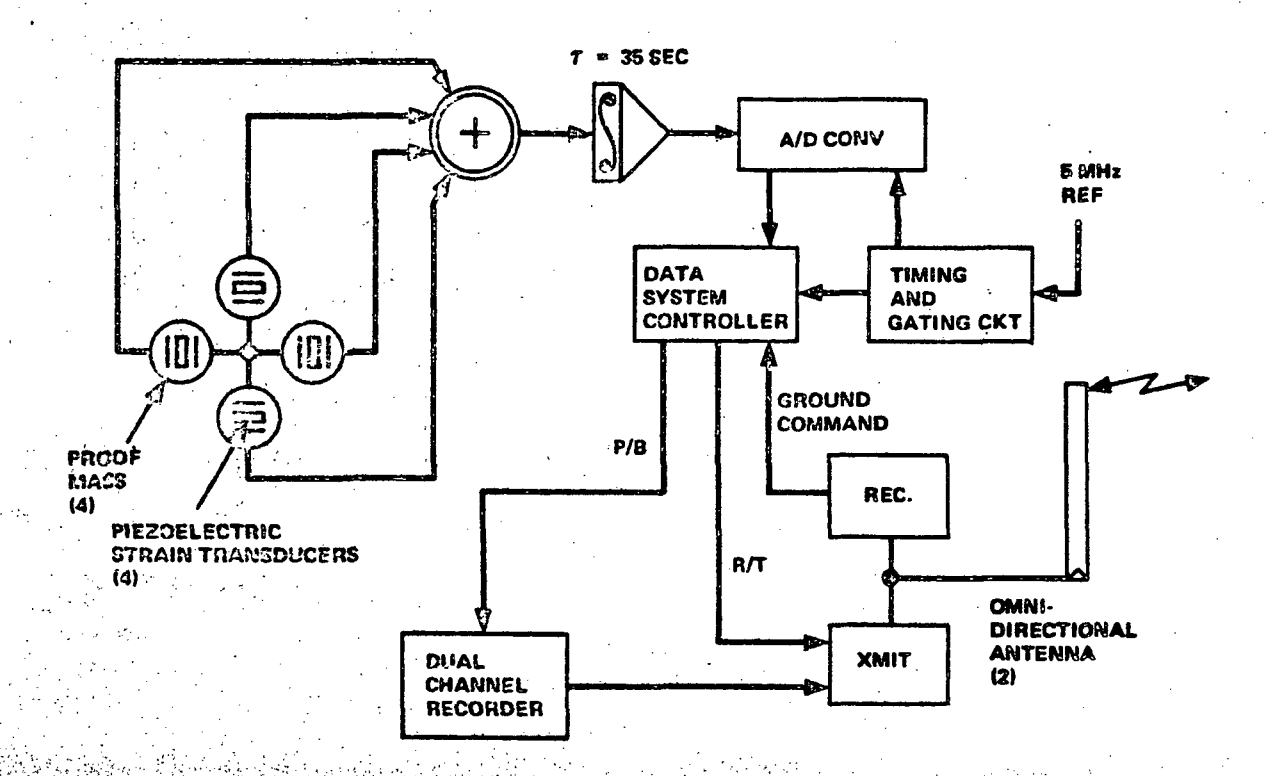
(7C) DETECTOR MEASUREMENTS CHARACTERISTICS: The Gradiometer is a resonant cruciform mass-spring system with a torsional vibration mode. In operation the sensor is rotated about its torsionally resonant axis at an angular rate of 2 revolutions per second (1/2 the torsional resonant frequency). Gradients in the gravity field excite the sensor structure at twice the rotational frequency. The differential torque ( $\Delta T$ ) is coupled into the central torsional flexture. The strains in this flexture are sensed with piezoelectric strain transducers which provide an electrical output. Measurement sensitivity is  $\pm 0.01$ E.U. The gravitational field signature is expected to be identifiable to crustal variations (mass concentrations) of the geoid.

SECTION NO.:

5.10

SENSOR CATEGORY: Field Measuring Sensors

#### (8) SENSOR DATA MEASUREMENT AND TRANSMISSION SYSTEM - BLOCK DIAGRAM:



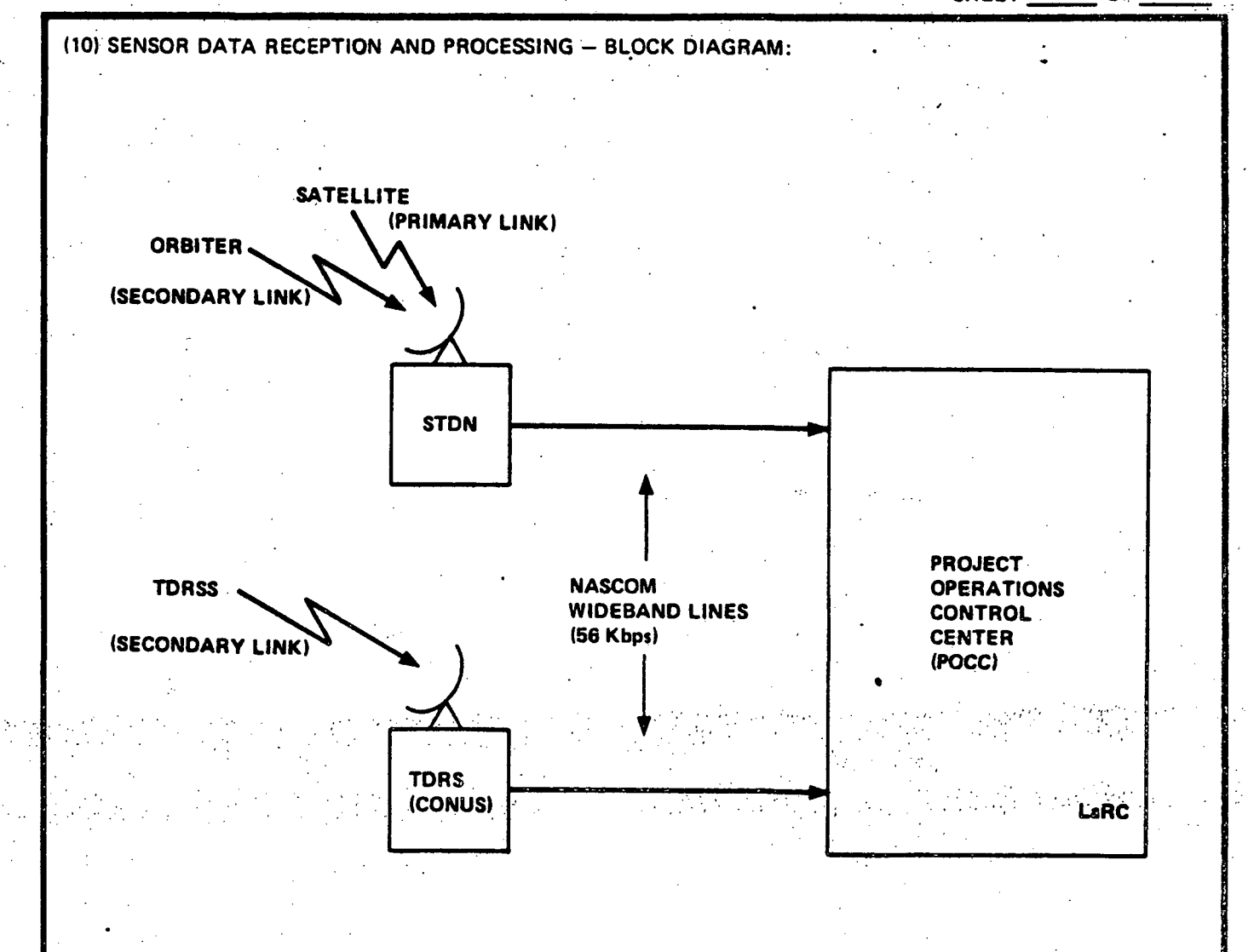
#### (9) MEASUREMENT AND TRANSMISSION SYSTEM - NARRATIVE:

The gradiometer resolution is defined as (nominally) equal to the satellite altitude, 300 km. Position determination of 300 m along-track and cross-track, and 50 m in the radial direction are required to maintain a data bias below 0.01 E.U. Orbital velocity is approximately 7.75 km/sec, therefore, one resolution element is passed during one integration period. The A/D converter samples the integrator output at 5 second intervals with ≥12 bit resolution which will produce a global gravity map at the 1 m gal level to degree and order 75 or better. The primary command, tracking, and telemetry link is accomplished through the STDN However, optional links with the TDRSS and/or the orbiter may be utilized. Transmit power is 20 W. Command, tracking and telemetry data are pulse-code modulated. The data rate is expected to be 1 kbps or less.

SECTION NO.: 5.10 SENSOR CATEGORY: Field Measuring Sensors

**REV. NO.:** 2

REV. DATE: 31 Jan 1978



#### (11) RECEIVING AND PROCESSING - NARRATIVE:

P/B data or R/T data received by either ground station is transmitted in near real-time to the POCC at LaRC. Transmissions are pre-scheduled and activity is expected to be at a 1 kbps data rate. Approximately 14 min. of P/B represents the longest required recording of gradient data prior to the satellite entering the FOV of an STDN station.

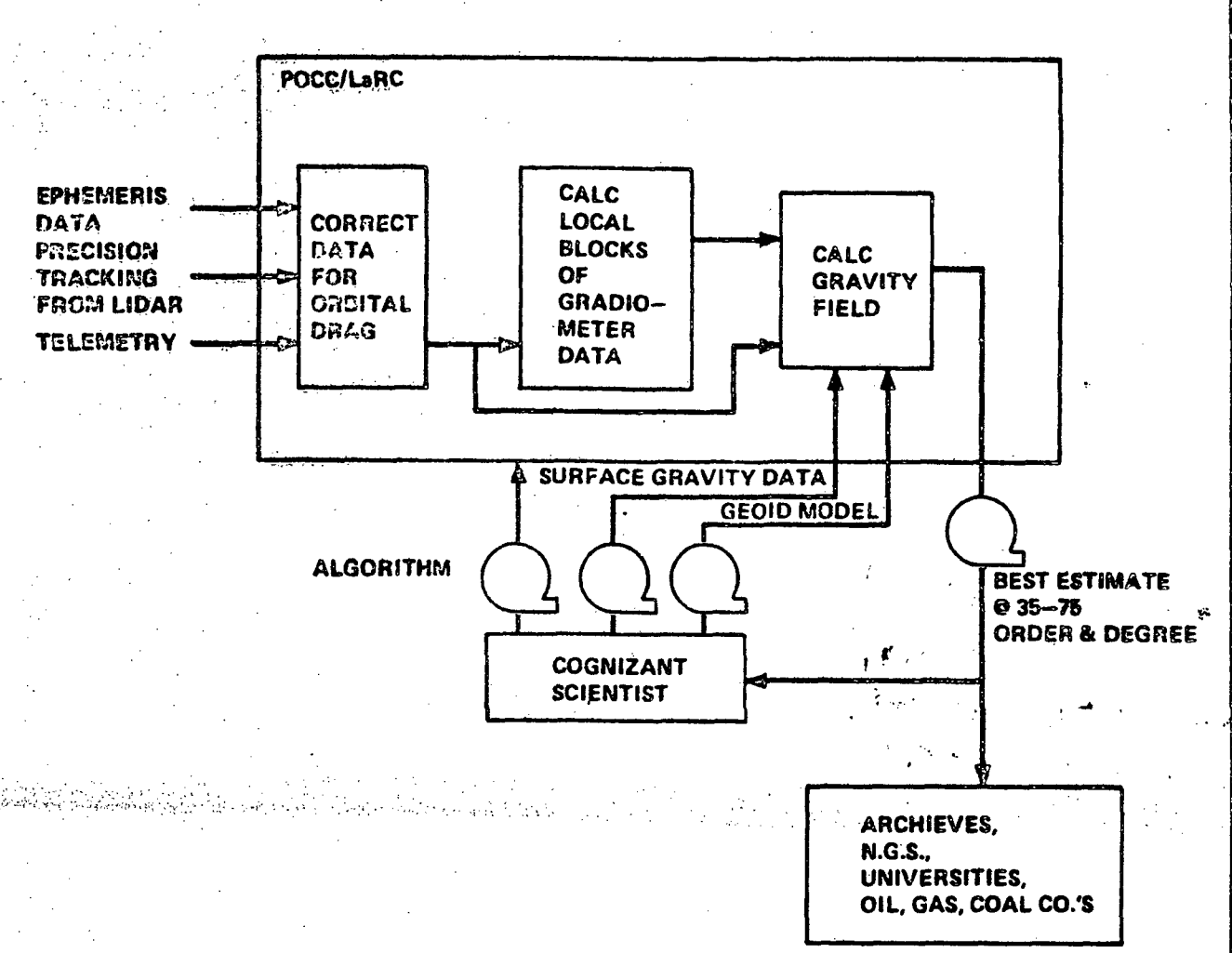
SECTION NO.: 5.10 SENSOR CATEGORY: Field Measuring Sensors

5.10 -37

**REV. NO.: 2** 

**REV. DATE: 31 Jan 1978** 





#### (13) DATA DISTRIBUTION - NARRATIVE:

Local blocks (localized areas) are calculated from the input parameters and combined to produce a representation of the global gravity field. Topoligical features as well as oil, gas, and coal deposits are some of the more important results expected from accurate data reduction of the gradiometer data.

5.10 SENSOR CATEGORY: Field Measuring Sensors SECTION NO .:

REV. NO.:

REV. DATE: 31 Jan 1978

APPENDIX A
REVISION CONTROL SHEET

SECTION	NUMBER PAGE	EFFECTIVE		
NUMBER	OF PAGES	NUMBER	REV. DATE	REV. NO.
Revision Control Sheet	1	A-i A-ii	31 JAN 78 31 JAN 78	2 2
Appendix A Table of Contents	2	A-iii A-iv	31 JAN 78 31 JAN 78	2 2
Appendix A Infrared Detectors	50	A-1 A-2 A-3 A-4 A-5 A-6 A-7 A-8 A-9 A-10 A-11 A-12 A-13 A-14 A-15 A-16 A-17 A-18 A-19 A-20 A-21 A-22 A-23 A-24 A-25 A-26 A-27 A-28 A-29 A-30 A-31 A-32 A-33 A-34 A-35 A-36 A-37 A-38 A-39 A-40 A-41	31 JAN 78	2 2 2 2 2 2 2 2 2 2 2 2 2 2 2 2 2 2 2 2

## APPENDIX A REVISION CONTROL SHEET

SECTION	NUMBER	NUMBER PAGE		VE
NUMBER	OF PAGES	NUMBER	REV. DATE	REV. NO.
Appendix A Infrared Detectors (continued)		A-42 A-43 A-44 A-45 A-46 A-47 A-48 A-49 A-50	31 JAN 78 31 JAN 78	2 2 2 2 2 2 2 2 2 2
		. <b>c</b>		*** ,.:
		•	•	
			• ·	
			·	

## Appendix A

## INFRARED DETECTORS

## Table of Contents

	Page
INTRODUCTION TO INFRARED DETECTORS	A-1
Definition and Evaluation of Detector Characteristics	A-2
THERMAL DETECTORS	A-4
Thermistor Bolometer	A-4
Radiation Thermopile	A-7
Pyroelectric	A-9
PHOTON DETECTORS	A-11
Photoconductive	A-13
HgCdTe	A-16
PbS & PbSe	A-17
Ge & Si (Extrinsic)	A-21
Photovoltaic	A-24
PbSnTe	A-26
Si (IR enhanced)	A-27
InSb & InAs	A-30
RECENT DEVELOPMENTS IN IR DETECTORS	A-31
DETECTOR COOLING DEVICES & TECHNIQUES	A-36
Thermoelectric	A-36
Joule-Thompson	A-37
Passive Radiators	A-40
Closed Cycle	A-42.

## Table of Contents (Continued)

SUM	MARY TABLES AND GRAPHS	Page
	Common Elements and Compounds used for Infrared Detectors	A-43
· ·	Spectral Response of Various Infrared Detectors	A-44
. 40	Typical Infrared Detector Characteristics	A-45
	Detector/Program Reference Table	A-46
REF	ERENCES	A-47
BIR	LIOGRAPHIES	A-48
TLL	USTRATION CREDITS	A-50

2 . .

# APPENDIX A INFRARED DETECTORS INTRODUCTION TO INFRARED DETECTORS

The domain of infrared energy in the electromagnetic spectrum extends from about .75  $\mu m$  to approximately 1000  $\mu m$  as shown in Figure 1.

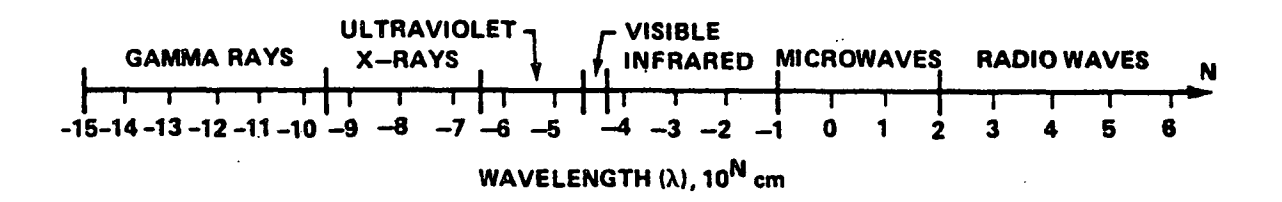


FIGURE 1 Electromagnetic Spectrum

The physical phenomena employed to measure infrared radiation incident upon a given area can be divided into two catagories; (1) thermal effects, or those which result from the heating of the device due to absorption of radiation, and (2) photon effects, which arise from direct interaction between the infrared radiation photons and the energy condition (or state) of the detector material [1].

For an ideal thermal detector, incident energy is absorbed uniformly at all wavelengths. The resulting increase in the temperature of the sensing element is thus wavelength invariant, and the signal produced by this temperature change, be it a change in resistance or voltage, is also wavelength invariant. In practice, the spectral response of all thermal detectors is not identical, since absorption by the sensing layer is wavelength dependent and since the energy usually passes through a protective window which will have its own characteristic absorption.

In the case of photon detectors, where incident photon flux interacts with electronic energy states, one might expect constant signal with wavelength for a fixed number of incident photons, followed by a rapid decrease in signal, when incident photons no longer have sufficient energy to excite charge carriers. This cutoff point, determined by the energy gap of the semiconductor material, may depend on such factors as element temperature, sample purity, and, for the most recent ternary compounds, on material composition. For actual detectors the shape of the response depends on a variety of conditions, such as, element thickness and preparation of its surface, but once the detector has been constructed, the shape of the spectral response at the operating temperature usually remains invariant, except for small changes produced by the aging of the material. [2]

#### Definition and Evaluation of Detector Characteristics

The design of detection systems is based on the performance of the detecting element. One needs, therefore, standards by which the capabilities of the basic components can be measured, not just to compare detectors of one kind, but for the selection of the type of sensing mechanism which best suits the design requirements.

One such performance parameter which is useful for the art of measurement in general is the noise equivalent power (NEP). This is a figure of merit which depends on operating conditions such detector area, wavelength, bandwidth, etc., and so must be specified along with NEP. The manner in which the NEP depends on these variables follows functional relationships which are the same for many (but not all) types of detectors.

Definitions and standards have, therefore, been introduced which refer to conditions of normalized variables and hence describe detector performance for at least one operating point, although not necessarily for the entire operating region.

Listed below are the more common expressions used to describe detector performance.

Responsivity (R)--detector output per unit power of incident radiation. The unit of measurement is volts/watt (or amperes/watt), or as the quantum efficiency, i.e., the number of transition events per incident quantum. The significance of this performance figure is the information it yields as to the required amplification or magnification; wavelength dependent.

Noise Equivalent Power (NEP)--a measure of the minimum power which can be detected. It indicates the power required to generate a signal-to-noise (S/N) ratio of 1, when the detector noise is referred to a one-cycle bandwidth. The NEP is given by the following expression:

$$NEP = \frac{Ed \cdot A \cdot N}{S \cdot (\Delta f)^{1/2}} \quad WATTS / (HZ)^{1/2}$$
 (1)

where

Ed = watts/cm<sup>2</sup> of surface radiation at the detector surface

A = area of detector sensitive surface in  $cm^2$ 

S = signal voltage developed by the detector in the radiation field

N = noise voltage developed by the detector

 $\Delta f = noise bandwidth$ 

When interpreting NEP values, careful attention must be given to the conditions under which the NEP is measured. Since most detectors are spectrally sensitive, it is necessary to specify the "type of radiation" employed in making the measurement. In most cases, the NEP will be evaluated either in the radiation field from a 500° Kelvin (K) blackbody source, or it will be referenced to a specific wavelength (e.g., 5 µm). In the former case, the given NEP will be an average sensitivity over all wavelengths emanating from the 500°K blackbody source, while in the latter instance the NEP represents an absolute sensitivity. The infrared radiation used in determining detector NEP values is normally modulated by means of a mechanical

¢5.2

ectors, both detector signal and noise will be frequency dependent, and it becomes necessary to specify the frequency at which the measurement was made. As a final requirement, all NEP values are (normally) specified for an equivalent noise bandwidth of 1 Hz. Symbolically, noise equivalent power is written as NEP (°K, Hz, 1), denoting the blackbody temperature, the chopping frequency, and the noise bandwidth, respectively.

Detectivity (D\*)--a term originally introduced to remove the dependence of NEP on the detector's sensitive area, and is related to NEP by the expression:

$$D^{*} (D-star) = \frac{(Detector Sensitive Area)^{1/2}}{NEP} cm-(Hz)^{1/2}/watt$$
 (2)

The use of D\* as a figure of merit has gained wide acceptance by the detector industry, and is usually the reference parameter in discussions of detector sensitivity. As with NEP, test conditions must be specified in complete detail. [3]

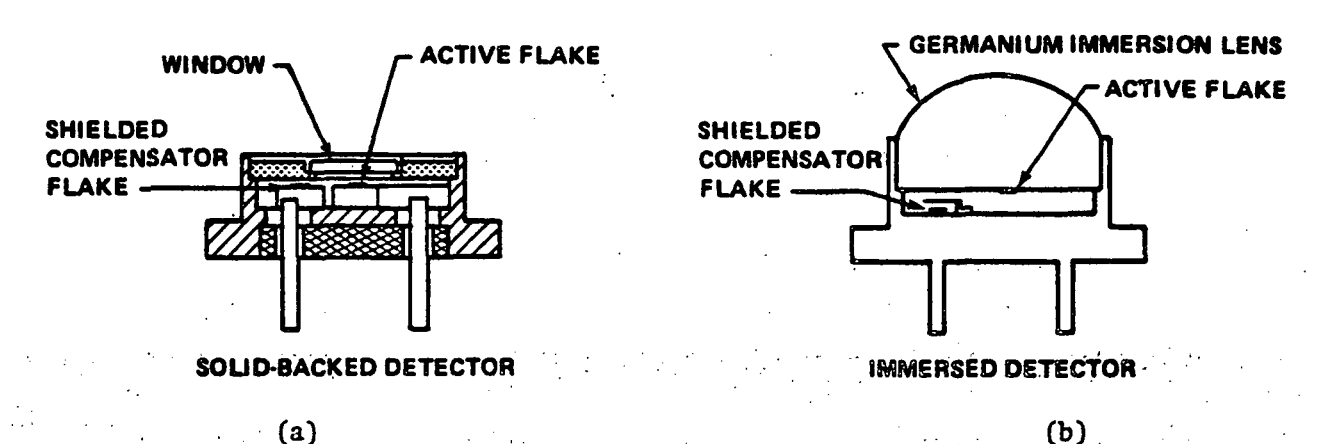
#### THERMAL DETECTORS

Thermal detectors are energy detectors, and their spectral response is dependent primarily upon the absorption properties of the detector. Associated with thermal detectors is a thermal mass which changes temperature as a function of the incident radiation. Three types of thermal detectors which are currently in use, and which are applicable to this document, are described below.

#### Thermistor Bolometer

Bolometer operation is based on changes in the electrical resistance of the detector as a function of temperature. Modern bolometer technology takes advantage of semicon Luctor materials which have a high temperature coefficient (c) of resistivity ( $\rho$ ), typically 3.5%/°C. These semiconductor bolometers are kn. m as

thermistor bolometers, i.e., thermally sensitive resistors. The two materials in common use are known as No. 1 and No. 2 thermistor material and are composed of sintered oxides of manganese (Mn), cobalt (Co) and nickel (Ni) formed into flakes, typically 10 µm thick. Two types of mounting structures common for infrared detection are solid-backed, and immersion as shown in Figure 2a and 2b respectively.



(a) FIGURE 2 Typical Mounting Structures for Thermistor Bolometers

The solid-backed thermistors are in the form of small flakes cemented to sapphire backing blocks. These assemblies are mounted, in turn, in a metal capsule and hermetically sealed. This construction provides an accurately controlled impedance between the flakes, as well as a good control of the detector time constant. The "active" flake is located in the center of the capsule and is exposed to the radiation to be detected (Figure 2a). The compensating flake is located off-center and is shielded from this outside radiation. Both flakes are connected in a bridge circuit (Figure 3) providing the active flake with compensation for resistance changes caused by ambient temperature variations. The immersed detector (Figure 2b) has its active flake optically attached to an infrared transmitting lens with a high index of refraction. A germanium (Gc) hemispheric lens is typically used for

this purpose and the flake is located at the center of the hemisphere's plano surface. The compensating flake is usually mounted in the detector base.

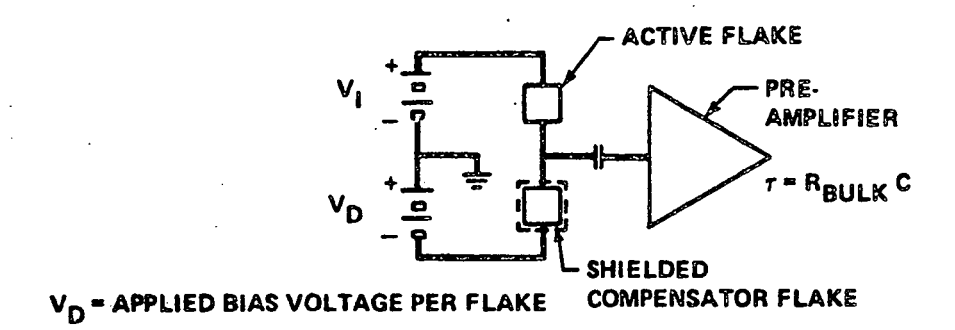


FIGURE 3 Conventional Bridge Circuit for Biasing
Thermistor Bolometer Detectors

Compared to a solid backed flake of the same size, detectivity (D\*) for the hemispherically immersed detector is improved by a factor of four. Also, for a given detectivity the required area is reduced by a factor of sixteen. Typical responsivity for both types is given in Figure 4.

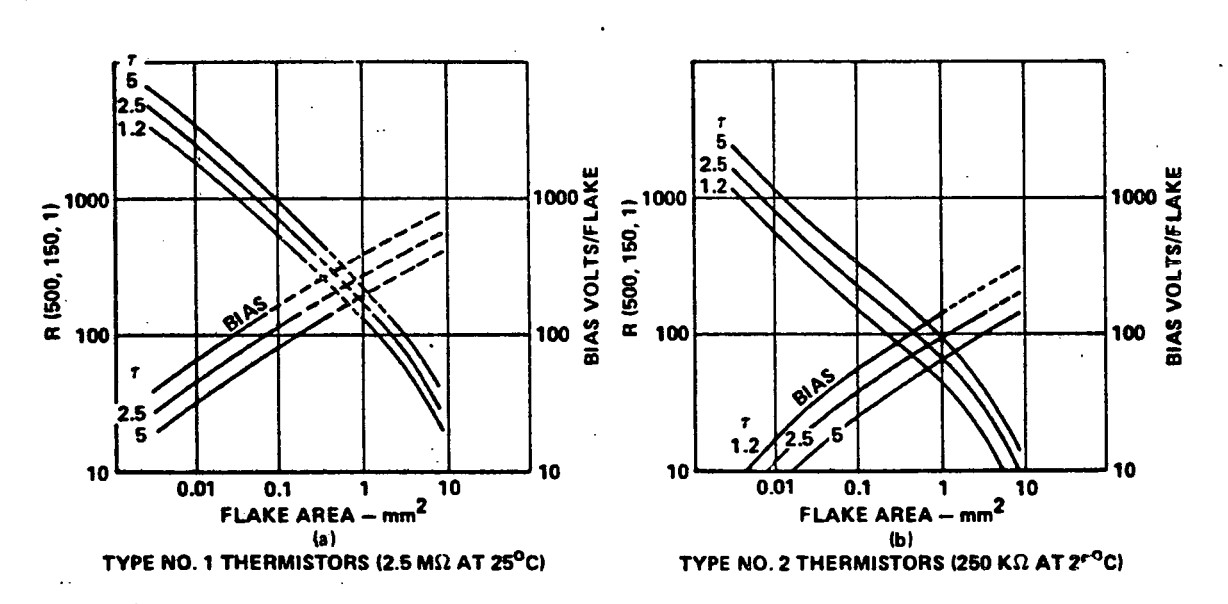


FIGURE 4 Typical Responsivity vs. Flake Area for Solid-backed and Immersed Thermistor Bolometers

#### Radiation Thermopile

The radiation thermopile can be defined as a collection of thermocouples of two dissimilar metals connected in series. The "hot" or active junctions of the detector are blackened to efficiently absorb radiation while the "cold" or reference junctions are maintained at the ambient temperature of the detector. The absorption of radiation by the blackened area causes a rise in the temperature of the hot junctions as compared to the cold junctions. The difference in temperature between the "hot" and "cold" junctions causes the detector to generate a voltage. The magnitude of this voltage is determined by the thermoelectric power of the materials used which is commonly characterized by the Seebeck coefficient defined below.

$$\alpha = \frac{\lim}{\Delta T} + \frac{\Delta V}{\Delta T} = \frac{dV}{dT} \quad (\mu V/^{\circ}C)$$
(3)

In general, radiation thermopiles can be classified into three types:

- 1. Bulk Type--These are made with wires for the active elements, typically silver and bismuth, manganese and constantan, or copper and constantan. In general, these devices are used for high radiation flux measurements. They are characterized by long response times, large physical dimensions, low impedance and good spatial uniformity.
- 2. Schwartz Type--Consists of two junctions using materials of high thermo-electric power and a thin gold leaf receiver. Characterized by high D\*, low impedance (usually requiring transformer coupling), medium speed but considered fragile, thus, limiting their application for the most part to laboratory use.
- 3. Thin Film Devices--The thin film thermopile allows for a high packing density of junctions within the detector area. The methods of construction used by the various manufacturers differ to some extent. However, they all use vacuum deposition techniques and evaporation masks to apply the thermoelectric materials--usually bismuth and antimony, which have a reasonable thermoelectric power and evaporate easily without changing state. Typically a manufacturer will utilize a high purity aluminum heat sink and support with an integral aluminum oxide less than .5 μm thick as the substrate. The hot junctions are evaporated over the

free standing film and the cold junctions are evaporated over the combined film-aluminum area. The "hot" junctions are covered by a black to increase the efficiency of collection of the radiation.

The following table summarizes the performance characteristics of some typical thin film devices.

TYPE L-22 S-15 S-60 GEOMETRY (mm)  $0.2 \times 0.2$  $1.5 \times 1.5$  $6.0 \times 6.0$ 4 x 10<sup>-3</sup>  $2.25 \times 10^{-2}$  $3.6 \times 10^{-1}$ ACTIVE AREA (cm<sup>2</sup>) NUMBER OF JUNCTIONS 20 28 120  $1.6-3.0x10^{8}$  $> 1.0 \times 10^8$  $0.3 - 1 \times 10^8$ D\* (500°K, DC) (cm(Hz)½/watt) NOISE EQUIVALENT POWER  $(w/Hz^{1}2)$  | 2 - 4 x  $10^{-10}$  $1 - 2 \times 10^{-9}$  $0.9 - 2.2 \times 10^{-8}$ 20 - 40 50 - 70 TIME CONSTANT (milliseconds) 20 - 30RESISTANCE (ohms) 2k - 4k8k - 14k 20k - 30kRESPONSIVITY (500°K, DC) 1 - 3 20 - 288 - 12 (volts/watt)

TABLE 1 Typical Performance Characteristics

The thin film thermopile compares favorably to other types of infrared detectors in many applications for a number of reasons, these include:

- Compact physical size offers minimal obscuration in tight optical systems.
- 2. Rugged construction makes them suitable for commercial and space applications.
- 3. All types of thermopiles act as voltage generators and do not require bias voltage.
- 4. The higher impedance levels of the thin film devices (typically 2k-30k, depending on the number of junctions) are easy to match to discrete low noise bi-polar amplifiers or low noise operational amplifiers.

- 5. The noise spectrum of all thermopiles is entirely determined by Johnson noise  $(4kTR\Delta f)^{1/2}$  making them ideal choices for low frequency or DC applications.
- 6. Thermopile detectors operate at ambient temperature and do not require cooling.
- 7. Thermopile detectors have a broad spectral response making them suitable for a variety of applications.

#### Pyroelectric Detectors

In its simplest form, the pyroelectric detector consists of a slab of pyroelectric material having two opposite face areas coated with conducting layers (Figure 5). A change in temperature ( $\Delta T$ ) generates a voltage change ( $\Delta V$ ) equal to

$$\Delta V = \frac{4\pi d}{\varepsilon} \left(\frac{dPs}{dT}\right) \Delta T \cdot 10^{12} \tag{4}$$

where

d = thickness of detector (cm)

 $\varepsilon$  = dielectric constant

dPs/dT = change in spontaneous polarization as a function of temperature change (pyroelectric coefficient in °C/(cm² · °K).

The expression for signal current is:

$$i = \frac{A}{d\varepsilon} \cdot \frac{dPs}{dT} \cdot \frac{dT}{d\tau}$$
 (5)

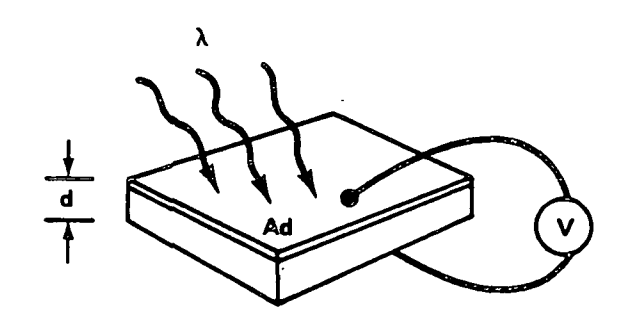


FIGURE 5 Simplified Detector Configuration.
The Incident Radiation Generates a Temperature Change that in turn Generates a Voltage Change.

To optimize the signal, a material should possess a low heat capacity, low dielectric constant, and a large pyroelectric coefficient. Further, since the signal current is proportional to the rate of change of the temperature, this detector is more attractive than other types of uncooled thermal detectors for higher frequency applications.

Most of the recent efforts on pyroelectric detectors has concentrated on triglycine sulphate (TGS). Since TGS is a ferroelectric crystal, it exhibits a spontaneous polarization (electric charge concentration) that is temperature dependent. Thus, as infrared radiation impinges upon detector surface, a voltage is generated which is proportional to the changes in radiant energy.

Table 2 gives a comparison of the more prominent pyroelectric materials.

TABLE 2 Typical Characteristics of Pyroelectric Detectors

	PVF <sub>2</sub>	LiTa0 <sub>3</sub>	TGS
Spectral Response (µm)	2-30	2-14	.1-300
Responsivity (μA/W-100 Hz)	1-2	1-2	>2
D* (500, 15, 1) (cm-Hz <sup>1/2</sup> /W)	1x10 <sup>8</sup>	1x10 <sup>8</sup>	3.5x10 <sup>8</sup>
Power Handling Capacity (W/cm <sup>2</sup> )	.2	10	1
Curie Point (°C)	55	80	49

The magnitude of the pyroelectric effect increases with temperature until what is known as the Curie point is reached. Beyond this, the polarization of the ferroelectric crystals disappear.

The detector equivalent circuit (Figure 6a) consists of a current generator in parallel with the capacitance of the detector. Tradeoffs between volume respon-

sivity and speed of response can be made by selecting different high impedance or low impedance terminations for the detector.

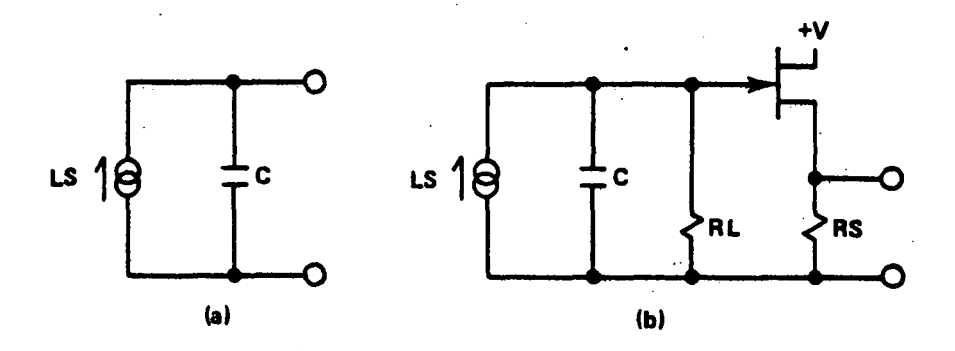


FIGURE 6 Equivalent Circuit (a), and Typical Circuit Configuration (b)

#### PHOTON DETECTORS

In all quantum detectors the release or transfer of charge carriers (e.g., electrons) can be directly associated with the absorption of quanta of radiation. The use of the photoconductive effect for infrared detection utilizes the change in resistance caused by hole-electron generation. There are two different classifications of photoconductive detectors depending upon whether the excitation of current carriers is intrinsic or extrinsic. In intrinsic excitation, hole-electron pairs are generated by exciting an electron from the valence to the conduction band. In extrinsic excitation, current carriers are produced by exciting electrons either from or to impurity doping levels which lie within the forbidden band of the semiconductor.

Review of Simple Band Theory--when two atoms approach one another, as in bonding, the levels must split so that there will be energy levels to accommodate all of the electrons of the system. When the system consists of a large number of atoms

bound together, as in the case in a crystalline material, the higher energy levels tend to merge and blend into two separate bands of allowed energies, which are often separated by an energy gap between the two allowed energy bands. This gap is often referred to as the forbidden band or forbidden gap. The lower band. called the valence band, is that band of energies occupied by the electrons that are bound between pairs of atoms, as part of a chemical bond between those atoms. The upper band is referred to as the conduction band. Electrons that occupy energy levels in the conduction band are free and, consequently, may take part in the conduction of electronic currents. The width of the energy gap is a sensitive measure of the energy needed by an electron to break a chemical bond, and is very closely related to the relative conductivity of various materials. The wider the gap, the lower the conductivity. As is shown in Figure 7a, crystalline quartz with a band gap of 6(eV), an insulator, shows a bulk resistivity on the order of  $2 \times 10^{20} \Omega$  cm. On the other hand, in a metallic conductor like silver (Figure 7b), the valence and conduction bands actually overlap, indicating that it is possible for electrons in the chemical bonds to conduct current. silver shows a bulk resistivity of approximately 1 x  $10^{-6}$   $\Omega$  cm. It is interesting to note that this resistivity spread of 26 orders of magnitude is one of the widest variations of any physical quantity ordinarily encountered.

In the region between these extremes is that class of materials known as "semiconductors." Unlike the conductors, these materials have a finite gap between the valence and conduction bands, but the gap is much narrower than that of the insulators. For example, pure silicon, Figure 7c, with a band gap of 1.1 eV, has a resistivity of about  $2 \times 10^5 \Omega$  cm. [15]

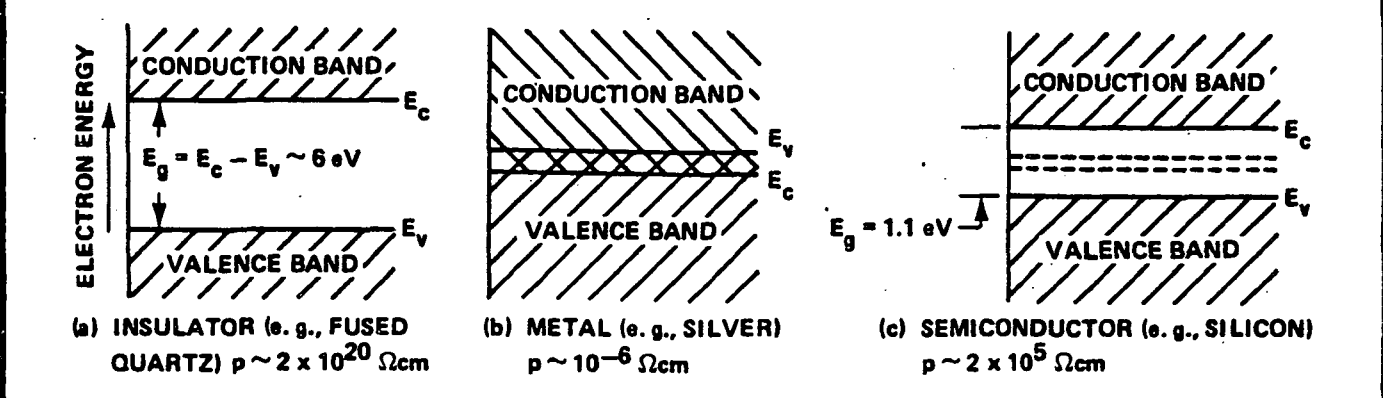


FIGURE 7 Element Characteristics

From the point of view of quantum mechanics, the energy of a quantum of radiation of frequency  $\nu$  is:

$$\varepsilon = hv,$$
 (6)

where  $h = 6.624 \times 10^{-27}$  erg sec is the Plank constant.

The wavelength associated with a quantum of energy & is accordingly:

$$\lambda = \frac{hc}{\varepsilon} . ag{7}$$

Since the energy of the radiation quantum is inversely proportional to the associated wavelength, it follows that a decrease in photoelectric activity at some long wavelength is due to the fact that the energy of the quanta is insufficient to set the electrons free.

#### Photoconductive Detectors

In photoconductive solids the electron becomes "free" for the conduction process only when the energy it gained from the absorbed quantum exceeds a certain level, i.e., the energy gap  $(E_g)$ . Hence, the photoeffect can occur only in energies greater or wavelengths shorter than a limit  $\lambda c$  given by,

$$\lambda c = \frac{hc}{E_g}. ag{8}$$

Solid state physicists measure  $E_g$  in electron volts rather than ergs. One electron volt is the energy which a particle carrying one unit of electrical charge  $(4.80 \times 10^{-10} \text{ electrostatic units, or } 1.62 \times 10^{-19} \text{ coulombs})$  acquires over a potential difference of one volt. In these terms one electron volt is equivalent to  $1.60 \times 10^{-13}$  erg, and the Planck constant has a value h =  $4.135 \times 10^{-15} \text{ eV-sec.}$  (8) may then be written as:

$$\lambda c = \frac{1.24 \times 10^{-4} \, \text{eV cm}}{E_g} \tag{9}$$

According to this formula, energy of one electron volt corresponds to that radiation of 1.24 µm wavelength. Energy gaps of some materials that are of significance in photoconductive detectors and their corresponding wavelength limits are listed in Table 3.

TABLE 3 Energy Gaps and Long-Wavelength Limits of Selected Materials

Material	$E_g(at 300^{\circ}K)$ , eV	$\lambda_{\circ}$ , micron
Si	1.1	1.13
Ge	0.68	1.82
Te	0.34	3.65
PbS	0.40	3.10
РЪТе	0.31	4.00
PbSe	0.25	4.95
InSb	0.18	6.90

All of the materials in Table 3 are so-called intrinsic semiconductors, that is, those in which the gap energy is determined by the nature of the material itself rather than by added impurities. Sometimes small amounts of impurities are present in the semiconducting material either naturally or by intentional addition (doping). These then are the so-called impurity semiconductors. Impurity atoms which may give off an electron when incorporated into the host crystal (e.g., as

in Si) produce a material with a slight excess of (negative) electrons (n-type semiconductors). Other atoms tend to accept electrons from the host material and thus produce an excess of positive "holes" (p-type semiconductors). Intermediate energy levels associated with impurities allow electron excitation to take place at smaller quantum energies than those required with the intrinsic semiconductors. Thus, by suitable doping the long-wavelength limit can be pushed quite far into the infrared. For instance, germanium doped with gallium is a p-type semiconductor with an impurity energy level of 0.65 eV, which makes it useful as a photoconductor detector to about 19 µm wavelength.

When a semiconductor is illuminated with radiation of quantum energy  $(hc/\lambda)$ greater than  $E_{\sigma}$ , some electrons are excited to the conduction band, and corresponding numbers of holes are left behind and made mobile in the valence band. the number of charge carriers is increased, and the conductivity of the material becomes temporarily greater. The responsivity of a photoconductive detector is then proportional to the excess of charge carrier concentration  $\Delta n$ . The steady state concentration is reached when the rate of generation of electrons by absorbed photons is equal to the rate at which they are removed from the conduction process by recombination with holes and by other mechanisms (trapping). If Q is the number of photons arriving per unit area per sec, a the optical absorption coefficient, and n the probability of electron excitation resulting from absorption of a photon (quantum efficiency), then the rate at which electrons are generated per unit volume is and, the recombination rate is directly proportional to the excess concentration  $\Delta n$  and inversely proportional to the average electron lifetime t in the conduction band. Thus in steady state  $\Delta n/t = \alpha \eta Q$ , and the (DC) responsivity is proportional to  $\Delta n/Q$ ,

$$R_0 \propto (\Delta n/Q) = \alpha n t. \tag{10}$$

In intrinsic semiconductors the absorption coefficient on the short-wavelength side of the energy gap is very high, typically of the order of  $10^{-4}$  cm. The radiation intensity or photon density decreases exponentially with the distance into the material. Consequently, there is no use making the semi-conducting photodetector much thicker than  $\alpha^{-1}$ , that is, about one micron. [4]

HgCdTe Detectors—the first successful intrinsic long-wavelength infrared detector was mercury cadmium telluride ( $\text{Hg}_{(1-x)}\text{Cd}_x\text{Te}$ ). This is an alloy consisting of a mixture of the compounds HgTe and CdTe. CdTe has a relatively wide bandgap (Eg=1.6eV) and HgTe is a semimetal having a negative energy bandgap of approximately 0.3eV. Alloy crystals made by mixing these two compounds will have an energy bandgap which is a function of x intermediate between these two end-point values.

For a value of x=0.2, detectors have a 13  $\mu$ m cutoff wavelength and require cooling to about 77°K. A typical plot of detectivity as a function of frequency for a good HgCdTe photoconductor, sensitive in the 8 to 13  $\mu$ m region is shown in Figure 8.

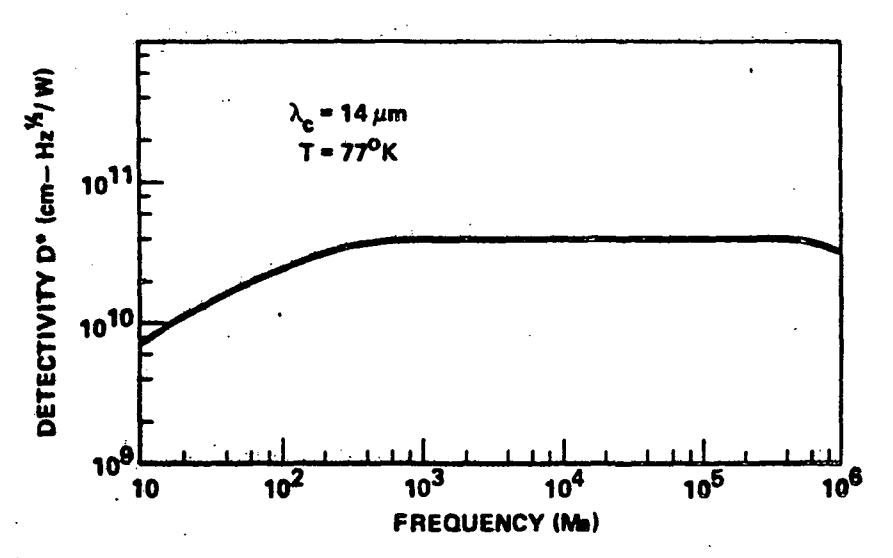


FIGURE 8 Plot of Detectivity as a Function of Frequency for a good HgCdTe Photoconductor

The device detectivity is degraded at low frequencies as a result of 1/f noise. At intermediate frequencies the detectivity is limited by generation-recombination noise induced by flunctuations of the incident background level. At high frequencies these background flunctuations roll off, like the signal, in a manner determined by the photoconductive gain. [5]

With normal incident backgrounds, and at operating temperatures in the vicinity of 77°K, photoconductors made from HgCdTe have two mobile carriers. The mobility ratio is such that the maximum photoconductivity gain is about 500. The devices are low impedance, about 50  $\Omega$  for a typical detector, and hence will operate effectively into any amplifier with an input impedance exceeding a few hundred ohms. But even with gain, the device output voltages across the low internal impedance are so small that a premium is placed on low-noise preamplification. Amplifiers with bipolar input stages and equivalent input noise voltages of about  $10^{-9} \text{V/Hz}^{1/2}$  are commonly used.

PbS and PbSe--are polycrystalline thin-film photoconductors sensitive in the 1 to 3 µm and 1 to 6 µm spectral regions, respectively. Both have high bulk resistance, generally exceeding 106 ohms per square at 200°K, which increase as the temperature is decreased. These high resistances are present because the granular nature of the films, and the oxide-rich layers connecting the grains, greatly reduce the effective majority carrier mobility. The detector is a thin film photoconductor chemically deposited onto a substrate. Photolithographic techniques are used to define the active area. Gold electrodes provide noise-free contact between the lead-out wires and the film. The photoelectric process involves absorption of photons from the incident radiant energy to generate free carriers in the Pb-S/Se crystals. A main-band transition occurs whereby an electron is raised from the

full band to the crystal's conduction band. This leaves a hole in the full band. Thus, conduction properties of the film are changed. As a circuit component, the sensor behaves like a variable resistor when connected to a bias supply. Photons induce changes in conductivity, which modulate the current flowing through the detector. Table 4 provides a comparison of the performance ranges of typical PbS and PbSe detectors.

TABLE 4 Typical PbS and PbSe Performance

Element Temp. (C°)	Spectral Response (µm)	$(x10^{10} \text{cm Hz}^{1/2} \text{W}^{-1})$	Resistance Per Sq. Area (megohms)	Time Constant (µs)
+25	1-3	1-15	0.1-10	30-1000
-20	1-3.2	2.5-20	0.15-25	60-2500
-30	1-3.4	3-30	0.2-35	75-3000
<b>-78</b>	1-4.0	10-10	0.4-100	100-10,000
-196	1-4.5	5-25	1-1000	500-50,000

#### Lead Sulfide

#### Lead Selenide

Element	Spectral	$D^*(\lambda_{pk}, 1500, 1)$ $(x10^8 \text{cm Hz}^{1/2} W^{-1})$	Resistance	Time
Temp.	Response		Per Sq. Area	Constant
(C°)	(µm)		(megohms)	(µs)
+25	1-4.8	5-80	0.05-20	0.5-10
-20	1-5	12-200	0.2-90	3-50
-30	1-5.2	15-250	0.25-120	5-60
-78	1-5.6	80-700	0.4-150	10-100
-196	1-7	80-600	0.5-200	15-150

(2π steradians field of view, 25°C background temperature)

The film can be deposited directly on high index optical materials to obtain the higher collection efficiency that results from optical immersion Direct immersion on high gain optics has become a standard production procedure.

The lead sulfide or lead selenide film is deposited directly on the plano-surface of a hemispherical lens as shown in Figure 9. There are limits to the extent of optical gain that can actually be achieved, but the marriage of PbS or PbSe to strontium titanate has provided excellent results. This optical material has high transmission, provides a good thermal match with the sensitive film, and has a reasonably high index of refraction (n = 2.268 at 2 µm). Referring to Figure 9, the image on the plane face is reduced by a factor of n in the linear dimensions (x and y) from that of the object. Strontium titanate allows the PbS film area to be reduced by approximately a factor of five. Since the signal-to-noise ratio is inversely proportional to the square root of the detector's active area, a gain of 2.2 results.

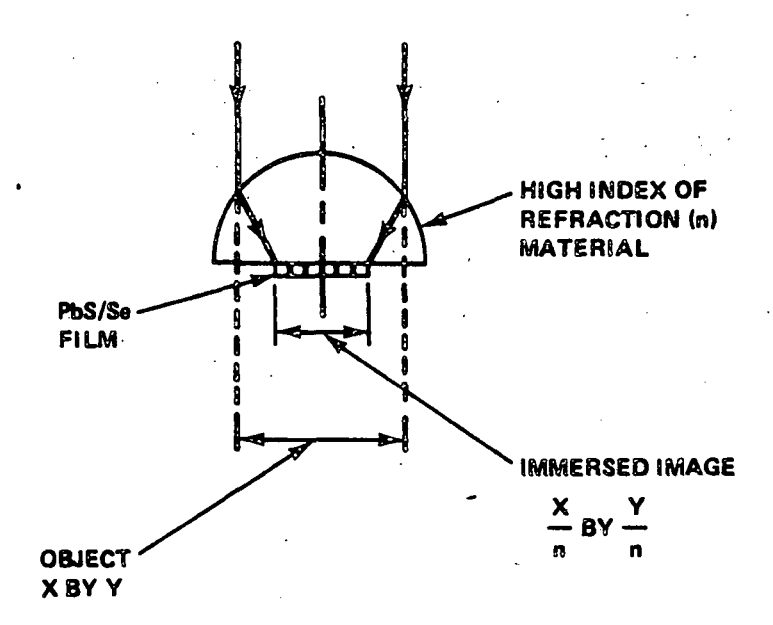


FIGURE 9 Detector Active Area Size Reduction
Afforded by Optical Immersion

As may be seen in Table 4, D\* improves significantly as the detector is cooled. An example of state-of-the-art packaging which provides for a cooled sensor without the inconvenience (and cost) of bulk or liquid cooling is shown

in Figure 10.

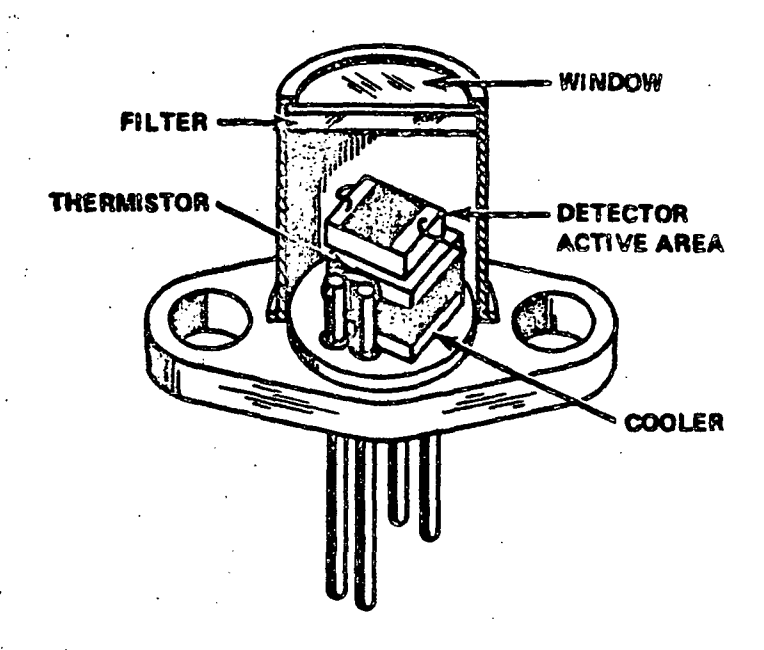


FIGURE 10 Detector Package--Window, Optical Filter,
Detector, Thermistor and One-Stage
Thermoelectric Cooler

Substantially better optical performance for wide angle systems can often be obtained with a spherical image surface rather than with a flat detector and associated field flatteners. Many years ago, researchers found that PbS and PbSe films could be deposited on very small diameter glass rods without exhibiting any abnormal behavior. Now, the detector industry provides both single-element detectors and multi-element arrays deposited on convex or concave configured substrates to system manufacturers routinely.

One-dimensional and two-dimensional detector arrays provide many advantages to the system designer and are very often the least expensive means of obtaining greater system performance. System sensitivity is proportional to the square root of the number of array elements (N). This results in search system range increases that are proportional to the fourth root of N. The time required to

scan a given field in space with a single detector element is determined by the time constant of the detector. This time is reduced by a factor of N for linear arrays and  $N^2$  for matrix arrangements. A multiplicity of elements enhances spatial resolution, which is particularly important in thermal imaging instrumentation.

A sixty-four element linear-single row array is typical of what is offered by the industry. Element active areas are typically 0.08 mm x 0.08 mm with element separation of 0.02 mm. Arrays may be optically filtered for a discrete wavelength or many filters of different wavelength can be employed to produce a simultaneous multi-wavelength observation. The multi-wavelength approach results in superior target identification.

The granular nature of the films, in addition to providing large detector resistances, also implies a large surface-to-volume ratio, and hence a large excess noise component, which constitutes the principal disadvantage of these detectors. Generally, the excess noise in PbS and PbSe detectors is at least an order of magnitude larger than that in HgCdTe detectors designed for the same spectral regions. The principal noise components observed in PbS and PbSe detectors are the excess (1/f) noise and, at higher temperatures, thermal generation-recombination noise. Background-limited operation at normal or reduced backgrounds is generally not attainable. [5]

Ge and Si Extrinsic Detectors--are impurity doped photoconductors. Both Ge:xx and Si:xx, where xx denotes the impurity symbol, exhibit both gain and a large internal resistance at normal background levels, and are thus excellant photoconductors [6], [7]. In use the devices are cooled until few of the hydrogenic impurities are thermally ionized. Photoconductivity is then observed when one of these

impurities is optically ionized, and persists until the freed charge carrier is recaptured by the ionized impurity center.

The principal problems with these devices are their low operating temperatures and the low impurity absorption coefficients available. The detector noise of thermal origin in these devices results from flunctuations in the majority carrier population. The impurity absorption coefficient is limited by the low solubilities of the impurities of interest in Ge. In Si, the solubilities are greater, but if too large an impurity concentration is used, the impurity energy levels begin to overlap. "Hopping" conductivity in the impurity band limits the applied field, hence the gain, and also contributes excess noise.

Table 5 lists the most fully developed Ge:xx and Si:xx photoconductors and their respective cutoff wavelengths. The range of cutoff wavelengths extends

TABLE Cutoff Wavelengths and Approximate Maximum
Operating Temperatures (300°K Background,
2π Field of View) for Various Extrinsic
Ge:xx and Si:xx Photoconductors

$^{\lambda}_{c}$	T <sub>MAX</sub> (300°K
. 9	60°K
14	35
22	24
31	14
40	10 '
125	4
24	. 20
17	25
	14 22 31 40 125 24

from about 10 µm to well over 100 µm for the various impurities. The approximate maximum temperatures of operation for room temperature (300°K) background radiation

with a 180° field-of-view falling on the detector are also given. (Note that as the cutoff wavelength increases, the maximum operating temperature decreases.) With these incident backgrounds, the resistance of a Ge:Hg detector would be of the order of 10<sup>5</sup> ohms, and the maximum gain might be as great as 200. Ge:Hg is one of the best developed and most useful of the extrinsic detectors. The basic material purity is good, the recombination time can be adjusted from about 10<sup>-7</sup> to 10<sup>-11</sup> sec by compensation, and bias fields in excess of 500 V/cm can be used. The upper limit on the gain is set in practice by the usable bias field, which will eventually cause field or impact ionization of the impurity centers. The gain theoretically saturates at the onset of space charge limited current flow, but the ionization limit is generally reached first.

The Hg solubility limit of somewhat less than 10<sup>16</sup> cm<sup>-3</sup> in Ge (using conventional growth techniques) implies that these detectors must be several millimeters thick to provide complete absorption. Small detectors are therefore very like tiny matchsticks in form. Nevertheless, staggered linear arrays of one to two hundred detectors as small as 0.1 mm by 0.1 mm are assembled, and operate very well.

Extrinsic silicon detectors, though reported first, have received less attention than Ge:xx until recently, and are still undergoing development. The primary reason for the renewed interest in Si:xx is the higher solubility of most of the impurities of interest (e.g.,  $\geq 10^{16} \, \mathrm{cm}^{-3}$ ) and the larger optical absorption cross section associated with them. The typical detector thickness required for total absorption in Si:xx detectors is on the order of 100  $\mu \mathrm{m}$ . These detectors are thus more amenable to large linear array and mosaic fabrication than Ge:xx detectors. The photoconductive gain in Si:xx detectors tends to be lower than that in Ge:xx due to lower carrier mobility, shorter recombination time, and

(at present) lower maximum bias fields. On the other hand, the resistance of a Si extrinsic detector will be somewhat larger than that of a comparable Ge extrinsic detector [5].

## Photovoltaic Detectors

Photovoltaic detectors possess no current gain mechanism. The detector capacitance is the diode junction capacitance, which is substantially larger than that of a photoconductor. The internal resistance of a photovoltaic detector (photodiode), if not determined by junction leakage, is a derived quantity related to the current-voltage characteristic of the junction by

$$\frac{1}{R} = \left(\frac{\partial I}{\partial V}\right). \tag{11}$$

Thus, to determine the internal resistance of those detectors, it is necessary to specify the bias voltage to be applied to the junction. To determine the optimim bias, several factors must be considered.

Since junction characteristics tend to saturate, or very nearly saturate, at reverse bias, it might seem desirable to operate the devices at reverse bias so as to obtain the largest possible internal detector resistance, and hence the largest possible output signal voltage. In practice, leakage currents paralleling the thermally generated junction currents are difficult to avoid at any other than zero bias. Surface passivation techniques designed to eliminate this problem in infrared detector materials are somewhat primitive and not entirely successful. Even when these leakage currents are smaller than the thermal junction currents, so that the junction resistance is not shunted, they often contribute large amounts of 1/f noise.

With no light incident, the thermal junction current in a pho odiode originates in part from hole-electron pairs which are thermally generated near the

junction, diffuse to the junction and are separated by the junction field. Pairs generated within the junction are separated immediately by the junction field and also contribute to the thermal junction current. When the diffusion mechanism dominates, the rms noise generated by the thermal junction current is, in theory, only half as great at large reverse biases as it is at zero bias; a reason often cited in support of reverse bias operation. However, photodiodes are most sensitive in the lower portions of their effective temperature ranges where their thermal junction currents are often dominated by pair generation in the junction region (called the generation-recombination regime, although recombination contributes current only at forward biases). In such cases more noise is generated by the device at reverse bias than at zero bias.

Finally, reverse bias operation is sometimes recommended to reduce the junction capacitance of the photodiode, extending its frequency response. The reduced detectivity which results from the increased diode noise at reverse biases unusually negates this improvement. Use of the photodiode as a high-speed detector is an exception. In such applications, the photodiode noise is often less than that of the preamplifier, and advantage may be taken of the improved reverse-bias frequency response without notice of the increased photodiode noise.

Thus, for maximum sensitivity at low to moderate frequencies it is preferable to operate photodiodes as near zero bias as possible. [2] When limited by flunctuations in the incident background radiation, the photodiode has one important advantage over the photoconductor. Background-induced noise in a photoconductor arises from fluctuations in carrier generation and recombination. In a photodiode, the carriers are swept across the junction before recombination can occur. Other things being equal, the rms noise from the photodiode is therefore

a factor of  $\sqrt{2}$  less than that from the photoconductor, and the detectivity is  $\sqrt{2}$  larger.

PbSnTe Detectors—are available only in the photovoltaic mode. Successful preparation has been accomplished by numerous methods including evaporation, sputtering, vapor epitaxy, liquid epitaxy, vapor bulk, solid state recrystalization, and others. Detectors produced thus far have  $D*\lambda p$  in the  $10^{10}\, \text{cmHz}^{1/2}\, \text{W}^{-1}$  range and time constants which are R-C limited in the 10-100 nS range. By using cooled filters, D\* values have been reported [13] which exceed the 180° FOV and 300°K background limited D\* values. (The cooled filter was an anti-reflection coating of ZnSe deposited directly onto the detector surface.) D\* values of  $10^{11}\, \text{cmHz}^{1/2}\, \text{W}^{-1}$  were reported for 10.6  $\mu m$  radiation at a detector temperature of 77°K. [2] Figure 11 indicates the range of spectral detectivity currently available.

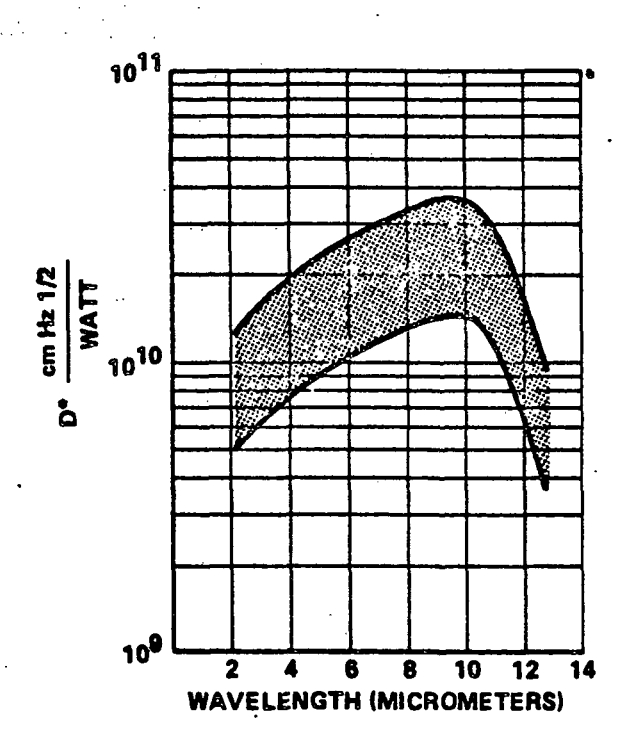


FIGURE 11 Range of Spectral Detectivity for PbSnTe (PV) Detectors at 77°K, 60°FOV

**REV. NO.:** 2

Silicon (IR Enhanced) Detectors--are often an economic choice for detection in the near infrared, i.e., .75 to 1.1  $\mu$ m. Detection is made difficult by the long optical absorption path length in silicon in the near IR range. In order to absorb all incident radiation the silicon thickness must be much greater than is necessary for shorter wavelength detection. Silicon is particularly reflective at about 1  $\mu$ m, therefore, an anti-reflection coating must be applied. Typically, a thick detector base with a  $1/4\lambda$  anti-reflection coating will provide approximately 38% quantum efficiency at 1  $\mu$ m.

Figure 12 shows the construction of two types of Si photodiodes. The Schottky barrier (Figure 12a) is formed by evaporating a transparent and conducting gold layer on one side of the silicon wafer and a thick aluminum layer on the opposite side. When a negative voltage is applied to the gold layer, it behaves like a step junction and a region depleted of charge is formed in the silicon over which an electric field exists. When a photon is absorbed, the minority carrier is swept to the junction, and the majority carrier to the ohmic contact, producing a current in the external circuit. The gold film thickness is critical in that it must exhibit maximum transmission of the illumination at the same time as maximum conductivity of the electrical current. The gold layer is typically 150°A thick and the silicon thickness ranges from 5 mils to 40 mils in different

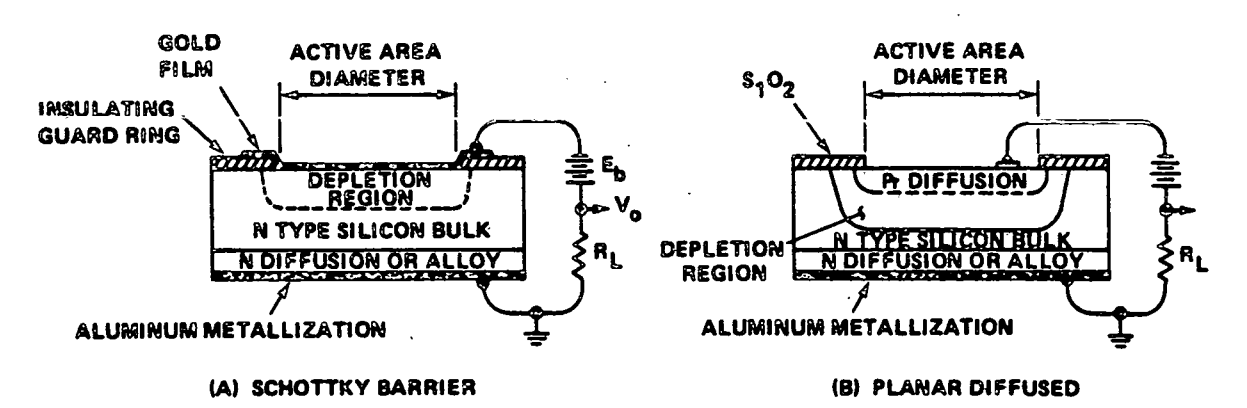
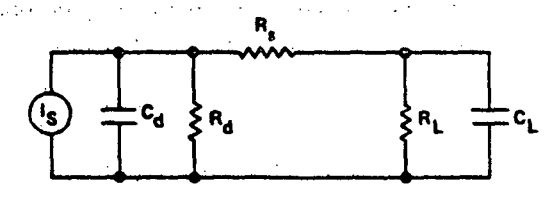


FIGURE 12 Construction of Si Photodiodes

detector types. The relationship between electric field penetration or depletion depth and applied voltage is  $d(\text{microns}) = 1/2\sqrt{\rho V}$ , where V = applied voltage and  $\rho = \text{resistivity}$  of silicon. For example, if 100 volts is applied to a junction made on 10,000 ohm-cm silicon, the depletion depth is 500 microns or 20 mils. This means the detector would be fully depleted at this voltage if the thickness was 20 mils (.020") or less.

The construction of a planar diffused Si photodiode is shown in Figure 12b. Here an oxide is grown on the silicon wafer, a hole etched in the oxide, and an impurity diffused into the silicon thru the oxide that forms a junction. The back side of the slice is then diffused with an ohmic plus contact. The depletion depth effect for the diffused device obeys the same equation as does the Schottky barrier. These two different construction techniques produce differences in spectral response, capacity, noise, high temperature and high light level operation.



te = SIGNAL CURRENT

C. = DEPLETION LAYER CAPACITANCE

R. = DEPLETION LAYER CONDUCTANCE

R. - SERIES RESISTANCE IN SILICON AND LEADS

R, - LOAD RESISTANCE

C, - LOAD CAPACITANCE

FOR MAXIMUM SIGNAL ACROSS R

 $R_s \ll R_L$   $R_s$  (TYPICAL) = 50~500  $\Omega$ 

R<sub>d</sub>>> R<sub>L</sub> R<sub>d</sub> (TYPICAL) > 10 MEG

FIGURE 13 Equivalent Circuit for Si Photodiode

Figure 13 shows the equivalent circuit for both the Schottky barrier and planar diffused devices. There is a junction depletion layer capacitance ( $C_d$ ), a junction parallel conductance ( $R_d$ ), which is the effective resistance of the

REV. NO.: 2

depletion region itself, and a series resistance  $(R_s)$ , which is the resistance of the undepleted silicon and any lead resistance. A constant light flux incident on the cell will generate a constant current.

The generation of current by light in a silicon cell is a quantum effect; i.e., one incident photon produces one electron hole pair. The incoming light beam thus represents a stream or current of photon particles that is converted to a stream of electrons or electrical current. The photon current flow has units of watts, since each photon is represented by a unit of energy expressed in joules, and a watt is the flow per second of a joule of energy. Thus the responsivity is a measure of the effectiveness of the light current to electrical current transduction process in a silicon cell. The responsivity will vary with changes in wavelength of the incident light and will also vary slightly with changes in applied voltage and changes in temperature. The reason for the responsivity change with wavelength is that the light reflection and absorption coefficients of silicon change with wavelength. The applied voltage affects the collection process of the photogenerated electron-hole pairs within the silicon and thus varies the responsivity. Temperature changes affect both the optical constants of the silicon cell and the collection process, thus varying the responsivity.

Figure 14 shows the characteristic I-V curves for both the Schottky barrier and planar diffused devices. A load line for the reverse bias mode or photoconductive mode is shown on the section of the graph to the right of the zero voltage line, and a load line for photovoltaic operation (i.e., no bias voltage) is shown to the left of the zero voltage line.

Several design considerations can be derived from close scrutiny of this curve. For the forward bias mode the device is acting as a photovoltaic (self generating) device. If the device is working into a short circuit, corresponding

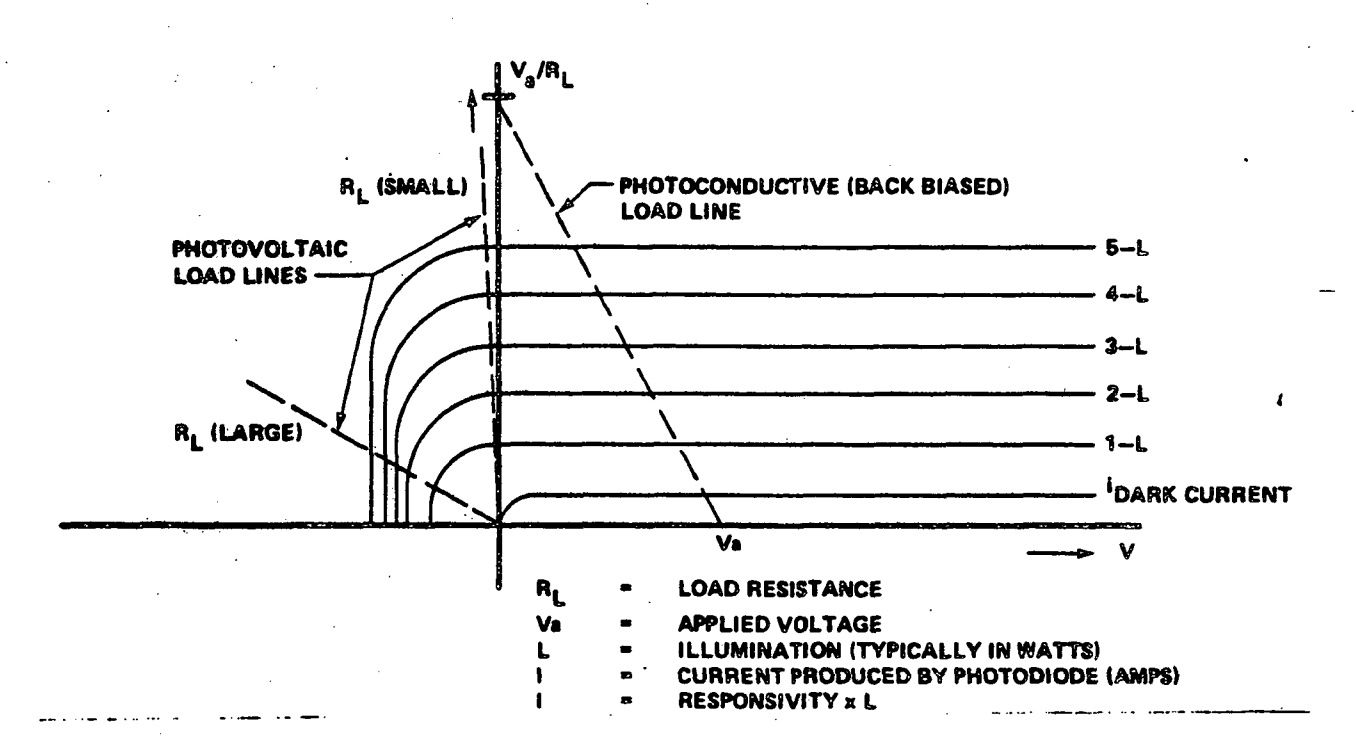


Figure 14 Shottky Barrier and Planar Difused Characteristic I-V Curves

to a vertical load line, the current output is linear with increases in incident illumination. As R<sub>L</sub> increases, operation becomes non-linear until the open circuit (load line horizontal) condition is obtained. At this point the open circuited voltage output is proportional to the log of the incident radiation. In this photovoltaic model of operation there is no dark current, making this ideal for low level measurements where changing dark currents are a significant portion of the final current output. This problem is especially significant where changing ambients can change the dark current by as much as 10% per 1°C. In the reverse bias mode linear operation is maintained so long as the saturation power is not exceeded, about 10 mw/cm² and the bias level remains higher than the product of the maximum signal current and the load resistance.

Indium Antiomonide & Indium Arsenide Detectors--are sensitive in the 1  $\cdot$  0 5.5  $\mu$ m and 1 to 3.5  $\mu$ m wavelength region respectively. Both are intrinsic detectors.

InSb detectors have been made for operation in the photoconductive and photovoltaic mode, but only the latter is commercially available. Typical  $D^*\lambda p$  values for InSb range from 0.55 x  $10^{11}$  to 1.0 x  $10^{11}$ cm  $Hz^{12}W^{-1}$ .

InAs have not progressed to the degree of perfection enjoyed by InSb. The material itself is more difficult to grow, and often contains a high concentration of low angle grain boundries. [5] The equivalent circuit of either type detector is the same as that for silicon detectors, discussed previously. Typical circuit operation provodes for a current mode preamplifier. The InSb and InAs detectors require cooling to liquid-nitrogen temperatures.

#### RECENT DEVELOPMENTS IN IR DETECTORS

Heterodyning--is a process by which light waves differing in frequency by  $\Delta f$  produce a photoemissive current modulated at  $\Delta f$ . The application of the scheme in the infrared region provides for a local (tunable) laser beam which is mixed in the photodetector with the incident radiation. The differential frequencies can then be analyzed by means of conventional microwave or rf circuitry.

The main requirements for a good heterodyne detector are a high quantum efficiency and a short response time. For video detection with photoconductors the responsivity is proportional to the lifetime and the most sensitive detectors are comparatively slow. For example Ge:Cu grown from extremely pure starting material (-10<sup>12</sup> impurities cm<sup>-3</sup>) has a lifetime of between 10<sup>-6</sup> and 10<sup>-7</sup> s. Such a photoconductor is an excellent video detector but has a limited bandwidth for heterodyne detection. By adding donor impurities such as antimony the lifetime can be reduced to less than 10<sup>-9</sup> s and the material is then suitable for heterodyne systems, but poor as a video detector. By suitable addition of compensating impurities all the doped germanium detectors can be made high speed.

Except at 10 μm where carbon dioxide lasers are available as local oscillators results with heterodyne detection have fallen far short of their theoretical performance. The chief problems appear to be lack of local oscillator power at wavelengths other than 10 μm, and the low quantum efficiency of the longer wavelength extrinsic detectors. Apart from Ge:Cu excellent results [8] have been achieved using HgCdTe and PbSnTe photovoltaic detectors at 10 μm and GaAs at 337 μm

At wavelengths beyond 125 µm the detectors normally considered for heterodyning are: (1) Josephson junctions, (2) Metal-oxide-metal and metal-semiconductor point-contact diodes, (3) Schottky diodes. Although good results have been achieved with all these devices the theoretical limit is a long way distant. Figure 15 shows the approximate state-of-the-art of heterodyne detection. The high NEP achieved by InSb electronic bolometer detectors is worth noting. They appear to have a good quantum efficiency, and reasonable power local oscillators are available in the millimeter region. The great disadvantage is the very limited bandwidth of less than 10 MHz. [9]

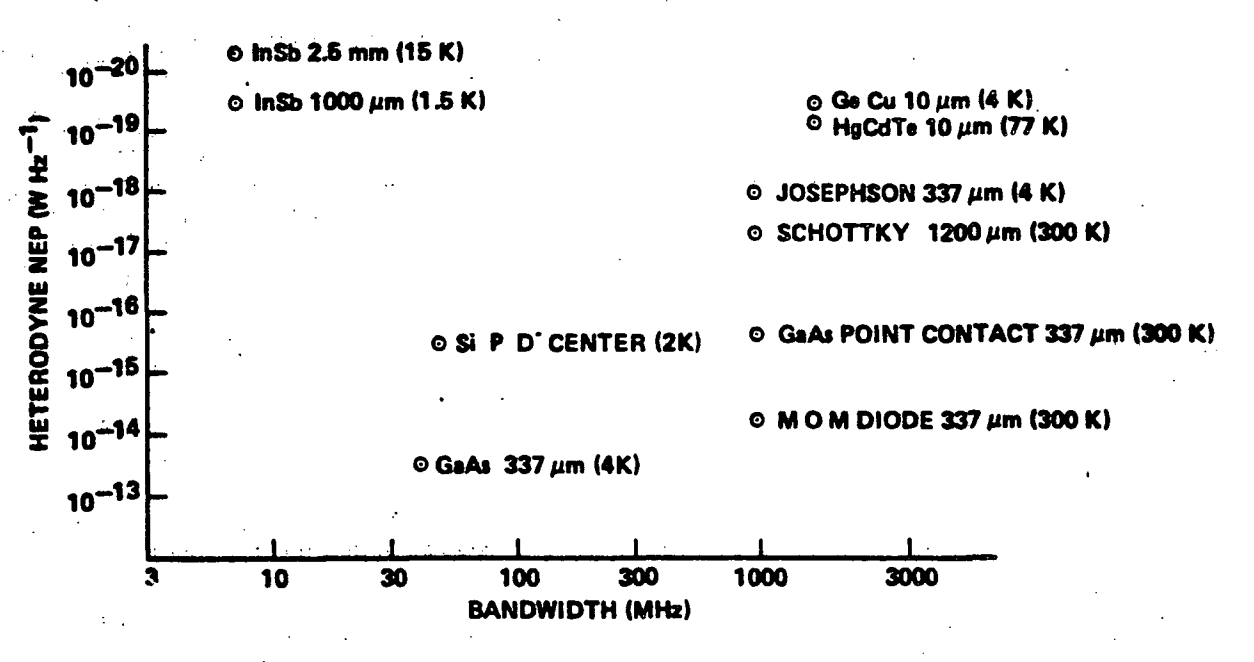


FIGURE 15 The Present State-of-the-Art of Infrared Heterodyne Detection

In Figure 15 one point is labled "Si: P D." This type of impurity photoconductor may offer an alternative to Josephson detectors and diodes in the submillimeter region for heterodyne detection. For a quantitative description of this detector, see [9].

Photon Drag--is a detection mechanism which relies on momentum transfer from photons to the free carriers in a semiconductor. p-Type germanium is widely used as a detector material for CO<sub>2</sub> lasers at 10 µm. Results obtained using an HCN laser at 337 µm and an H<sub>2</sub>O laser at 119 µm show that such detectors will be useful for measuring the output of CW and pulsed far infrared lasers. [10] The responsivity of a photon drag detector is proportional to the absorption coefficient of the free carriers in the semiconductor, and the absorption of germanium is some ten times greater in the 100-1000 µm region than at 10 µm. Figure 16 shows the expected performance of both n- and p-type germanium photon drag detectors of 2x2 mm area in the submillimeter region. The limited number of experimental points are in good agreement with theory. Table 6 gives details of a p-type detector under investigation at the present time. It has the advantage that with far infrared lasers pumped by CO<sub>2</sub> lasers it can measure the power of both lasers.

Photon drag detectors are very insensitive devices, but they have advantages as power measuring devices. They can be used from DC to about 10<sup>9</sup> Hz and their performance does not change with time. They are cheap and rugged, and operate at room temperature. More confirmation of their performance in the submillimeter region is required but potentially they appear to be useful comparison devices for the more sophisticated and much more sensitive detectors required in this region [9].

Charge-Coupled-Devices (CCD's)--with application in readout and signal processing techniques for infrared detector arrays, have been under investigation since about

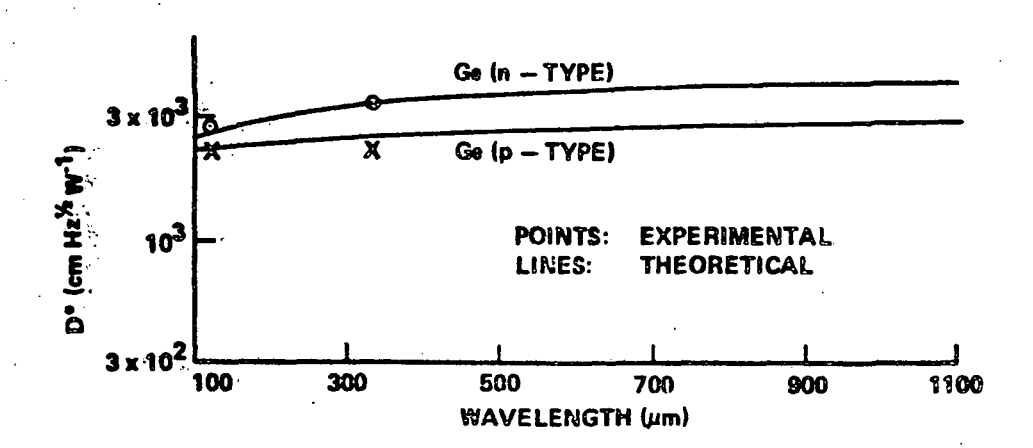


FIGURE 16 Performance of n- and p-Type Germanium
Photon Drag Detectors in the Far Infrared

TABLE 6 p-Type Germanium Photon Drag Detector

Active area	4 mm <sup>2</sup>
Length	10 mm
Resistance	400 ohms
10.6 µm Responsivity	$3 \times 10^{-6} \text{VW}^{-1}$
500 µm Responsivity	$2 \times 10^{-5} \text{VW}^{-1}$
10.6 μm NEP	$2.2 \times 10^{-3} \text{WHz}^{-1/2}$
500 μm NEP	$1.5 \times 10^{-4} \text{WHz}^{-1/2}$

1972. The charge-coupling principle basic to CCDs is very simple. Carriers are stored in the inversion regions (or potential wells) under depletion-biased electrodes and moved from under one electrode to under the next by appropriate pulsing of the electrode potentials. The neighboring electrodes must be close enough to allow the potential wells under them to couple and the charges to move smoothly from one well to the next.

In imaging, charges are introduced into the device when light from a scene is focused onto the device's surface. As in all semiconductors, the absorption of light quanta creates hole-electron pairs which under the influence of the potential beneath each storage electrode, are collected as a charge packet. The quantity of charge stored is proportional to the intensity of the image.

In this manner, a spatial charge representation of the scene is stored in the device. It is transferred off the device when clock voltages are applied to the electrodes, moving each charge packet serially from storage site to site until all charges reach the output diode.

In signal-processing and memory devices, the signal is not light-induced but is simply introduced into the device by a standard MOS element and then passed along by pulsing the appropriate electrodes sequentially.

Both hybrid and monolithic arrays of indium antimonide (InSb) and Si (CCD readout) have been fabricated, and reported [11] as significant improvements over current state-of-the-art. In the monolithic approach, the InSb infrared detectors and the CCD readout are integrated on the same InSb chip. The hybrid approach integrates InSb detectors and silicon CCD's in a modular assembly using advanced interconnection technology. Both techniques provide the means for incorporating self-scanned solid state detector arrays (so called "pushbroom mode") in earth oriented and planetary exploration remote sensing missions.

Table 7 compares conventional and InSb/CCD arrays. For further (quantitative) information the reader is referred to [11] and [12].

2 REV. DATE: 31 Jan 1978

REV. NO .:

TABLE Comparison of Conventional and InSb/CCD Arrays

Spectral Band (µm)	1.55 to 1.75		3.6 to 4.1	
Туре	InSb(PV)	InSb/CCD	InSb(PV)	InSb/CCD
Responsivity (A/W) R	1.0	1.0	2.3	2.3
Number of Detectors N	1 .	16	1	16
Scan Efficiency	0.8	0.4	0.8	0.4
IFOV Dwell Time (usec)	9.0	4.5	9.0	4.5
Bandwidth (KHz)	55	110	55	110
Detectivity (cm Hz $^{V2}/W$ ) D* $\lambda$	3.0x10 <sup>11</sup>	1.3x10 <sup>12</sup>	6x10 <sup>11</sup>	2.7x10 <sup>12</sup>

### DETECTOR COOLING DEVICES AND TECHNIQUES

In general, the long wavelength cutoff and detectivity, as well as other detector parameters, are determined by the operating temperature. Photodetectors operating in the 8 to 13 µm atmospheric window require lower operating temperatures than those operating in the 3 to 5 µm region. Intrinsic detectors, such as the ternary alloys, mercury cadmium telluride and lead tin telluride, can operate at higher temperatures than the extrinsic detectors, such as doped germanium. For remote sensing applications, future imagers and scanners particularly those operating in the 8 to 13 µm region will utilize intrinsic photodetectors cooled to 100 K or below to achieve background-limited performance. [12]

Several devices have been produced for the purpose of providing continuous cooling of detector elements to temperatures extending from 233° to 50°K. Each method has its own advantages and disadvantages.

## Thermoelectric

Thermoelectric cooling, utilizing the Peltier effect with dissimi ar metallic conductors (and variously called thermoelectric refrigeration, Peltier-effect

cooling, or electronic cooling), have found only modest acceptance as a detector cooling device because they are limited to requirements greater than 150°K. When designed in conjunction with an infrared detector package, a single-stage thermoelectric cooler will produce a temperature reduction of almost 50°K, with the hot junction at 293°K. A larger unit, incorporating two stages of thermoelectric junctions in cascade, will provide 79°K cooling from a hot-junction temperature of 298°K. [1] The electric power requirements of the thermoelectric coolers are in the nature of high, closely regulated DC current (5 to 20 amp), with low voltage. For development of various output capacities, the number of basic elements is proportionally increased; they all act in parallel, and their outputs add together. Semiconductor materials, such as bismuth-telluride - selenide and bismuth-antimony-telluride alloys, are the most common elements employed.

With an input to the device of low-voltage direct current and with heat continuously abstracted at one junction at ambient temperature, the other junction will cool. Essentially each of the two junctions become an "activity cell" in which at the lower refrigeration temperature level, heat is converted into electrical effect, and at the higher atmospheric temperature, the electrical effect is converted into heat. This establishes the basis of "heat pump" operation: the lower-temperature heat requirement must be supplied, essentially as in the evaporator of a vapor-compression system, by heat withdrawl via heat transfer, from all connected surroundings.

### Joule-Thompson

A Joule-Thompson (J-T) cooler (also called a demand flow cryostat) is a self-regulating device designed to reduce the temperature of a high-pressure gas by sudden adiabatic expansion. A thermostatic control element in the device senses the liquid level in the detector dewar (fused glass) and operates a self-contained

valve in response to changes in heat load and ambient temperature. The J-T device is passive: no electrical connections are required.

Figure 17 illustrates the functional components of an open-loop J-T system.

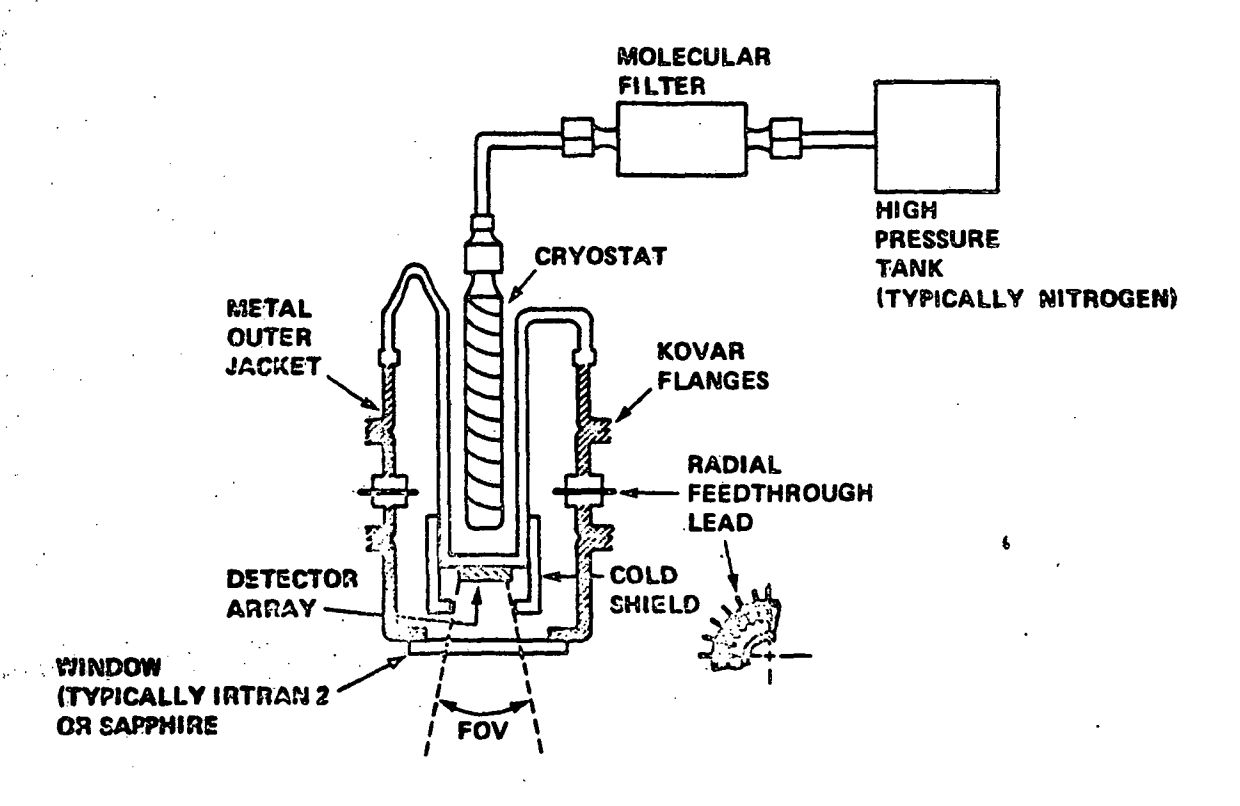


FIGURE 17 Functional Components of an Open-Loop J-T System

A major design problem with open-cycle liquid systems is to achieve the requisite thermal isolation in a sufficiently rugged dewar package. Extreme care with insulation systems and ingenuity in the design of mechanical supports are required to achieve the required thermal isolation. A further problem area with liquid systems is to determine the location of the vapor phase in the near zero-g environment, since it is necessary to vent only vapor in order to conserve refrigeration. Several schemes have been proposed for circumventing the vapor liquid separation problem, but none have been demonstrated, in a zero cenvironment.

In a solid-cryogen cooler, the detector is usually mounted on a pedestal which is thermally connected to a vacuum-insulated dewar containing a solidified cryogen. The ullage space above the stored solid is evacuated to maintain the cryogen in its solid state. Heat entering from the detector and the surroundings causes the cryogen to sublime, and the resulting vapor is vented. A solid-cryogen dewar comprises an inner vessel containing the cryogen, an insulation system, and a vacuum shell. A fill and vent tube permits initial filling of the cryogen vessel and venting of a vapor during operation. Auxiliary cooling lines, through which a liquid cryogen is circulated, are used during the filling operation and during prelaunch storage.

Depending on the application, a solid-cryogen cooler can offer several advantages over alternative systems. It offers a lower weight system compared with those using stored-liquid cryogens, since the latent heat of sublimation is greater than the latent heat of vaporization. Additionally, solid systems avoid the problem of locating the vapor phase under conditions of near-zero gravity.

There are several disadvantages to a solid-cryogen cooler in that it imposes restrictions on the detector mounting and, additionally, methane and hydrogen, both of which have excellent properties as solid coolants, are hazardous materials and require special handling.

The fact that the use of lower temperature cryogens results in a significantly higher weight, plus the fact that the weight of the cryogen is critically dependent upon the temperature of the external shell of the dewar, has led to the use of dual cryogen systems for applications where low detector temperatures are required. Such a system results in lower cooler weight at the cost of increased complexity. In such a system, a higher temperature cryogen, such as ammonia, is used to cool a thermal shield which completely surrounds a lower temperature

cryogen such as methane. A multilayer insulation system is placed between the shield and the outer shell of the cooler.

### Passive Radiators

Conceptually, the simplest way of developing cryogenic temperatures in space is to radiate power to the low-temperature heat sink of space by use of a suitably sized emitting surface. This concept is particularly attractive since such a system is completely passive, requires no continuous electrical power, and is potentially capable of high reliability for extended periods. Considerable effort has been devoted toward the design of passive radiators to maintain the temperature of detectors in electro-optical systems at temperatures in the 70 to 120 K region, and several such systems have flown.

The effective temperature of the star-speckled sky is less than 10 K. A suitably sized cold plate of high emittance to which one or more detectors are mounted can be made to radiate to this sink. It is, of course, necessary to shield the cold plate against heat inputs from the sun, the earth, and the space-craft. These considerations usually result in a radiator design which is tailored to a particular spacecraft system. The orbit plane, orbit altitude, and the location of the radiator on the spacecraft all significantly influence the design of the radiator.

A typical passive radiator design is shown schematically in Figure 18.

The assembly consists of a conical outer stage mounted to the optical instrument with low-conductance supports. The outer stage supports a disc-shaped, inner, low-temperature stage, also mounted with low-conductance supports. The cooled detectors are mounted on the low-temperature stage.

As shown in Figure 18, the inner stage has a clear-field-of-view to deep space. To achieve low inner-stage temperature, the clear-field-of-view is made

as large as possible--usually limited only by geometrical considerations prescribed by the orbit and the location of external appendages on the spacecraft.[12]

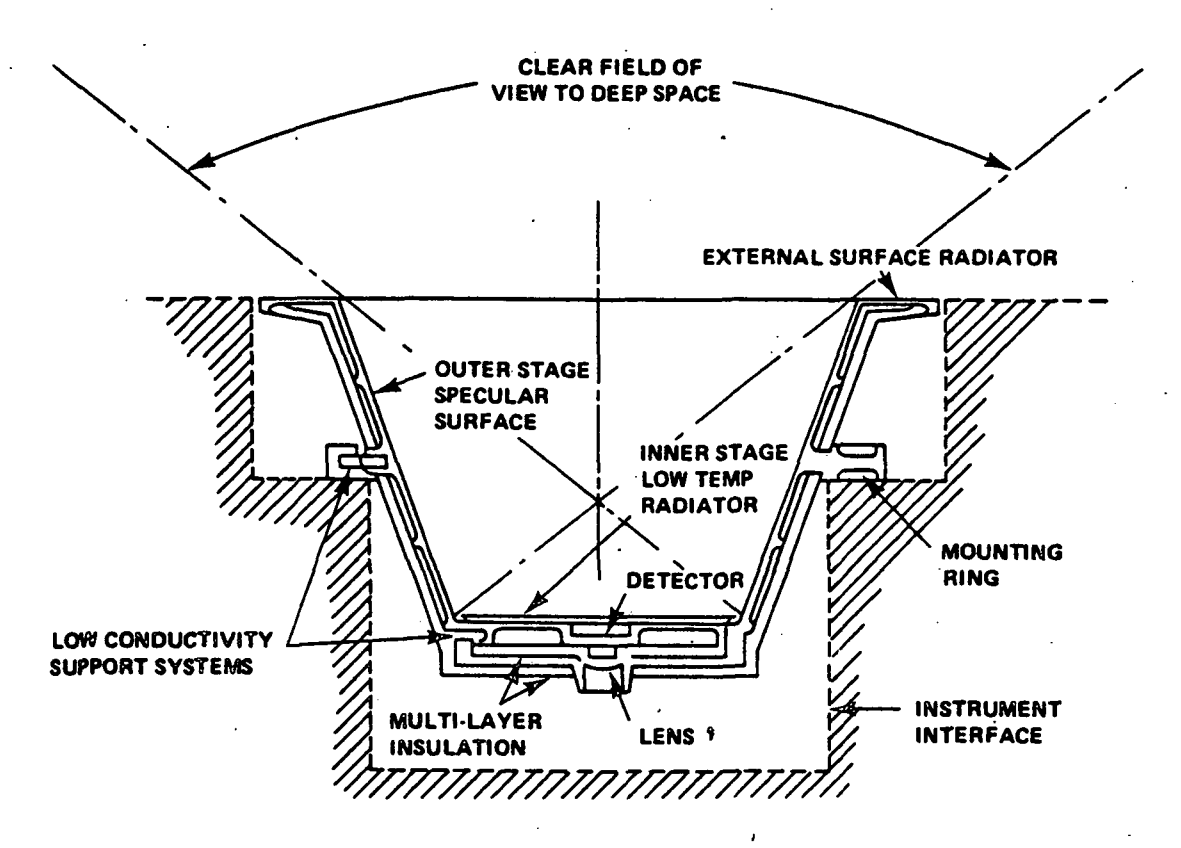


FIGURE 18 Schematic Diagram of a Passive Radiator

Although passive radiators are simple in principle, there are several important design problems associated with the development of flight hardware. The design of the support system is critical since it must support the low temperature stage with an extremely low thermal conductance and must maintain the detector in precise alignment with the room-temperature optical instrument.

Another fundamental design problem is that of preventing contamination of low-temperature optical surfaces, such as detector capsule windows, by outgassing from either the spacecraft or the radiator itself. Contaminants on the low-temperature surfaces can effect the optical signal throughput to detectors, and can also influence the detector operating temperatures by altering the emittance,

REV. NO.: 2 REV. DATE:

31 Jan 1978

solar absorptance, or specularity of critical thermal control surfaces. Current design practices are based on using protective covers and heaters to prevent contamination during prelaunch, launch and initial orbital operation.

# Closed-Cycle

A closed-cycle refrigeration system pumps the heat from the load temperature up to the temperature of the space radiator. The heat load, which includes all energy entering the system, is radiated to space by the heat rejection system. This system consists of a heat rejection radiator plus a means of transferring the heat generated in the refrigerator to the radiator. The transfer media may be conductive paths, heat pipes, or an active coolant loop in which a heat transfer fluid is circulated by a coolant pump.

Gryogenic refrigerators may be classified by two general types; intermittent flow and continuous flow. Intermittent flow refrigerators use regenerative heat exchangers and are distinguished by the thermodynamic cycle on which they operate. The Stirling, Gifford-McMahon, and Vuilleumier (VM) cycle refrigerators have been used for ground-based, airborne, and space missions. VM cycle refrigerators are heat-driven derivatives of the Stirling cycle refrigerators. The cycle is attractive for space use because of the ability for using solar or isotope thermal energy to drive the thermal compressor directly, thereby minimizing the electrical power input.

Continuous-flow refrigerators use counterflow heat exchangers. The units operate on the reversed Brayton thermodynamic cycle or derivatives of it. [12]

**REV. NO.:** 2

TABLE 8 Common Elements and Compounds used for Infrared Detectors

SYMBOL  MN  Manganese  Co  Cobalt  Ni  Nickel  Au  Gold  Ge  Germanium  Sb  Antimony  Te  Bi  Bismuth  PvF <sub>2</sub> Polyvinylidene Fluoride  SYMBOL  HgCdTe  HgCdTe  Cd  Ge(doped):  Zn  Cd  HgCdTe  Ge(doped):  PbSe  Ge(doped):  Zn  Cd  Hg  Hg  Hg  Au	NAME
MN Manganese HgCdTe  Co Cobalt Ni Nickel Au Gold Ge Germanium Sb Antimony Te Tellurium Bi Bismuth PvF <sub>2</sub> Polyvinylidene  HgCdTe  HgCdTe  HgCdTe  HgCdTe  FbS  Ge (doped): Zn  Cd  Cu  Hg	
LiTaO <sub>3</sub> Lithium Si (doped): Tantalate As Sb Sulfate  InAs InSb PbSnTe	Mercury Cadmium Telluride Lead Sulphide Lead Selenide Germanium  Cadmium Copper Mercury Gold Silicon Arsenic Antimony Indium Arsenide Indium Antimonide Lead Tin

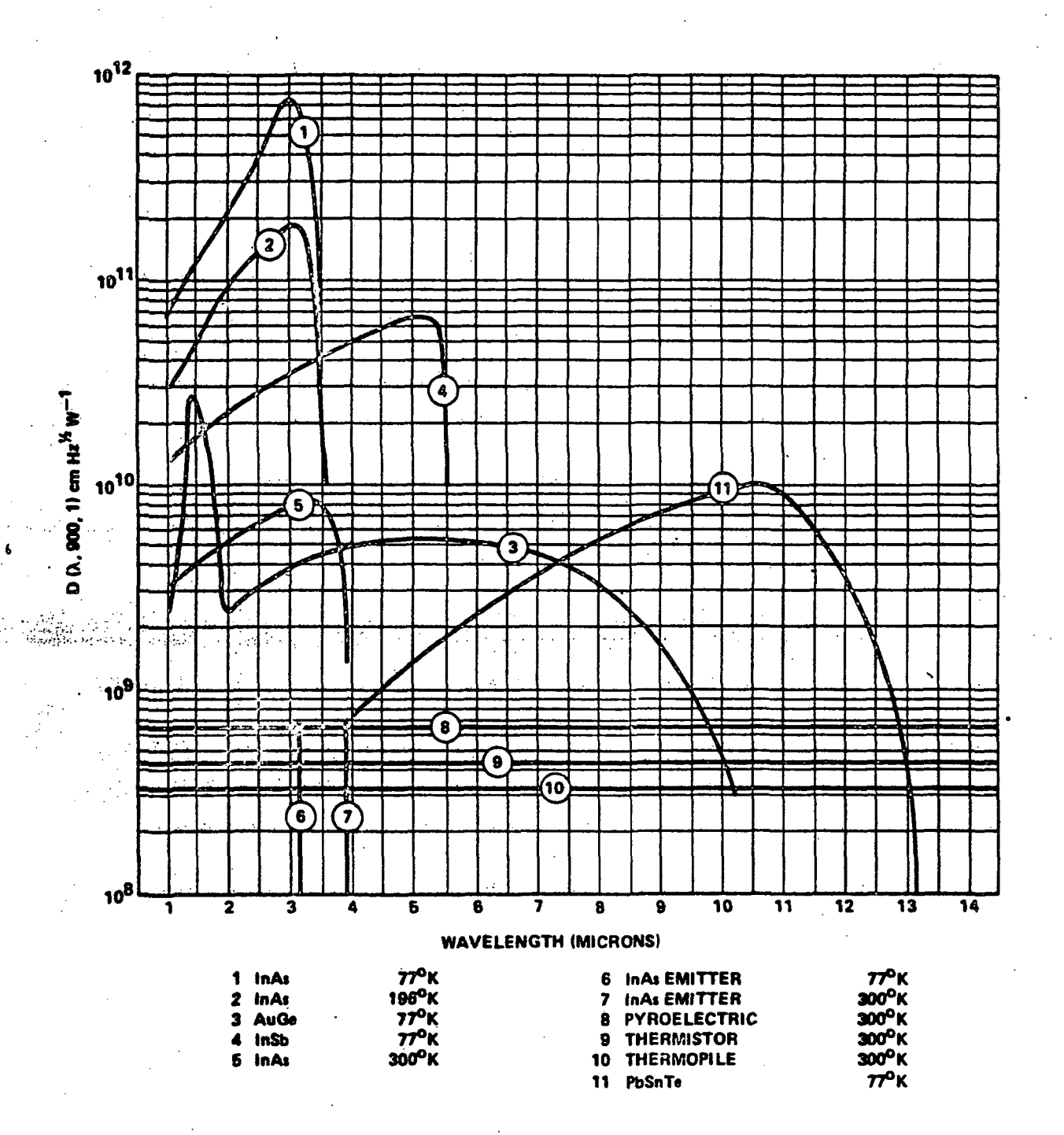


FIGURE 19 Spectral Response of Various Infrared Detectors

TABLE 9 Typical Infrared Detector Characteristics

ТҮРЕ	OPERATING TEMP. (°K)	λρ(μπ)	$(10^{10} \text{ cmHz}^{1/2} \text{W}^{-1})$	τ .
PbS	295 193 77	2.4 2.8 3.0	8.0 - 15.0	0.1 - 0.5 ms 2 - 5 ms 2 - 5 ms
InAs	77 193	3.0 3.2	60.0 - 80.0 60.0 - 80.0	5 μs 5 μs
PbSe	295 193 77	3.8 4.8 5.0	0.1 - 0.5 1.5 - 3.0 1.5 - 3.0	1 - 3 μs 10 - 40 μs 15 - 50 μs
InSb	77	5.0	8.0 - 20.0	20 - 200 ns
Ge:Au	77	5.0	0.3 - 0.7	10 - 100 ns
Ge:Hg	4	10.4	1.0 - 2.0	10 - 100 ns
PbSnTe	77	10.0	1.5 - 3.0	1 - 2 μs
HgCdTe	77	13.5	.5 - 2.0	0.2 - 0.8 μs
Ge:Cd	4	19.0	2.0 - 3.0	10 - 100 ns
Ge:Cu	4	21.0	1.3 - 2.0	10 - 100 ns
Ge:Zn	4	37.0	1.0 - 2.0	10 - 100 ns
Thermistor Bolometer	295	FLAT	0.6 - 0.8	0.2 - 1.0 ms
Carbon Bolometer	2	FLAT	4.3	10 - 100 ms
Thermocouple	295	FLAT	.02	10 - 50 ms
SbBi	295	> 40	>.01	20 - 40 ms
BiTe	295	> 50	0.009022	50 - 70 ms
PVF <sub>2</sub>	· 295	> 30.0	.01	0.1 - 0.8 μs
LiTa7 <sub>3</sub>	295	14.0	.01	.15 - 1.0 μs
TGS	295	20.0	.04	0.1 - 1.0 μs

# TABLE 10 Infrared Detector Types and Associated Sensor-Program\*

THERMAL DETECTORS	PHOTON DETECTORS
Thermistor Bolometer  • ERB - NIMBUS  • SR - ITOS  • THIR - NIMBUS  Radiation Thermopile  • IRIS - NIMBUS  • IRIS - MARINER  • NFR - PIONEER	Photoconductive  IRIS - NIMBUS CZCS - NIMBUS HIRS - ITOS VHRR - ITOS VISSR - GOES HCMR - AEM MSS - LANDSAT VAS - GOES
Pyroelectric  · VORTEX - PIONEER  · PMR - NIMBUS  · VTPR - ITOS  · BSU - TIROS  · SSU - TIROS	Photovoltaic  MAWD - VIKING  LIR - PIONEER  HIRS - ITOS  VAS - GOES  ASSIR - STORMSAT

<sup>\*</sup> e.g., Under the column titled THERMAL DETECTORS, see <u>Pyroelectric</u>. The Vertical Temperature Profile Radiometer (VTPR) incorporating a triglycine sulfate (TGS) detector was flown on an ITOS satellite.

#### REFERENCES

- [1] Jamieson, John A., et. al., <u>Infrared Physics and Engineering</u> (New York: McGraw-Hill, 1963), pp. 123-124.
- [2] Levinstein, Henry and Mudar, J., "Infrared Detectors in Remote Sensing," Proceedings of the IEEE, Vol. 63, No. 1, January 1975.
- [3] Thermal and Photon Detectors, Barnes Engineering Company, Bulletin 2-350A.
- [4] Simon, Ivan, <u>Infrared Radiation</u> (New Jersey: D. Van Nostrand Co., Inc., 1966), pp. 29-40.
- [5] Emmons, R.B., et. al., "Infrared Detectors: An Overview," Optical Engineering, Vol. 14, No. 1, January 1975.
- [6] Putley, E.H., "Far Infrared Photoconductivity," Phys. Stat. Soc., 6, 571 (1964).
- [7] Levinstein, H., "Extrinsic Detectors," App. Optics, 4, 639 (1965).
- [8] DeGraauw, T., Space Sci. Rev., Vol. 17, p. 709 (1975).
- [9] Kimmitt, M.F., "Recent Development of Infrared Detectors," <u>Infrared Physics</u>, Vol. 17, pp. 459-466 (1977).
- [10] Norton, P., J. of Appl. Phys., Vol. 47, p. 308 (1976).
- [11] Birch, J.R., et. al., Infrared Physics, Vol. 14, p. 189 (1974).
- [12] Phillips, J.D., Scorso, J.B., and Thom, R.D., "InSb Arrays with CCD Readout for 1.0 to 5.5 µm Infrared Applications," Conf. CCD Dev. Tech. & Appl., Washington, D.C., 1976, pp. 49-52 (JPL SP43-40).
- [13] "Advanced Scanners and Imaging Systems for Earth Observations," Report of a Working Group, NASA SP-335, 1972.
- [14] Rolls, W.H., and Eddolls, D.V., "High Detectivity Pb Sn<sub>1-x</sub> Te diodes," Appl. Phys. Lett., Vol. 9, pp. 304-306, October 1966.
- [15] "MOS Integrated Circuits," ed., William M. Penney, (Van Nostrand Reinhold Co.--New York), 1972, pp. 34-35.

#### **BIBLIOGRAPHY**

- (1) Long, D., and Schmit, J.L., "Semiconductors and Semimetals," <u>Infrared Detectors</u>, Vol. 5, Academic Press (New York, 1972).
- (2) Miller, B., "FLIR Gaining Wider Service Acceptance," Aviation Week and Space Technology, pp. 42-49, 7 May 1973.
- (3) Astheimer, R.W., "Infrared to Visible Conversion Devices," Photographic Science and Engineering, Vol. 13, pp. 127-133, May-June 1969.
- (4) Petrite, R.L., "Theory of Photoconductivity in Semiconductor Films," Phys. Rev., Vol. 104, pp. 1508-1516 (1956).
- (5) Wolfe, W.L., "Photon Number D\* Figure of Merit," Applied Optics, Vol. 12, pp. 619-621 (1973).
- (6) Kinch, M.J., et. al., "Recombination Mechanisms in 8-14 μm HgCdTe," J. App. Phys., Vol. 44, p. 1649 (1973).
- (7) Lee, E., and Bube, R.H., "Further Information on the Mechanism of Photoconductivity in Chemically Deposited Lead Sulfide Layers," J. App. Phys., Vol. 43, p. 4259 (1972).
- (8) Blouke, M.M., et. al., "Gain Saturation of Extrinsic Germanium Photoconductors at Low Temperatures," J. App. Phys., Vol. 43, p. 188, 1972.

Harrist Charles and the market and the state of

- (9) Johnson, M.R., Chapman, R.A., "Performance Limits for PbSnTe Photovoltaic Detectors," Proc. Iris-Detector Specialty Group, p. 101, 19 March 1974.
- (10) Putley, E.H., "The Pyroelectric Detector," Semiconductors and Semimetals, Infrared Detectors, Vol. 5, Academic Press (New York, 1970).
- (11) Anderson, L.K., et. al., "High Speed Photodetectors of Microwave Demodulation of Light," <u>Advances in Microwaves</u>, Vol. 5, Academic Press (New York, 1970).
- (12) Dimmock, J.O., "Capabilities and Limitations of Infrared Imaging Systems," Spie Seminar Proc., Vol. 32, p. 9 (1973).
- (13) Melngailis, I., "Small Bandgap Semiconductor Infrared Detectors," J. Luminesc, Vol. 7, pp. 501-523 (1973).
- (14) Annable, R.V., "Radiant Cooling," Applied Optics (1970).
- (15) Breckenridge, R.W. (Jr.), "A 3.6°K Reciprocating Refrigerator," Presented at the 1968 Cryogenic Engineering Conference, Cleveland, Onio (1968).

- (16) Gabron, F., McCullough, J.E., Merriam, R.L., "Spaceborne Passive Radiator for Detector Cooling," Proceedings of 20th National Infrared Information Symposium (IRIS) 1972.
- (17) Gessner, R.L., Colyer, D.B., 'Miniature Claude and Reversed Brayton Cycle Turbomachinery Refrigerators," Advances in Cryogenic Engineering, Vol. 13 (1968).
- (18) Maddocks, F.E., "Application of Turbomachinery to Small-Capacity, Closed-Cycle, Cryogenic Systems," Advances in Cryogenic Engineering, Vol. 13 (1968).
- (19) Prast, G., The Vuilleumier (VM) Cycle--Cryogenics and Infrared Detection, Boston Technical Publishers, Inc., Cambridge, Ma., 1970.
- (20) Schulte, C.A., Fowle, A.A., Heuchling, T.P., Kronauer, R.E., "A Cryogenic Refrigerator for Long-Life Application in Satellites," <u>Advances in Cryogenic Engineering</u>, Vol. 10, Plenum Press, New York, p. 477 (1965).

# Appendix A

# INFRARED DETECTORS ILLUSTRATION CREDITS

Figu	re No.	Page	Reference	Page
2	a.	A-5	Barnes Engr. Co. Bulletin No. 2-102	N/A
2	b	A-5	Barnes Engr. Co. Bulletin No. 2-101	N/A
3	,4	A-6	Barnes Engr. Co. Bulletin No. 2-102	N/A
6		A-11	New England Research Center Sudbury, Massachusetts Data Sheet: Li TaO3, Pyroelectric Infrared Detector	N/A
7	·	A-13	[15]	35
8	3	A-16	[5]	22
<b>9</b>	9,10	Λ-19,Α-20	Infrared Industries Inc. Bulletin: PbSMr. Versatility of The Detector World December 76	N/A
1	ú	A-28	Santa Barbara Research Center-Brochure	12
. 1	12,13,14	A-29,A-30, A-32	United Detector Technology "Silicon Photodetector Design Manual"	1,2,3
1	1:5	A-34	[9]	462
נ	16	A-36	[9]	465
1	18	A-43	[13]	135
1	19	A-46	[3]	6

#U.S. GOVERNMENT PRINTING OFFICE 1978- 640-081/226 REGION NO. 4

REV. NO.:

2